Universitat de Lleida

Dorsal Root Ganglion neurons as a model of Friedreich Ataxia: cellular alterations and therapeutic approaches

Elena Britti

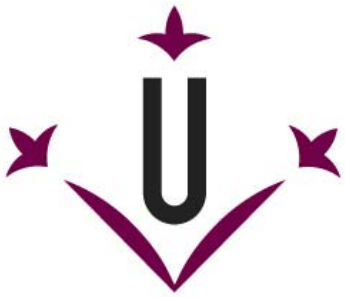

Universitat de Lleida

DORSAL ROOT GANGLION NEURONS AS A MODEL OF FRIEDREICH ATAXIA

CELLULAR ALTERATIONS AND THERAPEUTIC APPROACHES

Elena Britti

2021

Universitat de Lleida

TESI DOCTORAL

DORSAL ROOT GANGLION NEURONS AS A MODEL OF FRIEDREICH ATAXIA

CELLULAR ALTERATIONS AND THERAPEUTIC APPROACHES

Elena Britti

Memòria presentada per optar al grau de Doctor per la Universitat de Lleida

Programa de Doctorat en Salut

Director/Tutor

Joaquim Ros Salvador

2021

RESUM · RESUMEN · ABSTRACT

RESUM

L'atàxia de Friedreich (FA) és un trastorn cardio-neurodegeneratiu recessiu minoritari, sense cura. Es deu principalment a l'expansió del triplet GAA en el primer intró del gen *FXN*, que condueix a una disminució dels nivells de la proteïna mitocondrial frataxina (FXN). Els ganglis de l'arrel dorsal (GAD) son un dels teixits més afectats. Tot i que es desconeix la funció, la FXN participa en el metabolisme del ferro, en l'estrès oxidatiu i l'homeòstasi de Ca^{2+}. El nostre grup ha desenvolupat un model de cultiu primari de les neurones GAD de rata neonatal, basat en interferències d'ARN per disminuir les quantitats de FXN. Com a efecte inicial, vam observar una despolarització mitocondrial lleu, reducció dels nivells de l'intercanviador mitocondrial de $Na^{+}/Ca^{2+}/Li^{+}$ (NCLX) i augment de la concentració intracel·lular de Ca^{2+} $[Ca^{2+}]_i$ (probablement mitocondrial), que precedien la mort cel·lular. La lleu despolarització mitocondrial alenteix l'eflux de Ca^{2+} mitocondrial ($Ca^{2+}{}_m$) dependent de NCLX, tal com s'observa en cèl·lules permeabilitzades, augmentant la $[Ca^{2+}]_m$. El $Ca^{2+}{}_m$ activa calpaïnes mitocondrials que fragmenten NCLX; de fet, el quelant de Ca^{2+} BAPTA i els inhibidors de calpaïnes, MDL28170/Calpeptina, impedeixen la fragmentació de NCLX i milloren la supervivència. La sobrecàrrega de $Ca^{2+}{}_m$ i la despolarització mitocondrial afavoreixen l'obertura del porus de transició de permeabilitat mitocondrial (mPTP), alliberant Ca^{2+} i proteïnes pro-apoptòtiques al citosol, propiciant la proteòlisi del citoesquelet, l'activació del factors transcripcionals i mort cel·lular; en aquest sentit, s'observen beneficis quan s'utilitzen inhibidors/reguladors de mPTP com CsA/TRO19622. Amb l'objectiu principal de substituir/augmentar la quantitat de FXN, s'ha afegit el TAT-MTScs-FXN millorant la supervivència, la importació de proteïnes mitocondrials i els nivells de NCLX. Altres compostos explorats, com la leriglitazona, un agonista del factor transcripcional PPARγ, i el calcitriol, la forma activa de la vitamina D_3, augmenten els nivells de FXN, millorant el potencial de la membrana mitocondrial, la supervivència i els nivells de NCLX. L'ús de calcitriol es basa en l'observació de nivells reduïts de FDX1, una proteïna mitocondrial amb un centre ferro-sofre necessària per la síntesis de calcitriol. A més, el compost M indica que la modulació de l'expressió gènica pot ser beneficiosa en FA. En conclusió, la deficiència de FXN en GADs altera la funció mitocondrial i els nivells de Ca^{2+}, impacta en el metabolisme de la vitamina D_3 i incideix en la mort cel·lular apoptòtica, revelant que la dishomeòstasi de Ca^{2+} té un paper central en la FA.

RESUMEN

La ataxia de Friedreich (FA) es un trastorno cardio-neurodegenerativo recesivo raro, sin cura. Se debe principalmente a una expansión del triplete GAA en el primer intrón del gen *FXN*, que conduce a niveles reducidos de la proteína mitocondrial frataxina (FXN). Los ganglios de la raíz dorsal (GRD) son uno de los tejidos más afectados. Aunque se desconoce la función, la FXN participa en el metabolismo del hierro, estrés oxidativo y homeostasis del Ca^{2+}. Nuestro grupo ha desarrollado un modelo de cultivo primario de neuronas GRD de rata neonatal, basado en interferencia de ARN para disminuir las cantidades de FXN. Como efectos iniciales, hemos observado una leve despolarización mitocondrial, reducción de los niveles del intercambiador mitocondrial de $Na^{+}/Ca^{2+}/Li^{+}$ (NCLX) y aumento de la concentración de Ca^{2+} intracelular $[Ca^{2+}]_i$ (probablemente mitocondrial), que preceden la muerte celular. Esta leve despolarización mitocondrial ralentiza el eflujo de Ca^{2+} mitocondrial ($Ca^{2+}{}_m$) dependiente de NCLX, como se observa en células permeabilizadas, aumentando la $[Ca^{2+}]_m$. El $Ca^{2+}{}_m$ activa calpaínas mitocondriales que fragmentan NCLX; de hecho, el quelante de Ca^{2+} BAPTA y los inhibidores de calpaínas, MDL28170/Calpeptina, impiden la fragmentación de NCLX y mejoran la supervivencia. La sobrecarga de $Ca^{2+}{}_m$ y la despolarización mitocondrial promueven la apertura del poro de transición de permeabilidad mitocondrial (mPTP), liberando Ca^{2+} y proteínas proapoptóticas en el citosol, propiciando la proteólisis del citoesqueleto, la activación de factores de transcripción y la muerte celular; en este sentido, se observan beneficios cuando se usan inhibidores/reguladores del mPTP como CsA/TRO19622. Con el objetivo de reemplazar/aumentar la cantidad de FXN, el TAT-MTScs-FXN ha sido añadido, mejorando la supervivencia, la importación de proteínas mitocondriales y los niveles de NCLX. Otros compuestos examinados, como la leriglitazona, un agonista del factor de transcripción PPARγ, y el calcitriol, la forma activa de la vitamina D_3, aumentan los niveles de FXN, mejorando el potencial de membrana mitocondrial, la supervivencia y los niveles de NCLX. El uso de calcitriol se basa en la observación de niveles reducidos de FDX1, una proteína mitocondrial con un centro hierro-azufre necesaria para la síntesis de calcitriol. Además, el compuesto M indica que la modulación de la expresión génica puede ser beneficiosa en FA. En conclusión, la deficiencia de FXN en GRDs altera la función mitocondrial y los niveles de Ca^{2+}, impacta en el metabolismo de la vitamina D_3 e incide en la muerte celular apoptótica, revelando que la dishomeostasis de Ca^{2+} tiene un papel central en la FA.

ABSTRACT

Friedreich ataxia (FA) is a rare recessive cardio-neurodegenerative disorder, without a cure. It is mainly due to a GAA triplet expansion in the first intron of the *FXN* gene, leading to lower levels of the mitochondrial protein frataxin (FXN). Dorsal root ganglion (DRG) are one of the most affected tissues. Although the function is unknown, FXN is involved in iron metabolism, oxidative stress and Ca^{2+} homeostasis.

Our group has developed a neonatal rat DRG neurons primary culture model, based on RNA interference to reduce FXN amounts. As initial effects, we observed mild mitochondrial depolarisation, reduction of the mitochondrial $Na^{+}/Ca^{2+}/Li^{+}$ exchanger (NCLX) levels and increased intracellular Ca^{2+} concentration $[Ca^{2+}]_i$ (probably mitochondrial), prior to cell death. Mild mitochondrial depolarisation slows down the NCLX-dependent mitochondrial Ca^{2+} ($Ca^{2+}{}_m$) efflux, as observed in permeabilised cells, increasing $[Ca^{2+}]_m$. $Ca^{2+}{}_m$ activates mitochondrial calpains that cleave NCLX; in fact, the Ca^{2+}-chelator BAPTA and the calpains inhibitors, MDL28170/Calpeptin, they both prevent NCLX cleavage and improve survival. $Ca^{2+}{}_m$ overload and mitochondrial depolarisation promote mitochondrial permeability transition pore (mPTP) opening, releasing Ca^{2+} and pro-apoptotic proteins into cytosol, provoking cytoskeleton proteolysis, transcriptional factors activation and cell death; in this context, beneficial effects of mPTP inhibitors/regulators, such as CsA/TRO19622, are observed.

With the goal of replace/increase FXN amounts, TAT-MTScs-FXN has been added, showing beneficial effects on survival, mitochondrial protein import and NCLX levels. Other compounds screened, such as leriglitazone, a transcription factor PPARγ agonist, and calcitriol, the vitamin D_3 active form, increase FXN levels, improving mitochondrial membrane potential, survival and NCLX levels. The use of calcitriol is based on observed reduced levels of FDX1, a mitochondrial iron-sulfur protein necessary for calcitriol synthesis. Furthermore, compound M indicates that gene expression modulation may be beneficial in FA.

In conclusion, FXN deficiency in DRGs alters mitochondrial function and Ca^{2+} levels, impacts on vitamin D_3 metabolism and induces apoptotic cell death, revealing that Ca^{2+} dyshomeostasis has a central role in FA.

AGRADECIMIENTOS · ACKNOWLEDGEMENT · RINGRAZIAMENTI

La realización de esta tesis doctoral, para mí, es motivo de especial orgullo porqué representa el final de una etapa que empezó con mi entrada en España. Poco o nada queda de esa "chica desconcertada" que empezó l'Erasmus+ en Lleida. El deseo de empezar una nueva experiencia era grande y no me importaba comunicarme con dificultad en "italinglish" y no saber español/catalán. ¡¿Qué pensaba que serían 3 meses de Erasmus?! Finalmente, éste lugar me ha recibido durante 6 años. Gracias Chiara, por ese "¡me respondieron en Lleida!" cuándo enviamos emails para Europa. Gracias por ser mi hombro, confidente, solucionador de problemas burocráticos y compañera de aventuras: yo "navegador/GPS", tú "traductor". La respuesta a ése primer correo se la debo a Marta Llovera, mi mentora durante Erasmus+ y un modelo de investigadora a seguir. Gracias, porque con tu amabilidad, humildad, tranquilidad, precisión y paciencia me has enseñado tanto. Un equipaje que he necesitado durante todo mi doctorado.

Le debo un agradecimiento especial a él, mi Prof. Kim, quien logró brindarme cuidado, protección, estabilidad, confianza y autoestima. Gracias por los consejos, ayuda y esos "¡he encontrado un artículo!" que podrían iniciar interminables discusiones de viernes por la tarde buscando respuestas sobre frataxina, Ca^{2+}, poro... Tú creíste en mí cuando ni yo lo hacía, y entre "estem fututs, c'amu patutu y anar fent", hoy puedo decir la frase que me dijiste: "Hay prof. y Prof.". ¡Y tú eres Prof.! Sé que, aunque me vaya, siempre podré contar contigo. Gracias a las personas especiales que forman parte del grupo BQ. Gracias Fabien, por ayudarme en los primeros pasos del doctorado, en la disección de los DRGs, conversando sobre actualidad, futuro, Star Wars y series friki, por todos los cultivos de LCLs y por hacerme más autónoma y fuerte. Gracias Jordi, por las conversaciones durante el café en busca de respuestas sobre la frataxina o la vida y por haberme "abierto muchas veces la mente". Gracias Elisa, por tus momentos de "supermujer" y ayudarme a lanzarme a lo nuevo sin miedo. Gracias Roser, por las enseñanzas que me has dado, por ser la "manitas" que todo laboratorio quisiera y por resolver todo tipo de problemas. Gracias Rosa, David, Èlia, Celia, Núria por las risas en las pausas café, charlas, carnavales, calçotades y por estar siempre disponibles para ayudar. En particular Rosa por su ayuda en la burocracia y las aventuras en los congresos. Marta y Arabela por meterse en mi corazón muy rápido, por las risas a la hora del almuerzo y por ser la mejor compañía que podrías desear en un laboratorio y en la vida. Marta, mi "sestra", por la determinación y alegría que emana y por estar siempre disponible para echar una mano. Arabela por la paciencia, tranquilidad y dulzura que emana, por los cultivos de LCLs, por la ayuda con la disección de DRGs,

confocal y por ser la mejor sucesora que se podría tener. ¡Os quiero "pringadas 2 y 3"! Gracias a los alumnos que han estado en el lab y de los que he aprendido algo. Teresa por ser mi hombro en los primeros pasos de la tesis, siempre haciéndome sonreír en el lab como fuera y seguir siendo la amiga/compañera de lab/hermanita que a todo el mundo le gustaría. ¡Te quiero mucho! Ana M., Alba, Noelia, Lourdes, Maria(s), Lidia.

¡Gracias al grupo BQCC! Rosa S. por los consejos amables sobre problemas de doctorado y hacerme sonreír siempre durante el cachondeo. Ana por la ayuda sobre problemas con los DRGs y por las charlas a la hora del café. Sandra por la ayuda burocrática/científica que me diste, por estar siempre disponible, por las risas y el buen rollo durante los cursos de ingles, las pausas café y el cachondeo. Alba por los consejos, los abrazos/besitos de cada día, las risas, por el cuidado de mi pelo, los cotilleos y los "tinc gana"☺. Ambika, Sara, Ivan, Nuria, Diana, Oriol, Emma, Alex etc.

Gracias al grupo FPM que durante todo el doctorado me recibió con los brazos abiertos, almorzando juntos y haciéndome sentir parte del grupo. Gracias Manel por los consejos; Ricardo y Natàlia por l'alegría y las risas a carcajadas; Lara para hacerme sonreír y la ayuda burocrática y al respirometro; Mery por la ayuda en los primeros momentos del doctorado y las risas; Pascual para las conversaciones sobre temas científicos y no científicos; David y Cristian por las conversaciones de comida; Omar por ser mi compañero de campana; Ana, Josè, Anna, Reyna, Laia etc… para reír juntos.

Gracias a los demás miembros del IRBLleida: Isu por las comidas BQ; Anaïs y Alba por su ayuda con el confocal, sus consejos y amistad; Olga, Josep y Anna por la ayuda con los experimentos de Fura-2 y Neus(s) al cultivo; Marta y Leire por las conversaciones y las risas; Javi por las interminables conversaciones desde la autofagia hasta lo inesperable; Marc por las sonrisas a las 8:34 am en el estabulario; Aida y Gisel por la alegria compartiendo las ratas; Raúl, Cris, Pol por el cachondeo durante los carnavales y "al menjador"; Sílvia, Alaó, Sara, Sandra M., Coral, etc. Gracias Fernando por la sonrisa de la mañana y Loli por los consejos de mamá y sonrisa de la tarde☺.

Gracias a las personas que han sido parte del intercambio multicultural en mi casa. Maria Josè, nunca olvidaré nuestro primer encuentro, una mezcla de catalán, español, francés, italiano para poder comunicarnos. Youssouf por las emociones, las aventuras, la risa, la protección etc…Eres mi punto de referencia, fuerza, fuente de ideas, la persona con la que siempre he podido contar y más cercana a "família". Te quiero mucho y estás y siempre estarás en mi corazón. Los recuerdos que dejo en mi casa Lleidatana son innumerables cómo las cenas temáticas África/Italia con Youssouf, M.

Aznayn, M. Jawara y sus respectivos hermanos, amigos o niños del barrio, hasta acabar la cubertería disponible y comer arroz con estacas chinas☺. ¡Gracias "hermanos" porque estos momentos me hicieron sentir como en casa! Gracias a la madre de M. Aznayn, por esos deliciosos platos marroquíes que nos preparaste. Gracias a todos los demás compañeros de piso que pasaron por estas paredes, Fiona, Mary, Simone, Sercan, Ian, Juen, Tien Tien, Lei, Chari, Jocelyn, Luo, Ana, Enrique, Marcelo etc. Cada uno de ustedes me ha dejado algo, desde un plato chino, turco, alemán, mexicano, brasileño, catalán, italiano, hasta un gran bagaje cultural, nuevos descubrimientos, nuevos destinos para visitar y una mentalidad diferente. En concreto, Simone, por haber sido compañero de aventuras también en Londres, en la costa jurásica y Chari, por las aventuras con compañeros Erasmus, cenas mexicanas y conversaciones interminables.

Special thanks go to the people who welcomed me during my internship at UCL. First Prof. Abramov to enrich me with information on the dynamics of Ca^{2+} in neurons, to teach me "there are no failed experiments, but only experiments with unexpected results" and for advice on the areas of London to visit. Special thanks go to Noemi, my mentor during the internship and after. Thank you for teaching me so much with patience and for being a model of researcher to follow. Thanks also to Anna for being my companion during lunch times and adventures; Plamena, Sonia, Rosella for advices.

Thanks to the people I met during the internship: Simon for the walks in the London parks and adorable conversations; Matthew, Alexandre, Phil for the laughs together.

Grazie Laura, Elvy, Vale, Francesca, Rachele e tutte quelle persone che dall'Unical porto con me nel cuore. Laura per essere amica e sorella, per su(o)pportarmi e per i caffè virtuali. Elvy e Vale per caricarmi di allegria ed essere Uniche. Vi voglio bene!

Le persone a cui voglio dire infinitamente grazie sono mamma e papà, senza di voi non sarei qui. Papà per cercare fin da bambina di rispondere ai miei "Perché?" e iniziarmi alla scienza a modo tuo: abbracciati sul divano guardando documentari. Mamma per avermi insegnato i valori della determinazione, perseveranza e bastare a sé stessi. Mi sono serviti per essere forte durante la tesi. Grazie Giuseppe per essere sempre presente quando necessario e per gli scherzi, con te mi sento sempre bambina. Grazie zii e cugini per essere sempre al mio fianco, per quelle videochiamate di dozzine di persone, per commentare programmi TV in streaming e fantasticare con Bea. Grazie a tutti per essere la mia forza ogni volta che ritorno in Italia, a rigenerarmi nel cuore, nell'anima e nella pancia. *Famiglia*, non so cosa farei senza di voi!

¡Gracias de Corazón! Thanks! Grazie di cuore!

INDEX

INDEX

ABBREVIATIONS **XXXI**

INTRODUCTION **1**

1 FRIEDREICH ATAXIA (FA) **1**

1.1 History **1**

1.2 Pathology **2**
1.2.1 Neuronal pathology 3
1.2.1.1 Dorsal root ganglion alterations 3
1.2.1.2 Sensory peripheral nerves alterations 5
1.2.1.3 Spinal cord alterations 5
1.2.1.4 Dentate nucleus alterations 8
1.2.2 Cardiac and pancreatic pathology 9

1.3 Genetics **10**
1.3.1 Frataxin gene 10
1.3.2 Frataxin promoter 12
1.3.3 Frataxin expression 12

1.4 Epigenetic **13**

1.5 Frataxin protein **14**
1.5.1 Structure 14
1.5.2 Localisation 16
1.5.3 Frataxin function 16
1.5.3.1 Biosynthesis of iron-sulfur clusters 17
1.5.3.2 Heme group maturation 20
1.5.3.3 Iron binding/storage 22
1.5.3.4 Cellular iron homeostasis and modulation of Irp1 activation 23
1.5.3.5 Protection of cells against oxidative stress 24
1.5.3.6 OXPHOS system regulation 27
1.5.3.7 Cellular calcium homeostasis 28
1.5.3.8 Regulation of lipid metabolism 33
1.5.3.9 Mitochondrial biogenesis, fusion/fission and mitophagy control 34
1.5.3.10 DNA repair and tumour suppressor 35
1.5.3.11 Cell death and autophagy regulation 35
1.5.3.12 Summary of frataxin deficiency in neuronal cells 36

1.6 Friedreich ataxia models **37**
1.6.1 Yeast models 37
1.6.2 Invertebates models 38
1.6.3 Cellulars models 39
1.6.4 Mice models 40

1.7 Therapy **43**
1.7.1 Syntomatic 44

1.7.2 Improve mitochondrial function and reduce oxidative stress 44
1.7.3 Modulation of frataxin controlled metabolic pathways 46
1.7.4 Frataxin replacement, stabilizes or enhancers 47
1.7.5 Increase *FXN* gene expression 47
1.7.6 Stem cell and gene therapy 48

2 DORSAL ROOT GANGLION 49

2.1 Dorsal root ganglion sensory neurons 50
2.1.1 Structure and function 50
2.1.2 Embrionic development of DRG neurons 51
2.1.3 DRG neuron axon regeneration 52

2.2 DRG neurons subpopulations 53

2.3 Action potential in DRG neurons 56

2.4 Glial cells structure and communication 57
2.4.1 Satellite and schwann cells 57

2.5 Sensory neuropathy 58

2.6 DRG sensory neurons primary culture 58

3 CALCIUM AND DORSAL ROOT GANGLION 59

3.1 Cytosolic calcium 60
3.1.1 Cytosolic calcium influx 60
3.1.2 Cytosolic calcium efflux 62

3.2 Mitochondrial calcium 63
3.2.1 Mitochondrial calcium influx 63
3.2.1.1 Voltage-dependent anion channels (VDACs) 63
3.2.1.2 Mitochondrial calcium uniporter complex (MCUc) 64
3.2.2 Mitochondrial calcium efflux 68
3.2.2.1 Mitochondrial sodium (or lithium)/calcium exchanger (NCLX) 68
3.2.2.2 Regulation of NCLX activity 69
3.2.3 Mitochondrial calcium and respiration 71

3.3 Endoplasmic reticulum calcium and others 72
3.3.1 MAMs 73

3.4 Calcium binding proteins 73

3.5 Calcium differences among DRG subpopulations 74

4 CALCIUM AND MITOCHONDRIA IN NEURODEGENERATION 76

4.1 Mitochondrial permeability transition pore 76
4.1.1 Structure 76
4.1.2 Regulation 77

4.1.2.1 Mitochondrial membrane potential 77
4.1.2.2 Calcium 78
4.1.2.3 MATRIX pH and Pi 78
4.1.2.4 CypD and sirtuins 78
4.1.2.5 Others factors 80

4.2 Mitochondrial (intrinsic) apoptotic cell death 81
4.2.1 The mPTP opening and neurodegeneration 81
4.2.1.1 Caspases 82
4.2.1.2 Calpains 84
4.2.2 Inhibitors of mPTP opening 85

5 CROSSTALK MITOCHONDRIA-CYTOSOL-NUCLEUS 88

5.1 Phosphorylation state and gene expression alterations 88
5.1.1 CREB/ pCREB 88
5.1.2 NFAT/ pNFAT 89
5.1.2.1 Calcineurin inhibition 90
5.1.3 PTEN 91
5.1.3.1 PTEN canonical pathway 92
5.1.3.2 PTEN not-canonical pathway 92
5.1.4 PPARgamma 94
5.1.4.1 PPARγ/PGC1α pathway 95
5.1.4.2 PPARγ agonists 96
5.1.5 NRF2 97
5.1.5.1 NRF2 inducers 98

6 ACTIVE VITAMIN D_3 IN NEURONS 99

6.1 Vitamin D_3 metabolism 99
6.1.1 Ferredoxins and cytochromes 99
6.1.2 Calcitriol synthesis and degradation 100

6.2 Calcitriol actions 101
6.2.1 Non-genomic actions 102
6.2.2 Genomic actions 102
6.2.3 Calcitriol actions in target tissues 104
6.2.3.1 Calcitriol actions in Ca^{2+} and P_i metabolism 105
6.2.3.2 Calcitriol actions in neurons 106

6.3 Calcitriol and neurodegeneration 107
6.3.1 Calcitriol deficiency 107
6.3.2 Calcitriol supplementation 108

HYPOTHESES AND OBJECTIVES 111

1 HYPOTHESES 111

2 OBJECTIVES 111

MATERIALS AND METHODS **115**

1 EXPERIMENTAL ANIMALS **115**

2 MOLECULAR BIOLOGY TECHNIQUES **115**

2.1 Obtaining plasmids **115**
2.1.1 Plasmids 115
2.1.2 *Escherichia coli* culture and maintaining 118
2.1.3 *Escherichia coli* transformation 118
2.1.4 Obtaining plasmids 119
2.1.5 Plasmids quantification 120

3 CELLULAR BIOLOGY TECHNIQUES **121**

3.1 Preparation of plates **121**
3.1.1 Coating plates with collagen 121

3.2 Lentivirus production **122**
3.2.1 HEK293T cell culture 122
3.2.2 HEK293T transfection 123
3.2.3 Virus concentration 124
3.2.4 Virus titration 125

3.3 Post-natal rat DRG primary culture **126**
3.3.1 Dissection and isolation 126
3.3.2 Obtaining cell suspension of DRG neurons 127
3.3.3 Viral transduction 131
3.3.4 Viral transduction in time-course analysis 132
3.3.5 Efficiency of transduction 132
3.3.6 Treatments 133

3.4 Phase-contrast microscopy **134**
3.4.1 Axonal swelling analysis 134
3.4.2 Survival analysis 134
3.4.3 Size diameter analysis 135

3.5 Fluorescent microscopy **135**
3.5.1 TMRM 135
3.5.2 JC-1 assay 137
3.5.3 FLUO-8 and RHOD5N dye in whole cell 138
3.5.4 RHOD5N in membrane-permeabilised cells 140
3.5.5 Mitochondrial localisation of RHOD5N 143
3.5.6 FURA-2-AM ratiometric dye 143
3.5.7 Immunofluorescence 144

3.6 Lymphoblastoid cell lines (LCL) culture **146**

3.7 Oxygen consumption with Oroboros 2K **147**
3.7.1 Oxygen calibration 148
3.7.2 Medium background 149

3.7.3 Oxygen consumption 150

4 BIOCHEMICAL TECHNIQUES 151

4.1 DRG and LCL samples obtaining and preparation 151
4.1.1 Samples obtaining 151
4.1.2 Samples quantification and preparation 152

4.2 Electrophoresis methods 153
4.2.1 SDS-PAGE 153

4.3 Semi-dry western blot 154
4.3.1 Stripping conditions 158

4.4 Staining 158
4.4.1 Protein staining 158
4.4.2 Gel staining 160

4.5 Obtaining and analysis of bands 160

4.6 Enzymatic activity 160
4.6.1 Aconitase activity by fluorimeter 161
4.6.2 Citrate synthase activity by spectrophotometer 162
4.6.3 Ratio aconitase / cytrate synthase activity 163

5 COMPLEMENTARY TECHNIQUES 164

5.1 Baseline fluorescent level 164

5.2 Peak analysis 164
5.2.1 Calcium influx 164
5.2.2 Calcium efflux 164
5.2.3 Amplitude 165

5.3 Gauss-curve model for DRG subpopulation 165

6 STATISTICAL ANALYSIS 166

RESULTS 169

1 FXN-DEFICIENT DRG NEURONS AS A FA MODEL 169

1.1 RNA interference to decrease frataxin levels 169

1.2 Mitochondrial proteins remaining stable during FXN depletion 170

1.3 Frataxin deficiency alters the subpopulations of DRGs 172

1.4 Frataxin deficiency alters mitochondrial function 176
1.4.1 Frataxin deficiency reduces mitochondrial membrane potential 176
1.4.2 FXN deficiency maintains $\Delta\Psi_m$ by using ATP synthase working in reverse 179

1.4.3 NCLX decrease is an early consequence of FXN depletion 180
1.4.4 MICU1 and MICU3 protein levels decrease in FXN deficiency 180

1.5 Frataxin deficiency alters calcium dynamics 182
1.5.1 Progressive intracellular and mitochondrial Ca^{2+} overload in FXN deficiency 182
1.5.2 FXN deficiency decreases cytosolic Ca^{2+} buffer capacity 188

1.6 Frataxin deficiency induces mitochondrial import defects 193
1.6.2 Frataxin deficiency induces HSP60 import alterations 193
1.6.3 Frataxin deficiency alters Pink1 processing or import 195

1.7 Frataxin deficiency induces signs of apoptotic cell death 198
1.7.1 Mitochondrial pore opening and release of pro-apoptotic proteins 198
1.7.2 Progressive fodrin fragmentation during FXN depletion 202
1.7.3 Frataxin deficiency induces neurite degeneration and cell death 203

1.8 FXN deficiency alters phosphorylation state and gene expression 206
1.8.1 Frataxin deficiency alters PTEN protein levels 206
1.8.2 Frataxin deficiency dephosphorylates and activates NFAT 207

1.9 FXN deficiency induces changes in the iron-sulfur protein FDX1, but not Aco 208
1.9.1 FXN deficiency maintains aconitase activity and levels 208
1.9.2 Frataxin deficiency reduces FDX1 amounts 209

1.10 Frataxin deficiency alters Vitamin D_3 metabolism 210

2 COMPOUNDS CHELATING CALCIUM 211

2.1 Calcium chelator BAPTA protects FXN-deficient DRGs 211
2.1.1 BAPTA restores NCLX levels and Ca^{2+} homeostasis 211
2.1.2 BAPTA protects from apoptotic cell death 213

3 COMPOUNDS REPLACING FRATAXIN DEFICIENCY 213

3.1 TAT-MTScs-FXN replaces frataxin deficiency and improves altered markers 213
3.1.1 TAT-MTScs-FXN is targeted and processed into mitochondria 213
3.1.2 TAT-MTScs-FXN restores HSP60 import alterations 216
3.1.3 TAT-MTScs-FXN restores NCLX protein levels 217
3.1.4 TAT-MTScs-FXN restores pro-caspase 9 cleavage 218
3.1.5 TAT-MTScs-FXN decreases fodrin fragmentation 219
3.1.6 TAT-MTScs-FXN protects from neurodegeneration 221

4 COMPOUNDS INCREASING FXN LEVELS AND IMPROVING MITOCHONDRIAL FUNCTION 224

4.1 Calcitriol increase FXN levels and restores altered markers 224
4.1.1 Calcitriol restores enzymes levels involved in its own metabolism 224
4.1.2 Calcitriol increases frataxin levels 226
4.1.3 Calcitriol restores Ca^{2+} homeostasis 227
4.1.4 Calcitriol restores basal $\Delta\Psi_m$ and maintains it in response to inhibitors 232
4.1.5 Calcitriol decreases fodrin fragmentation 236

4.1.6 Calcitriol reduces neurodegeneration 236

4.2 Calcitriol synthesis alterations in FXN deficiency 237
4.2.1 Calcidiol has no effect on FDX1 and CYP27B1 levels 237
4.2.2 Calcidiol has no effect on FXN levels 239
4.2.3 Calcidiol amliorates Ca^{2+} homeostasis 239
4.2.4 Calcidiol reduces neurodegeneration 240

4.3 Leriglitazone protects FXN-deficient DRGs 241
4.3.1 Leriglitazone increases FXN levels 241
4.3.2 Leriglitazone protects NCLX Protein levels 242
4.3.3 Leriglitazone improves $\Delta\Psi_m$ 243
4.3.4 Leriglitazone does not increase aconitase activity 244
4.3.5 Leriglitazone protects FXN-deficient DRGs from apoptosis 245

5 COMPOUNDS MODULATING CALPAINS INHIBITION 247

5.1 Calpain activity inhibitors protect FXN deficient DRGs 247
5.1.1 MDL28170 and Calpeptin protect the cleavage of NCLX 247
5.1.2 MDL28170 treatment restores Ca^{2+} homeostasis 248
5.1.3 MDL28170 improves $\Delta\Psi_m$ 249
5.1.4 MDL28170 and Calpeptin protect fodrin fragmentation 250
5.1.5 MDL28170 and Calpeptin protect FXN-deficient DRGs from apoptosis 251

5.2 Calpain expression inhibition protects FXN-deficient DRGs 253
5.2.1 Calpain levels reduction by RNA interference 253
5.2.2 Lowering calpain 1 levels protects FXN-deficient DRGs 254

6 COMPOUNDS MODULATING MPTP OPENING 255

6.1 Cyclosporine A protects FXN-deficient DRGs 255
6.1.1 CsA protects from fodrin cleavage and apoptosis 255
6.1.2 CsA has no effect on NCLX protein levels 256
6.1.3 CsA has low effects in calcineurin activity inhibition 257

6.2 Olesoxime and Alisporivir actions on FXN-deficient DRGs 258
6.2.1 Olesoxime, but not Alisporivir, protects from apoptosis 258

7 COMPOUNDS MODULATING CALCINEURIN ACTIVITY 259

7.1 Tacrolimus, less then CsA, protects FXN-deficient DRGs 259
7.1.1 Tacrolimus has low protective effects 259
7.1.2 Tacrolimus has no effect on NCLX protein levels 260
7.1.3 Tacrolimus and CsA have no effect on calretinin 262

8 COMPOUNDS MODULATING GENE EXPRESSION 263

8.1 Compound M protects FXN-deficient DRGs 263
8.1.1 Compound M protects NCLX protein levels 263
8.1.2 Compound M restores $\Delta\Psi_m$ 264
8.1.3 Compound M protects fodrin fragmentation 265

8.1.4 Compound M protects FXN-deficient DRGs from apoptosis 266
8.1.5 Analogues have lower effect than Compound M 267

9 COMPARING NEURONS WITH LCLS FROM PATIENTS 269

9.1 LCLs from FA patients show frataxin reduction 269

9.2 LCLs from patients present NCLX reduction 270

9.3 Oxidative phosphorylation impaired in LCLs from patients 271

DISCUSSION 275

CONCLUSIONS 299

CONCLUDING REMARKS 303

LISTS OF FIGURES 307

LISTS OF TABLES 310

BIBLIOGRAPHY 315

SITOGRAPHY 349

PUBLICATIONS 353

ABBREVIATIONS

ABBREVIATIONS

$[Ca^{2+}]_c$: cytosolic calcium concentration

$[Ca^{2+}]_{free}$: free calcium concentration

$[Ca^{2+}]_i$: intracellular calcium concentration

$[Ca^{2+}]_m$: mitochondrial calcium concentration

$[O_2]$: O_2 concentration

·OH: hydroxyl radical

·OOH: peroxyl radical

8OH2'dG: C-8 hydroxylation of guanine

9-cis-RA: 9-cis retinoic acid

AAV: Adeno-Associated Virus

Aco: Aconitase

AD: Alzheimer Disease

Afg3l2: mAAA protease subunit

Aft1/2: iron-regulated transcription activator

AIF: apoptosis-inducing factor

AIS: axon initial segment-like structure

ALA: δ-aminolevulinic acid

Alb: albumin models

Alisporivir or Debio025: N-methyl-D-alanine-3-N-ethyl-valine-4-cyclosporine

ALS: Amyotrophic Lateral Sclerosis

ANT: adenine nucleotide translocase

ANT: ADP/ATP translocase

APAF-1: apoptotic protease activating factor 1

ARE: anti-oxidant response element

ATP: Adenosine triphosphate

AVED: ataxia with Vitamin E deficiency

Bax: Bcl-2-associated X protein

BBB: blood-brain barrier

Bcl-2: B-cell lymphoma protein 2

$Bcl\text{-}_{XL}$: B-cell lymphoma-extra large

BDB: blood DRG barrier

BDNF: Brain-derived neurotrophic factor

Bid: BH3-interacting domain death agonist

$Ca^{2+}{}_i$: intracellular calcium

$Ca^{2+}{}_m$: mitochondrial calcium

Calcidiol: 25-OH-vitamin D_3

Calcitriol: 1α,25-$(OH)_2$-vitaminD_3

CaMKII: Ca^{2+}/Calmodulin dependent Kinase II

CaMKIV: Ca^{2+}/Calmodulin dependent Kinase IV

cAMP: 3′,5′-cyclic adenosine monophosphate

Ca_V: voltage-gated Ca^{2+} channel

CBB: Coomassie Brilliant Blue

CBD: Ca^{2+}-binding domains

CBP: CREB Binding Protein

CCCP: carbonyl cyanide m-chlorophenyl hydrazone

CICR: Ca^{2+}-induced Ca^{2+} release

CNS: Central nervous system

CoQ_{10}: Coenzyme Q_{10}

COX-2: cyclooxygenase 2

CRACs: calcium-release activated channels

CRE: cAMP-responsive elements

CREB: cAMP responsive element binding protein

CS: Citrate synthase

CsA: Cyclosporine A

Cyp24a1: 25-hydroxyvitamin D-24-hydroxylase

Cyp27b1: 25-hydroxyvitamin D-1α-hydroxylase

CypD: Cyclophilin D

Cyps: cyclophilins

DAG: diacylglycerol

DBP: Vitamin D binding proteins

DFR: Deferiprone

DG: dentate gyrus

DMD: Duchenne Muscular Dystrophy

DMEM: Dulbecco's Modified Eagles Medium

DMF: Dimethyl fumarate

DN: dentate nucleus

DRG: Dorsal root ganglion

DRGO: DRG organoids

DRGs: Dorsal root ganglia

DRP1: dynein-related GTPase protein

DTNB: 5.5'-dithiobis-2-nitrobenzoic acid

ECG: Electrocardiogram

EGFR: epidermal growth factor receptor

EMRE: essential MCU regulator

EOFA: Early (or juvenile) Onset FA

EPO: Erythropoietin

ER: endoplasmic reticulum

ERK: Extracellular signal-regulated kinase

ETC: electron transport chain

EV: empty vector

FA: Friedreich Ataxia

FA-Acad: Acadian form

FARA: Friedreich's Ataxia Research Alliance

FAST-1: frataxin antisense transcription-1

FBS: fetal bovine serum

FCCP: Carbonyl cyanide-4-phenyl hydrazone

FDA: Food and Drug Administration

FDX1/2: ferredoxin

FECH: ferrochelatase

Fe-S: iron-sulfur

FGF-23: fibroblast growth factor

FK506: Tacrolimus

FKBPs: FK506-binding proteins

FM: medium factor

FOXO3: fork-head box O-3

FXDR: ferredoxin reductase

FXN: Frataxin

IHC: Immunohistochemistry

IMS: intermembrane space

Ins: insulin

IP_3: Inositol 1,4,5-trisphosphate

IP_3R: IP_3 receptor

iPSC: induced pluripotent stem cell

ISC: Iron-sulfur cluster

JC-1: 5,5′,6,6′-tetrachloro-1,1′,3,3′-tetraethylbenzimidazoly-carbocyanine iodide

JNK: c-Jun N-terminal kinase

JW47: Quinolinium-Cyclosporine A

***k*:** peak k-decay

Keap1: Kelch-like ECH-associated protein 1

KIKO: Knock-in/Knock out

LB: Luria Broth

LCL: Lymphoblastoid cell lines

Leriglitazone: MIN-102

LIAS: lipoic acid synthase

LOFA: Late Onset Friedreich Ataxia

LONP1: Lon peptidase 1

LV: Left ventricular

LV: lentivirus

MAM: mitochondria-associated membranes

MAPK: Mitogen-activated protein kinase

MAS: malate–aspartate shuttle

MCK: muscle creatine kinase

MCU: $_mCa^{2+}$ uniporter

MCUc: MCU complex

MCUR1: MCU regulator 1

Mef2: myocyte enhancer factor-2

MIM: mitochondrial inner membrane

MMPs: matrix metallopeptidases

MOM: mitochondrial outer membrane

MPP: mitochondrial processing peptidase

mPTP: Mitochondrial permeability transition pore

MS: Multiple Sclerosis

mtDNA: mitochondrial DNA

MTS: mitochondrial targeting sequence

MVP: major vault proteins

MW: molecular weight

NADPH: nicotinamide adenine dinucleotide phosphate

Na_V: voltage-gated Na^+ channel

NBM: Neuronal basal medium

NBMc: enriched NBM

NCLX: $Na^+/Ca^{2+}/Li^+$ exchanger

NCX: Na^+/Ca^{2+} exchanger

NFAT: nuclear factor of activated T cells

NGF: Nerve growth factor

NIM811: N-methyl-isoleucine-4-cyclosporine

NLS: nuclear localisation signal

NMN: nicotinamide mononucleotide

NOS: nitric oxide synthase

NOX: NADPH oxidase

NRF1: nuclear respiratory factors 1 and 2

NRF2: Nuclear factor (erythroid-derived 2)-like 2

NRVMs: neonatal rat ventricular myocytes

NSE: neuron-specific enolase

NT-3: Neurotrophin-3

$O_2^{\bullet-}$: superoxide

OD: Optical density

ON: Over night

OPA1: Optic atrophy 1

ORF: open reading frame

OSCP: oligomycin sensitivity conferring protein

OXPHOS: oxidative phosphorylation

PARL: presenilin-associated rhomboid-like protease

PD: Parkinson Disease

PDH: pyruvate dehydrogenase

Pdk1: 3-phosphoinositide dependent protein kinase-1

PEI: polyethylenimine

PES: Polyether sulfone

PGC1α: PPARγ coactivator 1α

PGZ: pioglitazone

P_i: inorganic phosphate

PI3K: phosphatidylinositol 3-kinase

P_iC: phosphate Pi carrier

Pink1: PTEN-induced putative kinase 1

PIP_2: phosphatidylinositol 4,5-bisphosphate

PIP_3: phosphatidylinositol 3,4,5-trisphosphate

PKA: cAMP-dependent Protein Kinase A

PLC: phospholipase C

PMCA: plasma membrane calcium ATPase

PNS: Peripheral nervous system

PP1/2A/2B: protein phosphatase 1/2A/2B

PPARγ: peroxisome proliferator-activated receptor gamma

PPIases: peptidyl-prolyl isomerases

PPRE: peroxisome proliferator response element

PRP: prion protein

Prph: Peripherin

PTEN: phosphatase and tensin homolog

PTEN-L: PTEN-long

PTH: parathyroid hormone

Pvalb: parvalbumin

PVDF: Polyvinyl difluoride

RGZ: rosiglitazone

rhuEPO: recombinant human erythropoietin

RNAi: RNA interference

RNS: reactive nitrogen species

ROCs: ligands activates receptor-operated channels

ROI: region of interest

ROS: radical oxygen species

RT: room temperature

RTA-408: Omaveloxolone

RXR: retinoic acid X receptor

RyRs: ryanodine receptors

***s*:** peak slope

SCA: spinocerebellar ataxia

Scr: Scrambled

SDH: succinate dehydrogenase

SDHB: succinate dehydrogenase subunit B

SERCA: sarco/endoplasmic reticulum Ca^{2+}-ATPase

SGC(s): Satellite glial cell(s)

shRNA: short hairpin RNA

Sirt3: sirtuin-3

SLP-2: stomatin-like protein 2

SMA: Spinal Muscular Atrophy

SMOCs: second-messenger operated Ca^{2+}-permeable ion channels

SOCs: store-operated channels

SOD: superoxide dismutase

SR: sarcoplasmic reticulum

SRF: serum response factor

STAR: steroidogenic acute regulatory protein

STAT-3: signal transducer and activator of transcription 3

TAT: Trans Activator of Transcription

TCA: tricarboxylic acid cycle

Tf: transferrin

TFAM: mitochondrial transcription factor A

TFAP2: transcription factor AP2

Tfr1: transferrin receptor

TM: transmembrane domains

TMRM: Tetramethylrhodamine methyl ester

TNFα: Tumour necrosis factor alpha

TRC: The RNAi Consortium

TrkA/B/C: tyrosine kinase receptors

TRO19622: Olesoxime

TRO40303: 3,5-Seco-4-nor-cholestan-5-one oxime-3-ol

TRP: transient receptor potential channel

TRPA1: Transient receptor potential cation channel ankyrin 1

TRPV1: Transient receptor potential cation channel subfamily V member 1

TSPO: translocator protein

TZD: thiazolidinediones

VDAC: voltage-dependent anion channel

VDR: vitamin D receptor

VDRE: VDR elements

Vitamin D_2: ergocalciferol

Vitamin D_3: cholecalciferol

Vitamin E: α-tocopherol

VOCs: voltage-operated channels

VSV: vesicular stomatitis virus

WB: western blot

YAC: yeast artificial chromosome

α-KGDH: α-ketoglutarate dehydrogenase

ΔF: peak amplitude

$\Delta\Psi_m$: mitochondrial membrane potential

***τ*:** tau or half-life

INTRODUCTION

INTRODUCTION

1 FRIEDREICH ATAXIA (FA)

1.1 History

Ataxia (from ancient Greek “without order”) indicates the loss of coordination or balance, a process that is the result of an alteration in any part of the complex network of neurons involving the central nervous system (CNS) and peripheral nervous system (PNS). Ataxia is usually a genetic disease, although it could be due to other causes, and can be divided in autosomal dominant and autosomal recessive inheritance (Akbar & Ashizawa, 2015).

Friedreich Ataxia (FA) is a rare hereditary neurodegenerative disease and the most common autosomal recessive ataxia with a prevalence of 1/50000 in the European population. It was described for the first time in 1863 by the German pathologist and neurologist Nikolaus Friedreich, which reported all the pathological characteristics of the disease: progressive loss of coordination (ataxia) in the arms and in the legs, sensory loss (especially proprioceptive sensation), and muscle weakness, often associated with kyphosis, scoliosis, foot deformity (*pes cavus*), and heart disease (Friedreich, 1863). Other symptoms of FA are: vision impairment (nystagmus), hearing loss (deafness), slurred speech (dysarthria), tendon reflex abnormalities while rarely tremor of the head, finger contractures, extensor plantar reflex (Babinski signs), cyanosis of the feet (Harding, 1981) and sphincter disturbances (Dürr et al., 1996). Other symptoms that may be associated with FA are: facial dysmorphia, seizures, myoclonus, mental retardation (Harding, 1981) and low bone mineral density and major incidence of fractures (Eigentler et al., 2014).

Major neurological symptoms of the disease are due to degeneration of **dorsal root ganglion (DRG) sensory neurons**, with sensory loss in lower limbs that occurs before upper limbs, position sense more affected than vibration sense and rarely abnormal pain, temperature appreciation and touch sensation (Harding, 1981). However, Friedreich Ataxia is also a multisystemic condition with frequent presence of cardiomyopathy and diabetes. In fact, myocardial failure or arrhythmias are the most common cause of premature death that occurs at a mean age of 38 years. On the other

hand, diabetes only occurs after neurological signs in about 10-20% of FA patients (Harding, 1981).

As FA is a rare and progressive disease, diagnosis usually occurs after several years from the onset of symptoms. The onset of symptoms usually occurs around puberty between the ages of 5 and 18 years, however less common cases present late onset of symptoms (Harding, 1981). Depending on the time in which the onset of symptoms occurs, FA has been divided in **Late Onset Friedreich Ataxia** (LOFA, after 25 years) and **Early (or juvenile) Onset FA** (EOFA, before 25 years). Another type of FA, which presents slower progression and no signs of cardiomyopathy and diabetes, is named **Acadian form** (FA-Acad). Whatever type is, nearly all patients became paraplegic, cannot perform daily tasks and need assistance and wheelchairs, 16 years after the onset of symptoms (Dürr et al., 1996; Harding, 1981), and present a shorter life expectancy to approx. 40-50 years.

Despite being described in 1863, nowadays the used treatments are limited to treating symptoms but no effective cure that can alter the natural course of the disease is present. This is principally because it is not know the function of its main protein frataxin and the mechanisms leading to the pathology. However, a connection between FA and iron has been supposed in 1980, when iron-positive granules were discovered in cardiomyocytes of FA patients (Lamarche, Côté, & Lemieux, 1980) and confirmed in 1997, when deficiency of iron-sulphur proteins was discovered in FA endocardial biopsies (Rötig et al., 1997). Nowadays, FA is considered a disease of iron dyshomeostasis, but, while the presence of iron has been confirmed in the heart of patients, its presence in the neuronal system is still a matter of debate.

1.2 Pathology

Friedreich Ataxia pathology is characterised by central and peripheral neuronal changes, cardiac alterations and diabetes. The involvement of myocardium and pancreatic β-cells indicates that Friedreich Ataxia is more a multisystem disease than only a neurodegenerative disease and points out a specific cell susceptibility in the nervous system, heart and pancreas. Why these specific organs are more affected is still a question to be investigated (González-Cabo & Palau, 2013). Although it is not known the reason of this specific cell susceptibility, it must be kept in mind that neuronal, cardiac and pancreatic cells, having a distinct embryonic origin, share many functional characteristics, such as electric excitability and a high level of metabolic activity. In

addition, neuronal and pancreatic cells share exocytosis triggered by a stimulus: neurotransmitters vesicles and granules of insulin, respectively (Cnop, Mulder, & Igoillo-Esteve, 2013).

1.2.1 Neuronal pathology

Most symptoms of Friedreich Ataxia are the consequence of neurological alterations; in fact, the first pathologic changes occur in the dorsal root ganglia with the loss of large sensory neurons. Then, it appears the degeneration of the sensory posterior (dorsal) columns, the spinocerebellar and corticospinal motor tracts and loss of large sensory fibers in peripheral nerves. Mild degeneration occurs in the medulla and cerebellum (Koeppen, 2011). **Figure 1** represents the most important neurological alterations in peripheral and central nervous systems.

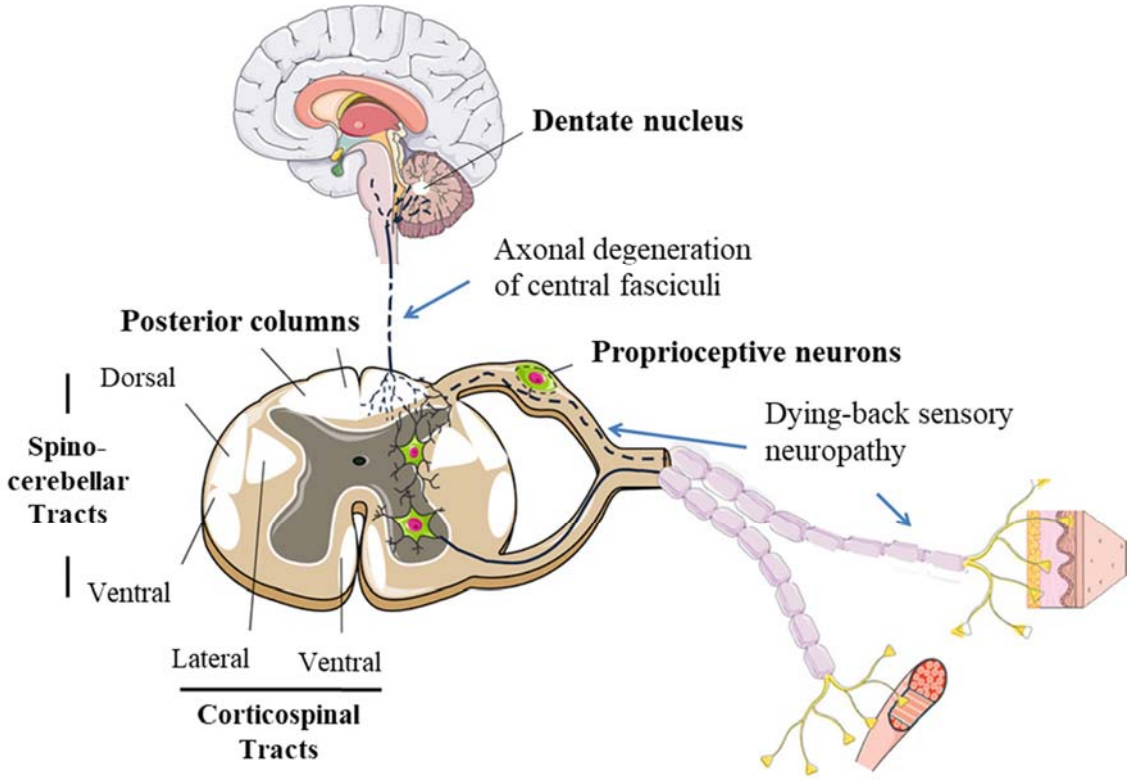

Figure 1. Axonal pathology in peripheral and central nervous systems. Degenerated fasciculi, tracts and nucleus are shown in white and loss of large myelinated axons are indicated in dashed black lines. Modified from (González-Cabo & Palau, 2013).

1.2.1.1 Dorsal root ganglion alterations

Neuro pathological characteristics of dorsal root ganglion (DRG) in FA are reduction in the size of the ganglion and its neurons, abundant presence of satellite cells surrounding, in an irregular multi-layer way, DRG neurons, and presence of residual nodules, as

shown in **Figure 2** (Koeppen & Mazurkiewicz, 2013)**.** The presence of residual nodules in DRG is not FA specific, as it has also been described in other pathologies and aging. The mechanism of sensory neurons loss is still unknown but, probably, it starts with satellite cells which mediate a total absorption of neurons leading to residual nodules and loss of sensory neurons, which, consequently, leads to alterations in dorsal roots and spinal cord (Koeppen et al., 2009; Koeppen & Mazurkiewicz, 2013).

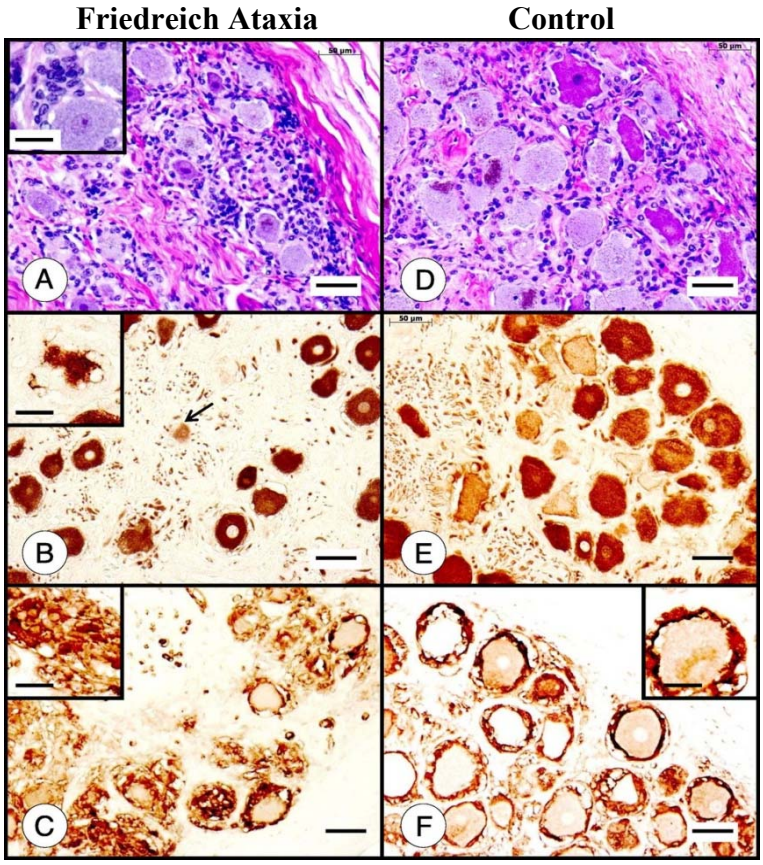

Figure 2. Dorsal root ganglia in Friedreich Ataxia (A-C) and Control (D-F). DRGs stained with hematoxylin and eosin (A, D) show in FA (A) a smaller size of its neurons and abundant satellite cells than in control DRG (D). Immunohistochemistry (IHC) for class III β-tubulin (B, E) shows smaller size of DRG neurons in FA (B) than in control (E) and the arrow indicate residual nodules. IHC for S100α (C, F) reveals a single-cell layer of satellite cells around DRG neurons in normal DRGs (F), while in FA (C) irregular multi-layers of satellite cells (Koeppen & Mazurkiewicz, 2013).

As FA is considered a disease of iron dyshomeostasis, iron-responsive proteins have been analysed in DRGs and satellite cells. An excess of iron stimulates the biosynthesis of ferritin and ferroportin. As ferritin is present only in satellite cells and normal DRG neurons display a single-layer of satellite cells while the number of layers increases in FA, patients display more immunoreactivity for ferritin than controls. While ferritin is

present only in satellite cells, ferroportin is present in satellite cells and neurons of normal DRG, but, in FA patients, it displays immunoreactivity only in satellite cells (Koeppen et al., 2009). High-definition X-ray fluorescence (HDXRF) maps of iron in DRG from FA patients show increased iron fluorescence in very restricted neuronal areas without changing the total amount of iron (Koeppen et al., 2009).

1.2.1.2 Sensory peripheral nerves alterations

FA patients present sensory peripheral nerves alterations such as progressive reduction of large myelinated fibers thought the course of pathology (McLeod, 1971). Loss of large myelinated fibers interests principally the Schwann cells of bigger nerves of spinal cord, such as the sural nerve in the legs (Koeppen & Mazurkiewicz, 2013). Transversal sections of sural nerves show not only reduction in number of large myelinated fibers, but also reduction in density (McLeod, 1971). In fact, normal mean density in sural nerves for individuals of 17-39 years is 6.13 ± 1.11 thousand fibers/mm^2 (O'Sullivan & Swallow, 1968), while FA patients show a mean density of 2.43 ± 1.10. These alterations lead to impairment of sensory conduction of vibration and position sense (McLeod, 1971). Apart from proprioceptive sensory nerves, also mechanoreceptors are involved in the pathology. In fact, Meissner's corpuscles, mechanoreceptor nerves termination involved in light touch, decreases area, diameter and density in skin (hands and feet) of FA patients (Creigh et al., 2019). In later stages of the disease it can also occur the reduction of small myelinated fibers, leading impairment of pain sensation (McLeod, 1971). For example, sensory action potentials in ulnar nerves are absent in all patients, while other nerves are reduced in amplitude and prolonged in latency (McLeod, 1971).

1.2.1.3 Spinal cord alterations

The diameter of spinal cord in FA patients is reduced at all levels; however, thinning is especially evident in the thoracic region, as shown in **Figure 3**. The thoracic region is the one that usually presents remarkable skeletal deformity (scoliosis) in most patients (Chevis et al., 2013).

Figure 3. Thoracic spinal cord in FA. Dorsal surface of the spinal cord shows thick white anterior roots (long arrows) and thin dorsal roots (short arrows). From (Koeppen, 2011).

The transverse slice of spinal cord displays means cord area greatly reduced in FA compared to a normal control and grey discoloration of the dorsal columns (Koeppen, 2011). While, mean cord eccentricity is significantly higher in FA patients than in controls. These means (reduced cord area and higher cord eccentricity), indicating cord atrophy with flattening, seem more associated with disease duration and loss of fibers than with length of GAA expansion (Chevis et al., 2013), suggesting that the cord damage is secondary to dorsal root ganglion damage (Koeppen & Mazurkiewicz, 2013).

- **Dorsal spinal roots and dorsal columns alterations**

The presence of gelatinous and thinner dorsal spinal root has been described by Friedreich in 1877 (Friedreich, 1877). As present in **Figure 4**, dorsal spinal roots in FA show loss of large axons without affecting axonal density, smaller myelinated fibers, degeneration of the dorsal column, dorsal spinocerebellar tract, and corticospinal tract and lack of cells in dorsal nucleus of Clarke column (Koeppen & Mazurkiewicz, 2013). While the dorsal spinal root is clearly affected in the disease, the ventral (motor) root displays a mild presence of smaller axons (Koeppen et al., 2009).

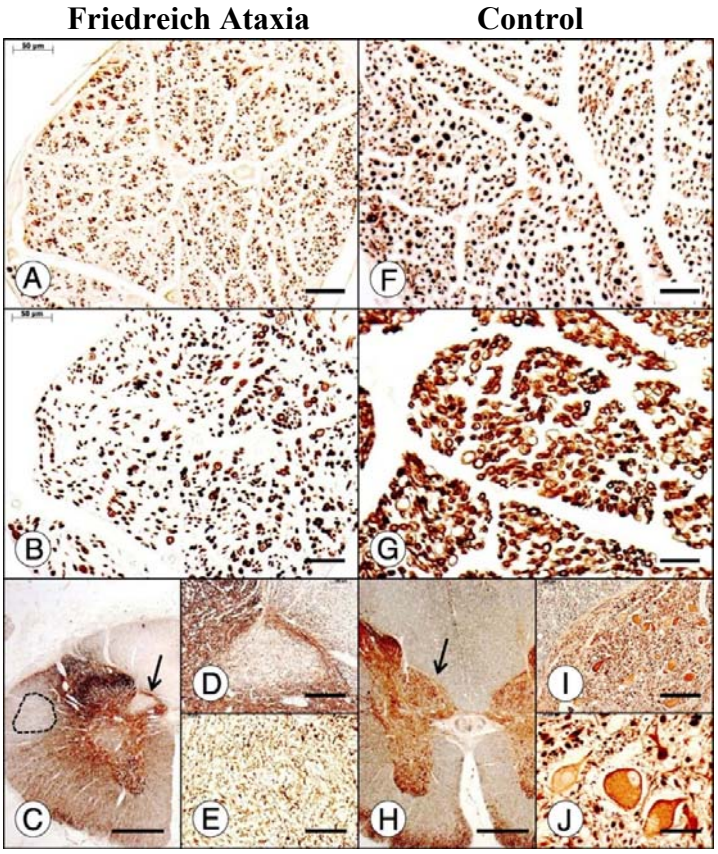

Figure 4. Dorsal spinal roots and dorsal nucleus of Clarke column in FA (A–E) and control (F–J) spinal cord. Immunohistochemistry (IHC) for phosphorylated neurofilament protein (A, F) show loss of large axon in FA (A) compared to control (F). IHC for myelin basic protein (B, G) show smaller myelinated fibers in FA (B) then control (G). IHC for class III β-tubulin (C–E, H–J) shows degeneration of the dorsal column, dorsal spinocerebellar tract, and corticospinal tract (interrupted line) in FA (C) and lack of cells in dorsal nucleus of Clarke column (arrow in C and magnification in D, E). In control the dorsal nucleus is larger and display round large nerve cells (arrow in H and magnification in I, J) (Koeppen & Mazurkiewicz, 2013).

The iron-responsive protein ferroportin has been analysed in ventral and dorsal roots of FA patients and controls. Ferroportin is present in large axons of dorsal root and ventral root in normal conditions, but, in FA patients, it does not displays immunoreactivity (Koeppen et al., 2009).

- **Corticospinal tracts degeneration**

Corticospinal tracts degeneration involves preferentially a myelin loss in the lateral area in the cervical spinal cord and in the entire area more caudally. Myelin loss is related to a selective degeneration of the distal ends of the longest and largest axons, a dying-back degeneration process. The major symptom due to degeneration of corticospinal tracts is diffuse muscle weakness (Murayama, Bouldin, Suzuki, 1992).

❖ **Spinocerebellar tracts degeneration**

Fiber loss in the anterolateral fields corresponding to spinocerebellar and corticospinal tracts may also be visible to the naked eye. The major symptom due to degeneration of spinocerebellar tracts is ataxia (Koeppen, 2011).

1.2.1.4 Dentate nucleus alterations

The major lesion in the CNS of FA patients combines the loss of large neurons of the dentate nucleus (DN) in cerebellum and proliferation of synaptic terminal named grumose degeneration (Koeppen & Mazurkiewicz, 2013). Although DN appearance is atrophic in almost all FA patients, this cerebellar lesion has been discovered later than spinal cord and DRG modifications. As shown in **Figure 5**, dentate nucleus of cerebellum in FA patients is smaller than normal condition, lacks the dentate grey mater ribbon and presents lower iron intensity (Koeppen et al., 2007).

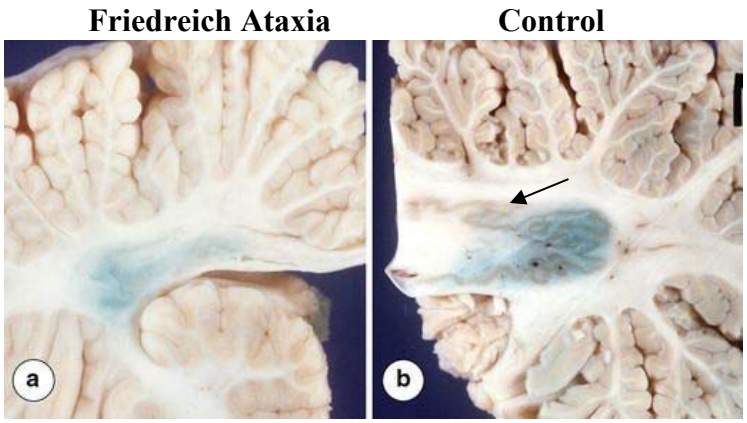

Figure 5. Dentate nucleus in FA (A) and control (B). The DN in FA patients (A) is smaller than in controls (B). It lacks the dentate grey matter ribbon of the normal nucleus (arrow), and the intensity of the iron staining using Perls's solution of 1% potassium ferrocyanide in 1% hydrochloric acid (Blue) is lower than normal (Koeppen et al., 2007).

When iron and ferritin were analysed by quantitative biochemical techniques, no significant changes were revealed between DN of FA patients and controls, although ferritin was more localised in microglia and astrocytes in FA patients and in oligodendroglia in controls (Koeppen et al., 2007). The dentate nucleus of cerebellum contains abundant iron. Probably, for this, the DN susceptibility in FA is high, but other neuronal iron-rich regions are not affected in the disease (Koeppen et al., 2007).

1.2.2 Cardiac and pancreatic pathology

Normal heart weights for adult men and women are 365±71g and 312±78g, respectively (mean ± SD) (De La Grandmaison, Clairand, & Durigon, 2001). In the case of FA patients, heart weights are usually 600–800g, presenting cardiomyopathy (Koeppen, 2011). FA cardiomyopathy is variable, as shown in **Figure 6** with two types of FA hypertrophic hearts (Koeppen, 2011). In fact, FA cardiomyopathy characteristics are thickness of the left ventricular (LV) walls, LV fibrosis and concentric/asymmetric hypertrophy, but also dilated cardiomyopathy. The most common abnormalities seen on the electrocardiogram (ECG) of FA patients (approximately 85%) are T-wave repolarisation abnormalities (Hanson, Sheldon, Pacheco, Alkubeysi, & Raizada, 2019).

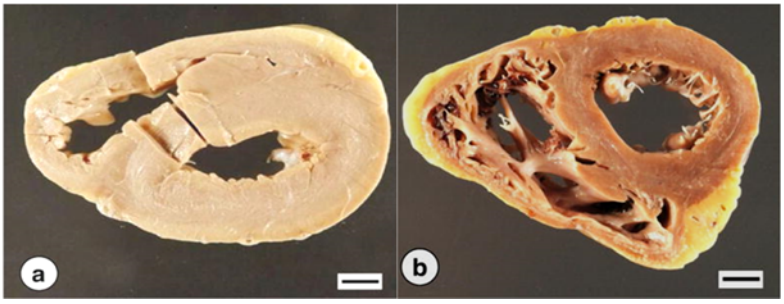

Figure 6. Aspect of two hearts of FA patients. (A) Concentric cardiac hypertrophy and discoloration of the myocardium. In this case, the ventricles are narrowed. (B) Cardiac hypertrophy affecting only the left ventricular wall and inter-ventricular septum. The right ventricle is dilated. Bars, 1 cm (Koeppen, 2011).

FA is also associated with pancreatic pathology, and diabetes in some cases. The percentage of diabetes in FA patients range from 8 to 32%. The main cells affected in FA and responsible for diabetes are pancreatic β-cells in the islets of Langerhans, which are reduced in number in post mortem pancreas sections of patients. β-cells are normally able to produce insulin when stimulated by glucose. As the β-cells number is lower in FA, diabetes seems consequent to lower insulin production in the islets, as indicated in **Figure 7** (Cnop et al., 2013).

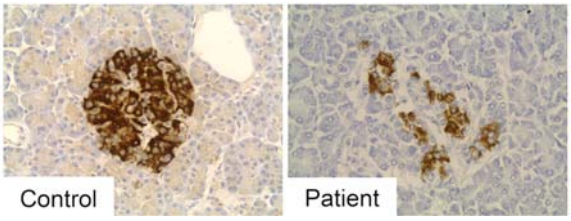

Figure 7. Insulin staining in the islets of Langerhans of a control and a FA patient post mortem sections. FA patients present islets of Langerhans with a lower β-cells content (insulin staining) and a lower islet area compared to control (Cnop et al., 2013).

1.3 Genetics

Genetic inheritance has been suggested since the FA discovery, but the demonstration did not occur until 1979 when 19 affected individuals were demonstrated descended of a single couple who married in 1786 in Quebec (Bouchard, Barbeau, Bouchard, Paquet, & Bouchard, 1979). In 1988 the locus for the genetic mutation was mapped in chromosome 9 (Chamberlain et al., 1988). Later, it was discovered that Friedreich Ataxia is a single gene disorder, caused by an unstable **Guanine-Adenine-Adenine (GAA) trinucleotide repeat expansion** in the first intron of frataxin, *FXN* (or *X25*), gene on chromosome 9q13. When a direct genetic test became available in 1996, the diagnosis started to be easier and the confusions with other similar pathologies stopped (Campuzano et al., 1996).

As an autosomal recessive disease, both parents must be carrier of the GAA repeats expansion for a 25% chance to have a child affected, carrying two mutated copies of the *FXN* gene. Carriers are clinically healthy and their frequency is about 1:50 – 1:100 in the affected populations and 1:120 in European populations. About 96% of affected individuals are homozygotes for the GAA repeats expansion, while about 4% are compound heterozygotes with a point mutation in one allele of the *FXN* gene and a GAA repeats expansion in the other. No patients homozygotes for a point mutation have been described (Campuzano et al., 1996).

1.3.1 Frataxin gene

FXN region contains five exons, named one to 5a, and an open reading frame (ORF) encoding a 210 amino-acid protein (the commonest protein). Another exon, exon 5b, presents an in-frame stop codon allows an alternative transcription of an isoform of 171 amino acids (alternate splicing). A non-coding exon 6 is also present (Campuzano et al., 1996). The region between 141-167 amino acids (exon 4 and 5a) is particularly conserved. Normal *FXN* gene presents between 8 and 22 repeats in the first intron of the gene, while a range of 120-1700 GAA repeats is present in the gene of FA patients with a major frequency of 700-800 repeats. The two alleles present, prevalently, GAA expansions of different sizes in the same individual (Dürr et al., 1996). The number of GAA repeats in the smaller allele of patients shows an inverse correlation with age at onset of FA, as shown in **Figure 8** (Dürr et al., 1996).

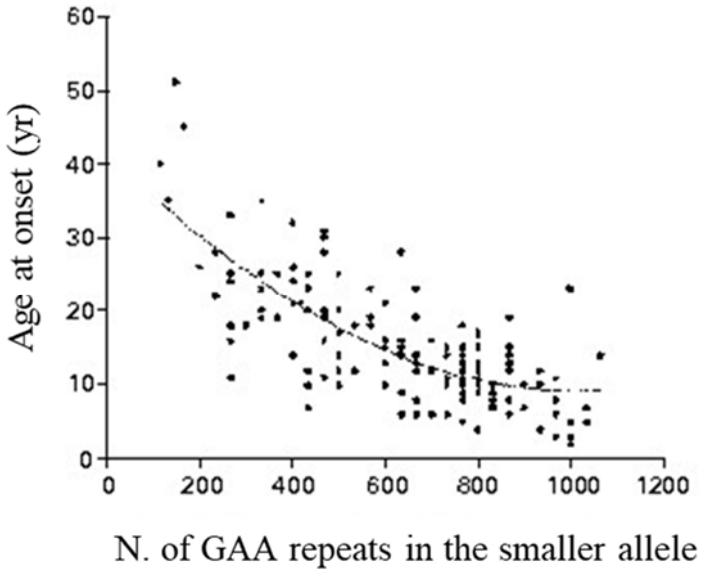

Figure 8. Correlation between age at onset and number of GAA repeats in patients. Larger number of GAA repetitions in the first intron of frataxin gene correlates with earlier age at onset for the patient in a study of 140 patients (Dürr et al., 1996).

Despite the fact that 96% of patients are homozygous for GAA repeats expansion, the 4% shows a **point mutation** in one allele of *FXN* gene and a GAA repeats expansion in the other, being heterozygous for the point mutation or compound mutations. More than 60 different mutations have been described for *FXN* gene; however, the more common point mutations are indicated in **Table 1**. In most cases, compound mutations produce a phenotype similar to GAA expansion in homozygosis or typical FA (I154F and W155R), however, some patients with point mutations show a milder phenotype or atypical FA (G130V and D122Y). All these genetic mutations are present in conserved residues of FXN protein, which could affect stability, alterations in interactions, folding, degradation etc (Pastore & Puccio, 2013).

Table 1. Point mutations in FA.

ID	Effect	Region	Nation	Clinic
L106X	Leu (**T**TA) > Stop (**T**GA)	Exon 3	France	Severe
Splice	Splicing (**AG**) > no spl. (**GG**)	Intron 3	Spain	Severe
I154F	Ile (**A**TC) > Phe (**T**TC)	Exon 4	Italy	Severe
G130V	GGT > GTT	Exon 4	France/USA	Mild
D122Y	GAC > TAC	Exon 3	Germany	Mild
W173G	TGG > GGG	Exon5a	Italy/USA	Severe

From (Campuzano et al., 1996; Pastore & Puccio, 2013).

1.3.2 Frataxin promoter

The promoter region of human *FXN* is extended for 1255 bp upstream the translation start site (AUG), however, only 221 bp of this sequence seems important for FXN expression (Greene, Entezam, Kumari, & Usdin, 2005). The regulatory elements of FXN expression are unknown. It has been demonstrated that the transcription factors **SRF** (serum response factor) and **TFAP2** (transcription factor AP2) bind directly to human *FXN* promoter sequences (in the 221 bp region), enhancing frataxin expression, with the difference that TFAP2 acts in several cell lines, while SRF seems to be cell-lines specific. SRF binds to serum response elements and can stimulate cell proliferation and cell differentiation, while TFAP2 is a developmentally regulated, retinoic-acid inducible transcriptional activator. The authors indicate that the overexpression of these factors can increase FXN protein levels (Li et al., 2010). Also, the same authors demonstrated a correlation between cellular iron status and frataxin expression, by showing that cellular iron depletion (demonstrated in FA cells) decreases frataxin expression, thus aggravating the protein deficiency (Li, Besse, Ha, Kovtunovych, & Rouault, 2008). Indeed, the expression of frataxin protein seems to be regulated not only from regulatory elements in promoter region, but also from elements present in the intronic region. In fact, **EGR3** factor seems to control the increase of frataxin expression by binding a transcription factor binding site in the intronic region downstream of exon 1 (Li et al., 2010).

1.3.3 Frataxin expression

FXN gene usually contains a dozen of GAA repeats (~8-22 GAA) in the first intron of the gene. FA patients present GAA repeated hundreds of times (expansion, ~120-1700 GAA), leading difficult the gene transcription and decreasing frataxin protein levels.
The *FXN* gene is expressed in all cells, but at variable levels in different tissues and during development. In fact, frataxin mRNA is highly expressed in tissue with high metabolic rate such as heart and the nervous system, and consequently these tissues are among the most affected in FA. DRG neurons express the highest frataxin levels and display a increased vulnerability to frataxin down-regulation (Koutnikova et al., 1997).

1.4 Epigenetic

Reduction of frataxin protein levels in FA seems to be due to epigenetic changes in the promoter region and/or the first intron of *FXN* gene, leading to heterochromatin formation. In fact, it has been demonstrated decreased presence of histones acetylation (hypo acetylation) and increased methylation (hyper methylation) of regions upstream GAA repeats at lysine 9 of histone H3 (H3-K9me3), especially CpG regions. In this scenario, the heterochromatin formation might impede the transcription of frataxin, leading to reduction of FXN protein levels, as shown in **Figure 9** (Al-Mahdawi et al., 2008; Greene, Mahishi, Entezam, Kumari, & Usdin, 2007). The long GAA repeats expansions adopt self-associated non-B DNA structures (triplex) leading to a sticky DNA, R-loop structures or DNA-RNA hybrids, which block the RNA polymerase II progression. It has been hypothesized that GAA repeats expansions lead to physiological formation of GAA·TTC·GAA DNA triplex structures in which the RNA polymerase II starts the transcription. Once the RNA polymerase II arrives at the DNA triplex site, the transcription is blocked, forming an R-loop structure; however, the nascent mRNA can anneal to the sticky DNA, forming a DNA_RNA hybrid structure that completely blocks transcription. Consequently, DNA_RNA hybrid structures could recruit histone deacetylases (HDAC) for deacetylation of amino-terminal tails of histones and histone methyl transferase (HMT) for tri-methylation of histone 3 at the lysine 9 position (H3-K9me3). Subsequently, heterochromatin protein 1 (HP1) could target H3-K9me3 residues and determine heterochromatin formation and *FXN* gene silencing (Marmolino & Acquaviva, 2009).

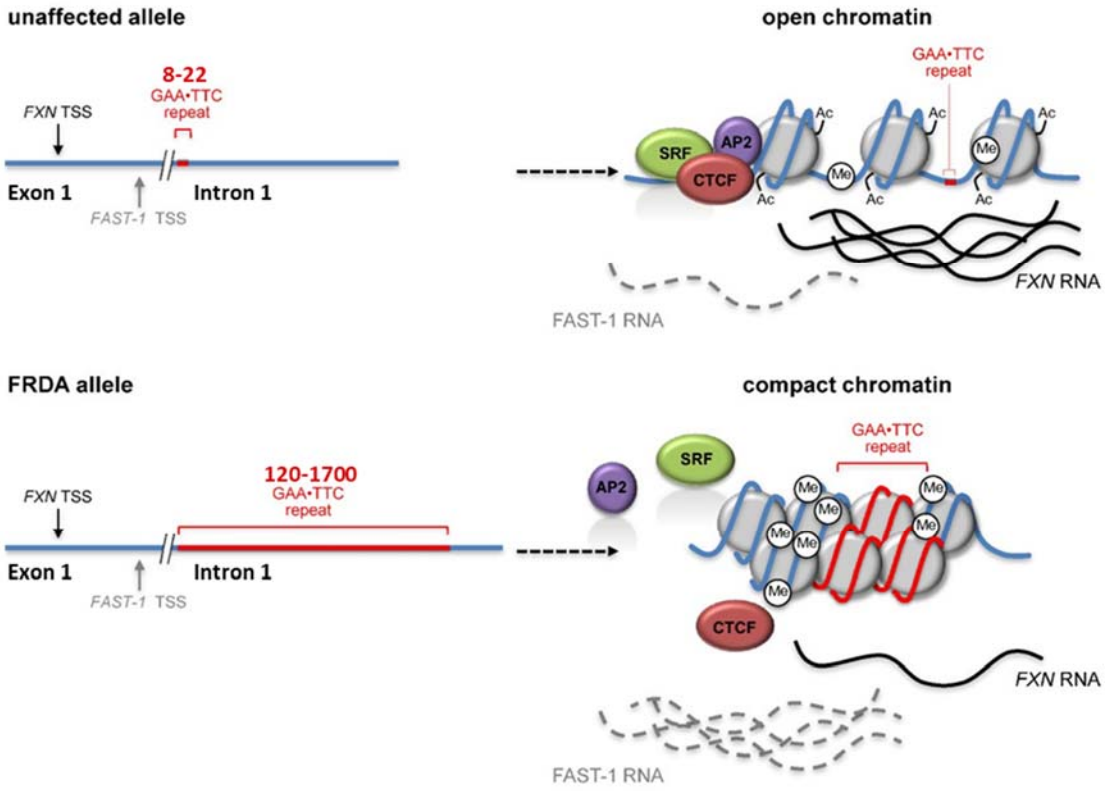

Figure 9. Epigenetic changes in FA. See text for details. Note the binding (or not) of transcription factors to promoter of *FXN* gene in control (or patients), thus the transcription (or lower). Note the presence of a frataxin antisense transcription-1 (FAST-1) RNA, with non-specified function in silencing and changing in acetylation and methylation leading to heterochromatin in patients. Modified from (Kumari & Usdin, 2012).

1.5 Frataxin protein

Frataxin is a highly conserved nuclear-encoded mitochondrial protein, ubiquitously present in prokaryotes and eukaryotes. The frataxin mature form of 14kDa comes from a precursor form of 210 amino acids and 23kDa. Despite the high conservation of frataxin mature form during evolution, some differences are present in structure (Pastore & Puccio, 2013).

1.5.1 Structure

Frataxin protein shows an α-β sandwich structure in which 2 α-helices form a plane and 5 anti-parallel β-sheets form the second plane, with another β-sheet (and in human frataxin one more) that intersects the planes, leading to the topology α1β1β2β3β4β5β6(β7)α2. Despite the presence of an extra β-sheet, the structures of Yfh1 (yeast), HsFtx (human) and CyaY (bacterial) frataxin are similar (Bencze et al., 2006), as shown in the **Figure 10**. These 3 structures show structural similarity due to

the high conservation of their amino acid sequences, however present differences in melting points (Yfh1 39°C, HsFtx 60°C and CyaY 54°C) and stability (Adinolfi, Trifuoggi, Politou, Martin, & Pastore, 2002). The α1 helix of Yfh1 shows surface-exposed acidic residues Glu71, Asp78, Asp79, Asp82, Asp86, Glu89, Glu90 and Glu93 that could bind cations. In fact, the conserved acidic residues (or acidic patch) on the α1/β1 regions of frataxin have been proposed binding iron metal (Bencze et al., 2006). Both forms of iron (Fe^{2+} and Fe^{3+}) are able to bind frataxin, but also others divalent cations by the fact that the binding does not seem related to cysteines or histidines, but to the weaker electrostatic charge (Huang, Dizin, & Cowan, 2008; Pastore & Puccio, 2013). Interestingly, iron binding is weak and not specific. In fact, frataxin can also bind others divalent and trivalent metals, for example, Mn^{2+}, but also Cu^{+} (Han et al., 2019).

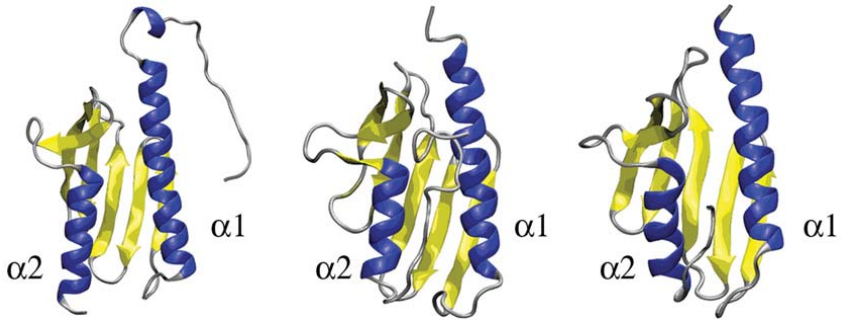

Figure 10. Frataxin structure. Ribbon diagram for yeast (Yfh1), human (HsFtx) and bacterial (CyaY) frataxin (from left to right). Note the two α helices and β-sheets structures. Modified from (Bencze et al., 2006).

In the case of absence of iron, all these frataxin shows a monomeric form. However, Yfh1 and CyaY have the tendency to oligomerize, *in vitro,* under controlled conditions in which iron is in excess. Iron presence seems to be the important factor for oligomerization in Yfh1, but not the only one for CyaY, in which aerobic state seems more important. Despite this tendency to oligomerize, *in vivo* oligomerization of frataxin seems to be due to stress conditions, such as mitochondrial iron uptake or heat stress, thus indicating the monomeric form of frataxin as functioning form. Interestingly, the N-terminal tail of human frataxin is non-conserved, flexible and intrinsically unfolded, but could become functional by interacting with other proteins (Pastore, 2013).

1.5.2 Localisation

Frataxin is a nuclear-encoded protein with mitochondrial localisation. The precursor protein (210aa in humans, 23kDa) targets the mitochondrial matrix, where an N-terminal targeting sequence is removed by the mitochondrial processing peptidase (MPP). The process includes two independent steps:

The **first step** generates an intermediate, a process in which mitochondrial processing peptidase cleaves the N-terminal residues of the protein or mitochondrial targeting sequence (MTS) of 41aa in humans (20aa in yeast) between Gly41 and Leu42, leaving a 19kDa form of frataxin (FXN $_{42\text{-}210}$);

The **second step** generates the 14kDa mature form of the protein, a process in which the peptidase removes more residues (or spacer) from the intermediate form between Lys80 and Ser81, leading to a 130aa form of frataxin, FXN $_{81\text{-}210}$. The spacer seems to be important to separate the basic residues of the MTS from the acidic residues of N-terminal domain of mature FXN and its cleavage seems to be the rate-limiting step in humans. Mitochondrial membrane potential is necessary for this process (Cavadini, Adamec, Taroni, Gakh, & Isaya, 2000; Condò et al., 2007; Gordon, Kogan, Knight, Dancis, & Pain, 2001). Another form of 17kDa, FXN $_{56\text{-}210}$, has also been demonstrated. This form of 155aa comes from the intermediate FXN$_{42\text{-}210}$ by a process in which a spacer of 31aa in yeast and 14aa in humans is removed out between residues Ala55 and Ser56. Although the FXN$_{81\text{-}210}$ is the form of frataxin more widely accepted as mature form, it has been proposed the presence of FXN$_{56\text{-}210}$ when the cleavage site for FXN$_{81\text{-}210}$ is blocked (Cavadini et al., 2000).

In mitochondria, the localisation of mature form ranges from matrix to cristae and in proximity to mitochondrial membranes. However, extra-mitochondrial forms of frataxin have been recently discovered (Condò et al., 2007).

1.5.3 Frataxin function

Although the function of frataxin is in an ongoing debate, its role in regulating mitochondrial function can be deduced by the fact that its deficiency most strongly affects tissues that are primarily involved in oxidative phosphorylation and are rich in mitochondria (*e.g.*, DRGs, cardiomyocytes and β-islet cells of the pancreas). In fact, frataxin deficiency impairs mitochondrial function, increases reactive oxygen species, and triggers the redistribution of iron in the mitochondria and the cytosol. However, the

specific role of frataxin in the cell is not known, but it has been related to different processes in which mitochondria are primarily involved: biosynthesis of iron-sulfur clusters; heme group maturation; iron storage; detoxification and modulation of iron regulatory protein-1 activation; OXPHOS system regulation and protection of cells against oxidative stress. Among them, iron-sulfur clusters' biosynthesis is the most studied and accepted (Pastore & Puccio, 2013).

1.5.3.1 Biosynthesis of iron-sulfur clusters

Many cellular processes require the presence of iron-sulfur (Fe-S) clusters (ISCs) cofactors, composed of iron and sulfur bound to three or more sulfhydryl groups of cysteine residues in proteins, such as [2Fe-2S], [3Fe-4S] and [4Fe-4S]. ISCs are essential in the mitochondrial respiratory chain (in fact, complex I shows 8 ISCs, complex II 3 ISCs and complex III only 1), in the storing of reducing power and in the binding of substrates for enzymes such as Aconitase (Maio, Jain, & Rouault, 2020). However, ISC-containing enzymes are not only present in mitochondria in the electron transport chain and Krebs cycle, but also in cytoplasm for ribosome biogenesis and in the nucleus for DNA repair mechanism and synthesis (Vaubel & Isaya, 2013).

The biosynthesis of Fe-S seems to be due to a complex formed by a **cysteine desulfurase NFS1**, a **scaffold protein ISCU** (Isu1 in yeast), **ISD11** and **ACP** proteins. Each of these four proteins is present twice in the complex, forming a symmetric hetero-octamer. A characteristic of this complex is the interaction between ACP and ISD11, in which the entire acyl chain (of at least 12 carbons) of ACP fits into a hydrophobic barrel created by ISD11 structure. It is unknown the function of this characteristic, but it has been speculated that ACP could link mitochondrial fatty acid biosynthesis to ISCs biogenesis, by the fact that disruption of ISCs biosynthesis leads to cytosolic lipid droplet accumulation (Maio et al., 2020).

The biosynthesis of Fe-S clusters starts on the main scaffold protein ISCU and needs the complex already mentioned. De novo assembled Fe-S cluster is then transferred from ISCU to other proteins through two processes: the **chaperone-mediated transfer to recipient proteins** and the **transfer by secondary carriers**. The first process needs the chaperone/cochaperone system (HSPA9/HSC20) to transfer ISCs into specific recipient apoproteins, such as SDHB (a subunit of complex II) or UQCRFS1 (Rieske protein of complex III). HSPA9 is a HSP70 chaperone, also known as glucose-regulated protein 75 (mortalin or GRP75). In the second process, ISCs can be transferred from ISCU to

secondary carriers that target other Fe-S recipient proteins, such as LIAS (lipoic acid synthase), as indicated in **Figure 11** (Maio et al., 2020).

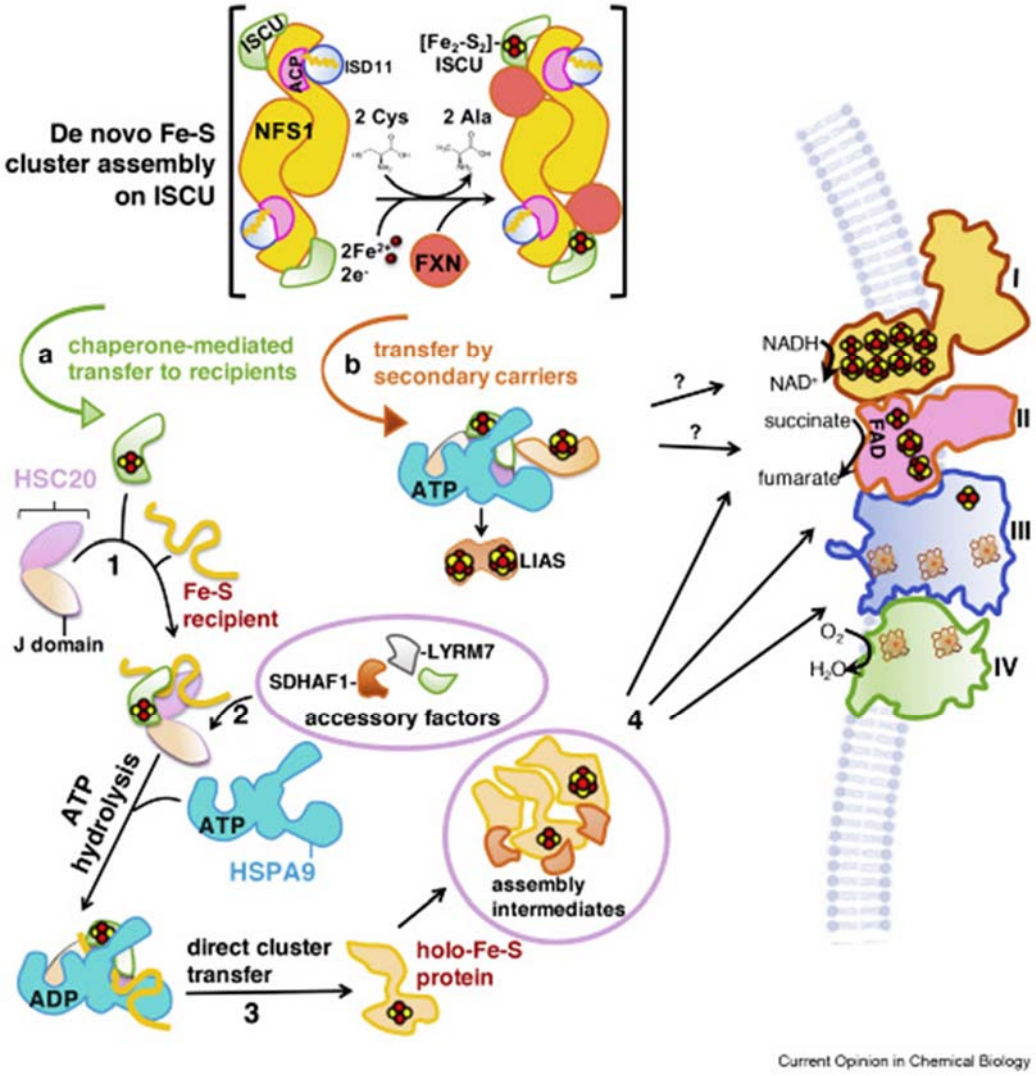

Figure 11. A model of Fe–S biogenesis pathway in mitochondria. See text for details. From (Maio et al., 2020). Note the presence of eight ISCs in complex I; three ISCs in succinate dehydrogenase subunit B (SDHB), which is the ISC-containing subunit of complex II and one ISC in complex III.

The first evidence of a correlation between FA and ISCs biogenesis comes from endomyocardial biopsy of FA patients, in which it was described a deficiency of complex I, II and III activities, but also aconitase (Rötig et al., 1997). After a decade of studies, nowadays, the role of frataxin in the Fe-S biosynthesis is unknown. Initial studies indicate frataxin as an iron donor for Fe-S cluster biogenesis (Yoon & Cowan, 2003). However, frataxin has been supposed to occupy a cavity between NFS1 and ISCU and act as an allosteric regulator that accelerates sulfur transfer from NFS1 to

ISCU (from Cys381 to Cys138). The proposed mechanism involves the ability of this complex to bind Zinc (Zn^{2+}). In the absence of frataxin, cysteine 381 of NFS1 binds Zn^{2+} leading an inactive state of NFS1. In the presence of frataxin, His137 of ISCU interacts with Trp155 of frataxin, leading to a conformational change in which the cysteine 381 of NFS1, not binding Zn^{2+}, is available for sulfur transfer, as schematised in **Figure 12** (Maio et al., 2020). This mechanism correlates with the fact that frataxin deficiency causes impairment of the ISCs-containing subunits of mitochondrial electron transport complexes I, II, and III and the iron-sulfur protein, aconitase. However, it should point out that frataxin seems not essential in ISCs biogenesis, but seems to modify its kinetics, catalysing the process. Indeed, the mechanism is complicated because **ferredoxin 2** (**FDX2**, a Fe-S clusters-binding protein) and **ferredoxin reductase** (**FDXR**) are necessary to provide electrons for the late steps of ISCs biogenesis. Thus, indicating a role in Fe-S cluster, but also heme, biogenesis for FDX2 and a separate role in mitochondrial cytochromes P450 function for ferredoxin 1 (FDX1) (Sheftel et al., 2010). However, a more recent study indicates that both FDX1 and FDX2 are important for Fe-S cluster biogenesis in several human cell lines and that loss of FDX1, FDX2 or FDXR induces cellular iron homeostasis defects. Nevertheless, the exact point in which these 3 proteins are necessary for Fe-S cluster biogenesis needs to be clarified (Shi, Ghosh, Kovtunovych, Crooks, & Rouault, 2012).

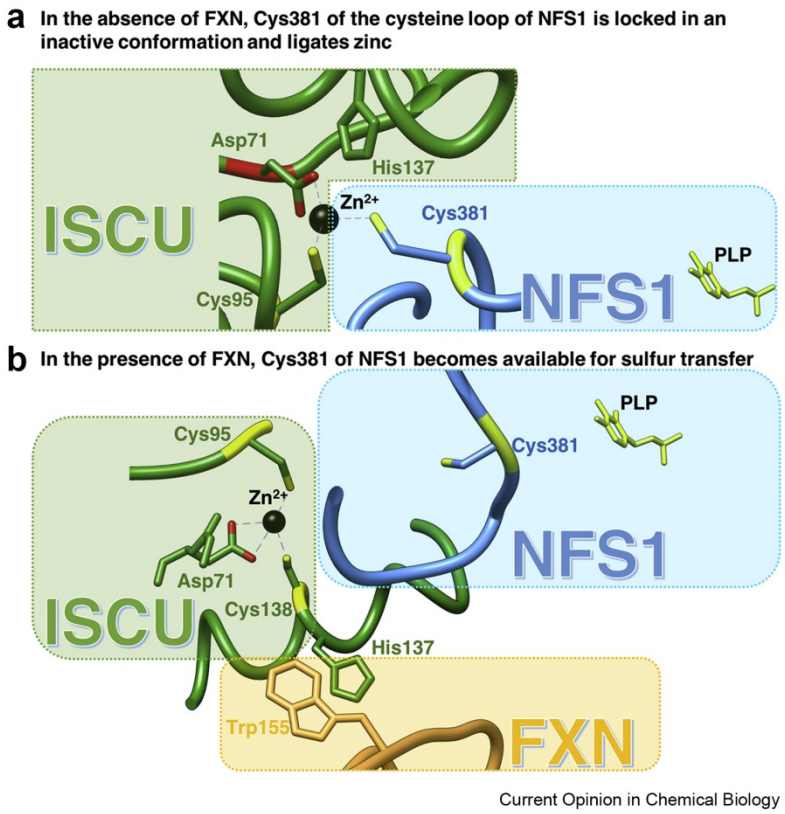

Figure 12. Supposed mechanism of action of frataxin in Fe-S clusters biogenesis. From (Maio et al., 2020).

1.5.3.2 Heme group maturation

Alterations in genes involved in Fe-S cluster biosynthesis, but also heme metabolism, are correlated to different types of ataxias. Heme, a complex of iron and protoporphyrin IX, is necessary for many cellular processes, including cell respiration, drug metabolism, gene regulation and ion channels function. Heme is present in hemoglobin, myoglobin and cytochromes. Its biosynthesis occurs in mitochondria; however, some steps are presents in cytosol or intermembrane space of mitochondria.

The first step requires the substrate succinyl-CoA, deriving from tricarboxylic acid cycle (TCA), and glycine to form δ-aminolevulinic acid (ALA), which is then converted into protoporphyrin IX. In the last step, which occurs in mitochondria, ferrous iron is inserted by ferrochelatase (FECH) into the protoporphyrin ring to form heme *b* (protoheme) (Chiabrando, Bertino, & Tolosano, 2020). Heme *b* is then used by cytochrome c lyases to form heme *c* or by heme *o* synthase to form heme *o*. Heme *o* is then converted in heme *a*. Heme *a*, *b*, and *c* can be used to form mitochondrial hemoproteins and/or can be exported by mitochondria, transported by chaperones and incorporated into different apoproteins to form cellular hemoproteins (Chiabrando et al.,

2020; Swenson et al., 2020). Interestingly, frataxin and ferrochelatase seem to interact, thus leading alterations in late steps of heme *b* biosynthesis in frataxin deficiency (Lesuisse et al., 2003; Yoon & Cowan, 2004). In this contest, it seems that the role of frataxin could be as a ferrous iron (Fe^{2+}) donor to ferrochelatase to produce heme and/or regulator of the metal that can be used by ferrochelatase (Vaubel & Isaya, 2013; Yoon & Cowan, 2004). Evidence of this mechanism comes from studies in which Yfh1-deficient yeast are not able to produce heme but instead produce Zn^{2+}-protoporphyrin, thus indicating an alteration in ferrochelatase action, by the fact that ferrochelatase can use Fe^{2+} or Zn^{2+} in the last step of this process (Lesuisse et al., 2003). An increase in Zn^{2+}-chelatase activity of ferrochelatase has also been confirmed in human FA lymphoblasts (Schoenfeld et al., 2005).

Furthermore, the situation appears more complex by the fact that Fe-S cluster biogenesis and heme biosynthesis are two processes interconnected, as showed in **Figure 13**. In fact, ferredoxin, a Fe-S cluster binding protein, and ferredoxin reductase provide electrons for the late step of heme *a* formation (Barros, Nobrega, & Tzagoloff, 2002). The ferrochelatase presents an ISC. Thus, alteration of heme pathway in FA, which determine heme *a* and *c* deficiency together with loss of heme-containing enzymes activity, could be an indirect mechanism due to ISC deficits (Napoli, Morin, Bernhardt, Buckpitt, & Cortopassi, 2007; Schoenfeld et al., 2005); but also exogenous heme administration increases the activity of ISC-containing proteins ferredoxin and aconitase (Napoli et al., 2007); succinyl-CoA derives from TCA, a cycle in which took part two Fe-S clusters proteins: succinate dehydrogenase B (SDHB) and aconitase 2. Indeed, heme is a cofactor for cytochromes c (heme *c*) and cytochromes in complexes II-III-IV of the mitochondrial electron transport chain (ETC), for example, IV or cytochrome c oxidase presents a heme *a*, while Fe-S clusters are cofactors for complex I, II and III (Chiabrando et al., 2020). Even though heme biosynthesis defects could be indirectly linked to frataxin loss, other diseases with heme deficiency present ataxic symptoms, for this reason, this mechanism needs further investigation also in FA (Chiabrando et al., 2020).

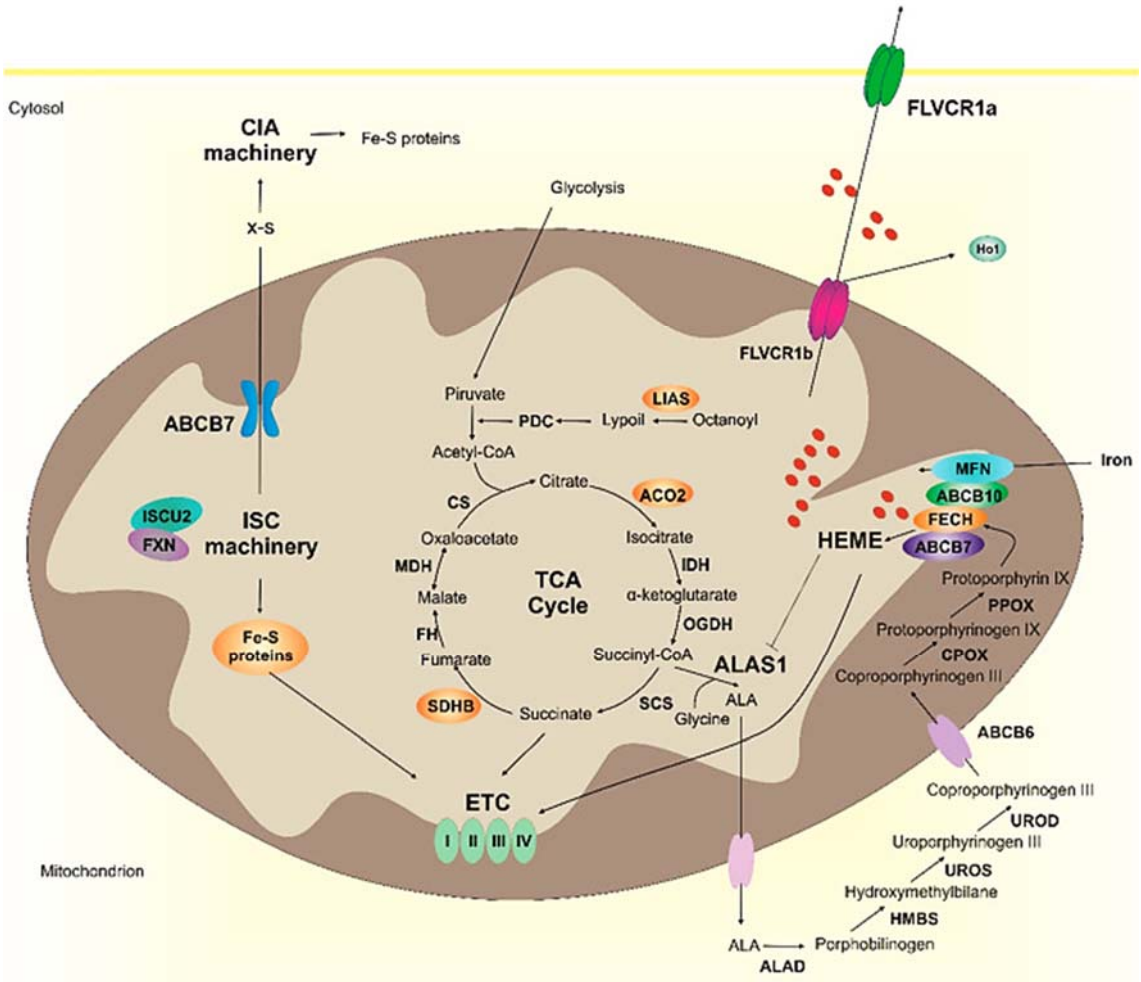

Figure 13. Fe-S cluster and heme biosynthesis are interconnected. In orange are represented Fe-S clusters proteins such as those of TCA cycle and ferrochelatase FECH. TCA is necessary to supply the metabolites for heme biosynthesis. ETC proteins present Fe-S clusters and heme. See text for details. From (Chiabrando et al., 2020).

1.5.3.3 Iron binding/storage

The ability of frataxin to bind iron and homooligomerize has suggested FXN as an iron-storage protein. In fact, under *in vitro* controlled conditions (low salt, O_2 presence and iron Fe^{2+} saturation), Yfh1 and CyaY can form a 48-multimeric homooligomer, that can bind up to 50 iron atoms/monomer. A structure that is similar to ferritin. Human frataxin does not show the same propriety (Bencze et al., 2006). However, it seems that the ability to store iron could be due to different isoforms of human frataxin. While FXN_{81-210} seems to be in a monomeric form and bind ISCs machinery only in the presence of ISCU, FXN_{42-210} seems to oligomerize, store iron and bind ISCs machinery also in the absence of ISCU *in vitro* (Vaubel & Isaya, 2013). The ability to bind iron could determine frataxin as an iron storage in normal condition and transform it into a scavenger protein in iron overloading conditions (Bencze et al., 2006). However, this

function does not seem that major frataxin action, because physiological concentrations of Ca^{2+} or magnesium can stabilize frataxin in the monomeric form (Adinolfi et al., 2002). Indeed, all these data remains undemonstrated *in vivo* and it could be possible that frataxin could be present mostly in a monomeric or oligomeric form depending on the state of the cell. In fact, it seems that in non-dividing cells FXN_{42-210} is predominantly cleaved in FXN_{81-210}, while in dividing cells FXN_{42-210} is mostly not processed (Vaubel, Rustin, & Isaya, 2011).

1.5.3.4 Cellular iron homeostasis and modulation of Irp1 activation

Frataxin deficiency causes iron accumulation in mitochondria (Foury & Cazzalini, 1997), a phenotype that could be a consequence of and early impairment of mitochondrial Fe-S cluster assembly and iron depletion in the cytosol (Li et al., 2008). In fact, mitochondrial ISC biogenesis defects can increase cellular iron uptake and distribution of iron between mitochondria and cytosol, leading to mitochondrial iron accumulation and cytosolic iron depletion (Rouault & Tong, 2005). The distribution of iron into the cell seems to be transcriptionally regulated. The effect of this mitochondrial iron accumulation could be the increase of the fraction of labile redox-active iron in mitochondria (Karthikeyan et al., 2003; Wong et al., 1999). However, iron is present in mitochondria under the form of insoluble nano-particle of ferric phosphate in Yfh1-depleted cells, which in turn could be not used for heme and ISCs synthesis (Lesuisse et al., 2003).

The **cellular iron homeostasis** involves iron-binding transferrin (Tf) that attaches transferrin receptor (Tfr1) onto plasma membranes, as shown in **Figure 14**. This process induces endocytosis of Tf-Tfr1 complex and the acids present in the endosome leads to iron release. Iron is then transported into the cytoplasm through DMT1 and stored into ferritin or imported into mitochondria through mitoferrin to be used for Fe-S cluster and heme biosynthesis or exported through ferroportin. This mechanism is regulated by IRP1 and IRP2, two iron regulatory proteins that act on mRNAs. IRP1 (or cytosolic aconitase), losing its Fe-S cluster, senses the iron status and becomes an IRE-binding protein, increasing or inhibiting the translation of mRNA containing IRE by binding onto 3' or 5' UTR, respectively. For example, Tfr1 contains a 3' UTR, while ferritin and ferroportin contain a 5' UTR. Thus, a decrease of Fe-S clusters can induce cytosolic iron depletion and an increase of Tfr1 and decrease of ferritin and ferroportin levels, while, when cytosolic iron is in excess, IRP1 presents its Fe-S cluster and loses

its affinity for IRE-containing mRNA. As IRP1 is a cytosolic protein, extramitochondrial frataxin should perform this function, by the fact that the export of Fe-S clusters from mitochondria to be used for cytosolic proteins is questioned. However, also the presence of frataxin in this compartment is still a matter of debate (Vaubel & Isaya, 2013).

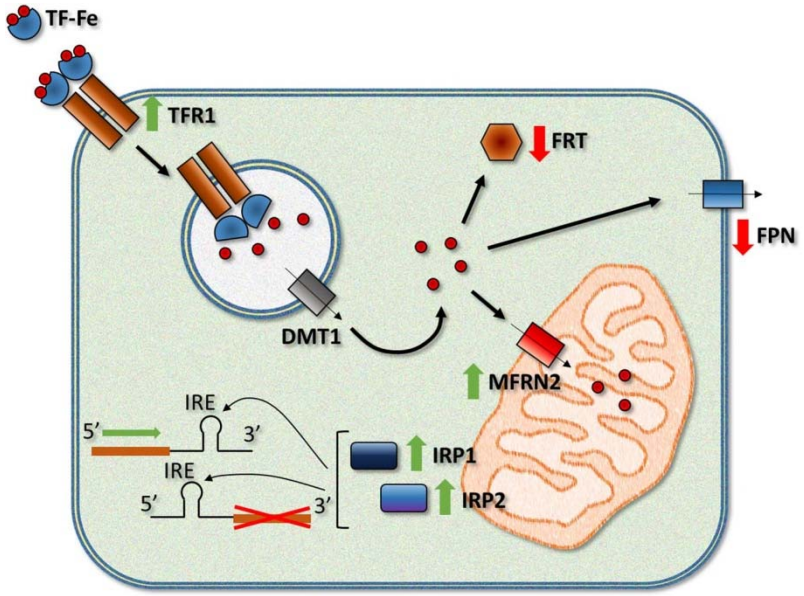

Figure 14. Iron homeostasis in FA. Arrows indicate the proteins upregulated and down-regulated by frataxin deficiency. See text for details. From (Llorens, Soriano, Calap-Quintana, Gonzalez-Cabo, & Moltó, 2019).

Nevertheless, in yeast model, Fe-S cluster deficiency has been shown as a consequence of **metabolic reprogramming**. Yfh1-deficient cells activate Aft1/2 (iron-regulated transcription activator, no orthologue has been found in mammals) transcription factors, which promote up-regulation of iron uptake and expression of Cth2 (tristetraprolin, TTP in mammals), an mRNA binding protein that degrades mRNAs of iron-containing proteins, indicating Fe-S cluster deficiency as a late event in the disease process. Indeed, Cth2 deletion in Yfh1-deficient cells maintains the activity of aconitase and SDH, indicating that the deficiency of Fe-S cluster-containing proteins is a consequence of this metabolic reprogramming consisting in a shift from respiratory to fermentative metabolism (Moreno-Cermeño, Alsina, Cabiscol, Tamarit, & Ros, 2013).

1.5.3.5 Protection of cells against oxidative stress

As iron (in the form of free iron or labile iron pool) is extremely reactive in redox chemistry and frataxin seems to regulate iron homeostasis, frataxin deficiency should induce oxidative damage to protein, DNA and lipids by **radical oxygen species** (ROS).

However, oxidative stress in FA is the most controversial topic, with studies indicating that it is the consequence of Fe-S cluster biogenesis defects and iron accumulation, studies indicating oxidative stress without or before Fe-S cluster defects and studies indicating no oxidative stress or a slightly increase. ROS, such as hydrogen peroxide (H_2O_2) or superoxide ($O_2^{\bullet-}$), are chemical reactive species of oxygen that are generally produced by oxidative phosphorylation. Anti-oxidant proteins, such as the metalloenzyme superoxide dismutases (SODs), can scavenge the superoxide anion and transform it into non-radical species. Cu/Zn-SOD (SOD1) is present in cytosol and mitochondrial membrane space, whereas Mn-SOD (SOD2) is the only superoxide dismutase found in mitochondrial matrix. An alteration in the balance between scavenger proteins and ROS production can induce oxidative stress (Tamarit, Obis, & Ros, 2016).

In yeast (Irazusta, Moreno-Cermeño, Cabiscol, Ros, & Tamarit, 2008), *C. elegans* (Vázquez-Manrique et al., 2006), *Drosophila* (Runko, Griswold, & Min, 2008), mouse (Al-Mahdawi et al., 2006), and FA patients fibroblasts (Wong et al., 1999) frataxin deficiency correlates with increased sensitivity to oxidative stress. In fact, increased levels of mitochondrial manganese superoxide dismutase Mn-SOD (SOD2), but decreased enzymatic activity, have been detected in Yfh1-depleted yeast, leading to more oxidative stress (Irazusta, Cabiscol, Reverter-Branchat, Ros, & Tamarit, 2006) and decreased total SODs activity in hearts of conditional frataxin knockout mice (Chantrel-Groussard et al., 2001). Interestingly, it has been described an interaction *in vitro* between Yfh1 and superoxide dismutase 1 (Cu/Zn-SOD or SOD1) and 2 and decreased activity of SOD1 in frataxin deficiency, but only slight affectation of SOD2. This mechanism, and the enzymatic activity, seems to be mediated by the binding of Yfh1 with different metals: no affinity between Yfh1 and SODs in the presence of Fe^{2+} or no metal; interaction and activity inhibited in the presence of Cu^{+}; interaction and activity increased in the presence of Mn^{2+} (Han et al., 2019).

One effect of oxidative damage during frataxin deficiency is the presence of **carbonylated proteins**, mainly present in the mitochondrial compartment. These proteins can be divided in different groups: anti-oxidant enzymes (catalase A, SOD1 and Thiol-specific peroxiredoxin); chaperones (mitochondrial heat shock protein SSC1, in mammalians mtHSP70/GRP75, mitochondrial matrix chaperone HSP78, in mammalians ClpB and cytoplasmic heat shock protein SSE1); metabolism enzymes (α-β subunits of mitochondrial ATP synthase, phosphoglycerate kinase, pyruvate kinase)

but also α chain of actin. Interestingly, there is selective oxidative damage for magnesium and/or nucleotide-binding proteins. This characteristic could be due to accumulation of free iron, which replace magnesium at the metal-binding site, thus inducing damage of these proteins. A mechanism known as **metal-catalysed oxidation**, which decreases functionality of these proteins, and eventually leads to degradation of the protein (Irazusta et al., 2008). Indeed, the NRF2/KEAP1 system, a signalling pathway regulating the response to oxidative stress, seems to be altered in FA by an H_2O_2-mediated process (Paupe et al., 2009). In the same line, H_2O_2 scavengers, but not those of $O_2^{\bullet-}$, protect *Drosophila* model of FA (Anderson, Kirby, Orr, Hilliker, & Phillips, 2008). H_2O_2 scavengers, but also intracellular and mitochondrial iron chelators, such as respectively deferoxamine and deferiprone, avoid the Fenton reaction. A reaction in which ferrous iron generates toxic reactive oxygen species by reducing oxygen to $O_2^{\bullet-}$ radical and reducing H_2O_2 to the hydroxyl radical. Another sign of oxidative stress in frataxin deficiency comes from the fact that FA is clinically similar to the ataxia with Vitamin E deficiency (AVED) and Vitamin E or (α-tocopherol) is an important anti-oxidant (Di Donato, Bianchi, & Federico, 2010), and the anti-oxidant EPI-A0001 improved neurological and cellular functions in FA (Lynch et al., 2012).

One of the different signs of oxidative damage is the **inhibition of aconitase activity**. In this case, oxidative damage precedes Fe-S clusters deficits. In fact, aconitase requires the ISC [4Fe-4S] for its activity, but, in the case of presence of $O_2^{\bullet-}$, its ISC is converted in the inactive [3Fe-4S]. However, this process seems reversible and avoided by the increased presence of citrate or by the oligomeric $FXN_{56\text{-}210}$, which *in vitro* converted [3Fe-4S] in the active [4Fe-4S]. Despite the fact that the aconitase activity seems to be related to frataxin amounts, the interaction between frataxin and aconitase, as well as if its activity is inhibited by ISCs biogenesis defects or oxidation, are still matters of debate (Vaubel & Isaya, 2013). Even though oxidative damage can occur without Fe-S cluster deficient proteins, indicating that ISCs deficiency could be the consequence of oxidative stress in frataxin-deficient yeast (Moreno-Cermeñ et al., 2010) and cardiomyocytes (Obis, Irazusta, Sanchís, Ros, & Tamarit, 2014).

Apart from all these data supporting oxidative stress in FA, other studies determine no oxidative damage in endogenous conditions, but higher cell death in response to exogenous oxidative stress or not even this. In fact, SODs should show an increased level, thus activity, in oxidative stress. Fibroblasts from patients skin show normal activity of SODs; however, in the presence of oligomycin (an inhibitor of ATP

synthase) addition, show increased cell death and decreased activity of SODs, indicating altered response to oxidative stress and higher susceptibility to cell death in stress conditions (Chantrel-Groussard et al., 2001). SODs levels are not affected in Yfh1-depleted yeast (Foury & Talibi, 2001) and SH-SY5Y neuroblastoma cell lines (Bolinches-Amorós, Mollá, Pla-Martín, Palau, & González-Cabo, 2014). However, the levels of SODs are not correlated with the activity, by the fact that this protein could be carbonylated, indicating loss of function, as commented before (Irazusta et al., 2008). Thus, deficits in SODs detoxification could lead to increased presence of superoxide.

Nevertheless, oxidative stress in patients can be analysed by measuring the presence of the **DNA base modification C-8 hydroxylation of guanine** (8OH2'dG) in the urine. When this study was performed, contradictory results were reported. Some studies indicate the presence of 8OH2'dG in FA patients and its decrease using anti-oxidant idebenone (Schulz et al., 2000) and other studies, although measuring significantly neurological improvement using the treatment, were not able to detect changes in the urinary marker (Di Prospero, Baker, Jeffries, & Fischbeck, 2007). All these characteristics indicate that further investigations are necessary to have a clearer understanding of the presence or not of the oxidative stress in FA (Schulz et al., 2009).

1.5.3.6 OXPHOS system regulation

Frataxin, apart from accelerating Fe-S clusters biosynthesis forming ISCs that are present in complex I, II and III of oxidative phosphorylation, seems to interact with some of those complexes. For example, it has been demonstrated an interaction *in vitro* between SDH (complex II) and frataxin, thus, contributing directly onto mitochondrial electron transport activity (González-Cabo, Vázquez-Manrique, García-Gimeno, Sanz, & Palau, 2005). In addition, the structure of frataxin is peculiar and there is only a protein that presents a similar structure in the complex I of *Thermus thermophiles*, thus suggesting a similar function (Sazanov & Hinchliffe, 2006). In support of this hypothesis, several studies indicate, respectively, boost or inhibition of ATP synthesis in frataxin overexpression (Ristow et al., 2000) or deficiency (Bolinches-Amorós et al., 2014), suggesting a role of frataxin as an activator of oxidative phosphorylation, thus modulating ATP content and $\Delta\Psi_m$, as shown in **Figure 15** (Ristow et al., 2000). Decreased ATP content in frataxin deficiency has been also related to decreased activity of complex IV (Bolinches-Amorós et al., 2014). However, why these complexes are affected by frataxin deficiency is still a matter of debate.

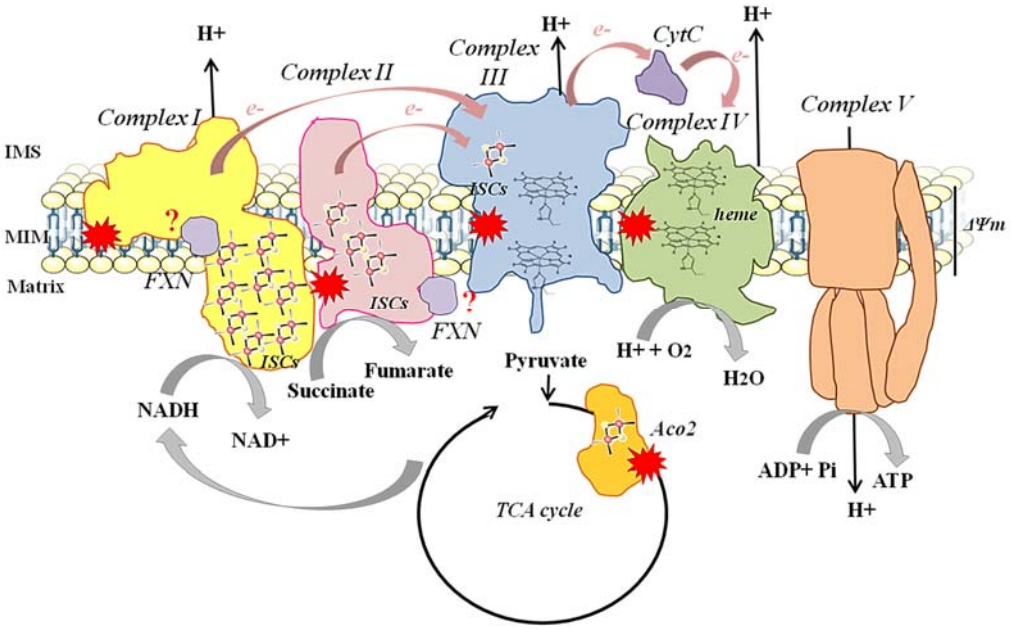

Figure 15. Defects of OXPHOS/TCA system in FA. See text for details. Note the presence of ISCs in complexes I/II and III of OXPHOS system and Aco2 in TCA cycle and the presence of heme in complexes III and IV. Based on (Maio et al., 2020).

1.5.3.7 Cellular calcium homeostasis

Mitochondrial function is directly related to cellular Ca^{2+} homeostasis, thus, frataxin deficiency, leading to mitochondrial dysfunction, has been linked to Ca^{2+} homeostasis deficits, indicating a role in this important cellular process. Ca^{2+} is the mediator of several cellular processes, such as heart contraction, cell signalling, axonal transport, axonal growth, generation of the action potential, synaptic transmission, autophagy, cell death etc. Thus, an alteration in Ca^{2+} pathway leads to different and irreversible consequences.

- **Heart**

Barbeau group discovered for the first time the connection between Ca^{2+} and Friedreich Ataxia in 1976 by looking at granular deposits of Ca^{2+} salts, together with iron, in myocardial cells from one FA patient. In this study, focal zones of calcification were detected near the conduction node (Sanchez-Casis, Cote, & Barbeau, 1976). These results were confirmed by Koeppen group, who indicates a significant increase of Ca^{2+} in right ventricular walls by analysing the presence of different metals in FA cardiac biopsies (Kruger et al., 2016). Generally, alterations in electrocardiograms (ECG) of patients, manifested as repolarisation abnormalities in which is detected a deep negative T-wave, are the most common reported cardiac phenotypes in FA (Kosutic &

Zamurovic, 2005). These changes in T-waves amplitude are related to increase serum Ca^{2+} or hypercalcaemia (Ahmed et al., 1989) and decrease in serum potassium or hypokalaemia (Wang, Han, & Li, 2018). Thus, when FA patients were treated with high-doses of β-blocker propranolol (60-120mg/24h), a drug capable of decreasing Ca^{2+} influx into the cells, no repolarisation abnormalities were detected but, on the contrary, positive T-waves in ECG (Kosutic & Zamurovic, 2005). Treatment with low doses of 40mg propranolol three times a day also induced benefits in motor performance and clarity in speech, indicating involvement of Ca^{2+} alterations in the disease (Braham, Sadeh, Turgman, & Sarova-Pinchas, 1979). On the same line, FA human induced pluripotent stem cells-derived cardiomyocytes show slower beating rates with reduced Ca^{2+} peak amplitude. These alterations have been prevented using nifedipine, a Ca^{2+}-channel blocker, but not a potassium-channel blocker (Crombie et al., 2017). Interestingly, these data have been reproduced by another group in FA iPSC cardiomyocytes only in the presence of exogenous iron (Fe^{2+}), in which slower Ca^{2+} transients are due to retard in Ca^{2+} reuptake by **sarcoplasmic reticulum** (SR) (Lee et al., 2014). Nevertheless, these alterations in contractility shown *in vitro* were also confirmed in a cardiac tissue model of FA patients without iron supplementation. In fact, 3-dimensional (3D) engineered cardiac tissues from FXN-deficient human pluripotent stem cell-derived ventricular cardiomyocytes (hPSC-hvCMs) show reduced contractile and relaxation rates (Wong et al., 2019). SR is the major Ca^{2+} store in cardiomyocytes and is involved in the mechanism of contraction. Ca^{2+} influx into SR is mediated by sarco/endoplasmic reticulum Ca^{2+}-ATPase (SERCA) pumps and its release through ryanodine receptors (RyRs), is due to a Ca^{2+}-induced Ca^{2+} release, a mechanism by which the presence of Ca^{2+} induces the emptying of SR store. In frataxin-deficient cardiomyocytes, the Ca^{2+} content in SR is lower and this mechanism could be due to an increase of RyRs or decrease of SERCA pumps functions. When treated with thapsigargin, mitochondrial Ca^{2+} ($Ca^{2+}{}_m$) uptake was slower, indicating a reduction of Ca^{2+} content in SR or decreased capacity of $Ca^{2+}{}_m$ influx. Interestingly, both RyRs and SERCA pumps have cysteine that can be affected by oxidative stress. Thus, the anti-oxidant vitamin E improved the phenotype, probably by preventing the oxidative damage of these channels (Abeti, Brown, Maiolino, Patel, & Giunti, 2018). However, frataxin deficiency also decreases the **$Ca^{2+}{}_m$ efflux**. Our group described a frataxin-deficient cardiomyocytes model in which decrease in NCLX levels, mitochondrial permeability transition pore (mPTP) opening and Nuclear Factor of Activated T cells

(NFATc4) activation have been detected (Purroy, Britti, Delaspre, Tamarit, & Ros, 2018). This exchanger, predominantly active in excitable cells such as cardiomyocytes and neurons, needs special attention by the fact that its functioning, providing Ca^{2+} for SR/ER, regulates the automaticity of HL-1 cardiomyocytes, due to Ca^{2+} oscillations, and the SR Ca^{2+} content (Takeuchi, Kim, & Matsuoka, 2013). Indeed, NCLX knockdown reduced uptake by SERCA pumps and ER Ca^{2+} content in β-lymphocytes (Kim, Takeuchi, Koga, Hikida, & Matsuoka, 2012) and HL-1 cardiomyocytes (Takeuchi et al., 2013), impairing ER/SR Ca^{2+} handling, thus, contributing to deregulate, respectively, antigen response and cardiac rhythmicity (Kim et al., 2012; Takeuchi et al., 2013). **Mitochondrial pore opening** has been demonstrated since cyclosporine A (CsA), an inhibitor of mPTP opening, has restored the phenotype in cardiomyocytes (Purroy et al., 2018). The rise of Ca^{2+} proceeding from damaged mitochondria contributes to activate calcineurin, a Ca^{2+}-activated phosphatase that dephosphorylates NFAT, allowing the nuclear translocation and **genetic expression** of hypertrophic signals in cardiomyocytes (Purroy et al., 2018).

❖ **Neurons**

The connection between Ca^{2+} and FA concerns not only heart pathology but also neuronal cells. In fact, frataxin silencing in SH-SY5Y human neuroblastoma cells (Bolinches-Amorós et al., 2014) and DRG neurons of the YG8R mouse model (Mollá et al., 2017) have been also linked with decreased **Ca^{2+}_m uptake** and $Ca^{2+}{}_m$ buffer capacity. Thus, frataxin could have an important role in the regulation of cellular Ca^{2+} homeostasis also in neurons. Mitochondria, together with endoplasmic reticulum, are important organelles for intracellular Ca^{2+} ($Ca^{2+}{}_i$) buffering. Thus, it is not surprising that mitochondria dysfunction provoke alterations in this process. For example, frataxin-deficient SH-SY5Y neuroblastoma cell lines failed to recover normal cytosolic concentration in response to a stimulus entering Ca^{2+} from extern or emptying Ca^{2+} from reticulum in $Ca^{2+}{}_{free}$ medium (Bolinches-Amorós et al., 2014). A mechanism that has been also demonstrated in YG8R cerebellar granular cells in response to KCl or thapsigargin, which suggests lower Ca^{2+} levels in ER, probably for an hyperactivation of the inositol-1,4,5-trisphosphate receptor (IP_3R) or RyRs or inactivation of SERCA pumps (Abeti et al., 2018). Indeed, ER stress has been also linked to frataxin deficiency. However, the chaperone Bip/GRP78, a protein related to ER stress, increases its levels only in the case of thapsigargin addition, thus, indicating no basal ER stress but a major

susceptibility to ER-related stress (Bolinches-Amorós et al., 2014). Interaction between mitochondria and ER or **mitochondria-associated membranes** (MAMs) creates a specific environment for Ca^{2+} homeostasis and these contacts are important for $Ca^{2+}{}_i$ buffering. Thus, Ca^{2+} stored in ER is released, through IP_3R, into mitochondria, where it is taken up by $Ca^{2+}{}_m$ uniporter (MCU) and extruded by mitochondrial Na^+/Ca^{2+} exchanger (NCLX), contributing to ER refilling. The chaperone glucose-regulated protein 75 (GRP75) links the two organelles. Interestingly, an extra-mitochondrial form of frataxin seems to interact with GRP75 and IP_3R, modulating MAMs and Ca^{2+} buffering (Rodríguez et al., 2020) and mitochondrial import of frataxin (Dong, McMillan, Clark, Lin, & Lynch, 2019). Thus, the function of MAMs is compromised in frataxin-deficient neuroblastoma cells, by the fact that the organelles are not properly connected, leading to increased cytosolic Ca^{2+} and decreased $Ca^{2+}{}_m$ buffering and uptake. Functions that seems to be restored by the use of anti-oxidants. In this scenario, MCU overexpression in frataxin-deficient Drosophila restores phenotypes due to frataxin deficiency (Rodríguez et al., 2020). A mechanism due to increase of MAMs or $Ca^{2+}{}_m$ uptake, as MCU is a mitochondrial player of both processes.

Our group described a frataxin-deficient DRG neurons model in which **increase in $Ca^{2+}{}_{free}$ concentration** ($[Ca^{2+}{}_i]_{free}$), activation of caspase-3 and calpains, alteration in Ca^{2+}-mediated signalling pathways such as cAMP response element-binding protein (CREB) and cell death (Mincheva-Tasheva, Obis, Tamarit, & Ros, 2014) have been detected, suggesting mPTP opening. The rise of Ca^{2+} proceeding from damaged mitochondria contributes to activate Ca^{2+}-dependent proteases, caspase 3 and calpains, which cleaves α-fodrin, a cytoskeletal protein and activate the nuclear transcription factors CREB by phosphorylation (Mincheva-Tasheva et al., 2014) that mediate **genetic expression** of apoptotic markers in neurons and cell death, as shown in **Figure 16** (Purroy et al., 2018). The apoptotic markers mediated by pCREB, such as Bax, have been restored by treating frataxin-deficient DRG neurons with the anti-apoptotic domain BH4 of Bcl-$_{XL}$ (Mincheva-Tasheva et al., 2014). Interestingly, Bcl-$_{XL}$ can mediate its anti-apoptotic function by closing the mitochondrial voltage-dependent anion channel (VDAC), thus, preventing Ca^{2+}-dependent mitochondrial outer membrane permeabilisation during apoptosis and cytochrome c release (Shimizu, Konishi, Kodama, & Tsujimoto, 2000) or by interacting with IP_3R, thus, inhibiting ER Ca^{2+} release, which, in turn, could prevent $Ca^{2+}{}_m$ overload and mPTP opening (Rong et al., 2009). In addition, treatment of fibroblast cells from patients (Wong et al., 1999) with

$Ca^{2+}{}_i$ chelator BAPTA-AM rescues the phenotype strengthening the hypothesis of a relation between Ca^{2+} and FA. Caspase-3 activation has been also detected, supporting the hypothesis of Ca^{2+}-induced mitochondrial or intrinsic apoptotic cell death (Wong et al., 1999). A process that has been also demonstrated in frataxin-deficient iPSC-derived neurons (Igoillo-Esteve et al., 2015), human neuronal like-cells (Palomo, Cerrato, Gargini, & Diaz-Nido, 2011), *in vitro* embryonic cerebral cortices and *in vivo* cerebellar granules neurons (Katsu-Jiménez, Loría, Carlos Corona, & Díaz-Nido, 2016). In this scenario, the treatment with pan-caspase inhibitors and calpeptin, a calpain inhibitor, in frataxin-deficient neuronal like-cells (Palomo, Cerrato, Gargini, & Diaz-Nido, 2011) and embryonic cerebral cortices (Katsu-Jiménez et al., 2016) improved apoptotic cell death. These results suggest that acting on the inhibition of **Ca^{2+}-activated proteases** could be beneficial.

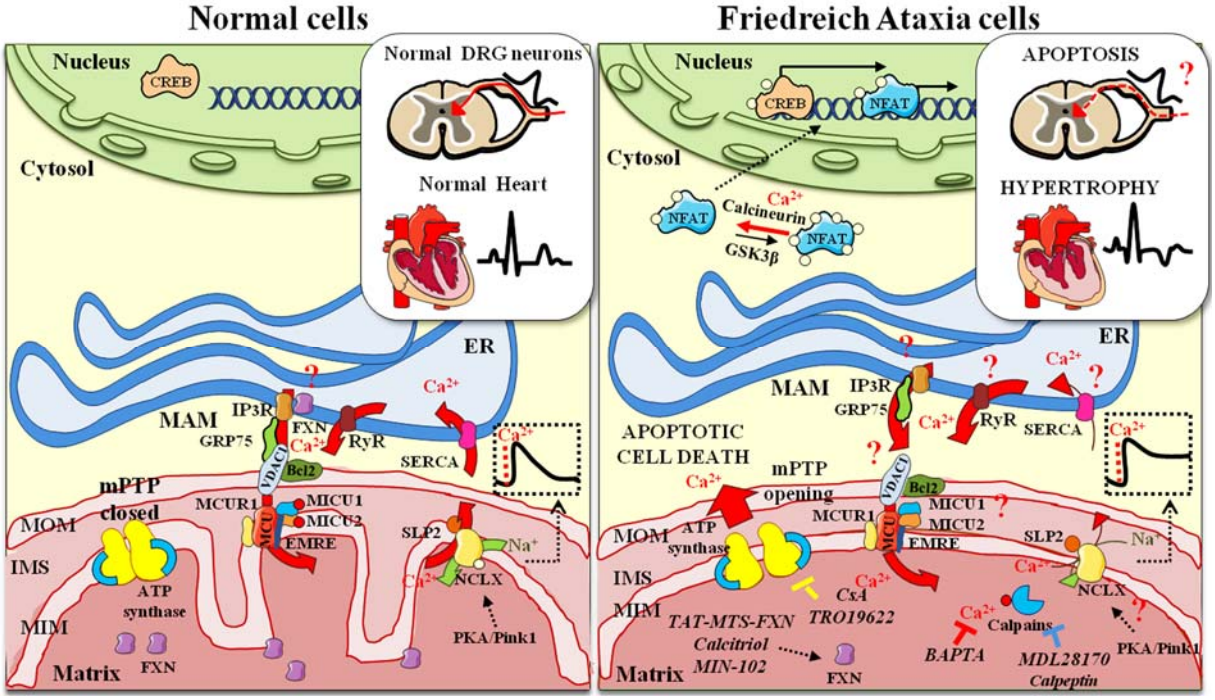

Figure 16. Ca^{2+} homeostasis in normal cells and frataxin-deficient cells. See text for details. From (Tamarit et al., 2021).

❖ Pancreas

Frataxin deficiency induces mitochondrial cell death not only in neurons but also in frataxin-deficient pancreatic β-cells. In fact, in this case, Ca^{2+}-dependent proteases activation such as caspase 3 and 9 have been also demonstrated, together with other pro-apoptotic factors (Igoillo-Esteve et al., 2015).

All these data are in agreement with alterations of Ca^{2+} homeostasis in FA, however, Ca^{2+} is not only linked to heart contraction and mitochondrial cell death in neurons and β-cells, but also with a variety of different situations. For example, defecation in *C. elegans* is controlled by Ca^{2+} oscillations in the gut cells, thus, frataxin-deficient worms show alterations in this process (Vázquez-Manrique et al., 2006). Ca^{2+} is linked to axonal transport, thus, frataxin deficiency could indirectly produce mitochondrial transport damage along axons. A process described in YG8R DRGs of mice, a frataxin knockout mice with a 90/190 GAA expansion form FA patients (Mollá et al., 2017). In addition, axonal growth is a dynamic process regulated by a continuous reorganisation of actin filaments (globular G-actin and filamentous F-actin) and microtubules, which is mediated by Ca^{2+}-binding proteins. As Ca^{2+} is involved in neurite growth, adult YG8R DRGs of mice show reduced neurite length associated with an increased F/G actin ratio and lower size/number of their growth cones (GC), the processes of neurons which allows forming neurites (Muñoz-Lasso et al., 2020). The same model shows Ca^{2+} imbalance, which causes axonal spheroids, retaining dysfunctional mitochondria, and impairs autophagy flux (Mollá et al., 2017). Although it is still unknown if Ca^{2+} deregulation is a cause or consequence of FA pathology and what are the initial steps of Ca^{2+} deregulation, the above data indicate a strong connection between this metal and FA. Thus, it is important to consider also Ca^{2+}-dependent mechanisms to test further therapeutic strategies.

1.5.3.8 Regulation of lipid metabolism

Dysregulation of lipid metabolism has been observed in several FA models, although this characteristic has not directly related to frataxin loss but to the consequences of this deficiency. The most accepted hypothesis is that frataxin-deficient mitochondria can not properly metabolise lipids, leading to an accumulation of intracellular lipid droplets (Tamarit et al., 2016). However, this accumulation could be also due to an increased synthesis. Even though it is unknown if this accumulation is a consequence of defect in catabolism or synthesis, the abundance of lipid droplets has been observed in heart of the muscle creatine kinase (MCK) and neuron-specific enolase (NSE) conditional mice, together with disorganised cristae and giant mitochondria (Puccio et al., 2001). In line with these observations, **lipid droplets accumulation** with balloon-like mitochondria has been also described in frataxin-deficient neonatal rat ventricular myocytes (NRVMs) (Obis et al., 2014), glial cells of a glial conditional *Drosophila* model

(Navarro et al., 2010), but also in liver of conditional mice (Alb). Recently, lipid droplets accumulation and enlarged mitochondria have been observed in brown adipose tissue of frataxin Knock-in/Knock out (KIKO) mice and frataxin-deficient T37i brown adipocytes (Turchi et al., 2020). Interestingly, as observed in patients (Huang, Nestruck, Barbeau, Bouchard, & Davignon, 1978), KIKO mice show a significant increase of cholesterol and triglycerides in blood (Turchi et al., 2020). Cholesterol is the most common steroid (lipid) taken up by mitochondria to form vitamin D, progesterone, cortisol etc. Its increased presence in blood could be due to impairment of its utilisation by different cytochromes P450, which need ferredoxin, a Fe-S protein, to convert cholesterol in the subsequent product. Thus, it is not surprising that frataxin deficiency, reducing ferredoxin activity, can impair **steroidogenesis** (Palandri, L'hôte, Cohen-Tannoudji, Tricoire, & Monnier, 2015). Another relation between iron and lipid metabolism comes from the fact that mitochondrial iron accumulation can increase **sphingolipids synthesis** (dihydrosphingosine, dihydroceramide, sphingosine), leading to an activation of 3-phosphoinositide dependent protein kinase-1 (Pdk1) and myocyte enhancer factor-2 (Mef2) PDK1/Mef2 pathway in frataxin-deficient *Drosophila* and neurodegeneration (Chen et al., 2016). In addition, excessive oxidative stress leads to oxidation of lipids, a process known as **lipid peroxidation** (Abeti et al., 2016).

1.5.3.9 Mitochondrial biogenesis, fusion/fission and mitophagy control

As indicated above, frataxin deficiency induces downregulation of the PPARγ transcription factor, leading to alteration in lipid metabolism. However, PPARγ is also a regulator of **mitochondrial biogenesis**. In fact, decreased number of mitochondria has been observed in several models such as patient-derived FA fibroblast cell models, the mouse model KIKO, whole blood collected from patients (Jasoliya, McMackin, Henderson, Perlman, & Cortopassi, 2017), frataxin-deficient SH-SY5Y human neuroblastoma cells (Bolinches-Amorós et al., 2014), but also brown adipose tissue (Turchi et al., 2020) and cerebellar homogenate of KIKO mice (Lin et al., 2017). However, this relation between frataxin and mitochondrial biogenesis is still a matter of debate, as this relation has not been observed in other models.

Frataxin deficiency in proliferative SH-SY5Y human neuroblastoma cells not only induces decreased number of mitochondria per cell, but also mitochondrial fusion with tubular and swollen morphology. Yfh1-deficient yeasts (Lefevre, Sliwa, Rustin, Camadro, & Santos, 2012) and muscle cells of a FA *Drosophila* model (Edenharter,

Schneuwly, & Navarro, 2018), on the contrary, show mitochondrial fragmentation, indicating that **regulation of fusion/fission** by frataxin is a complex phenomenon that needs further investigations. Interestingly, downregulation of mitofusin, a regulator of mitochondrial fusion, rescues the defects due to frataxin deficiency in muscle and glial cells of a FA *Drosophila* model, such as ER stress and lipid accumulation, indicating the control of mitochondrial morphology as an important target for future treatments (Edenharter et al., 2018).

Indeed, frataxin has been demonstrated to regulate also **mitophagy**, the degradation of damaged mitochondria. For example, frataxin deficiency in *C. elegans* induces iron starvation and a hypoxic-like response that, in turn, activate mitophagy, leading to lifespan extension. In line with this hypothesis, in mammalian cells, iron-chelators induce mitophagy, indicating that this event could be a consequence of iron dysregulation (Schiavi et al., 2015). In contrast, frataxin-deficient hepatic cell lines HepG2 show an inhibited Pink1/Parkin associated mitophagy, despite decreased iron content (Liu et al., 2018).

1.5.3.10 DNA repair and tumour suppressor

Nuclear DNA repair also seems to be a functionality of frataxin. However, this mechanism could occur as a consequence of other functions. For example, some specific nuclear DNA repair proteins and telomere-maintain proteins, contain ISCs, thus, deficiency of ISCs in FA could also affect DNA repair machinery (Thierbach et al., 2010) and telomere stability (Anjomani Virmouni et al., 2015).

Frataxin is a probable **tumour suppressor**, thus, its deficiency should induce tumour initiation (Thierbach et al., 2010). In this line, frataxin-deficient hepatocyte-specific Alb mice develop liver tumours in the early stage of their life (Thierbach et al., 2005) and FA patients at young ages show malignant formations, such as gastric carcinoma (Ackroyd, Shorthouse, & Stephenson, 1996), bowel ganglioneuroblastoma (Barr, Page, & Taylor, 1986) and breast cancer (Kidd et al., 2001). All these events have been related to ISCs deficiency, thus, indirectly due to frataxin deficiency, however, the presence of frataxin in nucleus questions this hypothesis (Guo et al., 2018).

1.5.3.11 Cell death and autophagy regulation

Cell death associated with frataxin deficiency has been reported in frataxin-deficient DRG sensory neurons (Mincheva-Tasheva et al., 2014), frataxin-deficient astrocytes

(Loría & Díaz-Nido, 2015), iPSCs-derived neurons from patients, frataxin-deficient pancreatic β-cells (Igoillo-Esteve et al., 2015), H_2O_2-treated fibroblasts from patients (Abeti, Baccaro, Esteras, & Giunti, 2018), human neuroblastoma SH-SY5Y cells (G. M. Palomo, Cerrato, Gargini, & Diaz-Nido, 2011) etc. In some of these FA models, an intrinsic (mitochondrial) apoptotic pathway has been observed with mPTP opening (Purroy et al., 2018) and activation of pro-apoptotic proteins such as caspase 3, Bax (Igoillo-Esteve et al., 2015; Mincheva-Tasheva et al., 2014; Palomo et al., 2011). In neuroblastoma cell lines, frataxin deficiency induces apoptosis or not, depending on the cellular phase. In fact, proliferating undifferentiated frataxin-deficient human neuroblastoma cell lines SH-SY5Y show cellular senescence and increased autophagy flux, but not apoptosis (Bolinches-Amorós et al., 2014), while differentiated ones present apoptosis, with chromatin condensation, nuclear fragmentation, p53 induction and activation of pro-apoptotic proteins such as caspase-3, PUMA, Bax, but not increased autophagy (Palomo et al., 2011). Interestingly, frataxin-deficient mouse P19 embryonic carcinoma cells, which can be induced to differentiate into a various cell types, including neurons and cardiomyocytes, show apoptosis in neuronal, but not cardiac, differentiated cells (Santos, Ohshima, & Pandolfo, 2001). These results highlight the relation between frataxin deficiency and intrinsic apoptosis in differentiated neuronal cells. Some frataxin-deficient cells, instead of apoptosis, display **autophagy alterations**. For example, undifferentiated frataxin-deficient human neuroblastoma cell lines SH-SY5Y (Bolinches-Amorós et al., 2014), lymphoblast derived from FA patients and *C. elegans* embryos induce autophagy. This process could be mediated by p53, a regulator of both apoptosis and autophagy (Schiavi et al., 2013).

1.5.3.12 Summary of frataxin deficiency in neuronal cells

In summary, frataxin deficiency seems to determine early defects in ISCs biogenesis, which, in turn, induce mitochondrial iron overload and, secondarily, oxidative stress (Vaubel & Isaya, 2013), but also oxidative damage can induce more ISCs deficiency and oxidative DNA damage in a vicious cycle. However, ISCs biogenesis defects seem to be clear in experiments *in vitro*, but not *in vivo* and oxidative damage can also occur without the alteration of ISC-containing enzymes. Thus, the function of frataxin is still a matter of debate. Nevertheless, from any point it starts, it is overall accepted that frataxin silencing provokes mitochondrial dysfunction, which, in turn, leads to alterations in energy production, Ca^{2+}_m homeostasis, $\Delta\Psi_m$, axonal transport and finally

autophagy deregulation or cell death (Tamarit et al., 2021). Some of these mechanisms are summarized in **Figure 17**. An intriguing question that needs to be solved is: *"How can an event like mitochondrial dysfunction lead to loss of specific neuronal cells such as DRG neurons?"*. The particular characteristic of this type of neurons being the longest in the body could be considered. However, major efforts should be performed to understand this selective vulnerability (Carletti & Piemonte, 2014).

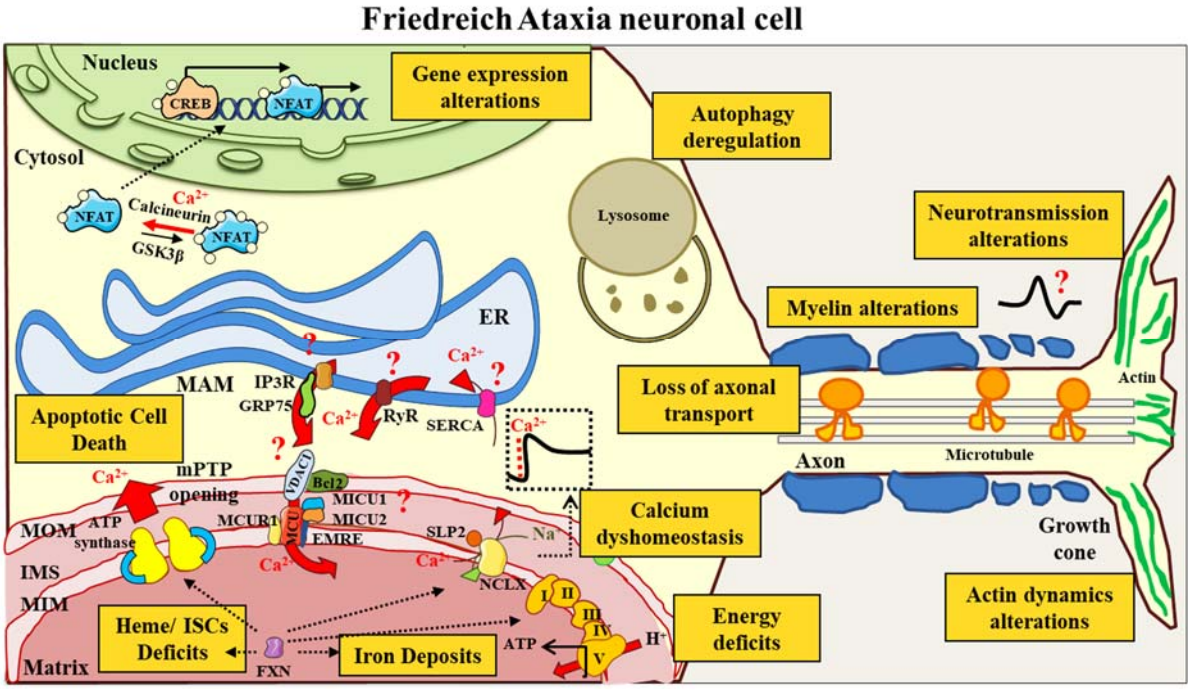

Figure 17. Pathophysiological effects of frataxin deficiency in neurons. Frataxin could determine Fe-S cluster deficiency, with consequently heme biosynthesis and energetic deficiency. In consequence, iron accumulates in mitochondria leading to oxidative stress. Iron can increase sphingolipids synthesis and activation of PDK1/Mef2 pathway. Furthermore, frataxin deficiency induces Ca^{2+} dyshomeostasis linked to retrograde axonal transport failure and actin dynamics in the neuronal growth cones. Autophagy alterations or intrinsic apoptosis have been also described. Based on (Chiabrando et al., 2020).

1.6 Friedreich ataxia models

Currently, there are no adequate models to study FA. On the one hand, this is due to the lethal phenotype in early embryonic stages in complete frataxin depletion. On the other hand, the models present in literature does not recapitulate all the characteristic phenotypes of the disease (Perdomini, Hick, Puccio, & Pook, 2013).

1.6.1 Yeast models

As frataxin is a conserved protein during evolution, its orthologs have been studies in several organisms such as *S. cerevisiae* yeasts, where frataxin is named Yfh1. Yfh1-

deficient yeast displays inability to grow in a non-fermentable medium, indicating defects in oxidative phosphorylation, but also iron accumulation and sensitivity to oxidative stress (González-Cabo, Llorens, Palau, & Dolores Moltó, 2009). Using this model, our group discovered that Yfh1-deficient yeast activates an iron-regulated transcription factor Aft1/2, which promote iron uptake and degrade mRNAs of iron-containing proteins through the expression of Cth2, an mRNA binding protein. Thus, Fe-S cluster deficiency could be a late event in consequence of this change in gene expression (Moreno-Cermeño et al., 2013).

1.6.2 Invertebates models

Frataxin deficiency has been also studied in the insect invertebrate ***Drosophila*** model trough a RNA interference systemic or tissue-specific downregulation of *fh*, the frataxin ortholog. For example, a *Drosophila* model, in which frataxin is ubiquitously decreased to 30% residual amounts shortens life span and impairs climbing activity. When this model has been maintained in hyperoxia (99.5% O_2) conditions, life span of frataxin-deficient animals has been even more shortened, indicating increased susceptibility to oxidative stress, as hyperoxia can recreate an unbalanced oxidative status (Llorens et al., 2007). Indeed, frataxin deficiency produces different phenotype in larvae or adult animals. In fact, systemic *fh* silencing produces giant, long-lived larvae, but also moribund, short-lived adults in relation to the moment in which the downregulation of frataxin is performed (Anderson, Kirby, Hilliker, & Phillips, 2005).

RNA interference has been also used to reduce the expression of frataxin in ***C. elegans***. When the frataxin ortholog *frh-1* is silenced induces reduction (Vázquez-Manrique et al., 2006) or extension of life span (Schiavi et al., 2013; Ventura et al., 2005), respectively, if the silencing is performed in larvae or adult worms. In the first case, animals display slow growth, lethargic behaviour, egg-laying defects, reduced brood size, abnormal pharyngeal pumping, altered defecation, and increased sensitivity to oxidative stress (Vázquez-Manrique et al., 2006). In the second case, small body size, reduced fertility, altered responses to oxidative stress (Ventura et al., 2005), reduced lipid accumulation and induced autophagy are the phenotypic characteristics (Schiavi et al., 2013).

1.6.3 Cellulars models

Cells derived from patients represent a good model to study FA because of the presence of GAA repeats expansion. These cells, such as **fibroblasts and lymphocytes from patients**, despite not presenting a clear phenotype, represent good models to screen new drugs increasing frataxin expression as they carry the human genetic mutation and are easy to obtain, but also to study the cause and consequence of GAA repeats expansion. Fibroblasts and lymphocytes have been collected directly from patients or immortalised generating a cell line (Perdomini et al., 2013). Immortalised cell lines are available in Coriell Institute biobank, in which a wide collection of biological samples is commercialized for medical research. Indeed, murine fibroblasts have been also "humanized" by depleting murine frataxin and replacing it with human missense-mutated frataxin ($hFXN^{G130V}$ or $hFXN^{I154F}$) to generate a model for point mutation FA (Calmels et al., 2009).

Nevertheless, the most affected tissues in FA are DRGs, cerebellar neurons, cardiomyocytes and pancreatic β-cells. None of them is accessible from patients, but to overcome this problem, human FA models based on **induced pluripotent stem cell (iPSC)** have been also generated. Using this technique, FA skin fibroblasts can be reprogrammed into iPSC and differentiated into the most affected cells, such as cardiomyocytes and neurons (Hick et al., 2013). Both models display impaired mitochondrial function with decreased $\Delta\Psi_m$ and progressive mitochondrial degeneration (Hick et al., 2013). As proprioceptive neurons are the most affected cells in DRGs, a lot of efforts have been made about the selective differentiation of iPSC into proprioceptive DRG neurons, including cell-sorting for pure culture (Dionisi, Rai, Chazalon, Schiffmann, & Pandolfo, 2020). This model can be used to study GAA repeats expansion and the phenotype in affected tissues, but also for drug screening. However, the limitation of this type of model is the difficulty to differentiate iPSC into the required cell and the instability of GAA repeats (expansion and contraction) during cell culture propagation (Perdomini et al., 2013).

To overcome differentiation protocols, some cellular models present frataxin reduction based on **RNA interference (RNAi)**, using siRNA or shRNA. In this case, the most affected tissues (heart, DRGs, cerebellum, pancreas) can be isolated from laboratory animals and primary cultures performed. Frataxin reduction is due to the use of siRNA or shRNA targeting mRNA of frataxin. This model is used to study the phenotype in the

most affected tissues and to test drugs. The limitation of these models is the non-human origin; the lack of GAA repeats expansion and the use of vehicle to introduce siRNA or shRNA into the cells such as viruses. Thus, frataxin-deficient cardiomyocytes (Obis et al., 2014) and DRG neurons (Mincheva-Tasheva et al., 2014) are generated by our laboratory as RNAi based cellular models of FA. Frataxin-deficient DRG neurons display Ca^{2+} dyshomeostasis and apoptotic cell death (Mincheva-Tasheva et al., 2014), while frataxin-deficient cardiomyocytes display lipid accumulation and mitochondrial swelling without affecting the activity of Fe-S cluster containing enzymes (Obis et al., 2014). Using the same technique, frataxin-deficient pancreatic β-cells, cortical neurons and astrocytes are also generated. All these models frataxin-deficient β-cells (Igoillo-Esteve et al., 2015), cerebral cortex neurons (Katsu-Jiménez et al., 2016) and astrocytes (Loría & Díaz-Nido, 2015) die for mitochondrial (intrinsic) apoptotic cell death.

All these models are based on a unique cellular type; however, frataxin deficiency interests all the cells of the human body, thus many efforts have been made to study FA in a 3D multicellular system *in vitro*. For this reason, human iPSC have been differentiated into **DRG organoids (DRGO)** to mimic the DRG organ *ex vivo.* This model contains all the subpopulation of DRG neurons and glial cells assembled to mimic the normal tissue and the physiological environment. When FA patient iPSC have been differentiated into FA DRGO, impairment of both survival and axonal spreading over the dish have been noticed, together with decreased number and altered size of mitochondria along axons (Mazzara et al., 2020).

1.6.4 Mice models

Complete deletion of frataxin in a KO mouse model results in embryonic lethality at embryonic day E6.5, while heterozygous $FXN^{+/-}$ mice have no pathologic phenotype, expressing 50% residual frataxin. This result agrees with the fact that the total loss of frataxin is not found in FA patients and no clinical characteristics are noticed in heterozygosis (Cossée et al., 2000).

Taken into account this characteristic, four different **conditional mouse models** have been generated, using the Cre-*loxP* system, in order to study frataxin depletion in a tissue-specific manner: muscle creatine kinase (MCK), neuron-specific enolase (NSE), prion protein (PRP), parvalbumin (Pvalb), insulin (Ins) or albumin models (Alb).

The MCK cardiac-specific model develops cardiac hypertrophy. A phenotype that reproduces clinical observations in the hearts of FA patients, but also biochemical features such as defects in ISCs containing enzymes and hyperacetylation of cardiac proteins. These biochemical characteristics occur early, prior to cardiac dysfunction. The NSE mouse model has been generated to recapitulate neuronal pathology. Interestingly, this model displays frataxin reduction not only in neurons but also in heart and liver, thus, apart from developing cardiomyopathy similar to MCK model; also develop ataxia with loss of proprioception. However, this model shows some limitations such as a severe phenotype that not properly reproduce the disease and the presence of characteristics not observed in FA patients such as spongiform lesions in cortex, probably because frataxin reduction occurs early when neurons are still immature.

To bypass this limitation, it has been generated an inducible conditional mouse model. This PRP mouse model decreases frataxin upon tamoxifen injection. This model induces frataxin deletion only in DRGs, spinal cord and cerebellum, and reproduces most of the neuronal characteristics of the pathology, such as degeneration of large DRG sensory neurons, with consequently loss of proprioception, and degeneration of cerebellum granule cells. In this model, DRG sensory neurons display autophagy processes such as lipofuscin and large vacuoles (Perdomini et al., 2013).

However, prion protein is present in several neuronal types. In order to specifically target proprioceptive neurons, another conditional neuronal mouse model has been developed in which frataxin is deleted in parvalbumin-positive cells, such as proprioceptive DRG sensory neurons, cerebellar deep nuclei and Purkinje neurons, but also interneurons in the brain. This new mouse, named Pvalb conditional model, recapitulates characteristics of the disease such as neuropathy and sensory ataxia with primary involvement of PNS and later cerebellar and cerebral dysfunction, however, displays a more rapid and severe phenotype. In fact, DRG neurons present large vacuoles with cytoplasmic material inside, mitochondrial dysfunction and cell degeneration, characteristics already noticed in other models. However, these mice present a premature death due to epileptic seizures, a phenotype not found in FA patients (Piguet et al., 2018).

As some FA patients shows diabetes, an Ins conditional mouse model has been generated to delete the amount of frataxin selectively in pancreatic β cells. These mice develop diabetes, probably for apoptosis of β-cells, as though for FA patients.

Even though liver is not affected in the disease, an Alb conditional mouse model that delete frataxin selectively in liver has been also generated. This model develops lobules in liver that could be tumours. (Perdomini et al., 2013). Even though these models are important to study the specific involvement of an organ in the disease, they show more severe characteristics due to the fact of complete deletion of frataxin in these organs, while FA patients display only reduction of frataxin level. Thus, mice models with residual frataxin levels should reproduce more properly the pathology.

Different **mice models based on GAA repeats expansion** with residual frataxin have been generated, such as KIKI, KIKO, YG8R and YG22R. KIKI mouse model is generated by introducing a $(GAA)_{230}$ sequence into both alleles of the endogenous frataxin intron 1 sequence ($FXN^{230/230}$), while KIKO mouse model is generated by crossing KIKI mice with frataxin knock-out ($FXN^{+/-}$) mice to obtain compound heterozygous mice ($FXN^{230/-}$). Both mice display a very mild phenotype, probably because the residual frataxin levels are 66-86% and 25-36% respectively for KIKI and KIKO mice, thus, up to the levels found in patients. Other mice models based on GAA repeats expansion are generated by substituting the endogenous mouse frataxin with a transgenic human frataxin produced in yeast artificial chromosome (YAC), producing the YG8 line with two GAA sequence of 90 and 190 repeats and YG22 line with one sequence of 190 repeats. Crossing these mice with heterozygous frataxin knockout mice ($FXN^{+/-}$) allows generating the YG8R and YG22R mice models that express only a single human frataxin transgene in a $FXN^{-/-}$ background. Nevertheless, even decreasing frataxin levels in all tissues, both models show a mild phenotype, probably due to the short GAA expansion. However, the limitation of this model is the difficulty to generate mice with large GAA repeats expansion. These mice can be used for studies on GAA instability, relation of repeat expansion with frataxin expression and therapeutic approach to upregulate frataxin (Perdomini et al., 2013).

Recently, an interesting model based on systemic inducible frataxin downregulation has been generated. These **inducible knock-down mice** (Transgenic FRDAkd), in which a shRNA targets frataxin mRNA upon doxycycline injection, displaying cardiac hypertrophy, neurodegeneration, scoliosis and ataxia, represent the best model to date for temporal studies on frataxin expression. However, it can not be used for GAA repeat expansion studies, as no GAA repeat expansions are present. Looking at DRGs of these

frataxin-deficient transgenic mice, condensed mitochondria, a type of mitochondria that display lower ATP production, has been found (Chandran et al., 2017).

1.7 Therapy

Currently, there is no effective cure for FA and the treatments in use provide the management of symptoms. However, different therapeutic strategies have been studied. Some of these are in Phase 1-2 (or preclinical stage), others in Phase 3 (or clinical trial), but none of them is still available to patients. Friedreich's Ataxia Research Alliance (FARA) groups the therapeutic candidates in large categories, as shown in **Figure 18** (see *http://www.curefa.org/pipeline.html*), such as:

- **Symptomatic;**
- **Improve mitochondrial function and reduce oxidative stress;**
- **Modulation of frataxin controlled metabolic pathways;**
- **Frataxin Replacement. Stabilizes or enhancers;**
- **Increase *FXN* gene expression;**
- **Gene Therapy;**
- **Stem cell therapy.**

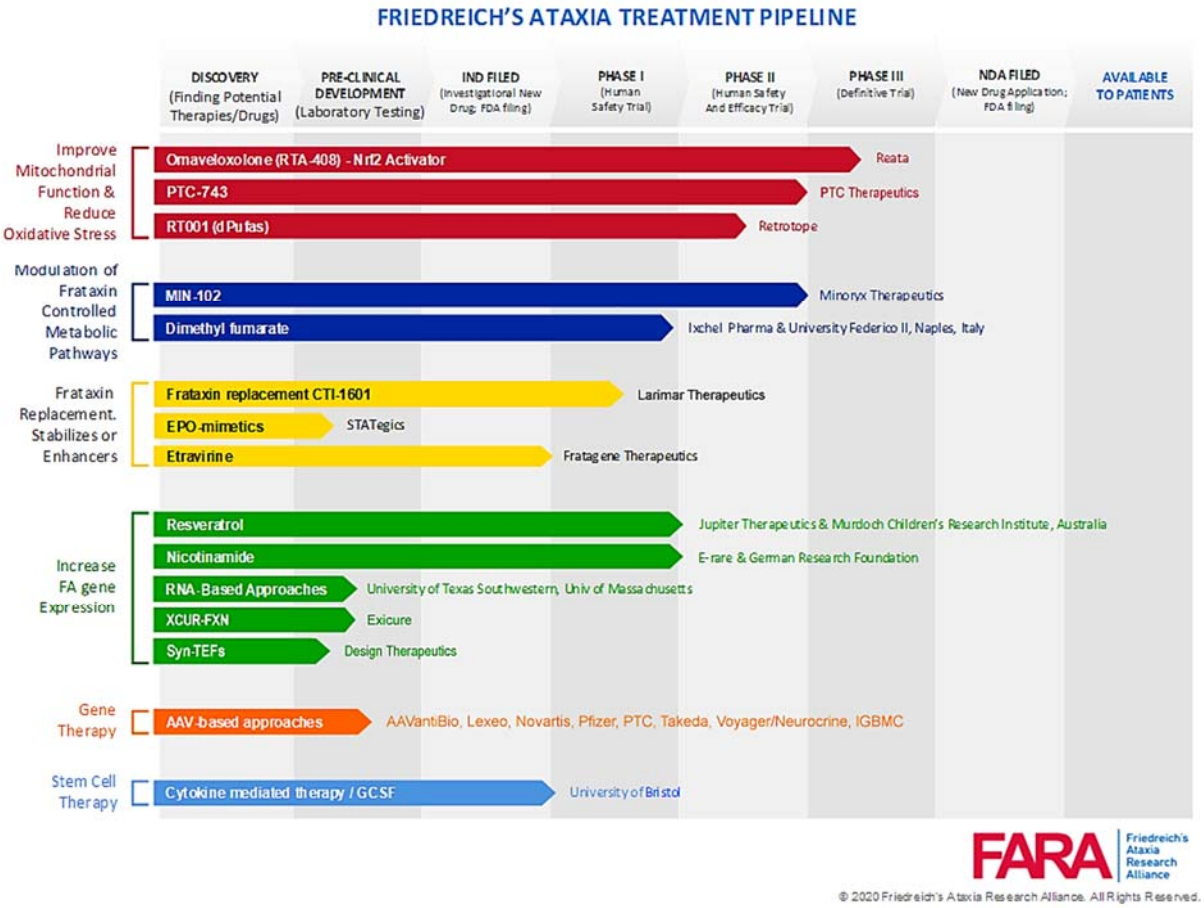

Figure 18. FA treatment pipeline. See text for details. From http://www.curefa.org.

1.7.1 Syntomatic

FA has no an effective cure. Meanwhile, many clinical trials are ongoing; pain symptoms are alleviated by using some painless drugs and palliative care are performed at end of life (Patel et al., 2019).

1.7.2 Improve mitochondrial function and reduce oxidative stress

Some of the FA characteristics are mitochondrial dysfunction and oxidative stress. For these reasons, anti-oxidant treatments have been studied. Some examples of drugs are:

Omaveloxolone (RTA-408): a synthetic drug created from Reata, which functions as an activator of NRF2 transcriptional factor, a pathway altered in FA cells. A randomised, placebo-controlled, double-blind study of 100 patients treated with 150mg/day of Omaveloxolone demonstrated an improvement in neurological rating scales used to establish the disease progression. This drug is currently in Phase III trial. http://www.curefa.org.

Coenzyme Q_{10} (CoQ_{10}): is an anti-oxidant molecule important in oxidative phosphorylation because transfer electrons from complex I and II into complex III. A clinical trial using CoQ_{10} showed beneficial effects when used in early stages of the disease (Cooper & Schapira, 2003).

Idebenone [2,3-dimethoxy-5-methyl-6-(10-hydroxydecyl)-1,4-benzoquinone]: a membrane-permeable anti-oxidant, analogue of CoQ_{10}. Idebenone decreased the cardiac hypertrophy in patients (Hausse et al., 2002); however, several studies show only a modest cardiac and neurological improvement. This drug is current used in clinical trials for other diseases. http://www.curefa.org.

Vitamin E (α-tocopherol): a lipid soluble anti-oxidant, present in mitochondrial membranes, obtained from diet (e.g. vegetable oils and nuts). Its deficiency induces AVED, a genetic ataxia linked to a mutation in the Vitamin E transferring protein. AVED shows similar symptoms to FA (Ouahchi et al., 1995). Vitamin E has been only used in clinical trials combined with CoQ or Idebenone for FA, showing modest beneficial effects (Cooper & Schapira, 2003).

EPI-A0001 (α-tocopheryl quinone): a potent anti-oxidant with similar structure to CoQ and idebenone, but major bioavailability. This anti-oxidant determined a dose-dependent improvement of neurological functions in a double-blind, randomised, placebo-controlled trial of 2 doses of EPI-A0001 (Lynch et al., 2012).

PTC-743 (EPI-743): an analogue of EPI-A0001 current in Phase II/Phase III trial. http://www.curefa.org. A 24-months randomised, placebo-controlled, double-blind trial of EPI-743 treated FA patients determined a significant improvement of neurological functions and disease progression (Zesiewicz et al., 2018).

Vitamin B1 (thiamine): an essential cofactor for some metabolic enzymes (e.g. PDH). This drug induces neurological, cardiac and motor improvements in clinical trials (Costantini et al., 2016).

Despite the presence of several clinical trials based on anti-oxidants, none of these shows clear and satisfactory results. Currently, only EPI-743 and Omaveloxolone are present in the annually updated FA treatments pipeline of FARA. http://www.curefa.org.

1.7.3 Modulation of frataxin controlled metabolic pathways

Although the function of frataxin is not known, some of the metabolic pathways that could occur in its deficiency have been discovered. Some examples of drugs targeting the modulation of these pathways are:

Leriglitazone (MIN-102): a synthetic compound generated by Minoryx Therapeutics, analogue of pioglitazone. As pioglitazone, leriglitazone is an activator of peroxisome proliferator-activated receptor-gamma (PPARγ) transcription factor, but can cross BBB better than its analogue. PPARγ coactivator 1 alpha (PGC-1α) pathway is considered altered in FA, leading to alterations in mitochondrial function and biogenesis, fatty acid storage and energy metabolism. Preclinical *in vitro* studies indicated that, in FA patients' fibroblasts, leriglitazone induces an increase in frataxin protein levels, together with other beneficial effects such as prevention of lipid droplet accumulation in frataxin-deficient cardiomyocytes. *In vivo*, leriglitazone treatment improved the motor function in YG8sR FA mice model (Rodríguez-Pascau et al., 2020). These results have encouraged clinical trial, in fact, leriglitazone is currently tested for a randomised, double-blind, placebo-controlled study evaluating the effects of leriglitazone on 32 FA patients in 4 European states (Phase II/III). http://www.curefa.org.

Dimethyl fumarate (DMF): a methyl ester of fumaric acid. The exact mechanism of action of DMF is unknown; however, this drug has been shown to modulate the Nuclear factor (erythroid-derived 2)-like 2 (NRF2) pathway, leading to NRF2-dependent mitochondrial biogenesis *in vivo* and *in vitro* (Hayashi et al., 2017). Recently, it has been demonstrated that DMF significantly increases *FXN* gene expression *in vivo* and *in vitro*, increasing the transcription initiation, leading to reduction of R-loop formation at the intronic GAA repeats sites in *FXN* gene (Jasoliya et al., 2019). This drug is currently in Phase I clinical trial. http://www.curefa.org.

Deferiprone (DFR): an iron-chelator for cytosolic and mitochondrial iron. However, its use should be considered with moderation as an excessive concentration or exposition could induce anemia (Marmolino & Acquaviva, 2009).

1.7.4 Frataxin replacement, stabilizes or enhancers

As FA is a disease of frataxin deficiency, many efforts have been done to deliver exogenous frataxin in cellular and animal models or stabilize/enhance endogenous levels. For example:

Frataxin Replacement: Despite the replacement approach seems to be the easiest, it is not at all. One of such replacement approaches involves the use of a TAT-FXN fusion protein, which presents the Trans Activator of Transcription (TAT) protein transduction domain (GRKKRRQRRRPQ) fused to the human frataxin protein. In a conditional frataxin-deficient mouse model, **TAT-FXN (CTI-1601)** can deliver exogenous frataxin into the mitochondria, increase body weight, improve cardiac functions and, consequently, extend the mean life span of 53% (Vyas et al., 2012). Actually, this study is in Phase I clinical trial for FA. http://www.curefa.org. Despite such promising data in the animal model, TAT domain allows frataxin entering into the mitochondria but also extruding from them. For this reason, Bioblast Pharma has proposed a new construct named **TAT-MTScs-FXN**, in which a MTS from citrate synthase is fused to the previous construct. The MTS domain improves the mitochondrial delivery of frataxin (Marcus et al., 2016).

Frataxin stabilizes or enhancers: A drug screening searching compounds able to increase FXN protein demonstrated that the **Erythropoietin (EPO)** significantly increases its levels. Different concentrations of **recombinant human erythropoietin (rhuEPO)** have been used to treat frataxin-deficient cells and lymphocytes, fibroblasts and myocytes from patients, showing that this compound increased FXN protein in all the cell lines studied (Sturm et al., 2005). However, they are not categorised in compounds able to increase frataxin expression because another study indicates that rhuEPO increases FXN without mRNA induction (Acquaviva et al., 2008).

1.7.5 Increase FXN gene expression

As FA is due to decreased levels of frataxin protein, many efforts have been done in order to increase gene expression. Some examples of drugs are:

Resveratrol: a compound naturally found in red grapes skins that is able to increase frataxin protein levels. A clinical trial has been started using this drug, showing

improvement in speech performance and neurological rating scales. However, side effects have been observed using this drug. http://www.curefa.org.

Histone deacetylase (HDACs) inhibitors: compounds used in order to inhibits HDACs, the enzymes responsible of deacetylation of histones. As *FXN* locus in FA shows hypoacetylation of histones and gene repression, HDACs inhibitors can improve *FXN* gene expression. Different HDACs inhibitors have been used *in vivo* and *in vitro* with a modest increase of frataxin protein levels (Marmolino & Acquaviva, 2009).

Nicotinamide (Vitamin B3): Vitamin B3 is a class III HDAC inhibitor able to upregulate *FXN* gene expression, reducing the heterochromatin modification at *FXN* locus, such as deacetylation of histone H3 (Libri et al., 2014). A clinical trial has been started using different concentrations of this drug. http://www.curefa.org.

RNA-based approaches (Antisense Oligonucleotides –ASOs): single strands of DNA or RNA that are complementary to a chosen sequence designed to increase specific gene expression. Nowadays, only preclinical *in vitro* studies have been performed, showing a ~2 fold-increase in FXN mRNA and protein levels (Shen et al., 2020).

1.7.6 Stem cell and gene therapy

An approach that has been considered to treat FA is the gene therapy. In fact, **Adeno-Associated Virus (AAV) carrying human FXN** has been administrated in MCK, NSE and Pvalb FA mouse models, showing improvement of cardiac and neurological functions (Gérard et al., 2014; Piguet et al., 2018). Another interesting approach is stem cell therapy to treat FA. The hypothesis is the use of genetic manipulated bone-marrow-derived mesenchymal stem cell (MSC) for autologous transplantation. MSCs obtained from FA patients can be genetically manipulated in order to remove GAA repeats expansion (e.g. CRISPR/Cas9 editing) or express neuroprotective factors (e.g. BDNF, GDNF) or express anti-inflammatory cytokines. These adult multipotent stem cells can differentiate into cardiac and neurological cells; thus, they are promising cells for replacement cell therapy in the case of GAA expansion editing and for re-stabling the correct environment for neurogenesis/neuroprotection or anti-inflammatory stimuli (Sadan, Melamed, & Offen, 2009; Tajiri et al., 2014).

2 DORSAL ROOT GANGLION

Humans interact with the environment and need to recognize and react to internal and external sensorial stimuli. These stimuli can be transported into spinal cord through afferent sensory dorsal axons (dorsal root) and propagated through motor ventral efferent axons (ventral root); both roots are component of spinal nerves. Dorsal root ganglion (DRG), presents at the distal end of the dorsal root, is the complex structure in charge of this function. Humans present 31 pairs of dorsal root ganglia, with a size depending on the vertebral level: Cervical DRGs are smaller than the others, increasing the size from C1 to C8 level; Thoracic DRGs (T1-T12) are similar; Lumbar DRGs increase from L1 to L5, and sacral DRGs decrease from S1 to S4, being S1 a very large ganglion. No age-correlated differences in the size of DRGs have been demonstrated, while individuals-correlated differences can be due to the fact that DRG size correlates with the number of neurons present within (Haberberger, Barry, Dominguez, & Matusica, 2019).

Each DRG is an ovoid and elongated, rather than round, structure encased by meninges including a layer of dura mater and contain cell bodies of sensory neurons which convey information from external or internal sites of the body such as actual or potential harm, temperature, touch, organ volume or muscle length to the central nervous system (Haberberger et al., 2019). Apart from sensory neurons, they contain a specific form of glia, named satellite glial cells (SGCs) that form an envelope around neuronal cell bodies and communicate with DRG sensory neurons. The surface of neuronal cell bodies extends forming structures named microvilli, in close relationship with the surrounding satellite cells (Haberberger et al., 2019). Neurons and the envelope of satellite cells form a unit, which is delimited by connective tissue, named perineurium. Moreover, DRG contains small blood vessels (endothelial and smooth muscle cells) to deliver energy and oxygen to the neurons in a unique manner. Since the blood DRG barrier is more permeable than a blood-brain barrier (BBB), it is known as BDB. In fact, this barrier, unique in neuronal system, allows more contacts between blood and DRG neurons/satellite cells (Reinhold & Rittner, 2020). This characteristic makes DRG neurons highly vulnerable to neurotoxic substances. In fact, capillaries in DRG are fenestrated, which means that many blood molecules can directly enter the DRG and interact with neuronal and non-neuronal cells. Non-neuronal cells are mainly

macrophages, T-lymphocytes and B-lymphocytes, which seem to be present in the absence of a pathological process (Haberberger et al., 2019).

2.1 Dorsal root ganglion sensory neurons

2.1.1 Structure and function

DRG neurons have a pseudo-unipolar morphology, a single axon that bifurcates into central and peripheral branch. Structurally, a DRG neuron is determinate by different parts: a cell body; a stem axon, which connects cell body to the axon; a single axon that bifurcates into a peripheral branch, which innervates peripheral tissue, and another central branch, which enters in the CNS to synapse with secondary neurons, as indicated in **Figure 19**.

C**ell body** of DRG neurons is typically circular to oval and of variable soma size diameter. The cell bodies of DRG neurons are completely wrapped by sheaths that may have one or several layers of SGCs.

S**tem axon** connects cell body to the two axons and can be myelinated or not, depending on the DRG neuron type. It seems important to differentiate this axon in two parts: Proximal and Distal. The proximal region is always unmyelinated, coated by a multilayer of SGCs in continuous with SGCs from cell body, and rich in mitochondria, ribosomes, microtubules and ER, while the distal part can be myelinated presenting Schwann cells. The length of the stem axon is variable, but the diameter is generally large. Long stem axons could be important to isolate large cell body and reduce the risk of spike propagation failure from peripheral to central axon. In this process, it could be important a triangular area at the level of bifurcation between stem axon and central and peripheral axons containing clusters of mitochondria (Nascimento, Mar, & Sousa, 2018). This area, where stem axon bifurcates into two axons, is generally named T-junction (Van Buyten, 2018).

DRG neurons axon can be myelinated or not, depending on the type of neuron and present differences between the central and the peripheral part. For example, the central axon in unmyelinated DRG neurons presents a smaller diameter than the peripheral axon and higher phosphorylation of neurofilaments. Generally, an axon with large diameter, both myelinated and unmyelinated, increases the nerve conduction velocity and presents higher amount of neurofilaments, but not phosphorylated, while small diameter axons present phosphorylated neurofilaments and delayed conduction. For

these reasons, peripheral axon conduction is faster than central. The differences between peripheral-central axons are so clear that DRG neurons have been considered as cell presenting central-peripheral polarity: the peripheral axon functions as dendrite-like, since the action potential is generated at its peripheral terminal and then propagates towards the bifurcation of the stem process, while the central axon is axon-like, since it conducts the signal from the bifurcation to the CNS. The central-peripheral polarity raises many questions about how the cells discriminate the selective transport of proteins and organelles in one branch or the other (Nascimento et al., 2018). In contrast, apart from differences, also similarities have been described for the two parts of the axon. For example, smooth ER-like structures have been shown in central and peripheral axons, with long ER tubule running parallel to the axon (Nascimento et al., 2018).

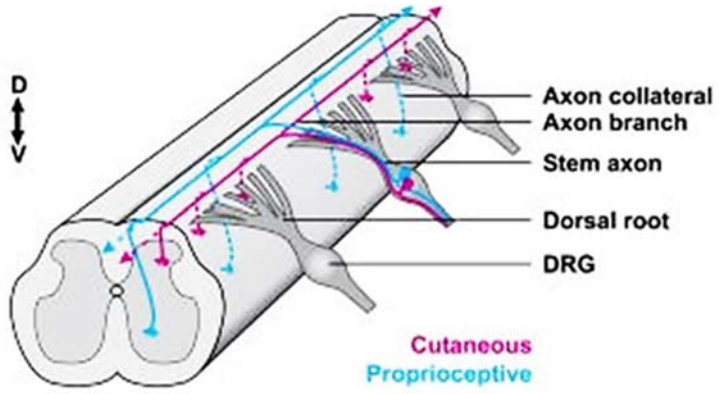

Figure 19. Disposition of DRG sensory neurons in dorsal roots of spinal cord. See text for details. From (Schmidt et al., 2007).

2.1.2 Embrionic development of DRG neurons

During embryonic development, the DRG neurons, which differentiate from neuronal crest, go through several morphological states, in this chronological order: spindle-shaped bipolar, eccentric bulged bipolar, bell-shaped bipolar or pseudo-unipolar, short-stem pseudo-unipolar and long-stem pseudo-unipolar. The analysis of thoracic rats DRGs reveals that the percentage of these morphological states changes during embryonic stages. This process, is schematized in **Figure 20** (Nascimento et al., 2018).

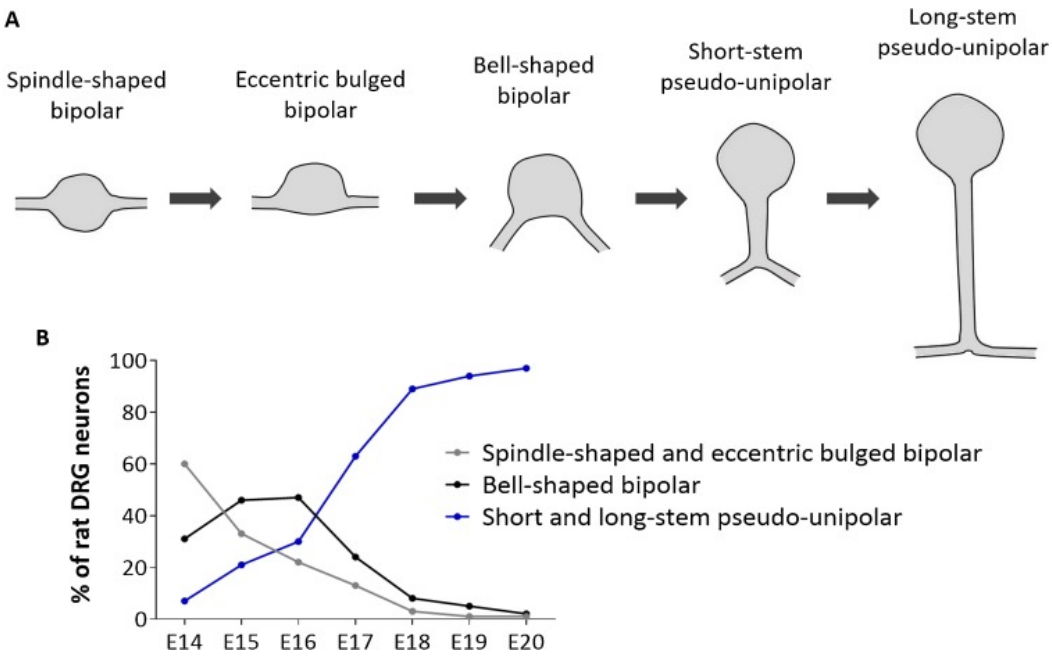

Figure 20. Embryonic development of DRG neurons. In A, morphological states of DRG neurons pseudo-unipolarization. In B, percentage of these morphological states during embryonic development of rats DRG neurons. See text for details. From (Nascimento et al., 2018).

2.1.3 DRG neuron axon regeneration

The fact that a unique cell body can generate and handle two different axons, with different proteins and functions, make DRG neurons intriguing cells. Even more impressive is the fact that the central and peripheral axons present differences in their ability to regenerate. After a nerve injury, a faster rate of regeneration has been demonstrated for peripheral axon than central axon, while if the injury interests the dorsal column of spinal cord or the dorsal root entry zone, the DRG central axon is not able to regenerate. Probably, the presence of Schwann cells in the peripheral axon contributes to regenerate. Also, a peripheral DRG neuron axon lesion could trigger the activation of injury signals, such as extracellular-signal-regulated kinase (ERK), c-Jun N-terminal kinase (JNK), signal transducer and activator of transcription 3 (STAT-3). These injury signals are transported, in retrograde manner, from the lesion site to the cell body, together with a back-propagating Ca^{2+} wave and an axonal transport of mitochondria, lysosomes and synaptic vesicles, leading to a transcriptional switch and the up-regulation of regeneration-associated genes (Nascimento et al., 2018).

2.2 DRG neurons subpopulations

The cell body of DRG contains different subpopulations of neurons that can be classified considering the function, the size and the diameter of axons.

The **classification considering the function** (each subpopulation responsible for a sensorial transmission) differentiates DRG neurons in proprioceptors, mechanoreceptors and nociceptors, which respectively allow position, movement and vibration senses; touch sensation and noxious stimulus, including mechanical, chemical, and thermal noxious stimuli (Berta, Qadri, Tan, & Ji, 2017).

The **classification considering the neurotrophic receptors** differentiates DRG neurons in tyrosine kinase receptors (Trk), which are activated by different neurotrophins (NGF, BDNF, NT-3/4) and controls the signalling of different transcription factors. As indicated in **Figure 21**, these receptors are:

- **TrkA** for noxious stimuli, thus nociceptors, including mechanical, chemical, and thermal noxious stimuli. This receptor is activated by NGF neurotrophin;
- **TrkB** for mechanical stimuli, thus mechanoreceptors. This receptor is activated by BDNF and NT-4;
- **TrkC** for proprioceptive stimuli and mechanical stimuli, thus proprioceptors and mechanoreceptors. This receptor is activated by NT-3 (Marmigère & Carroll, 2014).

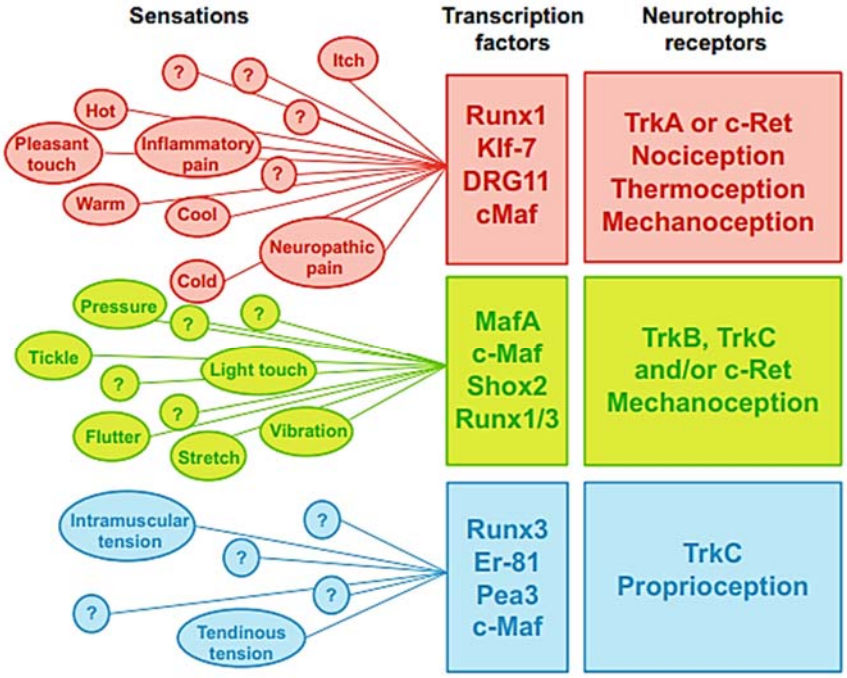

Figure 21. Sensorial stimuli and neurotrophic receptors in adult DRG neurons. See text for details. Modified from (Marmigère & Carroll, 2014).

The **classification considering the size** differentiates DRG neurons considering the size of their cell body. The soma size depends on the species analysed, the developmental stage, the use of neurotrophins, the days of culture maintaining and the operator's hand. Usually neonatal rats DRG neurons are categorised in <15µm (or <17µm) for small-diameter neurons, a range between 15-25µm (or 17-25µm) for medium-diameter and >25µm for large-diameter. The majority of neurons are intermediate-diameter (66.7%), while large and small-diameter neurons are respectively 14% and 19.3% in neonatal (P0-3) rat DRG primary cultures of lumbar and sacral zone at 0-2 days of culture (Bowie, Feltz, & Schlichter, 1994). Generally, proprioceptors neurons present a larger cell body, whereas nociceptors the smaller, as schematised in **Figure 22** (Berta et al., 2017).

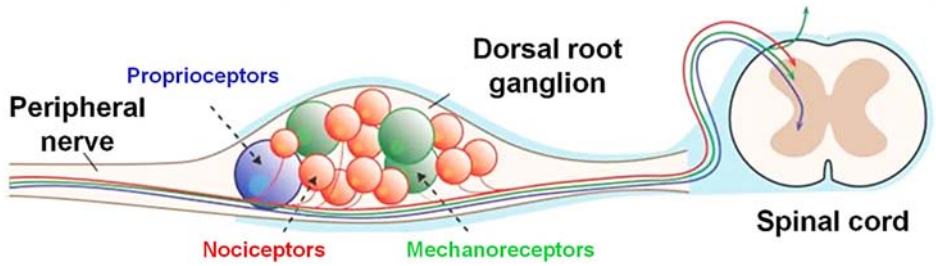

Figure 22. DRG neurons subpopulations classified considering function and size. Schematic figure of proprioceptors, nociceptors and mechanoreceptors sensory neurons in a dorsal root ganglion. Note the difference in size: proprioceptors > mechanoreceptors > nociceptors. Modified from (Berta et al., 2017).

The **classification considering the diameter of the axon** is an indication of the velocity of conduction as large-diameter axons are fast conducting. Generally, DRG neurons with large-medium cell bodies as proprioceptors and mechanoreceptors are low threshold, fast-conducting, and possess large-diameter myelinated Aα and Aβ fibers. In contrast, those with small cell bodies have either thinly myelinated medium-velocity Aδ fibers or unmyelinated slow-conducting C-fibers, with a high threshold for activation and smallest diameter (Berta et al., 2017).

Immunostaining for molecular markers may be performed to label specific subpopulations of DRG neurons and experiments should differentiate between subpopulations, when possible, as each of these subpopulations shows different characteristics (Nascimento et al., 2018). However, some of these characteristics are dynamic during development, such as the expression of Trk receptors, thus, complicating the categorization (Marmigère & Carroll, 2014).

❖ Nociceptors

Nociceptors are characterised by the expression of the neurofilament Peripherin (Prph), voltage-gated Na^+ channels (Nav), particularly Nav1.8 and Nav1.9, Ca^{2+} (Cav) channels, as well as transient receptor potential cation (TRP) channels, such as Transient receptor potential cation channel subfamily V member 1 (TRPV1) and Transient receptor potential cation channel ankyrin 1 (TRPA1) (Berta et al., 2017; Haberberger et al., 2019). Na_V channels are important to trigger an action potential, together with Ca^{2+}-activated potassium channels (K_{Ca}), while the channel important in the nociceptive stimulus, triggering action potential discharge and Ca^{2+} wave, is TRPV1, a channel protein that is activated by the vanilloid capsaicin, an ingredient of hot chilli peppers, by low pH and noxious heat. TRPV1 is not present only in nociceptors but also in mechanoreceptors and proprioceptors, and generally is present together with the TRPA1, a channel for irritant stimulus (Haberberger et al., 2019). These small-size neurons respond to capsaicin stimulation, a compound that induces cellular and $Ca^{2+}{}_m$ uptake, without the ER involvement (Wood et al., 1988). Nociceptors DRG neurons, as thermal, present small unmyelinated afferents and require NGF and the TrkA for proper functionality (Marmigère & Carroll, 2014).

❖ Mechanoreceptors

Low threshold mechanical stimuli such as light touch activate mechanoreceptors that specifically expressed neurofilament high (Nfh) and toll-like receptor 5 (Tlr5) (Berta et al., 2017). Na_V channels are present in lower levels than nociceptors, together with K_{Ca}, to trigger action potential (Haberberger et al., 2019). Mechanoreceptors DRG neurons present large myelinated afferents and require BDNF/NT-4 and the tyrosine kinase receptor TrkB, but also TrkC, for proper functionality (Marmigère & Carroll, 2014).

❖ Proprioceptors

Another type of DRG neuron is the proprioceptor that senses movement or vibration and it is generally characterised by the expression of the Ca^{2+}-binding protein parvalbumin (Pvalb) (Berta et al., 2017). In this particular sensory neuron, Na_V channels are present at lower level, together with K_{Ca}, to trigger action potential (Haberberger et al., 2019). Proprioceptive DRG neurons present large myelinated afferents and the survival of these neurons is mediated by Neurotrophin-3 (NT-3) and its high-affinity receptor TrkC (Zhou, Cameron, & Rush, 1998).

2.3 Action potential in DRG neurons

In DRG neurons, a sensorial stimulus activates transduction receptors that depolarize the peripheral terminal and convert the stimulus into an action potential discharge by activating voltage-gated Na^+ channels. The action potential (a Na^+ depolarisation followed by potassium repolarisation) is usually generated in a particular part of the axon named AIS (axon initial segment-like structure), enriched in voltage-gated Na^+ channels. However, in DRG neurons AIS is present in the stem axon and the action potential is generated in the peripheral axons. (Nascimento et al., 2018). Then, the action potential triggers $Ca^{2+}{}_i$ influx at the central terminal releasing glutamate or other signalling molecules, carrying the somatosensory information to the spinal cord. This action potential generates different types of currents, depending on the role of the T-junction (bifurcation). In fact, T-junction, as shown in **Figure 23**, can act as:

- a **barrier**, which impedes the action potential propagation to dorsal root;
- a **low-pass filter**, which reduces the action potential propagation;
- a **propagator of action potential**, with DRG participating in the process of current transport into dorsal horn (Van Buyten, 2018).

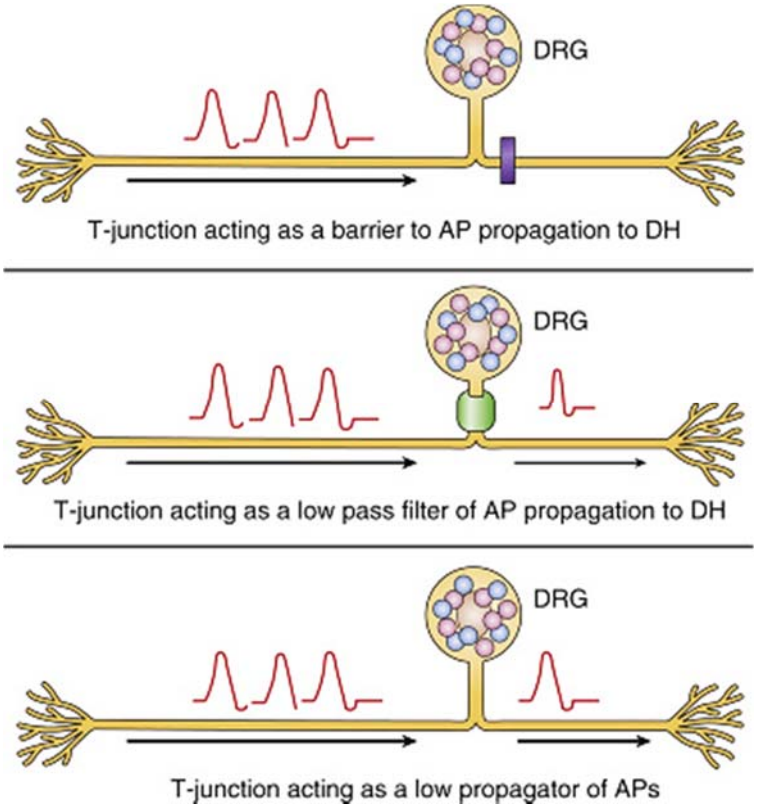

Figure 23. Role of T-junction in the propagation of action potential to dorsal horn. Action potential (AP) and dorsal horn (DH). See text for details. From (Van Buyten, 2018).

In some pathological conditions, such as a nerve injury, the AIS in the axon stem became sufficiently hyperexcitable to generate ectopic action potential, which can be propagated into dorsal horn. Each subpopulation of DRG neurons presents peculiar and characteristic channels and receptors, which allow specific action potential and conduction (Nascimento et al., 2018).

2.4 Glial cells structure and communication

2.4.1 Satellite and schwann cells

DRGs present a large amount of glial cells, such as **satellite glial cells**. Morphologically, satellite glial cells (SGCs) have an irregular shape and are not similar to any other glial cells present in the CNS (Nascimento et al., 2018). These cells are able to envelop the DRGs and modify the microenvironment of neurons, releasing and uptaking molecules and participating in immune-process (Haberberger et al., 2019). For example, DRG neurons can release ATP, TNFα and glutamate during stimulation. Such neurotransmitters can activate satellite cells. Interestingly, glutamate, released by glutamatergic DRG neurons, can be taken up by SGCs in order to be transformed into L-glutamine by glutamine synthetase. Then, glutamine can be taken up by neurons to be transformed into glutamate by glutaminase and packaged into vesicles to be released as neurotransmitter, as shown in **Figure 24**. Due to this important role of glial cells, changes in DRGs-SGCs communication are present in several pathological conditions (Miller, Hoffman, Sutharshan, & Schechter, 2011).

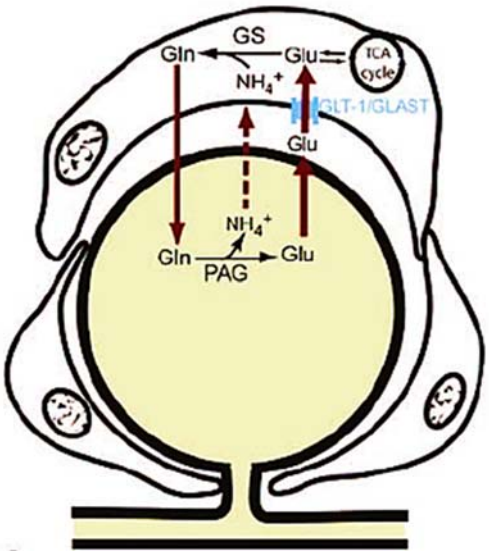

Figure 24. Schematic model of glutamate-glutamine cycle between DRG neurons and SGCs. See text for details. From (Ohara et al., 2009).

DRG neurons present also another type of glial cells named **Schwann cells**. These cells envelop DRG neurons at the distal part of the stem axon and in both (peripheral and central) axons and are responsible for myelin formation (Nascimento et al., 2018). These cells, as SGCs, are also interested in the conversion of glutamate into glutamine or glutamate-glutamine cycle (Miller et al., 2011).

2.5 Sensory neuropathy

In physiological situation, the action potential starts from peripheral axon; in pathological situations, could be generated from cell body and/or others parts of the axon (ectopic action potential) and DRG neurons became spontaneously active or hyperexcitable. This characteristic is an hallmark of neuropathic pain (Nascimento et al., 2018). In this situation, the layer of SGCs became multilayer and there is abnormal secretion of cytokines from macrophages, T-cells, glial cells and Schwann cells. These cells release inflammatory mediators, which sensitize and lower the threshold for action potential. This event involves changes in gene expression such as reduction in voltage-gated K^+ channel subunit expression in DRG neurons, but also changes in ion channels and currents, which involve Na^+ channels. Furthermore, inflammation changes the density of voltage-activated Ca^{2+} channels in different DRG subpopulations, thus, involving Ca^{2+} currents (Krames, 2015).

Sensory neuropathy occurs in several diseases. In FA, sensory neuropathy is associated with degeneration of large (proprioceptive), intermediate (mechanoreceptors) sensory neurons and Meissner's corpuscles, a neuronal corpuscle present in skin (hands and feet) and involved in light touch. These alterations induce an increased threshold for touch, vibration and cooling sensation, indicating a decrease in these sensorial characteristics and conduction velocity in sensorial nerves (Creigh et al., 2019).

2.6 DRG sensory neurons primary culture

To study, at cellular and molecular levels, physiological and pathological mechanisms occurring in DRG sensory neurons, it is important to use primary cell culture systems of embryonic and/or adult animals. However, the morphology of these cells cultured *in vitro*, do not recapitulate perfectly the *in vivo* organisation. Apart from that, DRG neurons monocultures in presence or not of Schwann cells and/or satellite cells can present different morphologies. For example, DRG neurons from newborn rats are bipolar in purified cultures, but are pseudo-unipolar when co-cultured with Schwann

and/or glial cells and NGF supplemented medium promotes the formation of somatodendritic microtubule-associated protein 2 (MAP2)-positive neurites, but NGF supplemented medium in the presence of SGCc does not allow the presence of MAP2 marker.

Apart from the morphology, it should be taken into account the heterogeneity of DRG neurons *in vivo*. Dorsal root ganglia contain different subtypes (or subpopulations) of neurons in a complex organisation. Culture conditions can bias the results by pushing the presence of a specific DRG neuron subpopulation. For example, in the presence of NGF, DRG neurons present a peptidergic phenotype typical of a specific subtype, while this process does not occur in NGF absence; moreover, the presence of neurotrophic factors such as NT-3 it is important for survival of proprioceptors. However, most DRG neurons cultures are performed in NGF supplemented medium alone, under-representing some DRG neurons subpopulations. Although the use of NGF alone allows us to better compare most of the studies carried out as *in vitro* cultures of DRG neurons and the neurochemical phenotype must always be considered when interpreting the data (Nascimento et al., 2018). Another limitation of DRG neuronal culture is the fact that the yield is generally low, limiting analysis. DRGs explants avoid this problem and the problem of morphology in culture since they contain, as *in vivo*, spindle-shaped bipolar DRG neurons, presenting central-peripheral asymmetry. However, the explants are not easy cultured and analysed (Nascimento et al., 2018).

3 CALCIUM AND DORSAL ROOT GANGLION

Calcium (Ca^{2+}) acts as a second messenger or signalling molecule within neurons to regulate different physiological processes: neurotransmitter release, excitability changes, enzyme activity and gene expression (Berridge, Lipp, & Bootman, 2000). Its concentration is deeply regulated by cells in order to maintain extracellular and cellular levels in millimolar (~1-2 mM) and nanomolar concentrations (~100nM), respectively. Organelles, such as mitochondria and endoplasmic reticulum (ER), compartmentalise and store Ca^{2+}, maintaining it at micromolar range (~250-600µM), and buffers it. Communication between extracellular space, cytosol, ER and mitochondria, through Ca^{2+}, is crucial for cells. For this reason, the intracellular Ca^{2+} concentration $[Ca^{2+}]_i$ is regulated by numerous mechanisms, such as influx pathways (ion channels); efflux

pathways (pumps and exchangers); uptake and release from intracellular stores (mitochondria and ER) and buffering mediated by Ca^{2+}-binding proteins (Patergnani et al., 2011).

3.1 Cytosolic calcium

Cytosolic Ca^{2+} concentration $[Ca^{2+}]_c$ depends on mechanisms of Ca^{2+} influx, mobilisation from intracellular stores such as ER and mitochondria and finally Ca^{2+} efflux to restore resting state (Patergnani et al., 2011). These mechanisms are controlled in order to maintain a low basal $[Ca^{2+}]_c$ (~100nM). Intracellular Ca^{2+} signals are generated by a stimulus that mobilises Ca^{2+} from extracellular space or ER/SR into cytosol. Once numerous Ca^{2+} -dependent processes are triggered, exchangers and pumps restore the resting state removing the excess of Ca^{2+} (Patergnani et al., 2011).

3.1.1 Cytosolic calcium influx

The Ca^{2+} channels in the plasma membrane responsible for Ca^{2+} influx into the cells are activated in different ways. For example, membrane depolarisation activates voltage-operated channels (VOCs), ligands activates receptor-operated channels (ROCs), second-messenger operated Ca^{2+}-permeable ion channels (SMOCs), transient receptor potential channels (TRP) and Ca^{2+} coming from intracellular stores activates store-operated channels (SOCs) or Ca^{2+}-release activated channels (CRACs), as indicated in **Figure 25**.

VOCs are Ca^{2+}-selective pores, activated and opened in milliseconds during action potential and found in neurons, muscle cells and endocrine cells. These channels are often involved in vesicles release and muscle contraction. The most common VOCs are the channels of the Ca_v1 family (Penner, Fasolato, & Hoth, 1993).

ROCs are channels activated by a ligand such as acetylcholine, glutamate, serotonin in excitatory cells and ATP and histamine in non-excitatory cells, caming from extracellular environment. The most common ROCs are glutamate receptor (GluR), NMDA, AMPA (Penner et al., 1993).

SMOCs are channels similar to ROCs, however, they are activated by second messengers, e.g. G-protein, coming from inside the cell (Penner et al., 1993).

SOCs/CRACs are activated by Ca^{2+} coming from intracellular stores, such as ER. These channels are present in non-excitable cells. The most common SOCs are STIM1/Ora1 channels. STIM1 in the ER has a sensor for ER Ca^{2+}, this channel interacts with Ora1 in the plasma membrane and allows the entry of Ca^{2+} from extracellular space into ER (Penner et al., 1993).

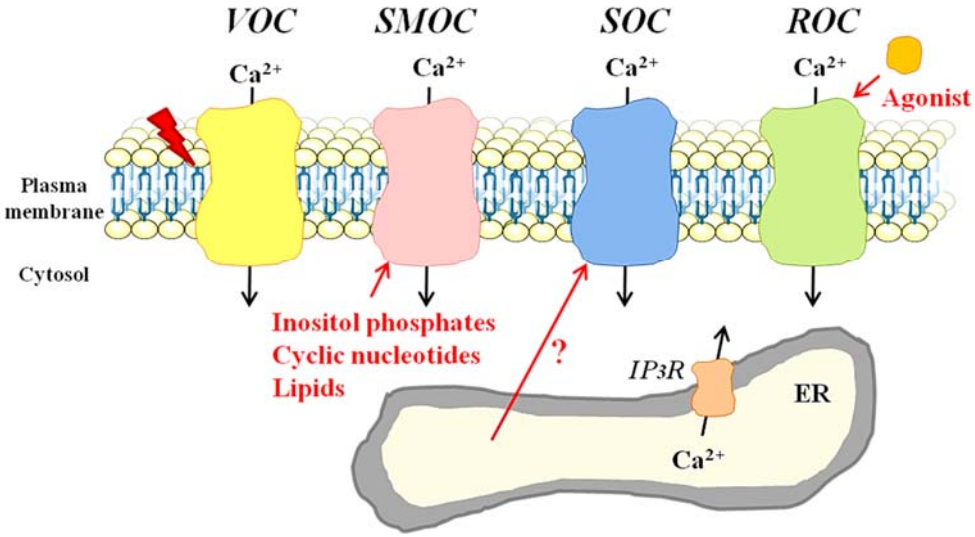

Figure 25. Channels for Ca^{2+} influx. See text for details. Based on (Penner et al., 1993).

TRPs are a particular family of channels that respond to external and internal stimuli, such as noxious stimuli, heat, pH, contact, light, growth factor, PIP_2 etc. There are different TRPs named TRPV, TRPM, TRPC, TRPA, with structural and functional differences etc. TRPVs are the most present channels in DRG neurons and respond to heat, inflammatory and noxious stimuli, but also capsaicin, as indicated in **Figure 26**, while TRPAs are mostly present in mechanoreceptors subpopulation. TRPMs are involved in control of insulin secretion in pancreatic β-cells and are regulated by Ca^{2+}, PIP_2 and voltage (Minke, 2006).

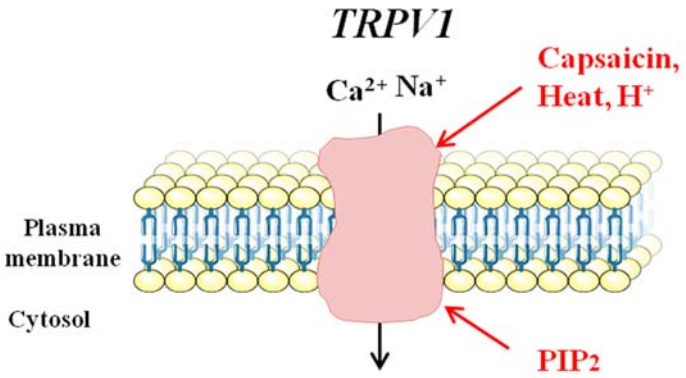

Figure 26. TRPVs mediates Ca^{2+} influx in DRG neurons. See text for details. Based on (Minke, 2006).

3.1.2 Cytosolic calcium efflux

Different channels present at the plasma membrane, such as Na^+/Ca^{2+} exchanger (NCX) and plasma membrane Ca^{2+} ATPase (PMCA), mediate cytosolic Ca^{2+} efflux, as shown in **Figure 27** (Brini & Carafoli, 2011).

PMCA, hydrolysing ATP, removes Ca^{2+} from cytosol into extracellular space. The pump operates with 1:1 Ca^{2+}/ATP stoichiometry. Some isoforms are present in brain (Brini & Carafoli, 2011).

NCX, mainly present in excitable tissues, e.g. heart and brain, determines the efflux of 1 Ca^{2+} for influx of 3 Na^+. This exchanger, with 9 transmembrane segments (TM) and a large intracellular loop containing 2 Ca^{2+}-binding domains (CBD1/2), has low affinity for Ca^{2+} and high capacity. In the case of lower concentration of Na^+ outside, this channel has the ability of changing its direction, transporting Ca^{2+} into the cells. There are 3 isoforms of NCX, NCX1 is present in all tissues but seems important in heart, NCX2 in brain and NCX3 in skeletal muscle (Patergnani et al., 2011). Despite NCX2 seems to be the neuronal isoform of NCX, NCX3 is highly expressed in cerebellum and PNS. In fact, NCX2-KO mice develop memory loss, while NCX3-KO mice reduces motor activity. NCX exchanger is regulated by Ca^{2+} and Na^+ gradient, but also ATP, PIP_2, redox agent and probably phosphorylation mediated by cAMP-dependent protein kinase A (PKA). Furthermore, Ca^{2+} regulates the expression of NCX during neuronal development. For example, a $[Ca^{2+}]_i$ increase induces the downregulation of NCX2 and up-regulation of NCX3 isoforms in cerebellar granule neurons (Brini & Carafoli, 2011). Another type of regulation has been also observed. In fact, in hippocampus neurons exposed to glutamate excitotoxicity, calpain-mediate cleavage of NCX3, and in minor part NCX1, has been observed, leading to cell death (Brustovetsky, Bolshakov, & Brustovetsky, 2010), while a calpain-mediated degradation of NCX1 has been observed in heart, leading to inactivation of the exchanger and heart failure (Wanichawan et al., 2014).

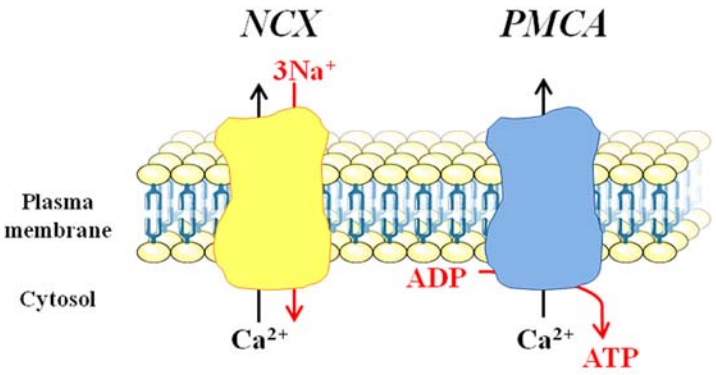

Figure 27. Channels for Ca^{2+} efflux. See text for details. Based on (Brini & Carafoli, 2011).

3.2 Mitochondrial calcium

Mitochondria are cellular organelles that present two membranes: mitochondrial outer membrane (MOM) and mitochondrial inner membrane (MIM). The space between these two membranes is named intermembrane space (IMS). An important characteristic of these membranes is that the MOM is largely permeable at small molecules, while MIM is permeable only at O_2, H_2O and CO_2. This peculiarity induces MIM to act as a barrier for H^+, which is responsible of the mitochondrial membrane potential ($\Delta\Psi_m$). Also, Ca^{2+} can easily pass the MOM, but needs the presence of the $Ca^{2+}{}_m$ uniporter complex (MCUc) to enter into the mitochondrial matrix (Patergnani et al., 2011).

3.2.1 Mitochondrial calcium influx

Deluca and Engstrom firstly described $Ca^{2+}{}_m$ uptake in 1961 (Deluca & Engstrom, 1961). Briefly, Ca^{2+} diffuses into the mitochondrial intermembrane space through voltage-dependent anion channels (VDAC1, VDAC2 and VDAC3) presents in the MOM and enters into the matrix through the MCUc, which is present in the MIM.

3.2.1.1 Voltage-dependent anion channels (VDACs)

VDACs are porin-like structures that allow Ca^{2+} to enter into IMS. VDACs protein interacts with anti-apoptotic proteins (e.g. Bcl-$_{XL}$ and Bcl-2) and glucose-regulated protein 75 (GRP75). GRP75 acts as a bridge for ER-mitochondria contacts or MAMs, allowing the Ca^{2+} mobilizing between both organelles (Patergnani et al., 2011).

3.2.1.2 Mitochondrial calcium uniporter complex (MCUc)

The $Ca^{2+}{}_m$ uniporter (MCU) complex (named MCUc) mainly regulates $Ca^{2+}{}_m$ influx into matrix (Baughman et al., 2011). The influx of Ca^{2+} through MCUc is $\Delta\Psi_m$-dependent; in fact, it depends on the highly negative charge in the matrix (~ -180mV). The flux of Ca^{2+} through MCUc, estimated ~10000 Ca^{2+} ions per second, renders the $\Delta\Psi_m$ less negative (Nemani, Shanmughapriya, & Madesh, 2018). The MCUc presents low affinity for Ca^{2+} and depends on $[Ca^{2+}]_i$ in a biphasic manner. This manner has been discovered in cells that show $Ca^{2+}{}_m$ oscillations in response to cytosolic ones. In fact, a stimulus triggering Ca^{2+} oscillation (micromolar range ~1-2μM) induces $Ca^{2+}{}_m$ uptake through MCUc, with a rapid rise of $[Ca^{2+}]_m$ that slowly return to basal signal. However, when Ca^{2+} oscillations are prolonged during the time, they are still visible in cytosol, but $Ca^{2+}{}_m$ uptake seems inhibited, indicating a maximum level reached. This means that $Ca^{2+}{}_m$ uptake is regulated by $[Ca^{2+}]_c$: low-$Ca^{2+}{}_i$ induces $Ca^{2+}{}_m$ uptake, while high-$Ca^{2+}{}_i$ inactivates the uniporter preventing further uptake. One explanation could be that the $Ca^{2+}{}_m$ overload induces mPTP opening, thus, failing the presence of the electron driving force for $Ca^{2+}{}_m$ uptake (Moreau, Nelson, & Parekh, 2006; Patergnani et al., 2011). Several proteins form this MCU complex: MCU, MCUb, MICUs family, essential MCU regulator (EMRE) and MCU regulator 1 (MCUR1) (Baughman et al., 2011).

MCU, the main protein of the complex, is a pore-forming protein of 35kDa in the MIM. It is formed by two transmembrane domains (TM1 and TM2) separated by a loop in the IMS that contains a DIME motif, amino acids negatively charged necessary for Ca^{2+} uptake. On the matrix side, MCU contains a NTD domain important for posttranslational modifications, such as phosphorylation of Ser^{92} or oxidation of Cys^{97}, both enhancing MCU activity (Feno, Rizzuto, Raffaello, & Vecellio Reane, 2021). In fact, the conserved cysteine 97 (Cys^{97}) on MCU can be S-glutathionylated. This MCU oxidation promotes oligomers formation and a higher $Ca^{2+}{}_m$ uptake (Dong et al., 2017).

MCUb is the dominant negative subunit of MCU that presents sequence similarity with MCU but opposite functions. Overexpression of MCUb reduces $Ca^{2+}{}_m$ uptake, while, silencing increases it. Thus, the ratio MCUb/MCU can indicate the $Ca^{2+}{}_m$ transients of the specific tissue (Feno et al., 2021).

EMRE, the essential MCU regulator, is a very small protein in the MIM that serves as a regulator of MCU activity and presents an N-terminal domain facing matrix and the C-

terminus facing intermembrane space. Its precursor of ~11kDa is cleaved by MPP in order to form the mature form of ~7kDa (König et al., 2016). Usually, 4 EMRE subunits bind the MCU tetramer. Its deletion changes the complex structure from tetrameric to monomeric and reduces Ca^{2+} uptake, indicating that EMRE is an essential protein for the complex (Feno et al., 2021). Its regulation depends on the protease Afg3l2, an m-AAA protease that, in the case of mutations, determines spinocerebellar ataxia (SCA). This ATP-dependent protease at the MIM is important for the correct assembling of EMRE on MCU, degrading the excess of EMRE non-assembled to MCU. In fact, when the Afg3l2-mediated proteolysis is not efficient, an excess of EMRE determines the formation of a MCU-EMRE constitutively active complex, which induces more Ca^{2+}_m uptake and renders neurons more sensitives to mPTP opening, as shown in **Figure 28** (König et al., 2016).

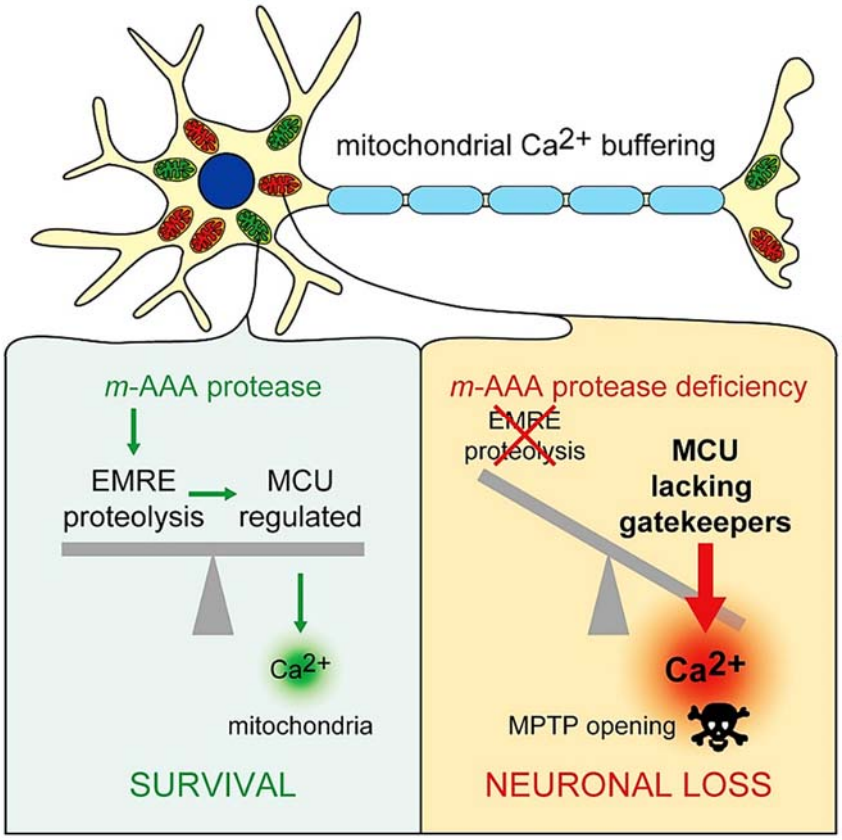

Figure 28. Afg3l2-mediated regulation of Ca^{2+}_m uptake. A scheme of MCU regulation in presence or loss of Afg3l2. Loss of the m-AAA protease induces MCU constitutive activation with increased Ca^{2+} uptake, sensitivity to mPTP opening and apoptosis (König et al., 2016).

MICUs family contains several regulatory subunits, such as MICU1 and MICU2, which contain two Ca^{2+}-binding domains and senses [Ca^{2+}] in the IMS (Pendin, Greotti, & Pozzan, 2014). MICU1, a 54kDa protein, is the first protein discovered of this family and deletion of this protein induces increased Ca^{2+}_m uptake and an ataxic phenotype in MICU1 KO mice (Liu et al., 2016). As shown in **Figure 29**, MICU1, but not the paralog MICU2, binds MCU at the IMS face. MICU1 and MICU2 generally form a heterodimer or a MICU1 homodimer, which is linked by a disulphide bond between two conserved cysteines. Both hetero and homodimer can bind the MCU tetramer with four EMRE subunits in a stoichiometry of 4:4:1:1 for the MCU-EMRE-MICU1-MICU2 complex (Feno et al., 2021), a complex of ~1.1MDa (König et al., 2016). Despite being observed as regulatory elements of MCU complex, the exact role of MICU1 and MICU2 is already under consideration. Nevertheless, it has been demonstrated that at low [Ca^{2+}]$_c$ the heterodimer binds MCU, while at high concentration the binding is avoided for conformational changes (Feno et al., 2021). Although MCU is expressed in all mammalian tissues, its activity is different among them, indicating that the regulatory subunits have a role in changing its function. In fact, in skeletal muscles, MICU1.1, a splice variant of MICU1, increases the sensitivity to Ca^{2+} concentration, while, in brain and neuronal tissues, MICU3, derived by a *MICU1* gene duplication, increases Ca^{2+} uptake (Feno et al., 2021).

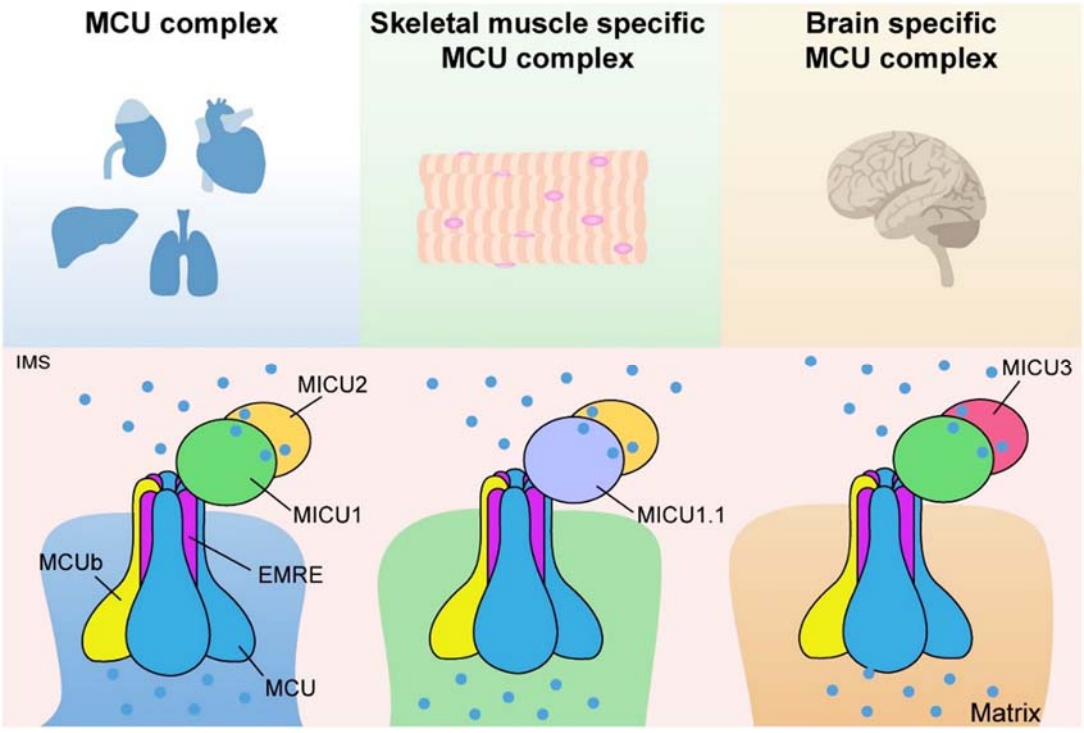

Figure 29. Tissue specificity of MCU complex. See text for details (Feno et al., 2021).

The assembling of MICU1-MICU2, MICU1.1-MICU2 or MICU1-MICU3 dimers on MCU tetramer seems regulated by the ATP-dependent m-AAA protease Afg3l2. As indicated in **Figure 30**, Afg3l2 protease limits EMRE protein levels removing the excess of non-assembled EMRE, in order to produce the same number of MICU1-MICU2-EMRE complexes as MCU tetramer. This situation leads to a regulated MCU complex. Interestingly, depletion of Afg3l2 protease, not only induces an excess of EMRE protein, but also avoids the interaction of MICU1-MICU2 complex on MCU for competition between EMRE and MICU1-MICU2-EMRE complex. This situation induces the simultaneous presence of a constitutively active ~400kDa MCU-EMRE complex and normally regulated ~1.1 MDa MCU-EMRE-MICU1-MICU2 complex (König et al., 2016).

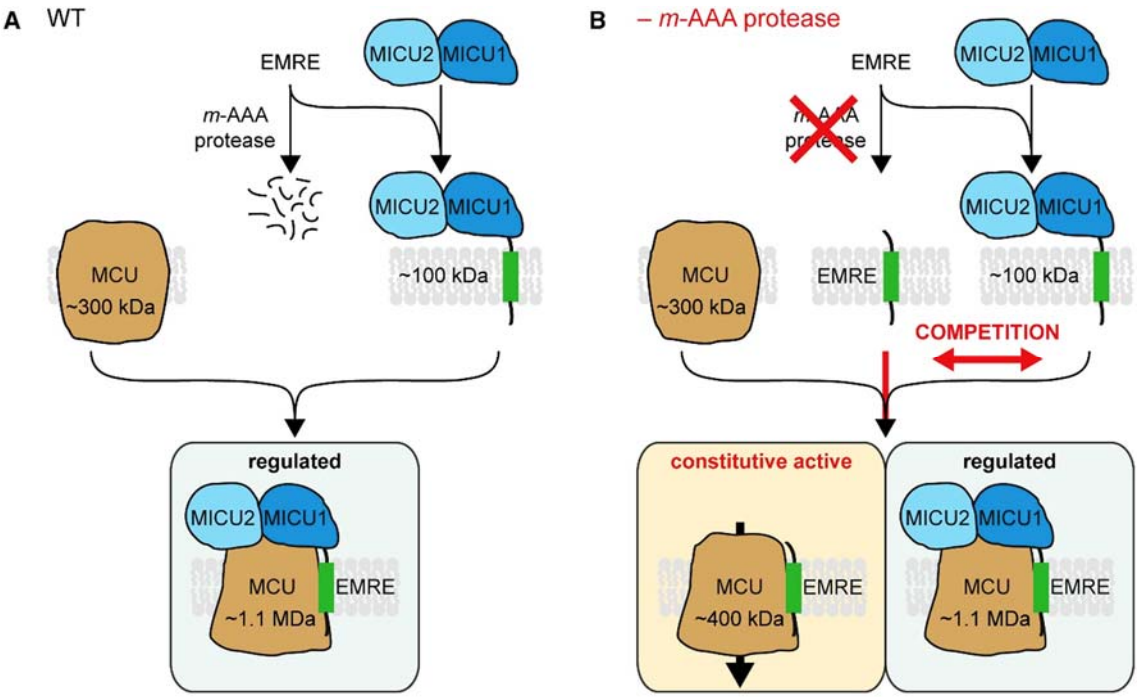

Figure 30. Schematic model of MCU complex assembling in wild type and Afg3l2-deficent cells. See text for details (König et al., 2016).

MCUR1 serves as a scaffold protein and positive regulator of MCU; in fact, its deficiency induces alterations in the formation of MCU-EMRE complex and decreases mitochondrial Ca^{2+} uptake, indicating its essential role for MCU activity (Tomar et al., 2016). Indeed, it seems to regulate the Ca^{2+} threshold for mPTP opening, in fact, loss of MCUR1 promotes resistance to Ca^{2+}-mediated mPTP opening, probably indirectly by regulating Ca^{2+} concentration (Chaudhuri, Artiga, Abiria, & Clapham, 2016). However,

some authors indicate this protein as a factor needed for cytochrome c oxidase assembling, indicating an indirectly relation with Ca^{2+} homeostasis (Paupe, Prudent, Dassa, Rendon, & Shoubridge, 2015).

3.2.2 Mitochondrial calcium efflux

Carafoli and collaborators firstly described Ca^{2+}_m extrusion. These pioneer results indicate that Ca^{2+}_m extrusion was proportional to medium concentrations of sodium and, in a minor manner, of lithium (Carafoli, Tiozzo, Lugli, Crovetti, & Kratzing, 1974).

3.2.2.1 Mitochondrial sodium (or lithium)/calcium exchanger (NCLX)

The main component for Ca^{2+}_m efflux is mitochondrial sodium (or lithium)/calcium exchanger, NCLX (or NCXK6 or SLC24A6), a multi-pass membrane protein localised in MIM at the level of cristae. This exchanger mediates Ca^{2+} extrusion from mitochondria in combination with influx of Na^+ (or Li^+), with a stoichiometry of $1Ca^{2+}$ for $3Na^+$ (or Li^+). The possibility of using Li^+ makes this exchanger different from the other NCX present in plasma membrane or ER (Cai & Lytton, 2004). Generally, NCLX-mediated Ca^{2+}_m efflux is slower than the uptake and the efflux activity is blocked by the benzodiazepine CGP37157 or mutations in the catalytic site, such as the threonine 468 (Thr^{468}) (Palty et al., 2010; Patergnani et al., 2011).

NCLX activity is very important in excitable cells such as neurons, cardiomyocytes and pancreatic β cells, being important respectively for viability and pain sensation, cardiac automaticity and insulin secretion (Kostic & Sekler, 2019). In fact, NCLX deficiency induces death of mice, correlated with heart failure, a phenotype related to Ca^{2+}_m overload and mPTP opening (Luongo et al., 2017). In nociceptive DRG neurons, NCLX activity is related to pain sensation, in fact, capsaicin, through TRPV1, can induce a Na^+ wave into the cytosol that promotes Ca^{2+} efflux through NCLX. The mechanism involves the interaction between TRPV1/MCU/NCLX. Thus, NCLX inhibition induces a lower response (small number of capsaicin-induced action potentials) of these sensory neurons to capsaicin (Kostic & Sekler, 2019; Nita et al., 2016). Inhibition of NCLX activity has been also observed in tauK18-treated co-cultures of neurons and astrocytes, indicating a possible involvement of this exchanger in tauophaties (Britti, Ros, Esteras, & Abramov, 2020). In B-lymphocytes, the inhibition of this exchanger increases

chemotaxis and motility through a mechanism related to mitochondria-ER Ca^{2+} refilling (Takeuchi, Kim, & Matsuoka, 2020).

3.2.2.2 Regulation of NCLX activity

Regulation of NCLX activity seems mediated by phosphorylation. This characteristic has been discovered in PTEN-induced putative kinase 1 (Pink1)-deficient neurons, a cellular model of PD (Kostic et al., 2015). The Pink1 protein, encoded by *PINK1* (*PARK6*) gene, is a serine/threonine kinase processed by different steps into mitochondria and rapidly degraded. The processing of 64kDa full-length Pink1 protein, depending on $\Delta\Psi_m$, involves different mitochondrial proteases: mitochondrial processing peptidase (MPP), presenilin-associated rhomboid-like protease (PARL), a subunit of mAAA protease (Afg3l2) and a subunit of heterodimeric matrix protease (ClpXP). MPP-mediate processing is important to remove the MTS, producing an intermediate form of 60kDa; PARL cleaves the N-terminal aa, generating a 55kDa form (Δ1), while Afg3l2/PARL seems essential to produce the 43kDa mature form (Δ2) (Greene et al., 2012; Pickrell & Youle, 2015). Both forms are released into the cytosol and rapidly degraded by proteasome (Pickrell & Youle, 2015). The 43kDa form of Pink1, localised in the cytosol and absent in Afg3l2-deficient *Drosophila* (Thomas, Andrews, Burman, Lin, & Pallanck, 2014), promotes Protein Kinase A (PKA)-mediated dendritic outgrowth and anterograde transport of mitochondria (Dagda et al., 2014). When mitochondria are damaged or depolarised, Pink1 processing is inhibited, leading accumulation onto mitochondria at MOM in order to mark mitochondria for removing (Becker, Richter, Tocilescu, Przedborski, & Voos, 2012; Greene et al., 2012).

Pink1 deficiency induces slower $Ca^{2+}{}_m$ efflux, indicating NCLX impairment, mitochondrial depolarisation and apoptotic cell death, but also lower activity of cAMP-dependent PKA, a Ser/Thr kinase as Pink1. All these phenotypes have been restored by PKA overexpression, since it has been demonstrated that PKA phosphorylates NCLX on Ser^{258}, activating the efflux of Ca^{2+}, as indicated in **Figure 31** (Kostic et al., 2015).

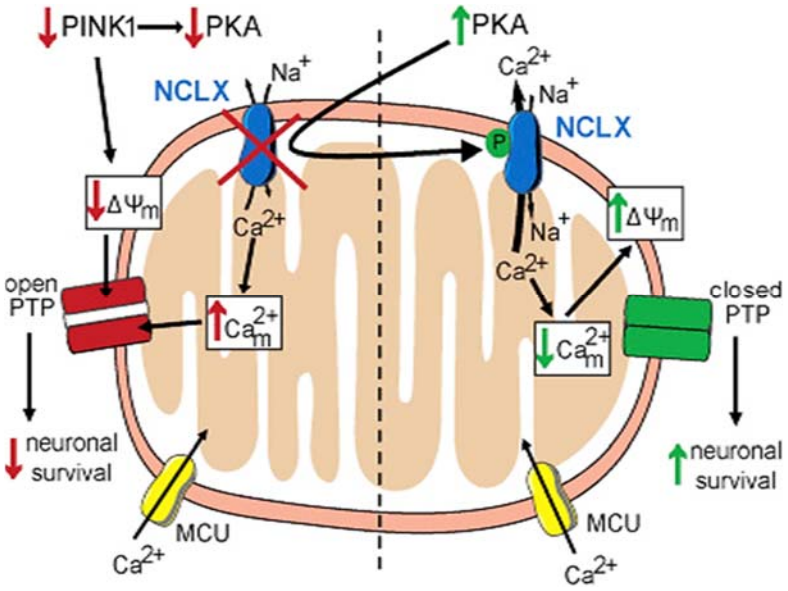

Figure 31. PKA-mediated phosphorylation of NCLX restores Pink1-deficient neurons. See text for details (Kostic et al., 2015).

Interestingly, mitochondrial membrane depolarisation can also regulate the activity of NCLX. In fact, complete depolarisation changes the mode of action of NCLX acting in a "reverse mode", thus, accumulating Ca^{2+} into the matrix, while a mild or partial mitochondrial membrane depolarisation decreases Ca^{2+} efflux, without affecting Ca^{2+} influx, a phenotype that can be rescue by Ser^{258} phosphorylation at the hydrophilic loop mediated by PKA. This means that NCLX activity can be dually regulated by two allosteric regulators that induce conformation changes of the exchanger: $\Delta\Psi_m$, acting on positively charged residues at the hydrophilic loop facing the matrix, and phosphorylation, acting on Ser^{258} near these charged amino acids. Thus, mild depolarisation prolonged during the time can decrease NCLX activity, promoting $Ca^{2+}{}_m$ overload and consequently decreasing $\Delta\Psi_m$ in a vicious cycle, triggering at the end the conditions for mitochondrial permeability transition pore opening (Kostic, Katoshevski, & Sekler, 2018).

The regulation of NCLX activity, mediated by PKA-phosphorylation at Ser^{258} and by $\Delta\Psi_m$ regulatory sites, makes this exchanger different from other members of NCX family. In fact, as indicated in **Figure 32**, NCLX lacks of allosteric Ca^{2+}-binding domains (CBD1 and CBD2), present in other NCX members, which induce activation of the exchangers (Katoshevski, Ben-Kasus Nissim, & Sekler, 2021).

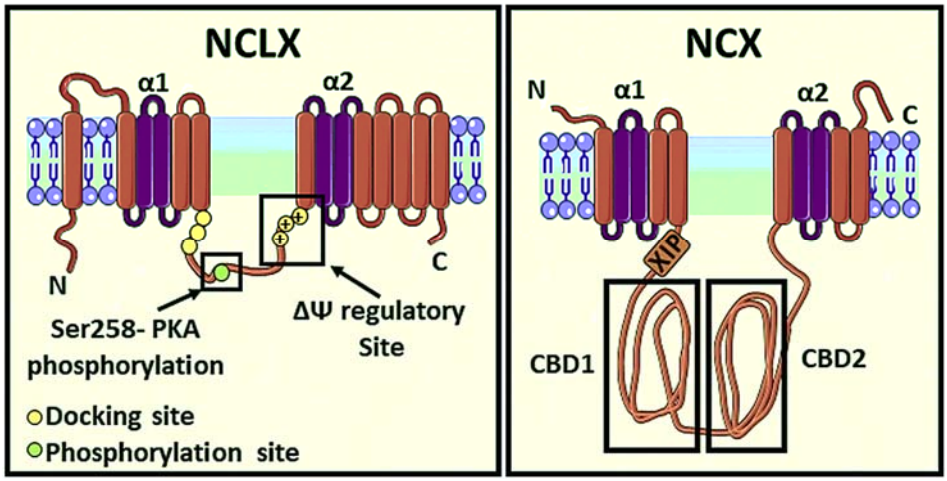

Figure 32. Structural differences between NCLX and NCX. Note the PKA-dependent phosphorylation and the $\Delta\Psi_m$ regulatory site in NCLX and the two regulatory sites in NCX. Modified from (Katoshevski et al., 2021).

Interestingly, some exchangers of NCX family are regulated by calpains, Ca^{2+}-activated proteins that mediate their degradation. For example, calpain-mediated degradation of NCX3 induces excitotoxicity in neurons (Bano et al., 2005). Similarly, NCLX seems to be regulated by calpains, in particular μ-calpains (Kar, Chakraborti, Samanta, & Chakraborti, 2009; Katoshevski et al., 2021).

Furthermore, NCLX seems also regulated by stomatin-like protein 2 (SLP-2), an inner mitochondrial membrane protein that might actuate as a negative regulator of NCLX, however, this effect seems to be indirect (Kostic & Sekler, 2019; Wai et al., 2016).

3.2.3 Mitochondrial calcium and respiration

Ca^{2+}_m uptake mediated by MCU is not only essential for Ca^{2+} buffering and apoptosis, but also many mitochondrial functions such as ATP production. The major pathway for ATP production is the oxidative phosphorylation (OXPHOS), in which the complexes I-IV pump H^+ across the MIM to generate an electrochemical gradient used for complex V, ATP synthase, to generate ATP, reducing O_2 to H_2O. Usually, an increase of Ca^{2+}_m boosts the OXPHOS and TCA cycle, consuming more O_2, to generate more ATP (Brookes, Yoon, Robotham, Anders, & Sheu, 2004). In fact, as shown in **Figure 33**, ATP synthase and TCA cycle dehydrogenases such as pyruvate dehydrogenase (PDH), iso-citrate dehydrogenase (IDH) and α-ketoglutarate dehydrogenase (α-KGDH) activities bind or use Ca^{2+} for ATP generation. Matrix Ca^{2+} also regulates OXPHOS by acting on complex III and IV of respiratory chain, F1Fo-ATP synthase and adenine

nucleotide translocase (ANT). In neurons, extra-mitochondrial Ca^{2+} can regulate other carriers such as Aralar/AGC1-MAS, an aspartate-glutamate mitochondrial carrier component of the malate–aspartate shuttle (MAS) and SCaMC-3 (Slc25a23), a mitochondrial ATP-Mg/Pi carrier. An increase in cytosolic Ca^{2+} can increase pyruvate supply into mitochondria by acting on Aralar/AGC1-MAS and enhance respiration in this cell type, increasing intra-mitochondrial NADH (Llorente-Folch et al., 2015).

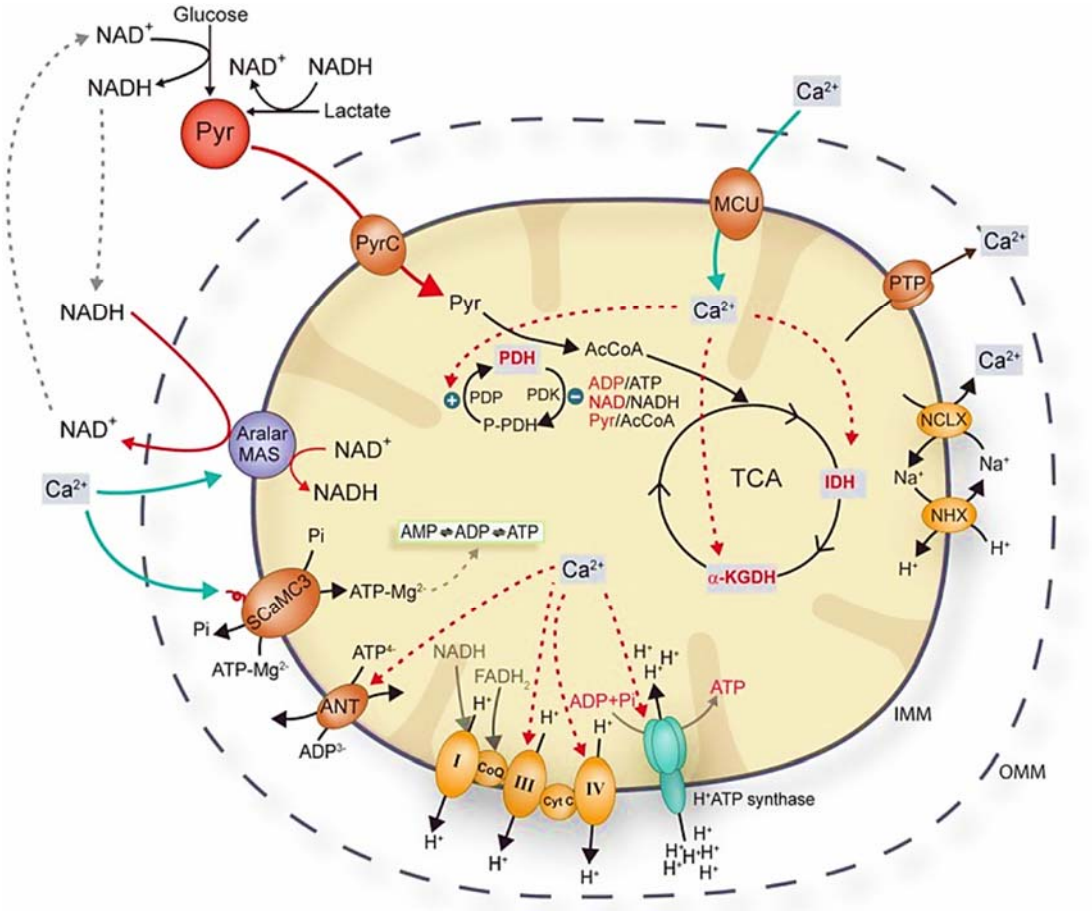

Figure 33. Ca^{2+} actions on mitochondrial respiration. In dashed red, enzymes regulated by matrix Ca^{2+}. In green, carriers regulated by cytosolic Ca^{2+}. See text for details. (Llorente-Folch et al., 2015).

3.3 Endoplasmic reticulum calcium and others

Endoplasmic reticulum (ER), usually stores Ca^{2+} at micromolar concentration. A stimulus (e.g. a ligand binds a specific receptor in plasma membrane) activates a series of signals that induce the hydrolysis of phosphatidylinositol 4,5-bisphosphate (PIP_2) in the plasma membrane. The hydrolysis induces the formation of two second messengers diacylglycerol (DAG) and inositol-1,4,5-trisphosphate (IP_3); IP_3 binds IP_3R on ER,

releasing Ca^{2+} contained in it and rising $[Ca^{2+}]_i$ to ~10μM (Patergnani et al., 2011). ER Ca^{2+} influx is regulated by the sarco/endoplasmic reticulum Ca^{2+} ATPase (SERCA), while efflux through the inositol-1,4,5-triphosphate receptors (IP_3Rs) and ryanodine receptors (RyRs) (Patergnani et al., 2011).

IP_3R is the principal Ca^{2+} channel responsible of Ca^{2+} release into the cytosol. This channel can be activated by IP_3 and Ca^{2+} and regulated by Ca^{2+}/CaM-dependent kinaseII (CaMKII), protein kinase C (PKC) and PKA (Patergnani et al., 2011).

SERCA is the Ca^{2+} channel responsible for Ca^{2+} influx into the ER/SR, coupling with ATP hydrolysis. This pump has 2 conformational states. In E1 state, the pump has high affinity for Ca^{2+} and binds Ca^{2+} coming from cytosol; In E2 state, the pump presents a conformational change that determines low affinity for Ca^{2+} and release of Ca^{2+} in the ER/SR. For each cycle, one ATP is hydrolysed to mobilise 2 Ca^{2+} ions (Patergnani et al., 2011).

3.3.1 MAMs

Apart from mitochondria, the other organelle involved in Ca^{2+} buffering is ER. The close contact between mitochondria and ER creates a particular space of 10-200nm, in which Ca^{2+} concentration increases, named mitochondria-associated membranes (MAMs) (Patergnani et al., 2011). In these MAM microdomains, VDACs, present in the MOM, and IP_3R, in the ER membrane, are in close relation through the interaction with GRP75, a molecular chaperone that acts as a bridge between MOM and ER. The proximity between the two organelles facilitates the mobilization of Ca^{2+}. The importance of MAMs in Ca^{2+} homeostasis became clear when it has been discovered that Ca^{2+} can enter into mitochondria directly from IP_3R (Patergnani et al., 2011).

3.4 Calcium binding proteins

Ca^{2+}-binding proteins are a family of proteins with the characteristic of buffering or sensing Ca^{2+} with different affinity. Calretinin, calbindin D28k and parvalbumin are members of this family (Schwaller, 2014). Calretinin is highly expressed in rat DRG neurons at the embryonic days E11-14, but is less present in post-natal days (Ambrus, Kraftsik, & Barakat-Walter, 1998). Interestingly, the expression of calbindin and parvalbumin or the number of neuronal subtypes expressing these proteins, but not calretinin, decrease in some neurodegenerative diseases (Barinka & Druga, 2010).

Parvalbumin (Pvalb), has the ability to bind Ca^{2+} at 2 EF-hands motifs with slow kinetics, being considered as a "slow" buffer (Barinka & Druga, 2010). This protein localises in DRG neurons, mainly in large-diameter subpopulation responding to NT-3 (Copray, Mantingh-Otter, & Brouwer, 1994) and highly expressed in DRGs of L3-L5 segments (Honda, 1995).

Calbindin D28k (CB), has the ability to bind Ca^{2+} at 4 EF-hands motifs with fast kinetics, being considered as a "fast" buffer (Barinka & Druga, 2010). This protein localises in excitatory neurons, cerebellar Purkinje cells (Barski et al., 2003) and DRG neurons, mainly in small-diameter subpopulation (Honda, 1995).

Calretinin (CR), initially discovered in retina, is a 31kDa Ca^{2+}-binding protein with 6 EF-hands motifs, of which only 5 can bind Ca^{2+} (Schwaller, 2014). Its ability to bind Ca^{2+} and buffer it shares characteristics with "slow" and "fast" buffers (Barinka & Druga, 2010). Calretinin, changing conformation upon Ca^{2+}-binding, could have a role as "sensor of Ca^{2+}", thereby activating or inactivating targets. Despite this possible role, it has been observed that calretinin can interact with the high-voltage activated Ca^{2+} channel $Ca_V2.1$ in neurons, indicating other possible functions that can affect $[Ca^{2+}]_i$ (Schwaller, 2014) and can modulate excitability in neurons (Camp & Wijesinghe, 2009). Its localisation is cytosolic; however, it has been observed a vitamin D_3-dependent nuclear localisation of calretinin and an alternatively spliced calretinin truncated form (22kDa) *in vitro* in colon cancer cells, which probably promote buffering of nuclear Ca^{2+} and proliferation inhibition (Schwaller, 2014). This Ca^{2+}-binding protein is highly expressed in GABAergic interneurons of brain (Barinka & Druga, 2010) and localises in DRG neurons, being present in medium-diameter subpopulation (Ren, Ruda, & Jacobowitz, 1993) as well as in small-diameter neurons and Schwann cells (Copray et al., 1994).

3.5 Calcium differences among DRG subpopulations

The mechanisms of cellular Ca^{2+} regulation can differ among subpopulations of DRGs (Lu, Zhang, & Gold, 2006). In fact, subpopulations of DRG neurons are heterogeneous in not only size, velocity conduction and action potential, but also in the Ca^{2+}-related stimuli responses. For example, small-diameter adult rat DRG neurons tend to increase the resting $[Ca^{2+}]_i$. Despite this characteristic, no statistically significant differences have been assessed in basal level of $[Ca^{2+}]_i$. However, the amplitude, analysed as the

$\Delta[Ca^{2+}]_i$ (peak value – baseline), and the decay of Ca^{2+} stimuli, analysed as the time to 50% of peak (half-life), are markedly different among subpopulations. High potassium (K^+)-stimulated or voltage-stimulated small-diameter rat DRG neurons show a larger $[Ca^{2+}]_i$ amplitude, dependent on extracellular Ca^{2+}, and slower decay rate; whereas large-diameter neurons a shorter amplitude and faster decay rate. Apart from these extracellular Ca^{2+}-dependent stimuli, peak amplitude and decay can depend on Ca^{2+}-induced Ca^{2+} release (CICR) from intracellular stores. Inhibition of RyR in internal stores, but not IP_3R, reduces K^+-stimulated peak amplitude in medium and large-diameter neurons. Moreover, SERCA inhibition increases peak amplitude and altered decay, also increasing Ca^{2+} baseline levels after stimulus, of large-diameter neurons. These results could suggest an increased ER filling capacity in large-diameter neurons than in others. In addition, a larger peak amplitude in medium-size neurons can be mediated by Ca^{2+} efflux processes, for example through the PMCA. Ca^{2+} efflux via NCX inhibition can also influence amplitude and decay in all subpopulations, with a great extent in small and medium-diameter neurons. CCCP disrupts mitochondrial proton gradient and blocks both uptake and release of Ca^{2+} from mitochondria, leading to understand the influence of mitochondria in peak amplitude and decay for each subpopulation. CCCP application increases peak amplitude and influences decay, being slower, in all subpopulations, with a great extent in medium and large-diameter neurons, but also caused an initial increase in resting $[Ca^{2+}]_i$, which declined with time, but did not return to the levels prior to CCCP application. In addition, Ca^{2+}-binding proteins are differentially distributed among sensory neurons, with parvalbumin preferentially expressed in neurons with a large soma, and calbindin expressed in neurons with a small soma; differences in the Ca^{2+}-affinity of these proteins could contribute to the heterogeneity of sensory neurons (Lu, Zhang, & Gold, 2006). Another characteristic of DRG subpopulations is the difference in voltage-dependent Ca^{2+} waves, which can be with low-threshold (T-type) or high-threshold (L and N-types) currents. In fact, large and small T-type Ca^{2+} currents are seen, respectively, in medium and small-size neurons, while none T-type Ca^{2+} current has been observed in large-diameter DRG neurons. L-type Ca^{2+} currents are observed mainly in small-diameter neurons, while N-type Ca^{2+} currents are present in all size of neurons in the same extent (Scroggs & Fox, 1992). These differences suggest different Ca^{2+}-related influx/efflux mechanisms among subpopulations and are important in order to understand why some subpopulations are more affected in some diseases (e.g. proprioceptors in FA).

4 CALCIUM AND MITOCHONDRIA IN NEURODEGENERATION

Neurodegenerative diseases are often related to alterations in Ca^{2+} concentrations, particularly in mitochondria. Even if mitochondrial dysfunction is an early alteration of the disease or a secondary process, the correlation between neurodegenerative diseases and altered mitochondria is often a key component (Monzio Compagnoni et al., 2020). A disease that involves as primary target mitochondria is considered a mitochondrial disease, being frataxin a mitochondrial protein; FA is considered one of those.

4.1 Mitochondrial permeability transition pore

The mitochondrial permeability transition pore (mPTP) is an inner membrane channel, which can promote mitochondrial dysfunctions and intrinsic apoptotic cell death when opened for long periods. Its opening has been described in many pathological conditions (e.g. neurodegenerative diseases) (Bernardi, Rasola, Forte, & Lippe, 2015).

4.1.1 Structure

The mPTP structure is controversial, however it is widely accepted the presence of dimers of F_0F_1 ATP synthase at the MIM (Giorgio et al., 2013). Other proteins have been included in the structure of mPTP complex, such as the mitochondrial phosphate P_i carrier (PiC) and ADP/ATP translocase (ANT) at the MIM, translocator protein (TSPO) and VDAC at the MOM and CypD in the matrix. Each of these proteins has been genetically removed to analyse mPTP function, observing that only F_0F_1 ATP synthase and CypD are essentials for mPTP formation (Bernardi et al., 2015). However, the interaction of CypD with oligomycin sensitivity conferring protein (OSCP), a member of F_0 subcomplex, is reversible, indicating that the ATP synthase is the essential part of the mPTP, as indicated in **Figure 34** (Giorgio et al., 2013).

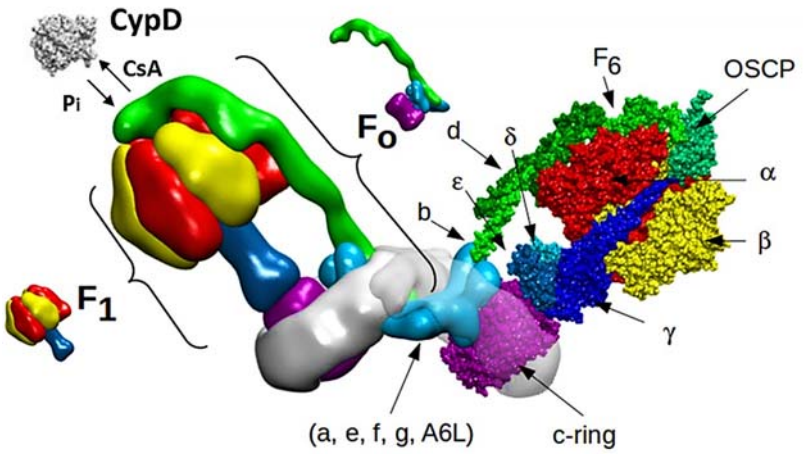

Figure 34. Structure of dimers of ATP synthase. Note the subcomplexs F0 and F1 and the subunits forming each of those subcomplexs. In particular, note in green OSCP and the CypD in grey. Modified from (Bernardi et al., 2015).

F_0F_1 ATP synthase (or Complex V of oxidative phosphorylation) produces ATP by using the H^+ gradient generated by OXPHOS. In fact, the translocation or flux of H^+ into matrix, mediated by the subcomplex F_0, is coupled with the synthesis of ATP from ADP and P_i, mediated by the catalytic subcomplex F_1. ATP synthesis is mediated by a rotatory mechanism of c-ring in F_1 subcomplex. However, ATP synthase can work in a "reverse mode" in which the extrusion of H^+ into the intermembrane space is coupled with hydrolysis of ATP. This mechanism can be induced by depolarisation, modifications of SH groups, ATP synthase inhibitors, Ca^{2+}-ATP etc. (Bernardi et al., 2015).

4.1.2 Regulation

The mPTP can change between open and closed states. A transient state is also seen, in which the mPTP can open and close continuously. Its opening requires matrix Ca^{2+}, together with mitochondrial membrane depolarisation. However, other factors inducing mPTP opening are pro-oxidants, pH alterations and modifications of mPTP regulators (e.g. CypD) (Bernardi et al., 2015).

4.1.2.1 Mitochondrial membrane potential

The mitochondrial membrane potential is important for the transition between opened and closed state of mPTP. In fact, mitochondrial membrane depolarisation favours mPTP opening, while a negative-inner membrane potential maintains mPTP in a closed state. This event seems mediated by critical Arg residues in the mPTP structure that

actuate as voltage-sensors (Bernardi et al., 2015; Linder, Morkunaite-Haimi, Kinnunen, Bernardi, & Eriksson, 2002). However, mitochondrial membrane depolarisation alone does not trigger mPTP opening (Brookes et al., 2004).

4.1.2.2 Calcium

As said above, mPTP opening can be triggered by mitochondrial depolarisation. However, partial or mild depolarisation is not sufficient for mPTP opening and $Ca^{2+}{}_m$ overload is also required for a two-hit opening mechanism (Brookes et al., 2004). Thus, Ca^{2+} is essential for mPTP opening, while Mg^{2+} and ADP inhibit it. Ca^{2+} can interact with ATP synthase in F_1 subunit and c-ring. Interestingly, the interaction of Ca^{2+} in regulatory sites of c-ring has been suggested to induce conformation changes, while, the catalytic sites in F_1 subunit can bind Mg^{2+} or Ca^{2+}, probably replacing Mg^{2+} sites with Ca^{2+} induces conformational changes that favour ATP hydrolysis and mPTP opening (Bernardi et al., 2015; Giorgio et al., 2017).

4.1.2.3 MATRIX pH and Pi

The **matrix pH** can modulate the mPTP opening. In fact, the optimum value for mPTP opening is pH 7.4, while upper or lower values favour the closing. Low pH values could inhibit mPTP opening by avoiding CypD interaction to OSCP, however, ATP synthase responds to pH also in CypD-deficient cells. ATP hydrolysis mediated by ATP synthase working in reverse seems to have optimal value at pH 8.0 (Bernardi et al., 2015).

The **matrix inorganic phosphate (P_i)** can also regulate mPTP by increasing the interaction between CypD and the subunit OSCP of ATP synthase, thus, favouring pore opening (Bernardi et al., 2015). However, P_i can also buffer the $Ca^{2+}{}_{free}$ presents in the matrix by forming $Ca_3(PO_4)_2$. Interestingly, P_i enters in mitochondria as $H_2PO_4^-$. This means that, when it became PO_4^{3}, loses $2H^+$, modifying $[Ca^{2+}]_m$ but also the pH in matrix (Hurst, Hoek, & Sheu, 2017).

4.1.2.4 CypD and sirtuins

Human cells express **cyclophilins (Cyps)** involved in several cellular processes, including protein folding, protein trafficking and cell signalling. Cyps are peptidyl-prolyl isomerases (PPIases), which catalyse the *cis* to *trans* conversion of proline-containing peptides. Despite having, generally, the same enzymatic activity, all

cyclophilins are different in structures and sequences. At least 16 Cyps have been discovered, of those only 7 binds to CsA.

The better-characterised are:

- CypA (Cyp18 or PPIA, 18 kDa) and Cyp40 (40 kDa) present in the cytosol;
- CypB (22 kDa) and CypC in the lumen of the ER;
- CypD in mitochondria;
- CypE and CypA in the nucleus (Naoumov, 2014).

CypA is normally a cytosolic protein, however, pro-inflammatory stimuli as infections, hypoxia, or oxidative stress can secrete it through vesicles (Bukrinsky, 2015). In fact, it is important for viral replication (e.g. Hepatitis C virus, HCV) and its inhibition is mediated by Alisporivir (Debio 025) (Quarato et al., 2012). However, it is not essential for survival (de Wilde, Pham, Posthuma, & Snijder, 2018).

CypB presents an N-terminal signal sequence important for its target into ER lumen. However, inflammatory stimuli, which cleave CypB, or the binding of CsA to CypB induces its release from cells (Naoumov, 2014).

Sirt3 is a 44kDa mitochondrial NAD^+-dependent conserved protein deacetylase, which is present in the mitochondrial matrix as 28kDa protein after cleavage by MPP. It is important for deacetylation of different proteins such as SOD2, CypD, p53, PGC1α etc. In fact, in normal conditions, SOD2 remains deacetylated by Sirt3 and, converting superoxide into H_2O_2, decreases superoxide levels. In pathological conditions with loss of Sirt3 activity two acetylations onto lysine K122 and K68 can inhibit its anti-oxidant function as ROS scavenger (Zou et al., 2017).

Sirt3 inactivation, leading to CypD acetylation, is related to increase susceptibility on mPTP opening and cell death. In fact, Sirt3 down-regulation seems related to age-associated disorders and neurodegenerative diseases such as AD and HD (Anamika, Khanna, Acharjee, Acharjee, & Trigun, 2019). Indeed, down-regulation of Sirt3 (mRNA and protein) has been also found in heart of FXN-KO mice, but not FXN mRNA and protein in Sirt3-KO mice, with consequently increased acetylation of mitochondrial proteins (Martin et al., 2017).

❖ **Posttranslational modifications of CypD**

The protein CypD is a regulator of mPTP, in fact, its deficiency determines cells that are resistant to apoptotic cell death because need higher matrix Ca^{2+} concentrations for opening. CsA, by binding CypD, can inhibit mPTP opening by avoiding the interaction with other pore members. This interaction can be promoted by P_i, but also by posttranslational modifications of CypD such as acetylation and phosphorylation. As shown in **Figure 35**, GSK-3β phosphorylates, while Sirt3 deacetylates CypD. Phospho-CypD favours, while the presence of Pink1 inhibits mPTP opening, by mechanisms not fully understood. Similarly, lower Sirt3 levels or/and activity induce acetylation of CypD, a mechanism that favours mPTP opening. Furthermore, the interaction between CypD and the signal transducer and activator of transcription 3 (STAT3), in phosphorylated state, avoids the binding of CypD to mPTP, thus, inhibiting mPTP opening (Bernardi et al., 2015).

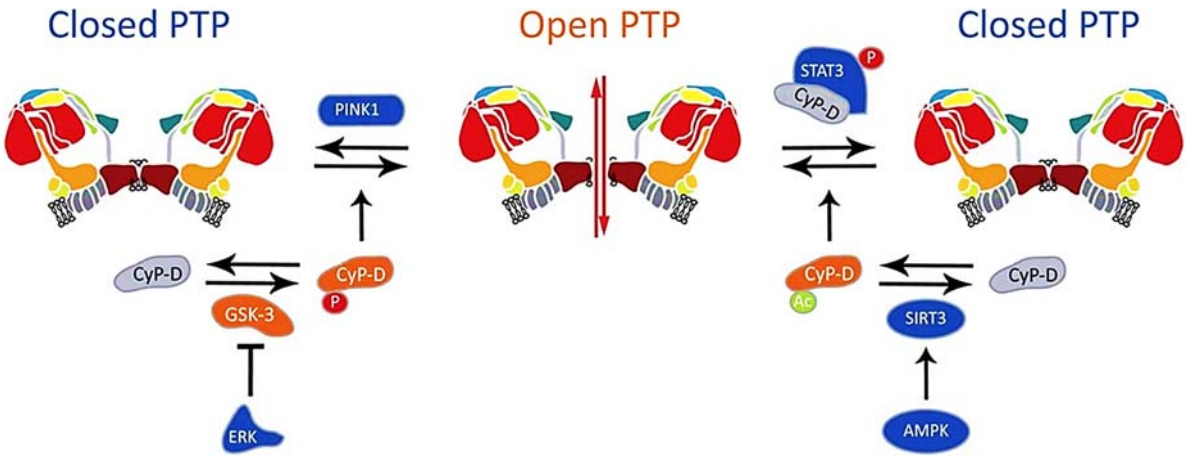

Figure 35. Posttranslational modifications of CypD regulate mPTP opening. Phospho-CypD and Acetyl-CypD induce mPTP opening, while Pink1 and phospho-STAT3 inhibit mPTP opening. See text for details. From (Bernardi et al., 2015).

4.1.2.5 Others factors

The mPTP opening is also sensitive to **oxidative stress**, such as the oxidation of critical thiols. For example, radical oxygen species (ROS), but also reactive nitrogen species (RNS), can modulate mPTP. This modulation can be direct by inactivating different subunits of the complex, in highly conserved residues (Bernardi et al., 2015) and indirect by modulating oxidative phosphorylation; intracellular and mitochondrial [Ca^{2+}] (Hurst et al., 2017) or anti-oxidant defences such as catalase, superoxide dismutase, and glutathione (Rasola & Bernardi, 2007). **Fatty acids** can also have a role

in modulating mPTP opening. For example, both palmitic acid and arachidonic acid can induce mPTP opening through a not fully understood manner (Penzo, Tagliapietra, Colonna, Petronilli, & Bernardi, 2002). **Anti-apoptotic proteins** such as Bcl-2 and Bcl-$_{XL}$, but also **metabolic ratios** such as ATP/ADP and NAD^+/NADH can modulate its opening (Rasola & Bernardi, 2007).

4.2 Mitochondrial (intrinsic) apoptotic cell death

Cell death (or apoptosis) occurs in physiological processes such as in development, but also upon cell damage. Internal (e.g. cytotoxic stress, heat shock, oxidative stress, and DNA damage) or external stimuli, respectively in intrinsic and extrinsic apoptotic cell death, can initiate a cascade of mechanisms that involve protein cleavage mediated by caspases and nuclear DNA breakdown. The involvement of mitochondrial damage and mPTP opening occur only in intrinsic apoptotic cell death (Cavalcante et al., 2019).

4.2.1 The mPTP opening and neurodegeneration

Under normal physiological conditions, mPTP opens transiently. These flickerings render mPTP as a Ca^{2+}-induced Ca^{2+} release channel. The opening interests individual pores; in fact, the same cell can have mitochondria simultaneously with mPTP in opened and closed states. Thus, depolarised mitochondria can release Ca^{2+} that can enter into healthy mitochondria. However, when many mitochondria in the cell persistently open their pores, this event triggers mitochondrial (intrinsic) apoptotic cell death, thus, neurodegeneration (Bernardi et al., 2015; Rasola & Bernardi, 2011). Mechanisms of mitochondrial apoptotic cell death have been demonstrated for several neurodegenerative diseases, such as PD, AD, HD, ALS (Rasola & Bernardi, 2011). Different models for mPTP closed/opened states have been theorized, however, the effects of such opening are more studied than the mechanisms of opening *per se*. In fact, it is widely accepted that mPTP opening induces $\Delta\Psi_m$ dissipation, inhibition of oxidative phosphorylation, influx of water into matrix resulting in mitochondrial swelling and rupture of MOM and efflux of matrix solutes/proteins leading to mitochondrial apoptosis (Gerle, 2016). The MOM integrity is influenced by the balance of anti-apoptotic stimuli, such as the presence of Bcl-2 (B-cell lymphoma protein 2, apoptosis regulator) or Bcl-$_{XL}$ (B-cell lymphoma-extra large) proteins, and pro-apoptotic stimuli, such as the presence of Bax (Bcl-2-associated X protein) or Bak (Bcl-2 antagonist) proteins. Thus, the activation of pro-apoptotic proteins induces MOM

rupture and the release in the cytosol of proteins present in the MIM like cytochrome c, apoptotic protease activating factor 1 (APAF-1) and pro-caspase 9. These released proteins, in the presence of ATP, form an apoptosome, and initiate the mechanisms of apoptotic cell death (Rasola & Bernardi, 2011).

4.2.1.1 *Caspases*

Caspases (cysteine-aspartic proteases) are inactive proteins that require a biochemical change to become active proteases, a cleavage at a specific Asp-X site. These proteases can be divided in 3 groups depending on their action: inflammatory caspases (caspases 1, 4, 5, 11-14), initiator (2, 8-10) and effector of apoptosis (3, 6-7) caspases (Lavrik, Golks, & Krammer, 2005). Among the proteins released by damaged mitochondria there are cytochrome c, APAF-1 and pro-caspase 9, which form the apoptosome, but also pro-apoptotic proteins like Smac/DIABLO and Omi/HtrA2. Cytochrome C and APAF-1, in the presence of ATP, oligomerize to form the apoptosome complex. The interaction of pro-caspase 9 to the apoptosome results in caspase 9 activation. This event converts the protein into one of the most important initiator caspases of intrinsic apoptosis that cleaves other effector caspases like pro-caspase 3 and pro-caspase 7, activating it. Proteins of IAP (inhibitor of apoptosis) family, such as XIAP, inhibit caspase 9, 3 and 7, however, the action of IAP proteins is inhibited by Smac/DIABLO and Omi/HtrA2, which, in turn, activate these caspases (Lavrik et al., 2005). As indicated in **Figure 36**, when the effector caspases are activated other proteins are cleaved, generating a cascade of events that degrade DNA/cytoskeletal proteins and induce morphological changes such as cell shrinkage, chromatin condensation and apoptotic bodies.

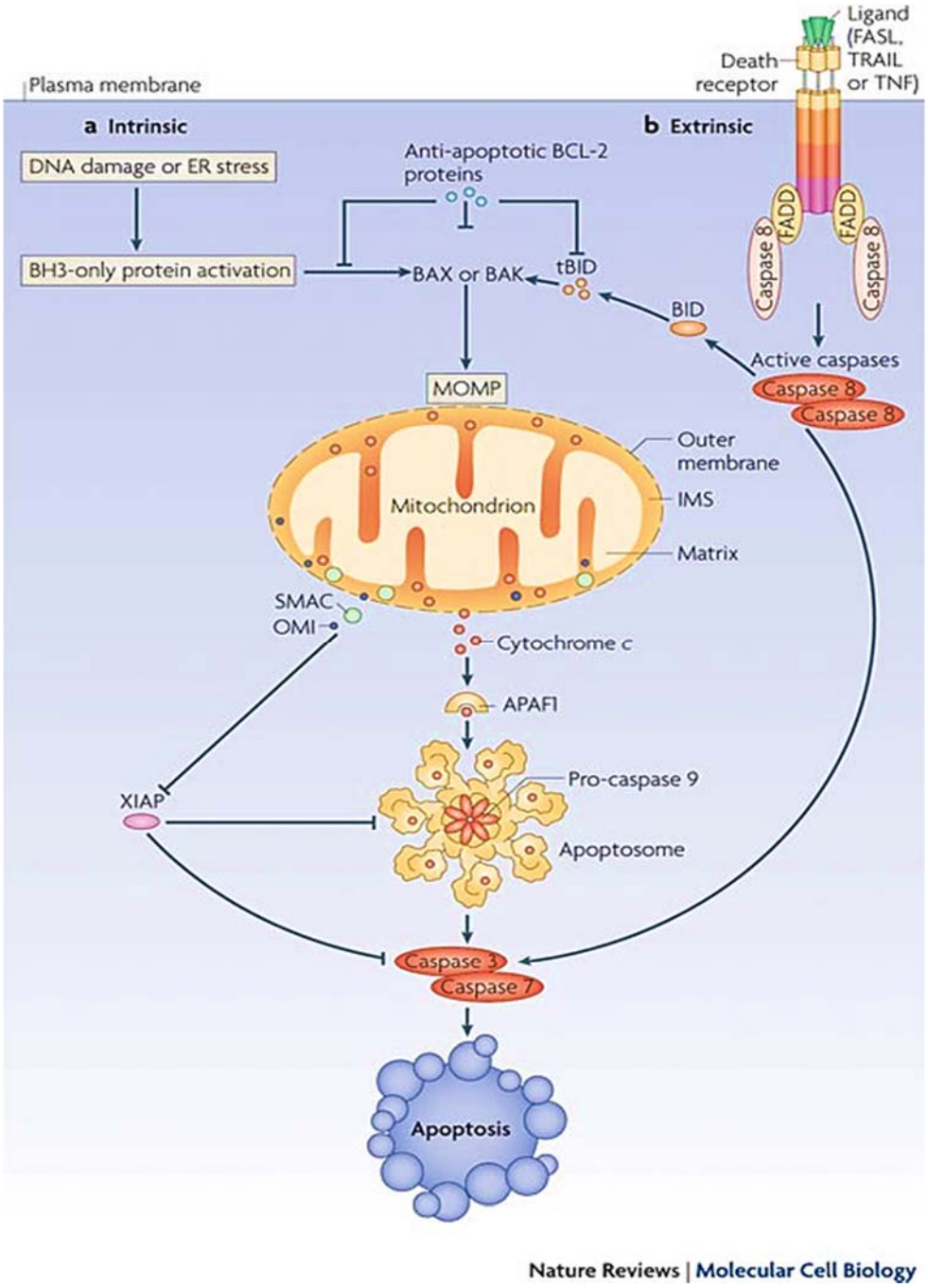

Figure 36. Intrinsic and extrinsic apoptotic cell death. See text for details. From (Tait & Green, 2010).

One of the most important effector caspases of intrinsic and extrinsic apoptosis is caspase 3, which induces the cleavage of CAD (caspase-activated DNAse) for DNA breakdown (Cavalcante et al., 2019), but also α-fodrin for cytoskeletal modifications (Jänicke, Ng, Sprengart, & Porter, 1998). This cytoskeletal protein is dually cleaved by caspase 3 and calpain 1, another type of cysteine protease (Siman, Baudry, & Lynch, 1984).

4.2.1.2 Calpains

Calpains are Ca^{2+}-activated cysteine proteases similar to caspases. In resting conditions, calpains are found as inactive pro-enzymes or bound to calpastatin, the endogenous inhibitor, while, when active, target and cleave different substrates. Both cysteine proteases, when active, induce apoptosis, nevertheless calpains are also involved in necrotic cell death (Wang, 2000).

Calpain family, containing 15 members, can be divided in classical and non-classical type, depending on the presence or not of a penta-EF hand. Thus, classical calpains (1, 2, 3, 8, 9, 11, 12 and 14) contain a penta-EF hand that binds to Ca^{2+}, while non-classical calpains (5, 6, 7, 10, 13, and 15) lack this domain. The most studied calpains are calpain 1 and calpain 2, respectively named μ-calpain and m-calpain for the Ca^{2+} concentration necessary to activate it. In fact, μ-calpain needs 3-50μM of Ca^{2+} for its activation, while m-calpain 0.4-0.8mM (Cheng, Wang, Lei, Wang, & Xiong, 2018). All these calpains, targeting different substrates, are localised in cytosol, mitochondria, ER etc (Smith & Schnellmann, 2012). For example, in cytosol, **PTEN** (phosphatase and tensin homolog), which converts $PI(3,4,5)P_3$ into $PI(4,5)P_2$, is considered a key substrate for calpain 2 since incubation of purified human PTEN with calpain 2 and Ca^{2+} for 1h at 37°C reduced PTEN levels giving several breakdown products of lower molecular weight. A slight decrease in MW, and the appearance of a long upper band, upon incubation with calpain 1 and Ca^{2+} for 1h at 37°C is also observed (Briz et al., 2013).

In mitochondria, calpain 10 is the only calpain that contains an MTS and is found in the matrix, while calpain 1 and 2 are found in the IMS, as shown in **Figure 37**. Calpain 10 cleaves **OXPHOS proteins**, such as Complex V (ATP synthase β) and subunities of Complex I (NDUFV2, NDUFB8) decreasing mitochondrial respiration. In contrast, calpain 2 seems to cleave **VDAC** (Smith & Schnellmann, 2012) and **Mortalin** (GRP75 or mitochondrial heat shock 70-kDa protein) (Ozaki, Yamashita, & Ishiguro, 2009), a mitochondrial chaperone, which has been described interacting with frataxin, *in vivo* in mouse cortex and *in vitro* in cortical neurons, (Dong et al., 2019). Although it has not been described a possible cleavage by calpain, an over expression of this stress response protein is related to survival increase and the interaction with calpain suggests a possible cleavage (Londono, Osorio, Gama, & Alzate, 2012). Meanwhile, **NCLX**, BH3-interacting domain death agonist (**Bid**) and apoptosis-inducing factor (**AIF**) seem to be substrates of calpain 1. Interestingly, the cleavage of Bid induces the formation of tBid,

a pro-apoptotic protein important for MOM rupture and mPTP opening during mitochondrial apoptotic cell death, while the cleavage of AIF induces the release in the cytosol of tAIF, a factor important for chromatin condensation and DNA fragmentation in apoptosis. Furthermore, the cleavage of NCLX and OXPHOS subunities can induce the conditions of Ca^{2+}_m overload and mitochondrial depolarisation for mPTP opening (Smith & Schnellmann, 2012). Thus, activation of calpains trigger events of mitochondrial apoptotic cell death.

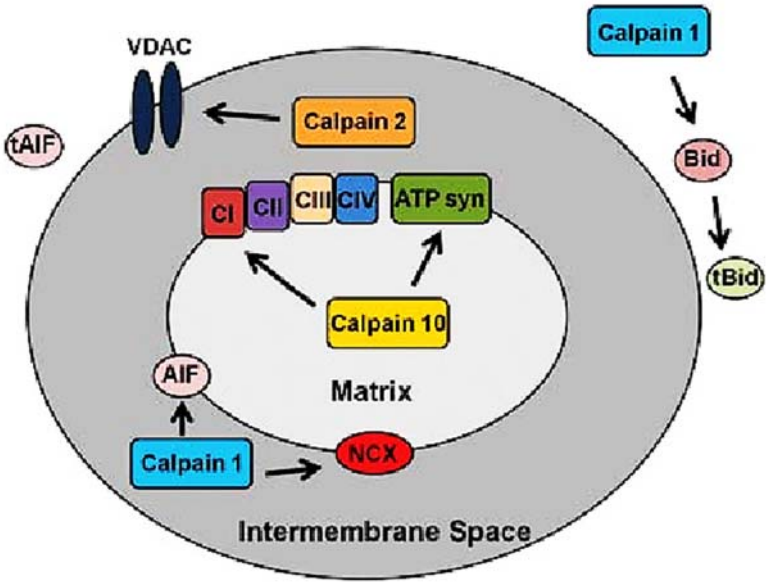

Figure 37. Substrates of mitochondrial calpains. See text for details. From (Smith & Schnellmann, 2012).

4.2.2 *Inhibitors of mPTP opening*

As mPTP opening is important in neurodegeneration and other diseases, many efforts have been directed towards the discovery of drugs capable of inhibiting it. However, neither the action neither the structure of this pore have been fully characterised, thus, the efforts are even harder. Even if the structure is controversial, the matrix cyclophilin D (CypD) is widely accepted as its main regulator. Hence, pharmacological regulation of CypD can modulate mPTP opening.

Different drugs have been detected as inhibitor of mPTP opening (**Figure 38**):

- Cyclosporine A (CsA);
- N-methyl-D-alanine-3-N-ethyl-valine-4-cyclosporine (Alisporivir or Debio025);
- N-methyl-isoleucine-4-cyclosporine (NIM811);

- Quinolinium-Cyclosporine A (JW47);
- Olesoxime (TRO19622);
- 3,5-Seco-4-nor-cholestan-5-one oxime-3-ol (TRO40303);

Even if the exact mechanism of action for each drug is not known, the first three molecules have been suggested as CypD inhibitors, being CsA the better characterised (Šileikytė & Forte, 2016).

CsA binds CypD, avoiding its interaction with mPTP. However, CsA, apart from its action on CypD, exerts immunosuppressive effects by forming a complex with CypA and calcineurin, a Ca^{2+}-activated phosphatase. This complex abolishes the calcineurin activity on nuclear factor of activated T cells (NFAT). Thus, promoting the phosphorylation of NFAT and its cytosolic localisation (details in the next sections). These immunosuppressive properties reduce the risk of organ rejection after organ transplantation (Naoumov, 2014).

Alisporivir (**Debio025**, licensed by Debiopharm Group) differs from CsA for two aminoacids. These artificial modifications abolish the affinity with calcineurin, increasing the affinity for Cyps, thus, conferring non-immunosuppressive effects. In fact, even if it binds CypA, Alisporivir cannot bind calcineurin, thus, being unable to inhibit calcineurin, it cannot exert immunosuppressive effects (Naoumov, 2014).

JW47 is a recently synthesized mitochondrial-targeting CsA, which carry a quinolinium cation to facilitates the mitochondrial import (Warne et al., 2016).

TRO40303 has been described as a modulator of mPTP opening by binding the cholesterol site of TSPO, an OMM-translocator protein also named Peripheral Benzodiazepine Receptor, which was earlier considered part of mPTP (Šileikytė & Forte, 2016).

TRO19622 is a cholesterol-like compound, which binds TSPO, and voltage-dependent anion channel (VDAC) and can cross the blood/brain barrier. Even if TSPO is no longer considered part of mPTP, the role of VDAC in mPTP structure is widely accepted. Interestingly, TRO19622 has been demonstrated to modulate mPTP opening in a variety of cells, in particular neurons, but not in isolated mitochondria. In fact, its neuroprotective role has been demonstrated in trophic factors-deprived motoneurons and K^+-deprived cerebellar granule neurons, in which, respectively, increase survival and neurite outgrowth and decreased cytochrome c release, but also in Amyotrophic

Lateral Sclerosis (ALS) and Spinal Muscular Atrophy (SMA) *in vivo* and *in vitro* models, but not isolated liver mitochondria. This characteristic suggests an indirect role of olesoxime in mPTP opening modulation, probably, mediated by reduced ROS production, thus, higher threshold of mPTP opening in response of Ca^{2+} (Bordet, Berna, Abitbol, & Pruss, 2010).

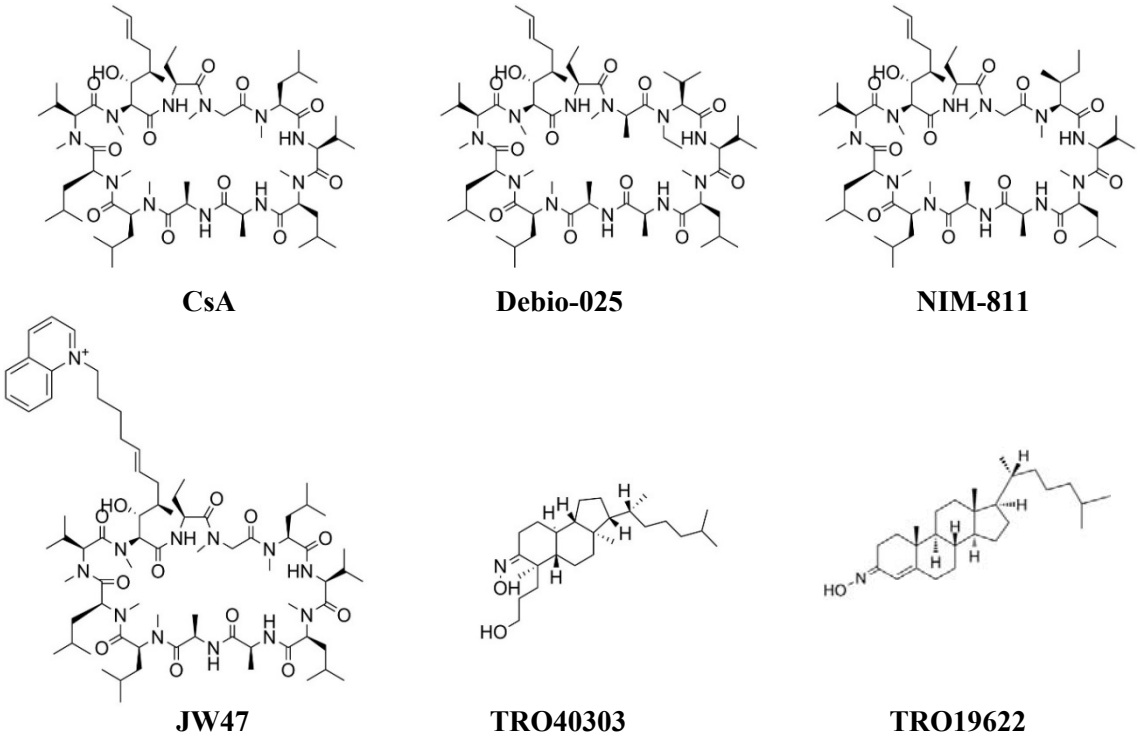

Figure 38. Chemical structures of mPTP inhibitors. Three of them (CsA, Debio-025 and TRO19622) have been used in this work. Modified from (Šileikytė & Forte, 2016). Structure of TRO19622 has been taken from https://www.medchemexpress.com/.

5 CROSSTALK MITOCHONDRIA-CYTOSOL-NUCLEUS

Variations in mitochondrial status are detected by the cells through a retrograde signal, in which mitochondria sends signals to other organelles and nucleus, changing gene expression, and starting mechanisms of mitochondrial biogenesis, mitophagy (removing damaged mitochondria), fusion/fission and mitochondrial movements.

Mitochondrial signalling can be mediated by ROS, Ca^{2+} and $\Delta\Psi_m$ but also sirtuin ($NADH/NAD^+$), AMPK (ATP/AMP), mTOR (ATP/ADP) or HIF1α (succinate/α-ketoglutarate). At least one of these signals can initiate mammalian retrograde signalling (from mitochondria to nucleus) (Cagin & Enriquez, 2015). The nuclear-cytoplasmic communication is often regulated by Ca^{2+}, by the fact that Ca^{2+} concentration can regulate opening ($+Ca^{2+}$) and closing ($-Ca^{2+}$) of the nuclear face of nuclear pore complex through its conformation change. Then, it can mediate the crossing of transcriptional factors leading to changes in gene expression (Stoffler, Goldie, Feja, & Aebi, 1999), such as activation of NFAT, NFKβ, mitogen-activated protein kinases (MAPK) and Ca^{2+}/Calmodulin (CaM)-dependent protein kinase type IV mediated activation of CREB (Cagin & Enriquez, 2015).

5.1 Phosphorylation state and gene expression alterations

5.1.1 CREB/ pCREB

CREB (Cyclic adenosine monophosphate-Response Element-Binding protein) is a transcription factor that, in neurons, is involved in neuronal survival, neuronal plasticity, excitability and memory. Upon increase of $[Ca^{2+}]_c$, PKA, CaM-dependent kinases, ERK or MAPK can activate CREB by phosphorylation. While CaMKII phosphorylates CREB at the activating site Ser133 and inactivating site Ser142, CaMKIV and PKA phosphorylate it only at the activating site. When activated, in nucleus, pCREB recruits co-activators such as CBP (CREB-binding protein) and binds CRE (cAMP Response Elements) sequence onto promoters of target genes. Thus, de-phosphorylation mediated by PTEN, protein phosphatase 2A or 1 (PP2A or PP1), turns back CREB to its inactive state (Steven et al., 2020). Thus, the duration of pCREB is important for a correct gene expression, in fact, a prolonged stimulus reduces the activity of phosphatases, allowing target genes expression (Belgacem & Borodinsky, 2017).

5.1.2 NFAT/ pNFAT

NFAT (Nuclear Factor of Activated T cells) is a transcription factor, which was firstly discovered in T lymphocytes, however, it is also expressed in sensory neurons (Kim & Usachev, 2009). Five NFAT isoforms (NFAT1-5) have been identified, specifically: NFAT1 (NFATc2); NFAT2 (NFATc1); NFAT3 (NFATc4); NFAT4 (NFATc3) and NFAT5. NFAT1-4 are generally regulated by Ca^{2+}, while NFAT5 by osmotic stress, with NFATc3 and NFATc4 are mainly associated with neurodegenerative changes (Kipanyula, Kimaro, & Seke Etet, 2016). In normal conditions, hyper-phosphorylated and inactive NFAT is localised in the cytosol. In the case of an increase of $[Ca^{2+}]_c$, Ca^{2+}-activated proteins such as calcineurin, a Ca^{2+}/calmodulin-dependent serine/threonine phosphatase also named protein phosphatase 2B (PP2B), dephosphorylates NFAT in multiple N-terminal phosphoserine sites and activates it. Generally, NFAT activation needs a massive amount of Ca^{2+}, in fact, the only release from ER does not seem to activate it, but ER can actuate together with Ca^{2+} influx from extracellular space (Kipanyula et al., 2016). For example, electrical stimulus (K^+), TRPV1 agonists or neurotrophins such as substance P, brain-derived neurotrophic factor (BDNF), nerve growth factor (NGF) and bradykinin, can increase $[Ca^{2+}]_c$ through plasmatic membrane, activating NFAT in neurons (Smith, 2009). In DRG neurons, upon external stimulus, Ca^{2+} enters into the cells and is rapidly buffered by mitochondria, slowly released back to the cytosol via NCLX and extruded from cells via PMCA or NCX. Blocking both, $Ca^{2+}{}_m$ uptake and $Ca^{2+}{}_m$ release, NFAT activation can be drastically decreased, while repetitive external stimulus triggers prolonged Ca^{2+} release from mitochondria facilitating de-phosphorylation of NFATs, indicating a role of mitochondria in its activation in DRGs (Kim & Usachev, 2009).

The hypo-phosphorylation of NFAT, mediated by calcineurin, allows activation of transcription factor by exposing a nuclear localisation signal (NLS), which determines its nuclear import (Hogan, Chen, Nardone, & Rao, 2003). NFAT translocation into the nucleus, which can have different velocity depending on the isoform (being NFATc4 the slowest) and can be cell type-specific (being NFATc3 and NFATc4 mainly present in DRG neurons), can be blocked by calcineurin inhibitors such as FK506 (tacrolimus) and cyclosporine A (CsA), which block the calcineurin interaction with its substrates for all the isoforms of NFATs (Vihma, Luhakooder, Pruunsild, & Timmusk, 2016). In DRG neurons, an electrical stimulation with 15mM K^+ for 20min rapidly increases the

amount of NFATc3 in nucleus, while NFATc4 needs 40mM K^+ for 180min for a gradual and slower nuclear import, indicating that NFATc3-dependent transcription occurs in response to mild depolarisation, while NFATc4-dependent in response to prolonged depolarisation. These variations can be ascribed to the fact that the isoforms are differently dephosphorylated in response to stimuli, being NFATc3 more rapidly dephosphorylated by calcineurin (Ulrich et al., 2012).

Once in the nucleus, different isoforms of NFATs, in complex with other transcription factors, regulate the expression of gene encoding for axonal growth, synaptic plasticity, neuronal survival, excitability, neuronal development, nociception (Vihma et al., 2016) and immune modulators or activators such as: gamma interferon (IFNγ); interleukins; Fas ligand; cyclooxygenase 2 (COX-2); and tumor necrosis factor alpha (TNF-α), but also Ca^{2+} regulators such as inositol 1,4,5-trisphosphate (IP_3) receptor (IP_3R) and pro-apoptotic signals (Kipanyula et al., 2016). For example bradykinin, a peptide secreted from the site of injury in acute pain, can bind receptors that stimulate Ca^{2+} influx and phospholipase C (PLC) to produce IP_3, which induces IP_3-dependent Ca^{2+} release from ER store and activates NFAT in DRG neurons, resulting in NFAT-dependent transcription of proinflammatory signals such as COX2 (Jackson, Usachev, & Thayer, 2007; Smith, 2009).

Once $[Ca^{2+}]_c$ is restored at basal levels, NFAT can be phosphorylated by protein kinases in the nucleus, such as glycogen synthase kinase (GSK3β), which requires a priming phosphorylation by PKA for its function, and pNFAT can be transported into the cytosol, however, a prolonged and persistent $[Ca^{2+}]_c$ retains NFAT in the nucleus (Hogan et al., 2003). Isoform-dependent variations in phosphorylation have been also detected in DRG neurons, in fact, NFATc4 translocation into the nucleus is more strongly regulated by a prolonged depolarisation together with GSK3β silencing, probably due to a persistent GSK3β-dependent phosphorylation, which can also occur in the cytosol and repress nuclear translocation (Ulrich et al., 2012).

5.1.2.1 Calcineurin inhibition

As NFAT induces the expression of proinflammatory signals, many drugs are used to inhibit calcineurin and maintain NFAT in phosphorylate state in order to suppress the immune system, such as cyclosporine and tacrolimus (FK506). Both antifungal drugs are normally used in post-transplantation to avoid organ rejection and other pathologies (Bierer, Holländer, Fruman, & Burakoff, 1993; Schreiber & Crabtree, 1992). As

indicated in **Figure 39**, calcineurin is formed by the enzymatic subunit A and the regulatory subunit B. When the subunit A binds to calmodulin and Ca^{2+}, a conformational change unmasks the catalytic active site important for phosphatase activity. When CsA binds the cyclophilin A or tacrolimus binds the FK506-binding protein 12 (FKBP-12), calcineurin changes its conformation, limiting the access to its active site (Hemenway & Heitman, 1999; Sieber & Baumgrass, 2009).

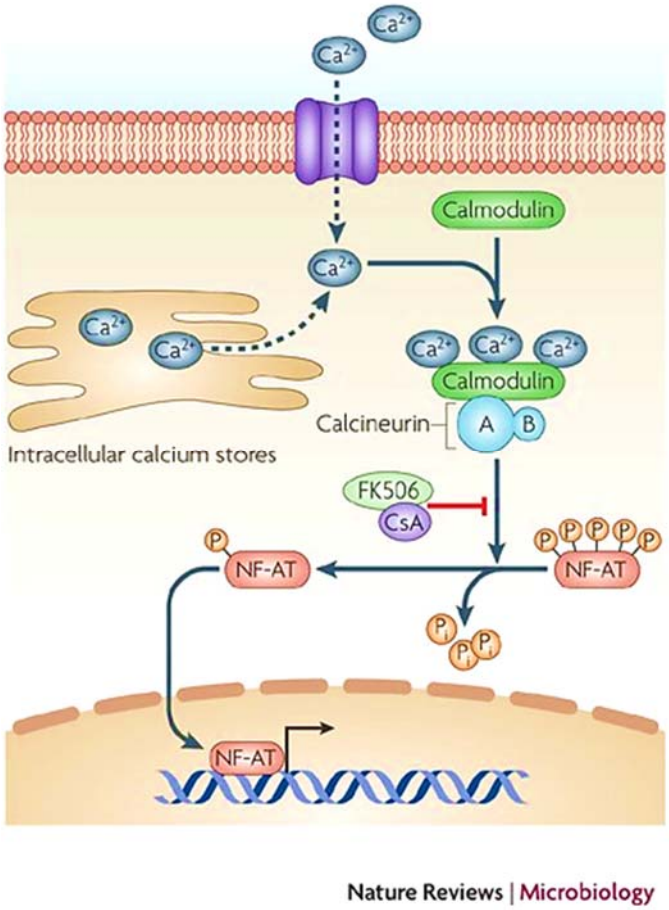

Figure 39. NFAT pathway and regulators. See text for details. From (Steinbach, Reedy, Cramer, Perfect, & Heitman, 2007).

5.1.3 PTEN

Phosphatase and Tensin homolog deleted on chromosome 10 (PTEN) is a potent tumour suppressor that regulates multiple cellular functions, not only in tumours but also in neurons, such as energy metabolism, survival, proliferation, cellular architecture, and motility (Worby & Dixon, 2014). PTEN is a dual phosphatase that is involved in a canonical and a not-canonical pathway. In the canonical pathway, PTEN localises in the cytoplasm, generally in neoplastic or actively dividing cells, and dephosphorylates lipid substrates, while in not-canonical pathway localises in nucleus, mainly in normal,

differentiated and quiescent cells, and dephosphorylates protein substrates (Worby & Dixon, 2014). However, in apoptotic cells, PTEN seems to localise more prominently in cytosol (Chung & Eng, 2005). This nuclear or cytoplasmic localisation of PTEN seems to be regulate by Ca^{2+} and magnesium concentrations, in fact, PTEN interacts with major vault proteins (MVP), proteins important for nuclear translocation in a Ca^{2+}-dependent manner and the interaction is inhibited in the presence of Mg^{2+} for a conformational change. Thus, nuclear localisation of PTEN is decreased by increasing Ca^{2+} levels in culture medium in a dose-dependent manner (Minaguchi, Waite, & Eng, 2006).

5.1.3.1 PTEN canonical pathway

In the cytoplasm, PTEN dephosphorylates its lipid substrate, phosphatidylinositol 3,4,5-trisphosphate (PIP_3) to produce phosphatidylinositol 4,5-bisphosphate (PIP_2), thus antagonising the phosphatidylinositol 3-kinase (PI3K)/AKT signalling pathway. PTEN deficiency, generally, induces increased levels of intracellular PIP_3 and activation of AKT, a serine/threonine kinase. Then, activated AKT phosphorylates and inhibits GSK3β activating glycogen synthase and regulating fatty acid synthesis; promotes glucose uptake by increasing the presence of glucose transporter GLUT4 on plasma membrane and activates mTOR (Worby & Dixon, 2014).

5.1.3.2 PTEN not-canonical pathway

Even though PTEN does not carry nuclear localisation signals (NLS), in the not-canonical pathway, PTEN localises in the nucleus, in a cell-cycle dependent manner, but also in oxidative stress conditions, where it plays important roles in chromosome stability, DNA repair and transcriptional regulation by de-phosphorylating transcription factors (Worby & Dixon, 2014). For example, CREB has been demonstrated to be a PTEN phosphatase target, in fact, PTEN deficiency leads to CREB phosphorylation independent of the PI3K/AKT pathway (Gu et al., 2011). The activity of PTEN is regulated at several levels: posttranslational modifications (e.g. ubiquitination), where PTEN downregulation via ubiquitin-mediated degradation is considered the main mechanism of loss of PTEN function; protein–protein interactions; transcriptional regulation, where PTEN is positively regulated by others transcription factors (e.g. PPARγ); microRNAs (miRNAs); long noncoding RNAs (lncRNAs) and antisense RNA (asRNA) (Worby & Dixon, 2014). For example, in rat DRG neurons, after nerve injury,

the up-regulation of a particular miRNA (miR-222) has been shown to reduce PTEN mRNA and protein levels, and, interacting with CREB, mediate PTEN-dependent CREB phosphorylation, probably leading to mechanisms of axonal regeneration (Zhou et al., 2012). During synaptic plasticity, it has been described that PTEN can be degraded by calpains in the brain (Briz et al., 2013). Another study has shown that a proteasome and calpain inhibitor I (A6185) blocks PTEN degradation and AKT activation, by increasing its nuclear localisation, after brain ischemia (Zhang, Wu, Han, & Zhang, 2007). Other authors indicate also PTEN at MAMs and ER, where seems to be important in Ca^{2+} signalling and apoptosis. In fact, a PTEN construct which increases its localisation in ER, increases Ca^{2+} release from ER, by de-phosphorylating IP_3Rs at MAMs, thus increasing Ca^{2+} transfer from ER to mitochondria and Ca^{2+}-induced mitochondrial apoptosis. Silencing PTEN, then, induces a slower release from ER to mitochondria upon ATP stimulus, which acts on plasma membrane receptors to produce IP_3, due to more phosphorylated IP_3R (Bononi et al., 2013). However, some authors indicate also that PTEN can localise to mitochondria and regulate mitochondrial-dependent apoptosis after staurosporine treatment, an unspecific inhibitor of protein kinases and apoptosis inductor (Zhu, Hoell, Ahlemeyer, & Krieglstein, 2006).

Recently, it has been identified a translational variant of PTEN, PTEN-long or PTEN-L, whose translation is initiated at a CUG codon 519 bp upstream and in frame with the known AUG translation start site for PTEN. PTEN-L adds 173 N-terminal aminoacids to the normal PTEN sequence (Worby & Dixon, 2014) and its synthesis is due to an eukaryotic initiation factor 2A (eIF2A)-dependent CUG initiation at the mRNA that determine an alternative translation (Liang et al., 2014). While PTEN is localised mainly in nucleus or cytosol, PTEN-L mainly in cytosol, secreted from cells (Worby & Dixon, 2014) or in mitochondria, where seems to target the complex IV of oxidative phosphorylation, enhancing its activity and inhibit Pink1 in the Pink1-Parkin mediated mitophagy (Liang et al., 2014). A summary of PTEN and PTEN-L functions is shown in **Figure 40**.

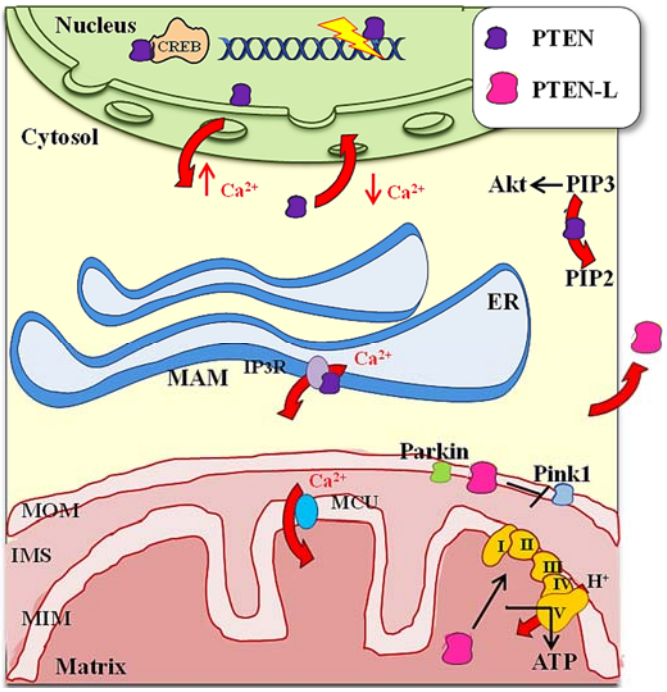

Figure 40. Localisation and functions of PTEN and PTEN-L. See text for details. Based on (Liang et al., 2014; Wang, Cho, et al., 2018; Worby & Dixon, 2014).

5.1.4 PPARgamma

The family of peroxisome proliferator-activated receptor (PPARs) is composed of PPARα, PPARβ/δ and PPARγ. The ligand-activated nuclear receptor PPARγ, mainly present in brain and heart, has been shown to regulate lipid/glucose metabolism, however, seems to regulate also anti-inflammatory responses, cell activation, differentiation, proliferation, and/or apoptosis (Lee et al., 2005). In neurons, PPARγ promotes neuronal differentiation, axon polarity, neurite outgrowth and pain signalling (Quintanilla, Utreras, & Cabezas-Opazo, 2014), but also plays a role in energetic metabolism by increasing mitochondrial biogenesis and mitochondrial functions such as ATP production (Landreth, Jiang, Mandrekar, & Heneka, 2008). In sensory neurons, it has been involved in response to injury. In fact, injury determined an increase of PPARγ transcript and protein, retrograde transport of PPARγ from axons to cell body and accumulation in the nuclei. These events seem involved in the mechanisms of axonal regeneration of sensory neurons (Lezana et al., 2016).

Natural ligands of PPARγ are linoleic acid and prostaglandin, both involved in the inflammatory response (Quintanilla et al., 2014). Ligand-activated PPARγ, together with other nuclear receptors such as retinoid X receptor (RXR) and coactivators, binds

particular regions in the DNA named peroxisome proliferator response elements (PPRE) in the promoter of genes. This binding induces the expression of target genes such as acyl-CoA oxidase, important for the β-oxidation of fatty acids (Dreyer et al., 1993), but also the inhibition of NFκB-dependent promoters such as inflammatory cytokines, chemokines, matrix metallopeptidases (MMPs), COX-2 and inducible nitric oxide synthase (iNOS), necessary for the inflammatory response (Landreth et al., 2008). PPARγ activation also stimulates the anti-oxidant NRF2/ARE pathway and the expression of proteins essential for cell survival, mitochondrial function and quality control. For example, some proteins important for TIM/TOM machinery. In the absence of ligands, PPARγ/RXR heterodimer on PPRE binds corepressors, such as nuclear receptor corepressor (NCoR), transducin β-like protein, and HDACs, which induce the gene repression (Cai et al., 2018).

5.1.4.1 PPARγ/PGC1α pathway

Peroxisome proliferator-activated receptor coactivator-α (PGC1α) is one of the most frequent PPARγ coactivators. Its expression seems to be stimulated by PPARγ (but also mTOR, CREB, p53) (Cagin & Enriquez, 2015). PGC1α activity is post-translational regulated by AKT and MAPK, and upon activation of PGC-1α by phosphorylation or de-acetylation, PGC-1α activates NRF1, NRF2 and PPARγ (Jiang et al., 2019). The PPARγ/PGC1α pathway regulates the energetic metabolism, in fact, its presence induces mitochondrial biogenesis and regulates mitochondrial function by stimulating the mitochondrial mass, the expression of OXPHOS proteins and by increasing DNA copy numbers (Landreth et al., 2008). PGC1α also regulates mitochondrial transcription factor A (TFAM), a transcription factor involved in transcription of mitochondrial DNA (mtDNA)'s genes. This function seems due to an interaction between TFAM and PGC1α in the mitochondria (Austin & St-Pierre, 2012). An increase in mitochondrial function and biogenesis should increase ROS, however, this pathway induces the expression of anti-oxidant enzymes such as SOD1, SOD2 and catalase, leading to a more efficient mitochondrial respiration (Corona & Duchen, 2016). Lower activity of PGC1α seems involved in ageing and several neurodegenerations such as AD, PD, ALS and HD (Austin & St-Pierre, 2012). PPARγ/PGC1α pathway is also deregulated in frataxin deficiency, thus, supporting PPARγ agonists as potential therapies for FA (Coppola et al., 2009; Marmolino et al., 2010).

5.1.4.2 PPARγ agonists

Benefits of PPARγ agonists have been observed in diabetes mellitus type 2 and several neurodegenerative conditions such as AD, ALS, ischemia and spinal cord injury. These agonists seem to actuate as anti-inflammatory, anti-apoptotic and anti-oxidant molecules (Corona & Duchen, 2016).

- **Thiazolidinediones (TZD)**

PPARγ agonists such as thiazolidinediones (TZD) are used to treat diabetes type 2 because these drugs reduce blood glucose levels. However, neuroprotective effects of these drugs are also observed (Quintanilla et al., 2014). PPARγ agonists **rosiglitazone (RGZ)** and **pioglitazone (PGZ)** are two TZDs drugs, which increase PPARγ activation and levels and up-regulate PTEN expression (Lee et al., 2005). In DRGs, PGZ reduces neuropathic pain by protecting against oxidative stress and Ca^{2+} alterations. The protective anti-oxidant effect is due to the increased activity of ROS-reducing enzymes (Khasabova et al., 2019) and reduced presence of pro-inflammatory cytokines such as TNFα and IL-6 (Maeda, Kiguchi, Kobayashi, Ozaki, & Kishioka, 2008). Also, the PPARγ agonists-mediated neuroprotection seems to involve other mechanisms. In fact, RGZ protects DRG neurons against an amyloid beta-mediated mitochondrial damage and apoptosis due to NGF deprivation. These anti-apoptotic effects involve Bcl-2 up-regulation (Fuenzalida et al., 2007). PPARγ agonists also have effects on Ca^{2+} homeostasis. In fact, in hippocampus neurons, RGZ reduces voltage-gated Ca^{2+} channel (VGCC)-mediated currents, while PGZ reduces NMDA receptor (NMDAR)-mediated Ca^{2+} currents, leading to decreased cellular Ca^{2+} entry (Pancani et al., 2009). Other actions mediated by PPARγ in CNS seem to be protection from demyelination and BBB disruption (Cai et al., 2018).

Despite the neuroprotective effects of PPARγ agonists, these drugs also have side effects. For example, in the case of FA, TZDs induces thrombosis and increases the incidence of heart failure (Quintanilla et al., 2014). For this reason, it has been produced by Minoryx Therapeutics **leriglitazone (MIN-102)**, a new brain-penetrating PPARγ agonist, selective for PPARγ and improved for CNS diseases. This novel drug is nowadays under a phase II clinical trial for FA in Europe for its effects in increasing FXN protein and up-regulating PGC1α, thus reducing oxidative stress probably by increasing NRF2 activation and SOD1/2 gene expression, restoring mitochondrial

function and consequently lipid metabolism, Ca^{2+} homeostasis and neuronal survival, as shown in **Figure 41** (Rodríguez-Pascau et al., 2020).

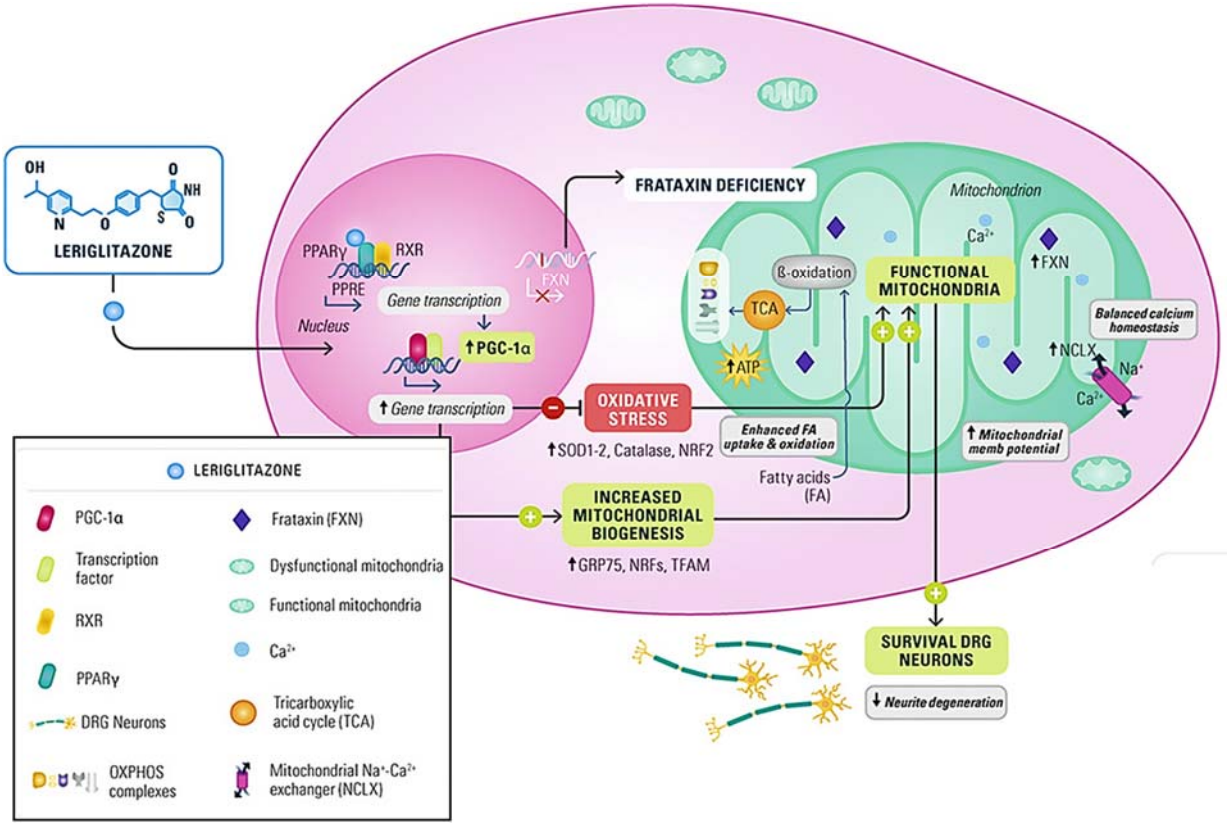

Figure 41. Actions of leriglitazone in frataxin-deficient cells. See text for details. Modified from (Rodríguez-Pascau et al., 2020).

❖ **Non-Thiazolidinediones (TZD) agonists**

PPARγ agonists different from TZDs are named as non-TZD agonists. In these groups are present: **ciglitazone, netoglitazone** and **rivoglitazone**. These group of PPARγ agonists is less studied (Corona & Duchen, 2016).

5.1.5 NRF2

Nuclear factor erythroid 2- related factor 2 (NRF2) is a transcription factor that confers cellular protection from oxidative insult and regulates gene expression by binding a particular region, named the anti-oxidant response element (ARE), in promoters or enhancers of several genes. For example induces the expression of anti-oxidant enzymes such as superoxide dismutase and glutathione. NRF2 induces the expression and activation of PPARγ, but also PPARγ induces the NRF2/ARE axis. These two axes,

NRF2-PPARγ actuate synergistically for anti-oxidant and anti-inflammatory response and some anti-oxidant enzymes, such as SOD, present ARE and PPRE elements (Cai et al., 2018). As represented in **Figure 42**, in cytosol, E3 ligase adapter Kelch-like ECH-associated protein 1 (Keap1) interacts with NRF2 and presents NRF2 for ubiquitination by E3 ligase and degradation by proteasome. When ROS oxidize cysteines present in a thiol-reach region of Keap1, the interaction between NRF2 and Keap1 is avoided and NRF2 can enter in the nucleus for the expression of ARE-target genes. The same NRF2 gene shows ARE regions, thus, NRF2 transcript levels are auto regulated (Robledinos-Antón, Fernández-Ginés, Manda, & Cuadrado, 2019). In frataxin-deficient DRGs, despite oxidative stress induces NRF2 activation, NRF2 transcript and protein levels are decreased and the accumulation of NRF2 in the nucleus is reduced (Shan et al., 2013).

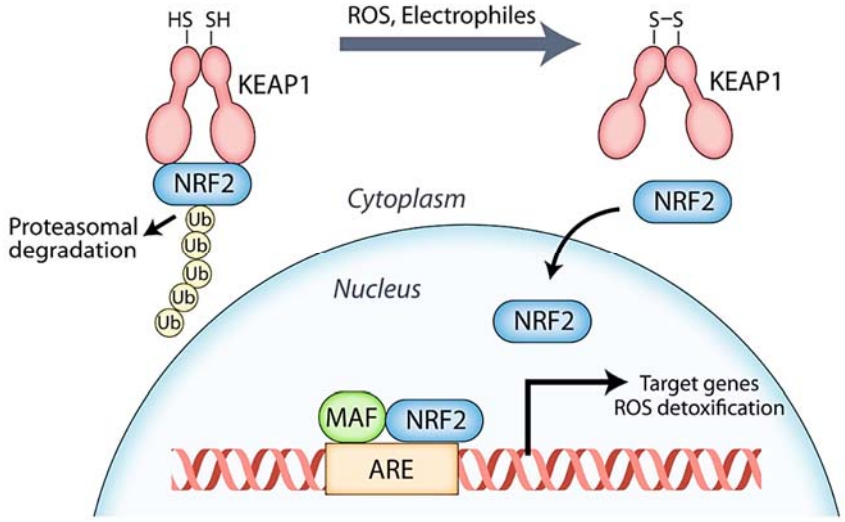

Figure 42. Scheme of NRF2 activation. See text for details. Modified from (Hiebert & Werner, 2019).

5.1.5.1 NRF2 inducers

NRF2 inducers are divided in different categories considering how NRF2 is activated:

Electrophilic compounds can modify cysteines present in the thiol-reach region of Keap1. One of the electrophilic NRF2 inducers is **omaveloxolone (RTA-408)**, which induces modifications in the cysteines of Keap1 and prevents the ubiquitination of NRF2, thus its degradation by proteasome. In this manner, more NRF2 can enter into the nucleus and target ARE-containing genes. Other drugs such as **dimethyl fumarate (DMF)**, **curcumin**, **genistein**, **sulforaphane**, **quercetin** and **resveratrol** induce NRF2-mediated gene expression using the same mechanism (Robledinos-Antón et al., 2019).

Protein-protein interaction inhibitors compounds can inhibit the interaction between NRF2 and Keap1. They are **truncated NRF2 peptides**, which bind Keap1, thus avoiding the degradation by proteasome of endogenous NRF2 (Robledinos-Antón et al., 2019).

6 ACTIVE VITAMIN D_3 IN NEURONS

Vitamin D_3 is a lipid-soluble steroid hormone also named sunshine vitamin because it is synthesized in the skin with the presence of sunlight. This hormone is essential for regulating body levels of Ca^{2+}, P_i, bone mineralisation and bone integrity, but also immune response (Kočovská, Gaughran, Krivoy, & Meier, 2017).

6.1 Vitamin D_3 metabolism

Vitamin D_3 needs several enzymatic steps for its activation, mediated by cytochromes P450 in the presence of ferredoxins and ferredoxin reductases. The last step induces the formation of the biologically active hormone (Miller, 2013).

6.1.1 Ferredoxins and cytochromes

Ferredoxins are small Fe/S cluster containing proteins, which are needed for different functions, and have been shown to interact physically with frataxin (Webert et al., 2014). Frataxin-deficient human granulosa cells display a deficient synthesis of progesterone, a steroid, for alterations in the transfer of electrons from a reductase to CYP11A1, mediated by the mitochondrial adrenodoxin (ferredoxin or FDX) for the conversion of cholesterol to pregnenolone (Palandri et al., 2015). FDX is also needed in other critical cellular functions, for example, calcitriol metabolism, by regulating the action of enzymes involved in its biosynthesis and degradation (Sakaki, Kagawa, Yamamoto, & Inouye, 2005). In fact, FDX and ferredoxin reductase (FDXR), a flavoprotein, donate electrons to the heme group of cytochrome P450 enzymes. In this reaction, nicotinamide adenine dinucleotide phosphate (NADPH) donates electrons to FDXR, which binding FDX, allows electrons transferring into the Fe/S cluster of FDX. Thus, FDX binds cytochrome P450 to transfer the electrons into the heme group of the enzyme. Then, the heme iron mediates the enzymatic reaction for the substrate conversion, as shown in **Figure 43**.

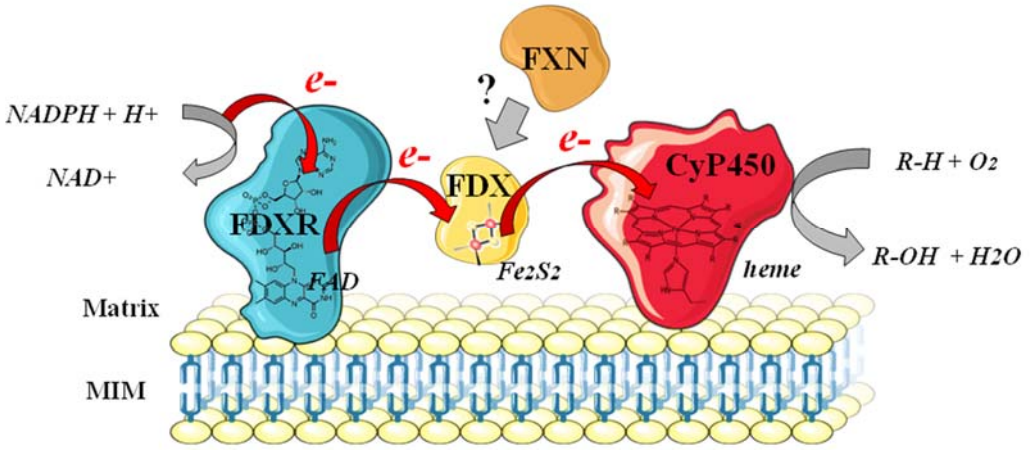

Figure 43. FDXR-FDX-CyP450 complex. See text for details. Based on (Miller, 2013).

6.1.2 Calcitriol synthesis and degradation

The 1α,25-$(OH)_2$-vitaminD_3 (or calcitriol) is the vitamin D_3 active form, which mediates the majority of intracellular actions. Its synthesis occurs in mitochondria when the precursor form 25-OH-vitamin D_3 (or calcidiol) is hydroxylated into calcitriol by the enzymatic activity of the 1α-hydroxylase (Cyp27b1), a heme-containing cytochrome P450 of 55kDa. In this reaction, ferredoxin 1 (FDX1) transfers electrons from FDXR to Cyp27b1 (Pedersen, Ghazarian, Orme Johnson, & DeLuca, 1976; Strushkevich et al., 2011). Historically, while calcidiol synthesis has been ascribed mainly in skin and liver, the synthesis of calcitriol in kidney. As represented in **Figure 44**, calcitriol biosynthesis starts in the skin where sunlight converts 7-dehydrocholesterol to vitamin D_3 (cholecalciferol). A small source of vitamin D_3 is also absorbed in the intestine through the diet. In fact, salmon, sardines, and tuna, contain relatively high amounts of cholecalciferol, while plants provide vitamin D_2 (ergocalciferol). In the blood, vitamin D binding proteins (DBP) are necessary to distribute vitamin D_3 to all organs. In the liver, the vitamin D-25 hydroxylase CYP27A1 adds a hydroxyl group to the C-25 position to form calcidiol, the immediate precursor for active vitamin D_3. Thus, in the kidney, the 1α-hydroxylase CYP27B1 adds another hydroxyl group to the 1 position to form the active hormone calcitriol. Recently, a local calcitriol synthesis has been discovered in many other extra-renal tissues, including brain (Garcion, Wion-Barbot, Montero-Menei, Berger, & Wion, 2002).

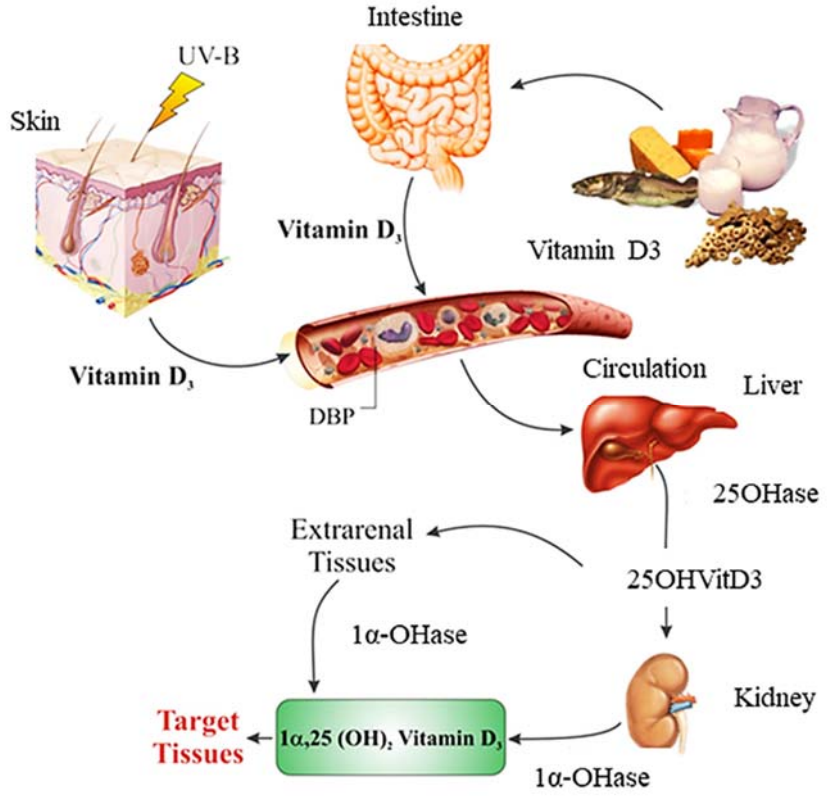

Figure 44. Organs involved in calcitriol biosynthesis. See text for details. Modified from (Zanatta et al., 2011).

Levels of calcitriol are regulated by the enzyme Cyp24A1, which mediates the conversion of calcitriol in 24,25-$(OH)_2$ vitamin D_3 or 1,25-$(OH)_2$ vitamin D_3-26,23 lactone and calcidiol in 25-(OH) vitamin D_3-26,23 lactone, decreasing calcidiol and calcitriol concentration. However, the serum half-life of these metabolites is very different, being 5-15h for calcitriol and 10-21 days for calcidiol. For this reason, but also for the physiological serum concentration of calcitriol ~1000-fold lower than calcidiol, despite being considered calcitriol the active hormone, calcidiol is usually detected in blood analysis (Faye et al., 2019).

6.2 Calcitriol actions

The intracellular actions of calcitriol are mediated by binding to the intracellular vitamin D receptor (VDR), which increases in levels in the presence of calcitriol (Gröschel, Tennakoon, & Kállay, 2015). In the cells, calcitriol can have non-genomic and genomic actions:

6.2.1 *Non-genomic actions*

Non-genomic actions of calcitriol are all the rapid signalling pathways that are triggered by this hormone in the first minutes of addition. In this case, VDR is present in plasma membrane or cytosol. In some cells, an increase of $[Ca^{2+}]_c$ is observed in the first minutes of calcitriol addition. This mechanism seems to involve IP_3, which binding IP_3R induces the release of Ca^{2+} from intracellular stores, but also the activation of PKC, which induces the activation ERKs, MAPKs or PKA. These kinases induce a cascade of signalling that triggers the translocation of VDR into the nucleus for its genomic actions (Hii & Ferrante, 2016).

6.2.2 *Genomic actions*

As indicated in **Figure 45**, calcitriol, by binding VDR and entering into the nucleus, in complex with retinoic acid X receptor (RXR) and coactivators (or corepressors), induces (or repress) the gene expression by binding particular regions of DNA named VDR elements (VDRE). For example, calcitriol represses the *CYP27B1* gene expression, and consequently protein levels, regulating its synthesis (Murayama et al., 1998), as well as regulates the expression of other proteins involved in cellular redox balance (e.g. NRF2) and Ca^{2+} signalling pathways (e.g. Klotho), but also signalling components for cell survival and histone demethylases for epigenetic changes (Forster et al., 2011; Nakai et al., 2014).

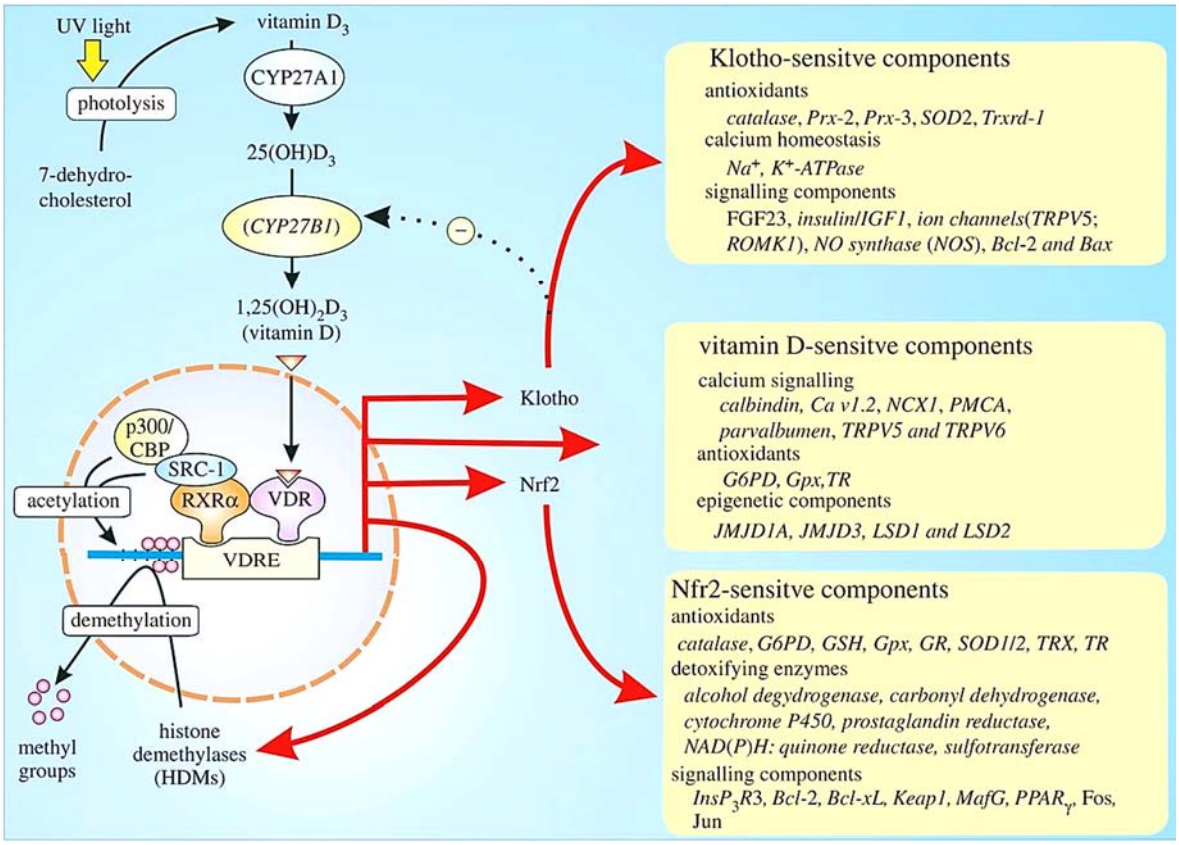

Figure 45. Genomic actions of calcitriol. See text for details. From (Berridge, 2016).

The calcitriol/Klotho/NRF2 pathway, shown in **Figure 46**, induces the expression of Ca^{2+} pumps and exchangers in order to maintain low levels of $[Ca^{2+}]_c$, for example, by upregulating Ca^{2+}-binding proteins for Ca^{2+} buffering, PMCA and NCX1 necessary for Ca^{2+} extrusion and reducing Cav1.2 channel expression in order to avoid Ca^{2+} entry. This pathway induces the expression of anti-oxidant proteins in order to maintain the normal reducing conditions in the cell, for example, by upregulating SOD1, SOD2 and catalase, glutathione peroxidases (Gpx) and reductase (GR) important for ROS scavenging, but also induces the expression of PTEN, which decreases the PIP_3 presence, leading to reduction of ROS. In fact, PIP_3 stimulates NADPH oxidase (NOX) for superoxide formation and calcitriol reduces ROS by down-regulating NOX and upregulating PTEN. Indeed, PTEN up regulation inhibits the PI_3K/Akt/mTOR pathway, leading to autophagy enhancing. Interestingly, ROS can act on RyR and IP_3R to stimulate Ca^{2+} depletion from ER and on PMCA and NCX1 to decrease Ca^{2+} efflux, leading to increased $[Ca^{2+}]_c$. Thus, ROS and Ca^{2+} in mitochondria can induce the opening of mPTP, leading to apoptosis. Calcitriol, by reducing ROS and cytosolic Ca^{2+} levels, but also inducing the expression of anti-apoptotic proteins, e.g. Bcl-2 and Bcl-$_{XL}$,

actuates in order to avoid cell death. Other proteins needed for epigenetic changes are also expressed to induce metabolic reprogramming (Berridge, 2015b, 2016). At the mitochondrial level, calcitriol increases the mitochondrial oxygen consumption rate, mitochondrial biogenesis, mitochondrial volume and induces the expression of pro-fusion proteins, e.g. OPA1, instead of pro-fission proteins, e.g. dynein-related GTPase protein (Drp1) (Ryan et al., 2016). Calcidiol can also bind VDR; nevertheless, the binding affinity is ~100-fold lower than those with calcitriol (Berridge, 2016).

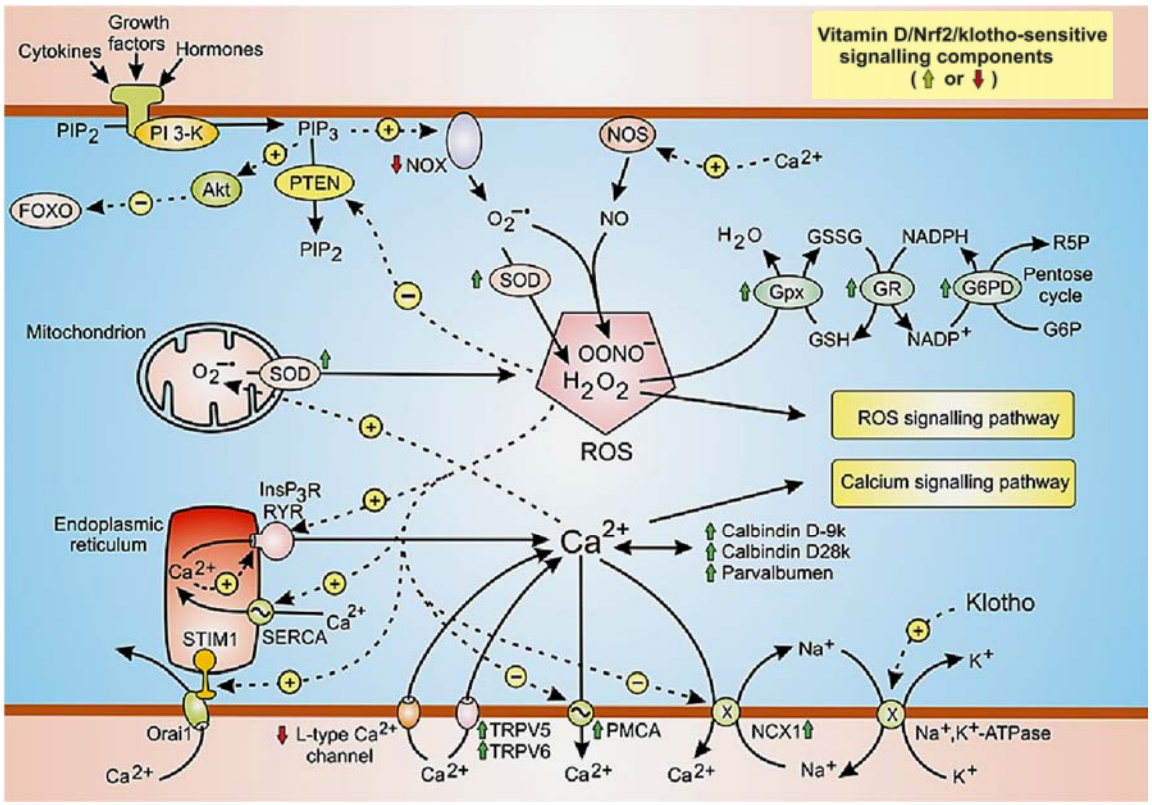

Figure 46. ROS and Ca^{2+} signalling pathways regulated by calcitriol. Arrows represent some of the components that are enhanced or decreased by calcitriol/NRF2/Klotho pathway. See text for details. Modified from (Berridge, 2015a).

6.2.3 *Calcitriol actions in target tissues*

The action of calcitriol involves several target tissues, such as:

- **Macrophages**, where calcitriol induces differentiation in immune cells;
- **Intestine,** where calcitriol increases the absorption in blood of Ca^{2+} and P_i;
- **Bone,** where calcitriol increases mineralisation and osteoclastic differentiation;
- **Parathyroid gland,** where calcitriol decreases parathyroid hormone (PTH) synthesis and release;
- **Vascular cells,** where calcitriol reduces inflammation;

- **Red blood cells,** where calcitriol improves hematopoiesis;
- **Heart,** where calcitriol decreases left ventricular hypertrophy;
- **Pancreas,** where calcitriol increases insulin secretion (Valdivielso, Cannata-Andía, Coll, & Fernández, 2009);

6.2.3.1 Calcitriol actions in Ca^{2+} and P_i metabolism

For its action in parathyroid glands and intestine, calcitriol is considered a "Ca^{2+} and P_i hormone". In fact, low serum Ca^{2+} levels stimulate Ca^{2+}-sensing receptors of parathyroid cells in the parathyroid glands for the release of PTH, which restores serum Ca^{2+} levels by acting on bone and kidneys. In bone, PTH stimulates osteoclasts to resorb bone and mobilise Ca^{2+} into the blood. In kidneys, PTH increases Ca^{2+} reabsorption in the blood and stimulates the synthesis of calcitriol, which induces Ca^{2+} absorption in the intestine. When Ca^{2+} levels are restored, calcitriol provides a negative feedback at the parathyroid glands to inhibit PTH release, as shown in **Figure 47** (Khundmiri, Murray, & Lederer, 2016).

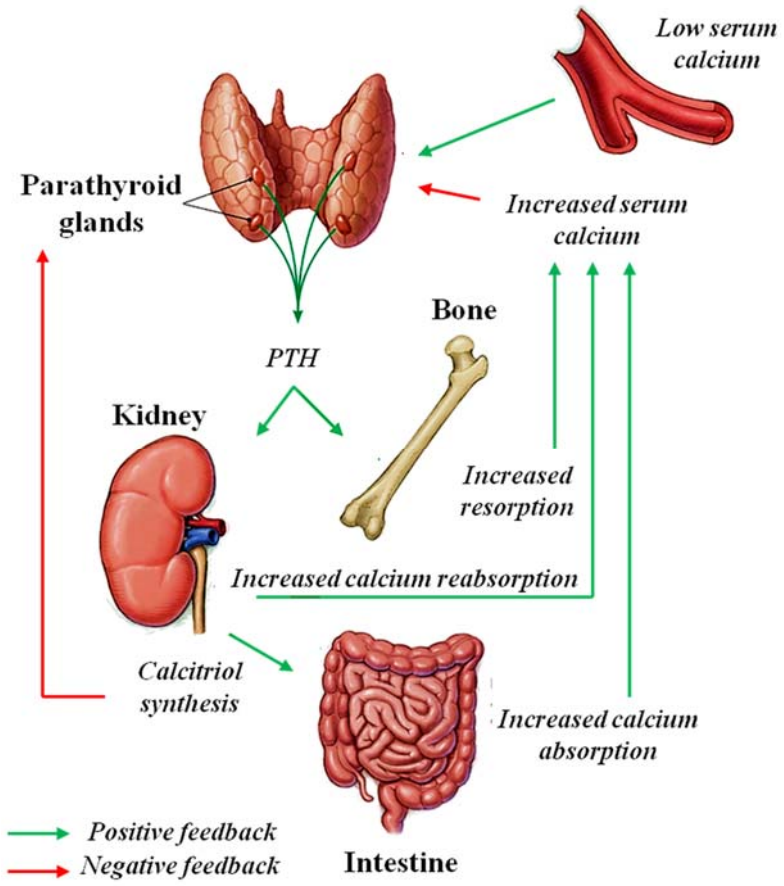

Figure 47. Calcitriol actions in Ca^{2+} metabolism. See text for details. Modified from (Michels & Kelly, 2013).

In the case of P_i metabolism, calcitriol increases P_i absorption in the intestine and the production of fibroblast growth factor (FGF-23) in bone, which promotes the P_i excretion and inhibits calcitriol synthesis in kidneys (Jacquillet & Unwin, 2019).

6.2.3.2 Calcitriol actions in neurons

Calcitriol is present not only in blood, but also in cerebrospinal fluid, indicating a role in CNS and PNS (Kočovská et al., 2017). In fact, VDR has been discovered in neurons, astrocytes and oligodendrocytes of basal ganglia, spinal cord, cerebellum and cerebral cortex, indicating that calcitriol action is also a neuronal mechanism. Interestingly, Cyp27b1 has been also discovered in endothelial cells, microglia, neurons and astrocytes, indicating that calcitriol synthesis can be an *in situ* process in CNS and PNS (Eyles, Smith, Kinobe, Hewison, & McGrath, 2005). The local and non-local synthesis of calcitriol in nervous system seem important for synaptic plasticity and regulation of neurotransmission, by modulating the synthesis of acetylcholine (Ach), dopamine (DA), and gamma-amino butyric (GABA) (Kočovská et al., 2017; Moretti, Morelli, & Caruso, 2018), for neuronal differentiation and neurite outgrowth, mediated by up-regulation of neurotrophins (Brown, Bianco, McGrath, & Eyles, 2003), but also for suppression of neuro-inflammation and neuroprotection (Lang, Ma, & Leibrock, 2019). In PNS, calcitriol has a role in neuronal differentiation, maintenance of axonal integrity and neuromuscular junctions. In Schwann cells, calcitriol up-regulates the expression of the myelin basic protein IGF-1, necessary for myelin formation, improving peripheral nerve conduction velocities and increasing axonal diameter (Faye et al., 2019). Improvement of myelination has been also observed *in vivo* in rats exposed to nerve injury and treated with vitamin D_3 (Chabas et al., 2013).

- **Calcitriol actions in DRG neurons**

VDR has been also identified in foetal (E12-E21) and adult DRG neurons (Johnson, Grande, Windebank, & Kumar, 1996; Tague & Smith, 2011), as well as Cyp27b1 and Cyp24a1, indicating that calcitriol synthesis, actions and degradation are also present in this neuronal type (Eyles et al., 2005; Tague & Smith, 2011). All DRG neurons subpopulations show the presence of VDR in nucleus, indicating that calcitriol affects mechanoreceptors, proprioceptors and nociceptors. In the case of NGF-dependent nociceptors, VDR is also present in cytoplasm, probably mediating the rapid non-genomic effects of calcitriol (Tague & Smith, 2011). In DRG neurons, calcitriol has

several functions such as axon genesis, increasing axonal diameter and neurite myelination, but also up regulation of neurotrophins (Faye et al., 2019). In fact, it increases NGF for development and maturation of nociceptors and regulates the expression of epidermal growth factor receptor (EGFR), both actions are important in modulating pain signalling, but also increases NT-3 and GDNF for development and maturation of proprioceptors neurons, thus modulating proprioception (Habib, Nagi, Thillaiappan, Sukumaran, & Akhtar, 2020). The up-regulation is because most of the genes of these neurotrophins, such as NGF, BDNF, NT-3, NT-4, GDNF, show a VDRE in the promoter (Chabas et al., 2013). For its action in pain signalling and for the fact that patients with chronic pain often show low serum calcitriol levels, calcitriol is often used as an analgesics to treat this disease (Habib et al., 2020) and for the treatment of diabetic neuropathy (Faye et al., 2019). Its function in proprioception is suggested by the fact that vitamin D_3 deficiency is correlated with an increased incidence of falls, indicating an altered function of large sensory fibers (Tague & Smith, 2011).

6.3 Calcitriol and neurodegeneration

Vitamin D_3 status is of particular interest because low serum levels (hypovitaminosis) or high levels of calcidiol (hypervitaminosis) are linked with unwanted effects. For example, hypovitaminosis induces an increased risk of rickets and osteomalacia, but also bone pain, weakness, diabetes mellitus and increased risk of cancer, while hypervitaminosis can deregulate the homeostasis of Ca^{2+} and phosphorus with hypercalcemia/hypercalcuria and hyperphosphatemia, leading to nausea, dehydration, constipation, polyuria and kidney stones. The optimal range of calcidiol in serum is ~25-80 ng/mL, while insufficiency is often ≤ 30ng/mL and deficiency ≤ 20ng/mL. The levels of calcitriol are rarely analysed and often indirectly considered based on serum calcidiol levels (Kennel, Drake, & Hurley, 2010).

6.3.1 *Calcitriol deficiency*

Calcitriol deficiency is a common risk factor in neurodegeneration (Buell & Dawson-Hughes, 2008). In fact, calcitriol deficiency, but also VDR mutations, have been related to aging and AD, MS, PD, ALS, HD (Berridge, 2016), as well as cognitive impairment, autism, schizophrenic-like disorders and other mental illnesses (Kočovská et al., 2017). In aging and neurodegenerative diseases, calcitriol deficiency induces an increase of $[Ca^{2+}]_i$ basal levels, mediated by IP_3R and RyR activation inducing release of Ca^{2+} from

ER intracellular store and/or decrease in Ca^{2+}-binding buffers, leading to a major incidence of mitochondrial damage and apoptotic cell death (Berridge, 2016, 2017). Interestingly, calcidiol insufficiency or deficiency, which is considered an indirect measure of calcitriol, has been observed in a small cohort of FA patients, a result that correlates with low bone mineral density and/or in some cases osteoporosis (Eigentler et al., 2014). Thus, calcidiol or calcitriol supplementation could be a potential therapy for all these diseases (Kočovská et al., 2017).

6.3.2 Calcitriol supplementation

All the form of vitamin D_3, such as cholecalciferol, calcidiol, calcitriol can be potentially used for supplementation. Cholecalciferol is mainly used for fortification of food, for its major stability, while calcidiol and calcitriol are generally used in treatment of diseases. However, calcidiol is not always properly converted into calcitriol. For example, in vitamin D resistant rickets type 1, a pathology with a genetic defect in the renal 1α-hydroxylase, the use of calcidiol is not useful for the treatment. Thus, it is crucial to utilize the correct form of vitamin D_3 in each case (Vieth, 2020). A beneficial role of calcitriol supplementation has been described in AD (Landel, Millet, Baranger, Loriod, & Féron, 2016; Morello et al., 2018), PD (Calvello et al., 2017), aging (Latimer et al., 2014), ALS (Libonati et al., 2017), where this supplementation has been associated with activation of vitamin D-NRF2-Klotho pathway, leading to reduction of oxidative stress and inflammatory biomarkers, restoration of $[Ca^{2+}]_i$ levels and mitochondrial function, attenuation of glutamate excitotoxicity and neuronal loss, but also re-myelination and enhancing of synaptic function (Berridge, 2017; Gianforcaro & Hamadeh, 2014).

HYPOTHESES AND OBJECTIVES

HYPOTHESES AND OBJECTIVES

1 HYPOTHESES

Taking into account the literature cited above and the localization of frataxin in mitochondria, the following hypotheses are proposed:

- The deficiency of frataxin may negatively affect Ca^{2+} homeostasis that would impair DRG neurons survival. The pathways in which Ca^{2+} is involved would affect specific mitochondrial functions that need to be defined.
- The increase of frataxin protein levels and the targeting of altered pathways would improve mitochondrial function and, consequently, neuronal survival.

2 OBJECTIVES

The aim of the project is to better understand the biological basis of Friedreich Ataxia, a rare neurodegenerative disease due to the decrease of the mitochondrial protein frataxin. Particularly, the project is focused on 3 distinct parts:

- Analysis of the connection between lack of frataxin and Ca^{2+} homeostasis, mitochondrial defects and apoptosis in frataxin-deficient DRG neurons;
- Evaluation of compounds that reverse the toxic effects of frataxin deficiency, in order to develop new therapeutic strategies to treat Friedreich Ataxia. In this context, several strategies and compounds outlined below will be assayed in frataxin-deficient DRG neurons to diminish or revert neurodegenerating traits:
    - chelating Ca^{2+};
    - replacing frataxin deficiency;
    - increasing FXN levels and improving mitochondrial function;
    - modulating calpain inhibition;
    - modulating mPTP opening;
    - modulating calcineurin activity;
    - modulating gene expression.
- As a proof of concept, frataxin-deficient DRG neurons will be compared with lymphoblastoid cell lines from patients.

MATERIALS AND METHODS

MATERIALS AND METHODS

1 EXPERIMENTAL ANIMALS

Experimental methods have been conducted in agreement with the *Real Decreto 53/2013*, in which recommendations and standard procedures, in relation to the use and protection of animals for experiments and teaching, are included. The *Ethical Committee of Animal Experimentation* (CEEA 02/08-17) from University of Lleida (UdL) approved and evaluated all the experimental procedures. For the experiments, male and female Sprague Dawley rats (*Rattus Norvergicus*) (RRID: RGD_70508) have been used. Rats were maintained in standard conditions of 12 hours cycles of light and darkness, a constant temperature of 20°C and eating and drinking *ad libitum*. Neonatal rats of three or four post-natal days were sacrificed with decapitation, following the guides of the *American veterinary medical association* (AVMA) *for euthanasia of animals*. No pre-registration was performed for the current study.

2 MOLECULAR BIOLOGY TECHNIQUES

2.1 Obtaining plasmids

In primary culture of dorsal root ganglion (DRG) neurons, lentivirus containing short hairpin RNA (shRNA) targeting frataxin mRNA has been used to decrease the amount of frataxin and scrambled shRNA that does not target any known mRNA as control. **Lentiviruses have been produced routinely in our laboratory by the laboratory technician Roser Pané Domenec using the following plasmids.**

2.1.1 Plasmids

A plasmid is a small, circular, double-stranded DNA molecule within a cell that is physically separated from chromosomal DNA and can replicate independently. Plasmid can also insert into the host chromosome, and these integrative plasmids are indicated as episomes. Artificially constructed plasmids are introduced into bacteria by a process called transformation and used as important tools to clone or express particular genes (inserts present in plasmids). The constructed plasmid usually contains an antibiotic resistance gene, which allows proliferating and selecting only the bacteria containing the plasmid DNA in a selective growth medium containing the particular antibiotic

(ampicillin) and an origin of replication to allow the bacterial cells to replicate the plasmid DNA. Three plasmids are needed in order to produce lentivirus:

- **Packaging plasmid** encoding components of the immunodeficiency virus human HIV-1 viral capsid (627). Provided from Addgene as transformed bacteria in stab culture, a type of Luria Broth (LB) Agar plate;
- **Envelope plasmid** encoding components of the vesicular stomatitis virus (VSV) envelope (628). Provided from Addgene as transformed bacteria in stab culture;
- **Transfer plasmid** encoding genetic material to be delivered to target cells:
  - **GFP**, a MISSION® **positive control** for transduction efficiency, which contains a gene encoding TurboGFP. Provided as 10µg of purified plasmid DNA, at [500ng/µL] in 10mM Tris-HCl (pH 8.0) and 1mM EDTA, it needs transformation in bacterial cultures and storing as glycerol stock at -80°C;
  - **Scr**, a MISSION® **negative control** containing a sequence not targeting any known mammalian genes. Provided as 10µg of purified plasmid DNA, at [500ng/µL] in 10mM Tris-HCl (pH 8.0) and 1mM EDTA, it needs transformation in bacterial cultures and storing as glycerol stock at -80°C for long-term storage;
  - **shRNAs** (FXN1/2) **to target FXN mRNA and decrease its protein levels** came from The RNAi Consortium (TRC) libraries of MISSION® shRNA bacteria harbouring shRNA plasmids for human and mouse genes cloned in pLKO.1-puro-TRC cloning vectors (RRID:Addgene_10878), as shown in **Figure 48**. Provided as transformed bacterial glycerol stock containing LB, Ampicillin at 100 µg/ml and 15% glycerol.

Detailed information for each plasmid is present in **Table 2**.

Table 2. Plasmids used to produce lentivirus.

ID	NAME	INSERT	Source	RefSeq	%&Sc
627	psPAX2	gag pol tat rev	RRID:Addgene_12260	No hairpin	
628	pMD2.G	vsv-g	RRID:Addgene_12259	No hairpin	
GFP	TRC1 pLKO.1-puro TurboGFP™ Positive Control	TurboGFP	Sigma, Cat# SHC003	No hairpin	
Scr	TRC1 pLKO.1-puro Non-Mammalian shRNA Control	CCGGCAACAAGATGAAGAGCACCAACTCGAGTTGGTGCTCTTCATCTTGTTGTTTTT	Sigma, Cat# SHC002	Non-target shRNA	
FXN1	TRCN0000197534 CloneID:NM_008044.1-600s1c1	CCGGCAAACTGGACTTGTCTTCATTCTCGAGAATGAAGACAAGTCCAGTTTGTTTTTTG	Sigma, Cat# SHCLNG-NM_008044	NM_008044 (Mouse FXN)	100% (CDS) & 3.375
FXN2	TRCN0000006137 CloneID:NM_000144.3-796s1c1	CCGGGCAGACGCCAAACAAGCAAATCTCGAGATTTGCTTGTTTGGCGTCTGCTTTTT	Sigma, Cat# SHCLNG-NM_000144	NM_000144 (Human FXN)	100% (CDS) & 7.560
EV			Gift Dr R. Soler's Lab		
shCALP1			Gift Dr R. Soler's Lab		

All plasmids present resistance to Ampicillin. Subtitled nucleotides indicate the target sequence. %= Percent match of the Specificity-Defining Region (SDR) of the hairpin sequence to transcript RNA. The SDR is defined as the initial 19 bases of the target sequence. 100%=19/19. The shRNAs FXN1/2 match with a coding region of the transcript (CDS). Sc=Adjusted score for a candidate targeting a particular gene calculated with a TRC algorithm. Larger numbers are better, and the scores range between 15 (best) and 0 (worst). From https://www.broadinstitute.org.

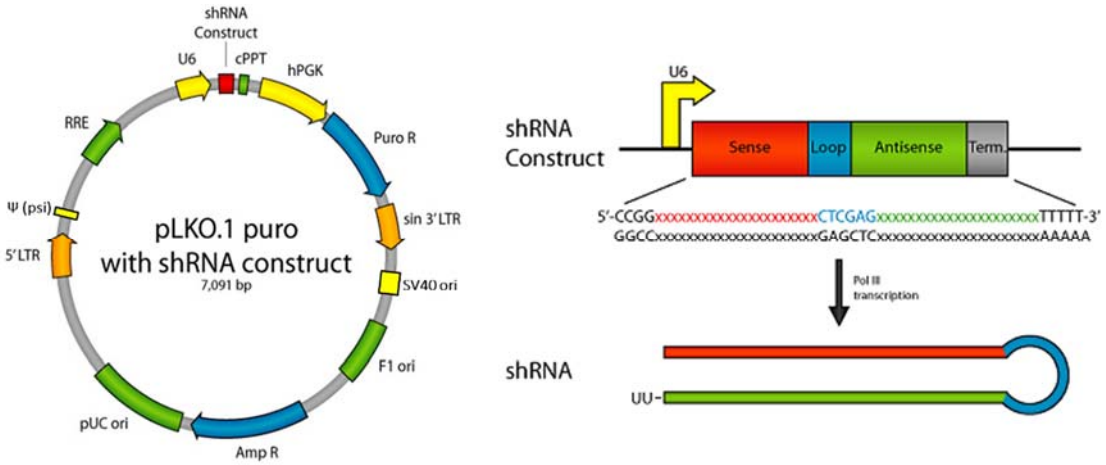

Figure 48. Map of pLKO.1-puro TRC cloning vector with shRNA construct and its transcription. Plasmid DNA (left panel) with: shRNA construct; f1 and pUC bacterial origin of replications; ampicillin resistance gene for selection of plasmid in bacteria; human U6 promoter (drives RNA Pol III transcription to shRNA); SV40 ori (induces replication in mammalian cells carrying SV40 large T antigen); Ψ sequence (involved in packaging the RNA genome into the viral capsid) etc. Transcription of shRNA construct (right panel) mediated by RNA Pol III. Modified from https://www.addgene.org/protocols/plko.

The plasmid DNA need to be purified from bacterial cultures. Subsequently, packaging cells (HEK293T), co-transfected with packaging, envelope and specific transfer plasmids, allow the production of self-inactivating replication incompetent viral particles, which are used in target cells (e.g. primary culture of DRG neurons).

2.1.2 Escherichia coli culture and maintaining

- **Transformed bacteria culture:**
  1. Using a sterile loop, touch the bacteria growing within the punctured area of the stab culture or the top of the glycerol stock.
  2. Place bacteria into a sterile culture tube containing 0.5 ml LB medium (yeast 5 g/L, tryptone 5 g/L, NaCl 10 g/L) without antibiotics.
  3. Incubate the culture at 37 °C with shaking for 15–30 minutes.
  4. Using a sterile loop, gently spread 25-50µL of the incubated bacterial culture onto freshly prepared plates containing LB agar and Ampicillin 50-100 µg/ml, to create streaks.
  5. Incubate plate with newly plated bacteria overnight (15-20 hours) at 37 °C.
  6. Isolate a single colony from the plate and use as a source inoculum for downstream applications (e.g., plasmid DNA expression and purification).
  7. Store bacterial glycerol stocks and stab cultures as a 20% glycerol stock for long-term storage at -80°C.
- **Not transformed bacteria culture:**
  1. Grow bacterial cultures in LB medium on an orbital shaker at 200 rpm and 37 °C without antibiotics.
  2. Use bacteria for transformation protocol and downstream applications.
  3. Freeze transformed and not transformed stock cells at -80°C in 20% glycerol for maintaining.

2.1.3 Escherichia coli transformation

In order to facilitate the transformation, introduction of exogenous DNA to the cells, "competent bacteria" are produced by membrane permeabilisation using the treatment with calcium chloride and thermic shock (Dagert & Ehrlich, 1979).

- **Obtaining competent bacteria:**
  1. Prepare a $CaCl_2$ solution: 60mM $CaCl_2$, 15% glycerol, 10mM HEPES, pH 7;

2. Sterilise $CaCl_2$ solution in the autoclave and keep it at 4ºC;
3. Incubate a DH5α bacteria strain ON at 37°C on an LB agar plate without antibiotics;
4. Dilute 1/100 the culture in fresh LB and allow to grow for 3-4 h up to 0.4 ODs;
5. Cool the culture for 10 min at 4ºC;
6. Centrifuge 250 mL of the culture at 3000 rpm for 7 min;
7. Re-suspend the pellet in 59 mL of $CaCl_2$ buffer (1/5);
8. Centrifuge at 4000 rpm for 5 min at 4°C;
9. Maintain on ice for 30 min;
10. Repeat step 8;
11. Re-suspend the pellet in 10 mL of $CaCl_2$ buffer (1/25), and rapidly make 200 µL aliquots on ice and keep it in -80°C;
12. The yield should be 105-107 units forming colony for µg of plasmid DNA transformed;

Once the competent bacteria are obtained, *E. coli* is transformed introducing the plasmid DNA of interest.

❖ ***E. coli* transformation:**

13. Thaw competent cells and plasmid DNA for 10min;
14. Use 5-10ng (until 50ng) of plasmid DNA, without exceed the 5% (v/v) of competent cells;
15. Mix by tapping *Eppendorf* tubes with finger and incubate for 20min on ice;
16. Perform a thermal shock of 45 sec at 42°C and incubate for 2 min on ice;
17. Add pre-heated (at 37°C) LB until 1 mL to facilitate cell recovering;
18. Incubate at 37°C for 45 min-1h with 170 rpm agitation;
19. Seed 15-20% of volume in a LB plate with 100 µg/mL ampicillin to allow the selective proliferation of bacteria with antibiotic resistance plasmids;
20. Next day, recover colonies that grown.

2.1.4 Obtaining plasmids

❖ **Plasmid expression:**

1. Seed a transformed *E. coli* colony, selected with the antibiotic, in a pre-culture of 2-10 mL LB with antibiotic Ampicillin 50-100 µg/ml;

2. Maintain growing for 8h;
3. Dilute pre-cultures 1/500-1/1000 in 250 mL selective medium;
4. Maintain growing for 12-16h at 300 rpm until saturation.

❖ **Obtaining purified plasmids:**

Obtain plasmids from bacteria using QIAGEN Plasmid Maxi Kit, following the protocol described by the commercial company.

5. Clear bacterial lysates by centrifugation;
6. Load cleared lysates onto the gravity-flow QIAGEN anion-exchange tip for efficient purification of plasmid DNA, where plasmid DNA selectively binds under appropriate low-salt and pH conditions;
7. Remove RNA, proteins, metabolites, and other low-molecular-weight impurities by a medium-salt wash;
8. Elute pure plasmid DNA in high-salt buffer;
9. Concentrate and desalt DNA by isopropanol precipitation and collect by centrifugation.

2.1.5 Plasmids quantification

❖ **Plasmid quantification:**

10. Measure the absorbance at 230, 260 and 280 nm using the spectrophotometer NanoDrop ND-1000;
11. Obtain DNA concentration and purity by considering that carbohydrates absorb at 230 nm, DNA/RNA at 260 nm, protein at 280 nm and contaminants give absorbance at 230 nm.

❖ **Analysis of DNA degradation:**

12. Prepare 1% agarose gel in TAE buffer: 20 mM Tris-HCl, 11.4% acetic acid (v/v), 1 mM EDTA, pH 8;
13. Prepare samples with loading buffer: 3% Ficoll (w/v), 20 mM EDTA pH 8, 0.05% blue bromophenol (v/v);
14. Load plasmid DNA in an agarose gel and perform electrophoresis run at 80V for about 1h;
15. Acquire the image in the DocEZGel of Bio-Rad and verify that plasmid DNA is not degraded.

3 CELLULAR BIOLOGY TECHNIQUES

3.1 Preparation of plates

3.1.1 Coating plates with collagen

- **Collagen stock solution:**
  1. Sterilise 1 L of milliQ water in the autoclave or filter using a 150 mL bottle top filter with 0.22 µm pore-size polyether sulfone (PES) membrane (Fisher scientific, FB12566508);
  2. Prepare a 0.1 N acetic acid solution with filtered milliQ water (285 µL of acetic acid in 50 mL of milliQ water);
  3. Open the vial with 50mg of collagen type one from rat-tail (Sigma-Aldrich, C7661) and add 7 mL of acetic acid and milliQ water solution.
  4. Wait until completely dissolved and transfer to a 50 mL tube, adding the acetic acid and milliQ water solution up to 50 mL;
  5. Dissolve the collagen in this solution for 4-6 hours by stirring;
  6. Store the stock solution of collagen (1 mg/mL) at 4°C for up to a year;
- **Collagen work solution and coating:**
  1. Prepare a solution with 0.02 N acetic acid and 75-100 µg/mL collagen in filtered milliQ water;
     a. For coating of HEK293T cell plates, use 13.3 mL:
        Add 12.3 mL of water and 16 µL of glacial acetic acid then mix well and add 1 mL of collagen.
     b. For coating of DRG neurons plates, use 9.6 mL:
        Add 8.6 mL of water and 11 µL of glacial acetic acid then mix well and add 960 µL of collagen, in this order.
  2. Coat the plates with the solution;
     a. For HEK293T cells, add 4 mL to each p100 plate;
     b. For DRG neurons, add 400 µL, 85 µL, 1.5 mL to each well in, respectively, a 24-well plate, 96-well plate and 6-well plate;
  3. Store closed plates at 4°C;
     a. In the case of HEK293T cells for maximum 1 week;
     b. In the case of DRG neurons attaching ON is preferred;
  4. Allow to dry collagen with the opened plates in the hood;

a. In the case of HEK293T cells ON the day before;
b. In the case of DRG neurons for at least 7h the same day of using it;

5. Inside the hood, move the plate occasionally in each side in order to allow the same degree of drying for all the wells of the plate or each side of the same well.

3.2 Lentivirus production

For transient knockdown of protein expression, plasmid DNA can directly transfect the target cells, but stable experiments need production of lentiviral particles in packaging cells and lentiviral transduction of target cells. Co-transfection of Human Embryo Kidney (HEK293T) cells, a cell for lentivirus packaging and production, with three plasmids (packaging, envelope and transfer), allowing plasmids to enter into the cells and nucleus, permits the plasmids expression in genetic RNA material and viral proteins to obtain lentivirus. Once produced, the genetic material present inside lentivirus is transduced to a target cell (e.g. DRG neurons).

3.2.1 HEK293T cell culture

HEK293T cells, deriving from HEK293, express the long T antigen of SV40 allowing episomal replication of transfected plasmids containing the SV40 replication origen.

1. Maintain HEK293T cell lines grow in p100 plates with a medium containing DMEM (Dulbecco's Modified Eagles Medium) 4.5 g glucose/L, 10% (v/v) FBS (GIBCO, Invitrogen) and 20 µg/ml penicillin/streptomycin in an incubator at 37°C and 5% CO_2.
2. Trypsinize mechanically when cells reach 70% confluence.
3. Centrifuge the cell suspension for 5 min at 1000 rpm and re-suspend the pellet with 1 ml of medium.
4. Seed cells in new p100 plates with a 1/20 dilution.
5. Repeat passages 2-3 and 4, after 3-4 days of incubation.
6. Count HEK293T cells with Burker chamber for downstream applications or store the stock of cells at -80°C for 1-3 days in cryotubes containing 2 million cells and then in liquid nitrogen.

3.2.2 HEK293T transfection

Co-transfecting HEK293T cells with a cationic lipid called polyethylenimine (PEI) and three different plasmids (envelope vector, pMD2.G; packaging vector, psPAX2 and the vector containing one of the shRNAs of interest: a shSCR control and two shFXNs that interfere with the mRNA of frataxin) produces lentiviral vectors. Cell membrane and DNA plasmids present negative charge, and then the lipid cation, PEI, binds plasmid DNA and allows DNA to enter into the HEK293T cells and nucleus, facilitating the transfection process.

- **PEI preparation:**
  1. Dilute PEI 20% in filtered milliQ water (Cf. 4.5 M) in the culture hood;
  2. Dilute PEI again to 0.2 M (1 mL of the 20% solution in 22.5 mL of milliQ water);
  3. Adjust to pH 5.6;
  4. Dilute 4 mL of the 0.2 M stock in 142.26 ml of milliQ water (Cf. 5.47 mM);
  5. Store at -20 ° C in aliquots of 1 mL.
- **Lentivirus production:**
  6. Use collagen-treated p100 plates to seed 1.5-2 million of HEK293T cells for each plate;
  7. Incubate ON cells at 37°C and 5% CO_2 ;
  8. Prepare a mix DNA-OPTIMEM: a sterile tube for a mix of each recombinant vector with packaging plasmid, envelope plasmid and OPTIMEM medium.
     a. For each p100 plate:
        i. 20 µg of one lentiviral vector (e.g. Scr-FXN1/2-GFP);
        ii. 13 µg of packaging plasmid (psPAX2);
        iii. 7 µg of envelope plasmid (pMD2.G);
        iv. 1.5 mL of OPTIMEM medium.
  9. Prepare a mix PEI-OPTIMEM:
     a. For each p100 plate:
        i. 1.260 mL of OPTIMEM;
        ii. 240 µL of PEI.
  10. Add the mix PEI-OPTIMEM drop by drop into the mix DNA-OPTIMEM: now the mix of two is the transfection solution;
  11. Vortex for 5 sec. at 1800 rpm;

12. Incubate for 10 minutes at RT;
13. During this time, wash plates containing HEK293T cells with 5 mL of OPTIMEM medium to be serum-free;
14. Add 3 mL of transfection solution drop-wise for each p100 plate, while gently swirling it;
15. Add 4mL of OPTIMEM for each plate;
16. Incubate at 37°C, 5% CO_2 for 1h (maximum 4h);
17. Replace media with complete DMEM media (4.5 g/L glucose, 10% FBS, P/S) and incubate at 37°C, 5% CO_2 for 3 days;
18. Collect media containing lentivirus in falcon tubes;
19. Maintain media at 4°C until virus concentration;

A similar protocol has been used for lentiviral production of empty vector (EV) and shCALP1 (shRNA for calpain 1) by Soler R.'s laboratory. Such viruses have been kindly given to us for the use in DRG neurons.

3.2.3 Virus concentration

Virus are concentrated using VIVASPIN 20 (Sartorius). This protocol allows concentrating 15-30 times virus.

20. Wash 100000 MW VIVASPIN 20 (Sartorius) column with 5mL milliQ water and centrifuge at 1000 rpm for 5min;
21. Centrifuge at 1000 rpm for 5 min the falcon tubes with the media containing lentivirus;
22. Filtrate the supernatant with a 0.45 µm filter;
23. 15mL of supernatant are added to each column VIVASPIN 20;
24. Centrifuge at 3500 rpm for 1h at 4ºC;
25. Aspirate and discard supernatant and repeat the centrifugation using the same column if more medium containing virus is collected;
26. Add 15mL of PBS to wash the column and centrifuge at 3500 rpm for 1h at 4ºC;
27. Aspirate and discard supernatant;
28. Once concentrated, store virus in tubs with screw caps at -80ºC for up then 3 months.

3.2.4 Virus titration

For the majority of lentivirus (**Scr, FXN1, FXN2** and **GFP**), virus titration has been performed using the QuickTiter™ HIV Lentiviral Quantitation Kit (HIV p24 ELISA) (Cell Biolabs, Cat# VPK-108-H). Such kit is an ELISA enzyme immunoassay developed for detection and quantification of the HIV-1 p24 core protein. A mouse monoclonal antibody to HIV-1 p24 is coated onto wells of the ELISA plate. The quantity of HIV p24 antigen, presents in lentiviral supernatant or purified virus, is determined by comparing its absorbance (measured at 450 nm) with that of known recombinant p24 antigen standard curve.

29. Prepare dilution series of HIV-1 p24 antigen standard and add 0.5% Triton-X for each dilution;
30. Dilute 1/500 – 1/5000 lentiviral supernatant in culture media and add 0,5% Triton-X for each sample;
31. Incubate 30 min. at 37°C;
32. Add sample or p24 antigen standard to anti-p24 antibody coated plate;
33. Cover the plate and incubate at 4°C ON;
34. Wash 3x the wells with 1X wash buffer;
35. A FITC-conjugated anti-p24 antibody is added at RT for 1h in an orbital shaker and binds to p24 antigen captured by the first antibody onto the plate;
36. Repeat step 26;
37. Add HRP-Conjugated anti-FITC antibody to all wells and incubate at RT for 1h in an orbital shaker;
38. Repeat step 26 to remove unspecific binding;
39. Add substrate solution for each well, which reacts with HRP giving a colorimetric product, and stop the reaction with the provided stop buffer;
40. Read the absorbance at 450nm in a spectrophotometer and calculate the concentration of p24 protein in each sample virus.

For the rest of lentivirus (**EV** and **shCALP1**), since such constructs carry a sequence for the expression of Green Fluorescent Protein (GFP), the titration has been performed counting the number of GFP-positive cells (transduced cells) on the total number of cells.

3.3 Post-natal rat DRG primary culture

After production and quantification, viruses are used to down-regulate the expression of frataxin in post-natal rat DRG primary cultures, in order to obtain the neuronal FA model of this thesis. Dissection and isolation of DRGs is a time-consuming process, for this reason, no more than 18 rats (usually 15-18 rats) are used for each day of culture. The dissection and isolation usually start at 8:30 am until ~13:30 am, followed by preparation of DRG neurons for culture (~14:30), 1h pre-plating, counting cells and plating in collagen-treated plates (~16:30). Neonatal rats at post-natal day 3 or 4 (P3-P4) are used (preferably P4 for easiest dissection and number of obtained cells). For 15-18 P4 rats, 1-1.4 millions of cells are usually obtained and seeded in different plates depending on the experiment. **Dr Llovera M., Dr F. Delaspre, T. Ximelis, Roser Pané or A. Sanz-Alcazár have kindly helped in dissection protocol.**

3.3.1 Dissection and isolation

- **Dissection:**
  1. Sterilise all dissection instruments with 70% ethanol in a hood for 10 min before using;
  2. Decapitate rats using scissors and soak up blood on paper towel;
  3. Immobilise rat using 4 needles and remove the skin using forceps from the dorsal part;
  4. Cut the dorsal part in the tail area and around the vertebral column (from tail to neck);
  5. Raise the dorsal part, trim away the adipose tissue from the shoulders and remove any excess tissue surrounding the dorsal part;
  6. Remove dorsal parts and keep it in a p100 dish, placed on ice, soaked in sterile and cold GHEBS to minimise the amount of blood;

- **Isolation of DRGs from dorsal parts:**
  7. Immobilise the dorsal block with 4 needles;
  8. Under the microscope, using small scissors, cut the middle line of the vertebral column along the spinal cord line (from neck to tail);
  9. Open the backbone and remove the spinal cord;
  10. Pick up DRGs with fine forceps and transfer it in a p60 dish with sterile GHEBS, on ice;

11. Clean DRGs from nerves and meninges and transfer ganglia to a new p60 containing sterile GHEBS on ice;

❖ **Cleaning of DRGs:**

12. In the laminar flow hood, wash a 1 mL pipette tip (with large inner diameter) with 0.1% BSA/GHEBS up and down 10 times (coating the tip with BSA prevents DRGs from adhering inside);
13. Cut off the end of the BSA-coated tip using scissors (UV-irradiated and sprayed with EtOH 70%);
14. Use the BSA-coated tip to collect the DRGs from p60 to one, two or three sterile tubes depending on the number of rats dissected (~ the same number of ganglia in each tube):
    a. For <15 rats → One 15mL centrifuge tube;
    b. For 15-18 rats → Two 15mL centrifuge tubes;
    c. For > 18 rats → Three 15mL centrifuge tubes;
15. Wash DRGs in each tube with sterile GHEBS (pH 7.4) 3 times;
16. Add the amount of GHEBS to arrive at 1 ml and use downstream protocol for each tube;

3.3.2 Obtaining cell suspension of DRG neurons

17. In the laminar flow hood, dissociate cleaned DRGs with cold 0.05% trypsin (Sigma-Aldrich) in 1mL of GHEBS;
18. Incubate for 35-40 min at 37ºC;
19. Gently flick tube every 10 min to prevent clumping and increase the enzyme penetration into the ganglia. Ganglia are still visible in a cloudy liquid;
20. In the case of ganglia attached on the top of the tube, spin down it for ~8 sec. in the centrifuge at 1300 rpm;
21. Remove as much trypsin/GHEBS as possible without disturbing DRGs;
22. Dilute trypsin concentration by washing ganglia with media, adding slowly enriched neurobasal culture media (Thermo Fisher Scientific—TFS, Madrid, Spain) (NBMc), pre-heated at 37°C, [consisting of 2% horse serum (TFS), 2% B27 supplement (TFS), 0.5 mM L-glutamine (TFS), 100 U/ml penicillin plus 100 ng/ml streptomycin (TFS) and supplemented with murine β-nerve growth factor at 50 ng/ml (PeproTech, New Jersey, USA) and the anti-mitotic

agent Aphidicolin (Sigma-Aldrich) at final concentration 3,4 µg/ml] and removing it without touching DRGs;

23. Add 1mL of NBMc in the same tube to prevent losing DRGs by attaching into the tip during the change;
24. Add 150µL of DNAse I grade II (Roche Diagnostics, Madrid, Spain) in 1mL NBMc (c.f. 3 mg/mL) for each tube;
25. Triturate mechanically DRGs with a 1mL pipette tip with large diameter (pipetting up and down until DRGs are no longer visible) without making foam;
26. Move the cell suspension of each tube to other new sterile tubes;
27. Add slowly 1mL of sterile BSA 7.5% (Sigma-Aldrich) to the bottom of each tube, allowing the cell suspension to form a phase onto BSA solution;
28. Centrifuge each tube for 5 min at 1300 rpm 800×g r.p.m. (302 rcf) with acceleration 1 and deceleration 0;
29. Discard the supernatant removing firstly the NBMc and then BSA;
30. Add gently 200µL of NBMc and slowly remove it without disturbing the cells on the bottom of the tube;
31. Re-suspend cellular pellet of each tube in 1 mL of NBMc medium and 150 µL of DNAse I grade II, pipetting several times (~10 times) to get an homogenous suspension;
32. Place 1 mL of NBMc into a p60 dish (Corning Inc., Fisher Scientific. Madrid. Spain) and add all cellular suspension into the same dish for 1h at 37ºC and 5% CO_2 mixing gently. The pre-plating allows satellite cells and glia to adhere and neurons to float.
33. Collect medium containing floating neurons in a new tube and count the cell suspension with a Burker chamber;
34. Pipetting frequently to keep the cellular density constant, seed cells in collagen-treated plates,:
    a. For survival analysis:
        i. Seed 10000 cells in the middle of the well as a ~50 µL drop in a cross-marked well of a 24-well plate (Corning Incorporated) and incubate 15 min. at 37°C/5%CO_2;
        ii. Gently, shake the plate using a horizontal movement;
        iii. Add 450 µL of NBMc medium and incubate at 37°C/5%CO_2.

b. For western blot analysis:
    i. Seed 10000 cells, 20000 cells or 30000 cells/well in the middle of the well as a maximum of 50 µL, 100 µL or 150 µL drop, respectively, of a 24-well plate pre-treated with 0,1 mg/ml collagen and incubate 15 min. at 37°C/5%CO_2;
    ii. Gently, shake the plate using a horizontal movement;
    iii. Add the rest of volume of NBMc to arrive at 500 µL.
c. For fluorescent microscope, neurodegeneration and size-diameter analysis:
    i. Use the same protocol for survival analysis, without cross-marked wells.
d. For TECAN analysis:
    i. Seed 10.000 cells/well as ~80µL in a 96-well plate with black wall and clear bottom (drop is not necessary), shake and incubate the plate at 37°C/5%CO_2.
e. For confocal and Fura2 analysis:
    i. Fluorescence: Seed 10000 or 20000 cells/well as a ~50µL or 100µL drop of a confocal plate (8 wells and 4 wells- plate respectively), incubate for 15 min, shake and incubate again. Alternatively, for confocal or Fura2 analysis, seed cells as a drop onto a collagen-treated 22-25mm diameter coverslip present in each well of a 6-well plate and incubate directly, without shaking.
    ii. Immuno-fluorescence: Seed 10000 or 20000 cells/well as a drop onto a collagen-treated round glass 12mm diameter coverslip of a 24-well plate and incubate directly, without shaking.

35. After 1–2 days, perform lentiviral transduction as described downstream and maintain the cells until the end of the experiment as explained in next sections. All passages are explained in **Figure 49**;

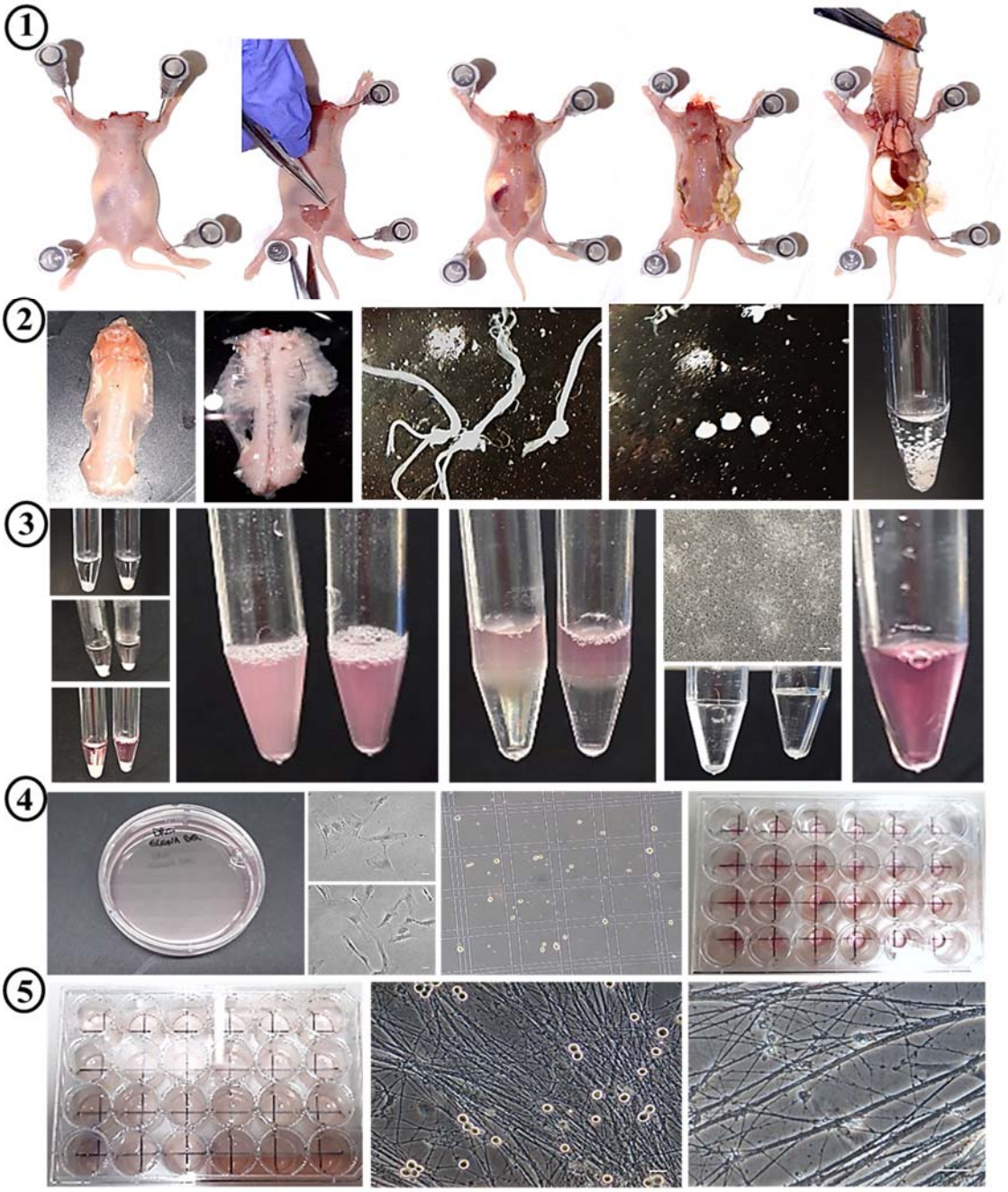

Figure 49. Protocol passages to obtain primary culture of neonatal rats DRG neurons. 1- Dissection of dorsal parts of P3-4 rats. From left to right: decapitate and immobilise rats using 4 needles; cut the dorsal part in the tail area; remove skin; cut dorsal part and remove it. 2- Isolation of DRGs from dorsal parts. From left to right: place dorsal part in GHEBS solution under microscope; remove the spinal cord; pick up DRGs; clean DRGs from nerves and collect in a tube. 3- Obtain cell suspension of DRG neurons. From left to right: Trypsinize DRGs (wash DRGs with GHEBS, add trypsin for 35 min at 37ºC, replace GHEBS/trypsin with NBMc); homogenise DRGs; add BSA at the bottom of the tube forming a phase and centrifuge to separate cells; Remove cell suspension and re-suspend pellet with NBMc. 4- Pre-plating, counting and plating cells. From left to right: pre-plate cells for 1h; collect cells and count cell suspension with Burker chamber; plate cells in a collagen-treated 24-wells plate (in the middle of each well). 5- Cell aspect 1-2 days after isolation. Allow DRG neurons to form neurites before lentiviruses transduction by waiting 1-2days after isolation. Phase-contrast photos using 10x + 1.6x objective are used for survival analysis (Scale bar= 30µm) and phase-contrast photos using 20x + 1.6x objective are used for neurite degeneration analysis (Scale bar= 30µm).

3.3.3 Viral transduction

Primary culture of frataxin-deficient DRG neurons are obtained using RNA interference (RNAi), that is the use of lentivirus carrying shRNAs targeting a specific mRNA (e.g. FXN). More in detail, the shRNA present in the lentivirus is flanked by *cis* elements necessary for its encapsulation, reverse transcription of RNA in DNA mediated by the reverse transcription complex and integration of such DNA into the target cell. Once the DNA insert is integrated into the host genome in the nucleus, RNA polymerase III transcribes the shRNA, which folds into the cell in a loop-shaped structure with two complementary sequences of RNA separated by a fork and is recognised by the machinery of RNAi: Drosha and DICER proteins. Both proteins process the shRNA, cutting and converting it into a small interference RNA (siRNA) that is recognised by RISC-AGO2 hybridising with the target mRNA. Then, the RISC-AGO2 complex cut the mRNA target, causing the expression silencing of the target gene, as shown in **Figure 50**.

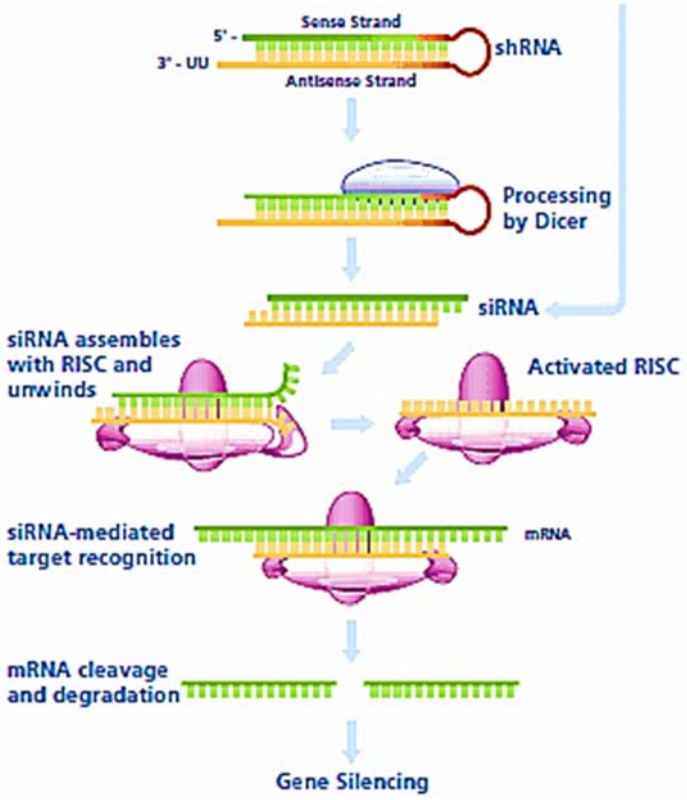

Figure 50. Passages of gene silencing using shRNAs. See text for details. From https://www.sigmaaldrich.com/.

36. Allow axonal growth of plated DRGs neurons, waiting 1-2 days after isolation;

a. Only for the experiments using EV and shCALP1, wait 1 day after isolation and add EV or shCALP1 lentivirus particles 14h before the Scr or FXNs transduction;

37. Perform Scr or FXNs lentiviral transduction adding 20 ng/1000 cells of lentivirus particles (~5-10 µL of the corresponding virus for each well);
38. Incubate cells with media containing lentivirus for 6h;
39. Leave some wells without adding viruses as a negative control (e.g. no lentivirus or no LV);
40. Substitute media by fresh NBMc culture media, in the presence of treatments or not depending on the experiment, in order to remove the virus;
    a. In the case of experiments using shCALP1 (or EV control) together with FXNs (or Scr control), both viruses are removed at the same time, reaching in total a 20h transduction for shCALP1 (or EV);

3.3.4 Viral transduction in time-course analysis

41. In the case of time-course analysis, perform lentiviral transduction, adding 20ng/1000 cells of lentivirus particles, in different days onto the same plate (e.g. the first day of transduction corresponds to day 5, while the last day to day 1);
42. Pay attention in adding the same set of viruses for each day, as the transduction efficiency can change between a stock and another;
43. Perform the experiment (e.g. fluorescence analysis) for each condition the same day.

3.3.5 Efficiency of transduction

For lentivirus carrying Scr or FXNs, the efficiency of transduction can be measured by using the same titration of lentivirus carrying GFP. At 5 days after GFP lentivirus transduction, fluorescent and phase-contrast images can be taken at the same field. The efficiency is thus calculated, using Image J software, by counting the number of GFP-positive cells on the total number of cells. For lentivirus carrying EV or shCALP1, the efficiency of transduction can be measured by counting directly the number of GFP-positive cells on the total number of cells, using Image J. This is due to the fact that such lentiviral constructs allow the expression of GFP protein.

3.3.6 Treatments

Perform experiments by adding treatments or changing media with treatments, as shown in the **Table 3**:

Table 3. Drugs screened in frataxin-deficient DRG neurons.

ID	0	1	2	3	4	Vehicle	Action	Source	RefSeq
TAT-MTS-FXN		↓	↓			PBS	FXN replacement	BioBlast	No comm.
Calcitriol			↓	↓	↓	EtOH	Neuroprotection	MEDCHEM	HY-10002
Calcidiol			↓	↓	↓	EtOH	Neuroprotection	SIGMA	H4014
MDL28170	↓	↓	↓	↓	↓	DMSO	Calpain inhibitor	TOCRIS	TO-1146
Calpeptin	↓	↓	↓	↓	↓	DMSO	Calpain inhibitor	Calbiochem	03-34-0051
BAPTA-AM	↓	↓	↓	↓	↓	DMSO	Ca^{2+} chelator	SIGMA	A1076
CsA	↓		↓		↓	DMSO	mPTP open. inhibitor	SIGMA	30024
TRO19622	↓		↓		↓	DMSO	mPTP regulator	SIGMA	T3077
DEBIO025	↓		↓		↓	DMSO	mPTP open. inhibitor	Debiopharm	NC
FK506	↓		↓		↓	DMSO	Calcineurin inhibitor	SIGMA	F4649
Leriglitazone	↓			↓		DMSO	PPARγ activator	Minoryx	NC
RTA-408	↓			↓		DMSO	NRF2 activator	Minoryx	Gift
Compound M			↓			DMSO	FT inhibitor	SIGMA	Patent
Compound S			↓			DMSO	FT inhibitor	Entrechem	Patent
Compound P			↓			DMSO	Kinase inhibitor	Quimigen	Patent
MG132					↓	DMSO	Proteasome inhibitor	Merk	474790

ID represents the name of each drug. 0-4 represents the day after lentivirus transduction in which the drug has been added changing the media. ↓ represents the moment in which the drug has been added. ↓ represents the moment in which the drug has been added comparing to ↓. Vehicle, drug action, source and reference have been also indicated. NC = non-commercial drug. FT= transcription factor. Patent= probable involvement in a use patent, thus, information is not releasable.

44. Warm up NBMc to 37°C and prepare the volume of NBMc + treatment or vehicle for each condition;
45. Change media using a gentle technique, such as aspiring media with a small-diameter Pasteur pipette connected to a vacuum pump and slowly replacing media with pipette tip, touching the wall of the well;
46. Incubate at 37°C/5%CO_2.

3.4 Phase-contrast microscopy

3.4.1 Axonal swelling analysis

Perform morphometric analyses of neurite degeneration at the desired days after lentivirus transduction, using the follow protocol:

47. Select an area in which neurites can be clearly distinguished;
48. Obtain phase-contrast images using a 20x lens and a zoom of 1.6x;
49. Create a grid over each image with NIH Image J software, using the grid plugin (line area ¼ 10000 pixels^2);
50. Took at least three images for each well, using at least three different wells for each condition, and repeating the experiment at least three times;
51. Count healthy and degenerated neurites (displaying axonal swelling and/or blebbing) at three power-fields per image;
52. Analyse data considering the ratio number of degenerated neurites over the total number of neurites.

3.4.2 Survival analysis

Perform survival analyses at the desired days after lentivirus transduction, using the follow protocol:

47. Plate cells in cross-marked wells;
48. Select the four fields per each cross-marked well at day zero and obtain phase-contrast images of each field using a 10x lens and a zoom of 1.6x;
49. Took at least four images per each well, using at least three different wells for each condition tested, and repeating the experiment at least three times;
50. Obtain phase-contrast images of the same field at the desired days after lentivirus transduction;
51. Compare all the images taken for each field with NIH Image J software;
52. Count the number of cells per each image at different time points, using the count cells plugin;
53. Analyse data comparing the number of cells presents at the desired day after lentivirus transduction on the initial number of cells.

3.4.3 Size diameter analysis

Size of cell body of DRG neurons was analysed, at the desired days after lentivirus transduction, from the phase-contrast images obtained as described above, using the follow protocol:

53. Compare the cells present in the phase-contrast images taken at different time-point, being sure of analysing always the same cell;
54. Perform manually a circle upon the cell body or soma by fitting the perimeter using Image J software;
55. Image J indicates the centre of the circle with a point, thus use this point to mark the diameter of the soma;
56. Calculate the size of the diameter by fitting a scale bar onto the diameter of the soma using Image J;
57. Categorise the values obtained into different range of DRG neurons populations:
    - >25; [22,5-25); [20-22,5); [17,5-20); [15-17,5); [12,5-15); [10-12,5); [7,5-10); <7,5µm;
    - >22; [15-22); <15µm.
58. Calculate the sum of cells for each condition and measure the number of cells for each interval on the total value of cells in percentage, in order to make a frequency distribution or use crude values in order to fit a Gauss curve model using OriginPro software, as described in Biophysical techniques.

3.5 Fluorescent microscopy

3.5.1 TMRM

- **$\Delta\Psi_m$ measurement:**

Tetramethylrhodamine, methyl ester assay (TMRM, ThermoFisher Scientific Cat#T668) ($\lambda_{ex\ 560nm}$ and $\lambda_{em\ 590nm}$) has been used to assess mitochondrial membrane potential ($\Delta\Psi_m$) in DRG neurons. TMRM is a cell-permeant and red-orange fluorescent dye, which accumulates in the negatively charge polarised mitochondria. Upon loss of $\Delta\Psi_m$, TMRM spreads throughout the cell cytosol and fluorescent signal decreases. The $\Delta\Psi_m$ analysis has been performed in DRG cultures plated in a ibiTreat 4-wells µ-slides

(ibidi, Cat# 80286), pre-treated with 0,1 mg/mL of collagen, at 5 days after lentivirus transduction, using the following protocol:

47. Prepare a working solution of 25nM TMRM in pre-heated at 37ºC HBSS + 10mM HEPES;
48. Wash 3 times cells with pre-heated HBSS +10mM HEPES;
49. Incubate cells at 37ºC 5%CO_2 with the working solution for 40min. in the dark and maintain it in this buffer (TMRM used in redistribution mode);
50. Obtain fluorescent Z-stack images using Olympus FV1000 confocal microscope (Alexafluor 568 filter, 60x objective and low laser power);
51. Analyse images with the NIH Image J software:
    a. Use a region of interest (ROI) per each cell, fitting each soma in a circle, or neurites, fitting some mitochondria in neurites in a rectangle;
    b. Calculate the mean intensity of each ROI;
    c. Subtract background fluorescence intensity from each ROI;

❖ **Dynamics changes of $\Delta\Psi_m$:**

TMRM analysis allows measuring the maintenance of $\Delta\Psi_m$ after addition of mitochondrial complex inhibitors. For this reason, video recording was performed and dynamics of $\Delta\Psi_m$ in response to inhibitors analysed using TMRM in the same conditions of above paragraph, with same differences:

51. Perform videos recording in multiarea time-lapse mode corresponding to 51 sec/photo and 8 fields for each well, using Olympus FV1000 confocal microscope (Alexafluor 568 filter, 60x objective and low laser power);
52. Record basal TMRM fluorescence for 5 min. and add directly to the buffer during video recording the following drugs:
    a. 2µg/mL of oligomycin for 15min;
    b. 2µM Rotenone for 10min;
    c. 10µM FCCP for 5 min;
53. Analyse videos with NIH Image J software, using bio format importer and time-series analysis plugin:
    a. Use a region of interest (ROI) per each cell, fitting each soma in a circle, or neurites, fitting some mitochondria in neurites in a rectangle;
    b. Calculate the mean intensity of each ROI;
    c. Subtract background fluorescence intensity from each ROI;

d. Normalise values (100;0) by using the formula:

$$\Delta F = (F - F_{FCCP}) / (F_0 - F_{FCCP}) \times 100$$

Where F= fluorescence intensity at any time point; F_0 = baseline fluorescence and F_{FCCP} = fluorescence intensity after 5 min of FCCP addition.

3.5.2 JC-1 assay

The $\Delta\Psi_m$ has been assessed using the dual-emission, mitochondrion-specific, lipophilic, cationic dye 5,5′,6,6′-tetrachloro-1,1′,3,3′-tetraethylbenzimidazoly-carbocyanine iodide (JC-1, Abcam ab141387) diluted in DMSO 1mg/mL. JC-1 is a cationic dye that accumulates and aggregates in energised mitochondria (high $\Delta\Psi_m$) as J-aggregate form yielding a red/orange emission (590±17.5 nm), while in depolarised mitochondria (low $\Delta\Psi_m$) is predominantly a monomeric form that yields green fluorescence with emission of 530±15 nm. Therefore, an increase in the ratio green fluorescence over the red fluorescence is indicative of depolarisation, whereas a decrease is indicative of hyperpolarisation. The $\Delta\Psi_m$ analysis has been performed in DRG cultures plated in a twenty-four-well tissue dish, at the desired day after lentivirus transduction (if not indicated, 72 hrs), using the following protocol:

47. Prepare a working solution of 5 µg/mL JC-1 in pre-heated at 37ºC NBM and vortex until no precipitates are seen;
48. Wash cells with pre-heated at 37ºC buffer (PBS or HBSS + 10mM HEPES);
49. Incubate the cells at 37ºC 5%CO_2 with the working solution for 30-35 min;
50. Wash cells with pre-heated at 37ºC buffer (PBS or HBSS + 10mM HEPES);
51. Maintain cells with 500µL of buffer;
52. Obtain fluorescent images, using an Olympus FluoView IX71 microscope with objective 10x + 1.6x;
53. Detect J-aggregate form of JC-1 using an excitation of 460-500 nm and an emission of 510-550 nm (filter Omega XF116-2), the monomeric form of JC-1 at an excitation of 520-550 nm and an emission higher than 510 nm (filter Olympus U-MWIB2) and both forms at an excitation of 460-490 nm and an emission higher than 510 nm (filter Olympus U-MWIG2). In the same field, obtain an image for each filter and analyse at least three fields per well, using three wells per condition and repeating experiment at least three times;

54. Analyse images with the NIH Image J software;
    a. Use as the ROI the entire image itself using the filter for both forms of JC-1 and the filter for aggregates;
    b. Split each image into three 8-bit grayscale images containing the red and green components of the original;
    c. Correct the fluorescence intensity using the above formula, as the split image taken with the filter for aggregates contained also the green component:
        i. Real green fluorescence intensity= Green fluorescence Intensity – (Red fluorescence intensity * factor X);
        ii. Where, factor X= green fluorescence intensity/red fluorescence intensity from the image with the filter for aggregates;
    d. Use the Real green fluorescence intensity for the ratio green fluorescence over red fluorescence, indicating an increase in the ratio intensity as depolarisation;

3.5.3 FLUO-8 and RHOD5N dye in whole cell

$Ca^{2+}{}_{i\ free}$ analysis has been performed with a green-fluorescent Ca^{2+} indicator Fluo8-AM (Abcam, Cat# Ab112129, $\lambda_{\sim 490nm}$ excitation, $\lambda_{\sim 525nm}$ emission), while $Ca^{2+}{}_{m}$ measurements with a low affinity red-fluorescent Ca^{2+} indicator Rhod5N-AM (Kd=19µM, $\lambda_{\sim 551nm}$ excitation, $\lambda_{\sim 576nm}$ emission) (Cayman Chemicals, Cat# 20442) and used as previously described in (Gandhi et al., 2009). Rhod5N fluorescent probe predominantly accumulates in mitochondria (Angelova et al., 2019), however is still visible in cytosol. Both probes were dissolved in DMSO (Sigma-Aldrich, Cat# D2650) and protected from light.

47. Prepare a solution of 0.005% Pluronic F127 (ThermoFisher Scientific, Cat# P6867) in pre-heated at 37ºC Hank's Balanced Salt Solution HBSS (156 mM NaCl, 3 mM KCl, 2 mM $MgSO_4$, 1.25 mM KH_2PO_4, 2 mM $CaCl_2$, 10 mM glucose) + 10mM HEPES (pH 7,4 adjusted with NaOH) and vortex it;
48. Prepare a working solution by adding 5µM Rhod5N-AM or 5µM Fluo-8-AM or both probes (depending on the experiment) into the above solution and vortex it;

49. Before starting the experiment, remove NBMc media and wash 1x DRG neurons with pre-heated at 37°C HBSS+10mM HEPES;
50. Incubate DRG neurons with the working solution at 37°C/ 5% CO_2 for 30 minutes;
51. Wash 1x DRG neurons with pre-heated at 37°C HBSS+10mM HEPES;
52. Detect fluorescence intensity by using:
    a. Olympus FluoView IX71 microscope, with an Omega XF116-2 filter and a 32x lens;
        i. Using a 24-well plate, take five images per well of at least three different wells for each condition and repeating the experiment at least 3 times.
        ii. Analyse each image with NIH ImageJ software, subtracting background (Rolling ball radius: 50 pixels) and measuring Rhod5N intensity in:
            - **Soma.** Measure basal intensity by using a circle selection upon each soma. Size of the circle has been changed in order to fit the edges of the cells. Attached cells whose edges are difficult to determine were not considered.
            - **Neurites.** Measure basal intensity by using a fixed neurite track equivalent to 100 pixels (at least five tracks per image and a total of 30 images per condition);
    b. Confocal microscope Olympus FluoView FV1000 (system version 4.1.1.5), maintaining controlled experimental conditions (37°C/5% CO_2) and 40x objective;
        i. Use a 4 or 8 well confocal plate directly or an AttoFluor Cell Culture chamber (ThermoFisher Scientific, Cat# A7816) with 22mm-diameter coverslips;
            - **4 or 8 well confocal plate.** Cells are seeded onto collagen pre-treated confocal plate.
            - **AttoFluor Cell Culture chamber.** Cells are seeded onto 22mm-diameter coverslips placed in a 6 well tissue dish (Corning Incorporated, Cat# 351146), pre-treated with 0.1 mg/mL of collagen (Sigma-Aldrich, Cat# C7661-25);

Each coverslip, on which DRG neurons have been cultured, is placed in an AttoFluor Cell Culture chamber (ThermoFisher Scientific, Cat# A7816) in preheated HBSS + 10mM HEPES.

ii. Images have been exported as TIF files and imported to NIH Image J software for subtracting background (Rolling ball radius: 100 pixels);

3.5.4 RHOD5N in membrane-permeabilised cells

Rhod5N-AM is a cationic dye that accumulates mainly in mitochondria, but also in the whole cell. Its presence in intracellular compartment can be easily discriminate by analysing only neurites in intact cells or by permeabilising plasma membrane using digitonin. Digitonin is a non-ionic detergent, which permeabilise plasma and nuclear membranes, depending on the presence of cholesterol. As mitochondrial membrane contains only low amounts of cholesterol, digitonin is usually used to isolate mitochondria *in sito* (Sudji, Subburaj, Frenkel, García-Sáez, & Wink, 2015). Furthermore, cell permeabilisation has been performed in a suitable solution for mitochondria, as described previously in (Abramov & Duchen, 2008).

47. Prepare a 0.5M stock EGTA solution in milliQ H_2O, adjusting pH until 8 with NaOH in order to obtain completely solubility, then, the solution is used into the pseudo-intracellular media;
48. Prepare a "pseudo-intracellular solution" containing 135 mM KCl, 10 mM NaCl, 20 mM HEPES, 5 mM pyruvate, 5 mM malate, 0.5 mM KH_2PO_4, 1 mM $MgCl_2$, 5 mM EGTA (from 0.5M stock) and 1.86 mM $CaCl_2$ (pH 7,1 adjusted with NaOH) to yield a $[Ca^{2+}]_{free}$ of 100 nM and to be used during and after permeabilisation of the cells with 60µM digitonin;
49. Prepare a stock solution of digitonin (Sigma-D141) in milliQ H_2O (1.84 mg/mL), heating at 98°C, vortexing until clear solution is obtained and cooling at RT to increase solubility, then store it at -20°C;
50. Prepare a solution of 0.005% Pluronic F127 (ThermoFisher Scientific, Cat# P6867) in pre-heated at 37ºC Hank's Balanced Salt Solution HBSS (156 mM NaCl, 3 mM KCl, 2 mM $MgSO_4$, 1.25 mM KH_2PO_4, 2 mM $CaCl_2$, 10 mM glucose) + 10mM HEPES (pH 7.4 adjusted with NaOH) and vortex it;

51. Prepare a working solution by adding 5µM Rhod5N-AM (for TECAN experiments) or 5µM Rhod5N-AM + 5µM Fluo-8 (for microscope) into the above solution and vortex it;
52. Before starting the experiment, remove NBMc media and wash 1x DRG neurons with pre-heated at 37°C HBSS+10mM HEPES;
53. Incubate DRG neurons with the working solution at 37°C/ 5% CO_2 for 30 minutes;
54. Wash 3x DRG neurons with pre-heated at 37°C HBSS+10mM HEPES;
55. Detect fluorescence intensity of whole cell by using:
    a. Olympus FluoView IX71 microscope, with an Omega XF116-2 filter (Rhod5N - red) and an Olympus U-MWIB2 filter (Fluo8 - green), using a 32x lens;
        i. Take red and green images at different time points for the same field of a well in a 24-well plate;
        ii. Subtract background (Rolling ball radius: 100 pixels) and compose merge images by using Image J software;
56. Alternatively, continue the experiment permeabilising cell membrane using 60µM digitonin for 13-15min in pseudo-intracellular solution at 37°C/ 5% CO_2 (for TECAN experiments) and RT (for Olympus FV1000 experiments).
57. Wash 2-3x permeabilised cells with pseudo-intracellular solution to remove digitonin;
58. Detect fluorescence intensity by using:
    a. TECAN Infinite® 200 PRO fluorescence microplate reader (i-control software 1.3.3.0), maintaining controlled experimental conditions (30°C, 1s shaking before reading in a Top mode) and manual Gain 90 from blank well;
        i. Seed 10000cells in a Falcon® 96-well Black/Clear Flat Bottom TC-treated Imaging Microplate (Ref# 655090) and perform the experiment at 3 days after lentivirus transduction by using 100µl of pseudo-intracellular solution;
        ii. Read the baseline fluorescence (Exc.= 557 nm and Em.= 579) for at least 5 minutes;
        iii. Collect solution of permeabilised cells and perform acetone precipitation;

1. Add 4 volumes of ice-cold acetone into the same eppendorf and incubate ON at -20°C;
2. Centrifuge for 10 min at maximum speed in a bench top centrifuge;
3. Discard the supernatant and air-dry the pellet;
4. Add 25µl of lysis buffer;

iv. Measure the concentration of mitochondria using Qubit (details in biochemical methods section);

v. Normalise fluorescent data on the µg of proteins present in 100µl of solution;

b. Olympus FluoView FV1000 confocal microscope (system version 4.1.1.5), using a x100 lens and Free-Run mode (corresponding to 2sec/photo);

i. Seed 10000 cells in ibiTreat 2-wells µ-slides (ibidi, Cat# 80426) pre-treated with collagen and perform the experiment at 5 days after lentivirus transduction by using pseudo-intracellular solution;

ii. Read the baseline fluorescence for at least 2 minutes;

iii. Stimulate mitochondria by adding $CaCl_2$ (5µM $[Ca^{2+}]_{free}$) to promote $Ca^{2+}{}_m$ uptake and release and record videos for 5 min. more;

iv. Analyse videos by using NIH Image J software (bioformat importer and time-series analysis) selecting ROIs in which cells are completely permeabilised and mitochondria responds to the stimulus;

v. Analyse peaks of $Ca^{2+}{}_m$ using Origin Pro 2017 program, fitting each peak with a linear or exponential model and measuring for each peak the amplitude (ΔF), Ca^{2+} influx (peak slope – s) and Ca^{2+} efflux (k-decay and tau), as described in the Biophysical Techniques section of Materials and Methods. **Dr Panosa Anaïs and A. Sanz-Alcazár and have kindly helped in obtaining confocal images.**

3.5.5 Mitochondrial localisation of RHOD5N

Localisation of Rhod5N in mitochondria was confirmed by using a mitochondrial control (Mitotraker green) and Rhod5N dye in DRG neurons at 5 days after lentivirus transduction, using the following protocol:

47. Plate DRG neurons in ibitTreat 4-well µ-slides (ibidi, Cat# 80286) pre-coated with collagen;
48. Wash 1x DRG neurons with HBSS+10mM HEPES;
49. Prepare a solution of 0.005% Pluronic F-127 in HBSS + 10mM HEPES;
50. Incubate cells with 5µM Rhod5N-AM and 10nM Mitotracker-green (λex ~490nm, λem ~316nm) in the above solution for 30 min at 37ºC/5% CO_2, protected from light;
51. Replace the buffer with fresh pre-warmed HBSS + 10mM HEPES and maintain cells in this solution for 15 min at RT protected from light;
52. Wash cells several times with HBSS + 10mM HEPES and take images with Olympus FV1000 confocal microscope and 100x objective + 3x zoom.

3.5.6 FURA-2-AM ratiometric dye

Fura-2-acetoxymethyl ester is a high affinity $Ca^{2+}{}_i$ sensitive dye, which is ratiometric and UV-excitable. Upon loading into the cells, esterases present in the cells hydrolyze the AM esters to liberate the probe. The probe can be excited at two wavelengths λ~340nm and λ~380nm, which are for Ca^{2+}-bound and Ca^{2+}-free detections, and the ratio 340/380 nm fluorescence intensity can be detected at λ~510 nm. **The experiment have been performed with the help of Dr Olga Tarabal.**

47. Use the autoclaved, sterilised with EtOH and dried 22 mm-diameter glass coverslips in 6-well dish pre-treated with collagen to plate DRG sensory neurons at the cell density of 30000 cells/well in the centre and follow above protocols to generate 4-days transduced FXN-deficient DRGs;
48. Prepare an EGTA stock solution with 400mM EGTA, 3M Tris and adjusting the pH at 8.7;
49. Prepare GHEBS buffer, as indicated in the dissection section, a normal (extracellular physiological solution) and a Ca^{2+}-free perfusion buffer, all buffers are pre-heated at 37°C:

a. Normal perfusion buffer: 150mM NaCl, 1mM $CaCl_2$, 1mM $MgCl_2$, 10mM glucose, 5mM KCl, 20mM HEPES, 0.1-1% BSA and adjust pH at 7.4;
b. Ca^{2+}-free perfusion buffer: dilute 1/100 the EGTA stock solution in the perfusion buffer without Ca^{2+} addition (pH 7.4) to a 4mM EGTA final concentration;

50. Prepare a 5µM Fura2-AM (Invitrogen) solution in perfusion buffer, protected from light;
51. Aspirate NBMc medium from neuronal cells and wash 1x with GHEBS buffer;
52. Wash 1x cells with perfusion buffer and incubate cells with 5µM Fura-2-AM solution for 30-45 min at 37°C, protected from light;
53. Wash 3x cells with Ca^{2+}-free perfusion buffer;
54. Leave at RT for 10-15 min, then at 4°C until the moment of use;
55. Remove coverslips from 6-well dish and place into a PH1 (Warner Instrument Corp, Hamden, CT) perfusion chamber, which allow continuously perfusion in Ca^{2+}-free buffer;
56. Connect the chamber with a Nikon Eclipse TE200 inverted fluorescence microscope, containing a monochromator and an Orca ER camera (Hamamatsu Photonics);
57. Perform Ca^{2+} imaging in the dark with Aquacosmos software (Hamamatsu Photonics);
58. Ratiometric signal was captured using a 40 1.3 NA Nikon S objective, oil-immersed;
59. CCCP addition was performed ~5 min after the initial recording, without removing CCCP during the experiment. **Dr Tarabal Olga and T. Ximelis have kindly helped in obtaining Fura-2 images.**

3.5.7 Immunofluorescence

Immunofluorescence has been performed in DRG cultures plated onto a coverslip in a twenty-four-well tissue dish, at five days after lentivirus transduction, using the following protocol:

❖ **Fix cells for immunofluorescence analysis:**

47. Place the cells on ice and throw away NBMc media;
48. Wash cells twice using 500µL PBS for each well;
49. Fix cells with 500 µL PFA 4% on ice for each well;
50. Incubate cells with PFA 4% for 20 min at RT;
51. Throw away PFA 4% and wash 3x cells with 500µL PBS/well;
52. Maintain cells with 500µL PBS/well;
53. Close the plate with parafilm and store plate at 4ºC for several weeks;

❖ **Prepare buffers for Immunofluorescence:**

54. Permeabilisation Buffer (PBS + Triton X-100 0,5%):
    a. Prepare 250µL of Triton X-100 in 50mL PBS 1x;
55. Blocking Buffer (BSA 1% + Triton X-100 0,2%):
    a. Prepare 0,5g of BSA and 100µL Triton X-100 in 50mL PBS 1x;

❖ **Prepare cells for Immunofluorescence:**

56. Take coverslips with forceps and place them in another plate, maintaining cells on the top;
57. Wash cells with 500 µL PBS 1x/well;
58. Incubate cells with 500 µL of Permeabilisation Buffer for 30 min at RT;
59. Throw away Permeabilisation Buffer and wash cells with 500 µL PBS 1x/well;
60. Incubate with 500 µL Blocking Buffer for 1h at RT or ON at 4ºC;
61. Throw away Blocking Buffer;
62. Add primary antibody for 2h at RT or ON at 4ºC in a dark humid chamber:
    a. Dilute primary antibody and use a 30µL drop of Blocking Buffer for each coverslip:
        i. Frataxin (Rabbit) 1:50;
        ii. OXPHOS (Mouse) 1:50;
        iii. β-Tubulin III (Mouse) 1:250;
    b. Place face-down coverslips for 2h at RT or ON at 4ºC on the drop, without agitation;
63. Wash cells 3x with 500 µL of Blocking Buffer/well;
64. Add secondary antibody for 2h at RT or ON at 4ºC in a dark humid chamber:
    a. Dilute secondary antibody in Blocking Buffer for each coverslip:
        i. Goat anti-rabbit (fluor 594) 1:300

ii. Goat anti-mouse (fluor 488) 1:300

65. Wash cells 3x with 500 µL of Blocking Buffer/well;
66. For Nuclear Staining use 500 µL/well of DAPI 1:2500 for 5 min at RT and wash 1x with 500 µL of ddH_2O;
67. Mount coverslip with Mowiol 4-88 and store at 4ºC;
60. Perform the immunofluorescence by taking images with fluorescent or confocal FV1000 microscope. **Dr F. Delaspre has kindly performed the last step of immunofluorescence analysis.**

3.6 Lymphoblastoid cell lines (LCL) culture

Lymphoblastoid cell lines, shown in **Table 4**, has been bought from Coriell Institute for Medical Research and initiated with frozen stocks in liquid nitrogen. In the table are indicated the cell line identification number and characteristics of the patient, carrier or control (gender, years, GAA repeats and other notes). Cells have been maintained with 10mL of RPMI 1640 medium (Gibco) supplemented with 15% fetal bovine serum (FBS), 1% penicillin/streptomycin and 2mM GlutaMAX (Gibco) in vented flasks (standing upright) at 37ºC/ 5% CO_2. Coriell Institute indications have been followed. **Dr F. Delaspre, T. Ximelis, A. Caparrós or A. Sanz-Alcazár have kindly performed cultures.**

Table 4. Lymphoblastoid cell lines characteristics.

ID	Control/ Carrier/FA	Gender	Years	GAA repeats	Note
GM22641	Control	Male	55		
GM22671	Control	Female	28		
GM22651	Control	Male	26		
GM15851	Control	Male	14		Brother of GM15850
LFA120	Control	Male	25-40		Gift
LFA195	Control	Female	30-45		Gift
GM12211	Carrier	Female	30	830	
GM16215	Carrier	Female	41	830	Mother of GM16214
GM16798	FA	Female	15	750/1000	
GM16203	FA	Female	29	670/830	
GM16205	FA	Male	30	530/530	
GM16223	FA	Male	41	400/630	
GM16209	FA	Female	41	800/800	
GM15850	FA	Male	13	630/1030	Brother of GM15851
GM16214	FA	Male	15	600/700	Son of GM16215

In the table are indicated the cell line identification number and characteristics of the patient, carrier or control (gender, years, GAA repeats and other notes). From https://www.coriell.org/.

3.7 Oxygen consumption with Oroboros 2K

The instrument Oxygraph Oroboros 2K has been used in this work to analyse the oxygen consumption of lymphoblastoid cell lines (LCL). This instrument allows to analyse the O_2 concentration ($[O_2]$) as a function of time in a closed Oxygraph chamber. The volume presents in each chamber is constant (2mL). The $[O_2]$ (the amount of O_2 per volume) is measured by a polarographic oxygen sensor (POS) as an electric current, which is converted into $[O_2]$ during time. The presence of cells in this closed system leads to oxygen consumption through mitochondrial respiration, thus, decreasing the $[O_2]$ with time. When cells are consuming O_2, the $[O_2]$ declines and a linear negative slope is shown in the Oroboros graph. A faster oxygen consumption rate leads to a steeper negative slope of $[O_2]$ with time. Then, this negative slope is proportional to the oxygen consumption rate per unit (oxygen flux). Before of performing the experiment

with Oroboros 2K, the instrument needs an oxygen calibration. Then, the background of medium is subtracted from the analysis. The Oroboros DatLab program is used for all these passages and for the analysis of the experiments, which can be measured as O_2 flow per cell expressed in pmol/(s*Mill) or normalised on maximal respiration of each experiment (flux control ratio).

3.7.1 Oxygen calibration

In order to analyse mitochondrial respiration of LCL, the Oxygraph instrument needs to be connected to Oroboros DatLab program, and the oxygen calibration performed using the following protocol:

1. Before oxygen calibration, perform a chemical sterilisation of Oxygraph chambers A and B:
    a. Wash chambers with 2 mL of EtOH 70%;
    b. Aspirate EtOH without touching the membrane inside each chamber;
    c. Add 2mL of EtOH 70% in each chamber;
    d. Wait between 30 minutes - 1 hour for chemical sterilisation of chambers and simultaneous temperature (37ºC) and barometric pressure (kPa) equilibration;
2. Wash chambers three times with mQH_2O, without touching the membrane;
3. Fill chambers with 2.5 mL of medium;
4. Perform oxygen calibration of each chamber:
    a. Close the chambers and remove the excess of medium;
    b. Select the calibration experiment in the DatLab4 program, which allows see the O_2 graph as an “uncorrected slope”;
    c. Put a key under the chamber to calibrate the oxygen;
    d. Inside the chamber, a trapped gas bubble should be present;
    e. Wait 30-45 minutes and be careful that the bottom graph in DatLab4 program, which indicate the Peltier Power (%), must be stable;
    f. Select a piece of the O_2 concentration graph (Blue line) that shows a stable signal and calibrate O_2;

3.7.2 Medium background

Medium background experiment or medium calibration is a procedure that should be due each time a new media is used. Once the media calibration is performed the values obtained can be used for all the cell experiments in which is used this particular medium. At the end of the media calibration, the O_2 flux is represented in function of O_2 concentration, in order to obtain the number **a (intercept)** and **b (slope)** of the linear regression. These two numbers need to be used in the setting of the cell experiment, together with the **O_2 solubility factor of the medium (FM)**. In the case of RPMI buffer, the FM of **0.89** has been selected from general guidelines of Oroboros-2K web site. Medium calibration is obtained using the following protocol:

5. After oxygen calibration, select the "uncorrected flux x Volume" plot and close the chambers containing RPMI medium without sample;
6. Wait 5-10 minutes;
7. Open the chamber and reduce O_2 concentration by using argon;
8. Look the O_2 concentration level, when the level is reduced by 50% the chamber is closed to measure the background O_2 flux;
9. Wait 5-10 minutes;
    a. Repeat the passages using argon 4 times (each time the level is reduced by 50%);
10. When the level of oxygen in the chamber is zero, select the background O_2 flux at 4 O_2 concentration levels;
11. Perform the linear regression **(y= bx – a)** with the flux (slope) in function of O_2 concentration values, as indicated in **Figure 51**;
12. Using RPMI 1640 medium supplemented with 15% FBS, 1% penicillin/streptomycin and 2mM GlutaMAX, the values a (intercept) and b (slope) of the linear regression measured are :
    - Chamber A

      a (intercept) = -1,5884 **b (slope) =** 0,0226
    - Chamber B

      a (intercept) = -1,7534 **b (slope) =** 0,0247

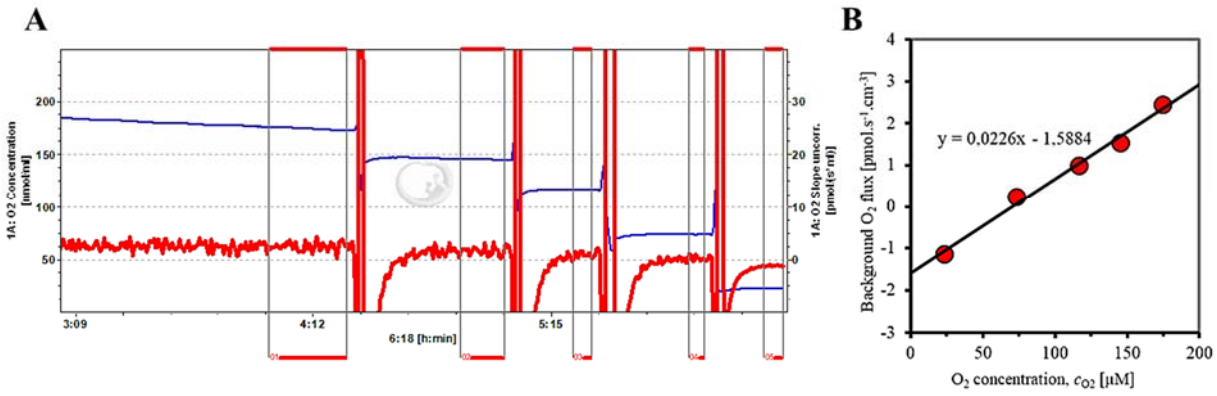

Figure 51. Measure of medium background using argon. See text for details. In A, representative image of medium background analysis using DatLab 4 program. In B, linear regression of background O_2 flux in function of O_2 concentration.

3.7.3 Oxygen consumption

Once oxygen and medium calibration are performed, the cells can be added into the chambers in order to measure the oxygen consumption, following these passages:

13. Count lymphoblastoid cell lines:
    a. LCLs, at the desired culture day (day 4-5), are centrifuged at 1000 rpm for 3 minutes and resuspended in 1 mL;
    b. Dilute cells with medium (1:10) and count cells with Neubauer chamber, considering the dilution factor;
    c. Calculate the number of cells in order to have 2-5 millions of cells in 2,4 mL and leave cells at 37ºC until the experiment is performed;
14. Select the "O_2 flux per units" plot in DatLab4 program and change the setting by adding the number of cells for each chamber, the solubility factor, the values of medium calibration etc.;
15. Add cells in each chamber and close the chamber;
    a. Wait until the O_2 flux per cell is stable, more or less 15-20 minutes, this represents the routine respiration or the resting state;
16. Add with Hamilton pipette 2µg/mL of Oligomycin (Stock 5mg/mL in DMSO) for each chamber;
    a. Wait ~10 minutes;
    b. Oligomycin inhibits the ATP synthase (Complex V), thus, arresting mitochondrial respiration;

17. Add with Hamilton pipette 0.5µM of FCCP for 5times (Stock 1mM in EtOH) for each chamber;
    a. Wait ~2minutes between each injection of FCCP;
    b. Uncoupler FCCP dissipates the $\Delta\Psi_m$ and consequently activates the electron transport chain to recycle protons from the matrix side across the inner mitochondrial membrane;
    c. The higher FCCP value of O_2 flux per cell is used in order to indicate the maximal respiration;
18. Add with Hamilton pipette 2.5µM of Antimycin A (Stock 2mg/mL in EtOH) for each chamber;
    a. Wait ~ 5minutes;
    b. This drug inhibits complex III and, by blocking completely mitochondrial respiration, allows to analyse the non-mitochondrial oxygen consumption;
19. Wash 3x the Hamilton pipette with EtOH 100% after each use and chambers with 100% EtOH;
20. Select stable portions of the graph in DatLab4 program in order to analyse the O_2 flow per cell;

4 BIOCHEMICAL TECHNIQUES

4.1 DRG and LCL samples obtaining and preparation

4.1.1 Samples obtaining

Obtaining samples has been performed in a BioIIA hood, following the protocol:

60. Prepare Eppendorf tubes and cool them on ice during the process;
61. Place the plate with cells on ice;
62. Perform 3 washes with ice-cold PBS 1x (pH 7.4 - GIBCO), maintaining the plate on ice;
63. During the last wash, maintain the plate in oblique position in order to discard any presence of PBS;
64. Add 25µL of Lysis Buffer, by changing its composition considering the next step:
    a. **For WB:** 2% SDS, 125 mM Tris pH 7.4, complete™, Mini, EDTA-free

protease inhibitors cocktail 1x (Roche, Cat# 04693159001) (prepared with 0.5M EDTA pH 8 to have a final concentration of 14mM EDTA) and PhosSTOP™ phosphatase inhibitors cocktail 1x (Roche, Cat# 4906845001);

i. In the case of WB analysis of acetylated proteins, deacetylase inhibitor cocktail 1x (Medchem express, Cat# HY-K0030), has been added to the previous cocktail.

b. **For enzymatic activity:** 50 mM Tris HCl pH 7.4; complete™, Mini, EDTA-free protease inhibitors cocktail 1x (Roche, Cat# 04693159001) (without adding EDTA); 0.5% Triton X-100 (v/v); 2.5 mM sodium citrate.

65. Use the same 25µL for more wells of the same condition, being careful not to make bubbles.

4.1.2 Samples quantification and preparation

Protein concentration of cells lysate is quantified using Qubit® protein assay kit (Thermofisher, Cat# Q33211), using the protocol of the kit. Briefly, a Qubit working solution is obtained by mixing the buffer and the fluorometer. All the passages are performed in the dark and using the reagents at RT. A curve calibration is performed quantifying the protein concentration of standards proteins and the concentration of samples is analysed by looking at the calibration curve. Samples (~1µL-1.5µL) are analysed in duplicate or triplicate and the average of these repetitions is used to obtain the sample stock concentration. WB has been performed using 10-25µg of protein. Thus, the amount of stock sample is mixed with lysis buffer and loading buffer 5X (50% glycerol, 10% SDS, 25% β-mercaptoethanol, 375 mM Tris-HCl pH 6.8, bromophenol blue) in order to equalize the volume of all samples. Then, the sample mix is incubated for 5 min at 98ºC to denature the proteins and centrifuged (short spin) at 14000 rpm. The sample mix is then immediately loaded into the gel. For each gel two wells are filled with a Marker (Precision Plus Protein™ All Blue Prestained Standards, Cat# 1610373, BioRad) presenting a standard MW. The reason of using two wells for Markers is due to the fact that, after transfer into membrane and before adding primary antibodies, the cutting of the membrane can be easily performed in order to use the same membrane for more antibodies of different MW.

4.2 Electrophoresis methods

4.2.1 SDS-PAGE

DRG neurons were rinsed three times in ice-cold PBS (pH 7.4) and lysed with 2% SDS, 125 mM Tris and protease inhibitors (Roche) to obtain crude extracts used for SDS–polyacrylamide gel electrophoresis. This technique allows separating protein by looking at MW, using SDS that denaturalise proteins and induces a negative charge onto proteins. Firstly, handmade gels are prepared, samples are loaded into electrophoretic chamber and semi-dry transfer into PVDF or Nitrocellulose membrane is performed. Secondly, antibodies detection is performed and bands quantified.

66. Prepare gels for electrophoresis.

    Two glasses for Mini protean Bio-Rad gels are rinsed with ddH_2O, dried and collocated into the support for Mini-protean Bio-Rad gels. The ddH_2O water is added to verified the correct position of the glasses. Acrylamide gels of 1.5 cm are handmade prepared by preparing solutions for separator and stacking gels:

    a. **Separator gel**: the portion of the gel that allows separation of proteins for MW is obtained by mixing 375 mM Tris-HCl pH 8.9, acrylamide/ bisacrylamide (30: 0.8) (w / w) 7-15% (v / v), SDS 0.1% (w / v), ammonium persulfate 0.005% (w / v) and TEMED 0.025% (v / v);
    b. **Stacking gel**: the portion of gel that allows concentration of proteins is obtained by mixing 125 mM Tris-HCl pH 6.8, acrylamide / bisacrylamide (30: 0.8) (w / w) 5% (v / v), SDS 0.1% (w / v), ammonium persulfate 0.005% (w / v) and TEMED 0.025% (v / v);

    Separator solution is added into the two glasses on the support. Isopropanol is added on the top and the solution is allowed to polymerise. Isopropanol is eliminated and stacking solution added. Before of polymerisation of stacking gel, a comb is inserted into the solution. Usually, combs of 15 wells are used, however, sometimes also of 10 wells.

67. Perform SDS-PAGE electrophoresis.

    Once gels are polymerised, they are equilibrated with an electrophoresis buffer composed of 25 mM Tris-HCl pH 8.8, 192 mM glycine, 0.1% SDS (w

/ v) into a support for SDS-PAGE electrophoresis. Samples, already prepared with loading buffer and lysis buffer, are loaded into the gels. Electrophoresis is maintained at 15mA/gel (constant amperage) until the bromophenol blue front runs off the stacking gel, then, the amperage is changed at 20mA/gel (constant amperage) until the end of the run.

4.3 Semi-dry western blot

The Western Blot (WB) technique allows detecting proteins in a PVDF (Polyvinyl difluoride) or Nitrocellulose membrane after being separated in the gel by SDS-PAGE electrophoresis and transferred from the gel to the membrane applying an electric field. Generally, PVDF membranes are used for this technique, however, when the proteins that need to be detected are less than 20kDa such as frataxin, ferredoxin, cleavage caspase 3 etc., nitrocellulose membranes are used. In the case of detecting low MW and high MW proteins with the same electrophoresis, gel is cut (generally between ~20-30kDa) in order to transfer proteins into a PDVF membrane (2/3 of the gel) and a nitrocellulose membrane (1/3 of the gel). The detection of the proteins is due to the use of a primary antibody, which binds the protein that needs to be detected in the membrane, and a secondary antibody, which binds the primary antibody and using a chemiluminescent reaction the protein is detected. This chemiluminescent reaction exploits the use of a secondary antibody labelled with the horseradish peroxidase (HRP) enzyme and the application of the substrate of this enzyme, luminol reagent and hydrogen peroxide solution. The reaction takes place at the site of the membrane where the secondary antibody binds the primary antibody and the protein, thus, the protein in study can be detected. More antibody binds the protein, more amounts of protein are present. Thus, the chemiluminescent bands can be quantified using ImageLab software and the levels of proteins can be normalised on a control condition, using the following protocol:

68. Transfer proteins from gel to membranes:
    a. Millipore PVDF Immobilon-P transfer membrane (Cat# IPVH07850) with pore size of 0.45µm:
        i. Membrane is hydrated with methanol for ~1-2 minutes;
        ii. Excess of methanol is removed by washing once the membrane with ddH_2O;

iii. The membrane is incubated with the transfer buffer until the transfer is performed: 48 mM Tris-HCl, 39 mM glycine, 0.0375% SDS (w / v) and 10% methanol (v / v).

b. Amersham TM Protran TM Nitrocellulose Blotting membrane (Cat# 10600093) with pore size of 0.45µm:
   i. The membrane is incubated directly with the transfer buffer until the transfer is performed: 48 mM Tris-HCl, 39 mM glycine and methanol 20% (v / v).

c. Wet two *Whatman* filter papers/gel with the transfer buffer that used depending on the membrane;
   i. In the case of gel which is cut to be transfer into PVDF (2/3 of the gel) and nitrocellulose membrane (1/3 of the gel), *Whatman* filter papers are also cut to obtain the same dimensions of the gel and 2 papers are used for each portion of the gel;

d. Before transfer proteins into membranes, equilibrate the gel into the chosen transfer buffer for few minutes.

e. Perform transfer using Trans-Blot Turbo Transfer System:
   i. Assemble the sandwich (papers, gel and membrane) in the centre of the bottom cassette, following order from bottom to top cassettes: anode – *Whatman* paper – membrane – gel – *Whatman* paper – cathode;
   ii. Insert the cassette into the instrument and perform the transfer:
      - **All PVDF membrane:** 0.2A – 25V and 90min;
      - **2/3 PVDF membrane:** 0.2A – 25V and 60min;
      - **1/3 Nitrocellulose membrane:** 0.2A – 25V and 45min.

69. Blocks membrane, using milk or I-Block, to avoid non-specific interactions in GenHunter PerfectWestern™ containers (Cat# B172):
   a. **Using milk:** The membrane is blocked for 1 h at room temperature with a 5% milk powder solution in the solution TBST: 20 mM Tris-HCl pH 8, 125 mM NaCl and 0.1% (v / v) Tween-20;

b. **Using Tropix I-Block ™ Thermo Fisher Scientific (Cat# T2015):** The membrane is blocked for 1h at RT with 0.3% (w/v) heated PBS and 0.1% (v/v) Tween-20;

70. Before antibodies incubation, cover the membrane with Parafilm PM-999 and cut the membrane by using a ruler on the top of the membrane, following the MW of the two Markers. Thus, use the different portions of the membrane to incubate different antibodies;
71. Incubate antibodies with the membrane for protein detection in GenHunter PerfectWestern ™ containers of different size depending on the dimension of the membrane:
    a. **Primary antibody:** The chosen primary antibody, shown in **Table 5**, is diluted in TBST + 5% I-Block solution (0.3% I-Block in PBS and 0.1% Tween-20) or 5% milk and incubated with the membrane ON at 4ºC in shaking;
    b. Wash membrane 3 times with TBST + 5% of I-Block solution for 3-5 minutes at RT.

Table 5. Characteristics of primary antibodies used.

ID	Dilut.	Second.	~kDa	Source	Ref.	Membr.
Aco2	1:500	Rabbit	85	SIGMA	HPA001097	PVDF
Afg3l2	1:500	Rabbit	70	Sigma Prestige	HPA004480	PVDF
Bax	1:1000	Rabbit	21	BD Biosc.	BD610982	Nitrocell
Bcl-2	1:1000	Rabbit	34	Cell signalling	2876	PVDF
Calretinin	1:200	Rabbit	29	Santa Cruz Biotech.	Sc-50453	PVDF
Cl. Casp. 3	1:1000	Rabbit	17	Cell signalling	9661	Nitrocell.
Cyp24A1	1:1000	Goat	50	Fisher	PA519406	PVDF
Cyp27B1	1:200	Rabbit	56	Santa Cruz Biotech.	Sc-67260	PVDF
Cyp27B1	1:200	Sheep	56	NordicM.	HYD001	PVDF
FDX1	1:500	Rabbit	14	Abcam	Ab108257	Nitrocell.
Frataxin	1:250	Rabbit	14	Santa Cruz	Sc-25820	Nitrocell.
Frataxin	1:1000	Rabbit	14	Abcam	Ab219414	Nitrocell.
GRP75	1:500	Mouse	74	Abcam	Ab2799	PVDF

GRP78bip	1:500	Rabbit	78	Abcam	Ab21685	PVDF
HSP60	1:4000	Mouse	60-65	ProteinTech	66041-1-Ig	PVDF
K68-SOD2	1:500	Rabbit	24	Abcam	Ab137037	Nitrocell.
Lonp1	1:1000	Rabbit	100	ProteinTech.	15440-1-AP	PVDF
MCU	1:500	Rabbit	36	Sigma Prestige	HPA016480	PVDF
MICU1	1:500	Mouse	54	Biorbyt	Orb323178	PVDF
MICU3	1:1000	Rabbit	60	Life Techn.	PA5107178	PVDF
NCLX	1:500	Rabbit	55	LifeSpan BioSci.	LS-C102072	PVDF
NCLX	1:1000	Rabbit	55	OriGene	TA351684	PVDF
NFATc4	1:500	Rabbit	~100	Santa Cruz Biotech.	SC-13036	PVDF
Pink1	1:500	Rabbit	64-55-45	NovusBio	BC100-494	PVDF
pNFATc4	1:500	Rabbit	~120	Santa Cruz Biotech.	SC-32630	PVDF
Procasp. 9	1:1000	Mouse	47	Cell signalling	9508	PVDF
PTEN	1:1000	Rabbit	54	Cell signalling	9188	PVDF
Sirt3	1:1000	Rabbit	28	ThermoFisher Sci.	MA5-14910	PVDF
SOD1	1:1000	Rabbit	18	Chemicon	Ab1237	Nitrocell.
SOD2	1:2000	Mouse	24	Abcam	Ab16956	Nitrocell.
VDR	1:200	Mouse	48	Santa Cruz Biotech.	Sc-13133	PVDF
α-Fodrin	1:1000	Mouse	250-150/145 - 120	ENZO	BML-FG6090-0100	PVDF
β-Actin	1:250000	Mouse	42	SIGMA	A1978	PVDF

Dilution; Secondary antibody; MW, Source; Reference and membrane used.

c. **Secondary antibody:** The secondary antibody, shown in **Table 6**, is diluted in TBST + 5% I-Block solution (0.3% I-Block in PBS and 0.1% Tween-20) or 5% milk and incubated with the membrane for > 3h at RT in shaking;

Table 6. Characteristics of secondary antibodies used.

ID secondary	Dilut.	Source	Ref.
ImmunoPure Goat **Anti-Mouse** IgG (H+L) HRP conj.	1:20000	Pierce	31430
ImmunoPure Goat **Anti-Rabbit** IgG (H+L) HRP conj.	1:10000	ThermoFisher	31402
ImmunoPure Rabbit **Anti-Goat** IgG (H+L) HRP conj.	1:5000	Pierce	HJ1035344
ImmunoPure Rabbit **Anti-Sheep** IgG (H+L) HRP conj.	1:5000	ThermoFisher	81-8620

Dilution; Source and Reference.

d. Wash membrane 5-8 times with TBST for 3-5 minutes at RT;

72. Add premixed, ready to use, Millipore Immobilon Forte chemiluminescent HRP substrate (Cat# WBLUF0100) or not-mixed luminol and hydroxide peroxide Millipore Immobilon Western chemiluminescent HRP substrates (Cat# WBKLS0100) for 5 minutes to the membrane. Generally, the Immobilon Forte is use in this work to optimise the range and sensitivity of detection; however, for some antibodies this increased sensitivity is not needed, thus, the other substrate is sufficient for detection.
73. Acquire WB images using Chemidoc MP (Bio-Rad) CCD chamber.

4.3.1 Stripping conditions

In the case of using the same membrane for more antibodies of similar MW, Restore™ Western Blot stripping buffer (Cat# UK290782) is used to remove the antibody and re-block the membrane. The membrane is washed with TBST, immersed in stripping buffer for 8 minutes (PVDF membrane) or 15 minutes (Nitrocellulose membrane) at RT; washed again and re-blocked for 1h with blocking buffer. In the case of PVDF membrane, methanol activation is performed before the blocking.

4.4 Staining

4.4.1 Protein staining

Once the protein detection has been performed, the membranes can be stained in order to analyse the total protein loading, as the staining intensity depends on the amounts of total protein. In this work, staining has been performed to confirm that the transfer protocol has been correctly performed. For this reason, protein staining in PVDF membranes has been performed using Coomassie Brilliant Blue (CBB) (for high

amount of µg) or India Ink solution (for low amounts of µg) while protein staining in Nitrocellulose membrane has been performed in Ponceau S solution (for high amount of µg) or India Ink solution (for low amount of µg) with pre-treatment.

- **Coomassie Brilliant Blue (CBB) protein staining** in PVDF membranes has been performed using this protocol:
  - Rinse the membrane with ddH_2O;
  - Add 100% methanol for few seconds to activate the membrane;
  - Stain the membrane with Coomassie Brilliant Blue (CBB) solution: 0.1% CBB (w / v), 50% methanol (v / v) and 10% acetic acid (v / v) for ~5 minutes;
  - Destain the membrane 3 times (about 15 minutes in total) with 50% methanol (v / v) and 10% acetic acid (v / v);
  - Wash the membrane with ddH_2O and dry the membrane.
- **Ponceau S protein staining** in Nitrocellulose membrane has been performed using this protocol:
  - Rinse the membrane with ddH_2O;
  - Directly stain the membrane with 0.1% Ponceau S solution (w / v) and 5% acetic acid (v / v) for ~5 minutes;
  - Decolorate the membrane 3x with ddH_2O and dry the membrane.
- **India Ink protein staining** in Nitrocellulose and PVDF membrane has been performed using this protocol:

  Only for Nitrocellulose membrane:

  - Pre-treat the membrane with 1% KOH for 5 min with shaking and rinse twice for 15 min with PBS with shaking;

  For Nitrocellulose and PVDF membranes:

  - Wash blotting membrane 3x for 10 min each in 37ºC Tween-20 Solution with shaking: 0.3% (v / v) Tween-20 in PBS, pH 7.4;
  - Wash the membrane 3x for 10 min each in RT Tween-20 solution with shaking:
  - Incubate membrane in India Ink solution ON with shaking: 0.1% India Ink (v / v) Pelikan 17 Black in TBST;
  - Rinse the membrane twice in RT Tween-20 solution;

- Rinse with ddH_2O and dry membrane.

4.4.2 Gel staining

In order to confirm that the transfer protocol has been correctly performed, the amount of protein remained into the gel is stained with a gel staining solution: 0.1% Coomassie Blue G250 (w / v), 10% acetic acid (v / v) and 25% isopropanol (v / v) for several hours. Thus, gel is destained using 10% acetic acid (v / v) and 10% isopropanol (v / v).
The gel staining has been frequently performed to confirm the transfer into the membrane of proteins with higher MW, more difficulty transferred into membranes.

4.5 Obtaining and analysis of bands

A Chemidoc MP device (BioRad) CCD camera has been used to acquire chemiluminescent images of protein bands in membranes. ImageLab ™ software, version 5.2.1 (BioRad), has been used for the analysis of the protein bands. The intensity of the studied protein and the intensity of β-actin is obtained and the ratio (intensity of studied protein / intensity of β-actin protein) is calculated. Finally, the ratio is normalised on the control value.

4.6 Enzymatic activity

Aconitase activity has been assayed by an indirect method using the reduction of nicotinamide adenine dinucleotide phosphate (NADPH) by isocitrate dehydrogenase, as described in (Kakhlon et al., 2008). Formation of NADPH is followed by fluorescence in 96-well plates (excitation $\lambda_{345\ nm}$, emission $\lambda_{550\ nm}$) at 37°C, using TECAN® apparatus, calculating the aconitase activity of whole cells by the slope of NADPH formation, recorded from the beginning of the experiment. Then, the value is normalised on the Citrate synthase activity, using the spectrophotometer Shimadzu UV-2401, which measures the amounts of mitochondria present in the extract.
Briefly, neuronal cells, plated in 24-well dish at the density of 10000 cells/well, 4-days after lentivirus transduction are processed using the following protocol:

47. Wash 3x cells with cold PBS, maintaining the plate onto ice;
48. Collect cells from 6-wells (~60000 cells) with pipette in 25µl of lysis buffer for each condition:
    a. Tris HCl 50 mM pH 7,4;

b. protease inhibitors (without EDTA);
c. 0,5% Triton X-100 (v/v);
d. 2,5 mM sodium citrate;

49. Mix with the pipette and incubate for 5 minutes on ice;
50. Centrifuge at 13000g for 5 min at 4°C, to remove insoluble materials, and fresh activity is measured in duplicate.

4.6.1 Aconitase activity by fluorimeter

Once cell extract in lysis buffer is ready, it has been analysed aconitase activity. Aconitase (Aco) is an enzyme that catalyse the formation of isocitrate from citrate, though the *cis*-aconitate intermediate, in the first step of tricarboxylic acid (TCA) cycle. Then, isocitrate is converted into α-ketoglutarate by isocitrate dehydrogenase, converting $NADP^+$ into NADPH, as shown in **Figure 52**. Formation of NADPH is followed by fluorescence in 96-well plates (excitation $\lambda_{345\ nm}$, emission $\lambda_{550\ nm}$) at 37°C in TECAN® apparatus, with the following protocol:

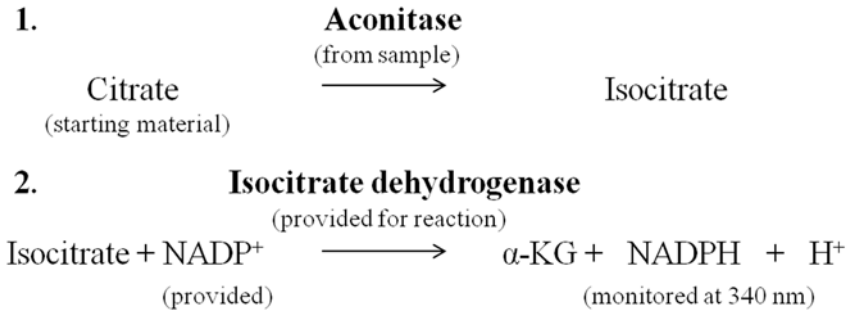

Figure 52. Aconitase and Isocitrate dehydrogenase reactions. See text for details.

51. Turn on TECAN® apparatus in order to allow the temperature reaching 37°C prior the experiment;
52. Prepare a suitable solution:
    a. 50 mM Tris-HCl (pH 7.4); 0,6 mM $MnCl_2$; 2,5 mM sodium citrate; 0,2 mM $NADP^+$;2 U isocitrate dehydrogenase.
53. The reaction is monitored by the presence of three controls in the above buffer:
    b. Positive control 0,38µM NADPH;
    c. Negative control without cell extract;
    d. Negative control without substrate sodium citrate;

54. Add 10µl of cell extract (~20µg) in the solution just prior the read (100µl/well) in a Falcon® 96-well Black/Clear Flat Bottom TC-treated Imaging Microplate (Ref# 353219);
55. Read the fluorescence with TECAN Infinite ® 200 PRO fluorescence microplate reader (i-control software 1.3.3.0), mantaining controlled experimental conditions (constant temperature at 37°C, a gain obtained from positive control NADPH (manual 145), excitation $\lambda_{345\ nm}$, emission $\lambda_{550\ nm}$);
56. Allow the experiment to continue for at least 40minutes, then analyse the slope (Fluorescence/min) of the curve subtracting blank;
57. Calculate the Specific Aconitase activity in U/mg (U=µmol/l), comparing the fluorescent value with the one obtained from positive control NADPH at concentration 0.38 µM and the protein concentration using Qubit (described elsewhere);

4.6.2 Citrate synthase activity by spectrophotometer

Once aconitase activity has been performed, citrate synthase activity has been analysed from the same sample in duplicate. Citrate synthase (CS), another TCA cycle enzyme, catalyses the formation of citrate using acetil-CoA and oxalacetate. Being a mitochondrial matrix enzyme, which remain constantly in mitochondria, it is considered a control of mitochondrial amount. The activity is calculated using the protocol described in (Shepherd & Garland, 1969) (**Figure 53**), in which the reduction of 5.5'-dithiobis-(2-nitrobenzoic acid) (DTNB or Ellman's reagent) allows to measure CS activity, expressed as µmol of reduced DTNB per min per ml using a DTNB molar extinction coefficient of ε_{412}= 13.8 mM^{-1} cm^{-1}. The enzymatic reduction of DTNB determines an increase of absorbance, which is calculated with the spectrophotometer Shimadzu UV-2401.

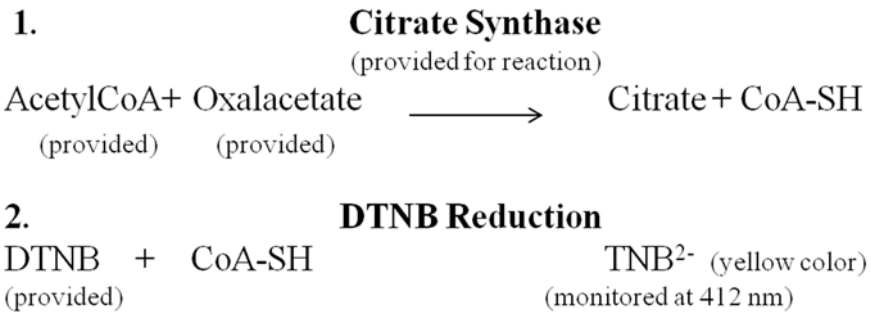

Figure 53. Citrate Synthase reaction and DTNB reduction. See text for details.

The activity has been analysed using the lineal part of the curve, using the follow protocol:

58. Add in a cuvette of 1 cm light-path:
    a. 810µl of milliQ water;
    b. 100µl of DTNB (0.4 mg/mL in 1M Tris HCl at pH 8.1);
    c. 10µl Acetyl-CoA (10mg/mL);
    d. 4µl of cell extract;
59. Measure the blank absorbance at 412 nm for 120 seconds at 25°C;
60. Add the substrate in the cuvette: 7µl Oxalacetate (8.5 mg/mL in milliQ water);
61. Measure the absorbance at 412 nm for 120 seconds at 25°C to analyse the citrate synthase activity (last linear minute);
62. Calculate the slope (Abs/min), subtracting the blank measure;
63. Then, calculate the enzymatic unit (U) as µmol of reduced DTNB per min per litre (U/l), using a DTNB molar extinction coefficient of ε_{412}= 13.8 mM^{-1} cm^{-1};
64. Convert U/l in specific activity (U/mg) by analysing the protein concentration with Qubit;

4.6.3 Ratio aconitase / cytrate synthase activity

The ratio total Aconitase/Citrate Synthase activity (Aco/CS, both in U/mg) allows calculate the Aconitase activity in relation to the amounts of mitochondria present in the extract. The ratio value is related to Scr control condition.

5 COMPLEMENTARY TECHNIQUES

5.1 Baseline fluorescent level

Raw data of images or videos ROIs (cell soma, neurite or mitochondria depending on the experiment) allow us to analyse baseline fluorescent levels for each ROI. In the case of images ROIs, fluorescent intensity was measured as mean in ImageJ software, upon subtraction of suitable background (Rolling ball radius: 50 or 100 pixels depending on the experiment), using a circle (for soma or mitochondria) or a constant segment parameter of 100 pixels or a rectangle (for neurites). In the case of videos ROIs, mean of the first 15 seconds (for Fura-2 analysis), for each cell, using a circle parameter, was used as baseline level, without subtracting background. Videos ROIs were detected directly with Aquacosmos software for Fura-2 ratiometric fluorescence intensity detection or ImageJ, using a Bioformat plugin and time-series analysis, for no-ratiometric dyes.

5.2 Peak analysis

In the case of videos ROIs for time-lapse experiments, normalization of fluorescent data (F) on the initial fluorescent value (F_0) is necessary for all peak measurements. Peak Analysis has been performed using OriginPro software, with data normalised F/F_0 and scaled on a constant time axis in seconds.

5.2.1 Calcium influx

For each ROI, a sparkline graph, normalised and scaled, was used to select an active plot, indicating the extremes of the region of interest or a range corresponding to Ca^{2+} influx. The region between the baseline fluorescent intensity just before the wave and the maximum fluorescent intensity (Peak) was considered as active plot in OriginPro and a lineal mathematical function was used to fit the curve and analyse the rate of Ca^{2+} influx between these two extremes. The resultant value of slope was used as influx rate parameter, using following equation: $y = a + b\ x$.

5.2.2 Calcium efflux

For each ROI, a sparkline graph, normalised and scaled, was used to select an active plot, indicating the extremes of the region of interest or a range corresponding to Ca^{2+}

efflux. The region between the maximum fluorescent intensity (Peak) and the end of the tail wave was considered as active plot in OriginPro and an exponential function (one-phase exponential decay Expdec1 function with time constant parameter and Levenberg Marquardt iteration algorithm) was used to fit the curve, until converged fit, and analyse the rate of Ca^{2+} efflux between these two extremes. The resultant values of Ca^{2+} efflux half-life (τ) and Ca^{2+} efflux decay rate (k) were used as derived efflux parameters, using the following equation: $y = A_1 * \exp(-x/t_1) + y_o$.

5.2.3 Amplitude

For each ROI, a sparkline graph, normalised and scaled, was used to find and select the peak of the stimulus (F_{max}) and the baseline level ($F_{baseline}$) using OriginPro. The amplitude is the ΔF calculated by subtracting F_{min} from F_{max} and corresponds to the amounts of Ca^{2+} present in the store at the moment of the stimulus for Fura-2 analysis, while indicates the uptake of $Ca^{2+}{}_m$ after stimulus for Rhod5N analysis in permeabilised cells.

5.3 Gauss-curve model for DRG subpopulation

DRG subpopulation shows a bell-shaped frequency distribution, in which medium-size DRG neurons represent the bigger proportion of cells than large or small-size soma. Histograms of frequency distribution can be fit with a Gauss model using OriginPro software. Fitting is performed until the model converge with histograms and the parameter x_c is obtained, which represents the mean (or centre) of the Gauss curve.

6 STATISTICAL ANALYSIS

For DRG neurons primary cultures, data has been obtained from at least three independent isolations (referred as n number). Each DRG isolation, in which an average of 15-18 rats have been used, it is usually performed between 8-13h a.m. followed by purification passages. For each experiment, at least 3 independent wells have been plated for each condition using a pool of cells obtained from one isolation.

For FA lymphoblastoid cells, 3 independent experiments have been performed at different passages of the cell line. Values were expressed as Mean ± SD for n=2 or Mean ± SEM (error bars) for $n \geq 5$. For all experiments, normality of data was assessed by using Kolmogorov-Smirnov and Shapiro-Wilk tests and equal variance by using Bartlett and Brown-Forsythe tests. Then, one-way ANOVA was used to assess differences between groups for variable treatment. If the ANOVA test was statistically significant, we performed post hoc pair-wise comparisons using the Bonferroni test. The *p*-values lower than 0.05 (*, #), 0.01 (**, ##) or 0.001 (***, ###) were considered significant, indicating (*) as frataxin-deficiency *vs* control condition and (#) as treatment *vs* vehicle. Graphpad Prism 5.0 was used for all above analysis. Grubbs' test (OriginPro 2017) was used to identify outliers, but no outlier, if existent, was eliminated from the analysis.

RESULTS

RESULTS

1 FXN-DEFICIENT DRG NEURONS AS A FA MODEL

1.1 RNA interference to decrease frataxin levels

This thesis project is based on the study of a neuronal model of Friedreich Ataxia previously developed in our laboratory (Mincheva-Tasheva et al., 2014). The cellular model of frataxin deficiency, based on RNA interference, using neonatal rat primary culture of sensory neurons from dorsal root ganglia, allows us studying the mechanisms that occur after frataxin depletion and screening different drugs in order to choose a better therapeutic strategy. In this model, three shRNAs are transduced in primary culture of dorsal root ganglia neurons, using lentivirus: FXN1 or FXN2 as shRNAs targeting frataxin mRNA and Scrambled (Scr) as a control, since it does not interfere with any known mammalian mRNA. To assess the efficiency of transduction for such shRNAs, lentivirus carrying the green-fluorescent protein (GFP) has been used at the same concentration (20ng/1000cells). By counting the number of GFP-positive cells on the total number of cells, it has been possible to measure the efficiency of viral transduction, which reached ~75% at the end of the experiment. Representative images are indicated in **Figure 54**.

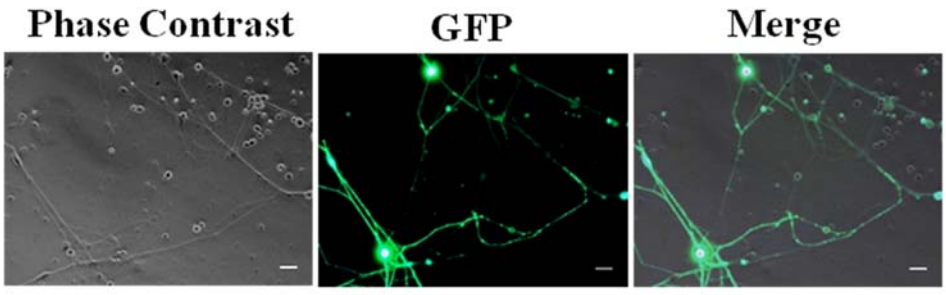

Figure 54. Transduction efficiency in DRG neurons. Representative images of DRG neurons, at 5 days, transduced with GFP. Phase-contrast and fluorescent images have been taken at the same field. The number of GFP-positive cells on the total number of cells has been counted on the merge image. Scale Bar= 30µm and objective= 16x.

This percentage of transduction, when applied to Scr and FXNs lentivirus, resulted in the progressive reduction of frataxin levels. **Figure 55** shows representative western blot images of frataxin depletion at several days after lentivirus transduction (**A**) and the

percentage of such reduction (**B**). As shown in the graph, FXN levels were reduced by 23-28%, mean values for shRNAs FXN1 and FXN2 respectively, as soon as 24hrs after transduction, while the residual percentage of frataxin, compared to the Scr control, is 30% for FXN1 and FXN2 shRNAs at the end of the experiment. The achieved reduction of 70-75% of Scr level is in close relation with the frataxin protein values observed in FA patients. For this reason, this model represents a good alternative for the study of neuronal alterations in FA.

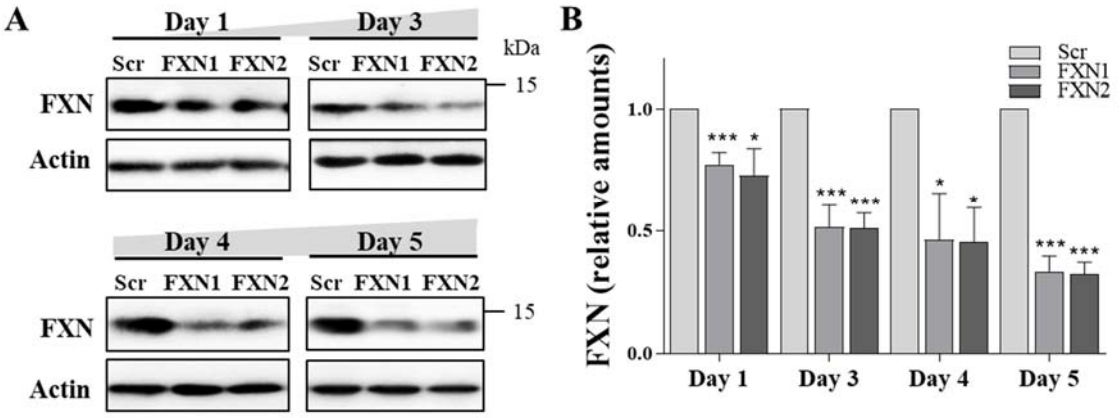

Figure 55. Frataxin depletion in DRG neurons. In A, WB analysis of frataxin mature protein in total lysates of frataxin-deficient DRG neurons (shRNA FXN1 and FXN2 *vs* scrambled control) at 1-3-4 and 5-days after lentivirus transduction as described in Materials and Methods. In B, histograms represent the percentage of frataxin depletion compared for each day. Frataxin values are normalised on β-actin and related to Scr control. Data are Mean ± SEM obtained from n=5 independent isolations. Scr conditions at each time point are indicated as 1 and significant values compared to each scrambled condition are indicated by (*).

1.2 Mitochondrial proteins remaining stable during FXN depletion

DRGs sensory neurons have been isolated from neonatal rats and transduced with lentiviral vectors carrying frataxin interfering shRNA (FXN1 or FXN2) or a non-interfering shRNA (Scr) as a FA model. As frataxin is a mitochondrial protein, and mitochondria have a central role in FA, it has been analysed in the model the content of two mitochondrial proteins, LONP1 (Lon peptidase 1) and MCU (Ca^{2+}_m uniporter). While the content of frataxin in frataxin-deficient DRG neurons decreases in a progressive manner, the content of LONP1 and MCU levels remain stable (as shown in **Figure 56 A-C** for intensity bands and **B-D** for quantification), indicating no alterations in mitochondrial number or biogenesis in this neuronal model.

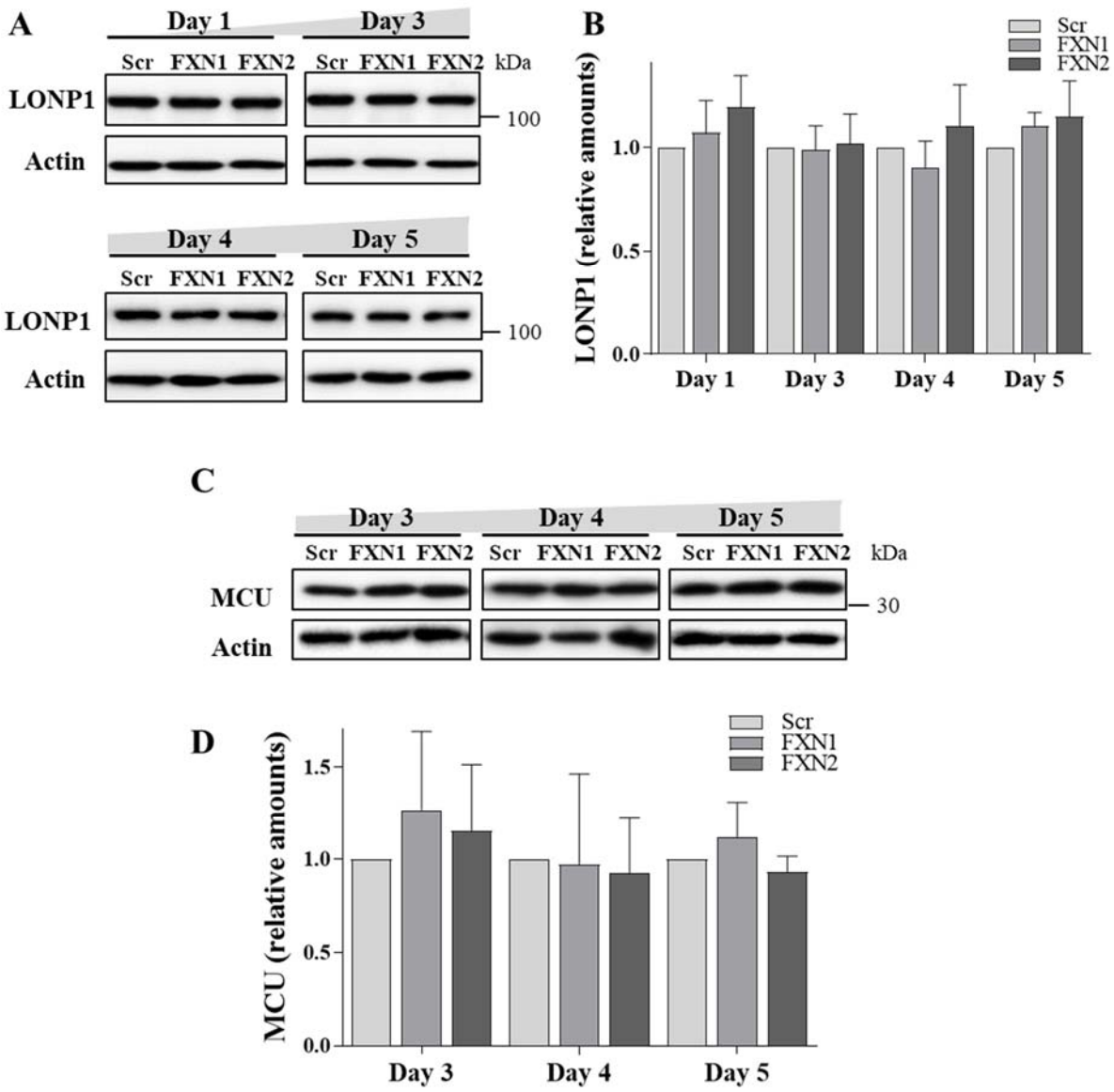

Figure 56. Mitochondrial proteins remain stable during frataxin depletion. In A, WB analysis of LONP1 protein in total lysates of frataxin-deficient DRG neurons at 1- 3- 4 and 5- days after lentivirus transduction Quantification is shown in B. Data are Mean ± SEM obtained from n=4 independent isolations. In C, WB analysis of MCU protein in total lysates of 3- 4 and 5-days transduced neurons. Quantification in D. Data are Mean ± SEM obtained from n=3 independent isolations. Scrambled (Scr) conditions at each time point are indicated as 1. As a mitochondrial control, no variation in both proteins LONP1 and MCU levels are shown.

1.3 Frataxin deficiency alters the subpopulations of DRGs

Frataxin deficiency induces degeneration of proprioceptive neurons of DRGs. These cells are a very small amount comparing on the total neurons present in a DRG and can be selected by looking at the soma size. In fact, proprioceptive neurons are the largest cells present in DRGs. In order to analyse if the Friedreich Ataxia model displays this characteristic, soma size has been calculated in Scr, FXN1 and FXN2 conditions, during the time in culture. Soma size have been categorised in different intervals of µm (>25; [22.5-25); [20-22.5); [17.5-20); [15-17.5); [12.5-15); [10-12.5); [7.5-10); <7.5) as indicated in Materials and Methods. Histograms in **Figure 57 A**, **C** and **E** indicate the percentage of neurons presents in each soma size interval in Scr, FXN1 and FXN2 conditions, respectively, for day 1, day 3 and day 5 after lentivirus transduction. Note the similarity in the gauss curves for each condition at day 1. The differences in the subpopulation of DRG neurons are more prominent at day 5 after lentivirus transduction, where the gauss curve peaks correspond to [15µm-17.5µm) soma size interval for Scr control, [12.5µm-15µm) for FXN1 and [10µm-12.5µm) for FXN2. Specifically, a gauss curve model has been fitted to histograms using Origin software, as mentioned in Materials and Methods, and the mean of the curve has been detected. Thus, the mean of the gauss curve in Scr condition is 17.34µm, 16.27µm and 15.34µm, while the mean in FXN1 condition is 16.46µm, 15.16µm and 13.78µm and the mean in FXN2 is 16.38µm, 13.97µm and 11.49µm, respectively, for day 1, day 3 and day 5. Histograms in **Figure 57 B**, **D** and **F** indicate the percentage of neurons presents in each soma size interval during time-course, respectively, for Scr, FXN1 and FXN2. Note that the gauss curves are similar for Scr conditions during time-course, while for FXN1 and FXN2 there is a switch into smaller DRG neurons population during the time in culture, indicating that larger and medium size soma neurons are lost during frataxin deficiency.

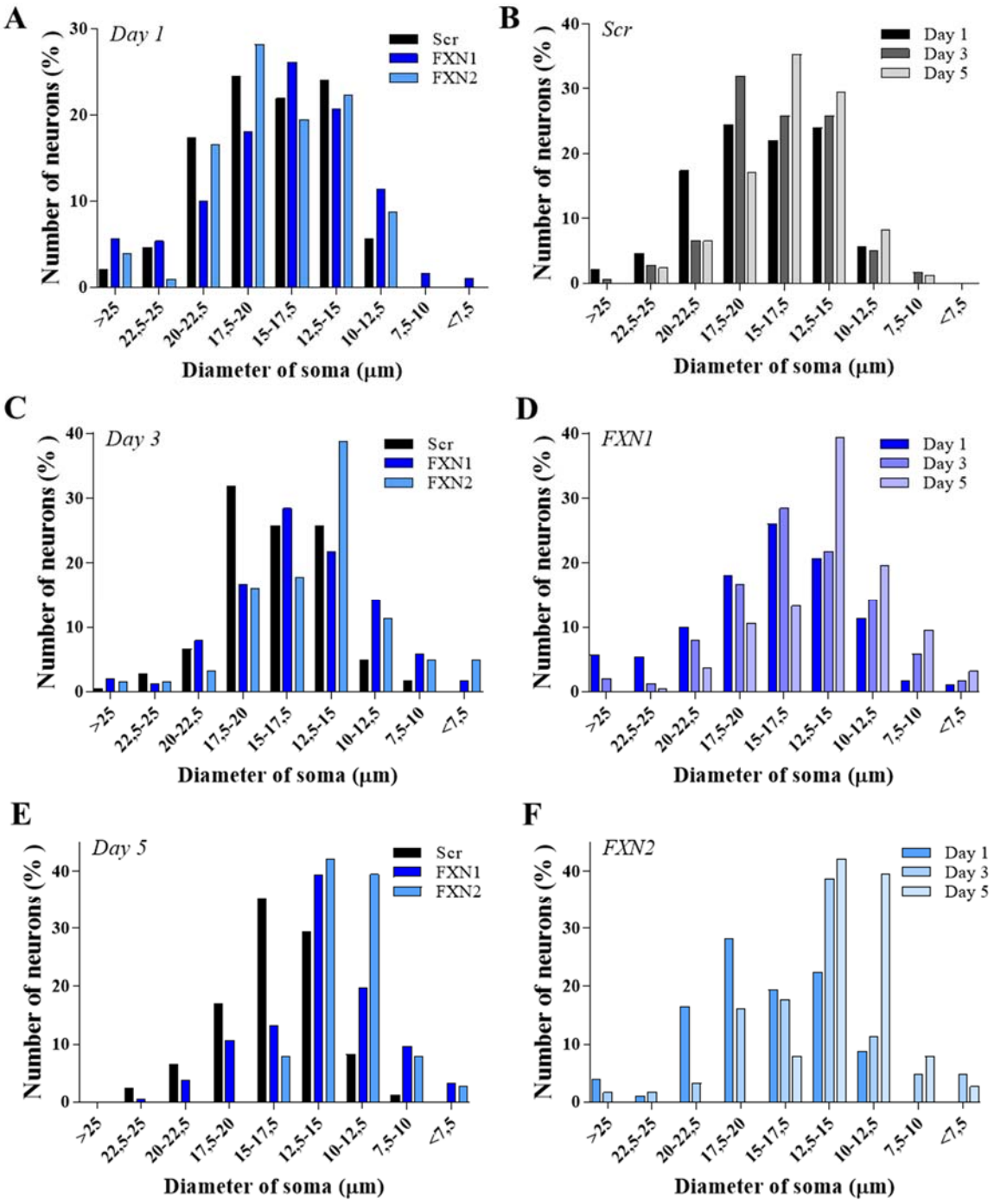

Figure 57. DRG neurons subpopulation changes in frataxin deficiency. DRG neurons are categorised in different size depending on soma diameter in µm (>25; [22.5-25); [20-22.5); [17.5-20); [15-17.5); [12.5-15); [10-12,5); [7.5-10); <7.5) as described in Materials and Methods. In A, C and E, histograms represent the percentage of soma diameters in Scr, FXN1 and FXN2 at different days after lentivirus transduction, respectively, day 1, day 3 and day 5, empathising the changes between control and frataxin deficiency. In B, D and F, histograms represent the percentage of soma diameters at different days after lentivirus transduction by analysing in a separated manner Scr, FXN1 and FXN2, empathising the changes during time-course. Data are the percentage obtained from n=3 independent experiments, analysing 196 soma for Scr, 299 soma for FXN1 and 103 soma for FXN2 at day 1 and followed until the end of the experiment.

As the size of DRG neurons indicates the characteristic of being proprioceptive, mechanoreceptor and nociceptor neurons, respectively, for large, medium and small DRG neurons, cells have been separated into 3 groups. Neonatal rat DRG neurons are categorised in small, medium and large depending on soma size, respectively, >22 µm (large, L), (22µm -15µm] (medium, M) and <15µm (small, S). Histograms in **Figure 58 A**, **B** and **C** indicate the percentage of L, M and S soma in Scr DRG neurons, respectively, at day 1, 3 and 5. Histograms in **Figure 58 D**, **E** and **F** indicate the percentage of L, M and S soma in FXN1 DRG neurons, respectively, at day 1, 3 and 5. Histograms in **G**, **H** and **I** indicate the percentage of L, M and S soma in FXN2 DRG neurons, respectively, at day 1, 3 and 5. Note the decrease in proprioceptive neurons and increase in nociceptor neurons during the time in all conditions, however, when analysing frataxin-deficient DRG neurons the differences are more prominent. In fact, the percentage fluctuates between ~9% (L), ~60% (M) and ~31% (S) DRG neurons at day 1 and 3% (L), 58% (M) and 39% (S) DRG neurons at day 5 for Scr condition, but 1% (L), 27% (M) and 72% (S) DRG neurons for FXN1 condition and 0% (L), 8% (M) and 92% (S) DRG neurons for FXN2 condition. Despite being preliminary data, as the number of cells analysed is low, the data perfectly match with previously reported results in which large and medium size neurons are more prone to die in FA.

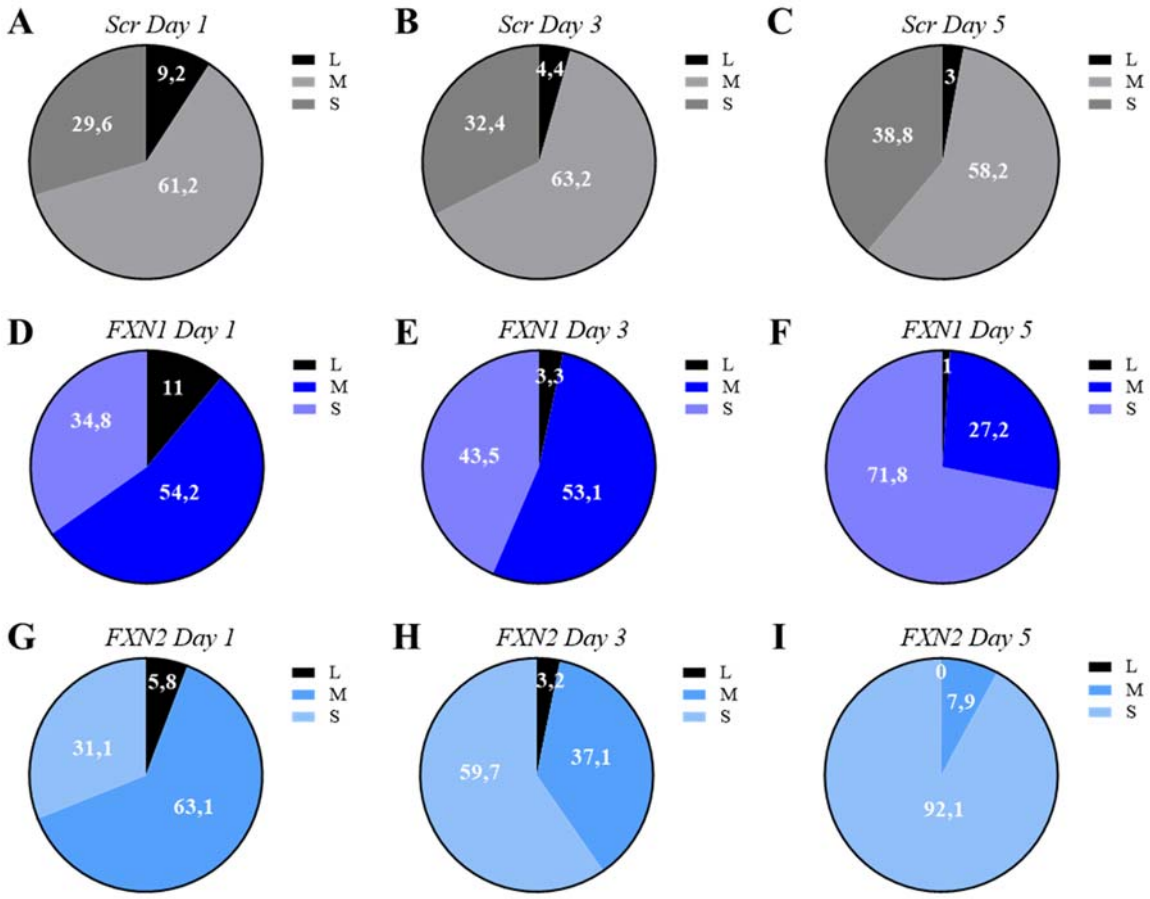

Figure 58. Percentage of small, medium and large DRG neurons in frataxin deficiency. DRG neurons are categorised in different size depending on soma diameter: >22 µm (large, L); (22µm -15µm] (medium, M); <15µm (small, S) as described in Materials and Methods. In A, B and C, histograms represent the percentage of S, M and L control cells on the total of neurons analysed, respectively, at day 1-3 and day 5 after lentivirus transduction. In D, E and F, histograms represent the percentage of S, M and L FXN1 cells on the total of neurons analysed, respectively, at day 1-3 and day 5 after lentivirus transduction. In G, H and I, histograms represent the percentage of S, M and L FXN2 cells on the total of neurons analysed, respectively, at day 1-3 and day 5 after lentivirus transduction. Data are the percentage obtained from n=3 independent experiments, analysing 196 soma for Scr, 299 soma for FXN1 and 103 soma for FXN2 at day 1 and followed until the end of the experiment.

1.4 Frataxin deficiency alters mitochondrial function

1.4.1 Frataxin deficiency reduces mitochondrial membrane potential

Numerous studies in the literature correlate frataxin deficiency with mitochondrial depolarisation (Abeti, Baccaro, et al., 2018; Bolinches-Amorós et al., 2014; Mincheva-Tasheva et al., 2014; Shidara & Hollenbeck, 2010). Using this FA model, previous results from our laboratory showed an increase of mitochondrial depolarisation at 5 days after lentivirus transduction with the JC-1 assay (Mincheva-Tasheva et al., 2014). However, no data were collected in early stages of frataxin depletion. Thus, in this work, JC-1 dye fluorescence has been analysed in a time-course study of mitochondrial depolarisation from 1 day to 5 days after lentivirus transduction in frataxin-deficient DRG neurons. Representative images of DRG neurons stained with JC1 are presented in **Figure 59A**. Histograms in **Figure 59B** represent the fluorescent intensity ratio of depolarised mitochondria (green) over polarised mitochondria (red), normalised to Scr control at day 1 (100%). Thus, a raise in this ratio indicates an increase of depolarised mitochondria in FXN-depleted neurons. Results show 28-24% more intensity of green/red fluorescence in the early stages of frataxin-depletion (FXN1-FXN2) and 42-200% at the end of the experiment. Dashed lines (**Figure 59B**) represent the mitochondrial depolarisation ratio obtained by treating Scr controls with 50µM and 100µM CCCP (dark and light lines, respectively), at three days after lentivirus transduction. Representative images of CCCP-treated Scr control cells are shown in **Figure 59C**. These results indicate that mild mitochondrial depolarisation in frataxin-deficient DRGs occurs at early stages of frataxin deficiency, although the content in mitochondria is not changing (**Figure 56**).

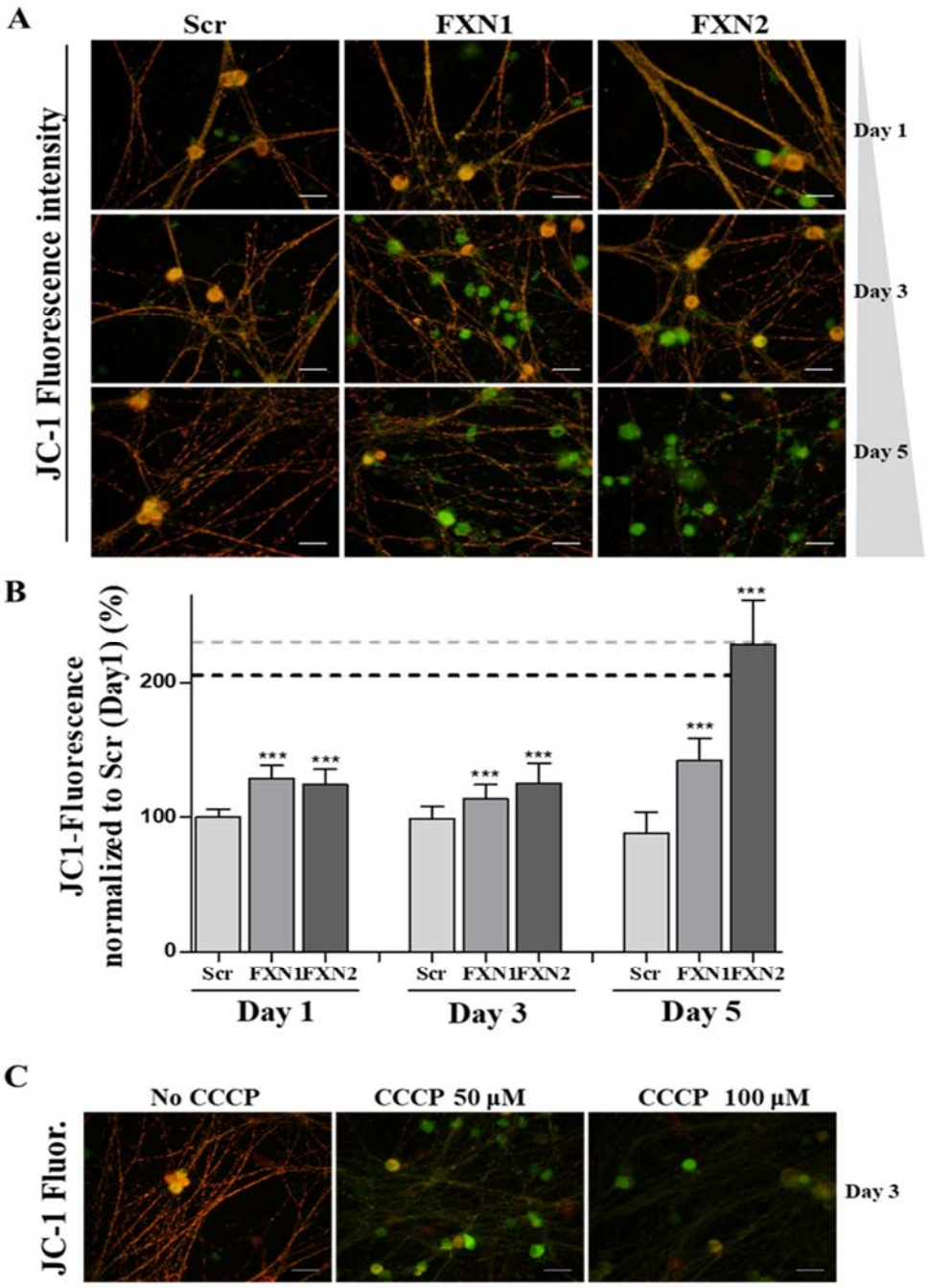

Figure 59. Small FXN reduction induces mild mitochondrial depolarisation. Representative images of fluorescent dye JC-1 in frataxin-deficient DRG neurons at day 1-3 and 5 after lentivirus transduction in **A**. Scale Bar= 30µm and objective= 32x. JC-1 images indicate mild depolarisation in FXN-depleted neurons. Histograms in **B** represent fluorescent green/red intensity ratio. Data are Mean ± SEM obtained from n=5 independent isolations. A range of 17-35 fields has been analysed for Scr conditions, a range of 20-40 fields for FXN1 conditions and 19-37 fields for FXN2 conditions. For each condition, three images per field have been taken. Scrambled condition at day 1 is indicated as 100%. Dashed lines indicate the values of green/red intensity ratio obtained in Scr controls using 50µM (bold line) and 100µM (light line) CCCP for 6h at three day after lentivirus transduction. Such values are the mean obtained from n=3 experiments and normalised to Scr at day three. Values: 209% (bold line) and 231% (light line). In **C**, representative images of CCCP-treated Scr conditions at day 3 after lentivirus transduction. Scale Bar= 30µm and objective= 32x.

Nevertheless, JC-1 fluorescence could produce some technical artefacts. Thus, $\Delta\Psi_m$ was also analysed with TMRM, as described in Materials and Methods, in order to confirm JC-1 results. TMRM was used in "re-distribution" mode, a manner in which depolarisation is indicated by decreased levels. Representative images of DRG neurons stained with TMRM are presented in **Figure 60A**. Histograms represent the basal TMRM fluorescent intensity in control and frataxin-deficient DRG neurons in soma (**Figure 60B**) and neurites (**Figure 60C**) normalised to Scr control as percentage, indicating mitochondrial depolarisation in frataxin deficiency. Results show 18% and 19% reduction of $\Delta\Psi_m$ in soma, respectively in FXN1 and FXN2 conditions, while, in neurites, a 22% and 39% reduction in FXN1 and FXN2, respectively. Although the values are not the same between the different methods (JC1 and TMRM), depolarisation by frataxin deficiency is confirmed by both probes.

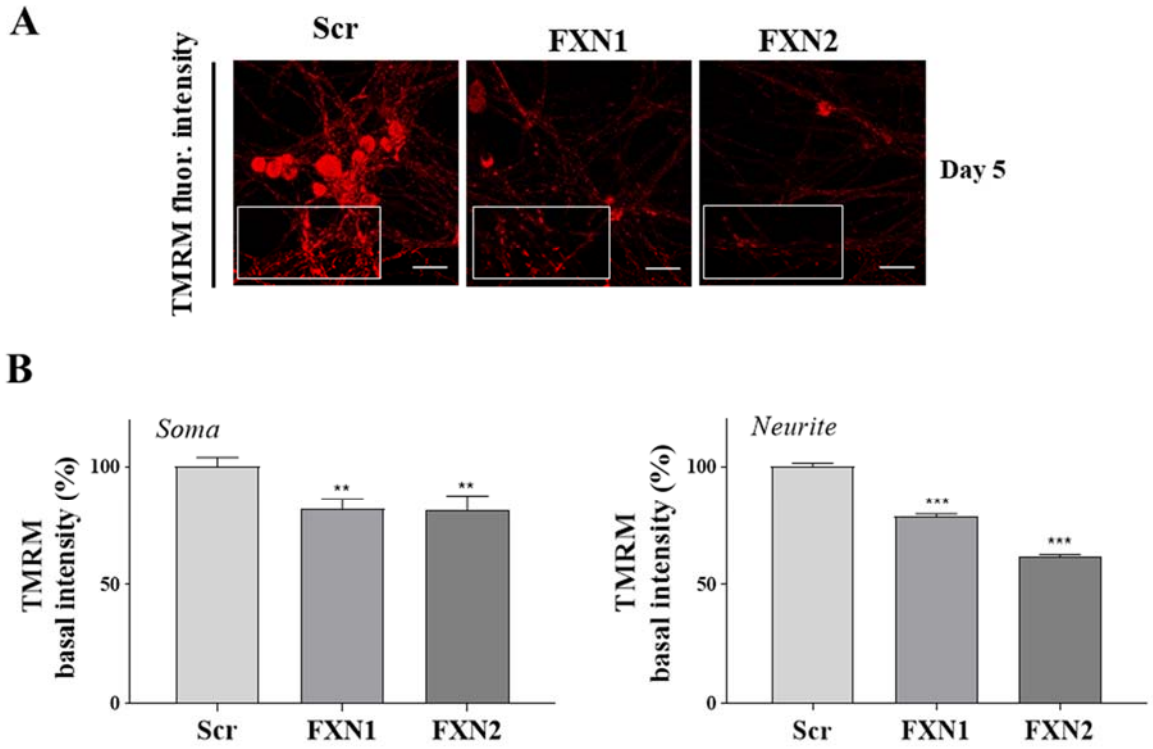

Figure 60. FXN deficiency induces mitochondrial depolarisation. Representative Z-stack images of fluorescent dye TMRM in frataxin-deficient DRG neurons at day 5 after lentivirus transduction in **A**. Scale Bar= 30µm. Images indicate depolarisation in FXN-depleted neurons, as TMRM 25nM is used in "re-distribution" mode. Histograms in **B** and **C** represent fluorescent intensity in soma and neurites, respectively. A range of 48-94 soma and 1912-2913 neurites were analysed for Scr; a range of 62-72 soma and 2471-2831 neurites were analysed for FXN1 and a range of 41-91 soma and 1994-2958 neurites were analysed for FXN2. Data are Mean ± SEM obtained from n=3-5 independent isolations. Scrambled condition is indicated as 100% in both graphs. Significant values compared to control conditions are indicated by asterisk (*).

1.4.2 FXN deficiency maintains $\Delta\Psi_m$ by using ATP synthase working in reverse

The decrease in $\Delta\Psi_m$, shown in the above paragraphs, points out the question if frataxin-deficient DRG neurons can maintain the $\Delta\Psi_m$ or not in response to inhibitors of mitochondrial complex. In a physiologic situation, when TMRM is used at 25nM in a re-distribution mode, the addition of oligomycin (complex V inhibitor) induces mitochondrial hyperpolarisation (visible by an increase of TMRM intensity), indicating that prior to drug addition ATP synthase was working in "forward" mode. In a pathological situation, oligomycin induces depolarisation (visible by a decrease of TMRM intensity), indicating that ATP synthase was working in "reverse" mode. Rotenone is used to inhibit the complex I, while FCCP is used to dissipate $\Delta\Psi_m$. Basal intensity (F_0) was considered as 100% and the end of the experiment (F_{FCCP}) was considered as 0% in each condition, in order to clearly analyse the dynamic changes in response to drug addition. The results in **Figure 61A** (soma) and **B** (neurites) indicate that frataxin deficiency induces ATP synthase working in reverse mode, thus consuming ATP instead of producing, in contrast to control condition where ATP is produced.

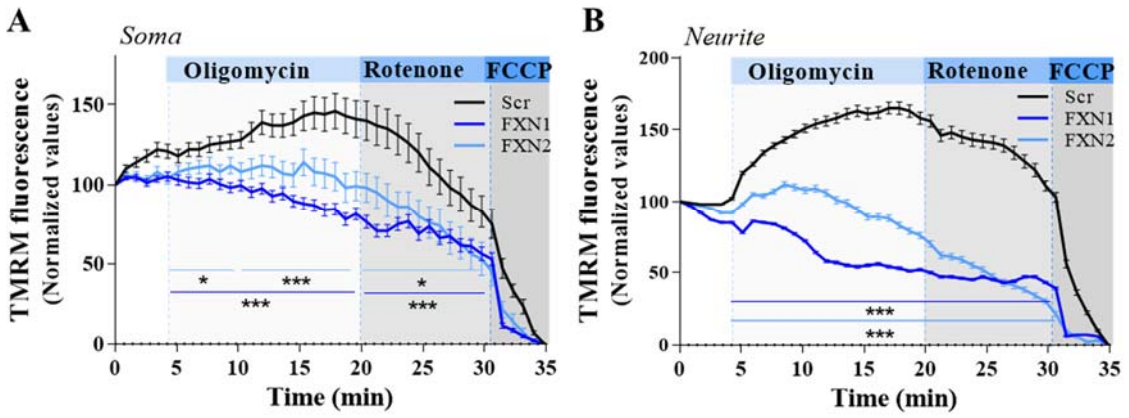

Figure 61. FXN deficiency induces ATP synthase working in "reverse" mode. Representative time-course curves of TMRM fluorescence intensity in response to drug addition in Scr controls and frataxin-deficient DRG neurons in soma (A) and neurites (B). Oligomycin 2µg/mL for 15 min, rotenone 2µM for 10min; FCCP 10µM for 5 min. Data are normalised by indicating the baseline of TMRM (F_0) as 100% and the value after 5 minutes of addition of FCCP (F_{fccp}) as 0%. A range of 48-94 soma and 1912-2913 neurites were analysed for Scr; a range of 62-72 soma and 2471-2831 neurites were analysed for FXN1 and a range of 41-91 soma and 1994-2958 neurites were analysed for FXN2. Data are Mean ± SEM obtained from n=3-5 independent isolations. Scrambled condition is indicated as 100% in both graphs. Significant values compared to control conditions are indicated by asterisk (*). **Data have been analysed with the help of A. Sanz-Alcazár.**

1.4.3 NCLX decrease is an early consequence of FXN depletion

Different uniporters and exchangers regulate Ca^{2+}_m content. For example, Ca^{2+} influx is mainly regulated by the Ca^{2+}_m uniporter (MCU). MCU level has been investigated by WB, observing not altered values comparing to the control Scr, as shown in **Figure 56A**. This result suggests a normal influx of Ca^{2+} into the mitochondria. However, the mitochondrial Na^+-Ca^{2+} exchanger (NCLX), which allows Ca^{2+} efflux in exchange with Na^+ or lithium influx, shows progressive decreasing levels (**Figure 62**) in frataxin-deficient DRG neurons, suggesting an altered Ca^{2+}_m efflux. At 24hrs after transduction, when FXN levels reduce by 23-28% (as indicated in **Figure 55**), NCLX levels decrease by 28-12% for shRNA FXN1 and FXN2, respectively, reaching, at 5-days after lentivirus transduction, a reduction by 50-70% compared to control DRG neurons. These results suggest an accumulation of Ca^{2+} within mitochondria. The same result has been shown by our laboratory for frataxin-deficient cardiomyocytes, strengthening the hypothesis of Ca^{2+}_m efflux alterations in FA (Purroy et al., 2018).

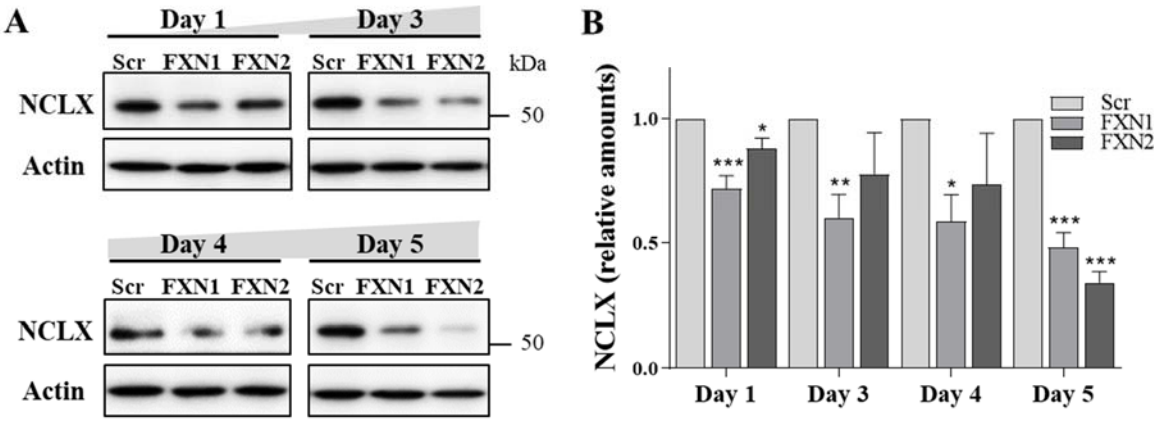

Figure 62. NCLX decrease initiates with a minor reduction of FXN levels. Amounts of the NCLX were analysed in time-course by WB, in A, showing a decrease that correlates with slight FXN reduction. Data are Mean ± SEM obtained from n=4 independent isolations. Quantification is shown in B. Scr conditions at each time point are indicated as 1 and significant values compared to each scrambled condition are indicated by (*).

1.4.4 MICU1 and MICU3 protein levels decrease in FXN deficiency

Despite the MCU protein levels remain stable in frataxin deficiency, proteins such as MICU1, MICU2, EMRE and in the case of neurons MICU3 are necessary for the activity of MCU complex. The stable amounts of MCU in frataxin deficiency (**Figure 56**) suggests a normal influx, however, both MICU1 and MICU3 show decreased

protein levels. Representative images in **Figure 63A** and **C** indicates the protein WB bands respectively for MICU1 and MICU3. Quantification in **Figure 63B** and **D** indicates a decrease in protein levels for both proteins. The decrease in these proteins does not necessary indicates a decrease in Ca^{2+}_m influx. These results indicate that alterations in Ca^{2+}_m influx are also detected. However, since many other proteins impact on MCU activity, many other proteins need to be analysed in order to understand the characteristics of Ca^{2+}_m influx in frataxin deficiency.

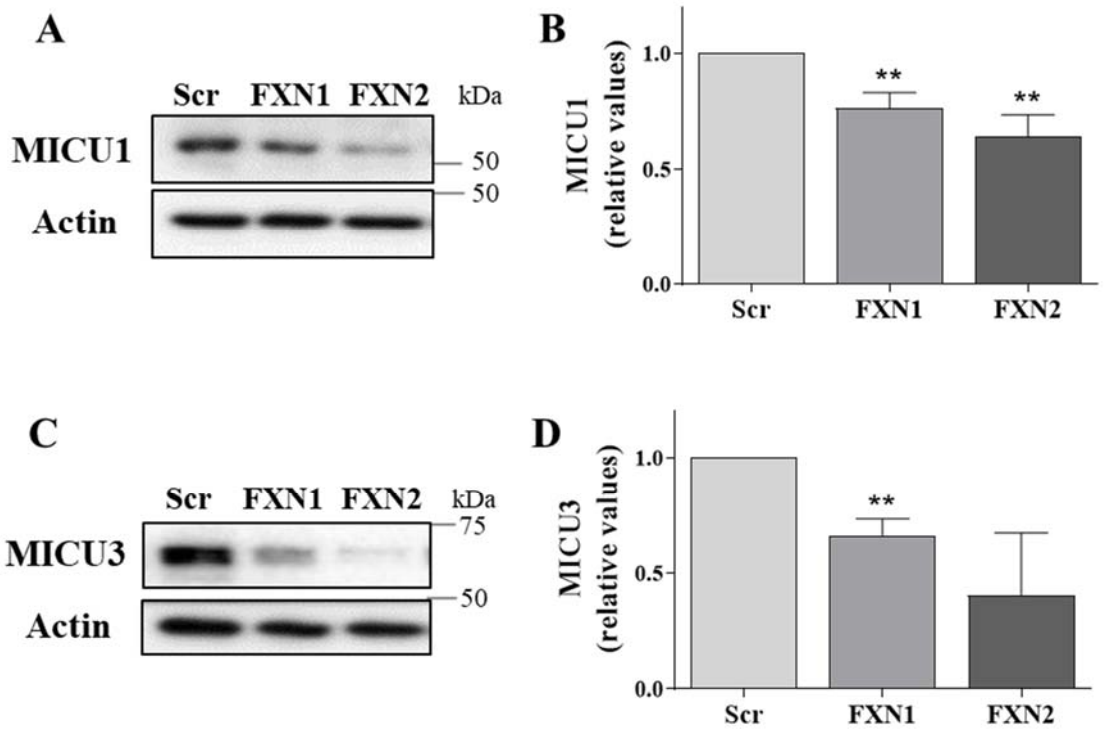

Figure 63. MICU1 and MICU3 protein levels decrease in frataxin deficiency. Amounts of the MICU1 protein levels were analysed by WB, in A, showing a decrease that correlates with FXN reduction. Data are Mean ± SEM obtained from n=7 independent isolations. Quantification is shown in B. Scr conditions at each time point are indicated as 1 and significant values compared to each Scr condition are indicated by (*). In C, representative images of MICU3 protein levels. Data are Mean ± SEM obtained from n=3 independent isolations. Quantification is shown in D. Scr at each time point is indicated as 1 and significant values compared to each Scr condition are indicated by (*).

1.5 Frataxin deficiency alters calcium dynamics

1.5.1 Progressive intracellular and mitochondrial Ca^{2+} overload in FXN deficiency

Previous results from our laboratory showed an increase of $[Ca^{2+}]_i$ at 5 days after lentivirus transduction using Fluo8 probe (Mincheva-Tasheva et al., 2014). However, no data were collected in early stages of frataxin depletion. Thus, in this work, it has been measured Ca^{2+} accumulation along the 5 days post-transduction. To that purpose, neurons were treated with Rhod5N-AM, a low-affinity Ca^{2+} indicator at days 1, 3 and 5 post-transduction. Representative images shown in **Figure 64A** and quantification in **B-C**, indicate that significant Ca^{2+} accumulation was observed as early as 1 day after transduction in FXN-deficient neurons compared to control cells. Rhod5N shows progressive and time-dependent Ca^{2+} accumulation in frataxin-deficient DRGs. The prevalence of mitochondria in neurites, the potential-driven uptake of the cationic dye Rhod5N by mitochondria and the punctate pattern in neurites indicate that the accumulation of Ca^{2+} in neurites is prevalently mitochondrial, while it cannot be distinguished in the soma ($Ca^{2+}{}_i$). Then, Rhod5N fluorescent intensity is shown in **Figure 64B** (soma) and **C** (neurites), respectively for $Ca^{2+}{}_i$ and an indication of $Ca^{2+}{}_m$. Results show an increase, as early as 1 day after lentivirus transduction, of Ca^{2+} accumulation of 7-22% for soma (**A**, $Ca^{2+}{}_i$) and 13-21% for neurites (**B**, $Ca^{2+}{}_m$). The results indicate an alteration in Ca^{2+} homeostasis in frataxin-depletion.

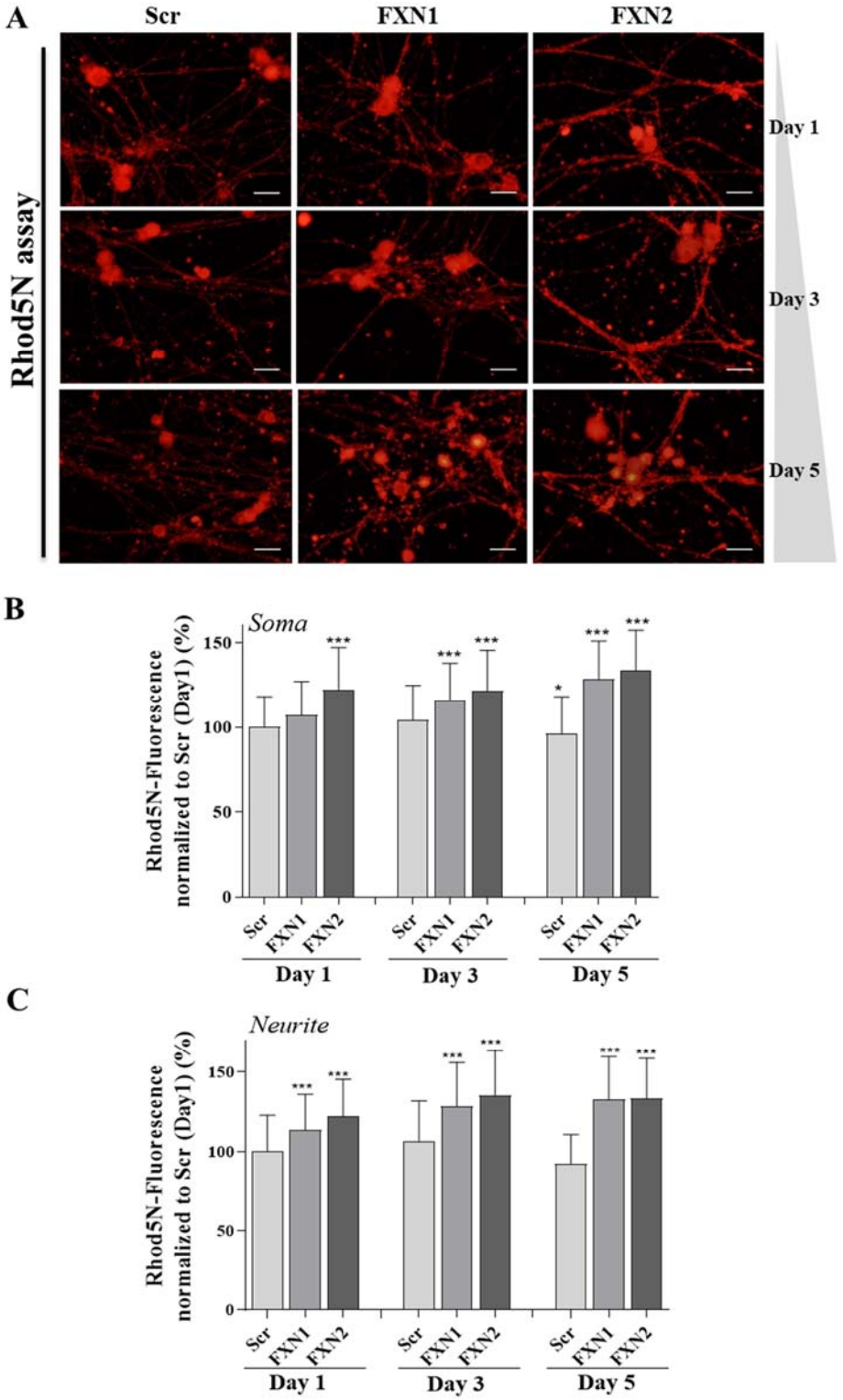

Figure 64. Early accumulation of Ca^{2+}_m in FXN-deficient DRGs. Representative images of fluorescent dye Rhod5N in FXN-deficient DRG neurons at day 1, 3 and 5 after lentivirus transduction in A. Scale Bar= 30µm and objective= 32x. Histograms in B and C, represent the intensity of the fluorescent dye Rhod5N in frataxin-deficient DRG neurons at day 1-3 and 5. Rhod5N shows progressive accumulation of Ca^{2+} in soma (A) and in neurites (B), respectively for Ca^{2+}_i and Ca^{2+}_m (see text for details). Data are Mean ± SEM obtained from n=3 independent isolations. A range of 315-421 neurites and 198-206 soma have been analysed for Scr conditions, 300-450 neurites and 218-313 soma for FXN1 conditions and 330-465 neurites and 215-285 soma for FXN2 conditions. Scr condition at day 1 is indicated as 100%. Significant values compared to Scr are indicated by (*).

To corroborate that the Rhod5N fluorescent intensity is prevalently mitochondrial, confocal images have been taken using at the same time two fluorescent (Fluo8 and Rhod5N) Ca^{2+}-sensitive probes, as shown in **Figure 65A**. The punctate pattern for red-fluorescent Rhod5N probe indicates a clear mitochondrial accumulation, while the more diffuse pattern for Fluo8 (green) dye indicates a $Ca^{2+}{}_i$ accumulation. Note the increase in Fluo8 fluorescence intensity in frataxin-deficient DRG neurons, indicating $Ca^{2+}{}_i$ accumulation, according to previously published data (Mincheva-Tasheva et al., 2014). However, in order to confirm the mitochondrial localisation, Rhod5N dye has been probed using a mitochondrial control (Mitotracker Green), as indicated in **Figure 65B**, showing a prevalently mitochondrial localisation.

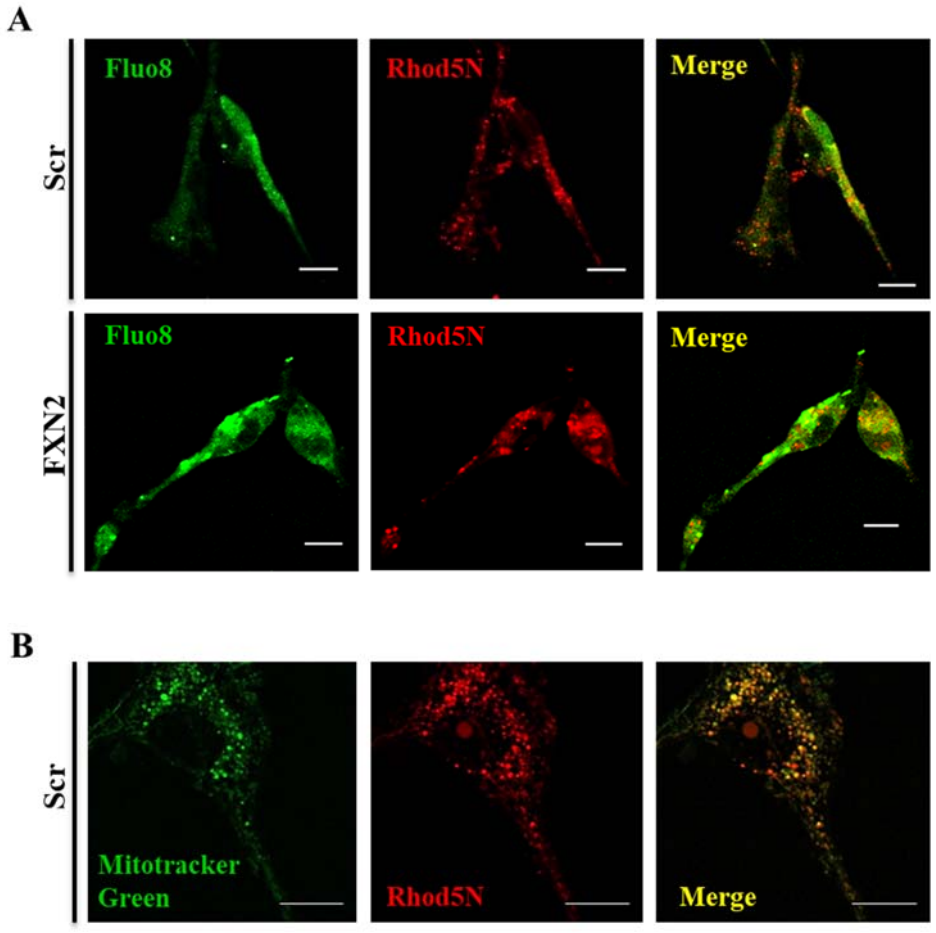

Figure 65. Punctate Rhod5N staining indicates the accumulation of Ca^{2+} in mitochondria. In A, representative images of Fluo8 and Rhod5N staining in Scr control and frataxin-deficient DRG neurons. Images are taken at the confocal microscope (see Material and Methods). Note the punctuate pattern which indicates $Ca^{2+}{}_m$ accumulation using Rhod5N, while a more diffuse pattern for Fluo8 indicates $Ca^{2+}{}_i$ accumulation. Note the increase in Fluo8 intensity in frataxin-deficient DRG neurons according to previously published work (Mincheva-Tasheva et al., 2014). Scale bar=10µm and objective= 40x. In B, representative images in Z-stack mode of mitochondrial localisation of Rhod5N. Rhod5N and Mitotracker green (mitochondrial control) have been probed in control DRG neurons as described in Material and Methods. Note the localisation of Rhod5N prevalently in mitochondria. Scale bar=10µm.

To confirm our data, Ca^{2+}_m has been also analysed in frataxin-deficiency in digitonin-permeabilised cells. Cell permeabilisation was visible at ~15min, as shown in **Figure 66A**. Rhod5N intensity was maintained at the same moment, preserving mitochondria. **Figure 66B** indicates the relative fluorescent values of Ca^{2+}_m in frataxin-deficient DRG neurons at 3 days after lentivirus transduction. As shown, frataxin-deficient DRG neurons display a 21% for FXN1 and 22% for FXN2 increase compared to Scr control values. Dashed lines indicate the value for untrasduced control, which is lower than Scr control. Once again, these data show an increase of Ca^{2+}_m in frataxin deficiency and confirm the above-mentioned results.

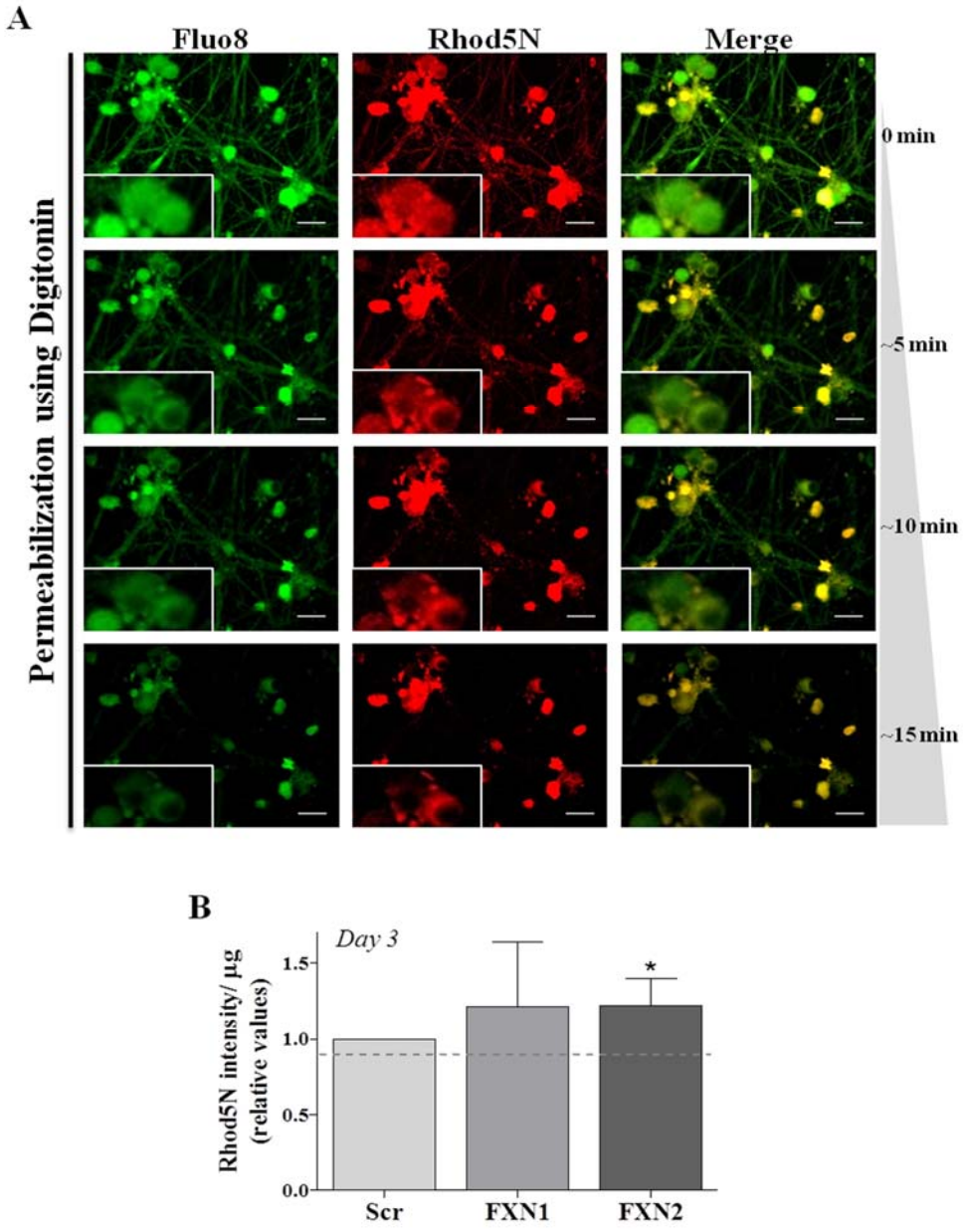

Figure 66. Digitonin-permeabilised cells show increase of Ca^{2+}_m in frataxin deficiency. In A, representative time-course images of permeabilised control cells using 60µM digitonin for

~15min. Fluo8 intensity decreases during the time indicating cell permeabilisation, while Rhod5N intensity is mainly maintained. Merge images indicates the time dependent shift from green-yellow color (Fluo8 and Rhod5N) to orange color, indicating a dramatic fall of Fluo8 intensity. Scale Bar= 30µm and objective= 32x. In B, histograms represent the relative values of Rhod5N fluorescence intensity of digitonin-permeabilised cells at 3 days after lentivirus transduction in pseudo-intracellular solution. Data are Mean ± SD obtained from n=3 isolations, 2 wells for condition. Dashed lines show the value for untransducted control relative to Scr condition indicated as 1 (value: 0.91).

Nevertheless, the analysis of basal Ca^{2+}_m is not clearly informative and could be affected by technical problems. Thus, Rhod5N signal in response to a stimulus of physiological Ca^{2+} ($[Ca^{2+}]_{free}$ of 5µM) has been analysed in permeabilised cells to avoid any technical problem and be confident that the signal analysed was present in mitochondria. For this reason, cells were permeabilised as indicated in Materials and Methods and representative images of cells before and after permeabilisation are present in **Figure 67B**. Note the decrease in Fluo8 signal upon digitonin addition and the maintenance of Ca^{2+}_m signal (Rhod5N). Normalised mean traces of permeabilised cells in response to a stimulus of Ca^{2+} are represented in **Figure 67A**, in which is possible to note the alteration in Ca^{2+}_m efflux. From these traces, it was possible to analyse the amplitude of the peak (**C**); the Ca^{2+}_m influx rate (**D**); Ca^{2+}_m efflux decay rate (**E**) and the peak half-life (**F**). Frataxin-deficient DRG neurons show significant increase in peak amplitude and alterations in κ-decay and τ parameters, which are compatible with decreased Ca^{2+}_m efflux. All these data are in agreement with previously reported data of NCLX decreased levels in frataxin-deficient DRG neurons (**Figure 62**).

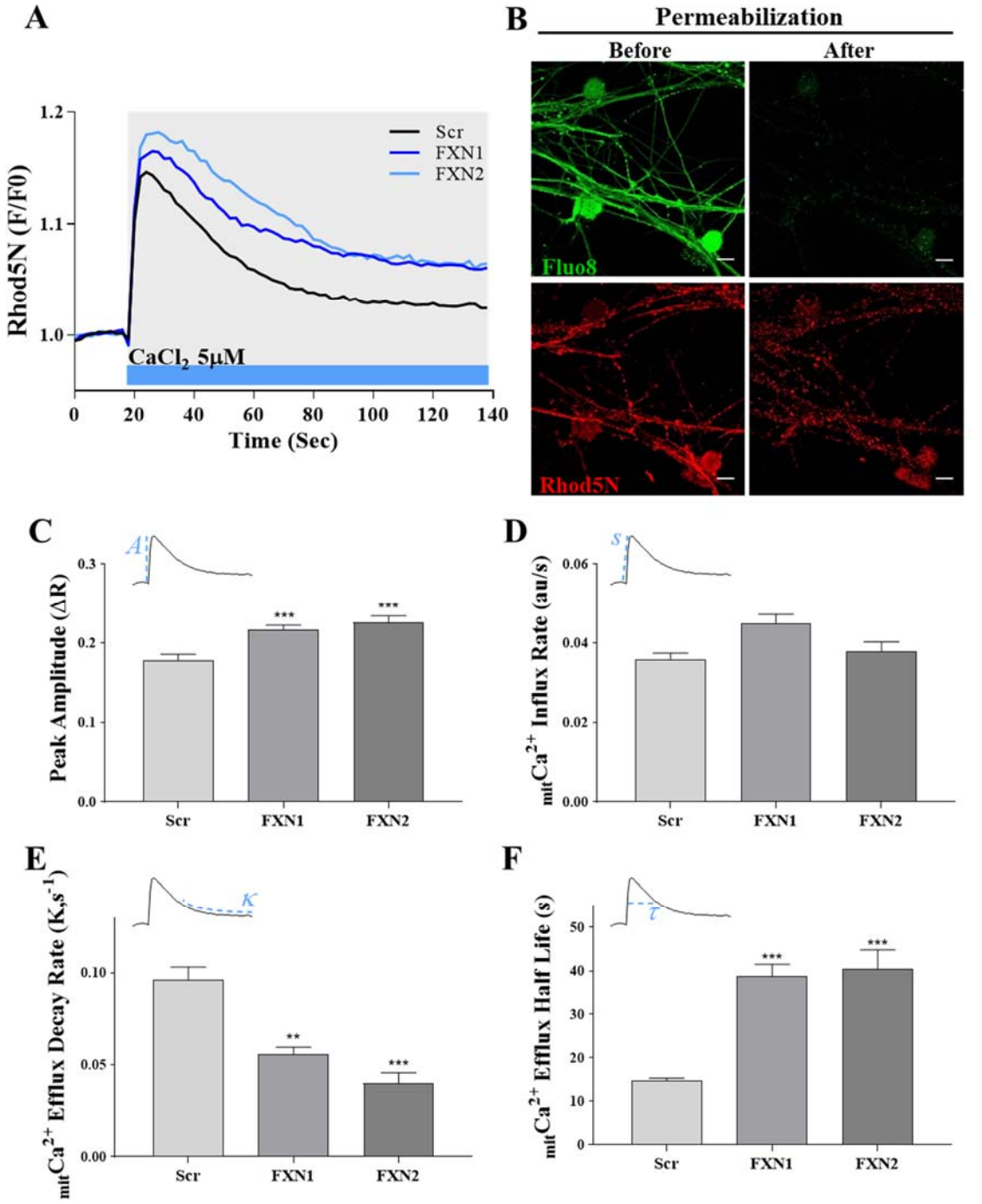

Figure 67. Frataxin-deficient digitonin-permeabilised cells show alterations in Ca^{2+}_m efflux. In A, mean traces of digitonin-permeabilised cells in response to physiological stimulus of Ca^{2+} (5µM $[Ca^{2+}]_{free}$). Normalised data are obtained from a range of 357-386 peaks for Scr conditions; a range of 348-578 peaks for FXN1 conditions and 234-391 peaks for FXN2 conditions. In B, representative images of permeabilised control cells using 60µM digitonin for ~15min. Fluo8 intensity (Ca^{2+}_i) decreases during the time indicating cell permeabilisation, while Rhod5N intensity (Ca^{2+}_m) is mainly maintained. Scale bar=10µm. Histograms in C indicate the amplitude of the peak (A); histograms in D indicate the Ca^{2+}_m influx rate (*s*) and histograms in E and F indicate respectively the Ca^{2+}_m efflux decay rate (k-decay, κ) and the peak half-life (tau, τ). Blue dashed lines in each graph represent all these parameters. Data are the mean ± SEM obtained from 5 independent experiments. Significant values compared to control conditions are indicated with (*).

1.5.2 FXN deficiency decreases cytosolic Ca^{2+} buffer capacity

A numerous number of previous study indicates that, in DRG neurons, mitochondria can buffer Ca^{2+} upon the entry from voltage and/or ligand gated plasmalemmal channels in order to limit the amount of Ca^{2+} that can enter into the cells. Then, Ca^{2+} can be released slowly and in regulated manner into the cytosol and stored into other intracellular stores (Shishkin et al., 2002; Svichar, Kostyuk, & Verkhratsky, 1997).

To analyse the Ca^{2+} buffer capacity in FXN-deficient DRGs, it has been used the proton ionophore carbonyl cyanide m-chlorophenyl hydrazone (CCCP), which uncouples mitochondrial respiration and ATP production by destroying the H^+ gradient across the MIM, giving a rise of $Ca^{2+}{}_i$ in resting cells. The rise of $Ca^{2+}{}_i$ has been analysed with Fura-2-AM ratiometric dye, which analyses the ratio 340/380 nm between Fura-2-bound Ca^{2+} ($\lambda_{\sim 340\ nm}$) and $Ca^{2+}{}_{free}$ ($\lambda_{\sim 380\ nm}$) detections.

When CCCP is used in Ca^{2+}-free buffers, the rise of $Ca^{2+}{}_i$ reflects the amount of $Ca^{2+}{}_m$ that was present prior to the stimulus, since no uptake of extracellular Ca^{2+} is allowed. Then, the $Ca^{2+}{}_i$ declines back to baseline levels. This decline could be ascribed to (i) re-uptake by mitochondria; (ii) uptake by intracellular stores (e.g. ER); (iii) extrusion into extracellular space (Shishkin et al., 2002) using Na^+/Ca^{2+} exchangers or ATP-driven Ca^{2+}-pumps. When CCCP is continuously present in the buffer, it avoids Ca^{2+} re-uptake by mitochondria (Herrington, Park, Babcock, & Hille, 1996), maintaining only the (ii) and (iii) explanation for transient Ca^{2+} waves.

However, the uncoupler, not only releases Ca^{2+} from mitochondrial stores, but also, slowly and to a lesser extent, from not mitochondrial ones (e.g. ER) in Ca^{2+}-free and normal Ca^{2+} buffers. In fact, protons (H^+) could be necessary to retain Ca^{2+} not only in mitochondria but also in ER (Jensen & Rehder, 1991).

Bearing in mind all these concepts, confocal fluorescence microscopy was used and the $Ca^{2+}{}_i$ indicator Fura-2-AM to analyse time-lapse traces of $[Ca^{2+}]_{free}$ in frataxin-deficient DRG neurons after the application of CCCP 1µM using free-Ca^{2+} buffer, as shown in **Figure 68**. Representative Fura-2 ratio videos for Scr control and FXN1 conditions are present in **A**. Each cell soma of these videos has been analysed with Aquacosmos for ROI detection and OriginPro 2017 for ROI processing. **Figure 68B** represents the average of different time-lapse ratios traces separated in CCCP-fast and slow response neurons for Scr, FXN1 and FXN2 conditions. The separation has been performed by the fact that the wave shape after CCCP stimulus is very different between CCCP- fast and

slow response neurons and, as the cell number analysed in this study is a limiting factor, the number of neurons for a type is over (or under) represented could misinterpret the data. Note the tendency of average baseline Fura-2 ratio level to be higher in CCCP-fast response cells, while lower in the other ones. However, no correlation between baseline Ca^{2+} concentration and Ca^{2+} influx rate has been found (data not shown), neither a correlation between baseline values and cell size by the naked eye (or cell diameter measured through ImageJ). However, the limiting number of cells analysed can mask a possible weak correlation. Also, note the average ratio level for Scr condition, which is lower than FXN-deficient DRGs. Nevertheless, further experiments are necessary to understand these different waves' shapes better. Normalizing time-lapse traces on their initial fluorescence F_0 for CCCP-fast and slow response, respectively shown in **Figure 68C** and **D**, allow to analyse different peak parameters, using OriginPro: the baseline ratio levels for each cell soma in control and frataxin-deficient DRG neurons, as shown in **Figure 68E**; the peak amplitude ($\Delta F=F_{max} - F_{baseline}$) for CCCP-fast response neurons in **F**, which indicates more $Ca^{2+}{}_m$ accumulation in frataxin deficiency at the time before the stimulus; the Ca^{2+} influx rate (slope) for this peak in **Figure 68G** and the Ca^{2+} efflux by two different manners, efflux half-life (τ) and rate (k decay), respectively present in **H** and **I**. Both, the lower τ and higher k parameters, indicates alteration in Ca^{2+} buffer capacity after CCCP addition in frataxin deficiency such as (i) decreased efflux of Ca^{2+} across plasma membrane; (ii) decreased influx into ER; (iii) more distance between mitochondria and ER contacts or (iv) decreased level of Ca^{2+}-binding proteins which could not properly buffer Ca^{2+}. All these data indicate impaired recovery to baseline levels upon stimulus in frataxin deficiency. Further experiments are necessary to understand the role of frataxin in Ca^{2+} buffering, for example using thapsigargin to inhibit Ca^{2+} uptake by ER or free-Na^+ buffers as Na^+/Ca^{2+} plasma membrane exchanger uses Na^+ gradient to allow Ca^{2+} extrusion (Herrington et al., 1996). These data are in agreement with a previous published study using cerebellar granule neurons (CGNs) from YG8R, a 190+82 GAA repeats FA mouse model, in which frataxin deficiency determines an impairment of the return to resting conditions upon KCl stimulus and presents decreased amounts of Ca^{2+} in ER upon thapsigargin stimulus, probably for impairment of Ca^{2+} influx into ER through SERCA pumps (Abeti, Brown, et al., 2018). However, such data could be also explained also for reduced mitochondria-ER contacts in frataxin deficiency, a recent finding which add a novel possible role in regulating MAMs for frataxin (Rodríguez et al., 2020).

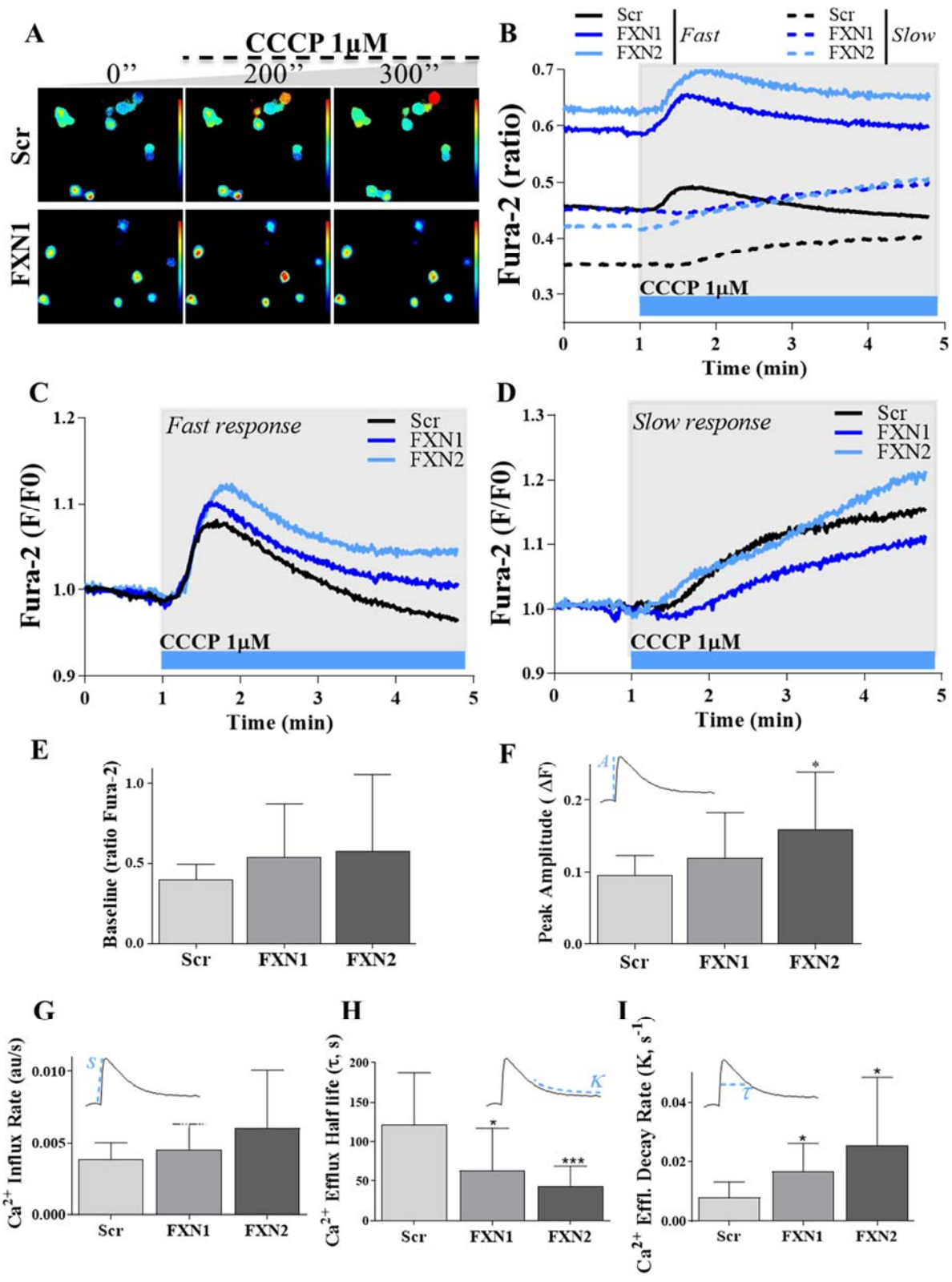

Figure 68. Ca^{2+} buffering alterations in frataxin-deficient DRG neurons. In A, representative confocal ratiometric 340/380 nm images of four-days transduced Scr control and FXN1 neurons loaded with Fura-2-AM at different time points before and after the addition of CCCP 1µM. In B, average of Fura-2 ratio 340/380 nm traces for DRG neurons responding to CCCP 1µM. CCCP-fast response cells and CCCP-slow response ones have been separated for the analysis. In C and D, average of Fura-2 ratio fluorescence (F) normalised to the initial fluorescence (F_0) in Scr, FXN1 and FXN2 conditions in response to CCCP stimulus, respectively for CCCP-fast

response and CCCP-slow response. Note the dashed blue lines near the peaks in each graph referring to the analysis performed in the graphs F-I: (A) amplitude of signal, F; (*s*) slope of Ca^{2+} influx, G; (τ) Ca^{2+} efflux half-life as τ (tau) parameter, H; (*k*) Ca^{2+} efflux decay rate as K parameter, I. In E, baseline levels for all cells analysed. In particular, 21 Scr cells (10 cells with CCCP-fast response and 11 cells with slow one), 20 FXN1 cells (12 cells fast response, 8 cells slow response) and 22 FXN2 cells (17 cells fast response, 5 cells slow response) have been analysed in OriginPro software for all analysis. Two cells indicated as outliners for Gribbs's test have been removed from analysis. Data are Mean ± SD from n=2 independent isolation. **Experiments performed with the help of Dr Olga Tarabal.**

One of the explanations for alteration in Ca^{2+} buffer capacity in frataxin deficiency that has been indicated before was a decreased level of Ca^{2+}-binding proteins, which could not properly buffer Ca^{2+}. Dorsal root ganglion shows different Ca^{2+}-binding proteins such as calretinin, calbindin and parvalbumin. These proteins show different affinity for Ca^{2+} and are differentially expressed among DRG subpopulations. While parvalbumin was impossible to detect in our hands, calretinin protein levels have been analysed in frataxin-deficient DRG neurons. The results in **Figure 69A** (quantification in **B**) indicate an increase of this Ca^{2+} buffer protein in frataxin deficiency. Despite this result is difficult to understand, besides suggesting alteration in Ca^{2+}-binding capacity, it could indicate an alteration in subpopulation distribution in frataxin deficiency. More experiments should be performed to understand this point better.

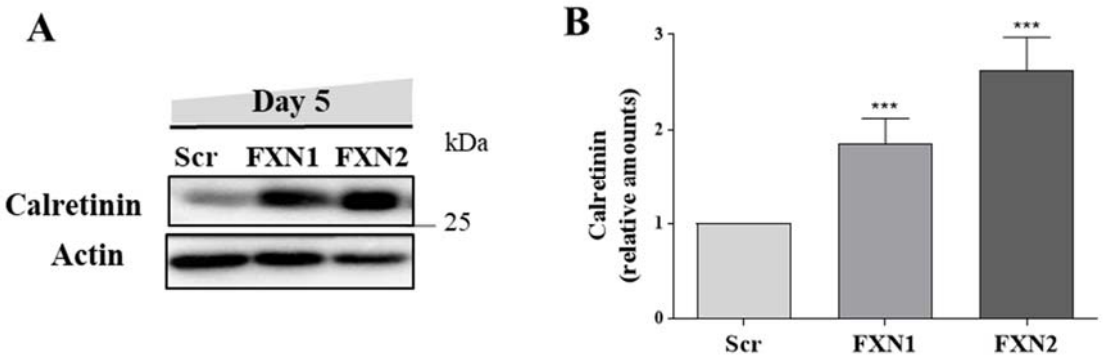

Figure 69. Calretinin Ca^{2+}-binding protein levels increase in frataxin deficiency. In A, WB bands of calretinin protein levels in frataxin-deficient DRG neurons. In B, histograms represent the amounts of calretinin relative to Scr control. Data are Mean ± SEM from n=17 independent experiments. Significant values compared to Scr control are indicated with (*).

Ca^{2+} buffer capacity alterations have been already postulated in frataxin deficiency and related to ER stress. In fact, ER stress susceptibility has been described in frataxin-deficient human SH-SY5Y neuroblastoma cell line, analysing a chaperone related to this mechanism (glucose-related protein-78/GRP78/Bip). GRP78/Bip is considered as

an ER stress marker and, in frataxin-deficient SH-SY5Y cell line, it increases in response to 1μM thapsigargin for 18h, but not in basal condition (Bolinches-Amorós et al., 2014). Thus, GRP78/Bip was analysed in frataxin-deficient DRG neurons and, as shown in **Figure 70A** and quantification in **B**, no changes were detected at 5 days after lentivirus transduction in basal condition, suggesting that no ER stress is present at the rest status. No data are available in the case of thapsigargin addition for our model.

While GRP78 chaperone levels remain invariant in resting conditions, the decreased amount of another mitochondrial chaperone, the glucose-related protein-75 (GRP75/Mortalin/HspA9), which physically interacts with frataxin (Shan, Napoli, & Cortopassi, 2007), has been previously related to frataxin deficiency. **Figure 70C** and quantification in **D** show a reduction to 78% (FXN1) and 60% (FXN2) compared to Scr control. GRP75 decreased levels have been previously shown in cerebellar tissue of FA KIKO mice, in which has been considered as a mitochondrial marker (Lin et al., 2017), human FA skin fibroblasts, HEK293 cells, in which is considered as a secondary effect of frataxin deficiency (Dong et al., 2019), and peripheral blood mononuclear cells (PBMCs) (Selak et al., 2011). Although GRP75 decrease has been related to a reduction in mitochondrial number, the previous results in **Figure 56** for LONP1 and MCU mitochondrial proteins do not support this hypothesis. Further studies are necessary to describe the correlation between frataxin deficiency and GRP75, considering the suggested functions as (i) facilitator of ER-mitochondria contacts in MAMs, which are decreased in number upon GRP75 deficiency (Honrath et al., 2017; Szabadkai et al., 2006); (ii) facilitator of protein import into the mitochondrial matrix; (iii) facilitator of iron-sulphur clusters in imported mitochondrial proteins (Shan et al., 2007). Then, our results could indirectly suggest more distance between MAMs and alterations in protein import in frataxin deficiency. Further studies are necessary to confirm directly these suggestions and to understand, in the case of confirmed suggestions, the role of frataxin deficiency in decreasing contacts ER-mitochondria and protein import.

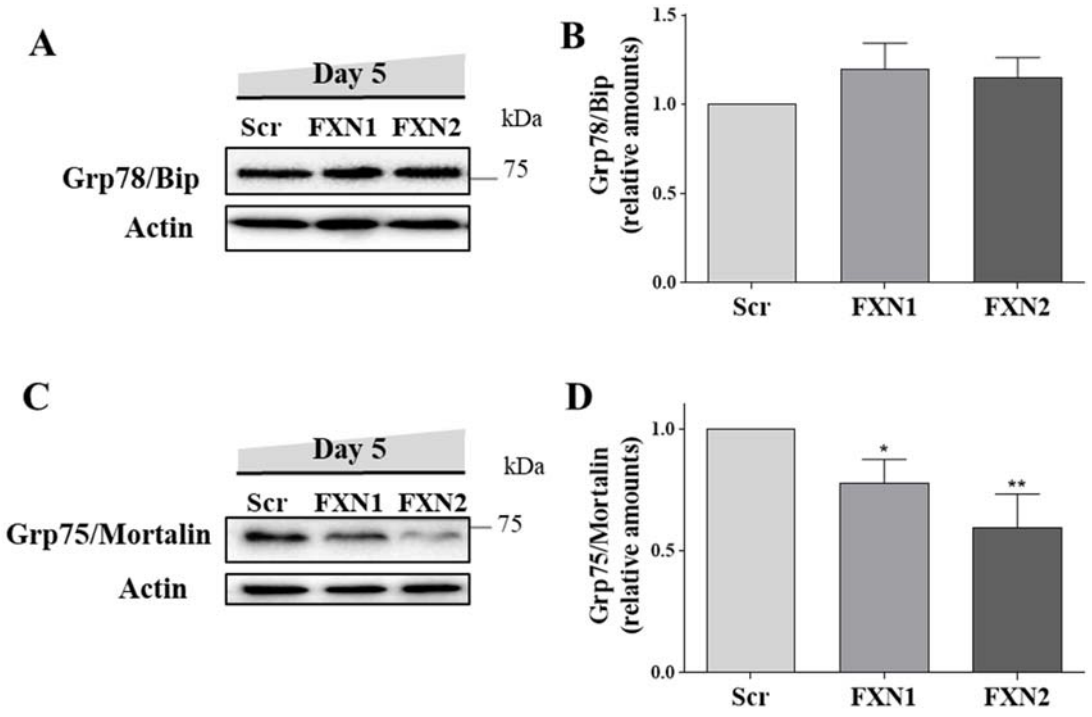

Figure 70. Frataxin deficiency determines decrease of GRP75/Mortalin, but not GRP78/Bip. In A, representative images of GRP78/Bip analysed by WB at 5 days after lentivirus transduction in frataxin-deficient DRG neurons. No changes are detected in B. Data are Mean ± SEM from n=14 independent isolations. In C, representative images of GRP75/Mortalin analysed by WB in frataxin-deficient DRG neurons at 5 days after lentivirus transduction. In D, histograms indicate the decrease of GRP75 relative amounts in frataxin deficiency. Data are Mean ± SEM from n=16 independent isolations. Scr condition is indicated as 1 and significant values referred to Scr are indicated as (*).

1.6 Frataxin deficiency induces mitochondrial import defects

1.6.2 Frataxin deficiency induces HSP60 import alterations

Despite the role in ER-mitochondria contacts, GRP75 is also the motor for mitochondrial protein import, in which an intact inner membrane potential is required for import into mitochondria of nuclear-encoded mitochondrial pre-proteins carrying MTS (e.g. frataxin). In fact, once inside the mitochondria, the N-terminal MTS of pre-proteins is cleaved off by mitochondrial processing peptidases (MPP) in a $\Delta\Psi_m$ and ATP-dependent manner. Thus, as we previously demonstrated a relationship between frataxin deficiency and mitochondrial membrane depolarisation, shown in **Figure 59** and **Figure 60** and a slightly depletion of GRP75 protein levels, shown in **Figure 70**, another protein imported into mitochondrial matrix has been analysed, the chaperone Hsp60. Hsp60 precursor form carries a MTS which allows it to be transported into mitochondria and MTS is cleaved by proteases releasing the mature form into the

matrix. **Figure 71A** shows defects in Hsp60 processing in frataxin-deficient DRG neurons; in fact, the precursor form is mainly present at 5 days after lentivirus transduction. Each isoform on Hsp60 total amount is shown in percentage in **B**, in which Scr, FXN1 and FXN2 conditions have respectively 9.7, 21 and 36% of Hsp60 (p) and 90.3, 79 and 64% of Hsp60 (m). Relative amounts on Scr condition are present in **C**, in which Hsp60 precursor form shows a 2-fold increase for FXN1 and 4-fold increase for FXN2, mature form is reduced by 15% (FXN1) and 30% (FXN2), while no changes are detected for total amount of Hsp60. All these data indicate defects in Hsp60 processing or import into mitochondria in frataxin deficiency.

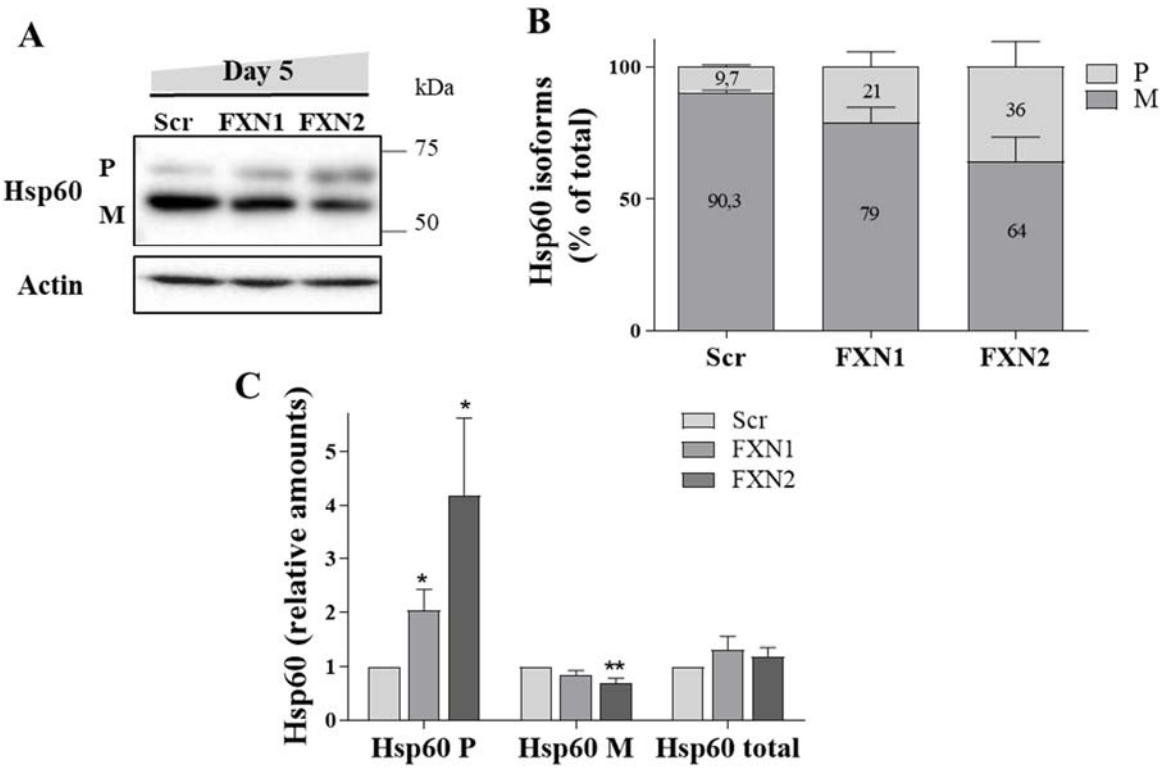

Figure 71. Frataxin deficiency determines defects in Hsp60 processing. In A, WB analysis of Hsp60 antibody in total lysates of frataxin-deficient DRG neurons at 5 days after lentivirus transduction. The antibody allows detect an upper band indicated as precursor Hsp60 (p) and a lower band as mature (m). In B, percentage of Hsp60 isoforms on Hsp60 total amount. In C, histograms represent Hsp60 isoforms normalised on Actin. Data are Mean ± SEM of n= 8 independent isolations. Scr condition are considered as 1 and significant values referred to Scr (Hsp60 p or m) are indicated with (*).

1.6.3 Frataxin deficiency alters Pink1 processing or import

Mitochondrial membrane potential is also required for import and processing of another nuclear-encoded mitochondrial and cytosolic protein: Phosphatase and tensin homologue (PTEN)-induced putative kinase 1 (Pink1). Pink1 processing, depending on $\Delta\Psi_{m,}$ represents a sensor for energy status of mitochondria since mitochondrial integrity is required for cleavage of the 64kDa full-length into different isoforms: intermediate form of 60kDa, which is rapidly converted in 55kDa (or Δ1) and 43KDa (or Δ2) mature forms (Becker et al., 2012).

Figure 72A shows defects in Pink1 processing in frataxin-deficient DRG neurons, in fact, 43kDa mature form levels are mainly reduced at 5 days after lentivirus transduction. Each isoform on Pink1 total amount is shown in percentage in **B**, in which Scr, FXN1 and FXN2 conditions have respectively 15.7, 27.3 and 33.6% of Pink1 full length or 64kDa; 34.9, 40 and 42.4% of Pink1 55kDa and 49.4, 32.5 and 24% of Pink1 43kDa. Note that, in normal conditions, the majority of Pink1 is processed into last-step isoform of 43kDa, while in frataxin deficiency remains mainly to the 55kDa and 64kDa isoforms. Relative amounts on Scr condition are present in **C**, in which Pink1 55kDa-form is reduced by 29% for FXN1 and 36% for FXN1, the 43kDa-mature form is reduced by 60% (FXN1) and 74% (FXN2), while no changes are detected for the full-length amount of Pink1.

Several proteases are involved in the cleavage of Pink1 protein: MPP, which cleaves MTS for import into mitochondria; PARL, presenilin-associated rhomboid-like protease; Afg3l2, a subunit of m-AAA protease and ClpP, a subunit of matrix protease ClpXP (Greene et al., 2012);

The specific protease responsible for the 43kDa fragment is not yet discovered, however, an elegant study in the literature screens different proteases, through RNAi, for the possibility of Pink1 cleavage. The study shows that Afg3l2 siRNA silencing, but also PARL silencing alone and in combination with Afg3l2, induces an increase of 52kDa form, indicating that Afg3l2/PARL can cleave this form, generating, probably, the 43kDa form (Greene et al., 2012). Furthermore, the 43kDa band is nearly absent in Afg3l2-deficient *Drosophila* fruit flies, once again suggesting Afg3l2 as the 43kDa-generating protease (Thomas et al., 2014). As mutations in Afg3l2 are responsible for spinocerebellar ataxia 28 (SCA28) (Di Bella et al., 2010), Afg3l2 protease levels have been analysed in our FA model at 1-3- and 5 days after lentivirus transduction. **Figure**

72E, and quantification in **F**, show decreased levels of Afg3l2 in the last steps of frataxin deficiency, being reduced by 16% in FXN1 and 38% in FXN2. The slightly decrease at the end of the experiment suggests the presence of other proteases, besides Afg3l2, involved in Pink1 processing, nevertheless, no data are currently available about its functionality and the question is still opened.

All these data indicate defects in Pink1 processing or import into mitochondria in frataxin-deficient DRG neurons. However, Pink1 total levels (in **Figure 72C**) are also reduced by 37% and 44%, indicating that the mechanism is more complex and could also rely on alterations in expression, stabilization or degradation.

Some studies indicate Pink1 55kDa degraded through proteasome machinery (Liu et al., 2017), but the 43kDa-form is not always present in cells, and being less studied, it is unclear if it is also degraded in the same way in our model. For this reason, the proteasome inhibitor MG132 has been used in not transduced controls. As it is shown in **Figure 72D**, MG132 5μM treatment for 10-15 and 20h in control induces an increase of 43kDa isoform, while no differences are detected for other isoforms, indicating that, in DRG neurons, endogenous Pink1 is prevalently in 43kDa-form and this form is even more dominant upon proteasome inhibition. However, MG132 treatment is not only specific to proteasome and can also inhibit calpains and cathepsins (Tsubuki, Saito, Tomioka, Ito, & Kawashima, 1996), rendering the study even more complex.

Apart from degradation pathways, Pink1 stability could also be related to frataxin deficiency. In fact, while the Pink1 precursor associates with mitochondria, Pink1 cleaved forms are found in the cytosol and stabilised by chaperones, such as Hsp90, but, loss of a cytosolic chaperone activity leads to decreased Pink1 level, in particular 43kDa cleaved form (Lin & Kang, 2008). No data about Hsp90 are available, however, previous results in **Figure 70** and **Figure 71**, indicate, respectively, alterations in GRP75 and Hsp60 chaperones, therefore, as both proteins have been discovered as Pink1 interacting partners (Rakovic et al., 2011), changes in Pink1 stability may also be taken into account.

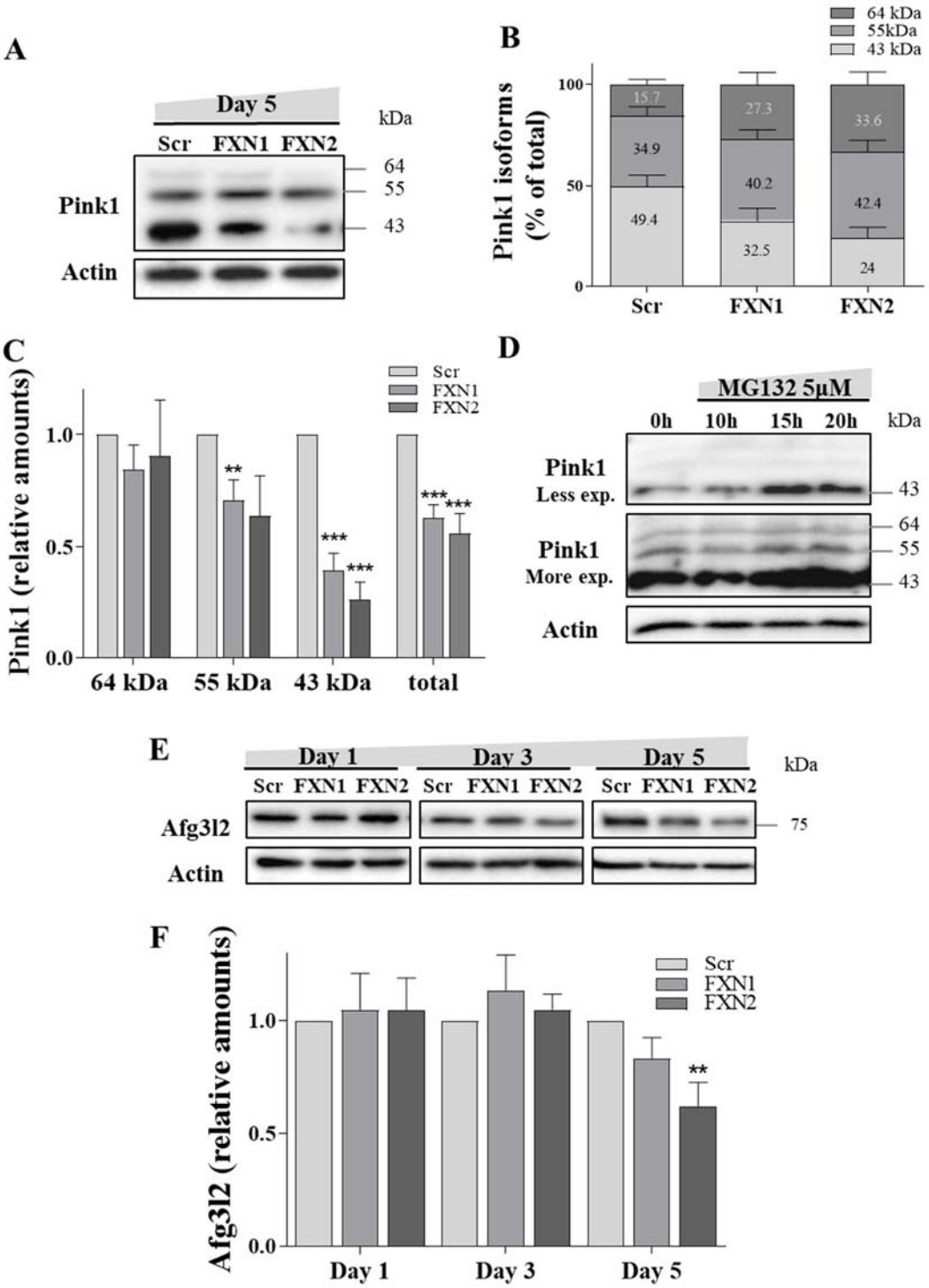

Figure 72. Pink1 processing is altered in frataxin-deficient DRG neurons. In A, WB analysis of Pink1 antibody in total lysates of frataxin-deficient DRG neurons at 5 days after lentivirus transduction. The antibody allows detect different isoforms (full length 64kDa; 55kDa-isoform and mature form 43kDa). In B, percentage of Pink1 isoforms on Pink1 total amount. In C, histograms represent Pink1 isoforms normalised on Actin. Data are Mean ± SEM of n= 12 independent isolations. In D, representative image of not transduced controls, not treated or treated with MG132 5µM for 10, 15 and 20h. Note the increase of 43kDa isoform using the proteasome inhibitor. In E, WB images of Afg3l2 antibody at day 1-3 and 5 after lentivirus transduction. Note the decrease of Afg3l2 at the end of the experiment. Quantification in F. Data are Mean ± SEM of n= 4 (day 1), n=8 (day 3) and n=14 (day 5) independent isolations. Scr conditions are considered as 1 and significant values referred to Scr are indicated with (*).

1.7 Frataxin deficiency induces signs of apoptotic cell death

1.7.1 Mitochondrial pore opening and release of pro-apoptotic proteins

Mitochondrial kinase Pink1 deficiency can contribute to mitochondrial transition pore opening (mPTP) (Kostic et al., 2015). The above results, impaired Ca^{2+}_m efflux in **Figure 67**, progressive Ca^{2+}_i and Ca^{2+}_m accumulation in **Figure 64**, mild depolarisation in **Figure 59** and Pink1 alterations in **Figure 72** in frataxin-deficient DRG neurons suggest mPTP opening. In fact, Ca^{2+}_m overload, mitochondrial depolarisation and NCLX impairment, probably due to loss of its phosphorylation or cleavage, decreases mPTP opening threshold (Gandhi et al., 2009), provoking mitochondrial Ca^{2+} release together with the release of pro-apoptotic proteins such as Bax, Caspase-3, pro-Caspase 9, Cytochrome C, which are all signs of the intrinsic (or mitochondrial) apoptotic cell death. Bax and cleaved Caspase-3 increased levels have been previously shown by our laboratory in frataxin-deficient DRG neurons at 5-days after frataxin depletion (Mincheva-Tasheva et al., 2014). The results in **Figure 73** are in agreement with the previous data. In fact, decreased levels of pro-Caspase 9 in **A** and quantification in **B** suggest its release from mitochondria, cleavage and, consequently, its activation. The 3-fold and 4-fold increase of cleaved-Caspase 3, respectively for FXN1 and FXN2, as shown in **Figure 73C** and **D**, is in line with this hypothesis. Furthermore, the pro-apoptotic protein Bax, shown in **G** and **H**, presenting a clear increase at 5-days after lentivirus transduction but not in early stage, indicates that apoptotic cell death occurs in late stages of the disease, when frataxin levels are very low. The anti-apoptotic protein Bcl2, shown in **E** and quantification in **F**, showing no differences in frataxin-depletion, strengthened this hypothesis. In addition, is generally accepted that the ratio between pro-apoptotic and anti-apoptotic proteins indicates in a more accurate manner the presence of apoptotic cell death; **Figure 73I** shows the ratio Bax/Bcl2 levels. Once again, the significant 3-fold and 4-fold increase for FXN1 and FXN2 indicate apoptotic cell death in frataxin-deficient DRG neurons at 5-days after lentivirus transduction.

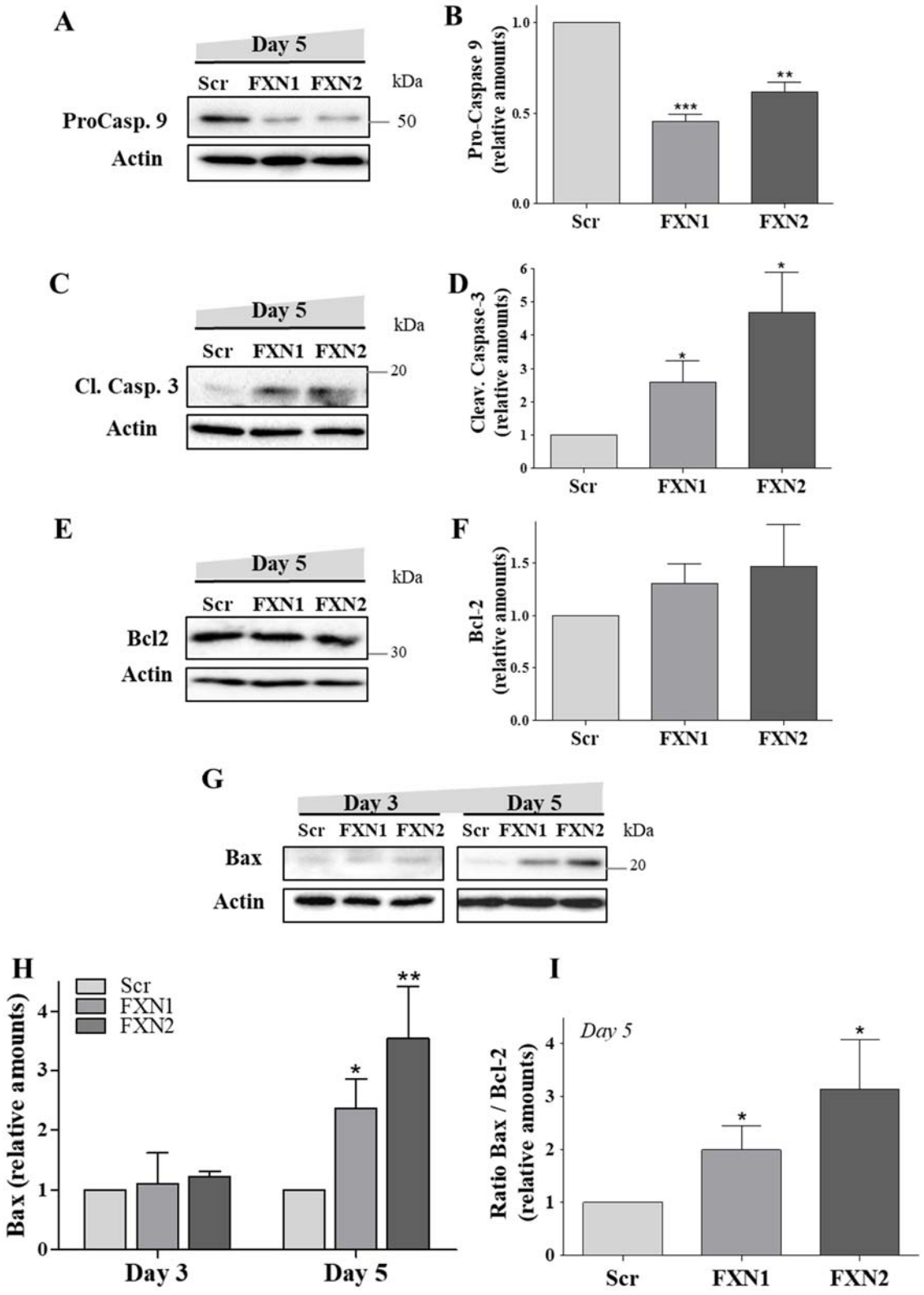

Figure 73. Alteration in pro-apoptotic and anti-apoptotic proteins levels indicates apoptotic cell death in frataxin deficiency. In A, C and E, amounts of pro-Caspase 9, cleaved Caspase 3 and Bcl2 are analysed by WB in frataxin-deficient DRG neurons at day 5 after lentivirus transduction. Quantification, respectively, in B, D and F. Data are Mean ± SEM obtained from n=5 (pro-Caspase 9), n=3 (cleaved-Caspase 3) and n=8 (Bcl2) independent isolations. In G, amounts of Bax are analysed by WB at 3 and 5-days after lentivirus transduction. Quantification

in H (n=3, day 3 and n=8 day 5). In I, ratio Bax/ Bcl2 at 5-days after lentivirus transduction. Data are Mean ± SEM, n= 8 independent isolations. Scr conditions are indicated as 1 and significant values compared to each Scr condition are indicated by (*).

The mPTP opening could be ascribed to modifications of its more important regulator Cyclophilin D (CypD). It has been described that acetylation of CypD (acetyl-CypD) can increase the susceptibility of mPTP opening. Nowadays, no antibodies to detect acetyl-CypD are commercially available, but it has been described that mitochondrial acetylation is mainly regulated by a sirtuin-3 (Sirt3), a mitochondrial deacetylase. For this reason, Sirt3 has been analysed in our model. **Figure 74A** and quantification in **B**, indicate a slightly reduction to 75% for FXN1 and 79% for FXN2 at 5 days after lentivirus transduction. A decrease in protein level could suggest a decrease in deacetylase activity, then increasing the mitochondrial acetylation of its substrates (e.g. CypD, SOD2 and others). As the acetyl-SOD2 (K68) antibody is commercially available, this acetylation has been analysed in our model, as indicated in **C**. Histograms in **D** indicates a tendency to increase in frataxin-deficient DRG neurons, however, more experiments are necessary to analyse if this difference is significant. The result has been then compared to SOD2 protein levels. WB bands in **E** and quantification in **F** indicate that the increase in acetylation is not ascribed to an increase in protein levels. **G** and **H** indicate, respectively, preliminary results for bands and quantifications of SOD1 protein.

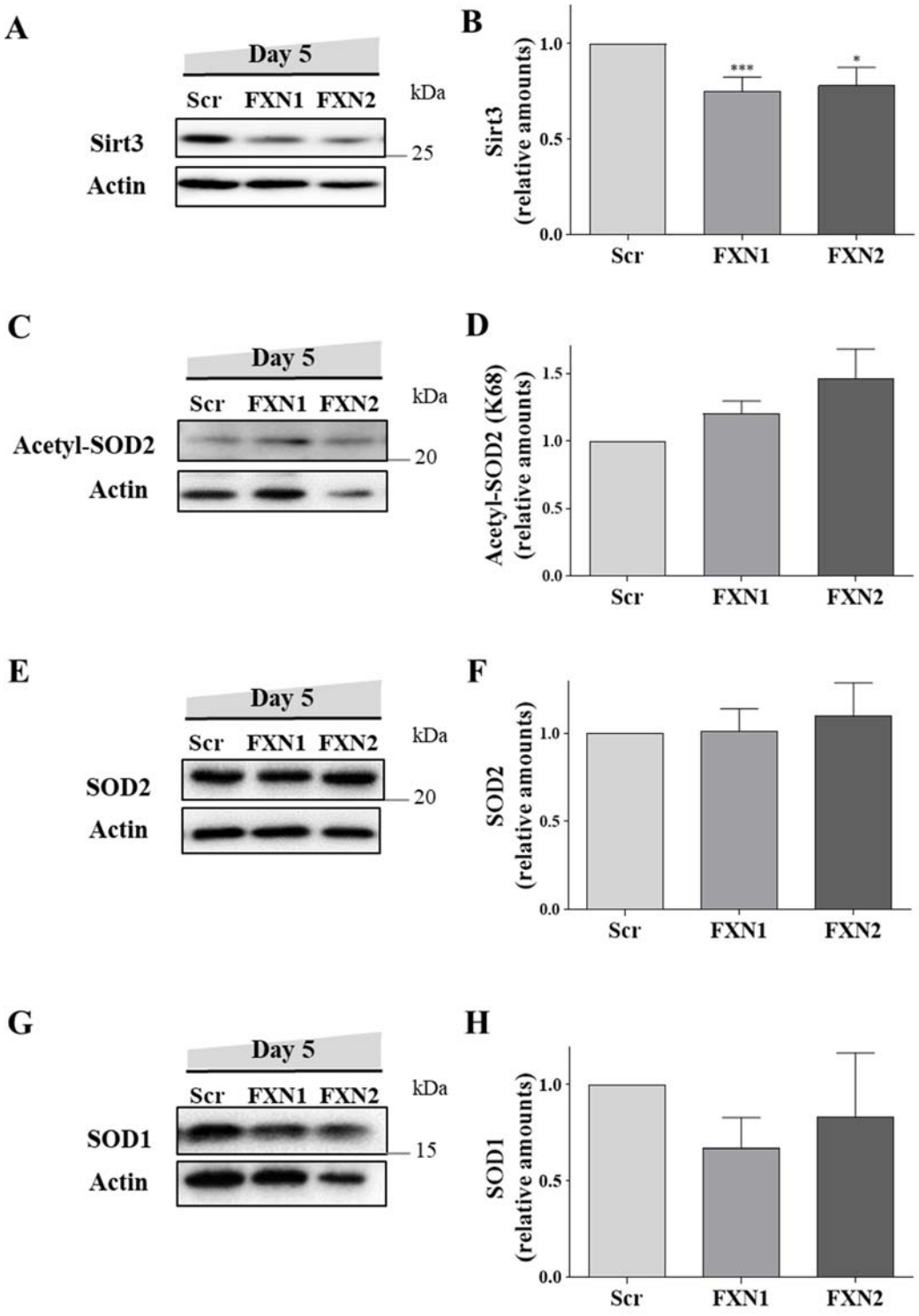

Figure 74. Mitochondrial Sirt3 deacetylase decreases in frataxin deficiency. In A, WB analysis of Sirt3 mature protein in total lysates of frataxin-deficient DRG neurons at 5 days after lentivirus transduction. In B, quantification of WB images. Data are Mean ± SEM of n=23 independent isolations. Scr condition is indicated as 1 and (*) is used for significant value respect Scr condition. In C, WB analysis of Acetyl-SOD2 (K68) and quantification in D. Data are Mean ± SEM from n=3 independent experiments. In E and G, WB bands for respectively SOD2 and SOD1 antibodies. SOD2 quantification in F. Data are Mean ± SEM from n=11 independent experiments. SOD1 quantification in H. Data are Mean ± SEM from n=3 independent experiments.

1.7.2 Progressive fodrin fragmentation during FXN depletion

An increase of $[Ca^{2+}]_i$, as shown in **Figure 64**, activates calpain and caspase proteases. Pro-Caspase 9 and Caspase 3 are cleaved in their active forms as shown in **Figure 73**, starting all the sign of intrinsic (or mitochondrial) apoptotic cell death. Both calpain and caspase proteases cleave the α-fodrin, a cytoskeletal protein of 250kDa, to produce a non-specific 150kDa fragment. A second cleavage results in a calpain-specific fragment of 145kDa, mediated by calpain-1 in the brain (Siman et al., 1984), or a caspase 3-specific product of 120kDa (Nath et al., 1996). Our laboratory previously showed that both fragments are present in frataxin-deficient DRG neurons at 5-days after transduction, suggesting activation of both caspase 3 and calpain. In this work, the fodrin fragmentation in FXN-deficient DRGs has been analysed by WB in early stages after frataxin depletion, observing a lineal and time-dependent increase of α-fodrin cleavage, starting 3 days after lentivirus transduction (**Figure 75A** and **B**).

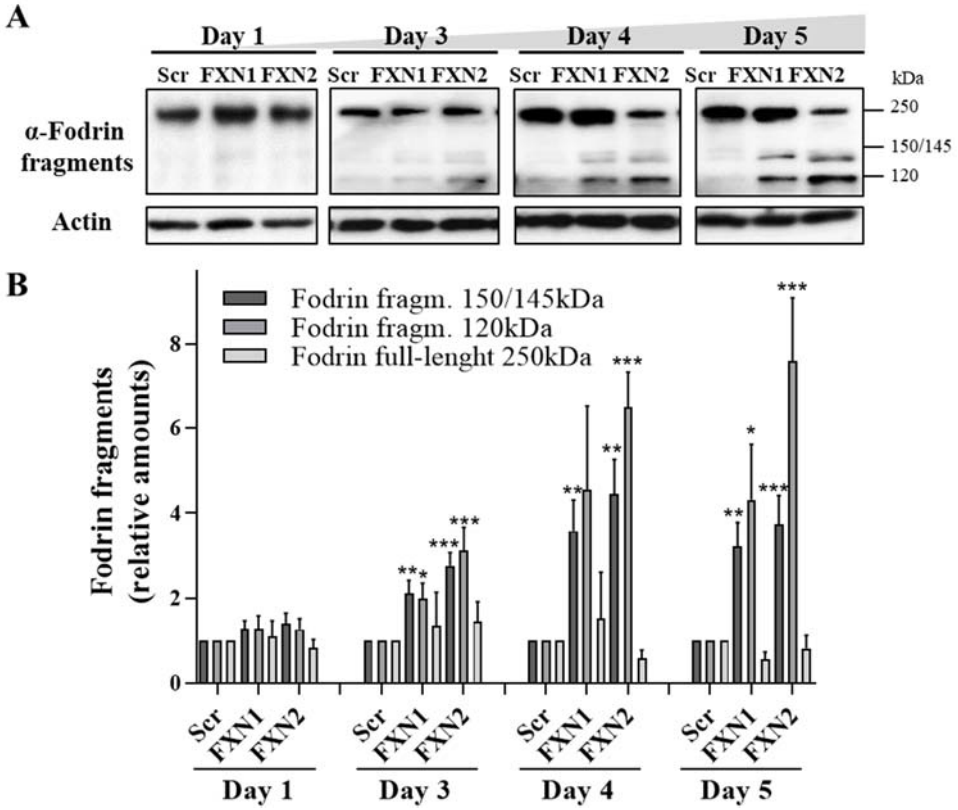

Figure 75. Progressive increase of calpain and caspase 3-cleaved fodrin fragments in frataxin-deficient DRG neurons. In A, amounts of fodrin fragments (145/150kDa and 120kDa) are analysed by WB in frataxin-deficient DRG neurons at day 1-3-4 and 5 after lentivirus transduction as described in Materials and Methods. Quantification for full-length α-fodrin and protease-specific fragments are shown in B. Note the progression of fragmentation during the time in frataxin deficiency. Data are Mean ± SEM obtained from n=5 independent isolations. Scr conditions at each time point are indicated as 1 and significant values compared to each Scr condition are indicated by (*).

1.7.3 Frataxin deficiency induces neurite degeneration and cell death

Previous results from our laboratory show that frataxin-deficient DRG neurons increase apoptotic cell death and neurite degeneration compared to control neurons at 5 days after lentivirus transduction (Mincheva-Tasheva et al., 2014). **Figure 76A** indicates representative images for same cross-marked culture well at different time points.

The number of neurons counted at day 2-3-4 and 5 *vs* the initial value is indicated as the percentage of survival in **B**, while histograms from the data at day 1-3 and 5 are presented in **C**.

Note the progressive decrease in cell survival for frataxin-deficient DRG neurons, which displays significant values compared to Scr condition at 3 days after lentivirus transduction, reaching the residual percentage of 65%-60% at such time point and 45%-30% (for FXN1 and FXN2, respectively) at the end of the experiment.

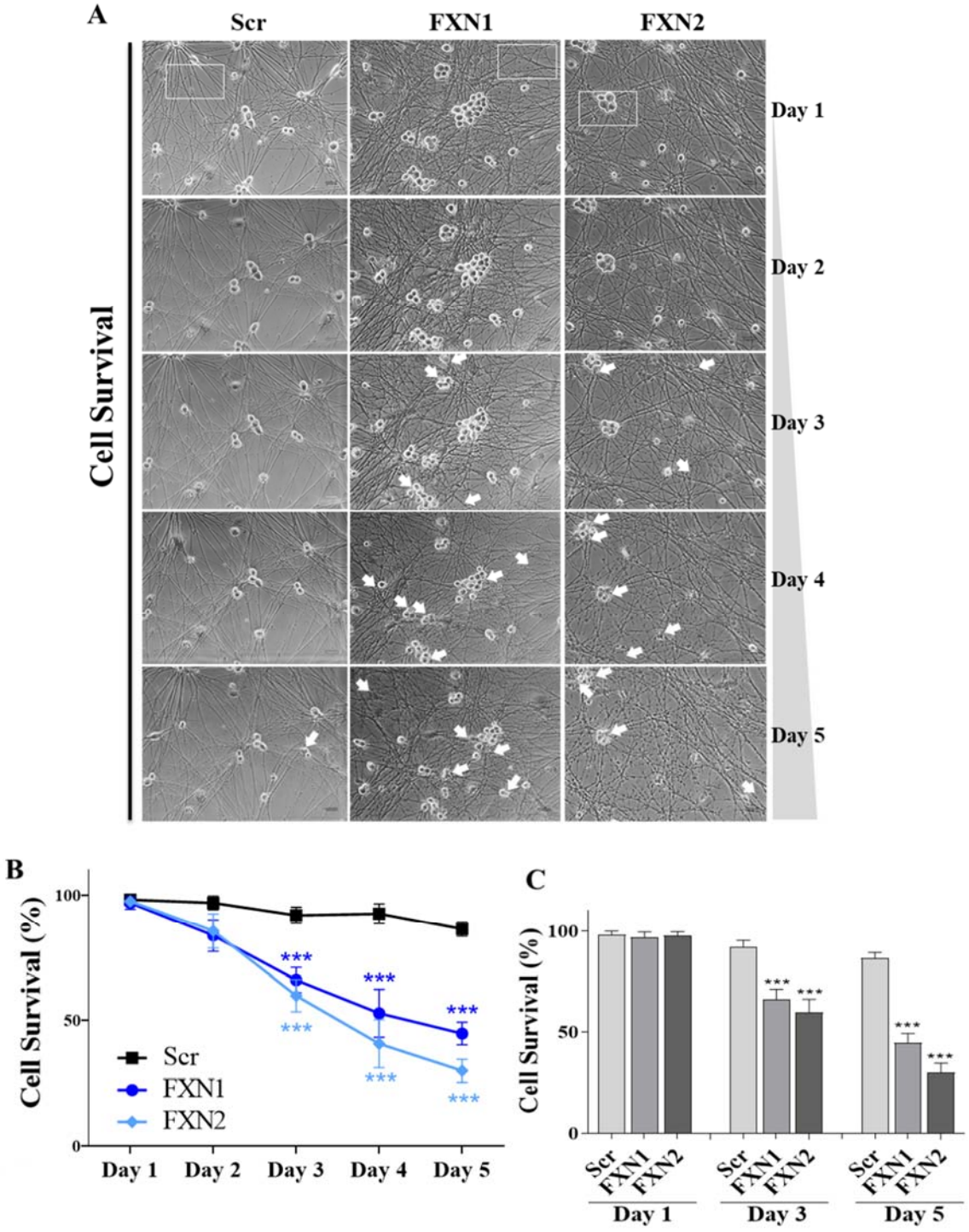

Figure 76. Frataxin-deficient DRG neurons show progressive apoptotic cell death. Representative phase-contrast images of the same field showing frataxin-deficient DRG neurons at days 1-2-3-4 and 5 after lentivirus transduction in A. Scale Bar= 30µm and objective= 16x. Arrows indicate apoptotic (detached) cells. The number of neurons at days 2, 3, 4 and 5 *vs* the initial value is indicated as percentage of survival in B. Data are Mean ± SEM obtained from n=6 independent isolations. In C, histograms represent the percentage of survival for neurons 3 and 5 days after lentivirus transduction. Data are Mean ± SEM obtained from n=6 independent isolations. A range of 1127-1200 neurons has been counted for Scr conditions, a range of 2388-2500 neurons has been counted for FXN1 conditions and a range of 2014-2100 neurons has been counted for FXN2 conditions at the initial value. Significant values compared to Scr condition are indicated by (*).

Furthermore, zoom-in in **Figure 77A** (of phase-contrast images in **Figure 76A**) shows a progressive presence of axonal swelling in neurites of frataxin-deficient DRG neurons. Representative images of neurodegeneration at several days after lentivirus transduction are quantified as the number of neurites with axonal swelling (or neurofilament aggregation) *vs* the total number of neurites. Values, indicated as percentage, are shown in **B**, while histograms from data at day 1, 3 and 5 after lentivirus transduction in **C**. Note the progressive increase in axonal swelling for frataxin-deficient DRG neurons, which displays significant values compared to Scr condition at 3 days after lentivirus transduction, reaching the residual percentage of 37%-46% at such time point and 68%-79% (for FXN1 and FXN2, respectively) at the end of the experiment. All these data indicate neurite degeneration with axonal swelling in frataxin deficiency.

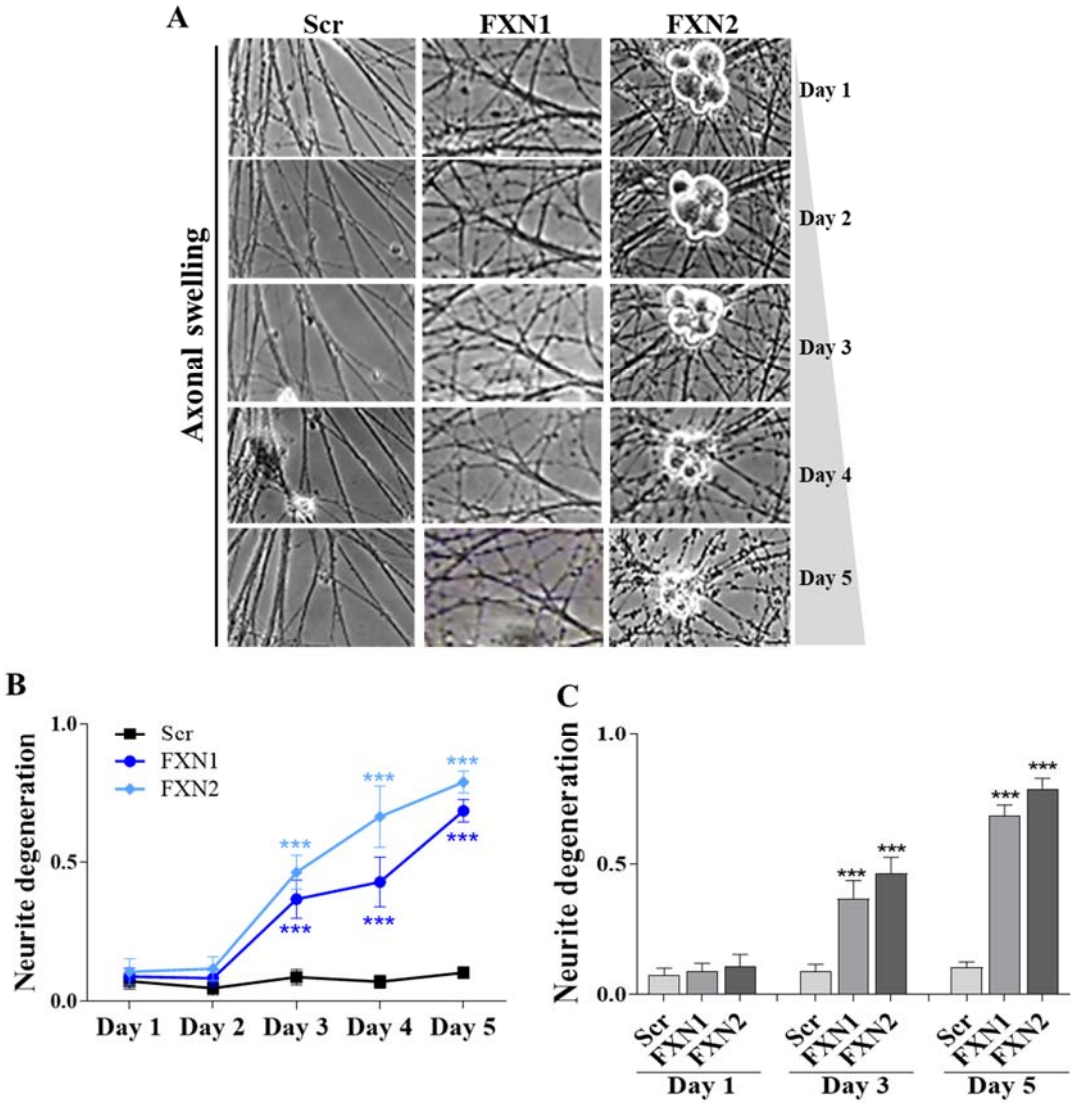

Figure 77. FXN-deficient DRGs show progressive axonal swelling. Representative phase-contrast images of the same field (marked in **Figure 76A**) showing axonal swelling of frataxin-deficient DRG neurons at days 1-2-3-4 and 5 after lentivirus transduction in A. Scale Bar= 30µm and objective= 32x. Note the progression of pointed pattern on neurites (axonal swelling)

during the time. Values in B and histograms in C represent the number of neurites with axonal swelling on the total number of neurites for each time point. Data are Mean ± SEM obtained from n=6 independent isolations. A range of 1184-2002 neurites have been analysed for Scr, a range of 1234-1633 neurites for FXN1 and a range of 1121-1551 neurites for FXN2 conditions. No selection between types of neurites has been made, meaning that large-diameter and small-diameter neurites have been analysed together. Significant values compared to Scr condition are indicated by (*).

1.8 FXN deficiency alters phosphorylation state and gene expression

Gene expression alterations in our model have been already detected, when the transcription factor CREB has been found phosphorylated in frataxin deficiency (Mincheva-Tasheva et al., 2014).

1.8.1 Frataxin deficiency alters PTEN protein levels

As the above results in **Figure 72** suggest alterations not only in processing but also expression of Pink1, the levels of another protein correlated to Pink1 expression have been analysed: the Phosphatase and Tensin homolog deleted on chromosome 10 (PTEN) protein. In fact, Pink1 is the PTEN-inducible putative kinase 1 for its increased expression in the presence of exogenous PTEN (Unoki & Nakamura, 2001). In addition, PTEN deficient mice develop seizures and ataxia (Backman et al., 2001). As, in our FA model, Pink1 total amounts decrease, PTEN deficiency was our initial hypothesis. For these reasons, PTEN was analysed by WB. **Figure 78A** shows PTEN bands of 55kDa in frataxin-deficient DRG neurons at several days after lentivirus transduction. Quantification on β-actin are indicated in **B**. PTEN levels decrease at 5 days, indicating that this reduction is a late event in frataxin deficiency.

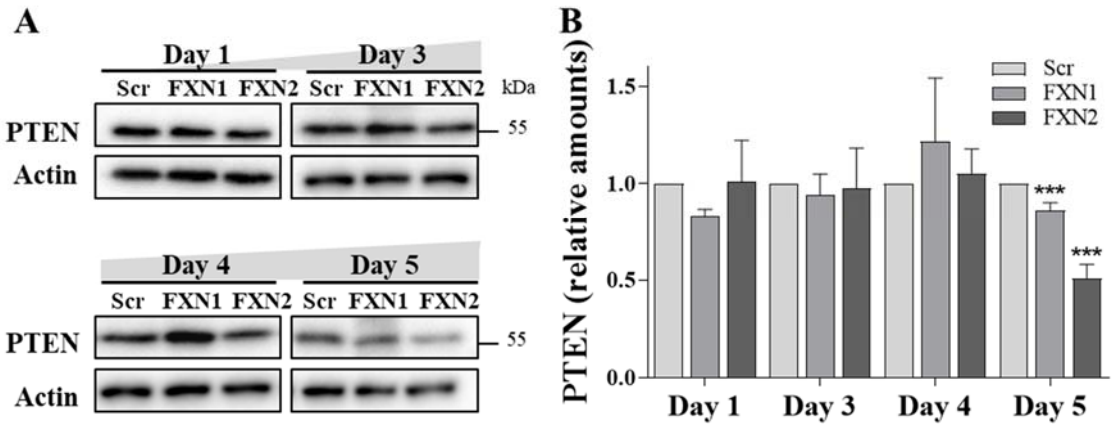

Figure 78. Frataxin deficiency induces decreased levels of PTEN. In A, WB images of PTEN 55kDa in total lysates of frataxin-deficient DRG neurons and controls at several days after

lentivirus transduction. Quantifications are shown in B. Scr for each time point is considered as 1 and (*) indicates significant values compared to Scr. Data are Mean ± SEM of n=2 (day 1), n=4 (day 3-4) and n=14 (day 5) independent isolations.

1.8.2 Frataxin deficiency dephosphorylates and activates NFAT

The data shown above indicate that frataxin depletion decreases NCLX (**Figure 62**) and triggers mPTP opening, which, thus, release $Ca^{2+}{}_m$ and pro-apoptotic proteins into the cytosol (**Figure 73**). In this context, Ca^{2+}-activated proteins such as calcineurin, a Ca^{2+}-dependent phosphatase, should be activated. One of the substrates of calcineurin is NFAT (Nuclear Factor of Activated T cells) transcription factor. The name is due to the fact that it was firstly discovered in T lymphocytes, however, it is also expressed in sensory neurons (Kim & Usachev, 2009). In normal conditions, hyper-phosphorylated and inactive NFAT is localised in the cytosol. When Ca^{2+}-activated phosphatases, such as calcineurin, dephosphorylate NFAT, allow activation of transcription factor and its nuclear import. Once $[Ca^{2+}]_c$ is restored at basal levels, NFAT can be phosphorylated by protein kinases, such as GSK3β, and transported into cytosol (Hogan et al., 2003). Then, in frataxin deficiency, NFAT should be activated. To test this hypothesis, firstly total levels of NFATc4 have been analysed. As shown in **Figure 79A** and quantification **B**, no changes are detected considering the total amount of NFAT. However, the hyper-phosphorylated (*) and dephosphorylated forms of NFAT have been detected, indicating a reduction of phosphorylated form in frataxin-deficient DRG neurons at 5 days after lentivirus transduction. Thus, the hypothesis has been confirmed using a second antibody, which detects phosphorylated form of NFATc4. As shown in **Figure 79C** and quantification in **D**, decreased levels of pNFAT have been detected in frataxin-deficiency at 5 days after lentivirus transduction, reaching a reduction to 40% for FXN1 and 35% for FXN2 of Scr control. However, the de-phosphorylation occurs in the last steps of frataxin deficiency, indicating, probably, that a massive increase of $[Ca^{2+}]_c$ is needed for NFAT activation, while at early stage of frataxin deficiency (e.g. day 1) the tendency seems to be opposite. De-phosphorylation of NFAT, together with activation of calcineurin, have been also detected in frataxin-deficient cardiomyocytes, strengthening this hypothesis (Purroy et al., 2018). More studies are necessary to understand what happens in the first steps of frataxin deficiency; however, all these data indicate NFAT activation (de-phosphorylation) at least in the last steps and point out the possibility of alteration of gene expression in frataxin deficiency.

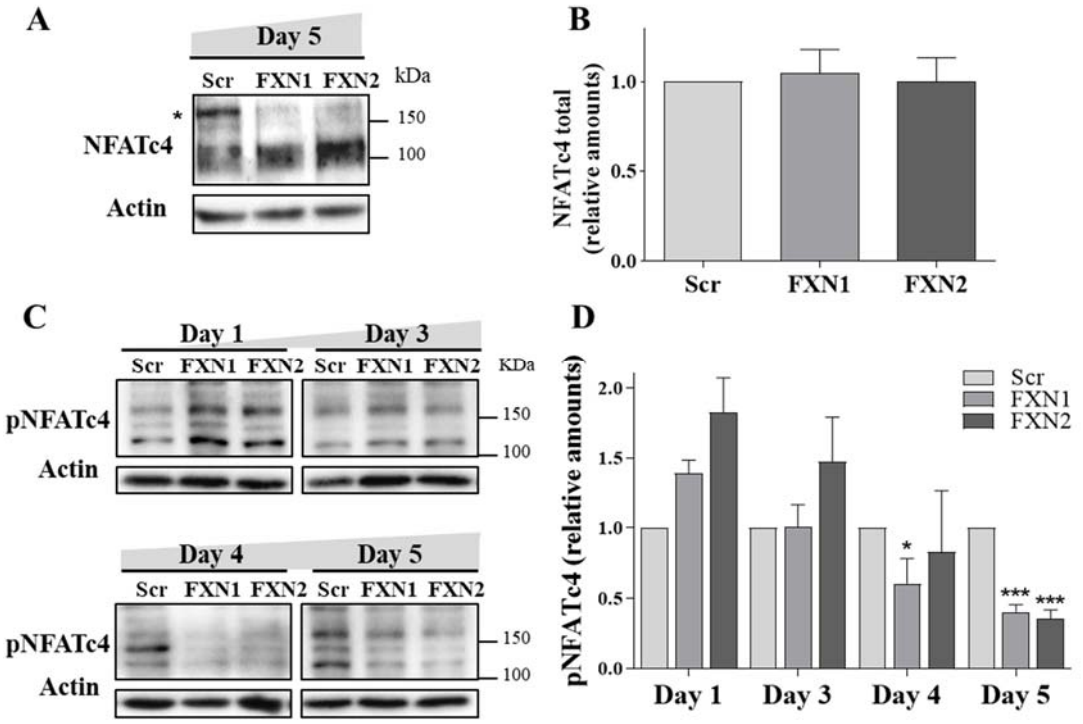

Figure 79. NFATc4 is activated, thus dephosphorylated, in frataxin deficiency. In A, representative WB images of total NFAT in FXN-deficient DRGs at 5 days after lentivirus transduction. The hyper-phosphorylated form of NFATc4 is indicated with (*), while the band around 100 kDa correspond to dephosphorylated NFATc4. Quantification of total amount of NFAT is shown in B. Data are Mean ± SEM from n=4 independent isolations. The phosphorylation state of NFATc4 transcription factor has been also tested in DRG neurons after frataxin depletion. WB Images in C, and quantification in D, show the decrease of NFATc4 phosphorylation levels at 5 days, but not in early stages. Quantification has been performed using the lower band of pNFAT of ~120kDa. Data are Mean ± SEM obtained from n=2 (day 1), n=4 (day 3 and 4) and n=18 (day 5) independent isolations. Scr conditions are indicated as 1 and (*) indicates significant values respect Scr condition.

1.9 FXN deficiency induces changes in the iron-sulfur protein FDX1, but not Aco

1.9.1 FXN deficiency maintains aconitase activity and levels

Despite being the role of frataxin ambiguous, some results suggest a role in iron-sulphur cluster biosynthesis. For this reason, two iron-sulphur cluster proteins have been analysed in this model: aconitase and ferredoxin 1 (FDX1). Frataxin-deficient DRG neurons display apoptotic cell death with axonal swelling and Ca^{2+} alterations, as above shown, but the amount in **Figure 80A** and **B** and the activity (compared to citrate synthase in **C**) of aconitase, an iron-sulphur protein, are comparable to the controls, indicating that Ca^{2+} alterations and apoptotic cell death are primary targets of frataxin deficiency. These results are in agreement with previously published data by our group

in which frataxin-deficient cardiomyocytes display normal activity and amount of aconitase, even though mitochondrial swelling and impairment of lipid metabolism is observed (Obis et al., 2014).

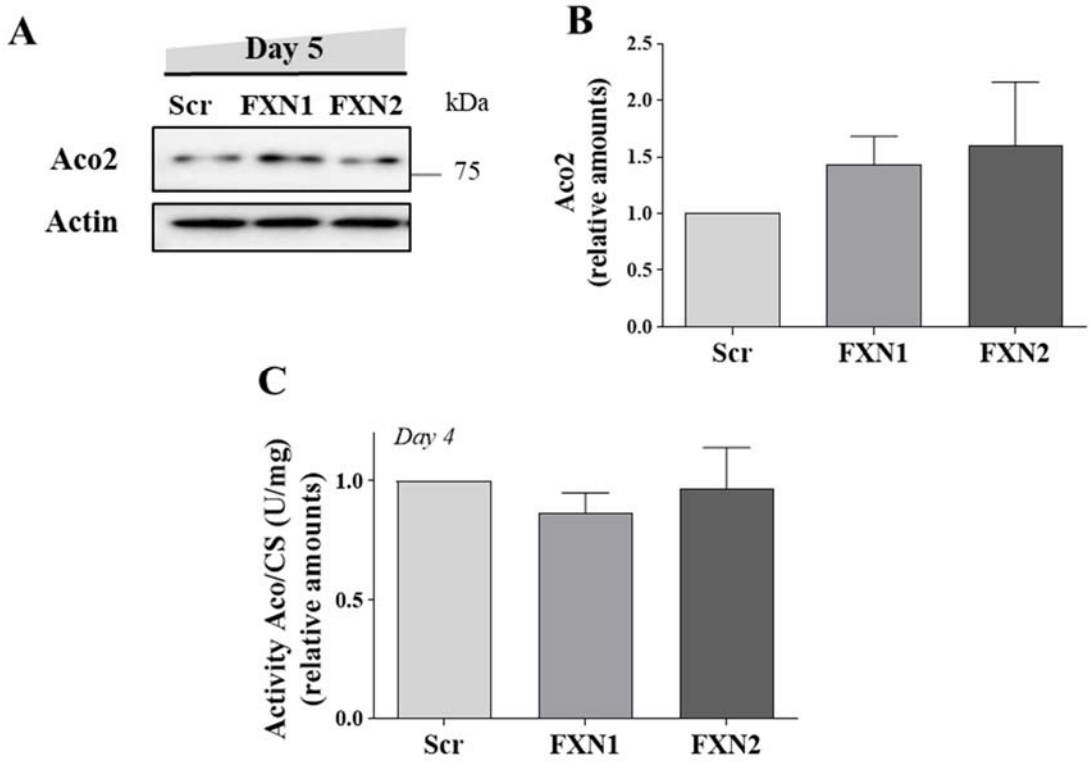

Figure 80. Frataxin-deficient DRG neurons show normal amounts and activity of Aconitase. In A, amounts of aconitase 2 are analysed by WB in frataxin-deficient DRG neurons at day 5 after lentivirus transduction as described in Materials and Methods. Quantifications for Aco2 are shown in B. Data are Mean ± SEM obtained from n=12 independent isolations. In C, relative amounts of ratio aconitase/citrate synthase activity in frataxin-deficient DRG neurons at 4 days after lentivirus transduction. Relative amounts of aconitase activity (Fluorescence) and citrate synthase activity (Absorbance), are indicated as U/mg in which Unit=µmol/min. Data are Mean ± SEM obtained from n=4 independent isolations. Scr conditions are indicated as 1.

1.9.2 Frataxin deficiency reduces FDX1 amounts

However, another protein carrying iron-sulphur cluster, FDX1 in **Figure 81A** and quantification in **B** shows reduced levels at 3 and 5 days after lentivirus transduction. For this iron-sulphur protein, the reduction to 68-65% at 3-days (respectively, FXN1 and FXN2) and to 50-48% of Scr level at 5 days after lentivirus transduction in frataxin deficiency could be ascribed to an alteration in iron-sulphur cluster biosynthesis and/or degradation. These results suggest that the role of frataxin in iron-sulphur cluster biosynthesis could be secondary to Ca^{2+} alterations.

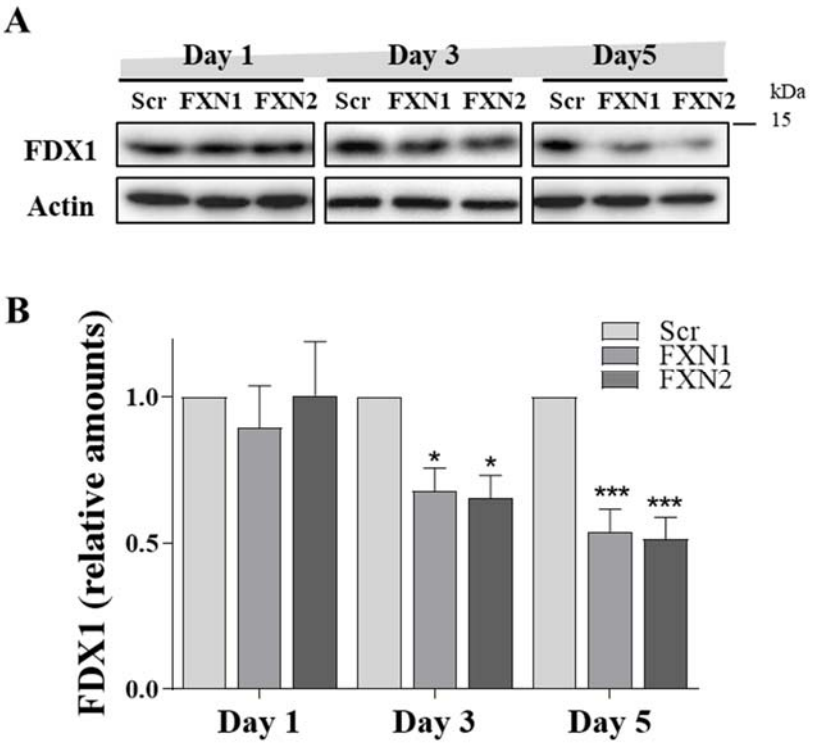

Figure 81. Frataxin deficiency decreases ferredoxin 1 protein levels. In A, amounts of ferredoxin 1 (FDX1) are analysed by WB in frataxin-deficient DRG neurons at day 1-3- and 5 after lentivirus transduction as described in Materials and Methods. Quantification for FDX1 is shown in B. Data are ± SEM obtained from n=3 independent isolations (day 1 and 3) and n=8 for day 5. Scr is indicated as 1 and significant values compared to Scr are indicated by (*).

1.10 Frataxin deficiency alters Vitamin D_3 metabolism

As above indicated in **Figure 81**, frataxin-deficient DRG neurons show low levels of FDX1. FDX1 is essential for Vitamin D_3 metabolism, regulating calcitriol (vitamin D active form) synthesis and degradation; it has been demonstrated to interact with frataxin (Cai, Frederick, Tonelli, & Markley, 2018). Then, the levels of two enzymes that, respectively, are responsible for calcitriol synthesis and degradation Cyp27b1 (25-hydroxyvitamin D-1α-hydroxylase) and Cyp24a1 (25-hydroxyvitamin D-24-hydroxylase) have been analysed. **Figure 82A** indicates the images and quantification (**B**) for Cyp27b1 levels. Note the 2-fold and 2.5-fold increase of Cyp27b1 in frataxin deficiency. **Figure 82C** and **D** show the images and quantification for Cyp24a1. Frataxin-deficient DRG neurons display a reduction by 26% for FXN1 and 29% for FXN2. Such results indicate alterations in calcitriol synthesis and degradation and point out the possibility of a calcitriol treatment in FA. In fact, the increase of Cyp27b1 levels, as its expression is regulated by calcitriol, suggest the possibility of calcitriol deficiency in FA.

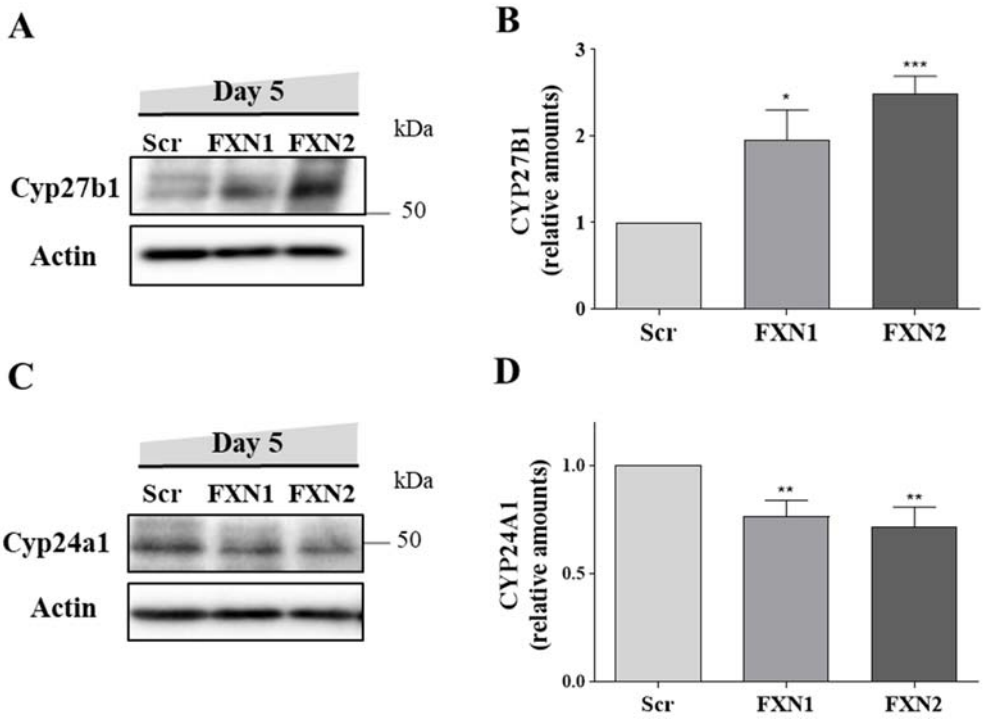

Figure 82. Enzyme levels for calcitriol biosynthesis and degradation are altered in frataxin-deficiency. In A, representative images of Cyp27b1 in total lysates of frataxin-deficient DRG neurons at 5 days after lentivirus transduction. Quantification in B. Data are Mean ± SEM, n=8. In C, representative images of Cyp24a1 in total lysates of frataxin-deficient DRG neurons. Histograms in D. Data are the Mean ± SEM of n=9 independent experiments. Scr is indicated as 1 and significant values compared to Scr are indicated with (*).

2 COMPOUNDS CHELATING CALCIUM

2.1 Calcium chelator BAPTA protects FXN-deficient DRGs

2.1.1 BAPTA restores NCLX levels and Ca^{2+} homeostasis

As mentioned in the previous sections, frataxin-deficient DRG neurons show alteration of Ca^{2+} homeostasis, in which NCLX is the major exchanger for Ca^{2+}_m efflux and MCU the major channel for Ca^{2+}_m influx. The correct function of these transporters mediates the balance of $[Ca^{2+}]_m$. Once demonstrated the reduced levels of NCLX in frataxin deficiency, the mechanism by which this reduction occurs become our intriguing question. When it has been demonstrated that the NCX, a member of Na^+/Ca^{2+} exchanger family, of the endoplasmic reticulum can be cleaved by Ca^{2+}-activated proteases (e. g. calpains) (Samanta, Kar, Chakraborti, & Chakraborti, 2010), it has been considered if the Ca^{2+}-dependent cleavage of NCLX could be the answer for our

question. For this purpose, NCLX protein levels have been analysed in the presence of a membrane-permeant Ca^{2+} chelator agent, BAPTA-AM, which sequestering intracellular Ca^{2+} reduces $[Ca^{2+}]_{free}$, even in mitochondria (Abramov & Duchen, 2008). For this reason, frataxin-deficient DRG neurons and controls have been daily treated with 12μM of BAPTA-AM or DMSO as vehicle. As shown in **Figure 83A** and **B**, NCLX protein levels are partially restored by BAPTA treatment, suggesting that increased $[Ca^{2+}]$ can contribute to NCLX reduced levels. In fact, BAPTA induces a 2-fold (for FXN1) and 4-fold (for FXN2) increase in NCLX levels. As a control of the chelating functions, it has been analysed also α-fodrin, a cytoskeletal protein, substrate of Ca^{2+}-activated proteases, which has been previously reported fragmented in our model. BAPTA treatment avoids α-fodrin fragmentation, by reducing the Ca^{2+}_{free} needed for proteases activation. Furthermore, to demonstrate that the increased NCLX protein levels are not ascribed to a general rise in mitochondrial protein amounts, the Ca^{2+}_m -uniporter, MCU, has been analysed as mitochondrial control as shown in **Figure 83C** and **D**. As expected, no differences have been detected in MCU levels by using the treatment. Taken together these results indicate that BAPTA treatment restores NCLX protein levels, suggesting a Ca^{2+}-dependent cleavage of NCLX in frataxin deficiency.

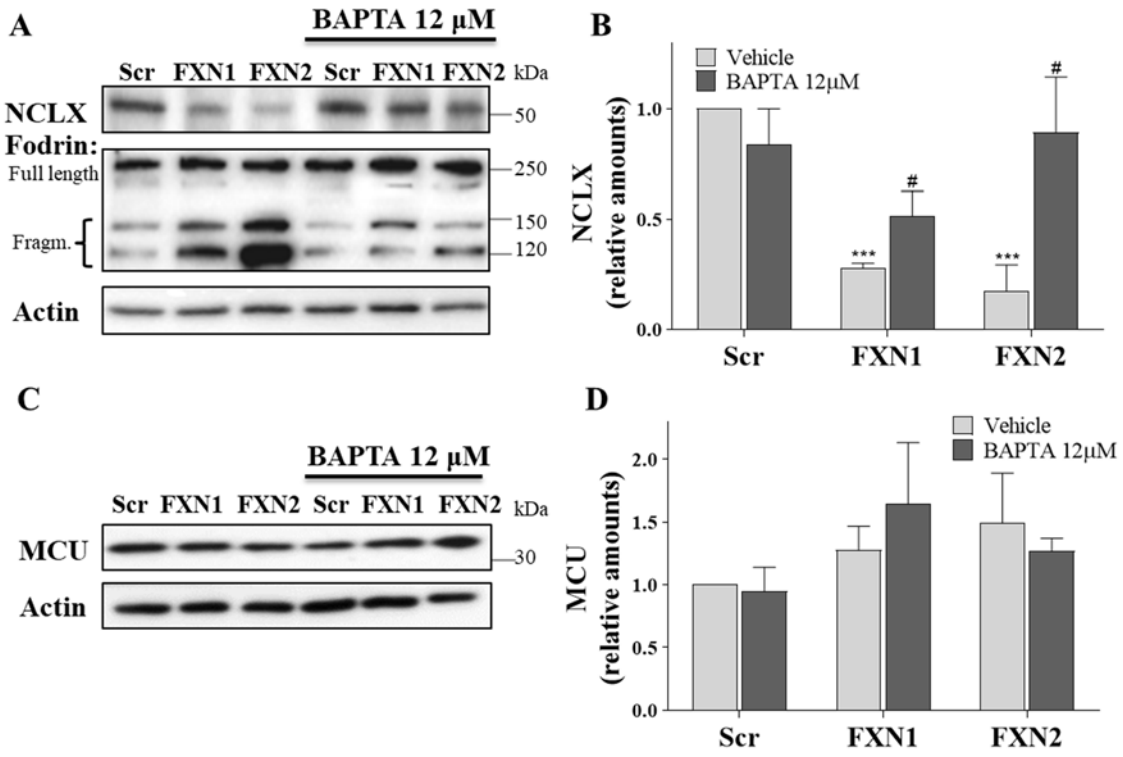

Figure 83. BAPTA treatment restores NCLX protein levels, without affecting mitochondrial protein amounts. In A, representative images of NCLX protein amounts and fodrin fragments in frataxin-deficient DRG neurons daily treated (or not) with BAPTA 12μM. Quantification in B.

Data are Mean ± SEM, n= 5 independent isolations. In C, representative WB images of MCU protein levels, used as a mitochondrial marker, normalised to β-actin in treated (or not) conditions. Quantification in D. Data are Mean ± SEM, n=4 independent isolations. Untreated Scr is indicated as 1 and significant values compared to Scr are indicated as (*), while compared to untreated conditions as (#).

2.1.2 BAPTA protects from apoptotic cell death

All the above results indicate that BAPTA 12μM protects frataxin-deficient DRG neurons from apoptosis. To corroborate this hypothesis, frataxin-deficient DRG neurons daily treated with BAPTA or vehicle have been tested for cell survival analysis. As expected and shown in **Figure 84**, BAPTA protects frataxin-deficient DRG neurons from cell death. In fact, cell survival reaches the 91 and 92% for both frataxin-deficient DRG neurons, FXN1 and FXN2, respectively. This result indicates that a Ca^{2+} chelator agent protects frataxin-deficient DRGs, suggesting that Ca^{2+}_{free} has an important role in DRG neurodegeneration.

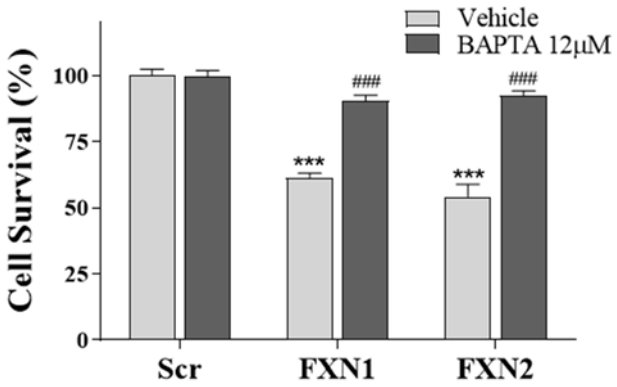

Figure 84. BAPTA treatment restores cell survival. The histogram indicates the percentage of cell survival in the presence of BAPTA 12μM or vehicle DMSO. Note the protection of frataxin-deficient DRG neurons using BAPTA treatment. Data are Mean ± SEM, n= 3 independent isolations. Untreated Scr conditions are indicated as 1 and (*) indicates significant values compared to Scr, while (#) significant values compared to untreated conditions.

3 COMPOUNDS REPLACING FRATAXIN DEFICIENCY

3.1 TAT-MTScs-FXN replaces frataxin deficiency and improves altered markers

3.1.1 TAT-MTScs-FXN is targeted and processed into mitochondria

TAT-MTScs-FXN is a TAT-fusion protein, which is used to deliver proteins into cells, in this case frataxin, carrying a MTS, which is used to deliver proteins specifically into

mitochondria, in this case MTS from the mitochondrial protein citrate synthase (MTScs) (Marcus et al., 2016). Thus, the construct is generated with the aim of replacing frataxin into mitochondria and is used in our frataxin-deficient neuronal model to test its efficiency. First of all, it has been tested the ability of TAT-MTScs-FXN to target mitochondria. **Figure 85A** shows the localisation of frataxin in cells treated with TAT-MTScs-FXN 7µg/mL 12h after transduction (red fluorescence). Immunofluorescent staining, using anti-OXPHOS antibody (green dots) was used as a mitochondrial marker. Merge images indicates a punctate pattern of frataxin signal in cell soma and along neurites, suggesting a mitochondrial localisation of TAT-MTScs-FXN. Once demonstrated that the construct penetrates into cells and targets to mitochondria, processing and maturation of frataxin was analysed by detecting the expected MW of its mature form (14kDa). TAT-MTScs-FXN 7µg/mL (or equal amount of vehicle) has been added to frataxin-deficient DRG neurons (or Scr controls) media, 48h after lentivirus transduction. As shown in **Figure 85B**, TAT-MTScs-FXN is processed into intermediate forms of frataxin above 20kDa and frataxin mature form of 14kDa, all of them detectable using frataxin antibody, while the last band in the WB indicates the kDa of TAT-fusion protein exempt from cells. Note the differences in TAT-MTScs-FXN processing between Scr controls and frataxin-deficient DRG neurons. As mitochondrial protein import is generally driven by $\Delta\Psi_m$ and as frataxin-deficient DRG neurons present mitochondrial depolarisation, it is conceivable that processing mechanisms in mitochondria would be dysfunctional in frataxin deficiency, therefore affecting TAT-MTScs-FXN import. In fact, histograms in **C** show a 3-fold increase in the unprocessed form of TAT-MTScs-FXN in frataxin-deficient DRG neurons, 1.3-fold (for FXN1) and 3.5-fold (for FXN2) increase in intermediate forms of frataxin, suggesting reduced ability of frataxin processing, and similar levels of frataxin mature form, suggesting degradation of excessive mature form in control conditions. These levels of frataxin mature form are much higher than endogenous frataxin signal corresponding to vehicle treated Scr controls, as shown in **D**. In fact, frataxin mature signal in untreated Scr controls is almost undetectable compared to TAT-MTScs-FXN 7µg/mL treated cells in the same WB exposure, and similar compared to TAT-MTScs-FXN 1µg/mL treated cells. However, **Figure 85E** indicates that processing alterations are present in frataxin-deficient DRG neurons even using lower amounts of TAT-MTScs-FXN 1 µg/mL and 3µg/mL. Nevertheless, all TAT-MTScs-FXN concentrations

in analysis are able to penetrate frataxin-deficient DRG neurons and increase frataxin mature levels.

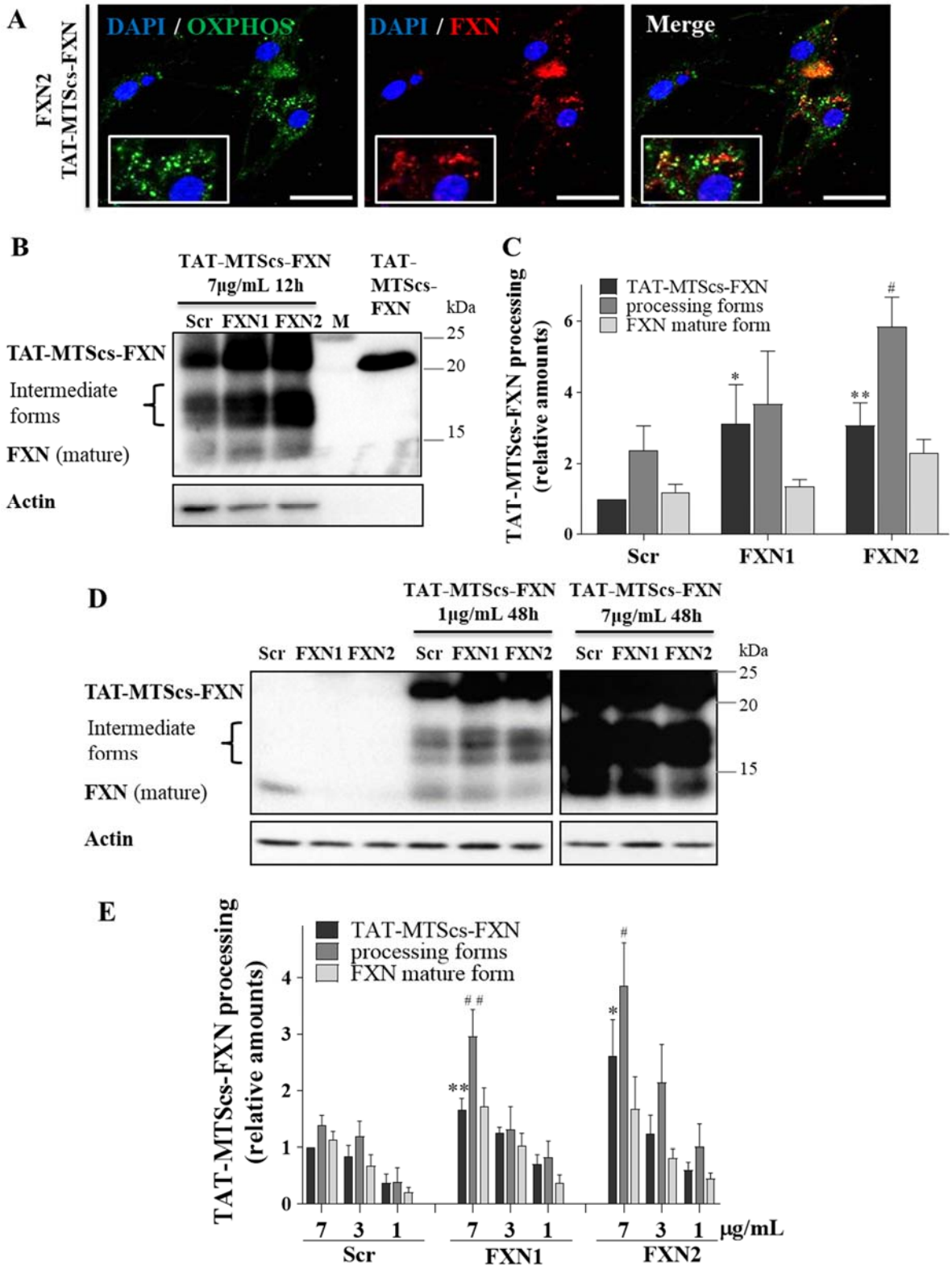

Figure 85. TAT-MTScs-FXN penetrates cells and targets mitochondria for processing, which is altered in frataxin deficiency. In A, immunofluorescent staining of anti-OXPHOS (in green) and anti-FXN (in red) antibodies in frataxin-deficient DRG neurons (FXN2) treated with TAT-MTScs-FXN 7µg/mL 12h after lentivirus transduction. Images have been taken at the end of the

experiment and nuclei stained with DAPI. Zoom-in allows to better note the co-localisation between the mitochondrial marker (anti-OXPHOS) and frataxin. Scale bar= 10µm and objectives= 20x. In B, representative WB images of frataxin protein levels in Scr controls and frataxin-deficient DRG neurons treated with TAT-MTScs-FXN 7µg/mL 12h after lentivirus transduction. Actin is used as control of protein loading. The band in the right corresponds to intact TAT-MTScs-FXN protein construct, free of cells. M= Marker 25kDa. Histograms in C correspond to the unprocessed, intermediate and mature form of frataxin bands (in B) normalised to unprocessed form in Scr condition indicated as 1. Data are Mean ±SEM of n=4 independent isolations. In D, representative images of TAT-MTScs-FXN 1 and 7µg/mL treated cells (Scr controls and frataxin-deficient) at 48h after lentivirus transduction. Histograms in E represent the unprocessed, intermediate and mature form of frataxin bands in cells treated with 1-3 and 7µg/mL of TAT-MTScs-FXN. Values are normalised to unprocessed form in Scr condition indicated as 1. Data are Mean ± SEM obtained from n=4 independent isolations.

3.1.2 TAT-MTScs-FXN restores HSP60 import alterations

The impairment of TAT-MTScs-FXN processing in FXN-deficient DRG neurons is in accordance with alterations of processing (or import) of other proteins (e.g. Hsp60 and Pink1 respectively shown in **Figure 71** and **Figure 72**). Deficiency of GRP75, the motor for mitochondrial protein import in **Figure 70**, and depolarisation of mitochondrial membrane in **Figure 59** agree with import alterations. Bearing in mind all these alterations related to mitochondrial import, it was analysed if the addition of exogenous frataxin could restore at least one of these alterations, the Hsp60 processing. The precursor form of Hsp60, in its process into the mitochondria, its MTS is cleaved by proteases, releasing the mature form into matrix. As shown in **Figure 86A**, frataxin-deficient DRG neurons at 5-days present defects in Hsp60 processing, which can be restored by TAT-MTScs-FXN 7µg/mL treatment. Each isoform, precursor (P) and mature (M) is shown in percentage of Hsp60 total amount in **B**. Precursor form shows 9.7 (Scr), 21 (FXN1) and 36% (FXN2), restored to 10.9 (Scr), 11.9 (FXN1) and 21.6% (FXN2) upon TAT-MTScs-FXN treatment. Mature form shows 90.3 (Scr), 79 (FXN1) and 64% (FXN2), restored to 89.1 (Scr), 88.1 (FXN1) and 78.4 (FXN2) upon treatment. Relative amounts on Scr condition are present in **C**, in which Hsp60 precursor form shows a 2-fold increase for FXN1 and 4-fold increase for FXN2, restored upon TAT-MTScs-FXN treatment. Mature form is reduced by 15% (FXN1) and 30% (FXN2), these values also restored by the treatment, while no changes are detected for total amount of Hsp60, even in treated conditions. All these data indicate that defects in Hsp60 processing or import into mitochondria in frataxin deficiency, can be restored by frataxin replacement.

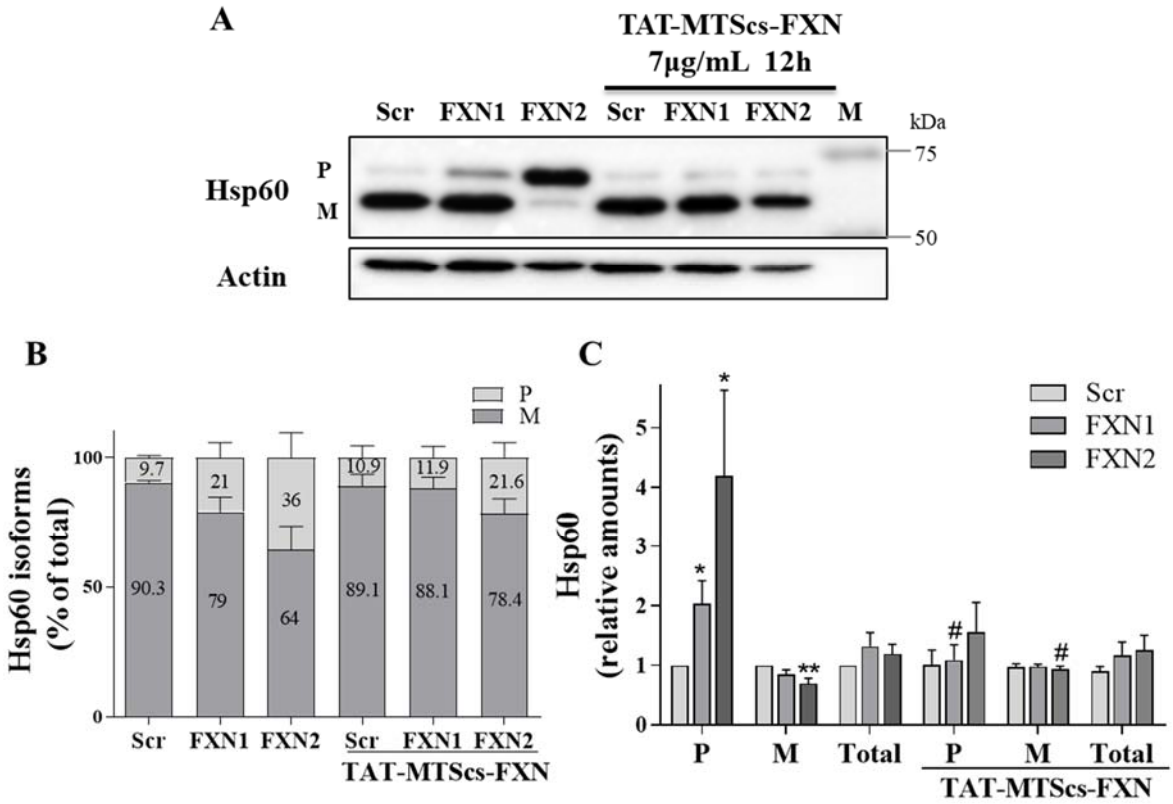

Figure 86. TAT-MTScs-FXN restores defects of Hsp60 import into mitochondria. In A, representative WB images of Hsp60 antibody in Scr controls and frataxin-deficient DRG neurons, treated or not with TAT-MTScs-FXN 7µg/mL at 12h after transduction. Antibody allows to detect two bands, a precursor (P) and mature (M) form of Hsp60, ~70 and 55kDa, respectively. M indicates the MW of Marker (75 and 50kDa). In B, Hsp60 isoforms are expressed as percentage on total Hsp60, while in C histograms represent relative amounts of isoforms and total Hsp60 values compared on untreated Scr conditions as 1. Data are Mean ± SEM obtained from n=8 independent isolations. Significant values compared to Scr or untreated conditions are indicated as (*) or (#) respectively.

3.1.3 TAT-MTScs-FXN restores NCLX protein levels

As previously described (**Page 180**), frataxin-deficient DRG neurons display decreased levels of the mitochondrial $Na^+/Ca^{2+}/Li^+$ exchanger, NCLX. A reduction that could result in Ca^{2+} alterations described elsewhere in this thesis, leading to $Ca^{2+}{}_m$ overload and consequently intrinsic apoptotic cell death. **Figure 87A** and quantification in **B** indicate that external addition of frataxin, 7µg/mL of TAT-MTScs-FXN at 12h, restores NCLX protein levels at those of controls: 2.9-fold increase for FXN1 and 3.5-fold for FXN2.

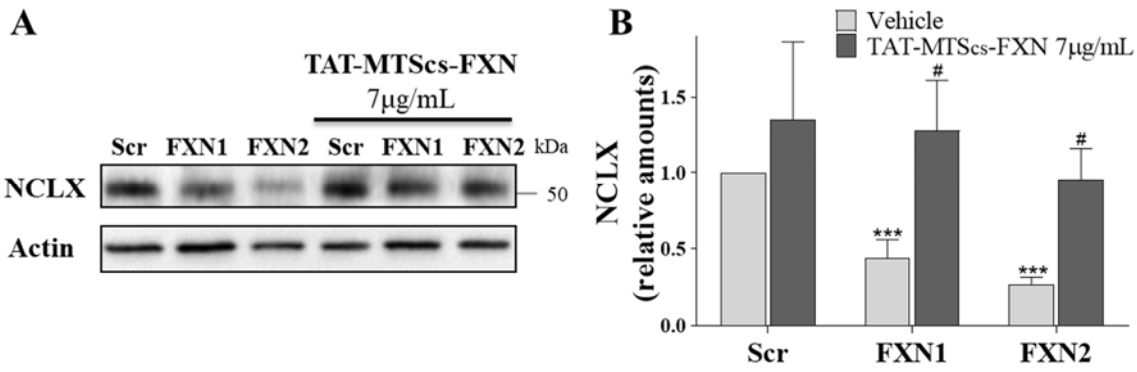

Figure 87. NCLX protein levels are restored by TAT-MTScs-FXN treatment. In A, representative WB images of NCLX protein levels of frataxin-deficient DRG neurons and controls treated (or not) with TAT-MTScs-FXN 7µg/mL at 12h. Histograms in B. Significant values compared to Scr controls are indicated as (*) and compared to untreated conditions as (#). Data are Mean ± SEM, n= 4 independent isolations.

3.1.4 TAT-MTScs-FXN restores pro-caspase 9 cleavage

Apart from mitochondrial import and Ca^{2+} alterations, frataxin-deficient DRG neurons present signs of mitochondrial (or intrinsic) apoptotic cell death (**Page 199**). Several proteins are extruded by mitochondria through the mPTP into the cytosol, therefore triggering a cascade of death signals. One of these proteins is pro-caspase 9, which, when extruded into the cytosol, is activated by cleavage and become ready for cleavage of its substrates. As shown in **Figure 88A**, frataxin-deficient DRG neurons present reduced levels of pro-caspase 9 protein, indicating the activation (cleavage) of this caspase in the cytosol, which are restored at controls levels once treated with 7µg/mL TAT-MTScs-FXN. Histograms in **B** indicates that pro-caspase 9 levels are reduced to 45% (FXN1) and 61% (FXN2) in frataxin deficiency and that TAT-MTScs-FXN 7µg/mL promotes a 2-fold increase in both frataxin-deficient DRG neurons (FXN1 and FXN2). These results suggest that caspase 9 is more active in frataxin deficiency and that the apoptotic cascade triggered by caspase 9 activation in frataxin deficiency could be prevented by TAT-MTScs-FXN addition, indirectly suggesting a closed-conformation for mPTP.

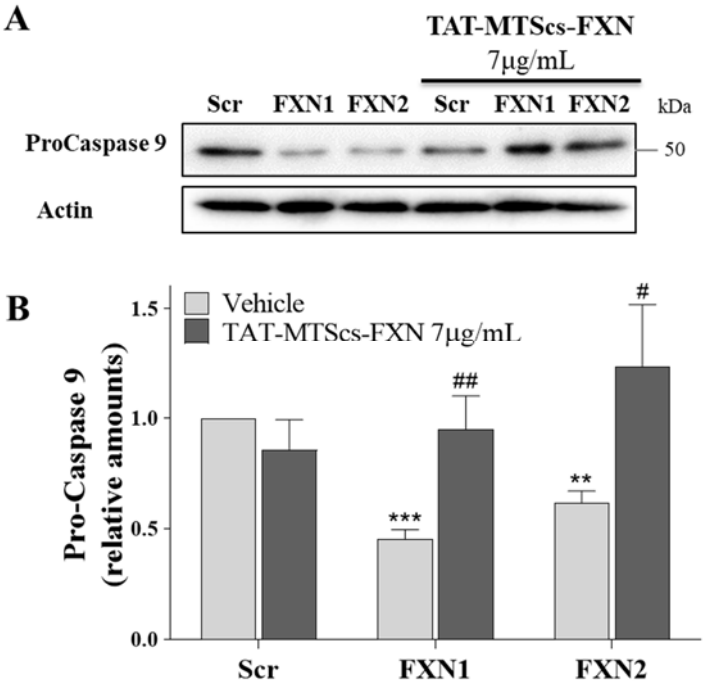

Figure 88. Pro-caspase 9 decreased levels in frataxin deficiency are restored by TAT-MTScs-FXN. In A, representative WB images of pro-caspase 9 antibody in frataxin-deficient DRG neurons treated or not with TAT-MTScs-FXN 7µg/mL at 12h after lentivirus transduction. In B, histograms indicate relative amounts of pro-caspase 9 normalised to β-actin and related to Scr untreated condition as 1. Data are Mean ± SEM, obtained from n=5 independent isolation. Significant values compared to Scr are indicated as (*), while compared to untreated conditions as (#).

3.1.5 TAT-MTScs-FXN decreases fodrin fragmentation

The above results in **Figure 88** suggest that TAT-MTScs-FXN can protect cells from intrinsic apoptotic death, by preventing mPTP opening. If this were the case, TAT-MTScs-FXN should also prevent α-fodrin fragmentation mediated by Ca^{2+}-activated proteases (caspase 3 and calpains), since Ca^{2+} and caspase 3 are extruded by mitochondria in this cell death pathway. To that purpose, different doses of TAT-MTScs-FXN (1-3-7µg/mL) have been used in frataxin-deficient DRG neurons and Scr controls at 48h after lentivirus transduction. As shown in **Figure 89A** for WB images and **B** for histograms, TAT-MTScs-FXN concentrations reduce α-fodrin cleavage in a dose-dependent manner, being 7µg/mL the best option among those analysed. However, when this concentration has been compared to the same concentration at 12h after lentivirus transduction, TAT-MTScs-FXN showed higher protective impact. **Figure 89A** and **B**, respectively for WB images and histograms, indicate the levels of fodrin fragments in frataxin-deficient DRG neurons, adding 7µg/mL of TAT-MTScs-FXN at 12h or 48h after transduction. These results are in agreement with those obtained for

pro-caspase 9 and indicates that TAT-MTScs-FXN can prevent signs of intrinsic apoptotic cell death.

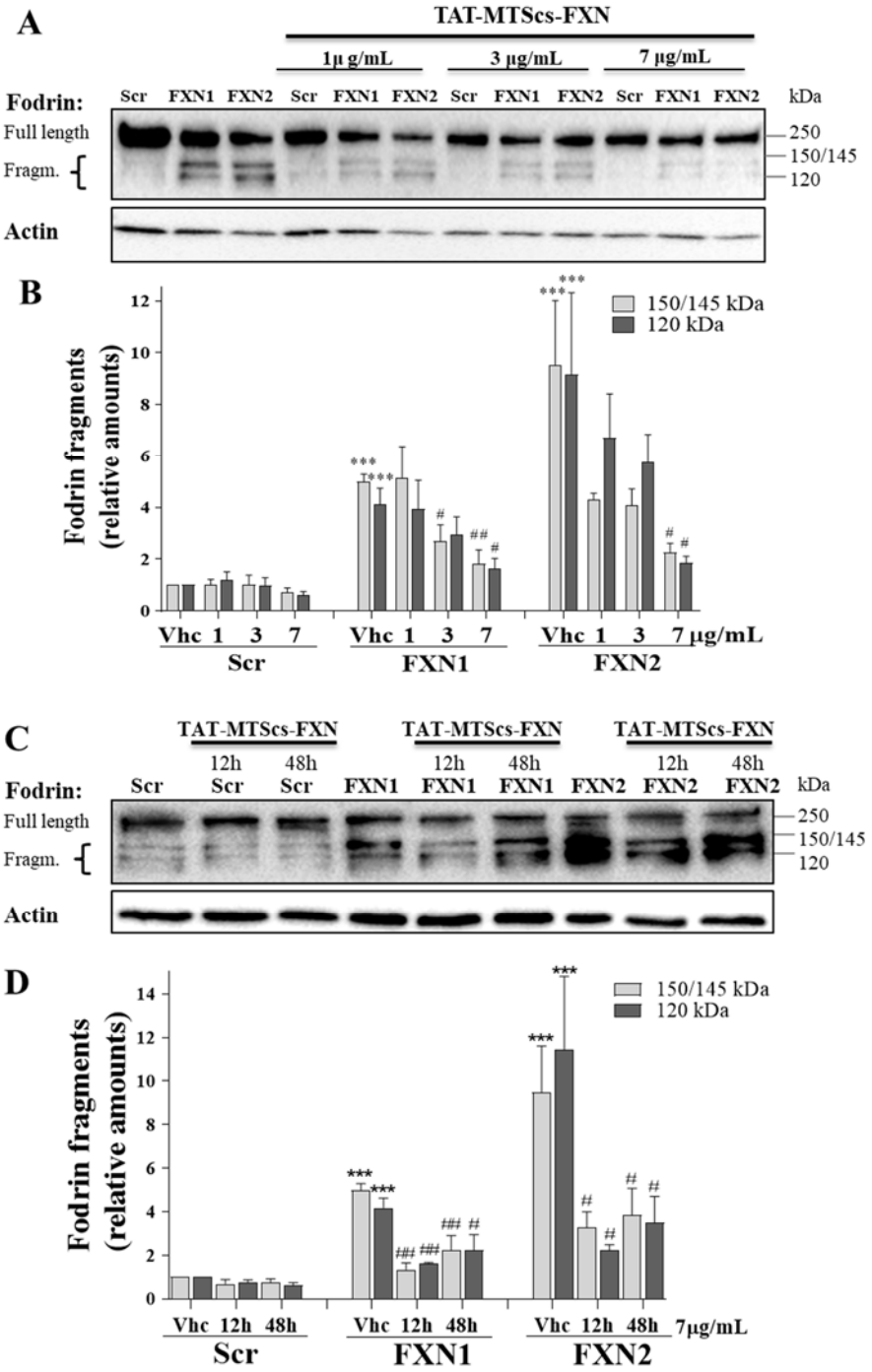

Figure 89. Fodrin cleavage is reduced by TAT-MTScs-FXN treatment. In A, representative images of α-fodrin fragmentation in frataxin-deficient DRG neurons treated or not with 1-3 or 7µg/mL of TAT-MTScs-FXN at 48h after transduction. Histograms in B indicates the relative amounts of fodrin fragments normalised to β-actin as a loading control and related to untreated Scr condition as 1. In C, representative WB images of α-fodrin fragmentation in frataxin deficient cells treated with 7µg/mL of TAT-MTScs-FXN at 12h or 48h after transduction. Histograms in D represent the values of fodrin fragments present in C. Untreated Scr condition is indicated as 1 and (*) indicates significant values *vs* Scr controls, while (#) *vs* the corresponding untreated conditions. Data are Mean ± SEM, obtained from n=5 independent isolations for both graphs (B and D).

3.1.6 TAT-MTScs-FXN protects from neurodegeneration

Frataxin-deficient DRG neurons show apoptotic cell death and neurite degeneration, indicated by the presence of axonal swelling within neurites prevented by TAT-MTScs-FXN. These beneficial effects were tested in terms of protection from neurodegeneration and cell death. **Figure 90A** shows representative images of neurites of cells treated with 7µg/mL of TAT-MTScs-FXN (or not), in which neurites with axonal swelling are signalised (marked) by arrows. The number of neurites presenting axonal swelling *vs* the total number of neurites has been shown as percentage in **B**, indicating as 100% both frataxin-deficient neurons (FXN1 and FXN2). TAT-MTScs-FXN reduces axonal swelling by 50% in FXN1 and 35% in FXN2. The reduction in axonal swelling is dose-dependent, as the concentration increases (1-3 and 7µg/mL of TAT-MTScs-FXN) neurite degeneration is reduced (**C**).

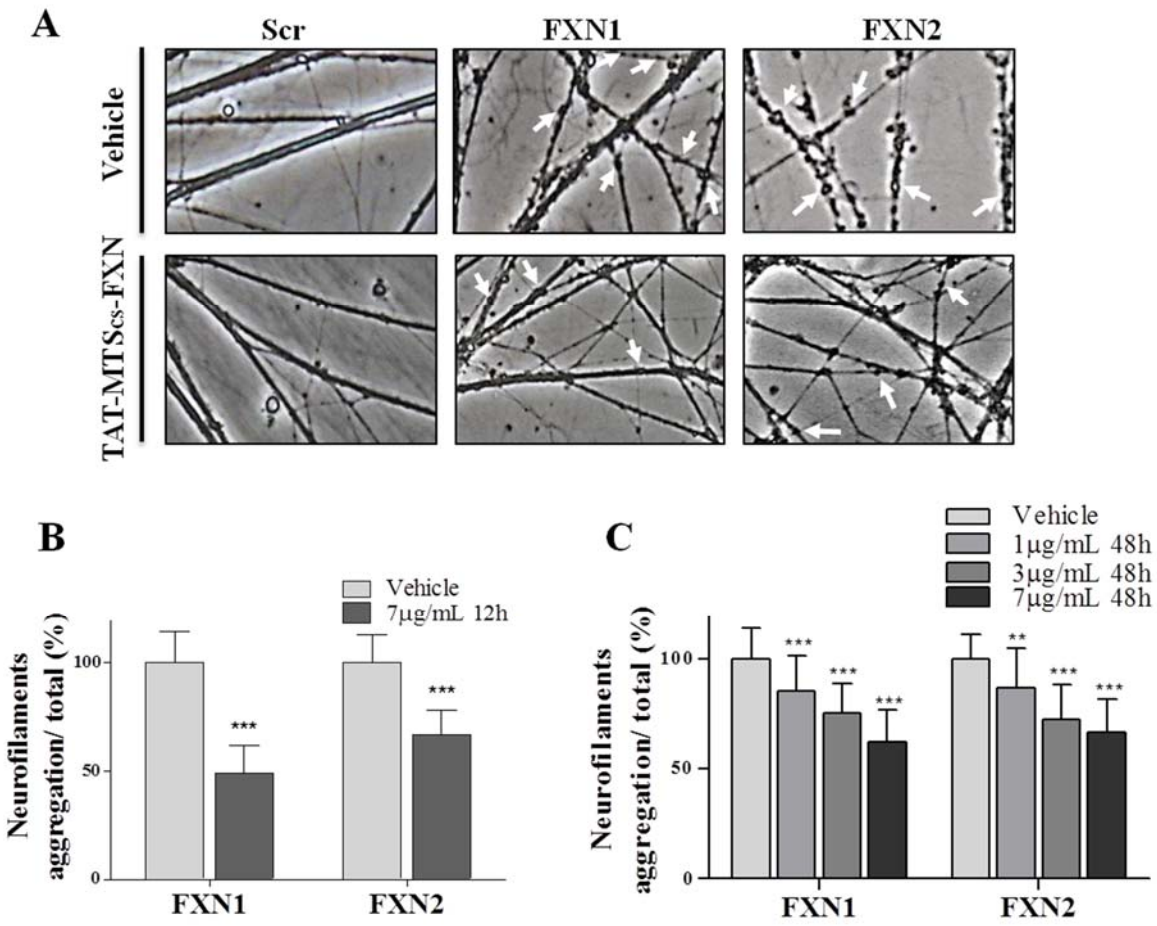

Figure 90. TAT-MTScs-FXN protects from neurite degeneration. In A, representative images of neurites in frataxin deficiency and treated cells, in which TAT-MTScs-FXN 7µg/mL is added to the cells 12h after lentivirus transduction. Arrows indicate neurites with axonal swelling (punctuate pattern onto neurites). In B and C, histograms indicate the percentage of axonal swelling (neurofilaments aggregation) on the total neurites, normalised onto frataxin-deficient

cells as 100%. TAT-MTScs-FXN 7µg/mL at 12h is used in B and 1-3 and 7µg/mL at 48h are used in C. Significant values compared to untreated frataxin-deficient DRG neurons is indicated as (*). Data are Mean ± SD, n= 4 independent isolations for both graphs B and C.

In agreement with the above-mentioned results, TAT-MTScs-FXN was tested for DRG neurons survival. **Figure 91A** indicates representative phase-contrast images of 7µg/mL of TAT-MTScs-FXN, added at 12h, treated neurons at day 0 and day 5 after lentivirus transduction, compared to untreated conditions. The number of cells at 5 days after lentivirus transduction on the initial value is shown as percentage in **B**, indicating an increased survival rate of 16.6% and 14.6%, for FXN1 and FXN2 respectively. As shown for neurite degeneration, **Figure 91C** indicates that TAT-MTScs-FXN, added at 48h after transduction, increases survival rate in a doses-dependent manner. In fact, 1µg/mL has no effect in cell survival; 3µg/mL increase cell survival by 9.2% and 6.8% and 7µg/mL by 14.9% and 11.4%, respectively for FXN1 and FXN2. Although the latter condition is able to protect neurons, the survival rate is lower than the values achieved using 7µg/mL at 12h, indicating that the addition of the construct in the early stages of frataxin deficiency leads to better protection. Taken together these results indicate that frataxin-deficient DRG neurons can have a slight protection from neurite degeneration and apoptotic cell death by frataxin replacement.

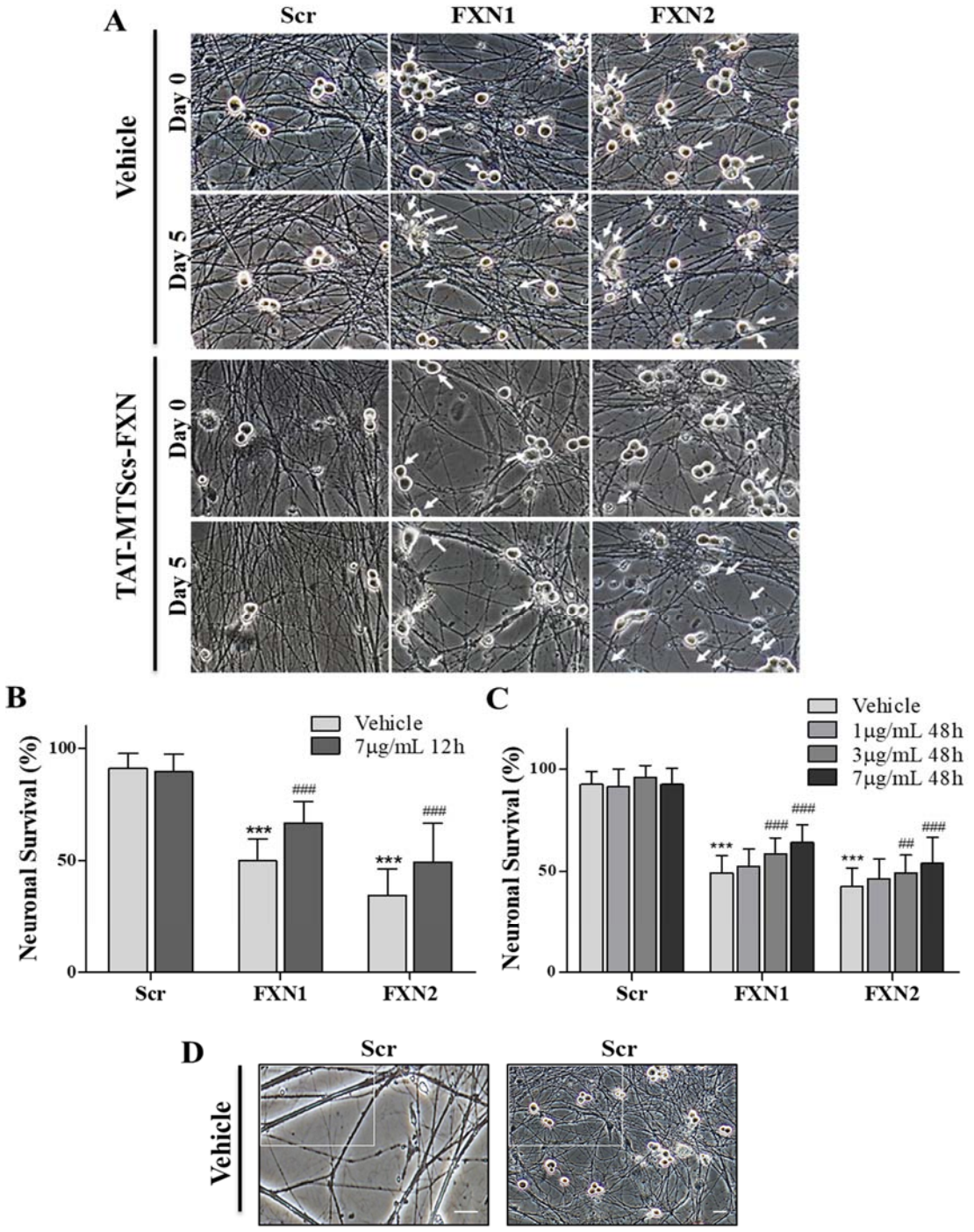

Figure 91. TAT-MTScs-FXN protects frataxin deficient DRG neurons from cell death. In A, phase-contrast images of cells in the same field at day 0 and 5 after lentivirus treated (or not) with TAT-MTScs-FXN 7µg/mL at 12h. Arrows indicate the cell bodies present at day 0 and absent at day 5. Histograms in B indicate the number of cells remaining at day 5 compared to the initial value in %. Data are Mean ± SD, n=4, counting a range of 956-1184 neurons for Scr and a range of 1397-1733 cells for each FXN1 and FXN2 conditions. In C, TAT-MTScs-FXN 1-3 and 7µg/mL at 48h have been used in frataxin deficiency to analyse survival. Data are Mean ± SD, n=4, counting a range of 436-1233 neurons for Scr and 867-1832 neurons for each FXN1 and FXN2 conditions. Significant values compared to Scr conditions are indicates as (*), while compared to untreated conditions as (#). In D is indicated the zoom-in for the representative images of Scr untreated condition, corresponding to 1/4th of full-size field, which is used in Fig. 90A and Fig. 91A, respectively for neurite degeneration and survival analysis. Scale bar= 30µm for both images, obtained with objective 32x (neurite) and 16x (survival).

4 COMPOUNDS INCREASING FXN LEVELS AND IMPROVING MITOCHONDRIAL FUNCTION

4.1 Calcitriol increase FXN levels and restores altered markers

4.1.1 Calcitriol restores enzymes levels involved in its own metabolism

As above indicated in **Figure 81**, frataxin-deficient DRG neurons display low levels of FDX1, a mitochondrial iron-sulfur cluster enzyme important in many cytochrome reactions. Upon analysing Cyp27b1 and Cyp24a1 levels, respectively calcitriol biosynthesis and degradation cytochromes that utilize FDX1 for their reactions, it was clear an alteration in calcitriol metabolism in frataxin deficiency, as indicated in **Figure 92**. Therefore, it was interesting known if supplementing calcitriol could be beneficial for frataxin-deficient DRG neurons. Thus, calcitriol, at the concentration of 20nM, was used as treatment for frataxin-deficient DRG neurons from 2-days after lentivirus transduction until the end of the experiment (daily added in fresh media). As indicated in **Figure 92C** and **D**, Cyp27b1 levels, which are induced of 2-fold and 2.5-fold in frataxin-deficiency, respectively for FXN1 and FXN2, return to the levels of Scr control upon the addition of 20nM calcitriol. Recovery of ferredoxin (**A** and **B**) levels and Cyp24a1 (**E** and **F**) has been also observed with calcitriol. **Figure 92G** and **H** indicate no variation for a mitochondrial protein LONP1. Then, it is clear that the treatment recovers both cytochromes, but also ferredoxin levels, without changing the values of LONP1, used as a mitochondrial protein control not related to the other enzymes.

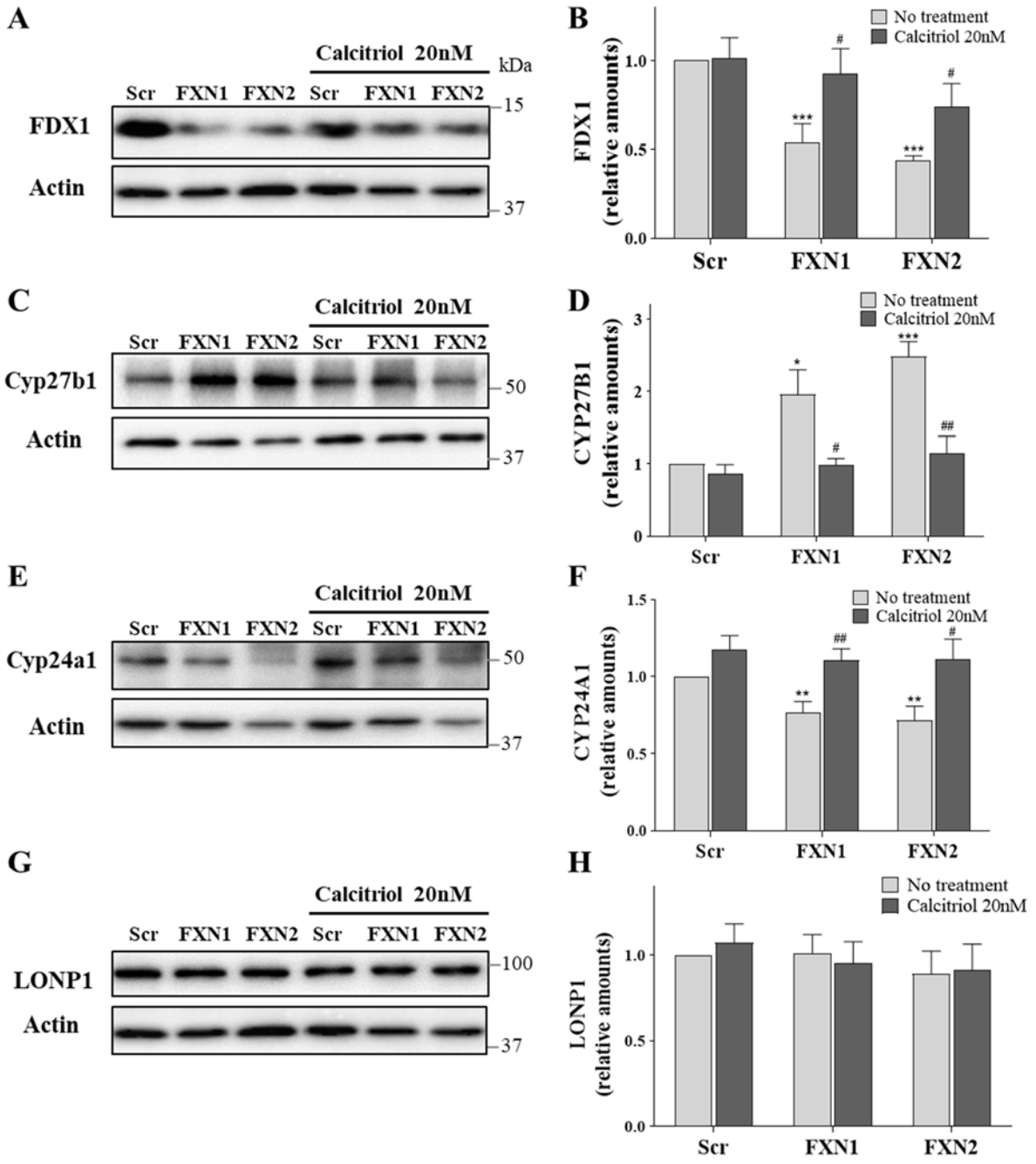

Figure 92. Calcitriol supplement reverts the alterations of its metabolism shown in frataxin deficiency. In A, representative images of FDX1 in total lysates of frataxin-deficient DRG neurons, at 5 days after lentivirus transduction, treated and not treated with calcitriol 20nM. Quantification in B. Data are Mean ± SEM of n= 6 independent experiments. In B, WB images of Cyp27b1 at the same conditions and quantification in D. Data are Mean ± SEM of n=8. In E, WB images of Cyp24a1 at the same conditions and quantification in F. Data are Mean ± SEM of n= 9. In G, WB images of LONP1 at the same conditions and quantification in H. Data are Mean ± SEM of n= 14. No treated Scr conditions are indicated as 1 and (*) indicates significant values compared to Scr, while (#) indicates significant values compared to no treated conditions.

4.1.2 Calcitriol increases frataxin levels

As ferredoxin has been described as an interacting protein of frataxin and the above results indicate restorations of this protein using calcitriol, it was interesting analyse the amounts of frataxin levels upon addition of calcitriol. **Figure 93A** indicates a small increase in frataxin amounts, in frataxin-deficient DRG neurons, upon calcitriol supplementation. As it is well documented that calcitriol supplementation induces an increase in vitamin D receptor (VDR), VDR levels were also used as a control of calcitriol supplementation. Note the clear increase in VDR amounts in frataxin-deficient treated cells. Histograms in **B** indicate that calcitriol 20nM determines a 1.7-fold (for FXN1) and 1.8-fold (for FXN2) increase of frataxin mature amounts in frataxin-deficient DRG neurons. Thus, the recovery effects of calcitriol onto FDX1, Cyp27b1 and Cyp24a1 protein levels, could be ascribed to the increased amounts of frataxin in our FA cell model.

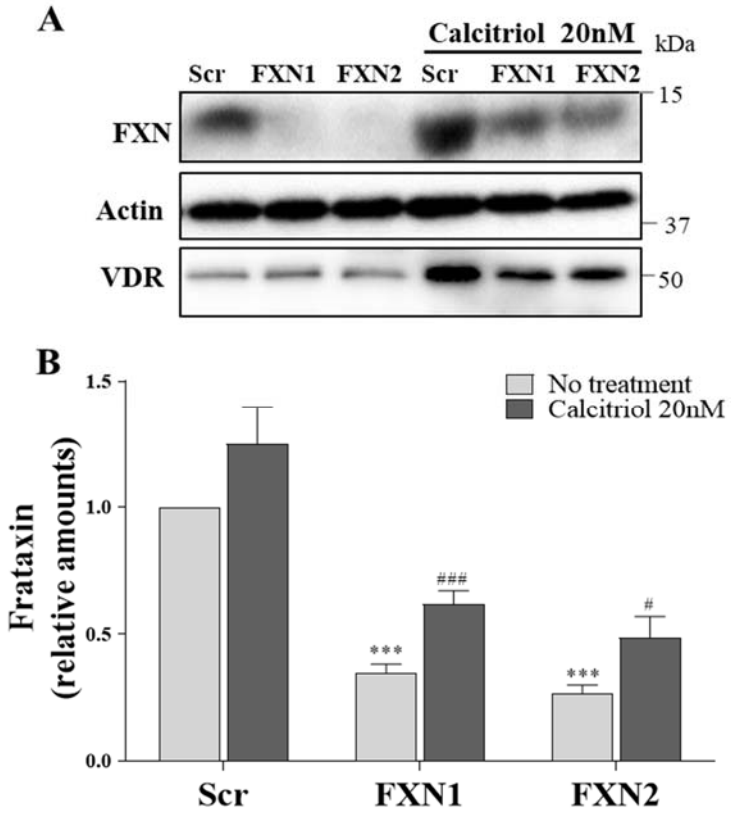

Figure 93. Calcitriol induces an increase in mature frataxin protein levels. In A, representative images of frataxin protein levels in total lysates of frataxin-deficient DRG neurons treated or not with calcitriol. VDR levels have been also analysed as a control of calcitriol supplementation, as calcitriol treatment determines a rise of VDR protein levels. In B, histograms of frataxin protein levels. Data are Mean ± SEM of n=12 independent isolations. No treated Scr condition is indicated as 1 and (*) or (#) indicate, respectively, significant values compared to Scr controls or no treated conditions.

4.1.3 Calcitriol restores Ca^{2+} homeostasis

The increase of frataxin levels upon calcitriol treatment gives us the basis to analyse the effect of calcitriol on already known markers of frataxin deficiency, for example Ca^{2+} homeostasis. $Ca^{2+}{}_m$ homeostasis is regulated by the action of mechanisms of Ca^{2+} influx and Ca^{2+} efflux (detailed in the introduction). NCLX mediates $Ca^{2+}{}_m$ efflux into cytosol; however, decreased levels of NCLX have been seen in our model, suggesting impairment of this mechanism (**Figure 62**). Calcitriol 20nM, by inducing an increase in frataxin amounts (**Figure 93**), avoids decrease NCLX protein levels, as shown in **Figure 94A** and **B**. Histograms indicate a 1.7-fold (for FXN1) and 2-fold (for FXN2) increase in frataxin-deficient DRG neurons upon calcitriol addition. However, MCU remains stable (**C** and histograms in **D**). As NCLX is important in Ca^{2+} homeostasis and its impairment determines Ca^{2+} accumulation in mitochondria, the levels of Rhod5N probe were analysed in our model in the presence of calcitriol. Representative images of the fluorescent Ca^{2+} indicator Rhod5N were shown in **E**. Note the difference in fluorescent intensity between the upper row (not-treated cells) and lower row (treated cells). Histograms representing such intensities are shown in **F** and **G**, in which, respectively, Rhod5N fluorescent intensity has been analysed in cell soma and neurites. Differences between cell soma and neurites Rhod5N fluorescence are explained in Materials and Methods. Then, cell soma fluorescent intensity, representing $Ca^{2+}{}_i$, is reduced by 19% (for FXN1) and 24% (for FXN2), while neurites fluorescence, representing prevalently $Ca^{2+}{}_m$, is reduced by 16% (for FXN1) and 23% (for FXN2) upon calcitriol treatment. These results indicate that calcitriol ameliorates Ca^{2+} homeostasis, probably through NCLX increase, by increasing frataxin protein levels.

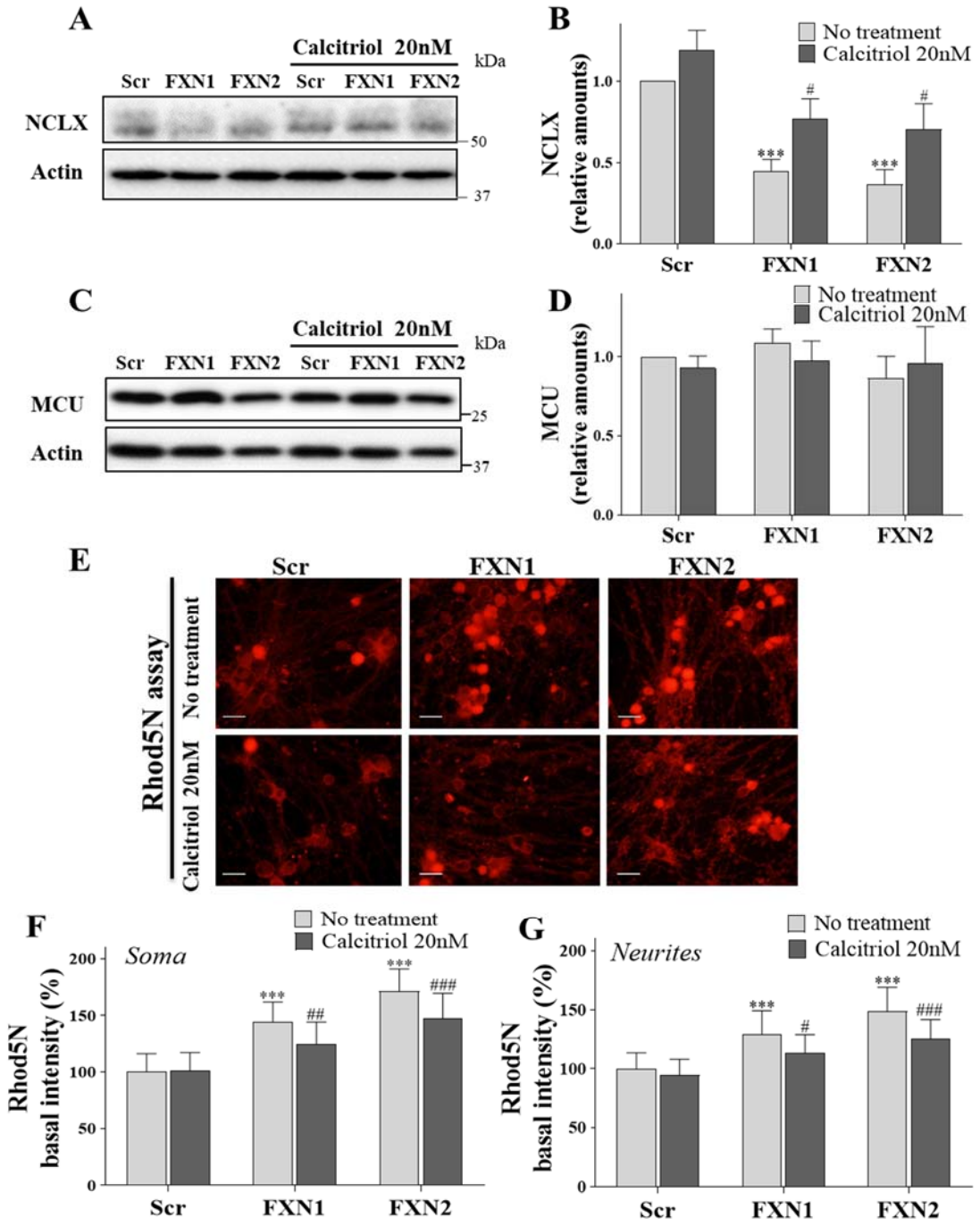

Figure 94. Calcitriol induces NCLX and Ca^{2+}_m recovery in frataxin deficiency. In A, WB images of NCLX in frataxin-deficient DRG neurons treated or not with calcitriol 20nM. Quantification in B. Data are Mean ± SEM of n= 10 independent isolations. In C, WB images of MCU and quantification in D. Data are Mean ± SEM of n= 12 independent isolations. In E, neuronal cells are stained with Rhod5N (see Materials and Methods) in order to analyse Ca^{2+}_m levels in treated and not-treated cells. Rhod5N has been analysed in cell soma and neurites, as indicated in F and G, respectively. Data are Mean ±SEM obtained from n= 3 independent isolation and a range of 216-225 soma and 205-251 segments (100 pixels) of neurite for Scr condition; a range of 178-331 soma and 233-245 segments of neurite for FXN1 condition and a range of 153-240 soma and 354-374 segments of neurite for FXN2 condition. Scale bar= 30µm. Significant values compared to control conditions (no treatment) are indicated (*) while (#) indicates significant values of calcitriol effects compared to the corresponding culture under non-treated conditions.

However, it is hard partitioning Rhod5N signal between cytosol and mitochondria, and a cytosolic signal could be still present. Thus, these data give us an indication of Ca^{2+} alterations in frataxin-deficient DRG neurons that can be improved by calcitriol, but Ca^{2+} dynamics upon a stimulus are more efficient methods to understand both arms of the Ca^{2+}_m pathway: Ca^{2+} uptake and release. To be confident that Ca^{2+}_m was analysed, permeabilised cells using 60µM digitonin were probed with Fluo8 for Ca^{2+}_i and Rhod5N for Ca^{2+}_m; subjected to a stimulus of physiologic Ca^{2+} (5µM $[Ca^{2+}]_{free}$) and the dynamic changes of Ca^{2+} were analysed in control and frataxin-deficient mitochondria as indicated in Materials and Methods. Dynamic changes upon the stimulus are represented in **Figure 95A**, in which it is possible to note that the recovering upon Ca^{2+} stimulus is lower in frataxin-deficient DRG neurons than in control. Details of this graph are represented in B, C and D, respectively for Scr, FXN1 and FXN2 compared to the respective treated conditions. These results show that although no significant variations were observed in the Ca^{2+}_m influx rate (**E**), the peak amplitude is significantly higher in FXN1 and FXN2 cells (**F**), the Ca^{2+}_m efflux decay rate (**G**) and half-life (**H**) are also significantly longer, indicating a slow efflux. Calcitriol supplementation improves the parameters of peak amplitude, efflux decay rate and half-life close to those found in control cultures. All these data are in agreement with the decreased levels of NCLX in frataxin deficiency and the partially recovering of NCLX levels using calcitriol 20nM. However, these data indicate that, although MCU levels are stable, changes in the peak amplitude could be ascribed to alterations in Ca^{2+}_m uptake, but could also be a consequence of decreased efflux.

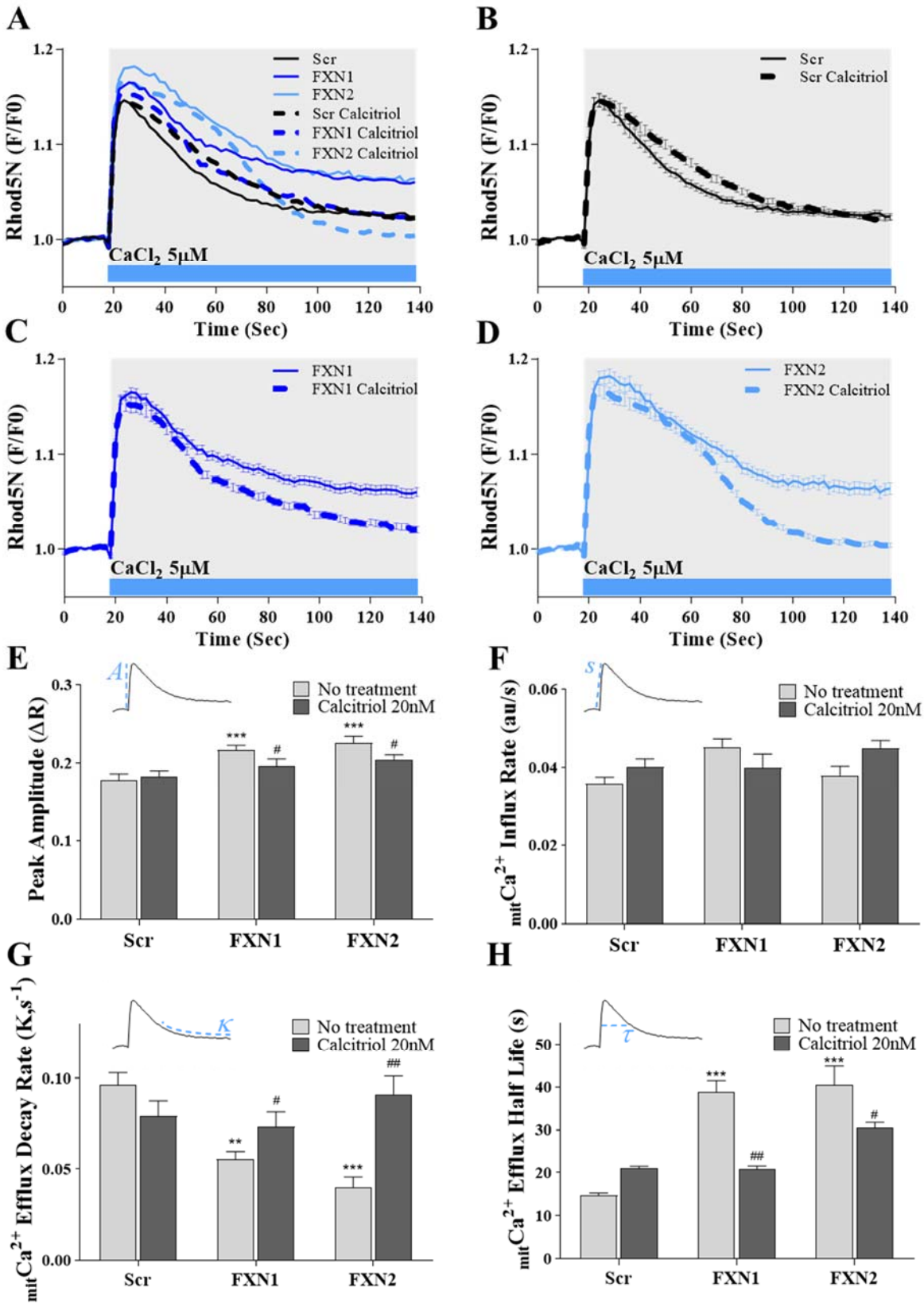

Figure 95. $Ca^{2+}{}_m$ efflux is improved by calcitriol. Digitonin-permeabilised DRG neurons are stimulated using 5µM of $CaCl_2$ ($[Ca^{2+}]_{free}$) in order to analyse the Ca^{2+} peak as described in Materials and Methods. Normalised mean traces of $Ca^{2+}{}_m$ changes (indicated by Rhod5N fluorescence) in permeabilised cells are shown in A, obtained from a range of 357-386 peaks for Scr; a range of 348-578 peaks for FXN1 and 234-391 peaks for FXN2 conditions. Peaks in B, C

and D are details of graph in A in order to note better the difference between treated and not treated cells. Data are Mean ±SEM. Graphs in E, F, G and H indicate the characteristics of the peaks present in A. Histograms in E indicates the peak amplitude. Histograms in F indicate the Ca^{2+}_m influx rate (or slope of the peak), while in G and H indicate the Ca^{2+}_m efflux decay rate and the peak half-life, respectively. The parameters analysed for each peak are indicated in blue dashed lines: A – amplitude; s – slope; τ – tau or half-life; κ – k-decay; Significant values compared to control conditions (no treatment) are indicated (*), while (#) indicates significant values of calcitriol effects compared to the corresponding culture under non-treated conditions. Data are the mean ± SEM obtained from 5 independent experiments.

The results shown above indicate alteration in Ca^{2+} homeostasis that can be restored by calcitriol. The alteration of the Ca^{2+}-binding protein calretinin in frataxin deficiency has been shown elsewhere in the text. The expression of this protein is regulated by calcitriol, as the promoter of calretinin gene presents VDRE elements. For this reason, calretinin protein amounts have been analysed in the presence of calcitriol 20nM. As indicated in **Figure 96A** and quantification in **B**, the amounts of this protein return to control levels when frataxin-deficient DRG neurons are treated with calcitriol.

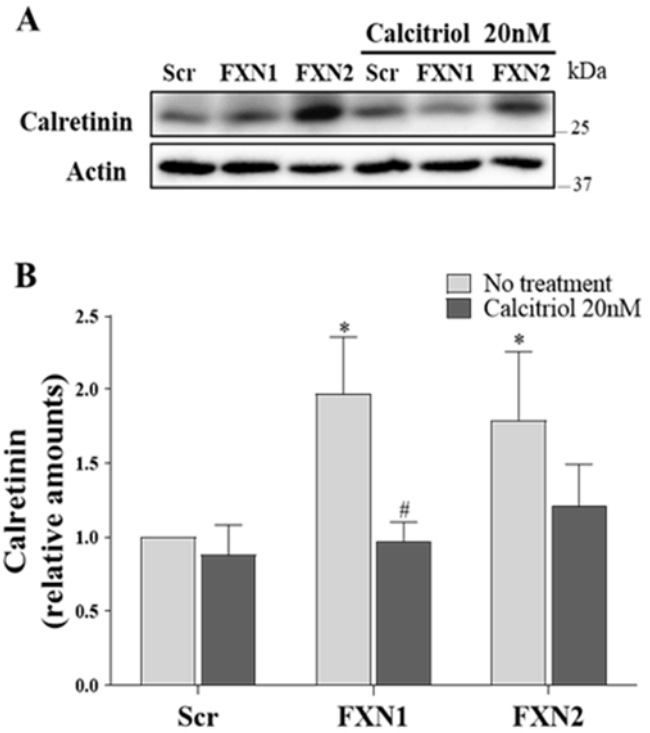

Figure 96. Calretinin protein levels decrease with calcitriol treatment. WB images of calretinin protein in frataxin-deficient DRG neurons treated or not with calcitriol 20nM. Histograms in B indicate the amounts relative to Scr control. Data are Mean ± SEM from n=6 independent experiments.

4.1.4 Calcitriol restores basal $\Delta\Psi_m$ and maintains it in response to inhibitors

As indicated above (**Figure 59**) and previously published in our model, frataxin-deficient DRG neurons display $\Delta\Psi_m$ (Mincheva-Tasheva et al., 2014). This altered marker was used (described in Materials and Methods) to test calcitriol treatment on this parameter. **Figure 97A** indicates a JC-1 yellow/green fluorescent color for frataxin-deficient DRG neurons, indicating depolarisation, which can be maintained at the levels of Scr control by calcitriol treatment. Histograms in **B**, indicate the percentage of fluorescent green/red intensity ratio for frataxin-deficient DRG neurons and controls, compared to treated conditions. In fact, the green/red intensity ratio increases by 29% (for FXN1) and 30% (for FXN2) in frataxin deficiency at 5 days after lentivirus transduction and is reduced by 15% and 24% upon treatment with calcitriol. Thus, these results indicate that calcitriol can maintain the $\Delta\Psi_m$ approximately at the levels of Scr controls. As a complement, cells were also probed with TMRM dye in order to confirm our results with JC1 assay. TMRM (25nM) was used in "re-distribution and non-quench mode" in order to analyse basal $\Delta\Psi_m$, as described in Materials and Methods, considering a decrease in fluorescence intensity as mitochondrial depolarisation. In **C** is shown the basal fluorescence intensity of TMRM in cells treated or not with calcitriol, in which it is possible to note lower intensity levels in FXN1 and FXN2 conditions (upper row) respect to Scr control (lower row). The fluorescence intensity was measured separately in soma (**D**) and neurites (**E**), showing that mitochondria in neurites are more depolarised than in soma. However, the phenotype is recovered by calcitriol in both compartments. The addition of inhibitors of different complexes allows understanding if $\Delta\Psi_m$ can be maintained or not. Thus, oligomycin, rotenone and FCCP were added in this order, as mentioned in Materials and Methods, and changes in TMRM fluorescence intensity upon drug addition were analysed separately in soma and neurites. As observed in both in **F** (soma) and **G** (neurites), frataxin-deficient DRG neurons reduced TMRM fluorescence in response to oligomycin. The depolarisation indicates that, prior to the drug addition; $\Delta\Psi_m$ was maintained by the F_1F_0 ATP synthase working in "reverse" mode, consuming ATP. While, in the presence of calcitriol, the hyperpolarisation upon oligomycin addition indicates that ATP synthase was working in "forward" mode, generating ATP. **Figure 98** indicates details of graphs **F** and **G**, considering error bars and statistical analysis.

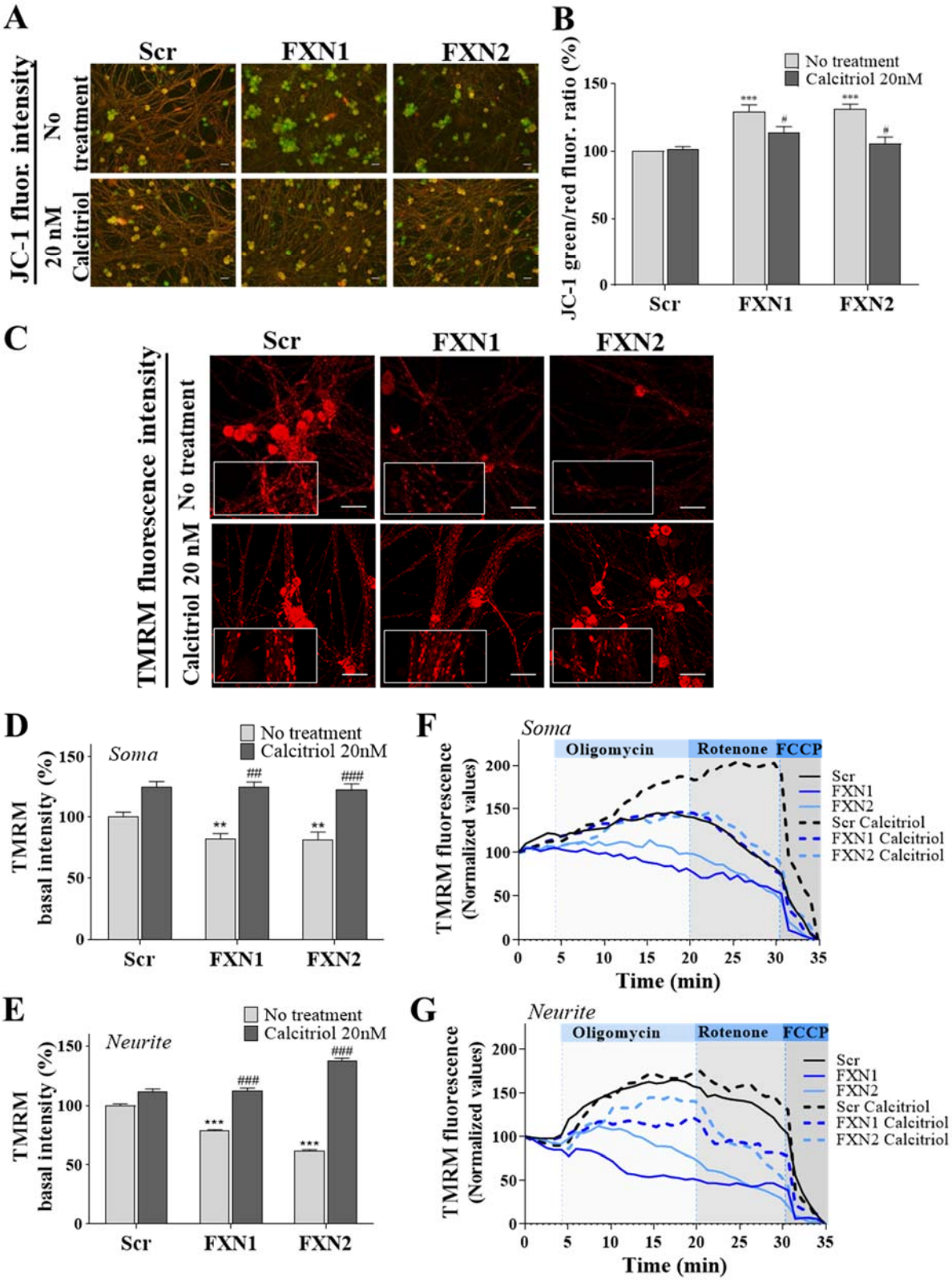

Figure 97. Calcitriol treatment restores $\Delta\Psi_m$ and allows complex V working in forward mode. In A, representative images of frataxin-deficient DRG neurons stained with JC-1 to analyse the $\Delta\Psi_m$. Scale bar= 30µm. Quantification in B. Histograms represent JC-1 fluorescence ratio (green/red), normalised to Scr condition (indicated as 100%) and expressed as percentage. Data are Mean ± SEM of n=6 independent experiments. A range of 56-65 fields has been analysed for Scr, a range of 65-68 fields for FXN1 and a range of 58-67 fields for FXN2. Controls and

frataxin-deficient DRG neurons treated or not with calcitriol were also probed with TMRM 25nM. A representative confocal image in Z-stack mode is shown in C. Scale bar= 30µm. Quantification, normalised to Scr condition and expressed as percentage, is shown in D for soma and E for neurites. Data are the mean ± SEM. A range of 48-94 soma and 1912-2913 neurites were analysed for Scr; a range of 62-72 soma and 2471-2831 neurites for FXN1 and a range of 41-91 soma and 1994-2958 neurites for FXN2. Results are obtained from n= 3-5 independent experiments. In F and G, representative mean traces of TMRM fluorescence intensity in response to drugs addition (Oligomycin 2µg/mL for 15 min; Rotenone 2µM for 10min; FCCP 10µM for 5 min) in Scr controls and frataxin-deficient DRG neurons treated or not with 20nM calcitriol are shown in soma (F) and neurites (G). Data are obtained from n= 3-5 independent experiments and normalised by indicating as 100 the first value of TMRM baseline and as 0 the values 5 minutes after FCCP addition. A range of 126-157 soma and 1101-4044 neurites were analysed for Scr conditions; a range of 148-166 soma and 2437-2642 neurites for FXN1 and a range of 103-124 soma and 294-1156 neurites for FXN2 conditions. Significant values compared to Scr control condition (no treatment) are indicated as (*), while (#) indicates the effect of treatment compared to no treatment condition. **Data have been analysed with the help of A. Sanz-Alcazár.**

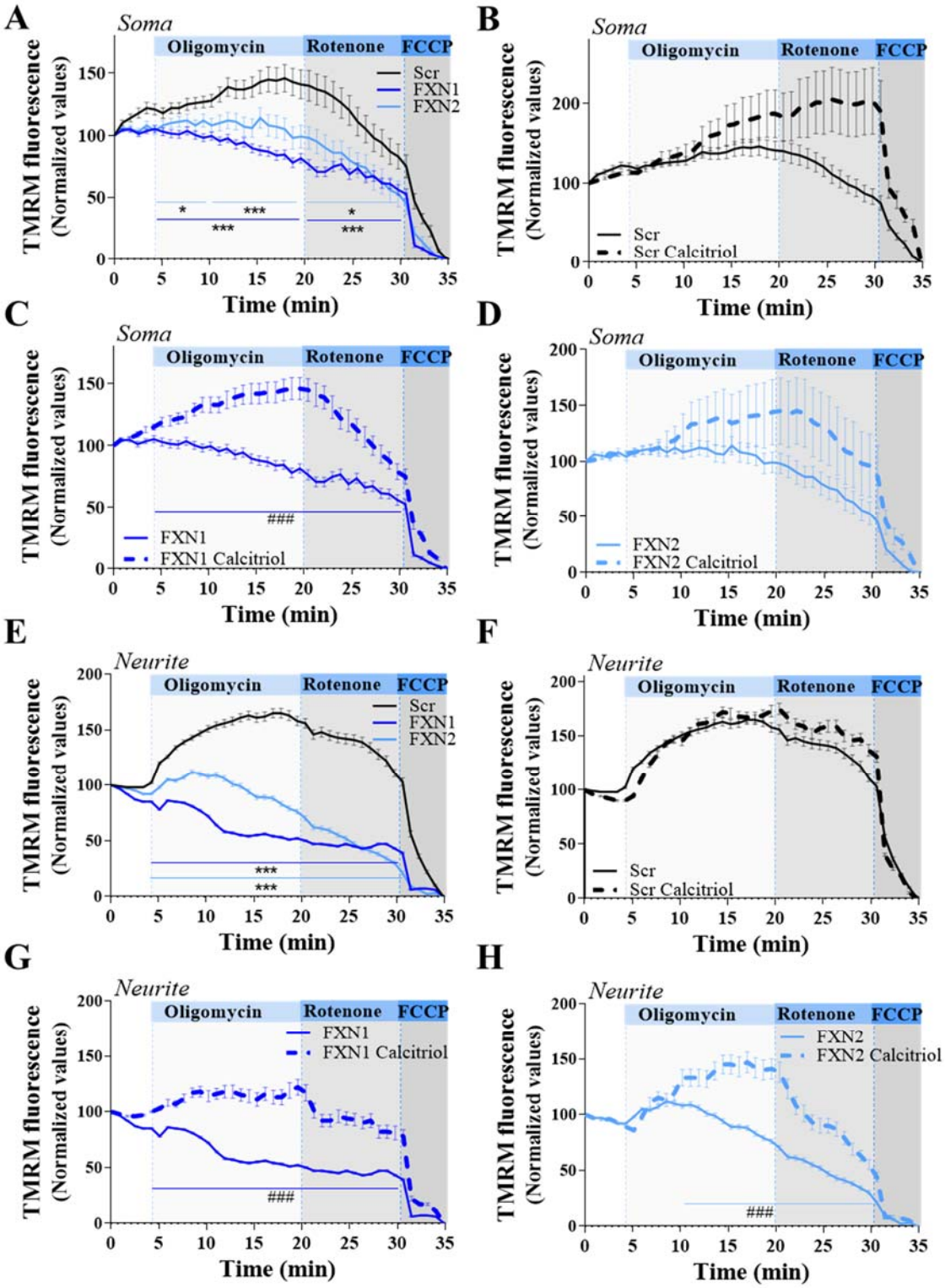

Figure 98. Detailed graphs of above figure with statistical analysis. Representative time-course curves of TMRM fluorescence intensity in response to drug addition in Scr controls and frataxin-deficient DRG neurons in soma (A-D) and neurites (E-H), considering differences between Scr, FXN1 and FXN2 in A and E, differences between treated and not treated condition in B and F for Scr, C and G for FXN1 and D and H for FXN2. Data are Mean ± SEM obtained from n=3-5 independent isolations. Scrambled condition is indicated as 100% in both graphs. Significant values compared to control conditions are indicated by asterisk (*) and (#) indicates treatment condition compared to untreated. **Data have been analysed with the help of A. Sanz-Alcazár.**

4.1.5 Calcitriol decreases fodrin fragmentation

As published (Mincheva-Tasheva et al., 2014), frataxin-deficient DRG neurons show α-fodrin cleavage, a marker of apoptotic cell death. **Figure 75** indicates the time-course of this Ca^{2+}-dependent process during frataxin depletion. The effect of calcitriol is shown in **Figure 99A**, in which fodrin fragments are clearly increased 2.5-fold and 3-fold respectively for FXN1 and FXN2; in contrast, 20nM calcitriol reduces the fodrin fragmentation. Quantification of fodrin (full-length and fragments) is shown in **B**.

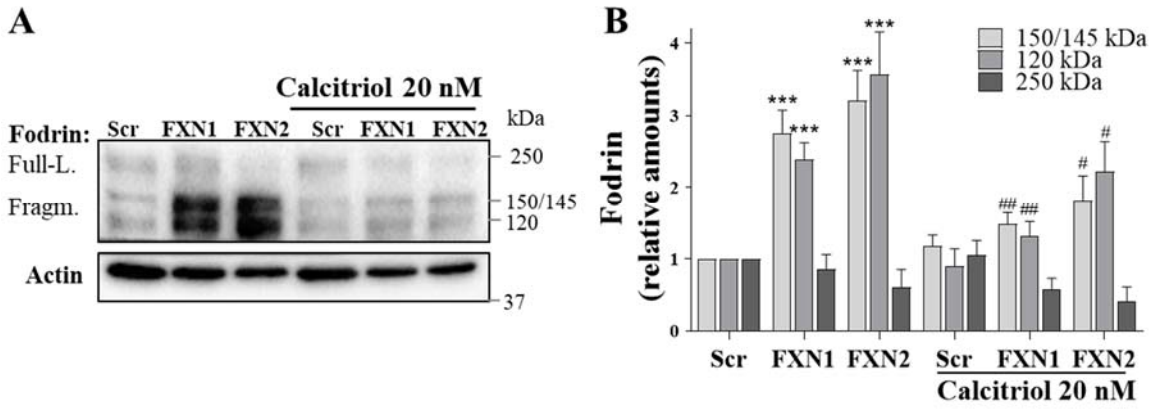

Figure 99. Calcitriol protects fodrin from fragmentation. In A, representative images of α-fodrin in total lysates of frataxin-deficient DRG neurons treated or not with calcitriol 20nM. Note the full-length of fodrin at 250kDa and fragments at 150/145 kDa and 120kDa. In B, quantification of fodrin full-length and fragments. Note the decrease in fragmentation up calcitriol addition. Data are Mean ± SEM of n= 14 independent isolations. No treated Scr from full-length and fragments is indicated as 1 and (*) indicates the significant values compared to Scr controls, while (#) compared to non-treated conditions.

4.1.6 Calcitriol reduces neurodegeneration

As published (Mincheva-Tasheva et al., 2014), frataxin-deficient DRG neurons show aggregation of neurofilaments that leads to neurite degeneration at 5 days after lentivirus transduction. **Figure 77** indicates the time-course of this process during frataxin depletion. **Figure 100A** and **B** indicate a clear reduction in neurite degeneration upon calcitriol supplementation by 54% (FXN1) and 42% (FXN2). Accordingly, cell survival analysis has been assessed in the same condition and, as indicated in **C**, calcitriol significantly increased survival of frataxin-deficient DRG neurons by 31% for FXN1 and 32% for FXN2. These results indicate that calcitriol induces neuroprotective effects in frataxin-deficient DRG neurons and suggest that could be useful as an easy supplementation in patients.

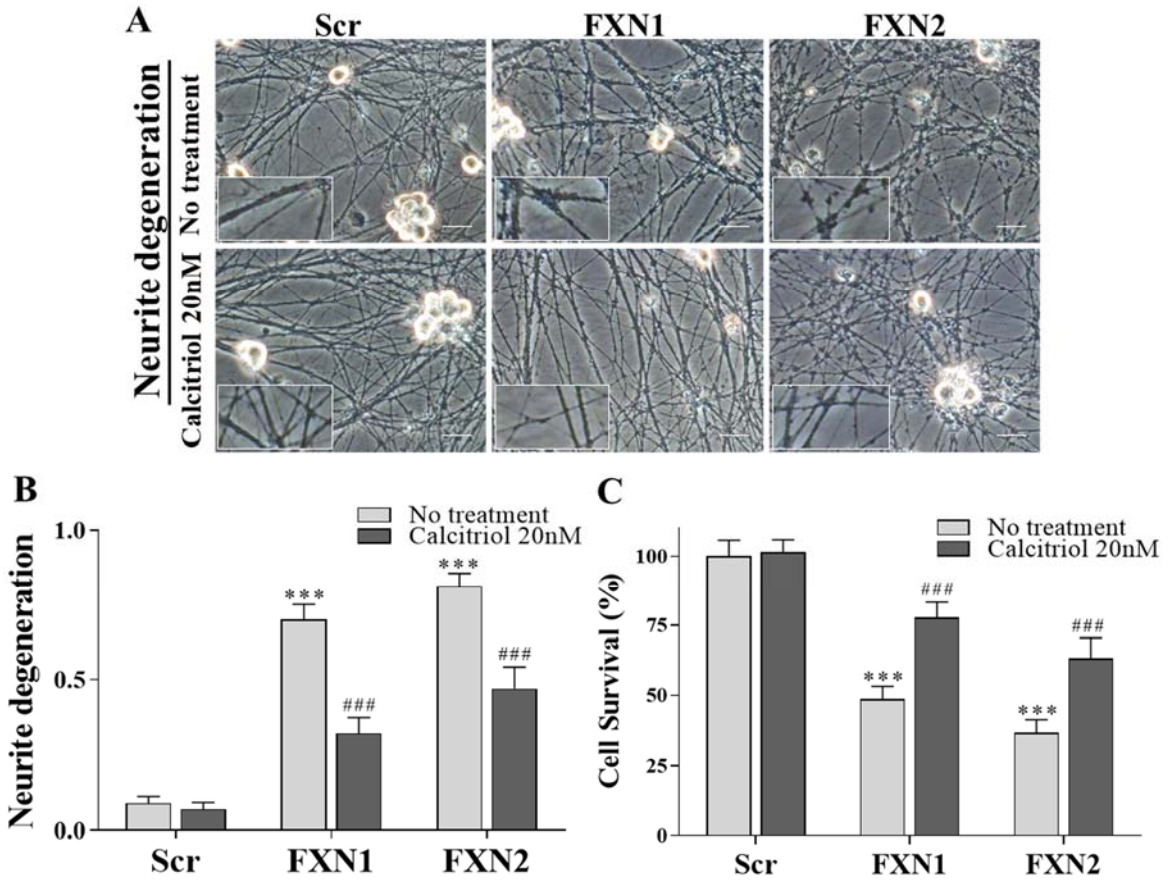

Figure 100. Calcitriol reduces neurite degeneration and improves cell survival. In A, representative images showing aggregation in neurites in frataxin-deficient DRG neurons (upper row) and with calcitriol addition (lower row). Scale bar= 30µm. In B, neurite degeneration is indicated as the number of neurites with axonal swelling *vs* the total number. Data are Mean ± SEM obtained from n=5 and a range of 2657-2692 neurites for Scr; a range of 2625-2842 neurites for FXN1 and a range of 1415-1615 neurites for FXN2 conditions. In C, cell survival analysis as described in Materials and Methods. Significant values compared to Scr control are indicated as (*), while (#) indicates significant values compared to non-treated conditions. Data are Mean ± SEM obtained from n=9 and a range of 961-1535 neurons for Scr; a range of 1691-2215 neurons for FXN1 and a range of 1189-1582 neurons for FXN2 conditions. Three independent individuals have performed survival analysis.

4.2 Calcitriol synthesis alterations in FXN deficiency

4.2.1 Calcidiol has no effect on FDX1 and CYP27B1 levels

The precursor form of calcitriol is calcidiol, which is converted in mitochondria into calcitriol through Cyp27b1 enzyme, using two electrons provided by ferredoxin, as explained in the introduction. Since it is known that calcitriol can be also produced in neurons, the use of its precursor (calcidiol) in FXN-deficient DRGs, if fully converted in calcitriol by Cyp27b1, should determine an equivalent effect at the same working concentration. Bearing this in mind, calcidiol 20nM has been added to FXN-deficient

DRG neurons in order to assess Cyp27b1 functionality. **Figure 101A** and **B** indicate no changes in FDX1 levels when neurons are treated with Calcidiol 20nM, accordingly, the same happens for Cyp27b1 levels in **C** and **D**, without changes in the amount of mitochondria (**E** and **F**). These results indicate a decreased Cyp27b1 enzymatic activity in frataxin deficiency, which could be ascribed to alterations of the heme group, used as a cofactor for its correct function.

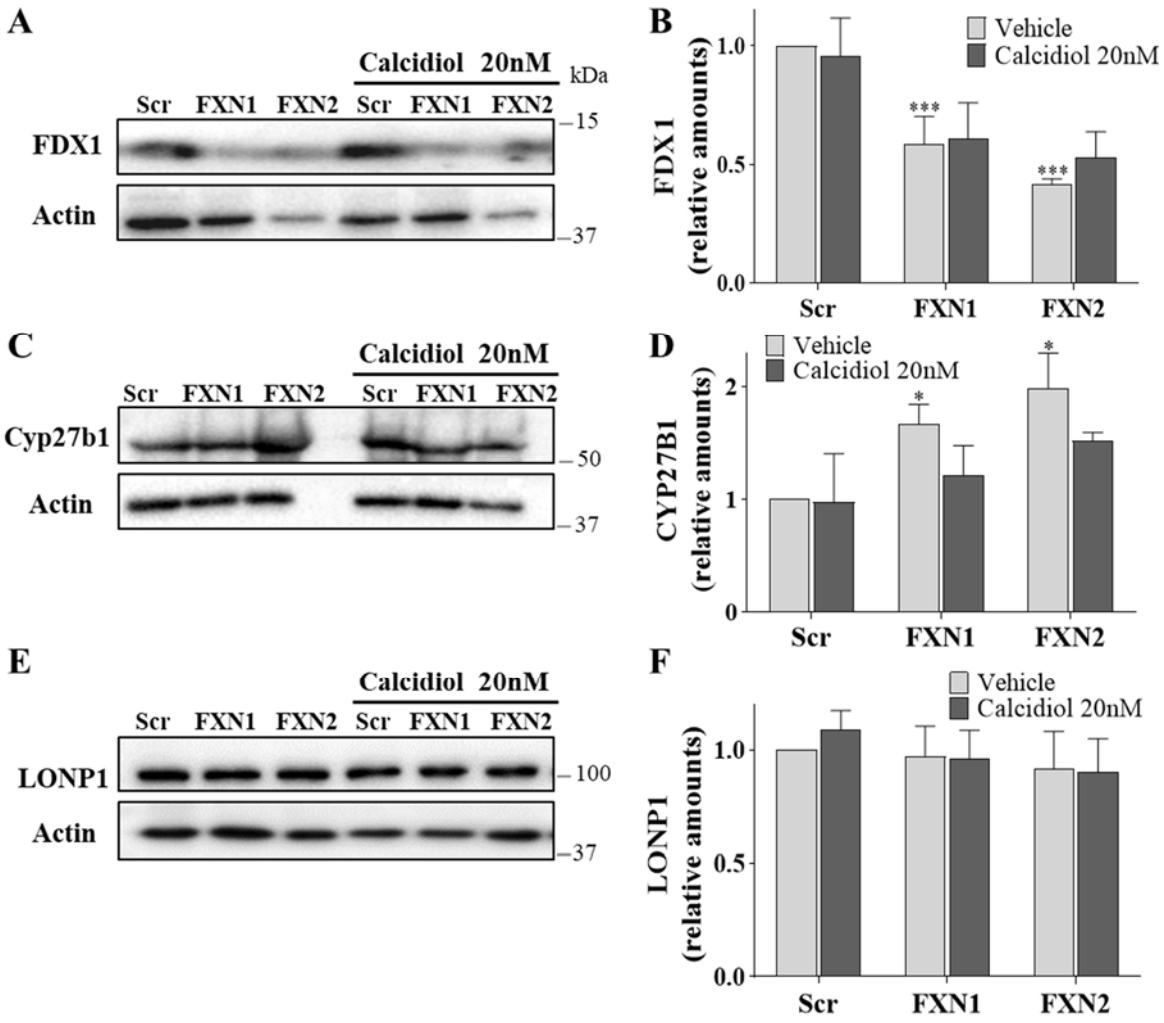

Figure 101. Calcidiol does not recover Cyp27b1 and FDX1 levels, indicating that could be not fully converted in calcitriol. In A, representative images of FDX1 in total lysates of frataxin-deficient DRG neurons, at 5 days after lentivirus transduction, treated and not treated with calcidiol 20nM. Quantification in B. Data are Mean ± SEM of n=5 independent experiments. In B, WB images of Cyp27b1 at the same conditions and quantification in D. Data are Mean ± SEM of n=3. In E, WB images of LONP1 at the same conditions and quantification in F. Data are Mean ± SEM of n=5. No treated Scr conditions are indicated as 1 and (*) indicates significant values compared to Scr.

4.2.2 Calcidiol has no effect on FXN levels

The above results indicate that the local neuronal synthesis of calcitriol is altered in frataxin deficiency, as the moment that frataxin-deficient DRG neurons supplemented with calcitriol or its precursor show different effects. The most important result obtained using calcitriol in frataxin deficiency was the increased expression of frataxin levels (**Figure 93**). For this reason, it has been checked if calcidiol has the same effect than calcitriol on their levels. As shown in **Figure 102A** and quantification in **B**, no changes have been detected. These results corroborate the deficiency of calcitriol synthesis in FXN-deficient DRGs and indicate that calcitriol, but not calcidiol, could be beneficial for FA patients.

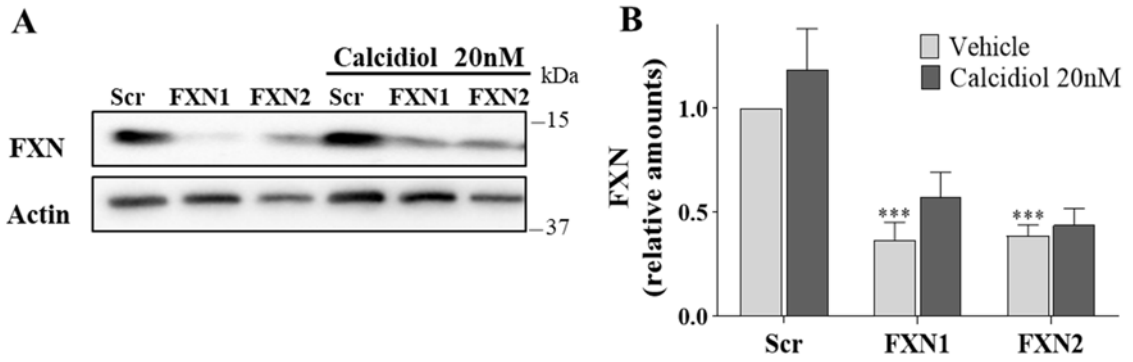

Figure 102. Frataxin levels are not increased by calcidiol supplementation. In A, representative images of frataxin levels in total lysates of frataxin-deficient DRG neurons treated or not with calcidiol. In B, histograms of frataxin protein levels. Data are Mean ± SEM of n=5 independent isolations. No treated Scr condition is indicated as 1 and (*) indicate significant values compared to Scr controls.

4.2.3 Calcidiol amliorates Ca^{2+} homeostasis

The effect of calcitriol on NCLX and fodrin fragmentation levels described in **Figure 94** and **Figure 99** points out the question if calcidiol could have a similar effect. For this reason, NCLX and fodrin protein levels have been checked in FXN-deficient DRGs treated with calcidiol 20nM. The results showed in **Figure 103A** and quantification in **B** indicate that NCLX protein levels are not altered by the treatment, despite a slight, not significant, increase. Even if these results could suggest no role of calcidiol in Ca^{2+} homeostasis, **C** and **D** indicate that fodrin fragmentation is avoided, thus indicating lower activation of caspase-3 and calpains, two Ca^{2+}-activated proteases. While the calpain-specific fragment of 145/150 kDa shows a significant decrease, those mediated by caspase-3 shows a not significant reduction. Taken together, the results obtained in

Ca^{2+} homeostasis with calcidiol addition indicate protective effects for frataxin-deficient DRGs, which are not comparable with those obtained using calcitriol. In fact, calcidiol protects in a very lower extent frataxin-deficient DRGs.

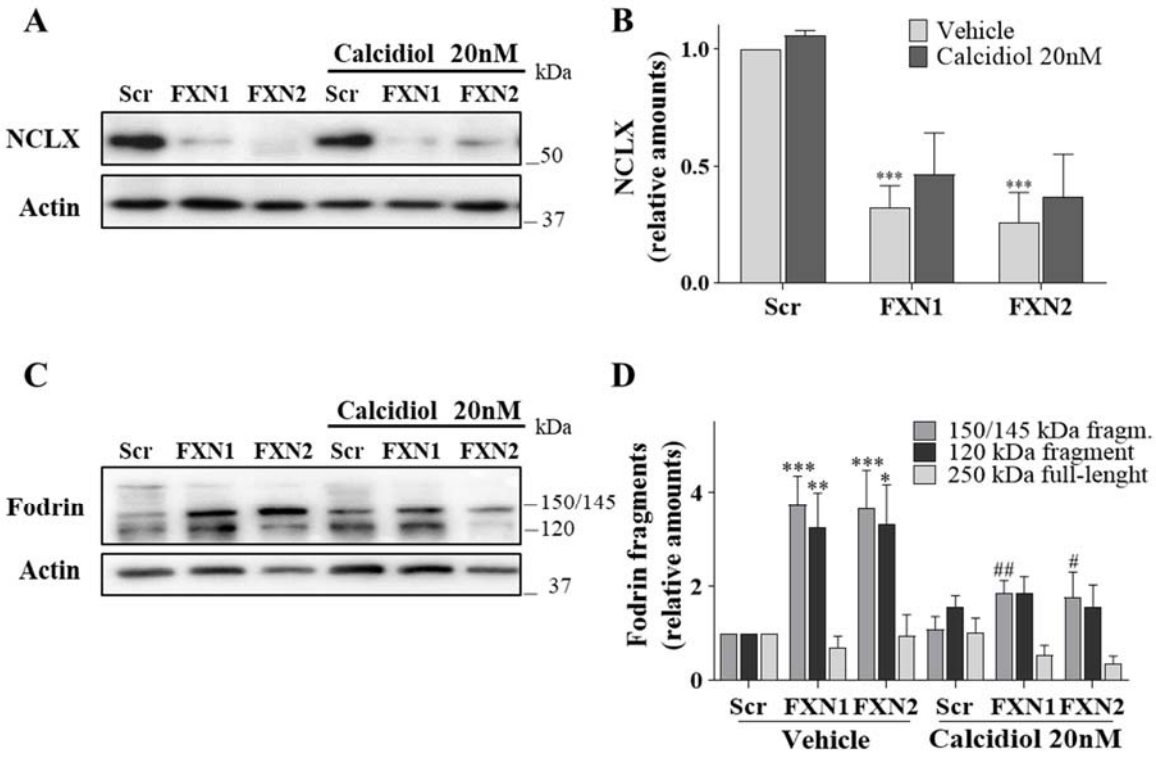

Figure 103. Calcidiol protects fodrin from fragmentations. In A, WB images of NCLX in frataxin-deficient DRG neurons treated or not with calcidiol 20nM. Quantification in B. Data are Mean ± SEM of n=4 independent isolations. In C, representative images of α-fodrin in total lysates of frataxin-deficient DRG neurons treated or not with calcidiol 20nM. Note the full-length of fodrin at 250kDa and fragments at 150/145 kDa and 120kDa. In B, quantification of fodrin full-length and fragments. Data are Mean ± SEM of n=7 independent isolations. No treated Scr from full-length and fragments is indicated as 1 and (*) indicates the significant values compared to Scr controls, while (#) compared to non-treated conditions.

4.2.4 Calcidiol reduces neurodegeneration

To assess if the slight effect in Ca^{2+} homeostasis shown in **Figure 103** induces neuroprotection, it has been analysed neurite degeneration and cell survival in frataxin-deficient DRG neurons treated with calcidiol 20nM. **Figure 104A** for neurite degeneration and **B** for cell survival indicates that calcidiol at 20nM protects frataxin-deficient DRG neurons from apoptosis. However, if compared to histograms in **Figure 100A** and **B** in which is analysed calcitriol, it stands out that these values, although significant, are below from those obtained with calcitriol treatment. These results demonstrate that calcitriol has more protective effects than calcidiol and corroborate the

outcome that Cyp27b1 enzyme functionality is damaged in frataxin deficiency, probably due to ferredoxin FDX1 lower levels or/and heme groups depletion. Nevertheless, no other concentrations have been assessed for calcidiol treatment and further experiments could be necessary in this direction.

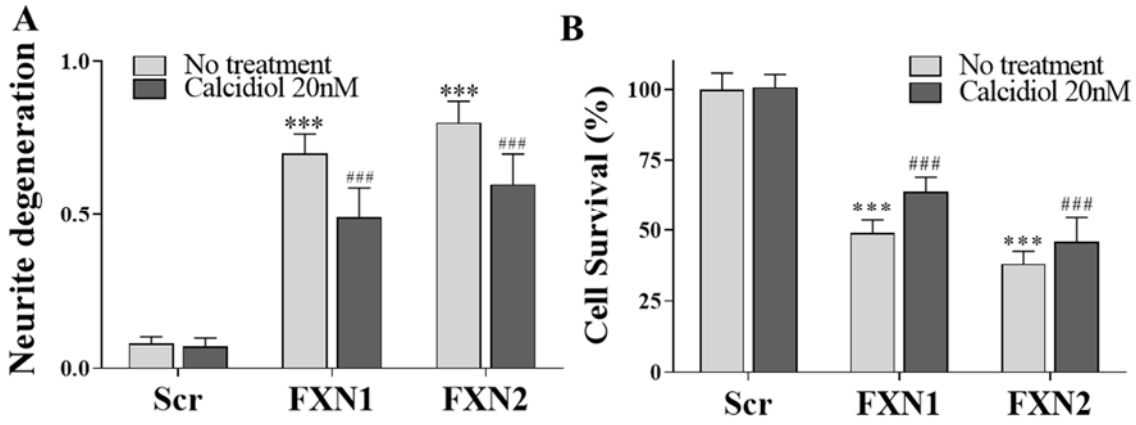

Figure 104. Calcidiol protects frataxin-deficient DRG neurons from apoptosis. In A, neurite degeneration is indicated as the number of neurites with axonal swelling *vs* the total number of neurites. Data are Mean ± SEM obtained from n=5 and a range of 2657-2692 neurites for Scr condition; a range of 2625-2842 neurites for FXN1 condition and a range of 1415-1615 neurites for FXN2 condition. In B, cell survival is analysed as indicated in Materials and Methods. Significant values compared to Scr control are indicated as (*), while (#) indicates significant values compared to non-treated conditions. Data are Mean ± SEM, counting a range of 961-1535 neurons for Scr condition; a range of 1691-2215 neurons for FXN1 condition and a range of 1189-1582 neurons for FXN2 condition. Note the improvement of frataxin-deficient DRG neurons upon calcidiol addition in cell survival and neurodegeneration, which is in lesser extent that using calcitriol treatment in the same conditions.

4.3 Leriglitazone protects FXN-deficient DRGs

4.3.1 Leriglitazone increases FXN levels

Leriglitazone is a novel and orally bioavailable peroxisome proliferator activated receptor gamma (PPARγ) agonist that has good brain penetration efficiency. As the PPARγ agonist Azelaoyl PAF increases frataxin protein and mRNA expression (Marmolino et al., 2009), it was analysed if these result can be observed also with leriglitazone. **Figure 105A** and quantification in **B** indicates a small increase (1.5-fold for FXN1) in frataxin amounts, upon 500nM leriglitazone supplementation. However, no changes for LONP1, a mitochondrial protein used as a control, as indicated in **C** and histograms in **D**. These results confirm that the activation of PPARγ increases frataxin protein levels and point out its use on Friedreich Ataxia.

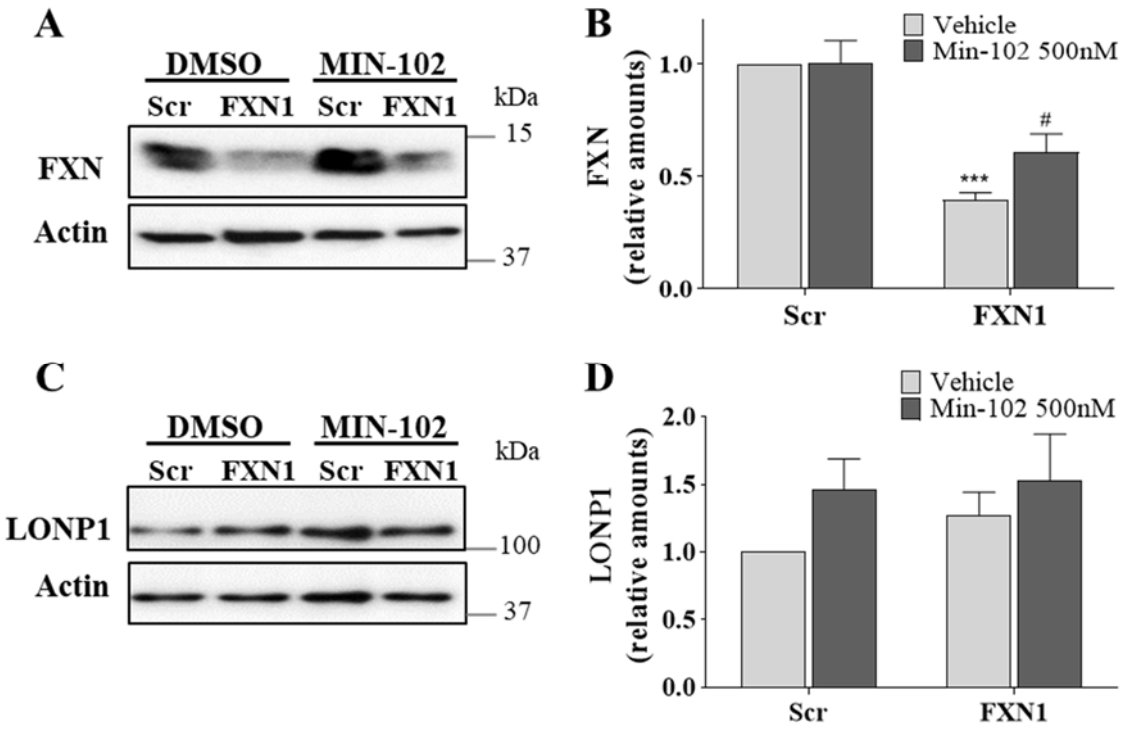

Figure 105. Leriglitazone 500nM induces an increase in mature frataxin protein levels. In A, representative images of frataxin levels in total lysates of frataxin-deficient DRG neurons treated or not with leriglitazone 500nM. In B, histograms of frataxin protein levels. Data are Mean ± SEM of n=7 independent isolations. In C, protein LONP1 has been used as mitochondrial control. Quantification in D. Data are the Mean ± SEM of n=5. No treated Scr condition is indicated as 1 and (*) or (#) indicate, respectively, significant values compared to Scr controls or no treated conditions.

4.3.2 Leriglitazone protects NCLX Protein levels

As previously observed, the replacement of frataxin in frataxin-deficient DRG neurons with TAT-MTScs-FXN induces an increase in NCLX protein level, indicating a positive correlation between the levels of these proteins. As leriglitazone increases frataxin protein levels, NCLX protein has been also analysed by WB. **Figure 106A** indicates a small increase in NCLX amounts, upon 500nM leriglitazone supplementation. Histograms in **B** indicate that leriglitazone promotes an increase of NCLX amounts (1.7-fold for FXN1) in frataxin-deficient DRG neurons.

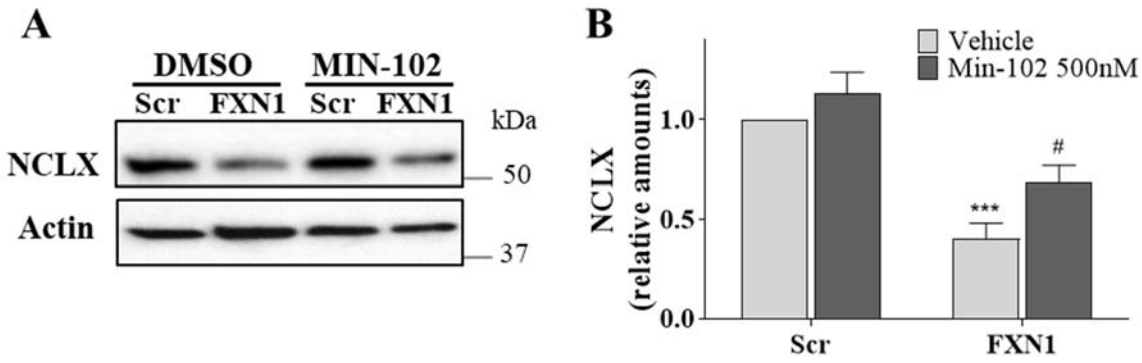

Figure 106. Leriglitazone 500nM induces an increase in NCLX protein levels. In A, representative images of NCLX protein levels in total lysates of frataxin-deficient DRG neurons treated or not with lerigliazone 500nM. In B, histograms of NCLX protein levels. Data are Mean ± SEM of n=7 independent isolations. No treated Scr condition is indicated as 1 and (*) or (#) indicate, respectively, significant values compared to Scr controls or no treated conditions.

4.3.3 Leriglitazone improves $\Delta\Psi_m$

As previously observed in this work, frataxin deficiency induces depolarisation of $\Delta\Psi_m$. A characteristic that has been improved by using treatments that increase frataxin endogenously, e.g. calcitriol treatment. Indeed, NCLX function and $\Delta\Psi_m$ are fine regulated, as indicated in the introduction (**Page 70**). Since leriglitazone increases frataxin protein levels, a consequently NCLX protein levels, $\Delta\Psi_m$ has been analysed. **Figure 107A** shows representative images of JC-1 fluorescence intensity assay. Note the increase in depolarised (green-yellow) mitochondria in frataxin-deficient DRG neurons that can be improved by using 500nM leriglitazone treatment. Histograms in **B** indicates the ratio of green-yellow/orange-red fluorescence intensity expressed in percentage. Note the significant decrease in green/red ratio by using leriglitazone, indicating an increase of $\Delta\Psi_m$.

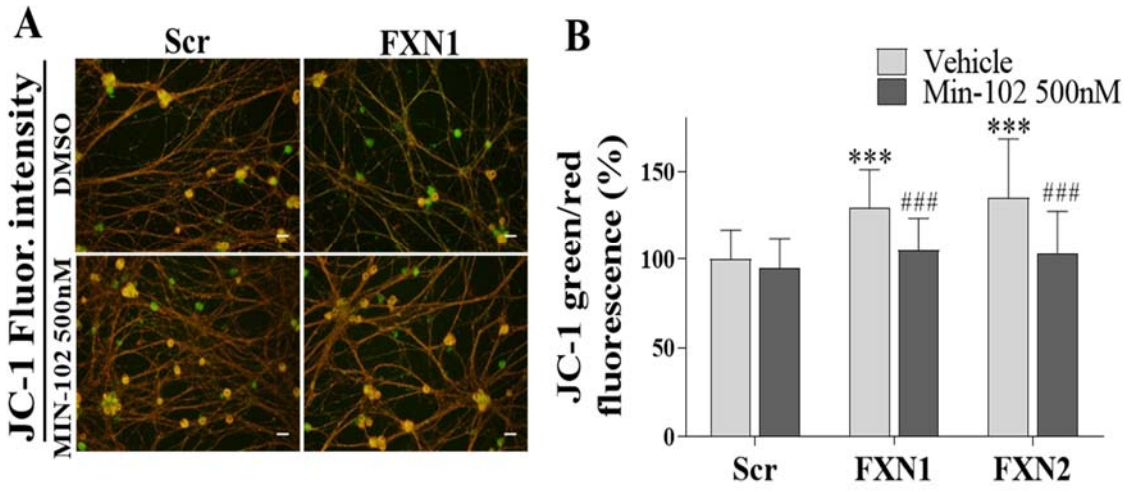

Figure 107. Leriglitazone treatment restores $\Delta\Psi_m$. In A, representative images of frataxin-deficient DRG neurons stained with JC-1 assay to analyse the $\Delta\Psi_m$ as described in Materials and Methods. Note the upper row (no treated cells) in which frataxin deficiency determines a greenish fluorescence, while the lower row (leriglitazone treated cells) shows an orange-red fluorescence, indicating restoration of $\Delta\Psi_m$. Scale bar= 30µm. Quantification in B. Histograms represent JC-1 fluorescence ratio (green/red), normalised to Scr condition (indicated as 100%) and expressed as percentage. Data are Mean ± SEM of n=3 independent experiments. Significant values compared to Scr control condition (no treatment) are indicated as (*), while (#) indicates the effect of treatment compared to no treatment condition.

4.3.4 Leriglitazone does not increase aconitase activity

The above paragraphs indicate that leriglitazone treatment improves mitochondrial function by increasing frataxin and NCLX protein amounts and restoring $\Delta\Psi_m$. In order to analyse if leriglitazone can boost mitochondrial function, the activity of aconitase has been analysed. The experiment has been performed at 4 days of lentivirus transduction and normalised on citrate synthase activity, as indicated in Materials and Methods. As indicated in **Figure 108**, no significant increase in aconitase activity has been observed using the treatment.

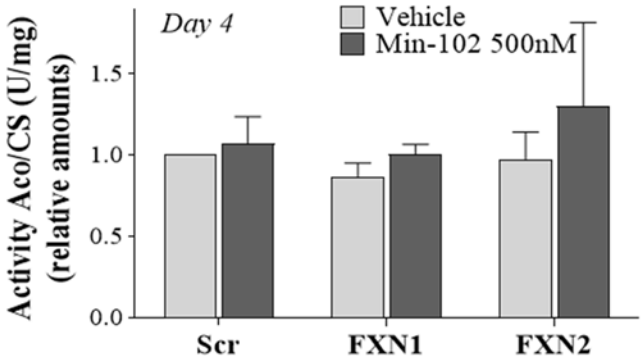

Figure 108. Leriglitazone (500nM) does not induce changes in Aconitase activity in frataxin-deficient DRG neurons. Relative amounts of ratio Aconitase/Citrate Synthase activity in

frataxin-deficient DRG neurons at 4 days after lentivirus transduction. Relative amounts of Aconitase activity (Fluorescence) and Citrate synthase activity (Absorbance), are indicated as U/mg in which Unit=µmol/min. Data are Mean ± SEM obtained from n=4 independent isolations. Scr conditions are indicated as 1.

4.3.5 Leriglitazone protects FXN-deficient DRGs from apoptosis

Improving mitochondrial function results in an increase of cell survival by ameliorating intrinsic pathways of apoptosis. Since leriglitazone treatment improves altered markers of frataxin deficiency, it has been analysed if this improving of mitochondrial function leads to restoration of apoptotic markers. The benefits exerted by leriglitazone, lead us to analyse its effect on apoptotic markers, such as α-fodrin fragmentation, neurite degeneration and survival. **Figure 109A** shows that the increase in fodrin fragmentation bands at 150/145 kDa (or calpain-dependent fragment) and 120kDa (or caspase 3-dependent fragment) in frataxin-deficient DRG neurons can be restored by using leriglitazone 500nM treatment. Histograms in **B** indicates the relative amounts of both fragments and 250kDa full-length protein in treated and untreated conditions. Note the significant decrease of fragmentation, indicating decrease of activation of caspase 3 and calpains by using leriglitazone. These results agree with data in **C** in which neurite degeneration has been analysed. Note the increase of neurite degeneration (the number of neurons with axonal swelling compared to the total amount of neurites) in frataxin deficiency that can be ameliorated by using 500nM leriglitazone treatment. However, different concentrations of the treatment have been used in frataxin-deficient DRG neurons (e.g. 300-500-1000 and 3000nM). Note the bell-shaped drug response in survival analysis, with 500nM concentration at the peak of the curve (**D**). All these results indicate that the activation of PPARγ prevents frataxin-deficient DRG neurons from apoptosis, by increasing frataxin levels and improving mitochondrial function, and point out leriglitazone as a possible treatment for Friedreich Ataxia. However, when 500nM leriglitazone has been analysed *vs* RTA-408 (Omaveloxolone), an NRF2 activator, at 500nM and 250nM concentrations, RTA-408 seems to have a better protection in frataxin-deficient DRG neurons than leriglitazone, as shown in **E**. Further studies are necessary to confirm or not this observation.

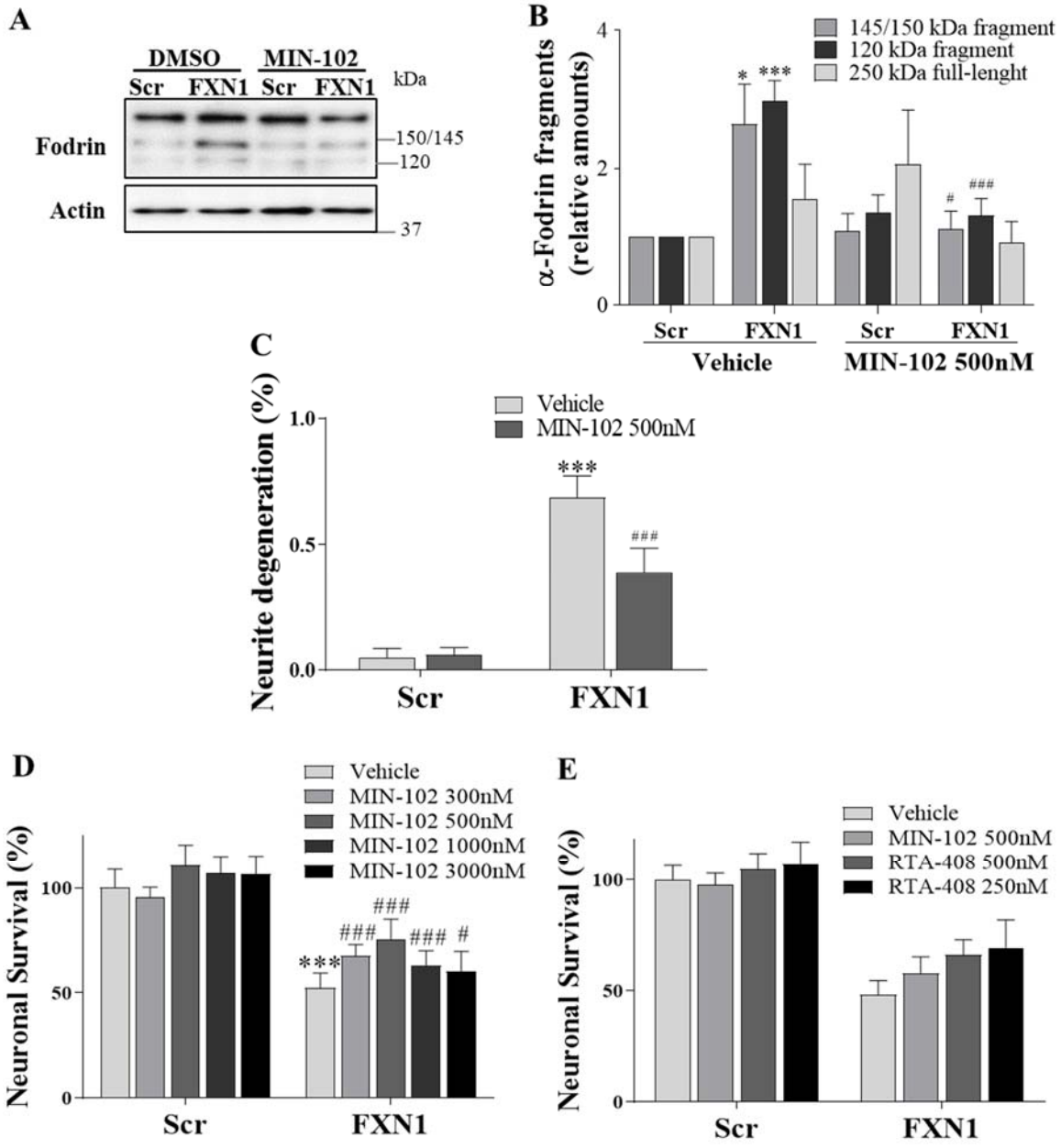

Figure 109. Leriglitazone reduces fodrin fragmentation, reduces neurite degeneration and improves cell survival. In A, representative images of α-fodrin fragments levels in total lysates of frataxin-deficient DRG neurons treated or not with leriglitazone 500nM. In B, histograms of 120kDa, 145/150kDa fragments and full-length protein levels. Data are Mean ± SEM, n=8. No treated Scr condition is indicated as 1. In C, neurite degeneration is indicated as the number of neurites with axonal swelling *vs* the total number of neurites. Data are Mean ± SEM obtained from n=3. In D, cell survival analysis with different concentrations of leriglitazone. Data are Mean ± SEM obtained from n=3. In E, leriglitazone has been analysed *vs* RTA-408 500nM and 250nM. Data are Mean ± SD from n=1 experiment. Significant values compared to Scr control are indicated as (*), while (#) indicates significant values compared to non-treated conditions.

5 COMPOUNDS MODULATING CALPAINS INHIBITION

5.1 Calpain activity inhibitors protect FXN deficient DRGs

Calpains are Ca^{2+}-activated proteases involved in cell death. As the alterations in Ca^{2+} homeostasis in frataxin-deficient DRG neurons is evident, calpains can play important roles in neurodegeneration. Then, we proceed to analyse whether inhibitors of calpains, such as MDL28170 and Calpeptin, could induce some beneficial effects.

5.1.1 MDL28170 and Calpeptin protect the cleavage of NCLX

Decreased levels of the mitochondrial Ca^{2+}/Na^{+} exchanger, NCLX, have been already analysed elsewhere in this thesis. However, why this exchanger shows low proteins levels it was an open question. As the involvement of μ-calpain has been demonstrated for the cleavage of NCLX in isolated mitochondria, in the presence of Ca^{2+} (Kar et al., 2009), inhibitors of calpains were tested as potential NCLX cleavage blockers. The NCLX content has been analysed in frataxin-deficient DRG neurons at 5-days after lentivirus transduction (**Figure 110A**), upon a daily addition of inhibitors of calpains MDL28170, Calpeptin or vehicle, showing that NCLX protein levels increase with both treatments. The 5μM MDL28170 treatment shows a 1.7-fold (FXN1) and 1.9-fold (FXN2) increase in NCLX levels and Calpeptin 25μM treatment shows a 1.4-fold (FXN1) and 2-fold (FXN2) increase, as quantified in **B**. These results indicate that frataxin deficiency induces a calpain-dependent NCLX cleavage.

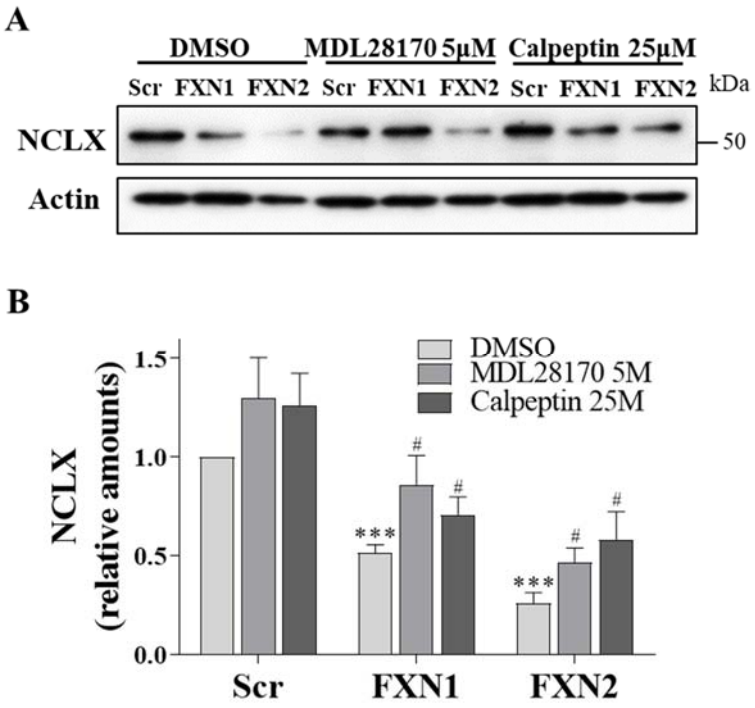

Figure 110. Calpain inhibitors protect NCLX from cleavage. In A, WB images of NCLX protein levels of total lysates of frataxin-deficient DRG neurons treated and not treated with MDL28170µM and Calpeptin 25µM. Quantification in B. Data are Mean ± SEM obtained from n=6 independent isolations. Significant values compared to scrambled condition are indicated with (*), while (#) indicates significant values of MDL28170 5µM or Calpeptin 25µM effects compared to the corresponding culture under non-treated conditions.

5.1.2 MDL28170 treatment restores Ca^{2+} homeostasis

The NCLX increase observed by calpain inhibition leads us to analyse if the effect of calpain inhibitors on NCLX protein levels could favour an improvement of Ca^{2+} homeostasis. For this purpose, Rhod5N fluorescence has been measured in frataxin-deficient DRG neurons at 1-3 and 5-days after lentivirus transduction in presence or not of MDL28170 5µM. Representative images are shown in **Figure 111A**. Quantification is present in **B** and **C**, respectively for Ca^{2+} accumulation in soma ($Ca^{2+}{}_i$) and neurite (prevalently $Ca^{2+}{}_m$). Histograms indicate that significant Ca^{2+} accumulation of 7-22% for soma (**B**, $Ca^{2+}{}_i$) and 13-21% for neurites (**C**, $Ca^{2+}{}_m$) has been observed in frataxin-deficient DRG neurons as early as 1 day after lentivirus transduction and such intensity increases in a progressive manner, while 5µM MDL28170 treated cells shows less accumulation. In fact, our results show that MDL28170 treatment can reduce $Ca^{2+}{}_i$ and $Ca^{2+}{}_m$ accumulation, supposedly by inhibiting calpains action on NCLX. Even if other substrates of calpains could be involved in the process, the improvement in Ca^{2+} homeostasis, by using this calpain inhibitor, is evident.

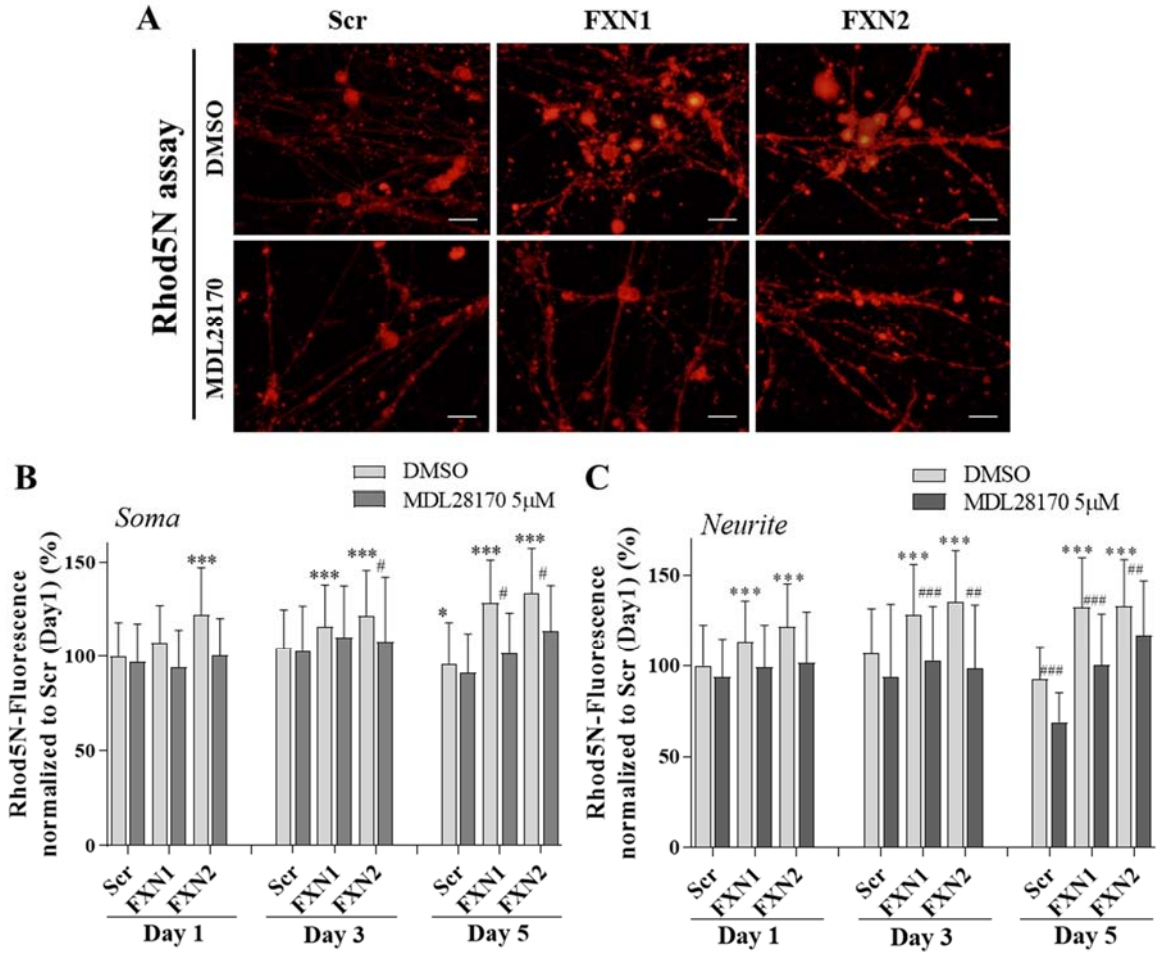

Figure 111. Ca^{2+} accumulation in frataxin deficiency is improved by using MDL28170. In A, representative images of Rhod5N fluorescent dye in frataxin-deficient DRG neurons at 5-days after lentivirus (upper row). Note the less accumulation of Rhod5N intensity using the treatment (lower row). Scale bar= 30µm and objective=32x. In B, histograms represent the intensity of the Rhod5N dye at 1-3 and 5 days after lentivirus. Images for frataxin-deficient DRG neurons at day 1 and 3 are present in **Figure 64**, while images for day 5 are present in **Figure 111**A. Data are Mean ± SEM obtained from n=3 independent isolations, analysing Rhod5N intensity in a range of 315-421 neurites and 198-206 soma for Scr, 300-450 neurites and 218-313 soma for FXN1 and 330-465 neurites and 215-285 soma for FXN2 conditions. Non-treated Scr condition at day 1 is indicated as 100% and significant values compared to Scr are indicated as (*), while (#) indicates significant values of MDL28170 5µM effect compared to non-treated conditions.

5.1.3 MDL28170 improves $\Delta\Psi_m$

As indicated above (**Page 177**), frataxin-deficient DRG neurons show a mild but progressive depolarisation starting at day 1 after lentivirus transduction. Considering depolarisation as a marker of frataxin deficiency, MDL28170 treatment at 5µM is also protective for $\Delta\Psi_m$, as shown in **Figure 112A**. Histograms in **B** represent the fluorescence green/red intensity ratio, in which a raise indicates more depolarised mitochondria and values are normalised to Scr control at day 1 indicated as 100%.

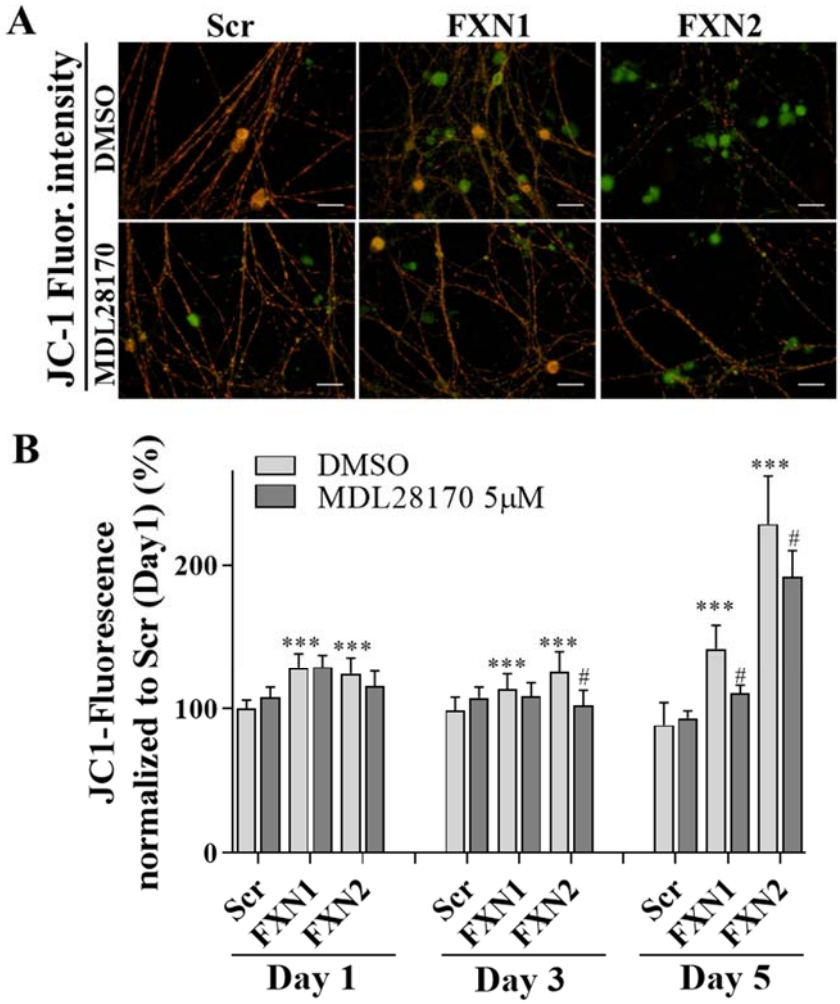

Figure 112. $\Delta\Psi_m$ in frataxin deficiency is ameliorated by the use of MDL28170. In A, representative images of JC-1 fluorescent dye in frataxin-deficient DRG neurons at day 5 after lentivirus transduction as described in Materials and Methods. Scale bar=30µm and objective= 32x. In B, histograms represent fluorescent green/red intensity ratio at day 1-3 and 5 after lentivirus transduction. Data are Mean ± SEM obtained from n=5 independent isolations. For each condition it has been taken 3 images per field and analysed a range of 17-35 fields for Scr conditions, a range of 20-40 fields for FXN1 and 19-37 fields for FXN2 conditions. Scr condition at day 1 is indicated as 100% and significant values compared to Scr are indicated with (*) and compared to non-treated conditions with (#).

5.1.4 MDL28170 and Calpeptin protect fodrin fragmentation

As the cleavage of α-fodrin is already published (Mincheva-Tasheva et al., 2014) and described in our model (**Page 202**), it has been analysed if calpain inhibitors, inhibiting calpains and reducing the signals for mPTP opening (Ca^{2+}_m overload and depolarisation), could be also protective for fodrin fragmentation, a marker of intrinsic apoptotic cell death. As expected, Calpeptin 25µM and MDL28170 5µM treatments have been used in frataxin-deficient DRG neurons, as shown in **Figure 113A** for WB

images and **B** for quantification, obtaining a decrease in fodrin fragmentation, thus, protecting fodrin from cleavage.

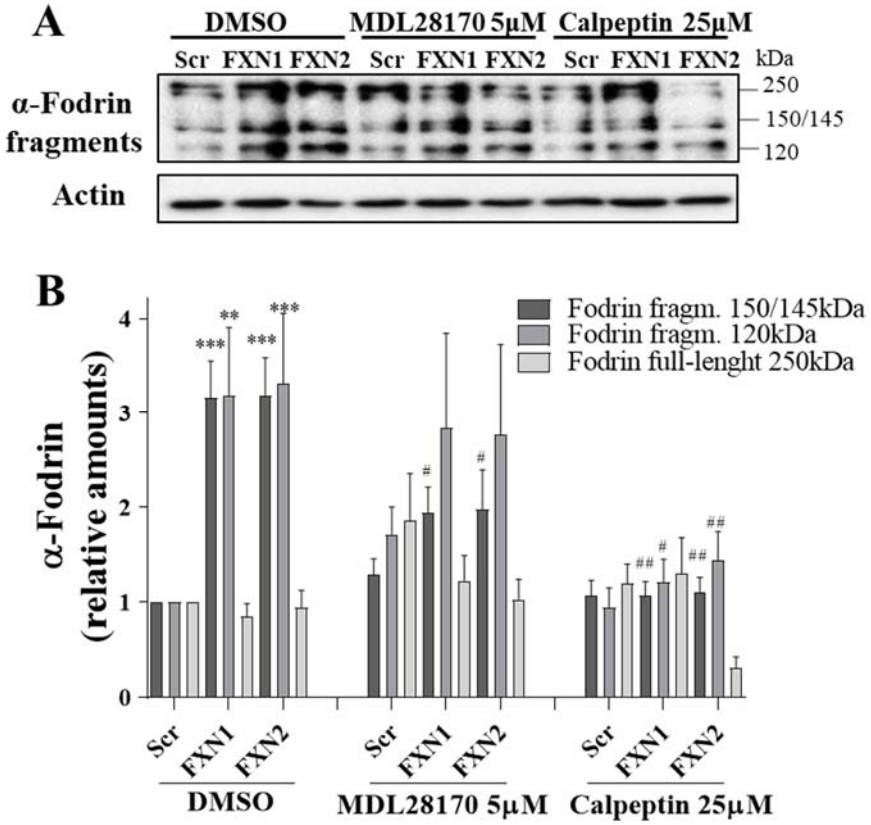

Figure 113. Calpain inhibitors protect fodrin from fragmentation. In A, WB images of α-fodrin antibody in frataxin-deficient DRG neurons in the presence of calpain inhibitors. The image shows full-length fodrin and fodrin fragments (145/150kDa and 120kDa) protein levels, which are quantified in B. Note the decrease in fodrin fragmentation using calpain inhibitors at 5-days after lentivirus transduction. Data are Mean ± SEM obtained from n=7 independent isolations. Scr conditions are indicated as 1 and significant values compared to Scr condition are indicated as (*), while (#) indicates values compared to non-treated conditions.

5.1.5 MDL28170 and Calpeptin protect FXN-deficient DRGs from apoptosis

Frataxin-deficient DRG neurons show apoptotic cell death and neurite degeneration, indicated by the presence of axonal swelling within neurites. As calpain inhibitors exert beneficial effects (restoring NCLX and decreasing fodrin fragmentation), indicating neuroprotection, it has been analysed if these positive effects result in protection from neurodegeneration and cell death in frataxin-deficient DRG neurons. For this purpose, Calpeptin 25µM and MDL28170 5µM treatments have been daily added in our model. **Figure 114A** shows representative images of neurites of treated (or not) frataxin-deficient DRG neurons. The number of neurites presenting axonal swelling *vs* the total number of neurites has been shown as percentage in **B** and **C**, indicating respectively

the changes in axonal swelling during the days or at day 5 after lentivirus transduction. The same has been made for survival analysis in **D** and **E**. Note the protection from apoptotic cell death using both calpain inhibitors during several days after lentivirus transduction, in **D**, and at the end of the experiment, in **E**.

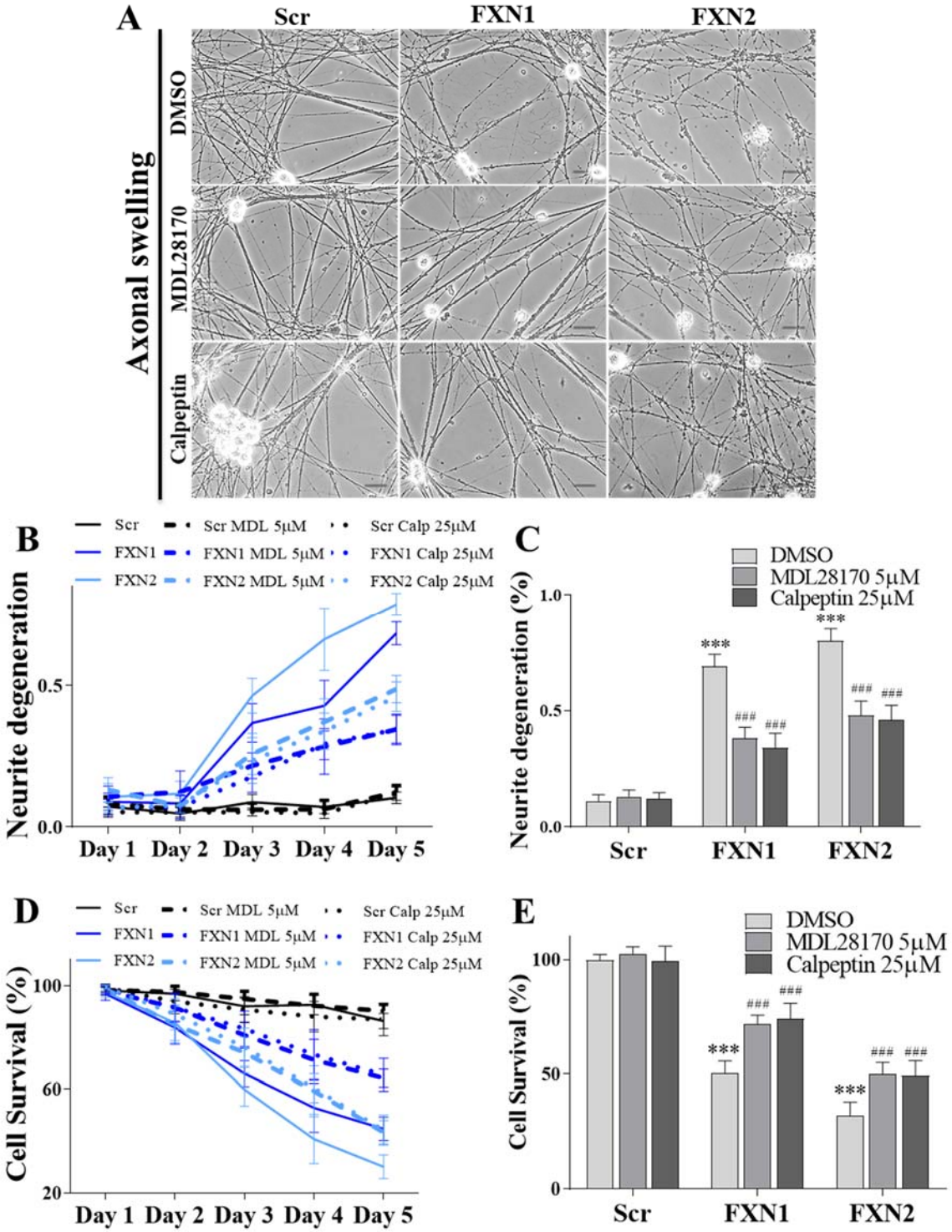

Figure 114. Calpain inhibitors protect FXN-deficient DRGs from apoptosis. In A, representative phase-contrast images of frataxin-deficient DRG neurons showing axonal swelling at 5 days after lentivirus in the presence of DMSO, MDL28170 5µM and Calpeptin

25µM. Scale bar=30µm and objective= 32x. Values in B and histograms in C represent the number of neurites with axonal swelling on the total number of neurites. In B, values are represented during the time, while, in C, histograms represent the analysis for the end of the experiment. MDL and Calp in graph legends refer to MDL28170 and Calpeptin. Data are Mean ±SEM obtained from n=6 independent isolations, analysing a range of 1184-2002 neurites for Scr, a range of 1234-1633 neurites for FXN1 and a range of 1121-1551 neurites for FXN2 conditions. In D, values represent the number of neurons at days 2, 3, 4 and 5 *vs* the initial value (DMSO *vs* treatments) in %, while, in E, histograms represent the % of survival at the end of the experiment. Data are Mean ± SEM from n=6 independent isolations, counting at time 0 a range of 1127-1200 neurons for Scr, a range of 2388-2500 neurons for FXN1 and a range of 2014-2100 neurons for FXN2 conditions. Significant values compared to Scr conditions are indicated as (*), while (#) indicates significant values compared to not treated conditions.

5.2 Calpain expression inhibition protects FXN-deficient DRGs

5.2.1 Calpain levels reduction by RNA interference

The above results for α-fodrin fragmentation, cell death and axonal swelling, restored by calpain inhibitors (**Pages 251, 252**), indicates that the inhibition of calpains can protect frataxin-deficient DRG neurons from apoptosis. In brain, the major calpain involved in α-fodrin fragmentation is considered the calpain 1 or µ-calpain (Siman et al., 1984). For this reason, it has been analysed if reducing calpain 1 levels by RNA interference could be also protective in frataxin deficiency. To test this hypothesis, DRG neurons have been transduced with both shFXN1 and shCALP1 and corresponding controls Scr and EV, as described in Materials and Methods. As indicated in the **Figure 115A**, transduction efficiency in Scr and FXN1 cells reached the 74% and 65% for EV and shCALP1, respectively. A 50% reduction of calpain 1 levels resulted from this RNA interference, as indicated in **B**.

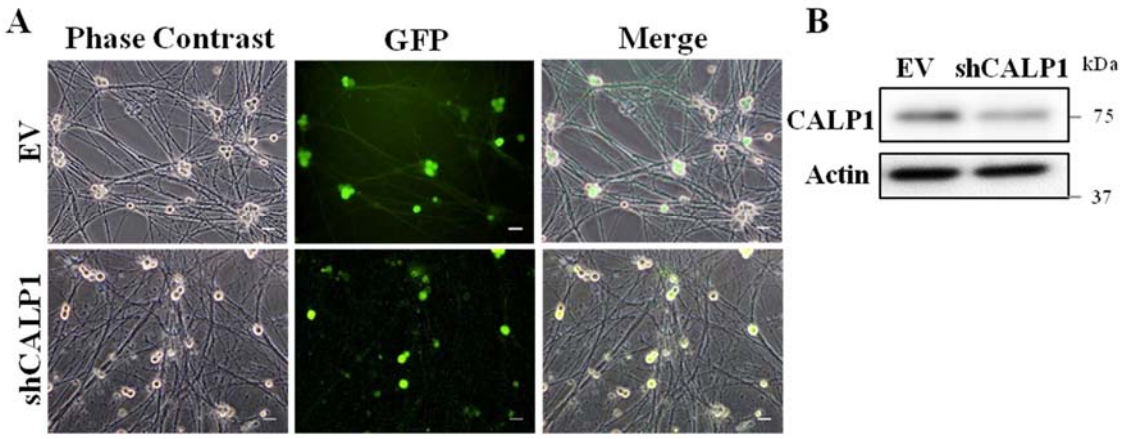

Figure 115. Transduction efficiency of shRNA for calpain 1. In A, representative phase-contrast and GFP fluorescent images of Scr controls 5-days after lentivirus transduction, transduced with empty vector (EV, upper row) and shRNA for calpain 1 (shCALP1, lower row). Merge images are representative of transduction efficiency, the number of GFP-positive cells on

the total number of cells in a field. Scale bar= 30µm and objective= 16x. In B, representative WB images of calpain 1 antibody in Scr controls transduced with EV or shCALP1, showing a 50% reduction of calpain 1 levels after shCALP1 transduction.

5.2.2 Lowering calpain 1 levels protects FXN-deficient DRGs

The role of calpain 1 in frataxin deficiency has been assessed using lentivirus carrying shRNA targeting calpain 1 (shCALP1) (or EV as control) and shRNA targeting frataxin (FXN1) (or Scr as control), as indicated in the above paragraph. In this manner, by lowering frataxin and calpain 1 levels together, it is possible to analyse the role of calpain 1 in frataxin deficiency for known marker of frataxin-deficient DRG neurons, axonal swelling and cell death. Neurite degeneration and cell survival have been analysed in frataxin-deficient DRG neurons and Scr controls transduced with shCALP1 or EV controls and compared to the values obtained using the calpain inhibitor MDL28170 (also transduced with EV lentivirus). **Figure 116A** shows the percentage of survival in DRG neurons (Scr controls and FXN1) transduced with EV, shCALP1 or EV plus MDL28170 5µM. Treatment has been resuspended in DMSO vehicle, which has been added in each condition for the analysis. Histograms represent the number of cells at 5 days after transduction compared to the initial value for each condition. The same conditions have been used for neurite degeneration analysis, shown in **B**. Note the similar values between frataxin-deficient DRG neurons transduced with shCALP1 and EV plus treatment for cell survival and axonal swelling, indicating that (i) lowering calpain 1 has similar effect than inhibiting it pharmacologically with MDL28170 5µM; (ii) calpain 1 contributes to neurodegeneration and (iii) the calpain inhibitor treatment might act on calpain 1 in this context.

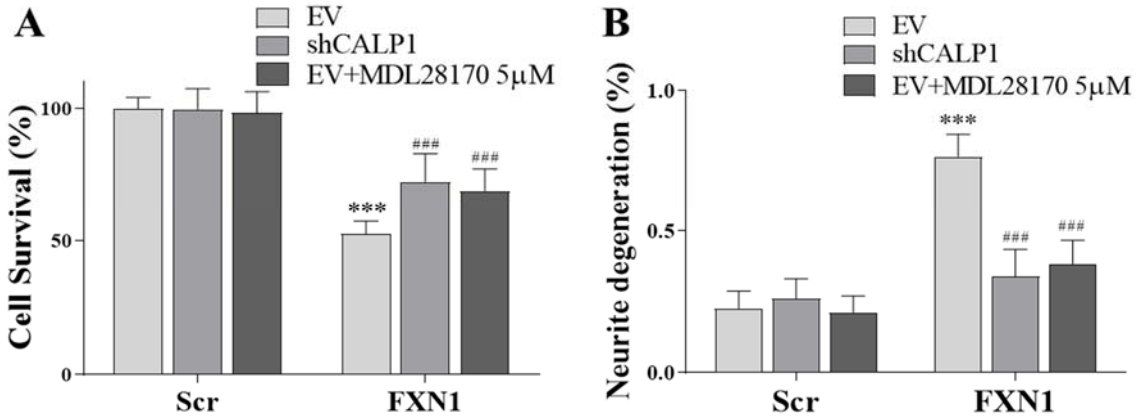

Figure 116. Pharmacological inhibition and RNAi reduction of calpain 1 give similar results in frataxin deficiency. In A, histograms show the % of survival of frataxin-deficient DRG neurons

at 5-days after transduction treated with EV, shCALP1 or EV plus MDL28170 5μM compared to Scr in the same conditions. Data are Mean ± SEM obtained from n=3 independent isolations, counting, at the time 0, a range of 466-643 cells for Scr and a range of 363-564 cells for FXN1 conditions. In B, for the same conditions has been analysed the number of neurites with axonal swelling on the total number. Data are Mean ± SEM obtained from n=3 independent isolations, analysing a range of 611-725 neurites for Scr and a range of 604-661 neurites for FXN1 conditions.

6 COMPOUNDS MODULATING MPTP OPENING

6.1 Cyclosporine A protects FXN-deficient DRGs

6.1.1 CsA protects from fodrin cleavage and apoptosis

Frataxin-deficient cardiomyocytes display mitochondrial swelling and lipid droplets accumulation. By treating these cells with Cyclosporine A (CsA), a Cyclophilin D (CypD) inhibitor, the formation of such phenotypes has been prevented (Purroy et al., 2018). CsA binds CypD and avoids mPTP opening. As mPTP is involved in the intrinsic way of the apoptotic cell death, CsA treatment has been also used in frataxin-deficient DRG neurons in order to avoid its opening. In this case, as indicated in **Figure 117**, CsA treatment 10μM increases survival (**C**) and prevents fodrin cleavage-mediated by calpains and caspase-3 (**A-B**), suggesting a decrease in cell death. These results suggest an intrinsic apoptotic cell death in frataxin deficiency and that the inhibition of mPTP opening can reduce these apoptotic traits.

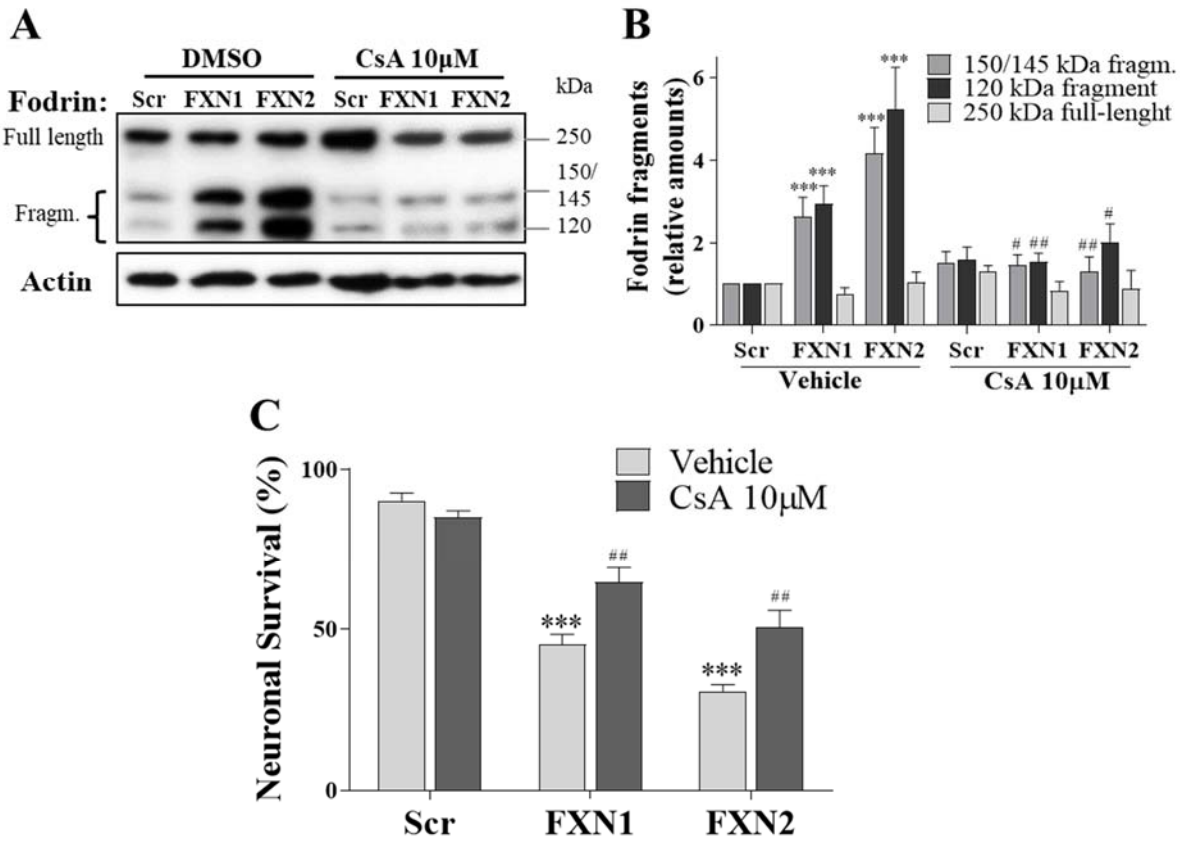

Figure 117. Fodrin fragmentation and cell death are decreased in CsA treated cells. In A, representative images of α-fodrin fragmentation in frataxin-deficient DRG neurons treated or not with CsA 10 μM at 0-2-4 days after transduction. Histograms in B indicate the relative amounts of fodrin fragments normalised to β-actin as a loading control and related to untreated Scr condition as 1. Data are Mean ± SEM, obtained from n=12 independent isolations. Histograms in C indicate the % of survival, the number of cells remaining at day 5 compared to the initial value in the presence of CsA or vehicle. Data are Mean ± SEM, n=7. Significant values compared to Scr conditions are indicates as (*), while compared to untreated conditions as (#).

6.1.2 CsA has no effect on NCLX protein levels

Different signals (e.g. Ca^{2+}_m overload, ROS, $\Delta\Psi_m$, pH etc.) can determine mPTP opening. Ca^{2+}_m overload and depolarisation have been demonstrated in our model, as previously mentioned in the text, and the increase of Ca^{2+}_m has been demonstrated as the cause (calpain-dependent cleavage) and speculated as the consequence (decreased Ca^{2+} efflux) of NCLX protein levels reduction. Hence, an NCLX reduction could decrease Ca^{2+}_m efflux, rise $[Ca^{2+}]_m$ and activate Ca^{2+}-dependent calpains, which in turn, by cleaving NCLX, exacerbate its loss. All mechanisms could terminate with mPTP opening. Thus, NCLX protein levels were checked in the presence of CsA treatment in order to corroborate that the inhibition of mPTP opening is secondary to NCLX levels

reduction, as speculated. **Figure 118A** and quantification **B** indicate that CsA treatment fails to protect NCLX protein levels, indicating that mPTP opening is secondary to NCLX reduction.

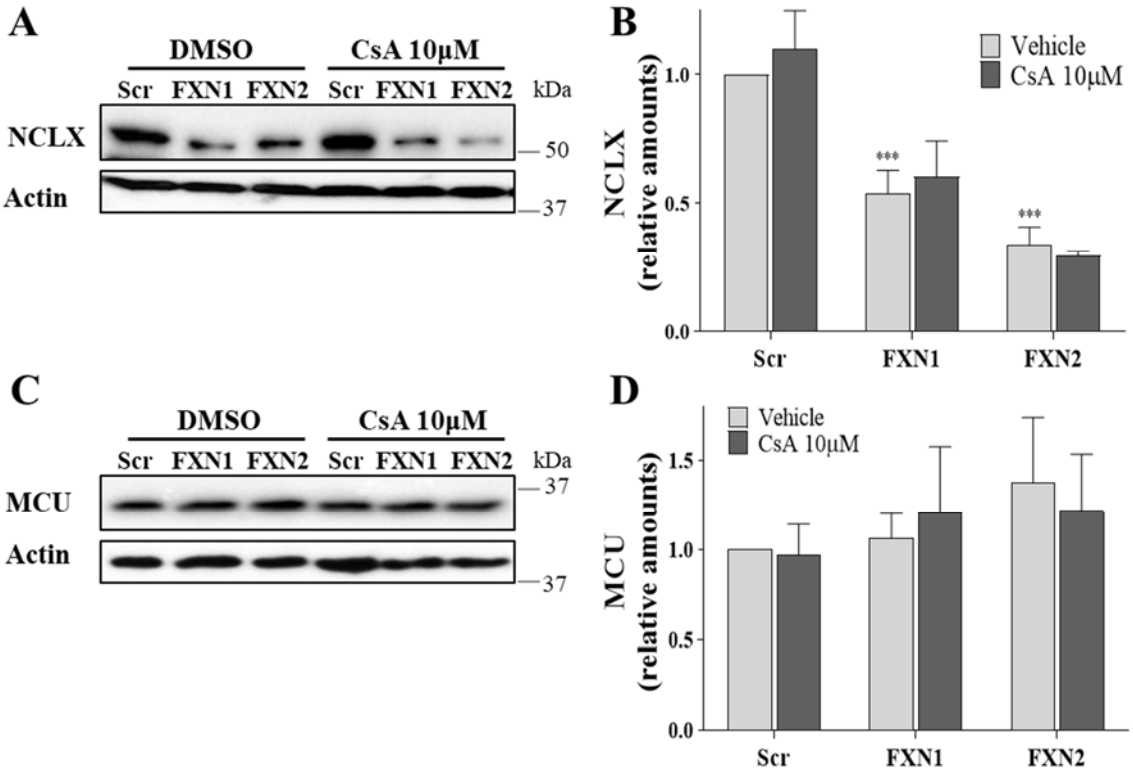

Figure 118. CsA fails to protect NCLX protein levels. In A, representative WB images of NCLX protein levels of frataxin-deficient DRG neurons and controls treated (or not) with CsA 10µM at 0-2-4days after lentivirus transduction. Histograms in B. Data are Mean ± SEM, n=10 independent isolations. In C, WB images for MCU protein levels and quantification in D. Data are Mean ± SEM, n=8 independent isolations. Significant values compared to Scr controls are indicated as (*) and Scr is indicated as 1.

6.1.3 CsA has low effects in calcineurin activity inhibition

Apart from being a CypD inhibitor, CsA also inhibits calcineurin activity, a Ca^{2+}-activated phosphatases. The phosphorylation state of NFATc4, a calcineurin-activated transcriptional factor, indicates the localisation of this transcription factor and indirectly the activation of calcineurin. In sensory neurons, when dephosphorylated, the active NFATc4 enters into the nucleus, transcribing genes involved in synaptic plasticity, axonal growth and neuronal survival (Kim & Usachev, 2009). In frataxin deficiency, NFATc4 is dephosphorylated and nuclear as described previously in the text. The treatment dose used in this study of CsA allows a slight inhibition of calcineurin activity, phosphorylating NFATc4, in the neuronal model, suggesting that the

improvement in survival and axonal swelling could be ascribed only to the inhibition of CypD in neurons, as indicated in **Figure 119**. However, previous results indicate that in frataxin-deficient cardiomyocytes NFATc4 is fully phosphorylated by CsA, indicating that this mechanism could be different between cell-types (Purroy et al., 2018).

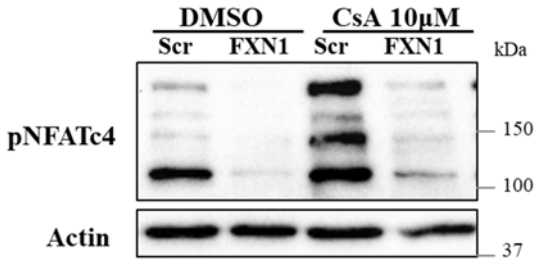

Figure 119. Slight increase in NFTAc4 phosphorylation using CsA in frataxin-deficient DRGs. Representative WB image of pNFATc4 antibody in frataxin-deficient DRGs at 5-days after lentivirus transduction treated with CsA 10µM or equal amount of vehicle.

6.2 Olesoxime and Alisporivir actions on FXN-deficient DRGs

6.2.1 Olesoxime, but not Alisporivir, protects from apoptosis

Apart from CsA, other compounds can modulate the mPTP opening, such as TRO19622 (Olesoxime) or Debio025 (Alisporivir). **Figure 120A** shows the percentage of survival in frataxin-deficient DRG neurons treated with 10µM and 30µM of TRO19622 or vehicle (DMSO). The drug has been added to the cells, by changing media, at 0-2 and 4 days after lentivirus transduction. Histograms indicate an increase in survival of 17% and 20% respectively for frataxin-deficient DRG neurons treated with 10µM and 30µM of TRO19622. These results are in line with those obtained using CsA treatment and indicate that the inhibition or modulation of mPTP opening has neuroprotective effects in frataxin deficiency. Alisporivir is a CsA analogue and Cyclophilin inhibitor, which presents non-immunosuppressive effects, in fact, it can desensitise mPTP, acting on CypD, but not inhibit calcineurin. Alisporivir protects muscle biopsies primary culture of Duchenne Muscular Dystrophy (DMD) patients by restoring the maximal respiratory capacity and mitochondrial cristae organisation in a DMD zebrafish model (Schiavone et al., 2017). Bearing in mind these protective effects on mitochondria, the addition of different concentrations of Alisporivir has been assessed to frataxin-deficient DRG neurons at 0-2-4 days after lentivirus transduction, as shown in **B**, indicating no protective effect. Although these results seem to be discordant to those obtained with CsA and TRO19622, similar results have been obtained in frataxin-deficient

cardiomyocytes in our lab testing mitochondrial swelling (unpublished data). However, a slight increase in survival has been detected using only one addition of 1,5µM Debio025 at 0h after lentivirus transduction and changing media at 2 and 4 days without further additions. Nevertheless, the few experiments performed do not allow testing the significance of the result. Moreover, it has been demonstrated a bell-shaped curve for Alisporivir doses-response in the DMD model, with decreased efficacy at 10µM concentration (using Alisporivir 2-weeks before analysis), suggesting that the concentrations tested in our model probably reflect the toxic doses of the bell curve (Schiavone et al., 2017). Hence, probably, lower concentrations (or early additions) could be protective and further studies are necessary to test these hypotheses.

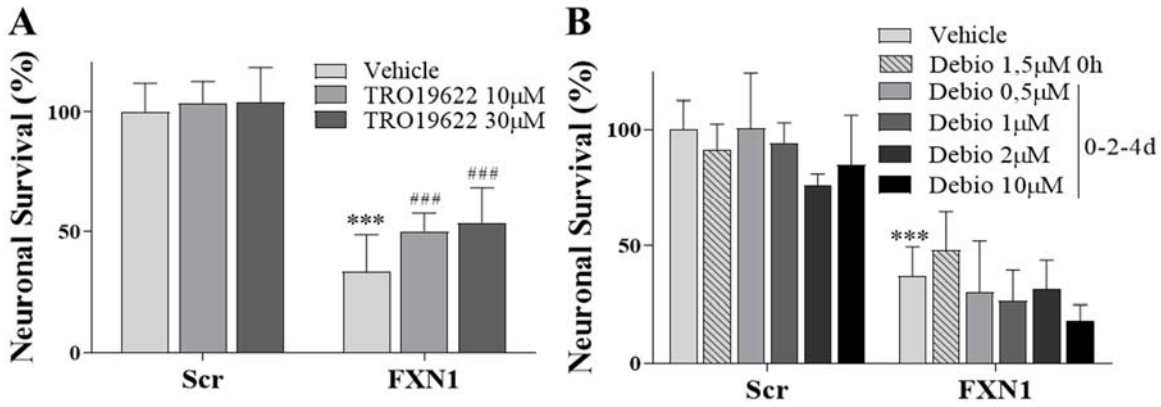

Figure 120. Olesoxime (TRO19622), but not Alisporivir (Debio025), reduces apoptotic cell death in frataxin-deficient DRG neurons. Histograms in A indicate the percentage of cell survival, the number of cells remaining at day 5 compared to the initial value in the presence of 10µM and 30µM of TRO19622 or vehicle (DMSO). Data are Mean ± SD, n=3. In B, different concentrations of Debio025 have been analysed in frataxin-deficient DRGs at 0h (1,5µM) and 0-2-4days (0,5-1-2-10µM) after lentivirus transduction. Data are Mean ± SD, n=2. Significant values compared to Scr conditions are indicates as (*), while compared to untreated conditions as (#).

7 COMPOUNDS MODULATING CALCINEURIN ACTIVITY

7.1 Tacrolimus, less then CsA, protects FXN-deficient DRGs

7.1.1 Tacrolimus has low protective effects

As mentioned before, CsA modulates mPTP opening but also calcineurin activity. Previous results in frataxin-deficient cardiomyocytes indicate that the inhibition of calcineurin fails to restore mitochondrial swelling, a phenotype reverted by CsA, indicating that the inhibition of mPTP opening has better effects than calcineurin

inhibition in frataxin deficiency (Purroy et al., 2018). To corroborate that, also in neurons, CsA protective actions were mainly ascribed to mPTP opening; Tacrolimus (FK506) has been used as a treatment in FXN-deficient DRGs at 0-2 and 4 days after lentivirus transduction (same conditions of CsA). This drug is a calcineurin inhibitor that has no role in mPTP opening. **Figure 121A** shows no beneficial effect of FK506 10µM treatment, same doses of CsA, in frataxin-deficient DRG neurons. However, a small survival increase of 12% has been detected using a lower concentration (100nM), as indicated in **B**. Nevertheless, this small increase is below the values obtained with CsA (20%) and TRO19622 (21%) treatments, indicating that the inhibition of calcineurin has lower protective effects than those obtained inhibiting or modulating mPTP opening. These results are in line with previous results in frataxin-deficient cardiomyocytes (Purroy et al., 2018).

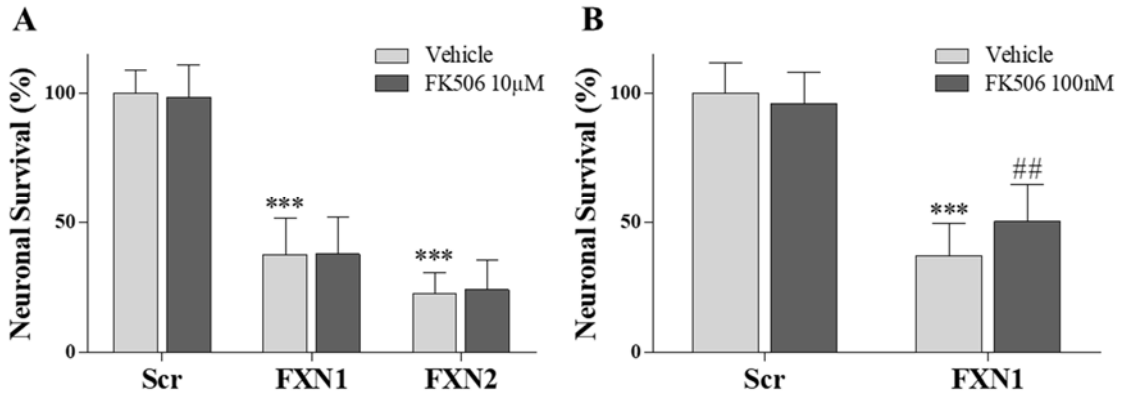

Figure 121. Tacrolimus (FK506) has low protective effect in neuronal survival of FXN-deficient DRGs. Histograms in A indicate the percentage of cell survival, the number of cells remaining at day 5 compared to the initial value in the presence of 10µM of FK506 or vehicle (DMSO), added at 0-2 and 4 days after lentivirus transduction. Data are Mean ± SD, n=4. In B, 100nM of FK506 is added to frataxin-deficient DRG neurons (FXN1). Note the low neuroprotective effect. Data are Mean ± SD, n=3. Significant values compared to Scr conditions are indicates as (*), while compared to untreated conditions as (#).

7.1.2 Tacrolimus has no effect on NCLX protein levels

As indicated before, CsA fails to protect NCLX protein levels. In order to understand mechanisms involved in NCLX reduction, this protein has been also checked in the presence of FK506 10µM, the inhibitor of calcineurin. As shown in **Figure 122A** no changes in NCLX protein levels, but also MCU levels, were detected. Quantification of NCLX and MCU are respectively present in **B** and **C**. These results indicate that pNFATc4 pathways do not regulate NCLX protein levels. As a control, pNFATc4 has been also checked in these conditions. **Figure 122D** and quantification in **E** indicate a

slight increase in the phosphorylation of NFATc4 in the conditions of this study. More experiments are necessary to assess if this slight increase is finally significant or not.

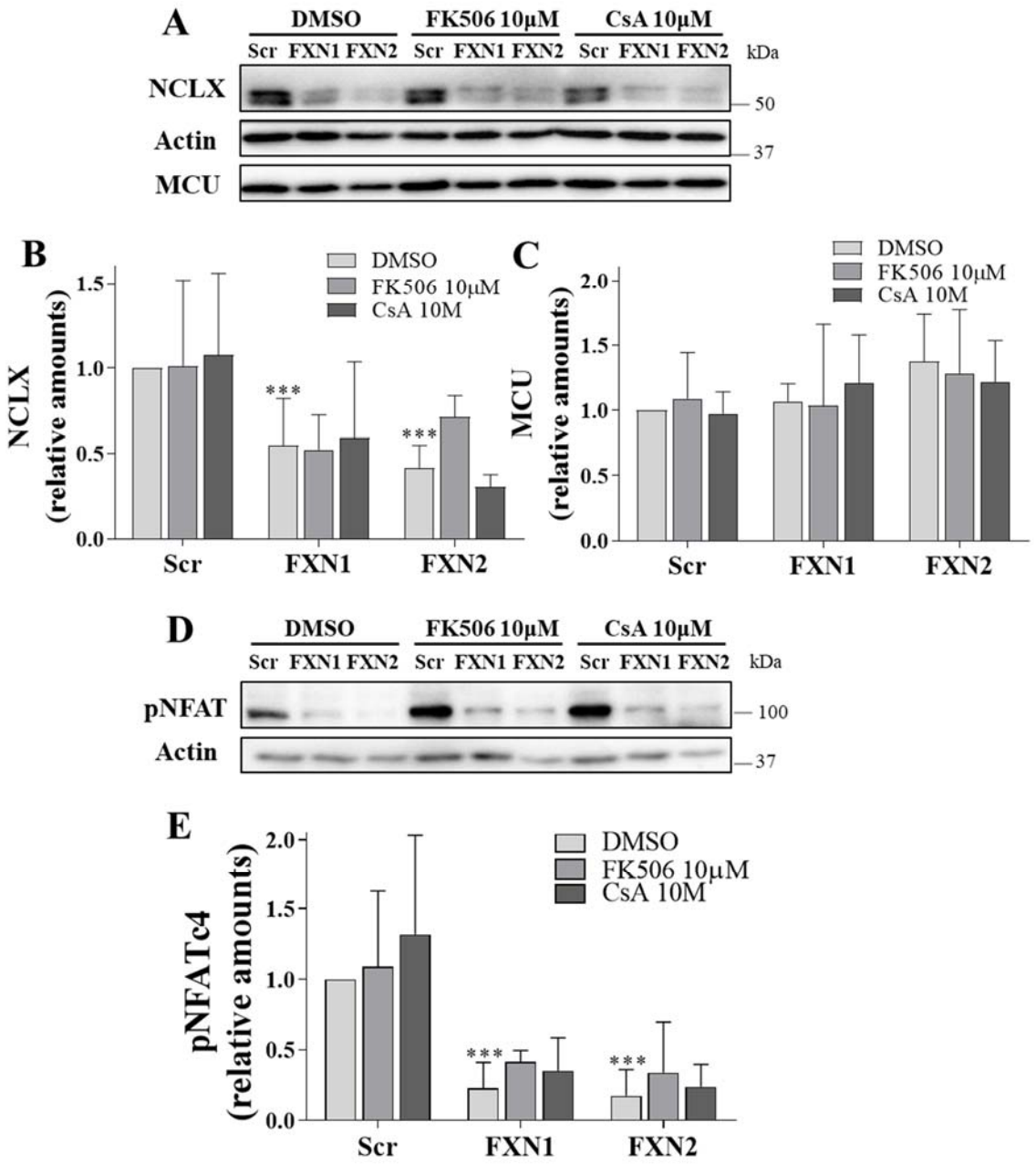

Figure 122. Tacrolimus fails to protect NCLX protein levels. In A, representative WB images of NCLX protein levels of frataxin-deficient DRG neurons and controls treated (or not) with CsA 10µM at 0-2-4days after lentivirus transduction. MCU levels are also showed. Histograms in B indicates NCLX, while in C MCU protein levels. Data are Mean ± SD, n=3 independent isolations in B and in C. In D, WB images of pNFATc4 protein levels and quantification in E. Data are Mean ± SD, n=3 independent isolations. Significant values compared to Scr are indicated as (*) and Scr is indicated with 1.

7.1.3 Tacrolimus and CsA have no effect on calretinin

The Ca^{2+}-binding protein calretinin has been detected increased in levels in frataxin deficiency, as indicated elsewhere in the text. However, the alteration of this protein has not detected before in frataxin deficiency. Then, in order to understand possible mechanisms of calretinin alteration, the protein has been analysed in the presence of Tacrolimus and CsA 10µM. As shown in **Figure 123A** and quantification in **B**, FK506 and CsA both fail to restore calretinin protein levels, thus, indicating that calretinin alteration in frataxin deficiency is not related to mPTP opening inhibition or calcineurin activity.

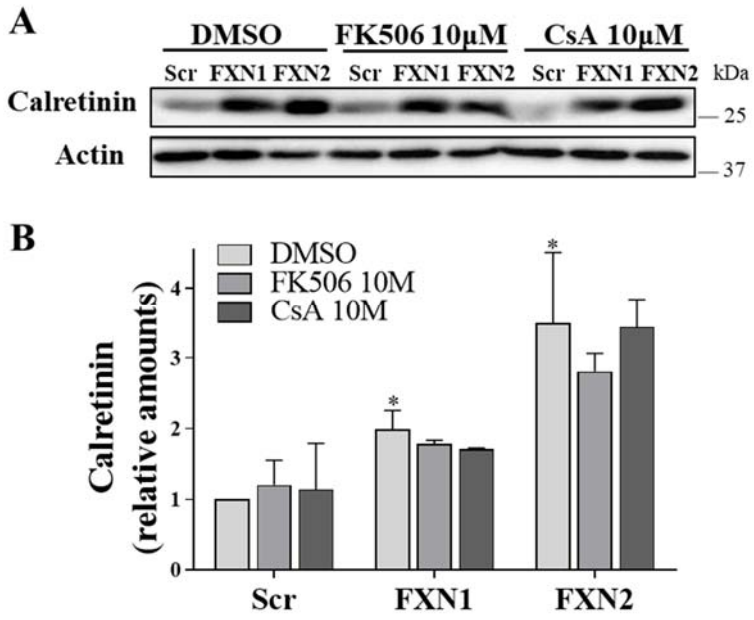

Figure 123. Tacrolimus and CsA fail to reduce calretinin at the levels of controls. In A, representative WB images of Calretinin protein levels of frataxin-deficient DRG neurons and controls treated (or not) with CsA 10µM and FK506 10µM at 0-2-4days after lentivirus transduction. Histograms in B. Data are Mean ± SD, n=2 independent isolations. Significant values compared to Scr are indicated as (*) and Scr is indicated with 1.

8 COMPOUNDS MODULATING GENE EXPRESSION

8.1 Compound M protects FXN-deficient DRGs

8.1.1 Compound M protects NCLX protein levels

The fact that altering gene expression with Calcitriol, a VDR and NRF2 activator, and leriglitazone, a PPARγ activator, can induce an increase of frataxin and NCLX protein levels in frataxin deficiency, points out the possibility of altering gene expression as a possible therapeutic strategy for FA. For this reason, a compound altering gene expression has been analysed. This drug, named in this work compound M, is already used as a treatment for other diseases and has been considered by our group as a repurposing drug for FA. The correct name is not revealed for the possibility of a patent of use in FA for this drug. Its use, yet in progress, is still at the preliminary phases but it has been decided to be included in this work for its great potential. First of all, it has been analysed if this drug can have an impact on frataxin protein levels. **Figure 124A** and quantification in **B**, despite being preliminary results; suggest no increase in frataxin protein levels using this compound at the concentration of 100nM. On the contrary, the preliminary results shown in **C** and quantification in **D** suggest that this drug could have an impact on NCLX, by increasing its levels. Further studies are necessary to confirm or discredit these preliminary observations.

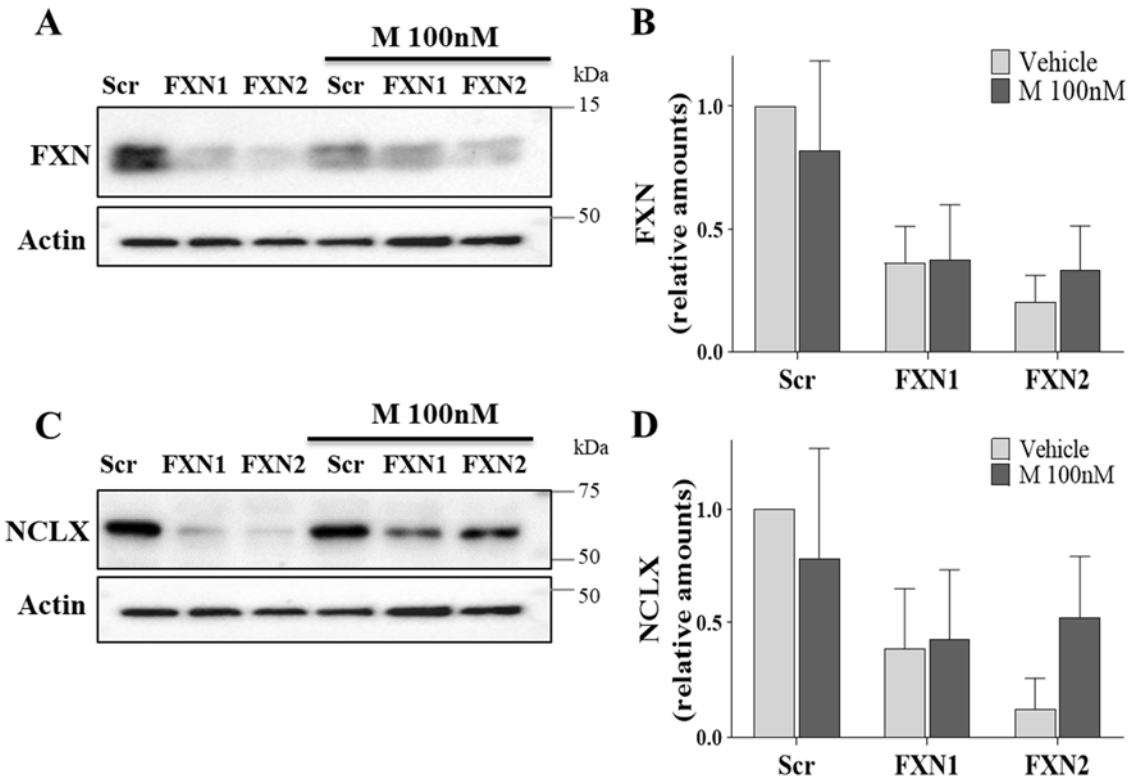

Figure 124. Compound M could protect NCLX protein levels without increasing FXN levels. In A, representative WB images of FXN protein in the presence of compound M. In B, quantification of FXN protein levels. Data are Mean ± SD from n= 2 independent experiments. In C, representative images of NCLX protein. Quantification in D. Data are Mean ± SD from n= 2 independent experiments.

8.1.2 Compound M restores $\Delta\Psi_m$

As NCLX function can be modulated by $\Delta\Psi_m$, the JC-1 fluorescent assay has been performed to analyse this important parameter in the presence of compound M 100nM. As indicated in **Figure 125**, frataxin deficiency induces an increase in mitochondrial membrane depolarisation that can be restored at the level of Scr control using 100nM compound M. This change is represented in the figure as the JC1 green/red fluorescence ratio in percentage, where an increase corresponds to mitochondrial depolarisation. This result indicates that compound M is able to restore $\Delta\Psi_m$ up to the control levels.

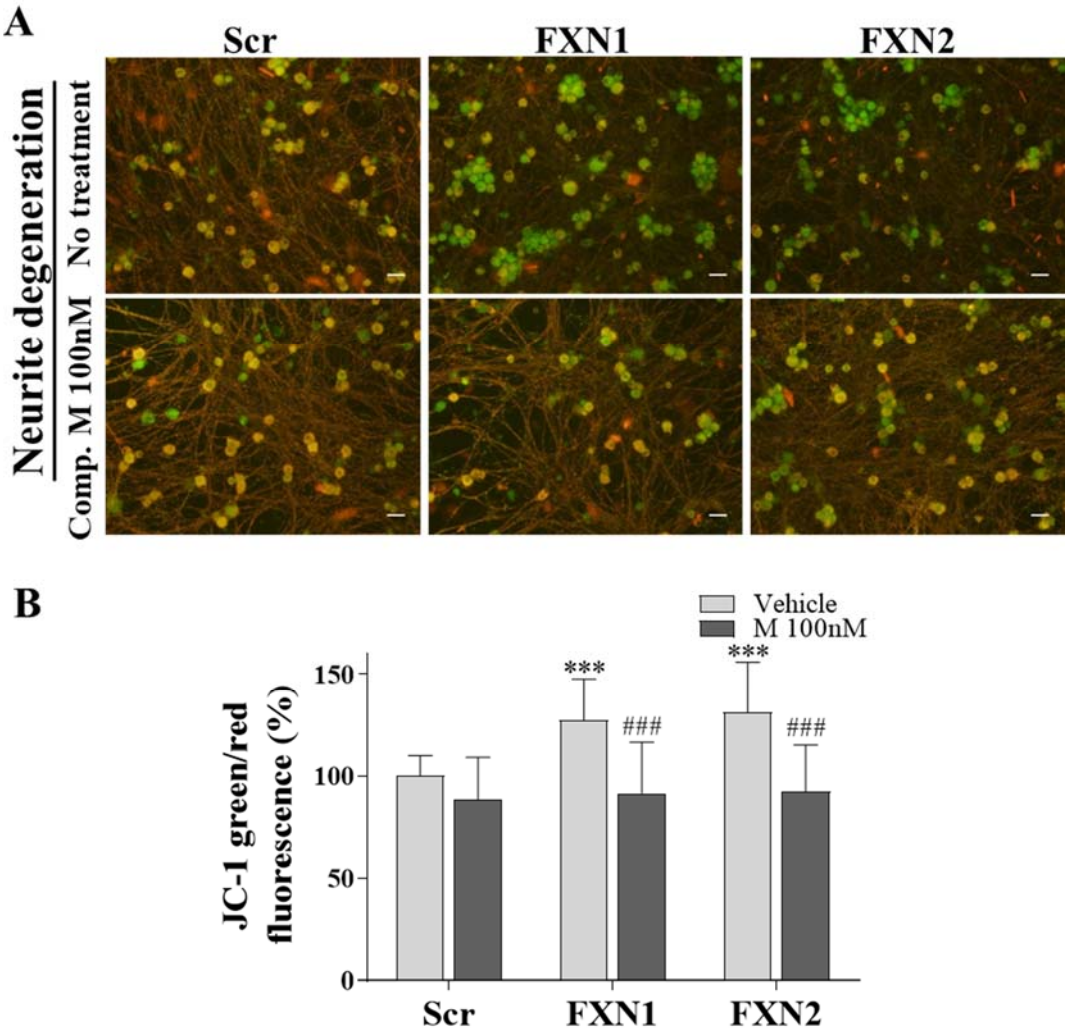

Figure 125. $\Delta\Psi_m$ in frataxin deficiency is restored by compound M treatment. In A, representative images of JC1 assay in DRG neurons treated with compound M or vehicle. Scale bar= 30µm. In B, histograms indicate the ratio of JC-1 green/red fluorescence in percentage. Significant values compared to Scr controls are indicated as (*) and Scr is indicated as 100%, while significant treated values compared to the respective untreated values are indicated as #. Data are Mean ± SEM, n= 3 independent experiments.

8.1.3 Compound M protects fodrin fragmentation

As indicated in the introduction, mPTP opening can occur when mitochondria are depolarised. In the process of mPTP opening different proteins and molecules are released into the cytosol, such as Ca^{2+} and caspase 3. Thus, the analysis of a substrate of activated caspase 3 could indirectly suggest an intrinsic apoptotic cell death. For this reason, α-fodrin fragmentation, due to the activation of caspase 3 and calpains, has been analysed in frataxin-deficient DRG neurons treated or not with compound M. As indicated in the **Figure 126**, compound M at 100nM seems to decrease fodrin

fragmentation. However, more experiments are necessary to study if these differences are statistical significant.

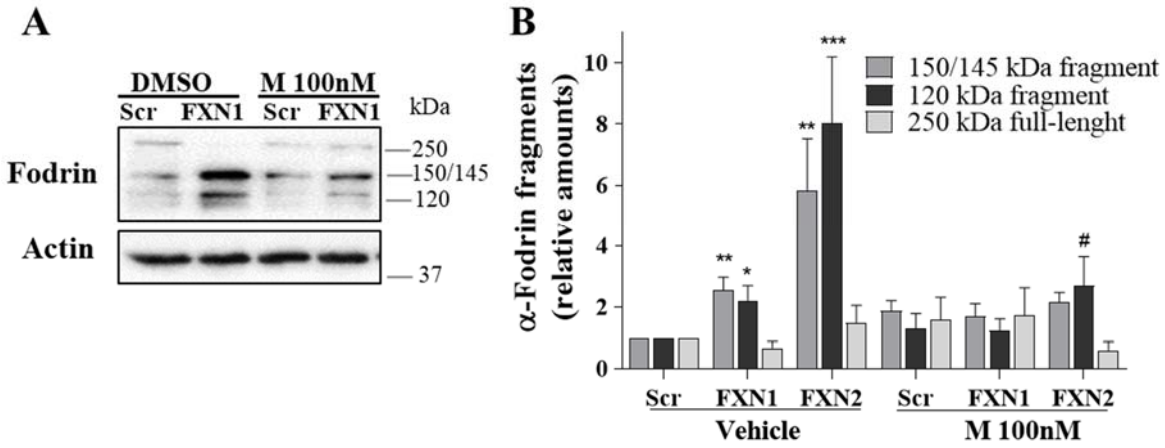

Figure 126. Fodrin fragmentation seems to decrease with compound M 100nM. In A, representative WB images of fodrin (full-length and fragments) protein in the presence of compound M 100nM. In B, quantification of fodrin protein levels. Data are Mean ± SEM from n= 3 independent experiments. In C, representative images of NCLX protein. Quantification in D. Data are Mean ± SEM from n= 3 independent experiments.

8.1.4 Compound M protects FXN-deficient DRGs from apoptosis

The results above suggest that compound M can protect α-fodrin fragmentation in frataxin-deficient DRG neurons, suggesting a protection from apoptotic cell death. In order to analyse this characteristic, the number of cells present after 5 days of lentivirus transduction has been compared to the initial number of cells in the presence of the vehicle or the treatment, compound M 100nM. The result in **Figure 127** indicates that compound M greatly protects frataxin-deficient DRG neurons from apoptotic cell death. Interestingly, compound M has been added once to the culture 48h after lentivirus transduction, when frataxin protein levels are already reduced. This result indicates that compound M has a great potential as a possible drug to be tested in FA. More studies are necessary; however, these results are promising.

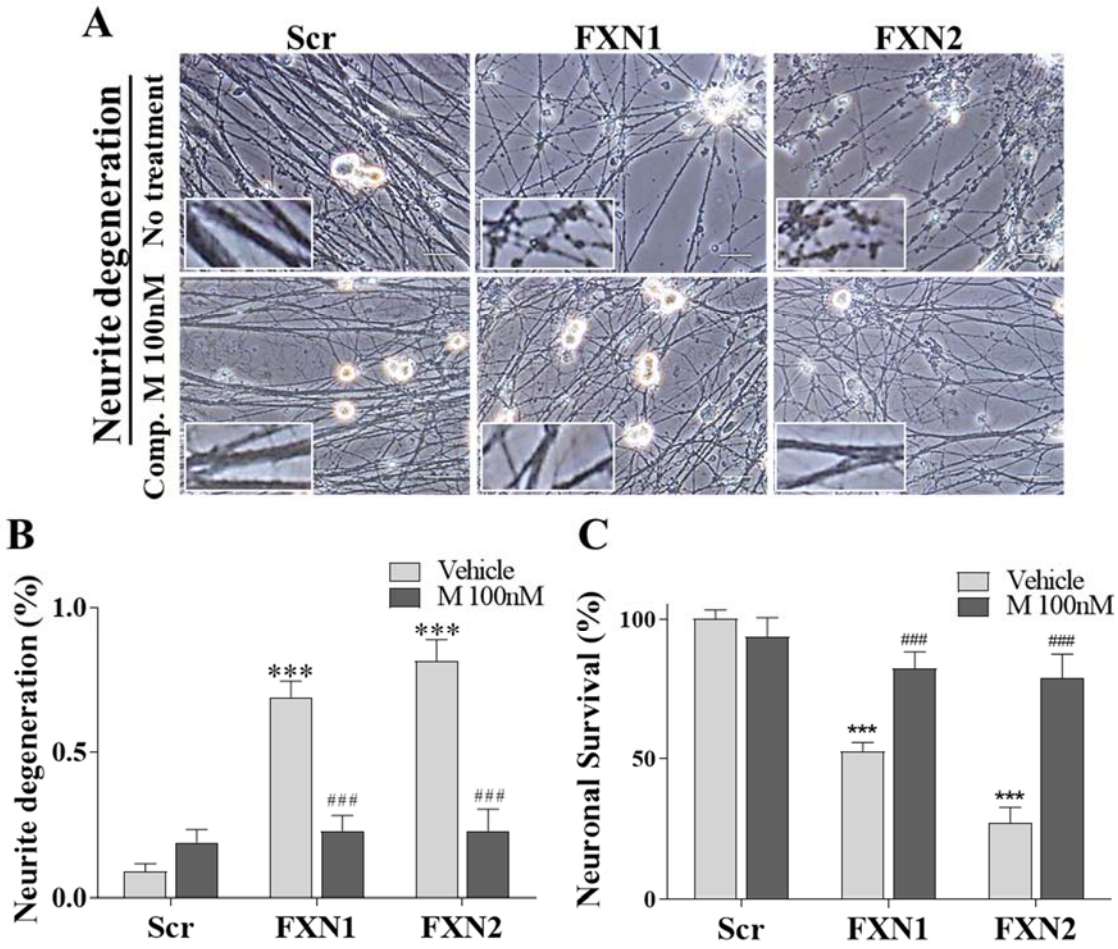

Figure 127. Compound M protects frataxin-deficient DRG neurons from apoptotic cell death. In A, representative phase-contrast images of DRG neurons treated with compound M or vehicle. Scale bar= 30µm. In B, histograms represent the number of neurites with axonal swelling on the total number of neurites. Data are Mean ± SEM from n= 3 independent experiments. Histograms in C represent the neuronal survival in percentage of frataxin-deficient DRG neurons treated or not with 100nM compound M. Data are Mean ± SEM from n= 4 independent experiments. Significant values compared to Scr controls are indicated as (*) and Scr is indicated as 100%, while significant treated values compared to the respective untreated values are indicated as #.

8.1.5 Analogues have lower effect than Compound M

One of the limitations of compound M is the binding to DNA. This characteristic could damage healthy cells. In order to analyse if an analogue of compound M, that has lower affinity to DNA and lower side effects, produces the same protection of frataxin-deficient DRG neurons, compound S has been analysed. As indicated in **Figure 128A** for survival and **B** for neurite degeneration, this compound, used at the same concentration that compound M, has lower ability to protect frataxin-deficient DRG neurons. However, more studies are necessary to understand if the characteristic of lower side effects can compensate this minor protection and if other concentrations can

have a different impact on these characteristics. Furthermore, compound M seems to act in the same manner than compound P, a kinase inhibitor. When 100nM compound M has been analysed *vs* 10µM compound P, even in this case compound M shows better protection of frataxin-deficient DRG neurons than compound P, indicating that the action of compound M could be different, as shown in **C** and **D** respectively for survival and neurite degeneration. Despite the mechanism of action of compound M in frataxin deficiency is not known, these results indicate that this compound has a great potential as a new strategy for FA patients. However, many studies need to be done in this direction.

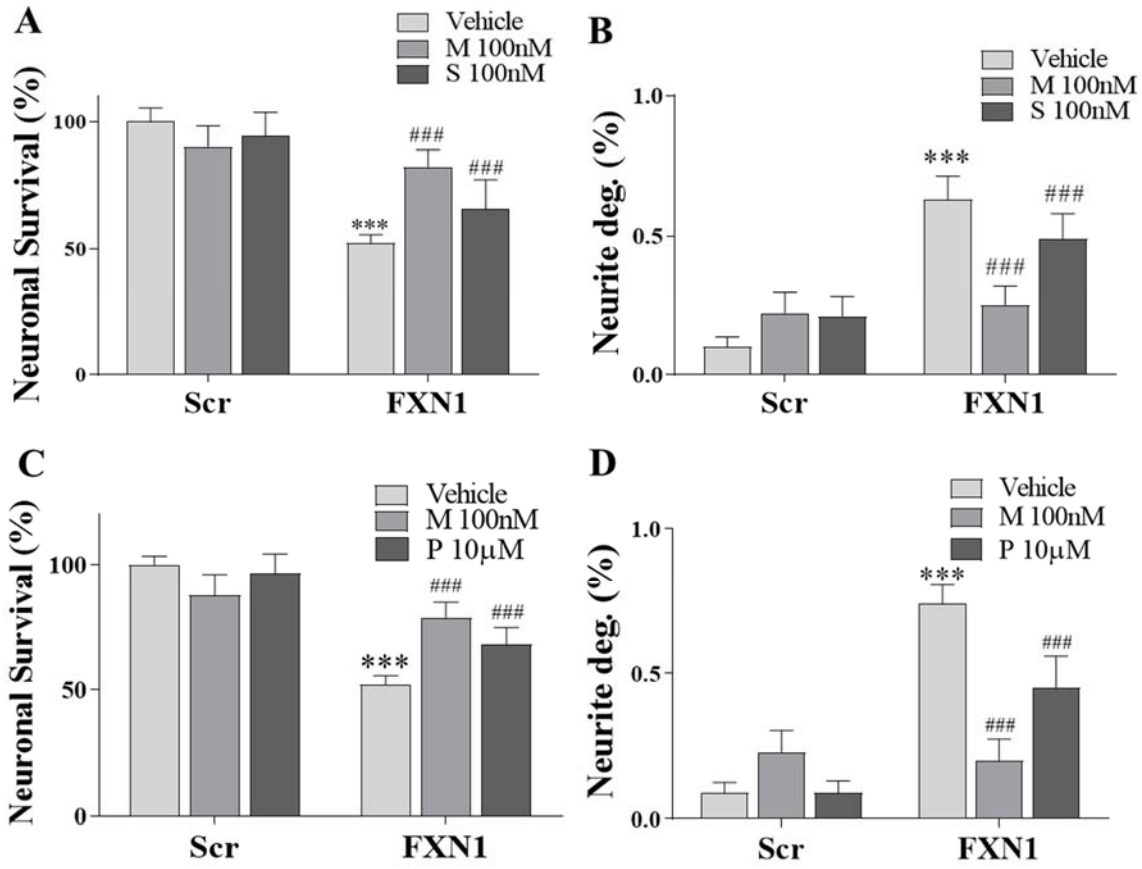

Figure 128. Analogues protect frataxin-deficient DRG neurons from apoptotic cell death in lesser extent than compound M. In A, histograms represent the neuronal survival in percentage of compound M *vs* compound S, all at 100nM. Data are Mean ± SEM from n= 3 independent experiments. In B, histograms represent the number of neurites with axonal swelling on the total number of neurites using the same conditions. Data are Mean ± SEM from n=4 independent experiments. Histograms in C represent the neuronal survival in percentage of frataxin-deficient DRG neurons treated or not with 100nM compound M *vs* 10µM of compound P. Data are Mean ± SEM from n= 3 independent experiments. In D, axonal swelling is analysed using the same conditions. Data are Mean ± SEM from n=4 independent experiments. In all graphs, significant values compared to Scr controls are indicated as (*), while significant treated values compared to the respective untreated values are indicated as #.

9 COMPARING NEURONS WITH LCLs FROM PATIENTS

9.1 LCLs from FA patients show frataxin reduction

Some of the points criticised regarding the frataxin-deficient DRG model indicated above is the lack of GAA expansions, the use of lentivirus and the rat origin. In order to analyse the correlation between NCLX and frataxin protein levels in a model obtained from patients, lymphoblastoid cell lines from healthy controls, carrier and patients have been purchased from Coriell Institute. These commercial immortalised cell lines represent a good model for studying biochemical alterations in frataxin deficiency; however, these cells are not useful for the lack of a clear phenotype and the fact that this cell type is not affected in the disease. For this reason, this human model has been used only to compare with the frataxin-deficient DRG model and confirm biochemical differences. First of all frataxin amounts have been analysed in LCLs. As expected, **Figure 129** indicates the decrease in frataxin protein levels in carrier and patients compared to control. Representative images are shown in **A** and quantification in **B**.

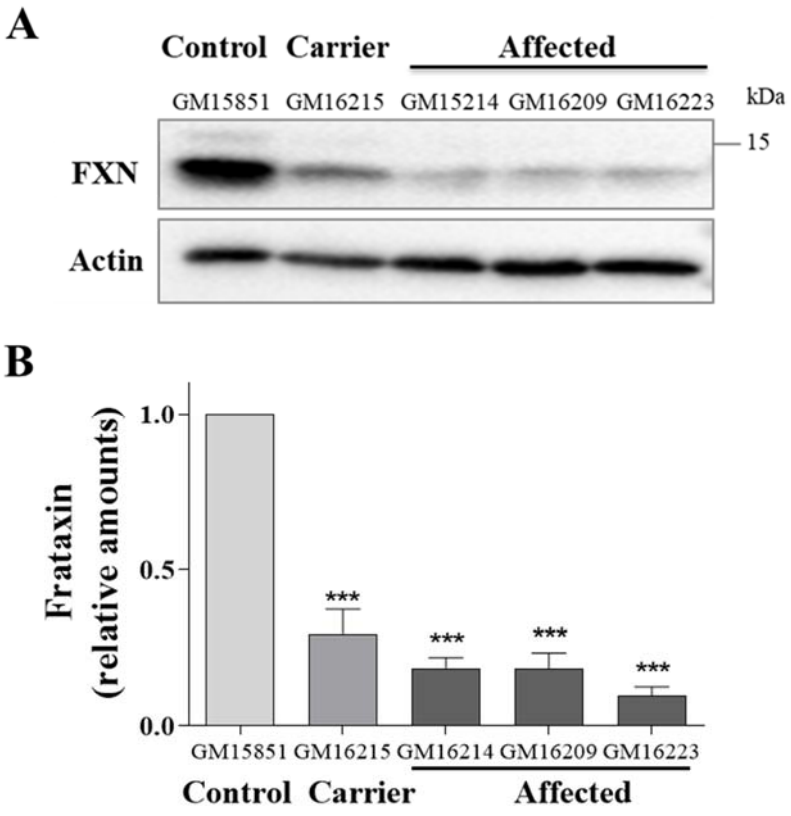

Figure 129. Frataxin amounts in LCLs from healthy controls, carrier and patients. In A, representative images of frataxin WB bands in LCLs for healthy controls, carrier and patients. In B, quantification of frataxin, relative to control amount. Data are Mean ± SEM from n= 6 independent experiments. Significant values compared to control are indicated as (*) and control is indicated with 1. **Dr F. Delaspre, T. Ximelis or A. Sanz-Alcazár have kindly performed cultures and T. Ximelis or A. Sanz-Alcazár participated in WB analysis.**

9.2 LCLs from patients present NCLX reduction

Once, as expected, it has been confirmed the decrease in frataxin protein amounts of FA patients and carrier, NCLX protein levels have been also observed in order to confirm the decrease of these levels in a model carrying GAA repeats expansion. Interestingly, despite LCLs from patients not displaying a clear phenotype, NCLX protein levels are decreased as observed in **Figure 130A** and quantification in **B**. Histograms in **B** shows that NCLX is reduced by ~30% in FA carrier and ~60% in FA patients. These observations are important because the reduction of NCLX in FA carrier involves this protein in the first steps of the disease, as already observed in frataxin-deficient DRG neurons. Thus, the results observed in frataxin-deficient DRG neurons are confirmed in LCLs from patients. These results are normalised on β-actin, a control for total protein amounts. In order to analyse if these decrease interests more mitochondrial proteins, a mitochondrial control has been also detected using the chaperone HSP60. Interstingly, this protein has been observed altered in frataxin-deficient DRG neurons, as indicated in the above Results section. When this protein has been analysed in FA carrier and patients, as shown in **C** and quantification in **D**, no changes have been detected. These results confirm the previous finding in frataxin-deficient DRG neurons.

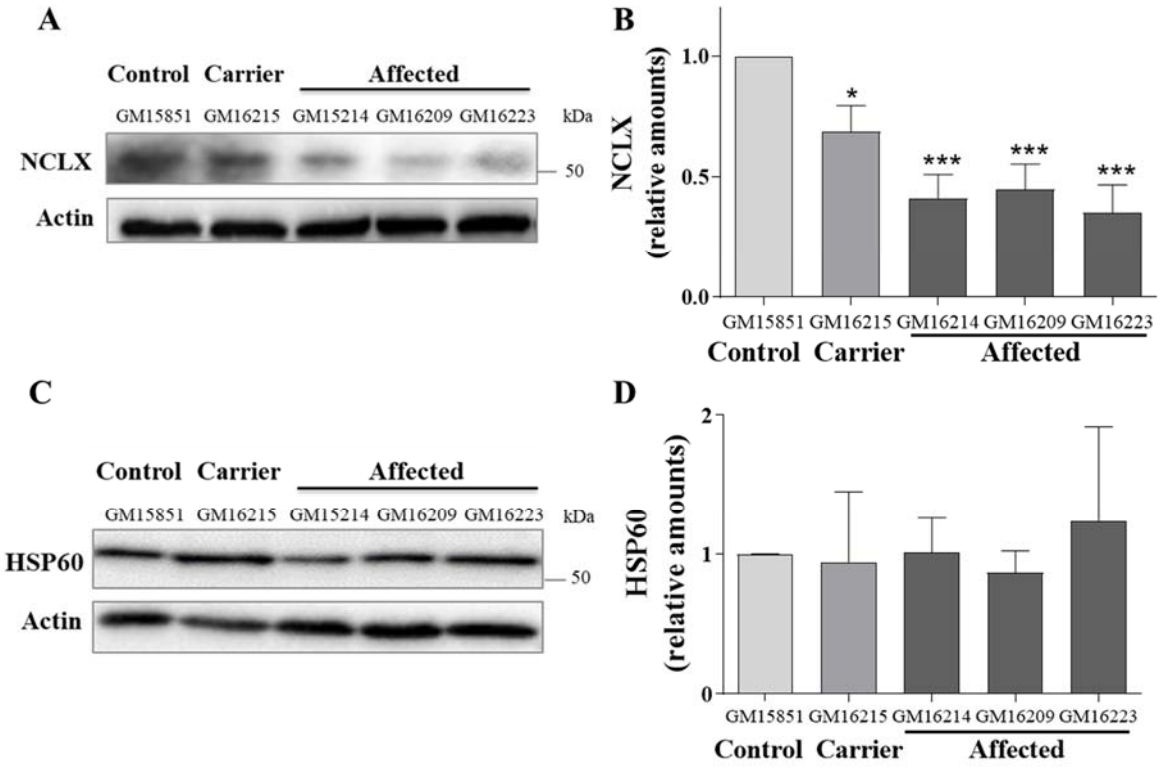

Figure 130. NCLX protein levels decrease in LCLs from FA carrier and patients. In A, representative WB images of NCLX protein amounts in LCLs from control, carrier and patients.

In B, quantification of WB bands. Data are Mean ± SEM from n=7 independent experiments. Significant values compared to control are indicated as (*) and control is indicated with 1. In C, representative WB images of HSP60 protein amounts in LCLs from control, carrier and patients. In D, quantification of WB bands. Data are Mean ± SEM from n=3 independent experiments. **Dr F. Delaspre and T. Ximelis have kindly performed cultures and T. Ximelis participated in WB analysis.**

9.3 Oxidative phosphorylation impaired in LCLs from patients

Some authors indicate an alteration in oxidative phosphorylation in frataxin-deficient cells (Abeti et al., 2016; Ristow et al., 2000). In order to analyse if this difference is present in our model, lymphoblastoid cell lines from controls, carriers and affected cells have been analysed in Oroboros-2K Oxygraph instrument as indicated in Materials and Methods. This apparatus allows analysing the mitochondrial respiration of cells in suspensions, thus, it has been used for LCLs but not for the neuronal model. **Figure 131A** indicates the O_2 flow normalised per cell during the time in a pool of controls, carriers and affected cells. In resting cells no differences are detected, however, a significant difference emerged upon addition of the protonophore FCCP, which is added 5 times. Cells from FA patients displayed a small respiratory increase using FCCP, meaning that these cells have a small mitochondrial respiratory capacity. These findings are in agreement with results in literature (Igoillo-Esteve et al., 2020; Ristow et al., 2000). Despite the significant values in FCCP addition, when cells are grouped for age and sex, as in **B** and **C**, no clear differences are noticed. Nevertheless, the tendency is similar indicating that more experiments are necessary for statistical analysis.

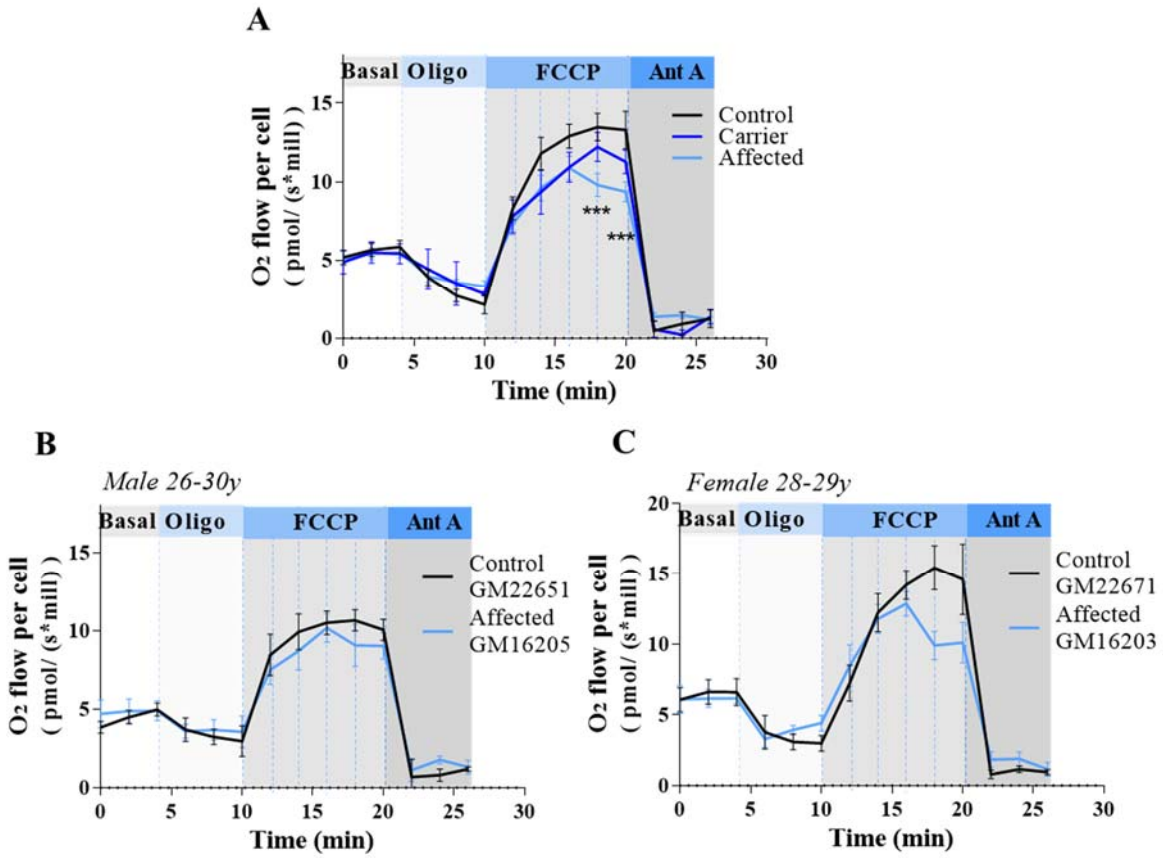

Figure 131. Mitochondrial respiration of a pool of LCL from controls, carriers and affected cells. In A, representative respirometry graph of LCL from controls, carrier and affected cells in Oroboros-2K Oxygraph instrument. An injection of 2µg/mL Oligomycin, 5 injections of 0,5µM FCCP and one injection of 2,5µM Antimycin A have been analysed during the time. Each experiment has been analysed with DatLab 4 program and normalised on cell number. Data are Mean ± SEM of n=18 independent experiment of controls (used a pool of GM22641- GM22671 - GM22651 - GM15851 - LFA120 - LFA195 controls cells), n=4 independent experiments of carriers (used a pool of GM12211 - GM16215 carrier cells) and n=20 independent experiments of affected cells (used a pool of GM16798 - GM16203 - GM16205 - GM16223 - GM16209 - GM15850 - GM16214 affected cells). In B and C, a control line and an affected line of similar age and sex (Male 26-30 years in B and Female 28-29 years old in C) is represented. Data are Mean ± SEM from n=5 independent experiments in B and n=6 in C. Significant values compared to control are indicated as (*). **Dr F. Delaspre, T. Ximelis or A. Sanz-Alcazár have kindly performed cultures.**

DISCUSSION

DISCUSSION

Nowadays, it is widely known that Friedreich Ataxia is a rare multi-organ disease, without a cure, affecting mainly the heart, neurons and pancreas, due to reduced levels of frataxin protein, a nuclear-encoded mitochondrial protein ubiquitously expressed (Campuzano et al., 1997). Despite it is generally accepted that GAA repeats expansion in the first intron of *FXN* gene and/or point mutations cause the reduction of frataxin, the functionality of this protein is still a matter of debate and many efforts are ongoing to improve quality of life and, hopefully, find a cure. Even if all cells in the organism express frataxin, these tissues, heart, neurons and pancreas, show the most abundant frataxin levels, indicating that its function is more critical there (Pastore, 2013). Many FA models exist decreasing frataxin in different ways and using yeast, mouse, rat, human cells etc. Despite the pros and cons of each FA model, the better models, ideally from humans and/or containing GAA repeats expansion, remain the ones that utilize these affected tissues (Perdomini et al., 2013). In particular, between different types of neurons, DRG neurons and cerebellar granule cells are the most affected neurons in the disease (Koeppen & Mazurkiewicz, 2013).

"*Why are these neurons more affected in FA?","What makes them so sensitive to the reduction of frataxin levels?","Why do these cells need more frataxin than other cells in the body?"*

These are the more intriguing questions that researchers in the field are still asking. However, there are some hypotheses. Neurons, cardiomyocytes and pancreatic β-cells are excitable cells in which a stimulus, external or internal, induces the propagation of an action potential, leading to the release of neurotransmitters (neurons), vesicles (β-cells) or contraction/relaxation cycle (cardiomyocytes). For these functions, these cells need more mitochondria than other cells, and the mitochondrial protein frataxin is essential for the correct function of this organelle (Miura, 2002). Among neurons, DRG sensory neurons represent the cells with the longest axons in the body (Nascimento et al., 2018). Axons are rich in mitochondria and ER organelles, but also microtubules for the movement of vesicles and mitochondria in the synaptic terminals, where mitochondria accumulate and together with vesicles are important for neuronal communication (Mironov & Symonchuk, 2006). Therefore, mitochondrial damage can reflect the alterations in synaptic function, especially for those neurons with longer

axons, for example, having problems in mitochondrial movements. Indeed, the presence of a fenestrate Blood-DRG-Barrier, allowing minor protection than other neurons in the body, renders DRG neurons more prone to external stimuli, which can also be toxic (Reinhold & Rittner, 2020).

"What is (are) the function(s) of frataxin?"

Frataxin seems to determine early defects in ISCs biogenesis, which, in turn, induce mitochondrial iron overload, heme group maturation dysfunction, energy deficits due to heme and iron-sulfur cluster containing proteins in TCA and ETC, alterations in mitochondrial membrane potential and Ca^{2+} homeostasis, gene expression alterations and oxidative stress. However, ISCs biogenesis defects are not always present in FA models, and more studies are necessary to determinate frataxin function. Although frataxin function(s) need to be better defined, whatever role it has, it seems clear that frataxin protects mitochondria. Consequently, it protects cells that need mitochondria for their functions, such as neurons where it is involved in axonal transport, growth cone and actin dynamics, neurotransmission, myelin protection, autophagy and apoptotic cell death (Carletti & Piemonte, 2014; Pastore, 2013).

Although this thesis will not solve these questions, it points out new functionalities for this protein in DRG neurons and suggests a flow-chart of events. Thus, it proposes a drug screening in these neurons and compares some results with lymphoblastoid cell lines from patients. To compare this work with others, it should be taken into account the use of aphidicolin to block satellite cells proliferation and only NGF in DRG neurons culture media.

- ***Analysis of the connection between lack of frataxin and calcium homeostasis, mitochondrial defects, apoptosis and iron alterations in frataxin-deficient DRG neurons.***

To this aim, the primary culture of neonatal rat DRG neurons have been isolated and frataxin has been decreased using RNA interference. The resulting frataxin-deficient DRG neurons show mitochondrial dysfunction, Ca^{2+} unbalance, mPTP opening, apoptotic cell death and neurodegeneration, but also alterations in vitamin D_3 metabolism and iron-sulfur proteins. Our group's previous results showed that reduction of frataxin, by using shRNA targeting frataxin mRNA, induces apoptotic cell death and

neurodegeneration after 5 days of interference (Mincheva-Tasheva et al., 2014). These results recapitulate some phenotypic features of the disease found in patients, such as the loss of DRG sensory neurons and presence of residual nodules where neurons are lost (Koeppen et al., 2013), but also some characteristics found *in vitro*, such as dying-back axonal degeneration in DRG neurons of FA mice (Mollá et al., 2017). By looking deeper at the soma diameter of neurons lost, it has been clear the apoptotic cell death of medium-large DRG neurons in frataxin deficiency and a general reduction of soma size of all subpopulations. The particular loss of medium-large DRG neurons recapitulates the disease' characteristics in which is present an early involvement of proprioceptive neurons, the biggest neurons in DRGs (Koeppen et al., 2009, 2013). Neuronal degeneration and apoptotic cell death are already visible on day 3 after viral transduction; meanwhile, pro-apoptotic proteins such as Bax are still not upregulated, probably indicating that neuronal degeneration occurs prior to the alterations in gene expression that provoke apoptosis, leading to, for example, an increased presence of Bax/Bcl-2 ratio at 5 days after transduction.

"How does frataxin protein induce apoptotic cell death?" "What are the early mechanisms in frataxin deficiency?"

To answer these questions, the alterations at day 1 after lentivirus transduction have been studied in order to indicate a flow-chart of events. The early events in frataxin deficiency observed in frataxin-deficient DRG neurons are mitochondrial depolarisation, NCLX reduction and Ca^{2+}_i increase (probably predominantly mitochondrial). These events indicate that the first mechanisms of frataxin depletion occurs in mitochondria and are linked with mitochondrial function and Ca^{2+} homeostasis. Interestingly, mitochondrial depolarisation, detected by using TMRM and JC-1 assays and already present in several FA models (Abeti et al., 2015, 2016; Bolinches-Amorós et al., 2014; Shidara & Hollenbeck, 2010), can affect NCLX function (Kostic et al., 2018) and NCLX dysfunction can affect the Ca^{2+} balance in the cell, but also mitochondrial membrane potential (Kostic & Sekler, 2018; Palty & Sekler, 2012). The link between Ca^{2+} and $\Delta\Psi_m$ is so interconnected that is difficult to understand which is the first event. Interestingly, mild depolarisation inhibits NCLX function, while complete depolarisation can reverse its mode of action (Kostic et al., 2018). Frataxin-deficient DRG neurons show mild depolarisation, compared with the effects of CCCP, suggesting $\Delta\Psi_m$-dependent inhibition of NCLX. Nevertheless, an

increase in Ca^{2+}_m could activate mitochondrial calpains that could cleave NCLX, reducing its function and exacerbating Ca^{2+}_m overload, and the rise of Ca^{2+} in mitochondria could affect the gradient of ions between matrix and IMS, rendering the $\Delta\Psi_m$ less negative inside (Kar et al., 2009). Thus, in frataxin deficiency, mild $\Delta\Psi_m$ could aggravate NCLX inhibition of remaining protein. Secondarily, depolarisation could also induce alterations in oxidative phosphorylation with ATP synthase working in reverse mode, consuming ATP instead of synthesising and extruding H^+ in the IMS in order to maintain the $\Delta\Psi_m$ (Nakamoto, Baylis Scanlon, & Al-Shawi, 2008). This event has been observed by analysing $\Delta\Psi_m$ dynamics upon addition of oligomycin in frataxin-deficient DRG neurons at 5 days after lentivirus transduction, but also in cerebellar granule cells of YG8R FA model (Abeti et al., 2016). ATP hydrolysis induces lower ATP content and could be due to depolarisation, but also modification of thiol groups and the presence of Ca^{2+}_m and Ca^{2+}-ATP (Bernardi et al., 2015).

"How does frataxin deficiency induce mitochondrial calcium dyshomeostasis?"

The balance between mechanisms of uptake and release regulates the Ca^{2+}_m content. The Na^+/Ca^{2+} exchanger NCLX is the main component responsible for Ca^{2+}_m efflux in excitable cells (Palty et al., 2010), inhibited by mild depolarisation (Kostic et al., 2018). Its progressive reduction in protein levels and mild depolarisation correlate with lower functionality observed at 5 days after lentivirus transduction. On the contrary, Ca^{2+}_m uptake is regulated by $\Delta\Psi_m$, by boosting the positive ions flux when mitochondria are more negative inside (hyperpolarised). However, low extra-mitochondrial Ca^{2+} levels (below 1-10µM) can provoke a kinetic modulation of the uptake, rather than thermodynamic (Nicholls, 1978), in which mild depolarisation could regulate the rate of Ca^{2+} efflux but no influx. Digitonin-permeabilised frataxin-deficient DRG neurons stimulated with a physiological $[Ca^{2+}]$ in a pseudo-intracellular solution (~100nM $[Ca^{2+}]_{free}$) allows us to understand the kinetic dynamics of Ca^{2+}_m in frataxin-deficiency when neurons are stained with Rhod5N-AM probe, a technique learned in the Dr A. Abramov laboratory (Abramov et al., 2007; Britti, Ros, et al., 2020; Gandhi et al., 2009). The resulting fluorescent peaks of Ca^{2+} indicate slower NCLX-mediated Ca^{2+}_m efflux and increased peak amplitude. Although this characteristic could indicate an increase of Ca^{2+} inside mitochondria, it could be a consequence of this slower Ca^{2+} efflux as well as technical issues, such as the increased Ca^{2+} ions per cell in frataxin deficiency due to a lower number of neurons/well.

However, the reduction in MICU1 protein levels, which in MICU1-KO mice provokes ataxia and Ca^{2+}_m uptake (Liu et al., 2016); MICU3 protein levels, which influences Ca^{2+}_m uptake in neuronal cells (Patron, Granatiero, Espino, Rizzuto, & De Stefani, 2019), but also lower levels of Afg3l2, which lead to the excess of EMRE-MCU complex, the formation of a MCUc constitutively open channel (König et al., 2016) and SCA disease (Di Bella et al., 2010), could indicate an alteration in Ca^{2+}_m influx. On the contrary, neither MCU nor LONP1 protein levels are affected by frataxin deficiency, indicating that these reductions do not generally affect mitochondrial proteins and that are directly related to alterations in Ca^{2+} balance.

"How does frataxin deficiency induce intracellular calcium dyshomeostasis?"

It should be taken into account that the dynamics of Ca^{2+} in digitonin-permeabilised cells could be different from those present in entire cells. In fact, ER, MAMs and $[Ca^{2+}]_c$ could influence the Ca^{2+} dynamics (Marchi et al., 2018; Patergnani et al., 2011), as observed in CCCP-stimulated Fura-2 stained frataxin-deficient DRG neurons, in which cytosolic Ca^{2+} buffer capacity is decreased, probably for decreased Ca^{2+}_m influx, more distance between ER-mitochondria contacts or decreased (or increased) ER Ca^{2+} uptake (release), or a combination of these events. Nevertheless, the CCCP stimulus releases Ca^{2+}_m content in the cytosol, revealing again that mitochondria in frataxin deficiency contain more Ca^{2+}. Interestingly, reduction of NCLX protein levels have been related to decreased ER Ca^{2+} content (B. Kim et al., 2012; Takeuchi et al., 2020), a characteristic noticed also in frataxin deficiency (Abeti, Brown, et al., 2018), suggesting that frataxin-deficient DRG neurons could show altered communication between these organelles, such as more distance between ER-mitochondria or altered ER uptake/release of Ca^{2+}. Both mechanisms are already observed in frataxin deficiency and probably due to oxidative stress and/or the recently finding of frataxin in MAMs (Abeti, Brown, et al., 2018; Rodríguez et al., 2020). Indeed, the glucose-related protein GRP75/mortalin, a member of MAMs proteins together with VDAC, Bcl-$_{XL}$ and IP_3R, shows decreased levels in frataxin-deficient DRG neurons, suggesting more ER-mitochondria distance. As observed for RyR and SERCA functions (Abeti, Brown, et al., 2018), also GRP75 levels and functions could be damaged by oxidative stress. In fact, this protein could be degraded by metal-catalysed oxidation (Irazusta et al., 2008) and/or by calpains (Ozaki et al., 2009). On the contrary, another glucose-related protein GRP78 present in ER and related to ER stress remains stable in this model.

Furthermore, TAT-BH4 treatment, a construct in which the anti-apoptotic domain BH4 of Bcl-$_{XL}$ is fused with TAT peptide for cellular internalisation (Mincheva-Tasheva et al., 2014), interacts with IP$_3$R, inhibiting ER Ca^{2+}release (Rong et al., 2009), thus, also suggesting in this model decreased ER Ca^{2+} content for activation of release mechanisms, which could affect $[Ca^{2+}]_c$ and $Ca^{2+}{}_m$ uptake.

"How does frataxin deficiency decrease calcium homeostasis protein levels?"

It is unknown the mechanism leading to a decrease in the proteins levels of MICU1, MICU3 and Afg3l2, significant for $Ca^{2+}{}_m$ influx. However, it has been observed that the reduction in MICU1 protein levels could occur due to proteasome degradation (Matteucci et al., 2018), gene expression repression in hypoxic conditions (Shanmughapriya et al., 2018), miRNAs-mediated mRNA regulation (Rao et al., 2020), but also mitochondrial Akt kinase-mediated phosphorylation which decreases its stability, thus the MICU1 levels. Interestingly, mitochondria-localised phosphatase PTEN counteract the action of Akt by inhibiting its activity and increasing MICU1, but also MICU2 levels (Marchi et al., 2019). In this work, the reduction of PTEN levels in frataxin deficiency could increase Akt-mediated phosphorylation of MICU1, reducing its levels, and it cannot be excluded a similar regulation for MICU3.

Furthermore, it has been shown that the deficiency in Afg3l2 protein levels is a late event in our model. This reduction could be due to secondary events of frataxin deficiency such as alteration in gene expression or, by being an ATP-dependent protease, could be linked to the metal-catalysed oxidation of nucleotide-binding proteins already observed in frataxin deficiency (Irazusta et al., 2008). Whatever the mechanism reducing Afg3l2 levels could be, its lower activity induces a constitutive $Ca^{2+}{}_m$ uptake and neurodegeneration, by increasing the presence of EMRE, thus, EMRE-MCU complex and avoiding the binding of MICU1-MICU2 heterodimer on MCU (König et al., 2016; Tsai et al., 2017), where free MICU1-MICU2 heterodimers in the IMS could be the target of proteins for degradation or Akt-mediated phosphorylation.

"How does frataxin deficiency induce mitochondrial protein import/processing defects?"

The deficiency of Afg3l2 protease also induces alterations in Pink1 protein processing in mitochondria, with decreased levels of 43kDa form (Thomas et al., 2014). This cytosolic form of Pink1 has been linked with PKA-dependent neurite outgrowth and regeneration (Dagda et al., 2014). However, the alteration in Pink1 processing could also be an indirect effect of mitochondrial protein import defects, as $\Delta\Psi_m$ and glucose-related protein mortalin/GRP75 are necessary for the correct mitochondrial import of several nuclear-encoded mitochondrial proteins, such as Pink1. In fact, mitochondrial depolarisation induces an augment of 64kDa-form Pink1 on the MOM, avoiding its import and generation of 43kDa-form (Becker et al., 2012; Jin et al., 2010). Frataxin-deficient DRG neurons show mitochondrial depolarisation but also decreased levels of GRP75, suggesting mitochondrial import defects, an event observed in frataxin deficienct-cells for the mitochondrial chaperone HSP60. Thus, mitochondrial depolarisation and lower levels of Afg3l2 and GRP75 proteins in frataxin-deficient DRG neurons correlate with cytosolic 43kDa-form Pink1 loss and neuronal degeneration.

"What are the functions of Pink1 in frataxin deficiency?"

The serine/threonine kinase Pink1 phosphorylates different substrates in mitochondria, regulating mitophagy (Eiyama & Okamoto, 2015), fission/fusion events (Kathrin Lutz et al., 2009) and mPTP (Gandhi et al., 2009; Gautier et al., 2012). Its deficiency has been linked with decreased phosphorylation of Ser^{258} in NCLX, thus, connecting Pink1 to Ca^{2+} unbalance events. Pink1-deficient cells, in fact, show lower pNCLX levels, leading to reduced activity and Ca^{2+}_m overload. The event can be restored by overexpressing PKA, which it has been considered the direct kinase for NCLX phosphorylation (Kostic et al., 2015). Despite the direct role of PKA phosphorylating NCLX, the deficiency of Pink1 induces an indirect event in this mechanism, probably involving the same PKA kinase. Frataxin-deficient DRG neurons not only show decreased levels of 43kDa form of Pink1 but also total levels, suggesting that the slower NCLX-mediated Ca^{2+}_m efflux could be due not only to reduction in NCLX levels and mild depolarisation but also to lower phosphorylation of the remaining protein. Deficiency of total Pink1 also correlates with lower levels of PTEN (Unoki &

Nakamura, 2001), a phosphatase provoking ataxia when depleted in mice (Backman et al., 2001) and substrate for calpains (Briz et al., 2013). For these reasons, reduction of PTEN protein levels have been observed in frataxin-deficient DRG neurons, and its reduction is a late event in the cell model of the disease. PTEN can localise near plasma membranes, in the nucleus, mitochondria, ER and secreted out of the cell, with different functions (Bononi et al., 2013; Chung & Eng, 2005). However, it is often observed in mitochondria and cytosol in apoptosis (Chung & Eng, 2005). No data are provided about its localisation in frataxin deficiency; however, some studies indicate that an isoform of PTEN, PTEN-L, which localises on MOM, can antagonise the function of Pink1, inhibiting mitophagy (Wang, Wang, et al., 2018). An event observed in frataxin-deficient liver cell lines, in which the inhibition of Pink1/Parkin-dependent mitophagy provokes an accumulation of damaged mitochondria and lipid droplets (Liu et al., 2018). Thus, deficiency of total Pink1 can inhibit mitophagy (Eiyama & Okamoto, 2015), promote fission instead of fusion events, by the fact that Drp1, an essential fission protein, is a substrate of Pink1 (Kathrin Lutz et al., 2009), but also, decreasing the PKA-dependent phosphorylation of NCLX, can promote mPTP opening and cell death (Gandhi et al., 2009).

"How does frataxin deficiency induce alterations in acetylation state and mPTP opening?"

The mPTP opening is regulated by $\Delta\Psi_m$, $Ca^{2+}{}_m$, matrix pH and Pi, but also oxidative stress and post-translational modifications of CypD, a protein involved in pore opening one component of the pore. In fact, Gsk3β-mediated phosphorylation or Sirt3-mediated acetylation of CypD promotes mPTP opening (Bernardi et al., 2015). Sirt3 is the main NAD^+-dependent deacetylase present in mitochondria, which shows low levels and activity in several frataxin deficiency models (Stram et al., 2017; Wagner, Melanie Pride, Babbey, & Mark Payne, 2012). Interestingly, an increase of $Ca^{2+}{}_m$ can activate the TCA cycle with the generation of NADH used by ETC for ATP production (Llorente-Folch et al., 2015). A lower Sirt3 activity has been linked with an accumulation of NADH generated from the TCA cycle that cannot be used by ETC proteins for defects in oxidative phosphorylation, leading to a decrease in ATP, NAD^+/NADH ratio (redox state) and lower activity of NAD^+-dependent Sirt3 (Wagner et al., 2012). For this reason, the use of nicotinamide mononucleotide (NMN), a precursor of NAD^+, in a FA mouse model shows Sirt3-dependent beneficial effects (Martin et al., 2017). Sirt3 can

de-acetylate and regulate the activity of different substrates, such as subunits of OXPHOS complexes, regulating oxidative phosphorylation and ATP production; LONP1, regulating the degradation of damaged proteins; fork-head box O-3 (FOXO3), a transcription factor regulating Pink1/Parkin mitophagy, fusion and fission mechanisms; OPA1, promoting fusion mechanisms; SOD2, involved in oxidative stress response; CypD regulating mPTP opening etc. Besides, it can indirectly induce Sirt1-mediated deacetylation of PGC1α, which interacts with NRF1/2 to activate TFAM, thus, promoting the synthesis of OXPHOS enzymes and mitochondrial biogenesis (Meng et al., 2019), but also PGC1α can interact with estrogen-related receptor α (ERRα) to induce a PGC1α-ERRα-mediated *SIRT3* gene expression and ROS scavenging (Kong et al., 2010). All these functions converge into protecting mitochondria. In this work, low levels of Sirt3 are observed at 5 days after lentivirus transduction, suggesting decreased activity, probably for decreased PGC1α-mediated expression since it has been noticed a strong correlation between *FXN* mRNA and PGC1α protein levels (Coppola et al., 2009). Therefore, Sirt3 deficiency can induce general mitochondrial damage, culminating with acetyl-SOD2-mediated oxidative stress and acetyl-CypD-mediated mPTP opening and apoptotic cell death (Anamika et al., 2019).

The analysis of the acetylation state of its substrates allows us to understand the activity of Sirt3. Antibodies detecting acetylated proteins are difficult to find commercially and generate. However, a commercially available antibody can detect the acetylation of lysine K68 in SOD2 protein. Preliminary results in this work indicate that the acetyl-SOD2 protein levels tend to increase compared to SOD2 total levels under frataxin deficiency, suggesting a lower activity of Sirt3 and a major exposure to oxidative stress in mitochondria. The preliminary results regarding the reduction of SOD1 protein levels, probably by degradation triggered by metal-catalysed oxidation (Irazusta et al., 2008), also suggest a major exposure to intracellular oxidative stress in frataxin deficiency. Despite these are only preliminary results, they are useful to suggest alterations in Sirt3 activity and pointing to acetyl-CypD formation, which, in turn, would trigger mPTP opening.

"How does frataxin-mediated mPTP opening induce cell death?"

All these events, mitochondrial depolarisation, Ca^{2+}_m overload, NCLX and Pink1 deficiency, but also mitochondrial acetylation state are related to mPTP opening. Thus, frataxin deficiency induces mitochondrial apoptotic cell death with the increased permeabilisation of MOM, release in the cytosol of Ca^{2+}, caspase 3, pro-caspase 9, cytochrome c, SMAC/Diablo etc. (Igoillo-Esteve et al., 2015; Mincheva-Tasheva et al., 2014; Santos et al., 2001). All these proteins and ions mediate the cascade of signals involved in apoptotic cell death, such as the auto-activation of pro-caspase 9 becoming caspase 9 and apoptosome formation (Martin, 2010). Some of these events have been seen in frataxin-deficient DRG neurons, by the fact that the TAT-BH4 treatment closes VDAC, avoiding MOM permeabilisation and apoptotic cell death (Mincheva-Tasheva et al., 2014), or by the detection of pro-caspase 9 and caspase 3 cleavages which, when activated, cleave substrate proteins. One of the substrates of the Ca^{2+}-activated caspase 3, but also calpain 1, is α-fodrin (Pike et al., 1998). The presence of 150/145kDa and 120kDa fragments of α-fodrin represent a useful apoptotic marker, as it indicates the presence of Ca^{2+}, activated caspase 3 and calpain 1 (Zhang et al., 2009). This marker has been used in frataxin-deficient DRG neurons, showing a progressive increase in fragmentations starting from day 3 after lentivirus transduction. Interestingly, Tau, a microtubule-associated protein, can also be fragmented by caspase 3 and calpain 1 and 2, generating toxic fragments leading to neurodegeneration (Liu et al., 2011). The portion named Tauk18, which is present in both fragments, can inhibit NCLX function, leading to Ca^{2+}_m overload and mPTP opening (Britti, Ros, et al., 2020); thus, it could exacerbate the effect due to reduced protein levels under frataxin deficiency.

Ca^{2+} released in the cytosol during mPTP opening can activate a series of signals to reprogram gene expression, inducing apoptotic cell death (Rasola & Bernardi, 2011). One of the transcription factors regulated by Ca^{2+} is CREB, which in some particular situations (e.g. hypoxia) can be phosphorylated to induce the up-regulation of Bax (Delivoria-Papadopoulos, Ashraf, & Mishra, 2007), an event mediated by nitric oxide synthase (NOS) (Mishra, Ashraf, & Delivoria-Papadopoulos, 2002). Previous results indicated that frataxin-deficient DRG neurons show increased neuronal NOS (nNOS), pCREB/CREB ratio and Bax up-regulation, suggesting that increased Bax levels could be mediated by pCREB (Mincheva-Tasheva et al., 2014). Interestingly, hypoxic/ROS conditions can inactivate PTEN, which cannot dephosphorylate CREB, leading to an

even more pCREB/CREB ratio (Steven et al., 2020). Thus, decreased levels of PTEN observed in this work could correlate with the up-regulation of Bax in the final steps of the disease.

Another Ca^{2+}-regulated transcription factor is NFAT. NFAT can be hyper-phosphorylated by Gsk3β (pNFAT) and hypo-phosphorylated by calcineurin (NFAT). The increased presence of Ca^{2+} in the cytosol can activate calcineurin, which hypo-phosphorylates and activates NFAT that can translocate into the nucleus and change gene expression by up-regulating (down-regulating) genes for pro-apoptotic (anti-apoptotic) proteins (Hogan et al., 2003). Frataxin-deficient DRG neurons show activation of the isoform NFATc4, in the late steps of frataxin deficiency, as well as frataxin-deficient cardiomyocytes (Purroy et al., 2018). Interestingly, in sensory neurons, NFATc4 is activated by prolonged Ca^{2+} release from mitochondria, suggesting mPTP opening (Kim & Usachev, 2009), and promotes apoptosis and inflammation in neurons (Shioda, Han, Moriguchi, & Fukunaga, 2007), while in cardiac models promotes hypertrophy (Wilkins et al., 2004). Caspase 3-mediated cleavage of α-fodrin is visible at 3 days after lentivirus transduction, suggesting mPTP opening, however, NFATc4 is still phosphorylated in this moment. The slower calcineurin-mediated dephosphorylation and nuclear import of NFATc4 in DRGs, compared to NFATc3 (Ulrich et al., 2012), could explain the later activation in frataxin-deficient DRG neurons.

"Is frataxin involved in iron-sulfur cluster biogenesis?"

All these results indicate a possible role of frataxin in Ca^{2+} homeostasis, mitochondrial function and apoptotic cell death; however, the function of frataxin has been often related to iron homeostasis, iron-sulfur cluster biogenesis and heme biosynthesis (Busi & Gomez-Casati, 2012). In this work, two iron-sulfur cluster proteins have been analysed in frataxin-deficient DRG neurons: FDX1 and Aco2. Deficiency in the activity of FDX1 has been previously described in frataxin deficiency (Napoli et al., 2007). Indeed, FDX1 has been observed in the mechanism of iron-sulfur cluster biogenesis (Shi et al., 2012) and in the pool of proteins interacting with frataxin (Cai et al., 2018). Deficiency in the activity of Aco2 has been observed in several models of frataxin deficiency (Bulteau et al., 2004; Rötig et al., 1997); however, not all the models show this phenotype (Obis et al., 2014), for this reason, the role of frataxin in regulating iron-

sulfur cluster biogenesis is still a matter of debate. In this work, frataxin-deficient DRG neurons show decreased protein levels of FDX1, which have also been observed in lymphoblastoid cell lines from patients (Britti et al., 2021), but neither the activity nor the levels of Aco2 became altered.

"*Why are FDX1 protein levels decreased in frataxin deficiency, but not aconitase?"*

Up to now, this question remains to be answered; nevertheless, oxidative stress-mediated degradation of Fe/S cluster proteins could be a hypothesis for FDX1, but not for Aco2 (Cabiscol, Tamarit, & Ros, 2014; Tamarit et al., 2016). In fact, as reported in this thesis, neither the levels nor the activity of aconitase seems to be affected by frataxin deficiency. These results indicate that frataxin role in iron-sulfur cluster biogenesis could be more entangled than already described and/or there would be mechanisms that can bypass the frataxin deficiency for some, but not for all iron-sulphur proteins. Nevertheless, the activity of aconitase analysed in this work does not discriminate between cytosolic (Aco1) and mitochondrial (Aco2) aconitase form; thus, the cytosolic activity could mask the inactivation of mitochondrial one. In addition, aconitase activity has been performed on day 4 after lentivirus transduction. Further work in these directions should indicate if the activity remains stable also in later steps of frataxin deficiency. However, apart from a selective oxidative stress-mediated degradation of Fe/S cluster proteins, alterations in *FDX1* gene expression could also be present. Interestingly, the *FDX1* promoter is upregulated by a steroidogenic factor (SF-1), which can be activated by cAMP/PKA pathway (Roumaud, Rwigemera, & Martin, 2017). SF1 regulates the expression of genes involved in steroidogenesis, such as steroidogenic acute regulatory protein (STAR) (Roumaud et al., 2017). STAR mediates the translocation of cholesterol from cytosol to mitochondria to be converted in pregnenolone by the cytochrome P450 Cyp11a1, that needs FDX1 for its action, and then in progesterone (Melcangi et al., 2014). In addition, SF1 has also been detected in neurons, where it mediates the steroidogenesis of progesterone and conversion in neuroprotective, myelin protective and anti-inflammatory metabolites. Lack of progesterone and these neuro-active metabolites has also been detected in neurodegenerative diseases (Melcangi et al., 2014). The fact that frataxin-deficient human ovarian cells produce less progesterone (Palandri et al., 2015) and that KIKO mice display impaired PKA-dependent lipolysis and high levels of cholesterol in the

blood (Turchi et al., 2020) are in line with ferredoxin activity and/or levels deficiency and steroidogenesis impairment in FA.

"What is the role of FDX1 and frataxin in vitamin D_3 metabolism?"

Apart from the role in iron-sulfur cluster biogenesis and progesterone synthesis, FDX1 has been observed in vitamin D_3 metabolism, by the fact that it has a role in releasing electrons used by cytochromes P450, such as Cyp27b1 and Cyp24a1. They, respectively, are the enzyme producing the active form of vitamin D_3 (calcitriol) and the enzyme regulating its levels (Estrada, 2018; Zalewski et al., 2016). The fact that FA patients show osteoporosis, often related to vitamin D_3 deficiency; these patients show lower blood levels of calcidiol, the precursor of the active form (Eigentler et al., 2014), and calcidiol and/or calcitriol are often reduced in the serum of patients with neurodegenerative diseases (Evatt et al., 2008); FDX1 is important for correct steroidogenesis and FA patients show steroids deficiency (Palandri et al., 2015); FDX1 is also needed for correct vitamin D_3 metabolism and FDX1 interacts with frataxin (Cai et al., 2018), all these facts moved our laboratory to study vitamin D_3 metabolism in frataxin-deficient DRG neurons. In fact, neurons can synthesize the active form of vitamin D_3 locally and express all the proteins necessary for its synthesis/degradation (Harms, Burne, Eyles, & McGrath, 2011). Thus, the levels of Cyp27b1 and Cyp24a1 have been analysed in frataxin-deficient DRG neurons, showing increased and decreased levels, respectively. Interestingly, Cyp27b1 and Cyp24a1 are heme-containing proteins (Annalora et al., 2010; Sawada, Sakaki, Kitanaka, Kato, & Inouye, 2001); thus, their function could be affected by frataxin deficiency and its increased and decreased levels, respectively, could not correspond to more calcitriol production. On the contrary, all these characteristics indicate a possible reduction of locally produced calcitriol in neurons.

- ***Evaluation of compounds that reverse toxic effects of frataxin deficiency in DRG neurons, in order to develop new therapeutic strategies to treat Friedreich Ataxia.***

The primary cultures of frataxin-deficient DRG sensory neurons have become a useful tool to study the basic mechanisms underlying apoptotic cell death and neurodegeneration in frataxin deficiency (Mincheva-Tasheva et al., 2014). Therefore, this model can contribute significantly to uncover new therapeutic approaches to treat FA.

"Why does BAPTA show beneficial effects under frataxin deficiency?"

Frataxin-deficient DRG neurons show alterations in Ca^{2+} homeostasis, with slower NCLX-mediated Ca^{2+}_m efflux, Ca^{2+}_m overload and mPTP opening. Thus, it is not surprising that the Ca^{2+} chelator BAPTA-AM shows protective effects from apoptotic cell death, such as protection of α-fodrin from Ca^{2+}-activated calpain and caspase 3. Interestingly, BAPTA also improves NCLX protein levels. This finding agrees with the fact that BAPTA can enter into mitochondria (Abramov & Duchen, 2008), where probably chelates Ca^{2+}_{free} inhibiting indirectly mitochondrial calpains.

"Why do calpain inhibitors show beneficial effects in frataxin deficiency?"

As calpains can cleave NCXs in the plasma membrane (Wanichawan et al., 2014) and NCLX in mitochondria (Kar et al., 2009), this possibility has been analysed in frataxin-deficient DRG neurons by using two non-specific calpain inhibitors: MDL28170, a cell-permeable calpain and cathepsin B inhibitor, and Calpeptin, a cell-permeable calpain and cathepsin K inhibitor (Donkor, 2015). Both calpain inhibitors protect NCLX from calpain-mediated cleavage, suggesting that frataxin deficiency promotes this cleavage, probably in an indirect manner by increasing Ca^{2+}_m for calpains activation. Ca^{2+}_m overload and depolarisation promote mPTP opening and apoptotic cell death (Rasola & Bernardi, 2007, 2011). Thus, it is not surprising that both treatments, improving Ca^{2+}_m efflux and avoiding overload, protect frataxin-deficient DRG neurons from α-fodrin fragmentation and from apoptosis. This neuroprotective effect has been confirmed by reducing calpain 1 levels using RNA interference, which shows a similar effect as MDL28170 treatment (Britti, Delaspre, Tamarit, & Ros, 2020).

"Why do mPTP opening and calcineurin modulators show beneficial effects in frataxin deficiency?"

The role of mPTP in frataxin deficiency has been confirmed by using compounds modulating mPTP opening, showing neuroprotective effects. Cyclosporine A (CsA) is the best characterised inhibitor of CypD, leading to mPTP opening inhibition (Warne et al., 2016). Its effect is not specific, by the fact that also inhibits CypA, modulating calcineurin activity and, consequently, NFAT/pNFAT pathway (Matsuda & Koyasu, 2000). Its use in frataxin-deficient DRG neurons reduces α-fodrin fragmentation and cell death, suggesting an intrinsic or mitochondrial pathway (Purroy et al., 2018). However, no effects are observed on NCLX protein levels, indicating that the mPTP opening is secondary to NCLX reduction/cleavage. In addition, preliminary results indicate lower effects on calcineurin inhibition, by the fact that pNFATc4 protein levels seem to be shortly improved by the treatment, indicating that the beneficial effects of CsA should be ascribed to its function on mPTP. Other mPTP opening modulators such as TRO19622 (Olesoxime) and Debio025 (Alisporivir) have been used in the model, showing that Olesoxime, but not Alisporivir, protects cells from apoptotic cell death. Interestingly, Alisporivir is a modified analogue of CsA, without effects on calcineurin activity (Quarato et al., 2012). This result contrasts with the role of mPTP opening in frataxin deficiency; however, the concentrations and the mode of administration could mask its effect.

To confirm that the effects of CsA are due to mPTP opening inhibition, the neuroprotective action of CsA has been compared with FK506 (Tacrolimus), a compound modulating calcineurin activity (Sieber & Baumgrass, 2009). Survival analysis in frataxin-deficient DRG neurons shows no effect using Tacrolimus at the same concentration as CsA, despite preliminary results show a similar low effect on pNFATc4 levels. This low effect on pNFATc4 could be due to the concentration of Tacrolimus assayed; however, the similar CsA result suggests that probably other isoforms of NFATs should be included to study phosphorylation levels, such as NFATc3, which is faster dephosphorylated by calcineurin. Nevertheless, a lower Tacrolimus concentration induces an improvement in survival, suggesting an action more centred on calcineurin, thus, pNFATc4 levels, but in a minor extent than using CsA. These results indicate that the calcineurin pathway is implicated in frataxin deficiency; however, its effects could induce cell death in lower measure than mPTP

opening. Similar effects have been observed on mitochondrial swelling, a phenotype for mPTP opening, in frataxin-deficient cardiomyocytes (Purroy et al., 2018). In addition, no effect on NCLX protein levels has been seen in Tacrolimus-treated frataxin-deficient DRG neurons, suggesting that the NCLX deficiency is not due to NFAT activation.

"Can frataxin levels be increased exogenously?"

Despite these interesting results about Ca^{2+} dyshomeostasis and mPTP opening in frataxin deficiency, the role of frataxin in these mechanisms is unknown. Thus, other strategies to treat FA involve the first characteristic of the pathology (frataxin deficiency) by using compounds replacing or increasing frataxin protein levels.

Many efforts are ongoing in order to increase frataxin protein levels. To this aim, TAT-MTScs-FXN, a fusion protein composed by mature form of frataxin, the mitochondrial targeting sequence of citrate synthase and the HIV peptide trans-activator of transcription TAT, has been developed (Marcus et al., 2016) and used in frataxin-deficient DRG neurons to replacing frataxin exogenously (Britti, Delaspre, Feldman, et al., 2018). TAT is necessary for the internalisation of frataxin into the cell, while MTS from citrate synthase is necessary for mitochondrial localisation. The use of MTS from citrate synthase has been shown to be more efficient than its own FXN MTS (Marcus et al., 2016). Other constructs using TAT are already present in literature, as well as a TAT-FXN construct (Kim et al., 2012; Vyas et al., 2012). However, TAT-MTScs-FXN allows frataxin to enter into mitochondria and remain there easily. This is true for control neurons; nevertheless, the frataxin deficiency induces alterations in mitochondrial protein import, probably due to mitochondrial depolarisation and GRP75 reduction, that impairs the construct entry. In fact, the processing and maturation of TAT-MTScs-FXN construct is slower in frataxin-deficient cells, leading that the fusion protein needs to be used in the early steps to be effectively transported into mitochondria. In fact, its use 12h after lentivirus transduction provokes major neuroprotection than the same concentration at 24h. Despite the alterations in mitochondrial protein import, the construct has protective roles in frataxin-deficient DRG neurons, such as reduction of apoptotic cell death, apoptotic markers (e.g. α-fodrin and caspase 9 cleavages) and neurodegeneration (Britti, Delaspre, Feldman, et al., 2018), but also improvement of NCLX protein levels (Purroy et al., 2018), thus, Ca^{2+} homeostasis and mitochondrial protein import of the mitochondrial chaperone HSP60

(Britti, Delaspre, Feldman, et al., 2018). Decreased HSP60 activity has been reported in several neurodegenerative diseases (Hansen et al., 2002; Magnoni et al., 2013); however, the impact of HSP60 alteration under frataxin deficiency remains to be explored. Nevertheless, TAT-MTScs-FXN shows protective effects *in vitro*, but also *in vivo*, by increasing survival of the MSK-conditional mouse model of FA (Britti, Delaspre, Feldman, et al., 2018).

"Can frataxin levels be increased endogenously?"

The problems in mitochondrial protein import of TAT-MTScs-FXN strengthens the hypothesis that the endogenously increase of frataxin can have more beneficial effects than the exogenous deliver. For this reason, leriglitazone, a synthetic activator of PPARγ, has been used in frataxin-deficient DRG neurons, because another PPARγ agonist, Azelaoyl-PAF, increased FXN mRNA and protein levels in fibroblasts (Marmolino et al., 2009). The use of leriglitazone increases frataxin protein in this model, but also FA fibroblasts, and protects frataxin-deficient DRG neurons from apoptotic cell death, improving mitochondrial function (e.g. $\Delta\Psi_m$ and NCLX protein levels) (Rodríguez-Pascau et al., 2020).

The effects of leriglitazone on mitochondrial function can be ascribed to the augment of frataxin, but also to the up-regulation of PPARγ target genes, which induce PGC1α and NRF2/ARE pathway and then their downstream targets (Cai et al., 2018), such as SODs containing PPRE and ARE regions into their promoters (Corona & Duchen, 2016). For example, in fibroblasts, leriglitazone induces PGC1α and its downstream target GRP75, by regulating mitochondrial function (Rodríguez-Pascau et al., 2020), but also frataxin import and processing (Dong et al., 2019).

Lower nuclear localisation, thus, activation of NRF2 (Shan et al., 2013) and beneficial roles of NRF2 inducers (Abeti, Baccaro, et al., 2018) have been already observed in frataxin-deficient cells, with some of these agonists in clinical trials (see http://www.curefa.org). One of them is RTA-408 (Omaveloxolone), used to improve mitochondrial function. Leriglitazone, by increasing frataxin and PPARγ, PGC1α and NRF2 target genes, should have better neuroprotective effects than the specific NRF2 activator, Omaveloxolone. However, preliminary data in this model do not seem to argument this hypothesis. Nevertheless, leriglitazone shows beneficial effects on lipid

metabolism in frataxin-deficient cardiomyocytes and on motor performance in YG8sR mouse model of FA (Rodríguez-Pascau et al., 2020). For its beneficial roles *in vivo* and *in vitro* and the up-regulation of frataxin protein levels *in vitro* (Rodríguez-Pascau et al., 2020), nowadays, leriglitazone is in Phase II clinical trial http://curefa.org.

Interestingly, *in silico* analysis using EPD new database (https://epd.epfl.ch//index.php) of *FXN* promoter shows different VDRE regions for the VDR binding onto the DNA. This characteristic moved our laboratory to study frataxin protein levels using calcitriol, the natural ligand of VDR and active form of vitamin D_3, revealing that calcitriol, but not calcidiol, its precursor, increases frataxin protein levels in frataxin-deficient DRG neurons. Thus, calcitriol shows major neuroprotective effects in apoptotic cell death, axonal swelling and α-fodrin fragmentation than its precursor indicating a problem in the last step of calcitriol synthesis in frataxin deficiency. Furthermore, calcitriol increases frataxin protein levels in frataxin-deficient cardiomyocytes, where it prevents lipid droplets accumulation and mitochondrial swelling, and lymphoblastoid cell lines from patients (Britti et al., 2021). Calcitriol synthesis and regulation of its levels need respectively the heme-containing enzymes Cyp27b1 and Cyp24a1, both in the presence of FDX1 (Sakaki et al., 2005). All these proteins are altered in frataxin-deficient cells and calcitriol supplementation, but not calcidiol, restores their levels to those of controls. Calcitriol supplementation in frataxin-deficient DRG neurons, in fact, down-regulates Cyp27b1 and upregulates Cyp24a1 and FDX1 up to control levels, but also VDR. These results agree with the finding that *Cyp27b1* and *VDR* genes show a VDRE element in their promoter, which in the presence of calcitriol-bound VDR, represses Cyp27b1 and induces VDR expression (Blomberg Jensen et al., 2010; Murayama et al., 1998). Regarding FDX1, calcitriol could protect FDX1 from oxidative stress degradation, FDX1 mRNA and protein levels can be upregulated by calcitriol addition (Nguyen et al., 2004) or its levels could be a consequence of frataxin up-regulation.

Regarding Ca^{2+} homeostasis, calcitriol, but not calcidiol, increases NCLX protein levels and improves NCLX-mediated Ca^{2+}_m efflux, probably indirectly by decreasing Ca^{2+}_m content and calpain activation, therefore avoiding Ca^{2+}_m overload and, consequently, mPTP opening. Thus, the lower activation of caspase 3 and the release of Ca^{2+}_m into cytosol protect α-fodrin from caspase 3 and calpains-mediated fragmentation in calcitriol-treated frataxin-deficient DRG neurons (Britti et al., 2021). Although calcidiol has no effect on NCLX or FXN protein levels, minor effects are still visible on α-fodrin

fragmentation, probably because even calcidiol can bind VDR in a lower extent. In addition, the analysis of Ca^{2+}_m dynamics indicates that calcitriol improves not only NCLX-mediated Ca^{2+}_m efflux but also peak amplitude. The decrease in peak amplitude could be a reflection of Ca^{2+}_m efflux improvement, lower Ca^{2+}_m entry or a technical issue. The involvement of Ca^{2+}_m uptake should be taken into account considering the fact that calcitriol can upregulate PTEN (Berridge, 2016), which can antagonise the Akt-mediated phosphorylation of MICU1, thus, reducing Ca^{2+} entry (Marchi et al., 2019).

Calcitriol also regulates the expression of vitamin D-dependent Ca^{2+}-binding proteins calretinin, calbindin and parvalbumin through the presence of VDRE in their promoters. Although some studies indicate an increase of these proteins by calcitriol addition (Berridge, 2016), in this work, it has been observed a decrease. This reduction could be cell-type-specific; due to indirect changes in $[Ca^{2+}]_c$ or variations between the pool of treated and not treated-DRG neurons subpopulations present at the end of the experiments, as calretinin is mainly present in medium and small-diameter subpopulations of DRG neurons (Copray et al., 1994; Ren et al., 1993). However, the VDR transcription factor is present in the nucleus of all subpopulations of DRG neurons and cytoplasm of nociceptors, suggesting that all these neurons are modulated by calcitriol (Tague & Smith, 2011). Therefore, another explanation of calretinin reduction in calcitriol-treated frataxin-deficient DRG neurons could be linked to neurotrophins secretion. In DRG neurons, calcitriol induces the expression of NGF, EGFR, NT-3, GDNF, BDNF, NT-4 by the presence of VDRE in their promoters (Chabas et al., 2013). However, BDNF and NT-4 down-regulate *calretinin* mRNA and up-regulate *calbindin* mRNA in cortical neurons, while NT-3 down-regulate only *calretinin* mRNA and no effects have been seen with NGF (Fiumelli, Kiraly, Ambrus, Magistretti, & Martin, 2000). These finding indicates that calcitriol can modify the neurotrophic environment and in response down-regulate calretinin protein levels. In addition, it can induce the expression of NT-3/4 and BDNF, which protect respectively proprioceptive and mechanoreceptor DRG neurons from cell death, which are the main DRG neurons affected in frataxin deficiency. Thus, the fact that frataxin-deficient DRG neurons increase calretinin protein levels could be due to selective cell death of medium-large diameter DRG neurons and/or an insufficient locally synthesis of calcitriol that can modify the neurotrophic environment, leading to the same effect. This effect has not

been observed by treating frataxin-deficient DRG neurons with Cyclosporine A or Tacrolimus, indicating that release of Ca^{2+} from mitochondria and Ca^{2+}-dependent activation of NFAT are not involved in this mechanism, thus, discarding the hypothesis of calretinin expression as an indirect effect of $[Ca^{2+}]_c$.

Apart from the regulation of Ca^{2+} homeostasis, calcitriol is also a potent anti-oxidant response inducer. Its effect seems due to the activation of NRF2 in the calcitriol/NRF2/Klotho pathway, by the presence of a VDRE in *NRF2* promoter, thus being a natural NRF2 inducer (Berridge, 2016). All these actions can result in the restoration of mitochondrial function, a characteristic seen in calcitriol-treated frataxin-deficient DRG neurons, which rescue $\Delta\Psi_m$ and probably the production of ATP, by involving mechanisms of ATP synthesis instead of hydrolysis (Britti et al., 2021). Even if the connection between calcitriol and frataxin in unknown, calcitriol mechanisms of action, therapeutic ranges and side effects are studied for decades, rendering this drug an easily therapeutic approach to treat FA.

"Can modulation of gene expression be beneficial in frataxin deficiency?"

Restoration of $\Delta\Psi_m$, α-fodrin fragmentation and apoptotic cell death has also been observed in this work using a new treatment, the compound here referred as M. This compound alters gene expression by binding guanine-cytosine rich regions of DNA and inhibiting the action of a specific transcription factor in these regions. Neither this compound nor the transcription factor inhibited has been never considered to treat FA; thus, the compound's name is protected for the possible involvement in a patent of use. As compound M strongly binds DNA, analogues of this drug have been developed for a lower DNA binding and, probably, minor side-effects. Compound M and analogue S have been tested in frataxin-deficient DRG neurons, indicating extraordinary protection from apoptotic cell death with only one single supplementing dose, particularly for compound M. In addition, compound M seems to be able to regulate the expression of a particular kinase involved in FA. Thus, the effect of compound M and the kinase inhibitor compound P have been compared, revealing better neuroprotection using compound M. The survival and axonal degeneration analysis indicate a major role of compound M protecting neurites than compound P. As compound M acts upstream compound P, it could involve axonal protection/ regeneration mechanisms.

In summary, frataxin-deficient DRG neurons have been used to screen several therapeutic approaches, revealing that the Ca^{2+} chelator BAPTA-AM and the compound M involved in gene expression, show major neuroprotection compared to compounds modulating calpain inhibition, mPTP opening, calcineurin activity and even frataxin increase. These results indicate that Ca^{2+} dyshomeostasis has a central role in the disease, at least in DRG neurons, and that the alterations in gene expression can revert the phenotype.

- ***Compare frataxin-deficient DRG neurons with lymphoblastoid cell lines from patients.***

Despite the fact that frataxin-deficient DRG neurons are a good model for studying the alterations due to frataxin deficiency, this model comes from rats and does not carry GAA repeat expansion. Therefore, several lymphoblastoid cell lines (6 controls, 2 carriers and 7 FA patients LCLs), carrying or not different GAA intronic expansions, have been used in this work to validate and compare disease alterations in patients. Interestingly, LCLs from patients, but also carriers in a minor measure, show decreased NCLX protein levels, indicating that reduction of NCLX is a common marker between these models. Decreased levels have also been detected in frataxin-deficient cardiomyocytes, strengthening the hypothesis (Purroy et al., 2018). In addition, the decreased NCLX levels in carriers, which present more frataxin than patients, indicate that even in this model NCLX reduction/cleavage is an early step in frataxin deficiency. As in frataxin-deficient DRG neurons, other mitochondrial proteins are not displaying such a reduction. In fact, no alterations in the chaperone HSP60 are observed in patients LCLs. Cell-type-specific mechanisms could explain the discrepancy between frataxin-deficient DRG neurons and patients LCLs regarding HSP60 processing/import. Furthermore, oxidative phosphorylation is often impaired in frataxin deficiency (González-Cabo et al., 2005; Lodi et al., 1999; Zarse, Schulz, Birringer, & Ristow, 2007) as well as in this work in LCLs from FA patients, where the analysis of O_2 consumption after FCCP addition using Oroboros oxygraph-2K indicates a lower respiration capacity under frataxin deficiency.

To sum up, Ca^{2+} dyshomeostasis, mitochondrial dysfunction, vitamin D_3 dysmetabolism, alterations in gene expression, mPTP opening and apoptotic cell death are mechanisms involved in the development of several neurodegenerative diseases.

This work provides enough data to confirm that Friedreich Ataxia should be added to this list for alterations in frataxin-deficient DRG neurons. At least in part, some of these alterations have been also found in lymphoblastoid cell lines from patients, not-affected cells in the disease. Thus, several treatments in this direction could have neuroprotective effects. Indeed, drug screening *in vitro* can select those drugs that can be futher used for *in vivo* analysis, accelerating clinical trials to find a cure.

CONCLUSIONS

CONCLUSIONS

I. Frataxin-deficient DRG neurons show alterations in Ca^{2+} homeostasis, provoked by alteration of NCLX, MICU1, MICU3, Afg3l2 protein levels; impaired NCLX function results in a decline of Ca^{2+}_m efflux, Ca^{2+}_m overload, and decrease in cytosolic Ca^{2+} buffer capacity.

II. Early events of frataxin deficiency are mitochondrial depolarisation, NCLX reduction and Ca^{2+}_m overload. Other mitochondrial proteins such as MCU and LONP1 remain stable.

III. Ca^{2+}_m overload and mitochondrial depolarisation induce mPTP opening and release of Ca^{2+} into the cytosol, starting the mitochondrial apoptotic cell death. Alteration in protein acetylation, due to decreased Sirt3 levels, could also play a role in this process.

IV. Ca^{2+}-activated calpain and caspase 3 mediate fragmentation of the apoptotic marker α-fodrin, which agrees with cell death and axonal degeneration in frataxin-deficient DRG neurons.

V. Cell death in frataxin deficiency mainly affects medium-large diameter DRG neurons, altering the pool of subpopulations presents in culture.

VI. Frataxin-deficient DRG neurons show alterations in mitochondrial function, such as mitochondrial depolarisation and maintaining $\Delta\Psi_m$ by ATP synthase working in reverse mode, but also in import or processing of mitochondrial proteins such as HSP60 and Pink1.

VII. Frataxin-deficient DRG neurons show late alterations in the phosphorylation state and gene expression, in fact, reduce the PTEN protein levels and dephosphorylate and activate NFATc4, suggesting an induction of apoptotic pathways.

VIII. Frataxin-deficient DRG neurons show decreased protein levels of the iron-sulfur protein FDX1, but not Aconitase levels and activity, indicating a selective reduction between iron-sulfur proteins.

IX. FDX1 is necessary for cytochromes functionality, such as Cyp27b1 and Cyp24a1, two mitochondrial enzymes of vitamin D_3 metabolism, indicating that frataxin deficiency alters this process.

X. The active form of vitamin D_3, calcitriol, shows major neuroprotective effects than its precursor, calcidiol.

XI. Calcitriol, but not calcidiol, and the PPARγ agonist leriglitazone increase frataxin protein levels.

XII. Ca^{2+} chelators (e.g. BAPTA), calpain inhibitors (e.g. MDL28170 and calpeptin), low expression of calpain 1 (shCALP1), frataxin replacement/increasing endogenously (e.g. calcitriol and leriglitazone) and exogenously (e.g. TAT-MTScs-FXN), mPTP opening modulators (e.g. cyclosporine A and olesoxime), calcineurin activity modulators (e.g. tacrolimus) and transcription factor inhibitors (e.g. compound M) show protective effects against apoptotic cell death. This screening indicates that BAPTA and compound M present major neuroprotection.

XIII. NCLX protein levels are increased by Ca^{2+}chelators (e.g. BAPTA) and calpain inhibitors (e.g. MDL28170 and calpeptin), indicating a possible calpain-mediated cleavage; by replacing frataxin endogenously (e.g. calcitriol and leriglitazone) and exogenously (e.g. TAT-MTScs-FXN), indicating that the process is reversible, but not modulating mPTP opening (e.g. Cyclosporine A) or calcineurin activity (e.g tacrolimus). Despite the improvement using all these compounds, restoration is observed only with TAT-MTScs-FXN treatment.

XIV. The $\Delta\Psi_m$ is improved by leriglitazone and MDL28170 treatments and restored by calcitriol and compound M.

XV. Lymphoblastoid cell lines from patients show decreased NCLX protein levels and lower mitochondrial respiratory capacity.

CONCLUDING REMARKS

CONCLUDING REMARKS

The research reported in this thesis has investigated the consequences of frataxin deficiency in DRG neurons and cells derived from patients indicating that both models show mitochondrial dysfunction with $Na^+/Li^+/Ca^{2+}$ exchanger reduced levels. The NCLX reduction induces slower Ca^{2+}_m efflux and Ca^{2+}_m overload, which, together with mitochondrial depolarization, provoke mPTP opening and, consequently, activation of Ca^{2+}-dependent proteases and apoptotic cell death. The mitochondrial Ca^{2+}-activated proteases calpains cleave NCLX, exacerbating its reduction, since Ca^{2+}-chelating agent and calpains inhibitors protect NCLX from cleavage. Interestingly, increasing frataxin (endogenously and exogenously) improves mitochondrial function and protect NCLX protein levels from cleavage, but not mPTP opening inhibitors, despite beneficial effects in neuronal survival. Overall, these results suggest the critical role of Ca^{2+} in FA. Furthermore, this thesis has also uncovered alterations in mitochondrial enzymes and proteins involved in Vitamin D_3 metabolism and transcription factors, indicating that calcitriol, the active form of Vitamin D_3, can be an easy therapeutic approach for FA and compounds such as leriglitazone, compound M and its analogues can be promising treatments for FA.

LISTS OF FIGURES · LISTS OF TABLES

LISTS OF FIGURES

Figure 1. Axonal pathology in peripheral and central nervous systems. 3
Figure 2. Dorsal root ganglia in Friedreich Ataxia (A-C) and Control (D-F). 4
Figure 3. Thoracic spinal cord in FA. 6
Figure 4. Dorsal spinal roots and dorsal nucleus of Clarke column in FA (A–E) and control (F–J) spinal cord. 7
Figure 5. Dentate nucleus in FA (A) and control (B). 8
Figure 6. Aspect of two hearts of FA patients. 9
Figure 7. Insulin staining in the islets of Langerhans of a control and a FA patient post mortem sections. 9
Figure 8. Correlation between age at onset and number of GAA repeats in patients. 11
Figure 9. Epigenetic changes in FA. 14
Figure 10. Frataxin structure. 15
Figure 11. A model of Fe–S biogenesis pathway in mitochondria. 18
Figure 12. Supposed mechanism of action of frataxin in Fe-S clusters biogenesis. 20
Figure 13. Fe-S cluster and heme biosynthesis are interconnected. 22
Figure 14. Iron homeostasis in FA. 24
Figure 15. Defects of OXPHOS/TCA system in FA. 28
Figure 16. Calcium homeostasis in normal cells and frataxin-deficient cells. 32
Figure 17. Pathophysiological effects of frataxin deficiency in neuronal cells. 37
Figure 18. FA treatment pipeline. 44
Figure 19. Disposition of DRG sensory neurons in Dorsal roots of spinal cord. 51
Figure 20. Embryonic development of DRG neurons. 52
Figure 21. Sensorial stimuli and neurotrophic receptors in adult DRG neurons. 53
Figure 22. DRG neurons subpopulations classified considering the function and the size. 54
Figure 23. Role of T-junction in the propagation of action potential to dorsal horn. 56
Figure 24. Schematic model of glutamate-glutamine cycle between DRG neurons and SGCs. 57
Figure 25. Channels for calcium influx. 61
Figure 26. TRPVs mediates calcium influx in DRG neurons. 61
Figure 27. Channels for calcium efflux. 63
Figure 28. Afg3l2-mediated regulation of mitochondrial calcium uptake. 65
Figure 29. Tissue specificity of MCU complex. 66
Figure 30. Schematic model of MCU complex assembling in wild type and Afg3l2-deficent cells. 67
Figure 31. PKA-mediated phosphorylation of NCLX restores Pink1-deficient neurons. 70
Figure 32. Structural differences between NCLX and NCX. 71
Figure 33. Calcium actions on mitochondrial respiration. In dashed red, enzymes regulated by matrix Ca^{2+}. 72
Figure 34. Structure of dimers of ATP synthase. 77
Figure 35. Posttranslational modifications of CypD regulate mPTP opening. 80

Figure 36. Intrinsic and extrinsic apoptotic cell death. 83
Figure 37. Substrates of mitochondrial calpains. 85
Figure 38. Chemical structures of mPTP inhibitors. 87
Figure 39. NFAT pathway and regulators. 91
Figure 40. Localisation and functions of PTEN and PTEN-L. 94
Figure 41. Actions of leriglitazone in frataxin-deficient cells. 97
Figure 42. Scheme of NRF2 activation. 98
Figure 43. FDXR-FDX-CyP450 complex. 100
Figure 44. Organs involved in calcitriol biosynthesis. 101
Figure 45. Genomic actions of calcitriol. 103
Figure 46. ROS and calcium signalling pathways regulated by calcitriol. 104
Figure 47. Calcitriol actions in calcium metabolism. 105
Figure 48. Map of pLKO.1-puro TRC cloning vector with shRNA construct and its transcription. 117
Figure 49. Protocol passages to obtain primary culture of neonatal rats DRG neurons. 130
Figure 50. Passages of gene silencing using shRNAs. 131
Figure 51. Measure of medium background using argon. 150
Figure 52. Aconitase and Isocitrate dehydrogenase reactions. 161
Figure 53. Citrate Synthase reaction and DTNB reduction. 163
Figure 54. Transduction efficiency in DRG neurons. 169
Figure 55. Frataxin depletion in DRG neurons. 170
Figure 56. Mitochondrial proteins remain stable during frataxin depletion. 171
Figure 57. DRG neurons subpopulation changes in frataxin deficiency. 173
Figure 58. Percentage of small, medium and large DRG neurons in frataxin deficiency. 175
Figure 59. Small FXN reduction induces mild mitochondrial depolarisation. 177
Figure 60. FXN deficiency induces mitochondrial depolarisation. 178
Figure 61. FXN deficiency induces ATP synthase working in "reverse" mode. 179
Figure 62. NCLX decrease initiates with a minor reduction of FXN levels. 180
Figure 63. MICU1 and MICU3 protein levels decrease in frataxin deficiency. 181
Figure 64. Early accumulation of $Ca^{2+}{}_m$ in FXN-deficient DRGs. 183
Figure 65. Punctate Rhod5N staining indicates the accumulation of Ca^{2+} in mitochondria. 184
Figure 66. Digitonin-permeabilised cells show increase of $Ca^{2+}{}_m$ in frataxin deficiency. 185
Figure 67. Frataxin-deficient digitonin-permeabilised cells show alterations in $Ca^{2+}{}_m$ efflux. 187
Figure 68. Ca^{2+} buffering alterations in frataxin-deficient DRG neurons. 190
Figure 69. Calretinin Ca^{2+}-binding protein levels increase in frataxin deficiency. 191
Figure 70. Frataxin deficiency determines decrease of GRP75/Mortalin, but not GRP78/Bip. 193
Figure 71. Frataxin deficiency determines defects in Hsp60 processing. 194
Figure 72. Pink1 processing is altered in frataxin-deficient DRG neurons. 197

Figure 73. Alteration in pro-apoptotic and anti-apoptotic proteins levels indicates apoptotic cell death in frataxin deficiency. 199
Figure 74. Mitochondrial Sirt3 deacetylase decreases in frataxin deficiency. 201
Figure 75. Progressive increase of calpain and caspase 3-cleaved fodrin fragments in frataxin-deficient DRG neurons. 202
Figure 76. Frataxin-deficient DRG neurons show progressive apoptotic cell death. 204
Figure 77. FXN-deficient DRGs show progressive axonal swelling. 205
Figure 78. Frataxin deficiency induces decreased levels of PTEN. 206
Figure 79. NFATc4 is activated, thus dephosphorylated, in frataxin deficiency. 208
Figure 80. Frataxin-deficient DRG neurons show normal amounts and activity of Aconitase. 209
Figure 81. Frataxin deficiency decreases ferredoxin 1 protein levels. 210
Figure 82. Enzyme levels for calcitriol biosynthesis and degradation are altered in frataxin-deficiency. 211
Figure 83. BAPTA treatment restores NCLX protein levels, without affecting mitochondrial protein amounts. 212
Figure 84. BAPTA treatment restores cell survival. 213
Figure 85. TAT-MTScs-FXN penetrates cells and targets mitochondria for processing, which is altered in frataxin deficiency. 215
Figure 86. TAT-MTScs-FXN restores defects of Hsp60 import into mitochondria. 217
Figure 87. NCLX protein levels are restored by TAT-MTScs-FXN treatment. 218
Figure 88. Pro-caspase 9 decreased levels in frataxin deficiency are restored by TAT-MTScs-FXN. 219
Figure 89. Fodrin cleavage is reduced by TAT-MTScs-FXN treatment. 220
Figure 90. TAT-MTScs-FXN protects from neurite degeneration. 221
Figure 91. TAT-MTScs-FXN protects frataxin deficient DRG neurons from cell death. 223
Figure 92. Calcitriol supplement reverts the alterations of its metabolism shown in frataxin deficiency. 225
Figure 93. Calcitriol induces an increase in mature frataxin protein levels. 226
Figure 94. Calcitriol induces NCLX and $Ca^{2+}{}_m$ recovery in frataxin deficiency. 228
Figure 95. $Ca^{2+}{}_m$ efflux is improved by calcitriol. 230
Figure 96. Calretinin protein levels decrease with calcitriol treatment. 231
Figure 97. Calcitriol treatment restores $\Delta\Psi_m$ and allows complex V working in forward mode. 233
Figure 98. Detailed graphs of above figure with statistical analysis. 235
Figure 99. Calcitriol protects fodrin from fragmentation. 236
Figure 100. Calcitriol reduces neurite degeneration and improves cell survival. 237
Figure 101. Calcidiol does not recover Cyp27b1 and FDX1 levels, indicating that could be not fully converted in calcitriol. 238
Figure 102. Frataxin levels are not increased by calcidiol supplementation. 239
Figure 103. Calcidiol protects fodrin from fragmentations. 240
Figure 104. Calcidiol protects frataxin-deficient DRG neurons from apoptosis. 241

Figure 105. Leriglitazone 500nM induces an increase in mature frataxin protein levels. 242
Figure 106. Leriglitazone 500nM induces an increase in NCLX protein levels. 243
Figure 107. Leriglitazone treatment restores $\Delta\Psi_m$. 244
Figure 108. Leriglitazone (500nM) does not induce changes in Aconitase activity in frataxin-deficient DRG neurons. 244
Figure 109. Leriglitazone reduces fodrin fragmentation, reduces neurite degeneration and improves cell survival. 246
Figure 110. Calpain inhibitors protect NCLX from cleavage. 248
Figure 111. Ca^{2+} accumulation in frataxin deficiency is improved by using MDL28170. 249
Figure 112. $\Delta\Psi_m$ in frataxin deficiency is ameliorated by the use of MDL28170. 250
Figure 113. Calpain inhibitors protect fodrin from fragmentation. 251
Figure 114. Calpain inhibitors protect FXN-deficient DRGs from apoptosis. 252
Figure 115. Transduction efficiency of shRNA for calpain 1. 253
Figure 116. Pharmacological inhibition and RNAi reduction of calpain 1 give similar results in frataxin deficiency. 254
Figure 117. Fodrin fragmentation and cell death are decreased in CsA treated cells. 256
Figure 118. CsA fails to protect NCLX protein levels.. 257
Figure 119. Slight increase in NFTAc4 phosphorylation using CsA in frataxin-deficient DRGs. 258
Figure 120. Olesoxime (TRO19622), but not Alisporivir (Debio025), reduces apoptotic cell death in frataxin-deficient DRG neurons. 259
Figure 121. Tacrolimus (FK506) has low protective effect in neuronal survival of FXN-deficient DRGs. 260
Figure 122. Tacrolimus fails to protect NCLX protein levels. 261
Figure 123. Tacrolimus and CsA fail to reduce calretinin at the levels of controls. 262
Figure 124. Compound M could protect NCLX protein levels without increasing FXN levels. 264
Figure 125. $\Delta\Psi_m$ in frataxin deficiency is restored by compound M treatment. 265
Figure 126. Fodrin fragmentation seems to decrease with compound M 100nM. 266
Figure 127. Compound M protects frataxin-deficient DRG neurons from apoptotic cell death. 267
Figure 128. Analogues protect frataxin-deficient DRG neurons from apoptotic cell death in lesser extent than compound M. 268
Figure 129. Frataxin amounts in LCLs from healthy controls, carrier and patients. 269
Figure 130. NCLX protein levels decrease in LCLs from FA carrier and patients. 270
Figure 131. Mitochondrial respiration of a pool of LCL from controls, carriers and affected cells. 272

LISTS OF TABLES

Table 1. Point mutations in FA..... 11
Table 2. Plasmids used to produce lentivirus..... 117
Table 3. Drugs screened in frataxin-deficient DRG neurons..... 133
Table 4. Lymphoblastoid cell lines characteristics. 147
Table 5. Characteristics of primary antibodies used. 157
Table 6. Characteristics of secondary antibodies used..... 158

BIBLIOGRAPHY

BIBLIOGRAPHY

Abeti, R., Baccaro, A., Esteras, N., & Giunti, P. (2018). Novel Nrf2-Inducer Prevents Mitochondrial Defects and Oxidative Stress in Friedreich's Ataxia Models. *Frontiers in Cellular Neuroscience*, *12*(188). https://doi.org/10.3389/fncel.2018.00188

Abeti, R., Brown, A. F., Maiolino, M., Patel, S., & Giunti, P. (2018). Calcium Deregulation: Novel Insights to Understand Friedreich's Ataxia Pathophysiology. *Frontiers in Cellular Neuroscience*, *12*(264). https://doi.org/10.3389/fncel.2018.00264

Abeti, R., Parkinson, M. H., Hargreaves, I. P., Angelova, P. R., Sandi, C., Pook, M. A., … Abramov, A. Y. (2016). Mitochondrial energy imbalance and lipid peroxidation cause cell death in friedreich's ataxia. *Cell Death and Disease*, *7*(5), e2237. https://doi.org/10.1038/cddis.2016.111

Abeti, R., Uzun, E., Renganathan, I., Honda, T., Pook, M. A., & Giunti, P. (2015). Targeting lipid peroxidation and mitochondrial imbalance in Friedreich's ataxia. *Pharmacological Research*, *99*, 344–350. https://doi.org/10.1016/j.phrs.2015.05.015

Abramov, A. Y., & Duchen, M. R. (2008). Mechanisms underlying the loss of mitochondrial membrane potential in glutamate excitotoxicity. *Biochimica et Biophysica Acta - Bioenergetics*, *1777*(7–8), 953–964. https://doi.org/10.1016/j.bbabio.2008.04.017

Abramov, A. Y., Fraley, C., Diao, C. T., Winkfein, R., Colicos, M. A., Duchen, M. R., … Pavlov, E. (2007). Targeted polyphosphatase expression alters mitochondrial metabolism and inhibits calcium-dependent cell death. *Proceedings of the National Academy of Sciences of the United States of America*, *104*(46), 18091–6. https://doi.org/10.1073/pnas.0708959104

Ackroyd, R., Shorthouse, A. J., & Stephenson, T. J. (1996). Gastric carcinoma in siblings with Friedreich's ataxia. *European Journal of Surgical Oncology*, *22*(3), 301–3. https://doi.org/10.1016/S0748-7983(96)80023-0

Acquaviva, F., Castaldo, I., Filla, A., Giacchetti, M., Marmolino, D., Monticelli, A., … Cocozza, S. (2008). Recombinant human erythropoietin increases frataxin protein expression without increasing mRNA expression. *Cerebellum*, *7*(3), 360–365. https://doi.org/10.1007/s12311-008-0036-x

Adinolfi, S., Trifuoggi, M., Politou, A. S., Martin, S., & Pastore, A. (2002). A structural approach to understanding the iron-binding properties of phylogenetically different frataxins. *Human Molecular Genetics*, *11*(16), 1865–1877. https://doi.org/10.1093/hmg/11.16.1865

Ahmed, R., Yano, K., Mitsuoka, T., Ikeda, S., Ichimaru, M., & Hashiba, K. (1989). Changes in T wave morphology during hypercalcemia and its relation to the severity of hypercalcemia. *Journal of Electrocardiology*, *22*(2), 125–132. https://doi.org/10.1016/0022-0736(89)90081-2

Akbar, U., & Ashizawa, T. (2015). Ataxia. *Neurologic Clinics*, *33*(1), 225–248. https://doi.org/10.1016/j.ncl.2014.09.004

Al-Mahdawi, S., Pinto, R. M., Ismail, O., Varshney, D., Lymperi, S., Sandi, C., … Pook, M. (2008). The Friedreich ataxia GAA repeat expansion mutation induces comparable epigenetic changes in human and transgenic mouse brain and heart tissues. *Human Molecular Genetics*, *17*(5), 735–746. https://doi.org/10.1093/hmg/ddm346

Al-Mahdawi, S., Pinto, R. M., Varshney, D., Lawrence, L., Lowrie, M. B., Hughes, S.,

… Pook, M. A. (2006). GAA repeat expansion mutation mouse models of Friedreich ataxia exhibit oxidative stress leading to progressive neuronal and cardiac pathology. *Genomics*, *88*(5), 580–590. https://doi.org/10.1016/j.ygeno.2006.06.015

Ambrus, A., Kraftsik, R., & Barakat-Walter, I. (1998). Ontogeny of calretinin expression in rat dorsal root ganglia. *Developmental Brain Research*, *106*(1–2), 101–108. https://doi.org/10.1016/S0165-3806(97)00201-0

Anamika, Khanna, A., Acharjee, P., Acharjee, A., & Trigun, S. K. (2019). Mitochondrial SIRT3 and neurodegenerative brain disorders. *Journal of Chemical Neuroanatomy*, *95*, 43–53. https://doi.org/10.1016 / j.jchemneu.2017.11.009

Anderson, P. R., Kirby, K., Hilliker, A. J., & Phillips, J. P. (2005). RNAi-mediated suppression of the mitochondrial iron chaperone, frataxin, in Drosophila. *Human Molecular Genetics*, *14*(22), 3397–405. https://doi.org/10.1093/hmg/ddi367

Anderson, P. R., Kirby, K., Orr, W. C., Hilliker, A. J., & Phillips, J. P. (2008). Hydrogen peroxide scavenging rescues frataxin deficiency in a Drosophila model of Friedreich's ataxia. *Proceedings of the National Academy of Sciences of the United States of America*, *105*(2), 611–616. https://doi.org/10.1073/pnas.0709691105

Angelova, P. R., Vinogradova, D., Neganova, M. E., Serkova, T. P., Sokolov, V. V., Bachurin, S. O., … Abramov, A. Y. (2019). Pharmacological Sequestration of Mitochondrial Calcium Uptake Protects Neurons Against Glutamate Excitotoxicity. *Molecular Neurobiology*, *56*(3), 2244–2255. https://doi.org/10.1007/s12035-018-1204-8

Anjomani Virmouni, S., Al-Mahdawi, S., Sandi, C., Yasaei, H., Giunti, P., Slijepcevic, P., & Pook, M. A. (2015). Identification of telomere dysfunction in Friedreich ataxia. *Molecular Neurodegeneration*, *10*(22). https://doi.org/10.1186/s13024-015-0019-6

Annalora, A. J., Goodin, D. B., Hong, W. X., Zhang, Q., Johnson, E. F., & Stout, C. D. (2010). Crystal structure of CYP24A1, a mitochondrial cytochrome P450 involved in Vitamin D metabolism. *Journal of Molecular Biology*, *396*(2), 441–51. https://doi.org/10.1016/j.jmb.2009.11.057

Austin, S., & St-Pierre, J. (2012). PGC1α and mitochondrial metabolism - emerging concepts and relevance in ageing and neurodegenerative disorders. *Journal of Cell Science*, *125*(21), 4963–71. https://doi.org/10.1242/jcs.113662

Backman, S. A., Stambolic, V., Suzuki, A., Haight, J., Elia, A., Pretorius, J., … Mak, T. W. (2001). Deletion of Pten in mouse brain causes seizures, ataxia and defects in soma size resembling Lhermitte-Duclos disease. *Nature Genetics*, *29*(4), 396–403. https://doi.org/10.1038/ng782

Bano, D., Young, K. W., Guerin, C. J., Lefeuvre, R., Rothwell, N. J., Naldini, L., … Nicotera, P. (2005). Cleavage of the plasma membrane Na+/Ca2+ exchanger in excitotoxicity. *Cell*, *120*(2), 275–85. https://doi.org/10.1016/j.cell.2004.11.049

Barinka, F., & Druga, R. (2010). Calretinin expression in the mammalian neocortex: A review. *Physiological Research*, *59*(5), 665–677. https://doi.org/10.33549/physiolres.931930

Barr, H., Page, R., & Taylor, W. (1986). Primary small bowel ganglioneuroblastoma and Friedreich's ataxia. *Journal of the Royal Society of Medicine*, *79*(10), 612–613. https://doi.org/10.1177/014107688607901018

Barros, M. H., Nobrega, F. G., & Tzagoloff, A. (2002). Mitochondrial ferredoxin is required for heme a synthesis in Saccharomyces cerevisiae. *Journal of Biological Chemistry*, *277*(12), 9997–10002. https://doi.org/10.1074/jbc.M112025200

Barski, J. J., Hartmann, J., Rose, C. R., Hoebeek, F., Mörl, K., Noll-Hussong, M., … Meyer, M. (2003). Calbindin in cerebellar Purkinje cells is a critical determinant of the precision of motor coordination. *Journal of Neuroscience*, *23*(8), 3469–3477. https://doi.org/10.1523/jneurosci.23-08-03469.2003

Baughman, J. M., Perocchi, F., Girgis, H. S., Plovanich, M., Belcher-Timme, C. A., Sancak, Y., … Mootha, V. K. (2011). Integrative genomics identifies MCU as an essential component of the mitochondrial calcium uniporter. *Nature*, *476*(7360), 341–345. https://doi.org/10.1038/nature10234

Becker, D., Richter, J., Tocilescu, M. A., Przedborski, S., & Voos, W. (2012). Pink1 kinase and its membrane potential (Δψ)-dependent cleavage product both localize to outer mitochondrial membrane by unique targeting mode. *Journal of Biological Chemistry*, *287*(27), 22969–22987. https://doi.org/10.1074/jbc.M112.365700

Belgacem, Y. H., & Borodinsky, L. N. (2017). CREB at the crossroads of activity-dependent regulation of nervous system development and function. *Advances in Experimental Medicine and Biology*, *1015*, 19–39. https://doi.org/10.1007/978-3-319-62817-2_2

Bencze, K. Z., Kondapalli, K. C., Cook, J. D., McMahon, S., Millán-Pacheco, C., Pastor, N., & Stemmler, T. L. (2006). The structure and function of frataxin. *Critical Reviews in Biochemistry and Molecular Biology*, *41*(5), 269–291. https://doi.org/10.1080/10409230600846058

Bernardi, P., Rasola, A., Forte, M., & Lippe, G. (2015). The mitochondrial permeability transition pore: Channel formation by F-ATP synthase, integration in signal transduction, and role in pathophysiology. *Physiological Reviews*, *95*(4), 1111–55. https://doi.org/10.1152/physrev.00001.2015

Berridge, M. J. (2015a). Vitamin D: A custodian of cell signalling stability in health and disease. *Biochemical Society Transactions*, *43*(3), 349–58. https://doi.org/10.1042/BST20140279

Berridge, M. J. (2015b). Vitamin D cell signalling in health and disease. *Biochemical and Biophysical Research Communications*, *460*(1), 53–71. https://doi.org/10.1016/j.bbrc.2015.01.008

Berridge, M. J. (2016). Vitamin D, reactive oxygen species and calcium signalling in ageing and disease. *Philosophical Transactions of the Royal Society B: Biological Sciences*, *371*(1700), 20150434. https://doi.org/10.1098/rstb.2015.0434

Berridge, M. J. (2017). Vitamin D deficiency accelerates ageing and age-related diseases: a novel hypothesis. *Journal of Physiology*, *595*(22), 6825–6836. https://doi.org/10.1113/JP274887

Berridge, M. J., Lipp, P., & Bootman, M. D. (2000). The versatility and universality of calcium signalling. *Nature Reviews. Molecular Cell Biology*, *1*(1), 11–21. https://doi.org/10.1038/35036035

Berta, T., Qadri, Y., Tan, P. H., & Ji, R. R. (2017). Targeting dorsal root ganglia and primary sensory neurons for the treatment of chronic pain. *Expert Opinion on Therapeutic Targets*, *21*(7), 695–703. https://doi.org/10.1080/14728222.2017.1328057

Bierer, B. E., Holländer, G., Fruman, D., & Burakoff, S. J. (1993). Cyclosporin A and FK506: molecular mechanisms of immunosuppression and probes for transplantation biology. *Current Opinion in Immunology*, *5*(5), 763–773. https://doi.org/10.1016/0952-7915(93)90135-F

Blomberg Jensen, M., Andersen, C. B., Nielsen, J. E., Bagi, P., Jørgensen, A., Juul, A., & Leffers, H. (2010). Expression of the vitamin D receptor, 25-hydroxylases, 1α-hydroxylase and 24-hydroxylase in the human kidney and renal clear cell cancer.

Journal of Steroid Biochemistry and Molecular Biology, *121*(1–2), 376–82. https://doi.org/10.1016/j.jsbmb.2010.03.069

Bolinches-Amorós, A., Mollá, B., Pla-Martín, D., Palau, F., & González-Cabo, P. (2014). Mitochondrial dysfunction induced by frataxin deficiency is associated with cellular senescence and abnormal calcium metabolism. *Frontiers in Cellular Neuroscience*, *8*, 124. https://doi.org/10.3389/fncel.2014.00124

Bononi, A., Bonora, M., Marchi, S., Missiroli, S., Poletti, F., Giorgi, C., … Pinton, P. (2013). Identification of PTEN at the ER and MAMs and its regulation of Ca 2+ signaling and apoptosis in a protein phosphatase-dependent manner. *Cell Death and Differentiation*, *20*(12), 1631–43. https://doi.org/10.1038/cdd.2013.77

Bordet, T., Berna, P., Abitbol, J. L., & Pruss, R. M. (2010). Olesoxime (TRO19622): A novel mitochondrial-targeted neuroprotective compound. *Pharmaceuticals*, *3*(2), 345–368. https://doi.org/10.3390/ph3020345

Bouchard, J. P., Barbeau, A., Bouchard, R., Paquet, M., & Bouchard, R. W. (1979). A Cluster of Friedreich's Ataxia in Rimouski, Québec. *Canadian Journal of Neurological Sciences / Journal Canadien Des Sciences Neurologiques*, *6*(2), 205–208. https://doi.org/10.1017/S0317167100119651

Bowie, D., Feltz, P., & Schlichter, R. (1994). Subpopulations of neonatal rat sensory neurons express functional neurotransmitter receptors which elevate intracellular calcium. *Neuroscience*, *58*(1), 141–9. https://doi.org/10.1016/0306-4522(94)90161-9

Braham, J., Sadeh, M., Turgman, J., & Sarova-Pinchas, I. (1979). Beneficial effect of propranolol in familial ataxia. *Annals of Neurology*, *5*(2), 207. https://doi.org/10.1002/ana.410050219

Brini, M., & Carafoli, E. (2011). The Plasma Membrane Ca2+ ATPase and the plasma membrane Sodium Calcium exchanger cooperate in the regulation of cell Calcium. *Cold Spring Harbor Perspectives in Biology*, *3*(2), a004168. https://doi.org/10.1101/cshperspect.a004168

Britti, E., Delaspre, F., Feldman, A., Osborne, M., Greif, H., Tamarit, J., & Ros, J. (2018). Frataxin-deficient neurons and mice models of Friedreich ataxia are improved by TAT-MTScs-FXN treatment. *Journal of Cellular and Molecular Medicine*, *22*(2), 834–848. https://doi.org/10.1111/jcmm.13365

Britti, E., Delaspre, F., Sanz-Alcázar, A., Medina-Carbonero, M., Llovera, M., Purroy, R., … Ros, J. (2021). Calcitriol increases frataxin levels and restores mitochondrial function in cell models of Friedreich Ataxia. *Biochemical Journal*, *478*(1), 1–20. https://doi.org/10.1042/BCJ20200331

Britti, E., Delaspre, F., Tamarit, J., & Ros, J. (2018). Mitochondrial calcium signalling and neurodegenerative diseases. *Neuronal Signaling*, *2*(4), 20180061. https://doi.org/10.1042/ns20180061

Britti, E., Delaspre, F., Tamarit, J., & Ros, J. (2020). Calpain-Inhibitors Protect Frataxin-Deficient Dorsal Root Ganglia Neurons from Loss of Mitochondrial Na+/Ca2+ Exchanger, NCLX, and Apoptosis. *Neurochemical Research*, *46*(1), 108–119. https://doi.org/10.1007/s11064-020-03020-3

Britti, E., Ros, J., Esteras, N., & Abramov, A. Y. (2020). Tau inhibits mitochondrial calcium efflux and makes neurons vulnerable to calcium-induced cell death. *Cell Calcium*, *86*, 102150. https://doi.org/10.1016/j.ceca.2019.102150

Briz, V., Hsu, Y.-T., Li, Y., Lee, E., Bi, X., & Baudry, M. (2013). Calpain-2-mediated PTEN degradation contributes to BDNF-induced stimulation of dendritic protein synthesis. *Journal of Neuroscience*, *33*(10), 4317–28. https://doi.org/10.1523/JNEUROSCI.4907-12.2013

Brookes, P. S., Yoon, Y., Robotham, J. L., Anders, M. W., & Sheu, S. S. (2004). Calcium, ATP, and ROS: A mitochondrial love-hate triangle. *American Journal of Physiology - Cell Physiology*, *287*(4), c817-33. https://doi.org/10.1152/ajpcell.00139.2004

Brown, J., Bianco, J. I., McGrath, J. J., & Eyles, D. W. (2003). 1,25-Dihydroxyvitamin D3 induces nerve growth factor, promotes neurite outgrowth and inhibits mitosis in embryonic rat hippocampal neurons. *Neuroscience Letters*, *343*(2), 139–43. https://doi.org/10.1016/S0304-3940(03)00303-3

Brustovetsky, T., Bolshakov, A., & Brustovetsky, N. (2010). Calpain activation and Na+/Ca2+ exchanger degradation occur downstream of calcium deregulation in hippocampal neurons exposed to excitotoxic glutamate. *Journal of Neuroscience Research*, *88*(6), 1317–28. https://doi.org/10.1002/jnr.22295

Buell, J. S., & Dawson-Hughes, B. (2008). Vitamin D and neurocognitive dysfunction: Preventing 'D'ecline? *Molecular Aspects of Medicine*, *29*(6), 415–422. https://doi.org/10.1016/j.mam.2008.05.001

Bukrinsky, M. (2015). Extracellular cyclophilins in health and disease. *Biochimica et Biophysica Acta - General Subjects*, *1850*(10), 2087–2095. https://doi.org/10.1016/j.bbagen.2014.11.013

Bulteau, A. L., O'Neill, H. A., Kennedy, M. C., Ikeda-Saito, M., Isaya, G., & Szweda, L. I. (2004). Frataxin acts as an iron chaperone protein to modulate mitochondrial aconitase activity. *Science*, *305*(5681), 242–5. https://doi.org/10.1126/science.1098991

Busi, M. V., & Gomez-Casati, D. F. (2012). Exploring frataxin function. *IUBMB Life*, *64*(1), 56–63. https://doi.org/10.1002/iub.577

Cabiscol, E., Tamarit, J., & Ros, J. (2014). Protein carbonylation: Proteomics, specificity and relevance to aging. *Mass Spectrometry Reviews*, *33*(1), 21–48. https://doi.org/10.1002/mas.21375

Cagin, U., & Enriquez, J. A. (2015). The complex crosstalk between mitochondria and the nucleus: What goes in between? *International Journal of Biochemistry and Cell Biology*, *63*, 10–15. https://doi.org/10.1016/j.biocel.2015.01.026

Cai, K., Frederick, R. O., Tonelli, M., & Markley, J. L. (2018). Interactions of iron-bound frataxin with ISCU and ferredoxin on the cysteine desulfurase complex leading to Fe-S cluster assembly. *Journal of Inorganic Biochemistry*, *183*, 107–116. https://doi.org/10.1016/j.jinorgbio.2018.03.007

Cai, W., Yang, T., Liu, H., Han, L., Zhang, K., Hu, X., … Chen, J. (2018). Peroxisome proliferator-activated receptor γ (PPARγ): A master gatekeeper in CNS injury and repair. *Progress in Neurobiology*, *163–164*, 27–58. https://doi.org/10.1016/j.pneurobio.2017.10.002

Cai, X., & Lytton, J. (2004). Molecular Cloning of a Sixth Member of the K+-dependent Na +/Ca2+ Exchanger Gene Family, NCKX6. *Journal of Biological Chemistry*, *279*(7), 5867–5876. https://doi.org/10.1074/jbc.M310908200

Calmels, N., Schmucker, S., Wattenhofer-Donzé, M., Martelli, A., Vaucamps, N., Reutenauer, L., … Puccio, H. (2009). The first cellular models based on frataxin missense mutations that reproduce spontaneously the defects associated with Friedreich ataxia. *PLoS ONE*, *4*(7), e6379. https://doi.org/10.1371/journal.pone.0006379

Calvello, R., Cianciulli, A., Nicolardi, G., De Nuccio, F., Giannotti, L., Salvatore, R., … Lofrumento, D. D. (2017). Vitamin D Treatment Attenuates Neuroinflammation and Dopaminergic Neurodegeneration in an Animal Model of Parkinson's Disease, Shifting M1 to M2 Microglia Responses. *Journal of Neuroimmune Pharmacology*,

12(2), 327–339. https://doi.org/10.1007/s11481-016-9720-7

Camp, A. J., & Wijesinghe, R. (2009). Calretinin: Modulator of neuronal excitability. *International Journal of Biochemistry and Cell Biology*, *41*(11), 2118–21. https://doi.org/10.1016/j.biocel.2009.05.007

Campuzano, V., Montermini, L., Lutz, Y., Cova, L., Hindelang, C., Jiralerspong, S., … Koenig, M. (1997). Frataxin is reduced in Friedreich ataxia patients and is associated with mitochondrial membranes. *Human Molecular Genetics*, *6*(11), 1771–80. https://doi.org/10.1093/HMG/6.11.1771

Campuzano, V., Montermini, L., Moltò, M. D., Pianese, L., Cossée, M., Cavalcanti, F., … Pandolfo, M. (1996). Friedreich's Ataxia: Autosomal Recessive Disease Caused by an Intronic GAA Triplet Repeat Expansion. *Science*, *271*(5254), 1423–1427. https://doi.org/10.1126/SCIENCE.271.5254.1423

Carafoli, E., Tiozzo, R., Lugli, G., Crovetti, F., & Kratzing, C. (1974). The release of calcium from heart mitochondria by sodium. *Journal of Molecular and Cellular Cardiology*, *6*(4), 361–371. https://doi.org/10.1016/0022-2828(74)90077-7

Carletti, B., & Piemonte, F. (2014). Friedreich's ataxia: A neuronal point of view on the oxidative stress hypothesis. *Antioxidants*, *3*(3), 592–603. https://doi.org/10.3390/antiox3030592

Cavadini, P., Adamec, J., Taroni, F., Gakh, O., & Isaya, G. (2000). Two-step processing of human frataxin by mitochondrial processing peptidase: Precursor and intermediate forms are cleaved at different rates. *Journal of Biological Chemistry*, *275*(52), 41469–41475. https://doi.org/10.1074/jbc.M006539200

Cavalcante, G. C., Schaan, A. P., Cabral, G. F., Santana-Da-Silva, M. N., Pinto, P., Vidal, A. F., & Ribeiro-Dos-Santos, Â. (2019). A cell's fate: An overview of the molecular biology and genetics of apoptosis. *International Journal of Molecular Sciences*, *20*(17), 4133. https://doi.org/10.3390/ijms20174133

Chabas, J. F., Stephan, D., Marqueste, T., Garcia, S., Lavaut, M. N., Nguyen, C., … Feron, F. (2013). Cholecalciferol (Vitamin D3) Improves Myelination and Recovery after Nerve Injury. *PLoS ONE*, *8*(5), e65034. https://doi.org/10.1371/journal.pone.0065034

Chamberlain, S., Shaw, J., Rowland, A., Wallis, J., South, S., Nakamura, Y., … Williamson, R. (1988). Mapping of mutation causing Friedreich's ataxia to human chromosome 9. *Nature*, *334*(6179), 248–250. https://doi.org/10.1038/334248a0

Chandran, V., Gao, K., Swarup, V., Versano, R., Dong, H., Jordan, M. C., & Geschwind, D. H. (2017). Inducible and reversible phenotypes in a novel mouse model of Friedreich's ataxia. *ELife*, *6*, e30054. https://doi.org/10.7554/eLife.30054

Chantrel-Groussard, K., Geromel, V., Puccio, H., Koenig, M., Munnich, A., Rötig, A., & Rustin, P. (2001). Disabled early recruitment of antioxidant defenses in Friedreich's ataxia. *Human Molecular Genetics*, *10*(19), 2061–2067. https://doi.org/10.1093/hmg/10.19.2061

Chaudhuri, D., Artiga, D. J., Abiria, S. A., & Clapham, D. E. (2016). Mitochondrial calcium uniporter regulator 1 (MCUR1) regulates the calcium threshold for the mitochondrial permeability transition. *PNAS*, *113*(13), E1872-80. https://doi.org/10.1073/pnas.1602264113

Chen, K., Lin, G., Haelterman, N. A., Ho, T. S. Y., Li, T., Li, Z., … Bellen, H. J. (2016). Loss of frataxin induces iron toxicity, sphingolipid synthesis, and Pdk1/Mef2 activation, leading to neurodegeneration. *ELife*, *5*, e16043. https://doi.org/10.7554/eLife.16043

Chevis, C. F., Da Silva, C. B., D'Abreu, A., Lopes-Cendes, I., Cendes, F., Bergo, F. P. G., & França, M. C. (2013). Spinal cord atrophy correlates with disability in

Friedreich's ataxia. *Cerebellum*, *12*(1), 43–47. https://doi.org/10.1007/s12311-012-0390-6

Chiabrando, D., Bertino, F., & Tolosano, E. (2020). Hereditary Ataxia: A Focus on Heme Metabolism and Fe-S Cluster Biogenesis. *International Journal of Molecular Sciences*, *21*(11), 3760. https://doi.org/10.3390/ijms21113760

Chung, J. H., & Eng, C. (2005). Nuclear-cytoplasmic partitioning of phosphatase and tensin homologue deleted on chromosome 10 (PTEN) differentially regulates the cell cycle and apoptosis. *Cancer Research*, *65*(18), 8096–100. https://doi.org/10.1158/0008-5472.CAN-05-1888

Cnop, M., Mulder, H., & Igoillo-Esteve, M. (2013). Diabetes in Friedreich Ataxia. *Journal of Neurochemistry*, *126*(1), 94–102. https://doi.org/10.1111/jnc.12216

Condò, I., Ventura, N., Malisan, F., Rufini, A., Tomassini, B., & Testi, R. (2007). In vivo maturation of human frataxin. *Human Molecular Genetics*, *16*(13), 1534–1540. https://doi.org/10.1093/hmg/ddm102

Cooper, J. M., & Schapira, A. H. V. (2003). Friedreich's Ataxia: Disease mechanisms, antioxidant and Coenzyme Q 10 therapy. *BioFactors*, *18*(1–4), 163–171. https://doi.org/10.1002/biof.5520180219

Coppola, G., Marmolino, D., Lu, D., Wang, Q., Cnop, M., Rai, M., … Geschwind, D. H. (2009). Functional genomic analysis of frataxin deficiency reveals tissue-specific alterations and identifies the PPARγ pathway as a therapeutic target in Friedreich's ataxia. *Human Molecular Genetics*, *18*(13), 2452–61. https://doi.org/10.1093/hmg/ddp183

Copray, J. C. V. M., Mantingh-Otter, I. J., & Brouwer, N. (1994). Expression of calcium-binding proteins in the neurotrophin-3-dependent subpopulation of rat embryonic dorsal root ganglion cells in culture. *Developmental Brain Research*, *81*(1), 57–65. https://doi.org/10.1016/0165-3806(94)90068-X

Corona, J. C., & Duchen, M. R. (2016). PPARγ as a therapeutic target to rescue mitochondrial function in neurological disease. *Free Radical Biology and Medicine*, *100*, 153–163. https://doi.org/10.1016/j.freeradbiomed.2016.06.023

Cossée, M., Puccio, H., Gansmuller, A., Koutnikova, H., Dierich, A., LeMeur, M., … Kœnig, M. (2000). Inactivation of the Friedreich ataxia mouse gene leads to early embryonic lethality without iron accumulation. *Human Molecular Genetics*, *9*(8), 1219–1226. https://doi.org/10.1093/hmg/9.8.1219

Costantini, A., Laureti, T., Pala, M. I., Colangeli, M., Cavalieri, S., Pozzi, E., … Fancellu, R. (2016). Long-term treatment with thiamine as possible medical therapy for Friedreich ataxia. *Journal of Neurology*, *263*(11), 2170–2178. https://doi.org/10.1007/s00415-016-8244-7

Creigh, P. D., Mountain, J., Sowden, J. E., Eichinger, K., Ravina, B., Larkindale, J., & Herrmann, D. N. (2019). Measuring peripheral nerve involvement in Friedreich's ataxia. *Annals of Clinical and Translational Neurology*, *6*(9), 1718–1727. https://doi.org/10.1002/acn3.50865

Crombie, D. E., Curl, C. L., Raaijmakers, A. J. A., Sivakumaran, P., Kulkarni, T., Wong, R. C. B., … Pébay, A. (2017). Friedreich's ataxia induced pluripotent stem cell-derived cardiomyocytes display electrophysiological abnormalities and calcium handling deficiency. *Aging*, *9*(5), 1440–1452. https://doi.org/10.18632/aging.101247

Dagda, R. K., Pien, I., Wang, R., Zhu, J., Wang, K. Z. Q., Callio, J., … Chu, C. T. (2014). Beyond the mitochondrion: Cytosolic PINK1 remodels dendrites through Protein Kinase A. *Journal of Neurochemistry*, *128*(6), 864–77. https://doi.org/10.1111/jnc.12494

Dagert, M., & Ehrlich, S. D. (1979). Prolonged incubation in calcium chloride improves the competence of Escherichia coli cells. *Gene*, *6*(1), 23–28. https://doi.org/10.1016/0378-1119(79)90082-9

De La Grandmaison, G. L., Clairand, I., & Durigon, M. (2001). Organ weight in 684 adult autopsies: New tables for a Caucasoid population. *Forensic Science International*, *119*(2), 149–154. https://doi.org/10.1016/S0379-0738(00)00401-1

de Wilde, A. H., Pham, U., Posthuma, C. C., & Snijder, E. J. (2018). Cyclophilins and cyclophilin inhibitors in nidovirus replication. *Virology*, *522*, 46–55. https://doi.org/10.1016/j.virol.2018.06.011

Delivoria-Papadopoulos, M., Ashraf, Q. M., & Mishra, O. P. (2007). Differential expression of apoptotic proteins following hypoxia-induced CREB phosphorylation in the cerebral cortex of newborn piglets. *Neurochemical Research*, *32*(7), 1256–63. https://doi.org/10.1007/s11064-007-9301-5

Deluca, H. F., & Engstrom, G. W. (1961). Calcium uptake by rat kidney mitochondria. *Proceedings of the National Academy of Sciences of the United States of America*, *47*(2), 1744–1750. https://doi.org/10.1073/pnas.47.11.1744

Di Bella, D., Lazzaro, F., Brusco, A., Plumari, M., Battaglia, G., Pastore, A., … Taroni, F. (2010). Mutations in the mitochondrial protease gene AFG3L2 cause dominant hereditary ataxia SCA28. *Nature Genetics*, *42*(4), 313–21. https://doi.org/10.1038/ng.544

Di Donato, I., Bianchi, S., & Federico, A. (2010). Ataxia with vitamin e deficiency: Update of molecular diagnosis. *Neurological Sciences*, *31*(4), 511–515. https://doi.org/10.1007/s10072-010-0261-1

Di Prospero, N. A., Baker, A., Jeffries, N., & Fischbeck, K. H. (2007). Neurological effects of high-dose idebenone in patients with Friedreich's ataxia: a randomised, placebo-controlled trial. *Lancet Neurology*, *6*(10), 878–886. https://doi.org/10.1016/S1474-4422(07)70220-X

Dionisi, C., Rai, M., Chazalon, M., Schiffmann, S. N., & Pandolfo, M. (2020). Primary proprioceptive neurons from human induced pluripotent stem cells: a cell model for afferent ataxias. *Scientific Reports*, *10*(1), 7752. https://doi.org/10.1038/s41598-020-64831-6

Dong, Y. N., McMillan, E., Clark, E. M., Lin, H., & Lynch, D. R. (2019). GRP75 overexpression rescues frataxin deficiency and mitochondrial phenotypes in Friedreich ataxia cellular models. *Human Molecular Genetics*, *28*(10), 1594–1607. https://doi.org/10.1093/hmg/ddy448

Dong, Z., Shanmughapriya, S., Tomar, D., Siddiqui, N., Lynch, S., Nemani, N., … Madesh, M. (2017). Mitochondrial Ca2+ Uniporter Is a Mitochondrial Luminal Redox Sensor that Augments MCU Channel Activity. *Molecular Cell*, *65*(6), 1014–1028.e7. https://doi.org/10.1016/j.molcel.2017.01.032

Donkor, I. O. (2015). An updated patent review of calpain inhibitors (2012 – 2014). *Expert Opinion on Therapeutic Patents*, *25*(1), 17–31. https://doi.org/10.1517/13543776.2014.982534

Dreyer, C., Keller, H., Mahfoudi, A., Laudet, V., Krey, G., & Wahli, W. (1993). Positive regulation of the peroxisomal β-oxidation pathway by fatty acids through activation of peroxisome proliferator-activated receptors (PPAR). *Biology of the Cell*, *77*(1), 67–76. https://doi.org/10.1016/S0248-4900(05)80176-5

Dürr, A., Cossee, M., Agid, Y., Campuzano, V., Mignard, C., Penet, C., … Koenig, M. (1996). Clinical and Genetic Abnormalities in Patients with Friedreich's Ataxia. *New England Journal of Medicine*, *335*(16), 1169–1175. https://doi.org/10.1056/NEJM199610173351601

Edenharter, O., Schneuwly, S., & Navarro, J. A. (2018). Mitofusin-Dependent ER Stress Triggers Glial Dysfunction and Nervous System Degeneration in a Drosophila Model of Friedreich's Ataxia. *Frontiers in Molecular Neuroscience*, *11*, 38. https://doi.org/10.3389/fnmol.2018.00038

Eigentler, A., Nachbauer, W., Donnemiller, E., Poewe, W., Gasser, R. W., & Boesch, S. (2014). Low bone mineral density in Friedreich ataxia. *Cerebellum*, *13*(5), 549–557. https://doi.org/10.1007/s12311-014-0568-1

Eiyama, A., & Okamoto, K. (2015). PINK1/Parkin-mediated mitophagy in mammalian cells. *Current Opinion in Cell Biology*, *33*, 95–101. https://doi.org/10.1016/j.ceb.2015.01.002

Estrada, D. F. (2018). The cytochrome P450 24A1 interaction with adrenodoxin relies on multiple recognition sites that vary among species. *Journal of Biological Chemistry*, *293*(11), 4167–4179. https://doi.org/10.1074/jbc.RA117.001145

Evatt, M. L., Delong, M. R., Khazai, N., Rosen, A., Triche, S., & Tangpricha, V. (2008). Prevalence of vitamin d insufficiency in patients with Parkinson disease and Alzheimer disease. *Archives of Neurology*, *65*(10), 1348–52. https://doi.org/10.1001/archneur.65.10.1348

Eyles, D. W., Smith, S., Kinobe, R., Hewison, M., & McGrath, J. J. (2005). Distribution of the Vitamin D receptor and 1α-hydroxylase in human brain. *Journal of Chemical Neuroanatomy*, *29*(1), 21–30. https://doi.org/10.1016/J.JCHEMNEU.2004.08.006

Faye, P. A., Poumeaud, F., Miressi, F., Lia, A. S., Demiot, C., Magy, L., … Sturtz, F. G. (2019). Focus on 1,25-dihydroxyvitamin D3 in the peripheral nervous system. *Frontiers in Neuroscience*, *13*, 348. https://doi.org/10.3389/fnins.2019.00348

Feno, S., Rizzuto, R., Raffaello, A., & Vecellio Reane, D. (2021). The molecular complexity of the Mitochondrial Calcium Uniporter. *Cell Calcium*, *93*, 102322. https://doi.org/10.1016/j.ceca.2020.102322

Fiumelli, H., Kiraly, M., Ambrus, A., Magistretti, P. J., & Martin, J. L. (2000). Opposite regulation of calbindin and calretinin expression by brain- derived neurotrophic factor in cortical neurons. *Journal of Neurochemistry*, *74*(5), 1870–7. https://doi.org/10.1046/j.1471-4159.2000.0741870.x

Forster, R. E., Jurutka, P. W., Hsieh, J.-C., Haussler, C. A., Lowmiller, C. L., Kaneko, I., … Kerr Whitfield, G. (2011). Vitamin D receptor controls expression of the anti-aging klotho gene in mouse and human renal cells. *Biochemical and Biophysical Research Communications*, *414*(3), 557–62. https://doi.org/10.1016/j.bbrc.2011.09.117

Foury, F., & Cazzalini, O. (1997). Deletion of the yeast homologue of the human gene associated with Friedreich's ataxia elicits iron accumulation in mitochondria. *FEBS Letters*, *411*(2–3), 373–7. https://doi.org/10.1016/S0014-5793(97)00734-5

Foury, F., & Talibi, D. (2001). Mitochondrial control of iron homeostasis. A genome wide analysis of gene expression in a yeast frataxin-deficient strain. *Journal of Biological Chemistry*, *276*(11), 7762–7768. https://doi.org/10.1074/jbc.M005804200

Friedreich, N. (1863). Ueber degenerative Atrophie der spinalen Hinterstränge. *Archiv Für Pathologische Anatomie Und Physiologie Und Für Klinische Medicin*, *26*(5–6), 433–459. https://doi.org/10.1007/BF01878006

Friedreich, N. (1877). Ueber Ataxie mit besonderer Berücksichtigung der hereditären Formen - Nachtrag. *Archiv Für Pathologische Anatomie Und Physiologie Und Für Klinische Medicin*, *70*(1), 140–152. https://doi.org/10.1007/BF01936635

Fuenzalida, K., Quintanilla, R., Ramos, P., Piderit, D., Fuentealba, R. A., Martinez, G.,

… Bronfman, M. (2007). Peroxisome proliferator-activated receptor γ up-regulates the Bcl-2 anti-apoptotic protein in neurons and induces mitochondrial stabilization and protection against oxidative stress and apoptosis. *Journal of Biological Chemistry*, *282*(51), 37006–15. https://doi.org/10.1074/jbc.M700447200

Gandhi, S., Wood-Kaczmar, A., Yao, Z., Plun-Favreau, H., Deas, E., Klupsch, K., … Abramov, A. Y. (2009). PINK1-Associated Parkinson's Disease Is Caused by Neuronal Vulnerability to Calcium-Induced Cell Death. *Molecular Cell*, *33*(5), 627–638. https://doi.org/10.1016/j.molcel.2009.02.013

Garcion, E., Wion-Barbot, N., Montero-Menei, C. N., Berger, F., & Wion, D. (2002). New clues about vitamin D functions in the nervous system. *Trends in Endocrinology and Metabolism: TEM*, *13*(3), 100–5. https://doi.org/10.1016 / s1043-2760 (01) 00547-1.

Gautier, C. A., Giaime, E., Caballero, E., Núñez, L., Song, Z., Chan, D., … Shen, J. (2012). Regulation of mitochondrial permeability transition pore by PINK1. *Molecular Neurodegeneration*, *7*, 22. https://doi.org/10.1186/1750-1326-7-22

Gérard, C., Xiao, X., Filali, M., Coulombe, Z., Arsenault, M., Couet, J., … Tremblay, J. P. (2014). An AAV9 coding for frataxin clearly improved the symptoms and prolonged the life of Friedreich ataxia mouse models. *Molecular Therapy - Methods and Clinical Development*, *1*, 14044. https://doi.org/10.1038/mtm.2014.44

Gerle, C. (2016). On the structural possibility of pore-forming mitochondrial FoF1 ATP synthase. *Biochimica et Biophysica Acta - Bioenergetics*, *1857*(8), 1191–1196. https://doi.org/10.1016/j.bbabio.2016.03.008

Gianforcaro, A., & Hamadeh, M. J. (2014). Vitamin D as a potential therapy in amyotrophic lateral sclerosis. *CNS Neuroscience and Therapeutics*, *20*(2), 101–11. https://doi.org/10.1111/cns.12204

Giorgio, V., Burchell, V., Schiavone, M., Bassot, C., Minervini, G., Petronilli, V., … Bernardi, P. (2017). Ca 2+ binding to F-ATP synthase β subunit triggers the mitochondrial permeability transition. *EMBO Reports*, *18*(7), 1065–1076. https://doi.org/10.15252/embr.201643354

Giorgio, V., von Stockum, S., Antoniel, M., Fabbro, A., Fogolari, F., Forte, M., … Bernardi, P. (2013). Dimers of mitochondrial ATP synthase form the permeability transition pore. *Proceedings of the National Academy of Sciences of the United States of America*, *110*(15), 5887–92. https://doi.org/10.1073/pnas.1217823110

González-Cabo, P., Llorens, J. V, Palau, F., & Dolores Moltó, M. (2009). Friedreich ataxia: An update on animal models, frataxin function and therapies. *Advances in Experimental Medicine and Biology*, *652*, 247–61. https://doi.org/10.1007/978-90-481-2813-6_17

González-Cabo, P., & Palau, F. (2013). Mitochondrial pathophysiology in Friedreich's ataxia. *Journal of Neurochemistry*, *126*(Suppl.1), 53–64. https://doi.org/10.1111/jnc.12303

González-Cabo, P., Vázquez-Manrique, R. P., García-Gimeno, M. A., Sanz, P., & Palau, F. (2005). Frataxin interacts functionally with mitochondrial electron transport chain proteins. *Human Molecular Genetics*, *14*(15), 2091–2098. https://doi.org/10.1093/hmg/ddi214

Gordon, D. M., Kogan, M., Knight, S. A. B., Dancis, A., & Pain, D. (2001). Distinct roles for two N-terminal cleaved domains in mitochondrial import of the yeast frataxin homolog, Yfh1p. *Human Molecular Genetics*, *10*(3), 259–269. https://doi.org/10.1093/hmg/10.3.259

Greene, A. W., Grenier, K., Aguileta, M. A., Muise, S., Farazifard, R., Haque, M. E., …

Fon, E. A. (2012). Mitochondrial processing peptidase regulates PINK1 processing, import and Parkin recruitment. *EMBO Reports*, *13*(4), 378–385. https://doi.org/10.1038/embor.2012.14

Greene, E., Mahishi, L., Entezam, A., Kumari, D., & Usdin, K. (2007). Repeat-induced epigenetic changes in intron 1 of the frataxin gene and its consequences in Friedreich ataxia. *Nucleic Acids Research*, *35*(10), 3383–3390. https://doi.org/10.1093/nar/gkm271

Greene, Entezam, Kumari, & Usdin. (2005). Ancient repeated DNA elements and the regulation of the human frataxin promoter. *Genomics*, *85*(2), 221–230. https://doi.org/10.1016/j.ygeno.2004.10.013

Gröschel, C., Tennakoon, S., & Kállay, E. (2015). Cytochrome P450 Vitamin D Hydroxylases in Inflammation and Cancer. *Advances in Pharmacology*, *74*, 413–458. https://doi.org/10.1016/BS.APHA.2015.03.002

Gu, T., Zhang, Z., Wang, J., Guo, J., Shen, W. H., & Yin, Y. (2011). CREB Is a Novel Nuclear Target of PTEN Phosphatase, *71*(8), 2821–5. https://doi.org/10.1158/0008-5472.CAN-10-3399

Guo, L., Wang, Q., Weng, L., Hauser, L. A., Strawser, C. J., Mesaros, C., … Blair, I. A. (2018). Characterization of a new N-terminally acetylated extra-mitochondrial isoform of frataxin in human erythrocytes. *Scientific Reports*, *8*(1), 17043. https://doi.org/10.1038/s41598-018-35346-y

Haberberger, R. V., Barry, C., Dominguez, N., & Matusica, D. (2019). Human dorsal root ganglia. *Frontiers in Cellular Neuroscience*, *13*, 271. https://doi.org/10.3389/fncel.2019.00271

Habib, A. M., Nagi, K., Thillaiappan, N. B., Sukumaran, V. K., & Akhtar, S. (2020). Vitamin D and Its Potential Interplay With Pain Signaling Pathways. *Frontiers in Immunology*, *11*, 820. https://doi.org/10.3389/fimmu.2020.00820

Han, T. H. L., Camadro, J. M., Barbault, F., Santos, R., El Hage Chahine, J. M., & Ha-Duong, N. T. (2019). In Vitro interaction between yeast frataxin and superoxide dismutases: Influence of mitochondrial metals. *Biochimica et Biophysica Acta - General Subjects*, *1863*(5), 883–892. https://doi.org/10.1016/j.bbagen.2019.02.011

Hansen, J. J., Dürr, A., Cournu-Rebeix, I., Georgopoulos, C., Ang, D., Nielsen, M. N., … Bross, P. (2002). Hereditary spastic paraplegia SPG13 is associated with a mutation in the gene encoding the mitochondrial chaperonin Hsp60. *American Journal of Human Genetics*, *70*(5), 1328–32. https://doi.org/10.1086/339935

Hanson, E., Sheldon, M., Pacheco, B., Alkubeysi, M., & Raizada, V. (2019). Heart disease in Friedreich's ataxia. *World Journal of Cardiology*, *11*(1), 1–12. https://doi.org/10.4330/wjc.v11.i1.1

Harding, A. E. (1981). Friedreich's ataxia: a clinical and genetic study of 90 families with an analysis of early diagnostic criteria and intrafamilial clustering of clinical features. *Brain : A Journal of Neurology*, *104*(3), 589–620. https://doi.org/10.1093/brain/104.3.589

Harms, L. R., Burne, T. H. J., Eyles, D. W., & McGrath, J. J. (2011). Vitamin D and the brain. *Best Practice and Research: Clinical Endocrinology and Metabolism*, *25*(4), 657–69. https://doi.org/10.1016/j.beem.2011.05.009

Hausse, A. O., Aggoun, Y., Bonnet, D., Sidi, D., Munnich, A., Rötig, A., & Rustin, P. (2002). Idebenone and reduced cardiac hypertrophy in Friedreich's ataxia. *Heart*, *87*(4), 346–349. https://doi.org/10.1136/heart.87.4.346

Hayashi, G., Jasoliya, M., Sahdeo, S., Saccà, F., Pane, C., Filla, A., … Cortopassi, G. (2017). Dimethyl fumarate mediates Nrf2-dependent mitochondrial biogenesis in mice and humans. *Human Molecular Genetics*, *26*(15), 2864–2873.

https://doi.org/10.1093/hmg/ddx167
Hemenway, C. S., & Heitman, J. (1999). Calcineurin: Structure, function, and inhibition. *Cell Biochemistry and Biophysics*, *30*(1), 115–51. https://doi.org/10.1007/BF02737887
Herrington, J., Park, Y. B., Babcock, D. F., & Hille, B. (1996). Dominant role of mitochondria in clearance of large Ca2+ loads from rat adrenal chromaffin cells. *Neuron*, *16*(1), 219–228. https://doi.org/10.1016/S0896-6273(00)80038-0
Hick, A., Wattenhofer-Donzé, M., Chintawar, S., Tropel, P., Simard, J. P., Vaucamps, N., … Puccio, H. (2013). Neurons and cardiomyocytes derived from induced pluripotent stem cells as a model for mitochondrial defects in Friedreich's ataxia. *Disease Models & Mechanisms*, *6*(3), 608–21. https://doi.org/10.1242/dmm.010900
Hiebert, P., & Werner, S. (2019). Regulation of wound healing by the nrf2 transcription factor—more than cytoprotection. *International Journal of Molecular Sciences*, *20*(16), 3856. https://doi.org/10.3390/ijms20163856
Hii, C. S., & Ferrante, A. (2016). The non-genomic actions of vitamin D. *Nutrients*, *8*(3), 135. https://doi.org/10.3390/nu8030135
Hogan, P. G., Chen, L., Nardone, J., & Rao, A. (2003). Transcriptional regulation by calcium, calcineurin, and NFAT. *Genes and Development*, *17*(18), 2205–32. https://doi.org/10.1101/gad.1102703
Honda, C. N. (1995). Differential distribution of calbindin-D28k and parvalbumin in somatic and visceral sensory neurons. *Neuroscience*, *68*(3), 883–92. https://doi.org/10.1016/0306-4522(95)00180-Q
Honrath, B., Metz, I., Bendridi, N., Rieusset, J., Culmsee, C., & Dolga, A. M. (2017). Glucose-regulated protein 75 determines ER–mitochondrial coupling and sensitivity to oxidative stress in neuronal cells. *Cell Death Discovery*, *3*, 17076. https://doi.org/10.1038/cddiscovery.2017.76
Huang, J., Dizin, E., & Cowan, J. A. (2008). Mapping iron binding sites on human frataxin: Implications for cluster assembly on the ISU Fe-S cluster scaffold protein. *Journal of Biological Inorganic Chemistry*, *13*(5), 825–36. https://doi.org/10.1007/s00775-008-0369-4
Huang, Y. S., Nestruck, A. C., Barbeau, A., Bouchard, J. P., & Davignon, J. (1978). Plasma Lipids and Lipoproteins in Friedreich's Ataxia and Familial Spastic Ataxia — Evidence for an Abnormal Composition of High Density Lipoproteins. *Canadian Journal of Neurological Sciences / Journal Canadien Des Sciences Neurologiques*, *5*(1), 149–56. https://doi.org/10.1017/S0317167100024951
Hurst, S., Hoek, J., & Sheu, S. S. (2017). Mitochondrial Ca2+ and regulation of the permeability transition pore. *Journal of Bioenergetics and Biomembranes*, *49*(1), 27–47. https://doi.org/10.1007/s10863-016-9672-x
Igoillo-Esteve, M., Gurgul-Convey, E., Hu, A., Romagueira Bichara Dos Santos, L., Abdulkarim, B., Chintawar, S., … Cnop, M. (2015). Unveiling a common mechanism of apoptosis in β-cells and neurons in Friedreich's ataxia. *Human Molecular Genetics*, *24*(8), 2274–2286. https://doi.org/10.1093/hmg/ddu745
Igoillo-Esteve, M., Oliveira, A. F., Cosentino, C., Fantuzzi, F., Demarez, C., Toivonen, S., … Cnop, M. (2020). Exenatide induces frataxin expression and improves mitochondrial function in Friedreich ataxia. *JCI Insight*, *5*(2), e134221. https://doi.org/10.1172/jci.insight.134221
Irazusta, V., Cabiscol, E., Reverter-Branchat, G., Ros, J., & Tamarit, J. (2006). Manganese is the link between frataxin and iron-sulfur deficiency in the yeast model of Friedreich ataxia. *Journal of Biological Chemistry*, *281*(18), 12227–

12232. https://doi.org/10.1074/jbc.M511649200
Irazusta, V., Moreno-Cermeño, A., Cabiscol, E., Ros, J., & Tamarit, J. (2008). Major targets of iron-induced protein oxidative damage in frataxin-deficient yeasts are magnesium-binding proteins. *Free Radical Biology and Medicine*, *44*(9), 1712–1723. https://doi.org/10.1016/j.freeradbiomed.2008.01.014
Jackson, J. G., Usachev, Y. M., & Thayer, S. A. (2007). Bradykinin-induced nuclear factor of activated T-cells-dependent transcription in rat dorsal root ganglion neurons. *Molecular Pharmacology*, *72*(2), 303–310. https://doi.org/10.1124/mol.107.035048
Jacquillet, G., & Unwin, R. J. (2019). Physiological regulation of phosphate by vitamin D, parathyroid hormone (PTH) and phosphate (Pi). *Pflugers Archiv European Journal of Physiology*, *471*(1), 83–98. https://doi.org/10.1007/s00424-018-2231-z
Jänicke, R. U., Ng, P., Sprengart, M. L., & Porter, A. G. (1998). Caspase-3 is required for α-fodrin cleavage but dispensable for cleavage of other death substrates in apoptosis. *Journal of Biological Chemistry*, *273*(25), 15540. https://doi.org/10.1074/jbc.273.25.15540
Jasoliya, M. J., McMackin, M. Z., Henderson, C. K., Perlman, S. L., & Cortopassi, G. A. (2017). Frataxin deficiency impairs mitochondrial biogenesis in cells, mice and humans. *Human Molecular Genetics*, *26*(14), 2627–2633. https://doi.org/10.1093/hmg/ddx141
Jasoliya, M., Sacca, F., Sahdeo, S., Chedin, F., Pane, C., Morra, V. B., … Cortopassi, G. (2019). Dimethyl fumarate dosing in humans increases frataxin expression: A potential therapy for Friedreich's Ataxia. *PLoS ONE*, *14*(6). https://doi.org/10.1371/journal.pone.0217776
Jensen, J. R., & Rehder, V. (1991). FCCP releases Ca2+ from a non-mitochondrial store in an identified Helisoma neuron. *Brain Research*, *551*(1–2), 311–314. https://doi.org/10.1016/0006-8993(91)90947-T
Jiang, X., Jin, T., Zhang, H., Miao, J., Zhao, X., Su, Y., & Zhang, Y. (2019). Current Progress of Mitochondrial Quality Control Pathways Underlying the Pathogenesis of Parkinson's Disease. *Oxidative Medicine and Cellular Longevity*, *2019*, 4578462. https://doi.org/10.1155/2019/4578462
Jin, S. M., Lazarou, M., Wang, C., Kane, L. A., Narendra, D. P., & Youle, R. J. (2010). Mitochondrial membrane potential regulates PINK1 import and proteolytic destabilization by PARL. *The Journal of Cell Biology*, *191*(5), 933–42. https://doi.org/10.1083/jcb.201008084.
Johnson, J. A., Grande, J. P., Windebank, A. J., & Kumar, R. (1996). 1,25-Dihydroxyvitamin D3 receptors in developing dorsal root ganglia of fetal rats. *Developmental Brain Research*, *92*(1), 120–4. https://doi.org/10.1016/0165-3806(95)00204-9
Kakhlon, O., Manning, H., Breuer, W., Melamed-Book, N., Lu, C., Cortopassi, G., … Cabantchik, Z. I. (2008). Cell functions impaired by frataxin deficiency are restored by drug-mediated iron relocation. *Blood*, *112*(13), 5219–27. https://doi.org/10.1182/blood-2008-06-161919
Kar, P., Chakraborti, T., Samanta, K., & Chakraborti, S. (2009). μ-Calpain mediated cleavage of the Na+/Ca2+ exchanger in isolated mitochondria under A23187 induced Ca2+ stimulation. *Archives of Biochemistry and Biophysics*, *482*(1–2), 66–76. https://doi.org/10.1016/j.abb.2008.11.024
Karthikeyan, G., Santos, J. H., Graziewicz, M. A., Copeland, W. C., Isaya, G., Van Houten, B., & Resnick, M. A. (2003). Reduction in frataxin causes progressive accumulation of mitochondrial damage. *Human Molecular Genetics*, *12*(24),

3331–42. https://doi.org/10.1093/hmg/ddg349
Kathrin Lutz, A., Exner, N., Fett, M. E., Schleke, J. S., Kloos, K., Lämmermann, K., … Winklhofer, K. F. (2009). Loss of parkin or PINK1 function increases Drp1-dependent mitochondrial fragmentation. *Journal of Biological Chemistry*, *284*(34), 22938–51. https://doi.org/10.1074/jbc.M109.035774
Katoshevski, T., Ben-Kasus Nissim, T., & Sekler, I. (2021). Recent studies on NCLX in health and diseases. *Cell Calcium*, *94*, 102345. https://doi.org/10.1016/j.ceca.2020.102345
Katsu-Jiménez, Y., Loría, F., Carlos Corona, J., & Díaz-Nido, J. (2016). Gene Transfer of Brain-derived Neurotrophic Factor (BDNF) Prevents Neurodegeneration Triggered by FXN Deficiency. *Molecular Therapy : The Journal of the American Society of Gene Therapy*, *24*(5), 877–89. https://doi.org/10.1038/mt.2016.32
Kennel, K. A., Drake, M. T., & Hurley, D. L. (2010). Vitamin D deficiency in adults: When to test and how to treat. *Mayo Clinic Proceedings*, *85*(8), 752–7. https://doi.org/10.4065/mcp.2010.0138
Khasabova, I. A., Khasabov, S. G., Olson, J. K., Uhelski, M. L., Kim, A. H., Albino-Ramírez, A. M., … Simone, D. A. (2019). Pioglitazone, a PPARγ agonist, reduces cisplatin-evoked neuropathic pain by protecting against oxidative stress. *Pain*, *160*(3), 688–701. https://doi.org/10.1097/j.pain.0000000000001448
Khundmiri, S. J., Murray, R. D., & Lederer, E. (2016). PTH and vitamin D. *Comprehensive Physiology*, *6*(2), 561–601. https://doi.org/10.1002/cphy.c140071
Kidd, A., Coleman, R., Whiteford, M., Barron, L. H., Simpson, S. A., & Haites, N. E. (2001). Breast cancer in two sisters with Friedreich's ataxia. *European Journal of Surgical Oncology*, *27*(5), 512–4. https://doi.org/10.1053/ejso.2000.1093
Kim, B., Takeuchi, A., Koga, O., Hikida, M., & Matsuoka, S. (2012). Pivotal role of mitochondrial Na+–Ca2+ exchange in antigen receptor mediated Ca2+ signalling in DT40 and A20 B lymphocytes. *The Journal of Physiology*, *590*(3), 459–474. https://doi.org/10.1113/jphysiol.2011.222927
Kim, M. J., Kim, D. W., Jeong, H. J., Sohn, E. J., Shin, M. J., Ahn, E. H., … Choi, S. Y. (2012). Tat-Frataxin protects dopaminergic neuronal cells against MPTP-induced toxicity in a mouse model of Parkinson's disease. *Biochimie*, *94*(11), 2448–56. https://doi.org/10.1016/j.biochi.2012.07.005
Kim, M. S., & Usachev, Y. M. (2009). Mitochondrial Ca2+ cycling facilitates activation of the transcription factor NFAT in sensory neurons. *Journal of Neuroscience*, *29*(39), 12101–14. https://doi.org/10.1523/JNEUROSCI.3384-09.2009
Kipanyula, M. J., Kimaro, W. H., & Seke Etet, P. F. (2016). The Emerging Roles of the Calcineurin-Nuclear Factor of Activated T-Lymphocytes Pathway in Nervous System Functions and Diseases. *Journal of Aging Research*, *2016*, 5081021. https://doi.org/10.1155/2016/5081021
Kočovská, E., Gaughran, F., Krivoy, A., & Meier, U. C. (2017). Vitamin-D deficiency as a potential environmental risk factor in multiple sclerosis, schizophrenia, and autism. *Frontiers in Psychiatry*, *8*, 47. https://doi.org/10.3389/fpsyt.2017.00047
Koeppen, A. H. (2011). Friedreich's ataxia: Pathology, pathogenesis, and molecular genetics. *Journal of the Neurological Sciences*, *303*(1–2), 1–12. https://doi.org/10.1016/j.jns.2011.01.010
Koeppen, A. H., Kuntzsch, E. C., Bjork, S. T., Ramirez, R. L., Mazurkiewicz, J. E., & Feustel, P. J. (2013). Friedreich ataxia: metal dysmetabolism in dorsal root ganglia. *Acta Neuropathologica Communications*, *1*(1), 26. https://doi.org/10.1186/2051-5960-1-26
Koeppen, A. H., & Mazurkiewicz, J. E. (2013). Friedreich Ataxia: Neuropathology

Revised. *Journal of Neuropathology & Experimental Neurology*, *72*(2), 78–90. https://doi.org/10.1097/NEN.0b013e31827e5762

Koeppen, A. H., Michael, S. C., Knutson, M. D., Haile, D. J., Qian, J., Levi, S., … Lamarche, J. B. (2007). The dentate nucleus in Friedreich's ataxia: the role of iron-responsive proteins manifesta-tion of mitochondrial iron dysmetabolism in the terminals. *Acta Neuropathol*, *114*, 163–173. https://doi.org/10.1007/s00401-007-0220-y

Koeppen, A. H., Morral, J. A., Davis, A. N., Qian, J., Petrocine, S. V., Knutson, M. D., … Li, D. (2009). The dorsal root ganglion in Friedreich's ataxia. *Acta Neuropathologica*, *118*(6), 763–776. https://doi.org/10.1007/s00401-009-0589-x

Kong, X., Wang, R., Xue, Y., Liu, X., Zhang, H., Chen, Y., … Chang, Y. (2010). Sirtuin 3, a new target of PGC-1α, plays an important role in the suppression of ROS and mitochondrial biogenesis. *PLoS ONE*, *5*(7), e11707. https://doi.org/10.1371/journal.pone.0011707

König, T., Tröder, S. E., Bakka, K., Korwitz, A., Richter-Dennerlein, R., Lampe, P. A., … Langer, T. (2016). The m-AAA Protease Associated with Neurodegeneration Limits MCU Activity in Mitochondria. *Molecular Cell*, *64*(1), 148–162. https://doi.org/10.1016/j.molcel.2016.08.020

Kostic, M., Katoshevski, T., & Sekler, I. (2018). Allosteric Regulation of NCLX by Mitochondrial Membrane Potential Links the Metabolic State and Ca2+ Signaling in Mitochondria. *Cell Reports*, *25*(12), 3465–3475.e4. https://doi.org/10.1016/j.celrep.2018.11.084

Kostic, M., Ludtmann, M. H. R., Bading, H., Hershfinkel, M., Steer, E., Chu, C. T., … Sekler, I. (2015). PKA Phosphorylation of NCLX Reverses Mitochondrial Calcium Overload and Depolarization, Promoting Survival of PINK1-Deficient Dopaminergic Neurons. *Cell Reports*, *13*(2), 376–386. https://doi.org/10.1016/j.celrep.2015.08.079

Kostic, M., & Sekler, I. (2018). Function, regulation and physiological role of the mitochondrial Na+/Ca2+ exchanger, NCLX. *Current Opinion in Physiology*, *3*, 63–70. https://doi.org/10.1016/j.cophys.2018.02.007

Kostic, M., & Sekler, I. (2019). Functional properties and mode of regulation of the mitochondrial Na+/Ca2+ exchanger, NCLX. *Seminars in Cell and Developmental Biology*, *94*, 59–65. https://doi.org/10.1016/j.semcdb.2019.01.009

Kosutic, J., & Zamurovic, D. (2005). High-dose beta-blocker hypertrophic cardiomyopathy therapy in a patient with Friedreich ataxia. *Pediatric Cardiology*, *26*(5), 727–730. https://doi.org/10.1007/s00246-005-0930-7

Koutnikova, H., Campuzano, V., Foury, F., Dollé, P., Cazzalini, O., & Koenig, M. (1997). Studies of human, mouse and yeast homologues indicate a mitochondrial function for frataxin. *Nature Genetics*, *16*(4), 345–351. https://doi.org/10.1038/ng0897-345

Krames, E. S. (2015). The dorsal root ganglion in chronic pain and as a target for neuromodulation: A review. *Neuromodulation*, *18*(1), 24–32. https://doi.org/10.1111/ner.12247

Kruger, P. C., Yang, K. X., Parsons, P. J., Becker, A. B., Feustel, P. J., & Koeppen, A. H. (2016). Abundance and significance of iron, zinc, copper, and calcium in the hearts of patients with Friedreich ataxia. *American Journal of Cardiology*, *118*(1), 127–131. https://doi.org/10.1016/j.amjcard.2016.04.024

Kumari, D., & Usdin, K. (2012). Is Friedreich ataxia an epigenetic disorder? *Clinical Epigenetics*, *4*(1), 2. https://doi.org/10.1186/1868-7083-4-2

Lamarche, J. B., Côté, M., & Lemieux, B. (1980). The cardiomyopathy of Friedreich's

ataxia morphological observations in 3 cases. *The Canadian Journal of Neurological Sciences. Le Journal Canadien Des Sciences Neurologiques*, *7*(4), 389–96. https://doi.org/10.1017/s0317167100022927

Landel, V., Millet, P., Baranger, K., Loriod, B., & Féron, F. (2016). Vitamin D interacts with Esr1 and Igf1 to regulate molecular pathways relevant to Alzheimer's disease. *Molecular Neurodegeneration*, *11*, 22. https://doi.org/10.1186/s13024-016-0087-2

Landreth, G., Jiang, Q., Mandrekar, S., & Heneka, M. (2008). PPARγ Agonists as Therapeutics for the Treatment of Alzheimer's Disease. *Neurotherapeutics*, *5*(3), 481–9. https://doi.org/10.1016/j.nurt.2008.05.003

Lang, F., Ma, K., & Leibrock, C. B. (2019). 1,25(OH)2D3 in Brain Function and Neuropsychiatric Disease. *Neuro-Signals*, *27*(1), 40–49. https://doi.org/10.33594/000000182

Latimer, C. S., Brewer, L. D., Searcy, J. L., Chen, K.-C., Popović, J., Kraner, S. D., … Porter, N. M. (2014). Vitamin D prevents cognitive decline and enhances hippocampal synaptic function in aging rats. *Proceedings of the National Academy of Sciences of the United States of America*, *111*(41), E4359-66. https://doi.org/10.1073/pnas.1404477111

Lavrik, I. N., Golks, A., & Krammer, P. H. (2005). Caspase: Pharmacological manipulation of cell death. *Journal of Clinical Investigation*, *115*(10), 2665–72. https://doi.org/10.1172/JCI26252

Lee, K. S., Park, S. J., Hwang, P. H., Yi, H. K., Song, C. H., Chai, O. H., … Lee, Y. C. (2005). PPAR-gamma modulates allergic inflammation through up-regulation of PTEN. *The FASEB Journal*, *19*(8), 1033–5. https://doi.org/10.1096/fj.04-3309fje

Lee, Y. K., Ho, P. W. L., Schick, R., Lau, Y. M., Lai, W. H., Zhou, T., … Siu, C. W. (2014). Modeling of Friedreich ataxia-related iron overloading cardiomyopathy using patient-specific-induced pluripotent stem cells. *Pflugers Archiv European Journal of Physiology*, *466*(9), 1831–1844. https://doi.org/10.1007/s00424-013-1414-x

Lefevre, S., Sliwa, D., Rustin, P., Camadro, J. M., & Santos, R. (2012). Oxidative stress induces mitochondrial fragmentation in frataxin-deficient cells. *Biochemical and Biophysical Research Communications*, *418*(2), 336–41. https://doi.org/10.1016/j.bbrc.2012.01.022

Lesuisse, E., Santos, R., Matzanke, B. F., Knight, S. A. B., Camadro, J. M., & Dancis, A. (2003). Iron use for haeme synthesis is under control of the yeast frataxin homologue (Yfh1). *Human Molecular Genetics*, *12*(8), 879–889. https://doi.org/10.1093/hmg/ddg096

Lezana, J. P., Dagan, S. Y., Robinson, A., Goldstein, R. S., Fainzilber, M., Bronfman, F. C., & Bronfman, M. (2016). Axonal PPARγ promotes neuronal regeneration after injury. *Developmental Neurobiology*, *76*(6), 688–701. https://doi.org/10.1002/dneu.22353

Li, K., Besse, E. K., Ha, D., Kovtunovych, G., & Rouault, T. A. (2008). Iron-dependent regulation of frataxin expression: Implications for treatment of Friedreich ataxia. *Human Molecular Genetics*, *17*(15), 2265–2273. https://doi.org/10.1093/hmg/ddn127

Li, K., Singh, A., Crooks, D. R., Dai, X., Cong, Z., Pan, L., … Rouault, T. A. (2010). Expression of human frataxin is regulated by transcription factors SRF and TFAP2. *PLoS ONE*, *5*(8), e12286. https://doi.org/10.1371/journal.pone.0012286

Liang, H., He, S., Yang, J., Jia, X., Wang, P., Chen, X., … Yin, Y. (2014). PTENα, a PTEN isoform translated through alternative initiation, regulates mitochondrial function and energy metabolism. *Cell Metabolism*, *19*(5), 836–48.

https://doi.org/10.1016/j.cmet.2014.03.023
Libonati, L., Onesti, E., Gori, M. C., Ceccanti, M., Cambieri, C., Fabbri, A., … Inghilleri, M. (2017). Vitamin D in amyotrophic lateral sclerosis. *Functional Neurology*, *32*(1), 35–40. https://doi.org/10.11138/FNeur/2017.32.1.035
Libri, V., Yandim, C., Athanasopoulos, S., Loyse, N., Natisvili, T., Law, P. P., … Festenstein, R. (2014). Epigenetic and neurological effects and safety of high-dose nicotinamide in patients with Friedreich's ataxia: An exploratory, open-label, dose-escalation study. *The Lancet*, *384*(9942), 504–513. https://doi.org/10.1016/S0140-6736(14)60382-2
Lin, H., Magrane, J., Rattelle, A., Stepanova, A., Galkin, A., Clark, E. M., … Lynch, D. R. (2017). Early cerebellar deficits in mitochondrial biogenesis and respiratory chain complexes in the KIKO mouse model of Friedreich ataxia. *DMM Disease Models and Mechanisms*, *10*(11), 1343–1352. https://doi.org/10.1242/dmm.030502
Lin, W., & Kang, U. J. (2008). Characterization of PINK1 processing, stability, and subcellular localization. *Journal of Neurochemistry*, *106*(1), 464–474. https://doi.org/10.1111/j.1471-4159.2008.05398.x
Linder, M. D., Morkunaite-Haimi, S., Kinnunen, P. K. J., Bernardi, P., & Eriksson, O. (2002). Ligand-selective modulation of the permeability transition pore by arginine modification: Opposing effects of p-hydroxyphenylglyoxal and phenylglyoxal. *Journal of Biological Chemistry*, *277*(2), 037-42. https://doi.org/10.1074/jbc.M107610200
Liu, J. C., Liu, J., Holmström, K. M., Menazza, S., Parks, R. J., Fergusson, M. M., … Finkel, T. (2016). MICU1 Serves as a Molecular Gatekeeper to Prevent In Vivo Mitochondrial Calcium Overload. *Cell Reports*, *16*(6), 1561–1573. https://doi.org/10.1016/j.celrep.2016.07.011
Liu, M. C., Kobeissy, F., Zheng, W., Zhang, Z., Hayes, R. L., & Wang, K. K. W. (2011). Dual vulnerability of tau to calpains and caspase-3 proteolysis under neurotoxic and neurodegenerative conditions. *ASN Neuro*, *3*(1), e00051. https://doi.org/10.1042/AN20100012
Liu, P., Lin, H., Xu, Y., Zhou, F., Wang, J., Liu, J., … Yao, P. (2018). Frataxin-Mediated PINK1–Parkin-Dependent Mitophagy in Hepatic Steatosis: The Protective Effects of Quercetin. *Molecular Nutrition and Food Research*, *62*(16), e1800164. https://doi.org/10.1002/mnfr.201800164
Liu, Y., Guardia-Laguarta, C., Yin, J., Erdjument-Bromage, H., Martin, B., James, M., … Przedborski, S. (2017). The Ubiquitination of PINK1 Is Restricted to Its Mature 52-kDa Form. *Cell Reports*, *20*(1), 30–39. https://doi.org/10.1016/j.celrep.2017.06.022
Llorens, J. V, Navarro, J. A., Martínez-Sebastián, M. J., Baylies, M. K., Schneuwly, S., Botella, J. A., & Moltó, M. D. (2007). Causative role of oxidative stress in a Drosophila model of Friedreich ataxia. *The FASEB Journal*, *21*(2), 333–44. https://doi.org/10.1096/fj.05-5709com
Llorens, J. V, Soriano, S., Calap-Quintana, P., Gonzalez-Cabo, P., & Moltó, M. D. (2019). The role of iron in Friedreich's ataxia: Insights from studies in human tissues and cellular and animal models. *Frontiers in Neuroscience*, *13*, 75. https://doi.org/10.3389/fnins.2019.00075
Llorente-Folch, I., Rueda, C. B., Pardo, B., Szabadkai, G., Duchen, M. R., & Satrustegui, J. (2015). The regulation of neuronal mitochondrial metabolism by calcium. *Journal of Physiology*, *593*(16), 3447–3462. https://doi.org/10.1113/JP270254
Lodi, R., Cooper, J. M., Bradley, J. L., Manners, D., Styles, P., Taylor, D. J., &

Schapira, A. H. V. (1999). Deficit of in vivo mitochondrial ATP production in patients with Friedreich ataxia. *Proceedings of the National Academy of Sciences of the United States of America*, *96*(20), 11492–5. https://doi.org/10.1073/pnas.96.20.11492

Londono, C., Osorio, C., Gama, V., & Alzate, O. (2012). Mortalin, apoptosis, and neurodegeneration. *Biomolecules*, *2*(1), 143–64. https://doi.org/10.3390/biom2010143

Loría, F., & Díaz-Nido, J. (2015). Frataxin knockdown in human astrocytes triggers cell death and the release of factors that cause neuronal toxicity. *Neurobiology of Disease*, *76*, 1–12. https://doi.org/10.1016/j.nbd.2014.12.017

Lu, S.-G., Zhang, X., & Gold, M. S. (2006). Intracellular calcium regulation among subpopulations of rat dorsal root ganglion neurons. *The Journal of Physiology*, *577*(1), 169–190. https://doi.org/10.1113/jphysiol.2006.116418

Luongo, T. S., Lambert, J. P., Gross, P., Nwokedi, M., Lombardi, A. A., Shanmughapriya, S., … Elrod, J. W. (2017). The mitochondrial Na+/Ca2+ exchanger is essential for Ca2+ homeostasis and viability. *Nature*, *545*(7652), 93–97. https://doi.org/10.1038/nature22082

Lynch, D. R., Willi, S. M., Wilson, R. B., Cotticelli, M. G., Brigatti, K. W., Deutsch, E. C., … Sciascia, T. (2012). A0001 in Friedreich ataxia: Biochemical characterization and effects in a clinical trial. *Movement Disorders*, *27*(8), 1026–1033. https://doi.org/10.1002/mds.25058

Maeda, T., Kiguchi, N., Kobayashi, Y., Ozaki, M., & Kishioka, S. (2008). Pioglitazone attenuates tactile allodynia and thermal hyperalgesia in mice subjected to peripheral nerve injury. *Journal of Pharmacological Sciences*, *108*(3), 341–7. https://doi.org/10.1254/jphs.08207FP

Magnoni, R., Palmfeldt, J., Christensen, J. H., Sand, M., Maltecca, F., Corydon, T. J., … Bross, P. (2013). Late onset motoneuron disorder caused by mitochondrial Hsp60 chaperone deficiency in mice. *Neurobiology of Disease*, *54*, 12–23. https://doi.org/10.1016/j.nbd.2013.02.012

Maio, N., Jain, A., & Rouault, T. A. (2020). Mammalian iron–sulfur cluster biogenesis: Recent insights into the roles of frataxin, acyl carrier protein and ATPase-mediated transfer to recipient proteins. *Current Opinion in Chemical Biology*, *55*, 34–44. https://doi.org/10.1016/j.cbpa.2019.11.014

Malaney, P., Uversky, V. N., & Davé, V. (2017). PTEN proteoforms in biology and disease. *Cellular and Molecular Life Sciences*, *74*(15), 2783–2794. https://doi.org/10.1007/s00018-017-2500-6

Marchi, S., Corricelli, M., Branchini, A., Vitto, V. A. M., Missiroli, S., Morciano, G., … Pinton, P. (2019). Akt-mediated phosphorylation of MICU 1 regulates mitochondrial Ca 2+ levels and tumor growth. *The EMBO Journal*, *38*(2), e99435. https://doi.org/10.15252/embj.201899435

Marchi, S., Patergnani, S., Missiroli, S., Morciano, G., Rimessi, A., Wieckowski, M. R., … Pinton, P. (2018). Mitochondrial and endoplasmic reticulum calcium homeostasis and cell death. *Cell Calcium*, *69*, 62–72. https://doi.org/10.1016/j.ceca.2017.05.003

Marcus, D., Lichtenstein, M., Cohen, N., Hadad, R., Erlich-Hadad, T., Greif, H., & Lorberboum-Galski, H. (2016). Heterologous mitochondrial targeting sequences can deliver functional proteins into mitochondria. *The International Journal of Biochemistry & Cell Biology*, *81*, 48–56. https://doi.org/10.1016/j.biocel.2016.10.013

Marmigère, F., & Carroll, P. (2014). Neurotrophin signalling and transcription

programmes interactions in the development of somatosensory neurons. *Handbook of Experimental Pharmacology*, *220*, 329–53. https://doi.org/10.1007/978-3-642-45106-5_13

Marmolino, D., & Acquaviva, F. (2009). Friedreich's ataxia: From the (GAA) n repeat mediated silencing to new promising molecules for therapy. *Cerebellum*, *8*(3), 245–259. https://doi.org/10.1007/s12311-008-0084-2

Marmolino, D., Acquaviva, F., Pinelli, M., Monticelli, A., Castaldo, I., Filla, A., & Cocozza, S. (2009). PPAR-γ agonist azelaoyl PAF increases frataxin protein and mRNA expression. new implications for the Friedreich's Ataxia Therapy. *Cerebellum*, *8*(2), 98–103. https://doi.org/10.1007/s12311-008-0087-z

Marmolino, D., Manto, M., Acquaviva, F., Vergara, P., Ravella, A., Monticelli, A., & Pandolfo, M. (2010). PGC-1alpha down-regulation affects the antioxidant response in friedreich's ataxia. *PLoS ONE*, *5*(4), e10025. https://doi.org/10.1371/journal.pone.0010025

Martin, A. S., Abraham, D. M., Hershberger, K. A., Bhatt, D. P., Mao, L., Cui, H., … Hirschey, M. D. (2017). Nicotinamide mononucleotide requires SIRT3 to improve cardiac function and bioenergetics in a Friedreich's ataxia cardiomyopathy model. *JCI Insight*, *2*(14), e93885. https://doi.org/10.1172/jci.insight.93885

Martin, L. J. (2010). Mitochondrial and Cell Death Mechanisms in Neurodegenerative Diseases. *Pharmaceuticals*, *3*(4), 839–915. https://doi.org/10.3390/ph3040839

Matsuda, S., & Koyasu, S. (2000). Mechanisms of action of cyclosporine. *Immunopharmacology*, *47*(2–3), 119–25. https://doi.org/10.1016/S0162-3109(00)00192-2

Matteucci, A., Patron, M., Reane, D. V., Gastaldello, S., Amoroso, S., Rizzuto, R., … Calì, T. (2018). Parkin-dependent regulation of the MCU complex component MICU1. *Scientific Reports*, *8*(1), 14199. https://doi.org/10.1038/s41598-018-32551-7

Mazzara, P. G., Muggeo, S., Luoni, M., Massimino, L., Zaghi, M., Valverde, P. T. T., … Broccoli, V. (2020). Frataxin gene editing rescues Friedreich's ataxia pathology in dorsal root ganglia organoid-derived sensory neurons. *Nature Communications*, *11*(1), 4178. https://doi.org/10.1038/s41467-020-17954-3

McLeod, J. G. (1971). An electrophysiological and pathological study of peripheral nerves in Friedreich's ataxia. *Journal of the Neurological Sciences*, *12*(3), 333–349. https://doi.org/10.1016/0022-510X(71)90067-0

Melcangi, R. C., Giatti, S., Calabrese, D., Pesaresi, M., Cermenati, G., Mitro, N., … Caruso, D. (2014). Levels and actions of progesterone and its metabolites in the nervous system during physiological and pathological conditions. *Progress in Neurobiology*, *113*, 56–69. https://doi.org/10.1016/j.pneurobio.2013.07.006

Meng, H., Yan, W. Y., Lei, Y. H., Wan, Z., Hou, Y. Y., Sun, L. K., & Zhou, J. P. (2019). SIRT3 Regulation of Mitochondrial Quality Control in Neurodegenerative Diseases. *Frontiers in Aging Neuroscience*, *11*, 313. https://doi.org/10.3389/fnagi.2019.00313

Michels, T. C., & Kelly, K. M. (2013). Parathyroid disorders. *American Family Physician*, *88*(4), 249–57. https://doi.org/10.1201/9780138719128-69

Miller, K. E., Hoffman, E. M., Sutharshan, M., & Schechter, R. (2011). Glutamate pharmacology and metabolism in peripheral primary afferents: Physiological and pathophysiological mechanisms. *Pharmacology and Therapeutics*, *130*(3), 283–309. https://doi.org/10.1016/j.pharmthera.2011.01.005

Miller, W. L. (2013). Steroid hormone synthesis in mitochondria. *Molecular and Cellular Endocrinology*, *379*(1–2), 62–73.

https://doi.org/10.1016/j.mce.2013.04.014
Minaguchi, T., Waite, K. A., & Eng, C. (2006). Nuclear localization of PTEN is regulated by Ca2+ through a tyrosil phosphorylation-independent conformational modification in major vault protein. *Cancer Research*, *66*(24), 11677–82. https://doi.org/10.1158/0008-5472.CAN-06-2240
Mincheva-Tasheva, S., Obis, E., Tamarit, J., & Ros, J. (2014). Apoptotic cell death and altered calcium homeostasis caused by frataxin depletion in dorsal root ganglia neurons can be prevented by BH4 domain of Bcl-xL protein. *Human Molecular Genetics*, *23*(7), 1829–1841. https://doi.org/10.1093/hmg/ddt576
Minke, B. (2006). TRP channels and Ca2+ signaling. *Cell Calcium*, *40*(3), 261–75. https://doi.org/10.1016/j.ceca.2006.05.002
Mironov, S. L., & Symonchuk, N. (2006). ER vesicles and mitochondria move and communicate at synapses. *Journal of Cell Science*, *119*(Pt 23), 4926–34. https://doi.org/10.1242/jcs.03254
Mishra, O. P., Ashraf, Q. M., & Delivoria-Papadopoulos, M. (2002). Phosphorylation of cAMP response element binding (CREB) protein during hypoxia in cerebral cortex of newborn piglets and the effect of nitric oxide synthase inhibition. *Neuroscience*, *115*(3), 985–91. https://doi.org/10.1016/S0306-4522(02)00275-0
Miura, R. M. (2002). Analysis of excitable cell models. *Journal of Computational and Applied Mathematics*, *144*(1–2), 29–47. https://doi.org/10.1016/S0377-0427(01)00550-7
Mollá, B., Muñoz-Lasso, D. C., Riveiro, F., Bolinches-Amorós, A., Pallardó, F. V., Fernandez-Vilata, A., … Gonzalez-Cabo, P. (2017). Reversible Axonal Dystrophy by Calcium Modulation in Frataxin-Deficient Sensory Neurons of YG8R Mice. *Frontiers in Molecular Neuroscience*, *10*, 264. https://doi.org/10.3389/fnmol.2017.00264
Monzio Compagnoni, G., Di Fonzo, A., Corti, S., Comi, G. P., Bresolin, N., & Masliah, E. (2020). The Role of Mitochondria in Neurodegenerative Diseases: the Lesson from Alzheimer's Disease and Parkinson's Disease. *Molecular Neurobiology*, *57*(7), 2959–2980. https://doi.org/10.1007/s12035-020-01926-1
Moreau, B., Nelson, C., & Parekh, A. B. (2006). Biphasic Regulation of Mitochondrial Ca2+ Uptake by Cytosolic Ca2+ Concentration. *Current Biology*, *16*(16), 1672–1677. https://doi.org/10.1016/j.cub.2006.06.059
Morello, M., Landel, V., Lacassagne, E., Baranger, K., Annweiler, C., Féron, F., & Millet, P. (2018). Vitamin D Improves Neurogenesis and Cognition in a Mouse Model of Alzheimer's Disease. *Molecular Neurobiology*, *55*(8), 6463–6479. https://doi.org/10.1007/s12035-017-0839-1
Moreno-Cermeñ, A., Obis, L., Bellí, G., Cabiscol, E., Ros, J., & Tamarit, J. (2010). Frataxin Depletion in Yeast Triggers Up-regulation of Iron Transport Systems before Affecting Iron-Sulfur Enzyme Activities, *285*(53), 41653–64. https://doi.org/10.1074/jbc.M110.149443
Moreno-Cermeño, A., Alsina, D., Cabiscol, E., Tamarit, J., & Ros, J. (2013). Metabolic remodeling in frataxin-deficient yeast is mediated by Cth2 and Adr1. *Biochimica et Biophysica Acta - Molecular Cell Research*, *1833*(12), 3326–3337. https://doi.org/10.1016/j.bbamcr.2013.09.019
Moretti, R., Morelli, M. E., & Caruso, P. (2018). Vitamin D in neurological diseases: A rationale for a pathogenic impact. *International Journal of Molecular Sciences*, *19*(8), 2245. https://doi.org/10.3390/ijms19082245
Muñoz-Lasso, D. C., Mollá, B., Calap-Quintana, P., García-Giménez, J. L., Pallardo, F. V. V., Palau, F., & Gonzalez-Cabo, P. (2020). Cofilin dysregulation alters actin

turnover in frataxin-deficient neurons. *Scientific Reports*, *10*(1), 5207. https://doi.org/10.1038/s41598-020-62050-7

Murayama, S. Bouldin, T. W. Suzuki, K. (1992). Pathological study of corticospinal-tract degeneration in Friedreich's ataxia. *Neuropathology and Applied Neurobiology*, *18*(1), 81–86. https://doi.org/10.1111/j.1365-2990.1992.tb00766.x

Murayama, A., Takeyama, K. I., Kitanaka, S., Kodera, Y., Hosoya, T., & Kato, S. (1998). The promoter of the human 25-hydroxyvitamin D3, 1α-hydroxylase gene confers positive and negative responsiveness to PTH, calcitonin, and 1α,25(OH)2D3. *Biochemical and Biophysical Research Communications*, *249*(1), 11–6. https://doi.org/10.1006/bbrc.1998.9098

Nakai, K., Fujii, H., Kono, K., Goto, S., Kitazawa, R., Kitazawa, S., … Nishi, S. (2014). Vitamin D Activates the Nrf2-Keap1 Antioxidant Pathway and Ameliorates Nephropathy in Diabetic Rats. *American Journal of Hypertension*, *27*(4), 586–595. https://doi.org/10.1093/ajh/hpt160

Nakamoto, R. K., Baylis Scanlon, J. A., & Al-Shawi, M. K. (2008). The rotary mechanism of the ATP synthase. *Archives of Biochemistry and Biophysics*, *476*(1), 43–50. https://doi.org/10.1016/j.abb.2008.05.004

Naoumov, N. V. (2014). Cyclophilin inhibition as potential therapy for liver diseases. *Journal of Hepatology*, *61*(5), 1166–1174. https://doi.org/10.1016/j.jhep.2014.07.008

Napoli, E., Morin, D., Bernhardt, R., Buckpitt, A., & Cortopassi, G. (2007). Hemin rescues adrenodoxin, heme a and cytochrome oxidase activity in frataxin-deficient oligodendroglioma cells. *Biochimica et Biophysica Acta - Molecular Basis of Disease*, *1772*(7), 773–780. https://doi.org/10.1016/j.bbadis.2007.04.001

Nascimento, A. I., Mar, F. M., & Sousa, M. M. (2018). The intriguing nature of dorsal root ganglion neurons: Linking structure with polarity and function. *Progress in Neurobiology*, *168*, 86–103. https://doi.org/10.1016/j.pneurobio.2018.05.002

Nath, R., Raser, K. J., Stafford, D., Hajimohammadreza, I., Posner, A., Allen, H., … Wang, K. K. (1996). Non-erythroid alpha-spectrin breakdown by calpain and interleukin 1 beta-converting-enzyme-like protease(s) in apoptotic cells: contributory roles of both protease families in neuronal apoptosis. *The Biochemical Journal*, *319 (Pt 3)*, 683–90. https://doi.org/10.1042/bj3190683

Navarro, J. A., Ohmann, E., Sanchez, D., Botella, J. A., Liebisch, G., Moltó, M. D., … Schneuwly, S. (2010). Altered lipid metabolism in a Drosophila model of Friedreich's ataxia. *Human Molecular Genetics*, *19*(14), 2828–40. https://doi.org/10.1093/hmg/ddq183

Nemani, N., Shanmughapriya, S., & Madesh, M. (2018). Molecular regulation of MCU: Implications in physiology and disease. *Cell Calcium*, *74*, 86–93. https://doi.org/10.1016/j.ceca.2018.06.006

Nguyen, T. M., Lieberherr, M., Fritsch, J., Guillozo, H., Alvarez, M. L., Fitouri, Z., … Garabédian, M. (2004). The rapid effects of 1,25-dihydroxyvitamin D3 require the vitamin D receptor and influence 24-hydroxylase activity: Studies in human skin fibroblasts bearing vitamin D receptor mutations. *Journal of Biological Chemistry*, *279*(9), 7591–7. https://doi.org/10.1074/jbc.M309517200

Nicholls, D. G. (1978). The regulation of extramitochondrial free calcium ion concentration by rat liver mitochondria. *The Biochemical Journal*, *176*(2), 463–74. https://doi.org/10.1042/bj1760463

Nita, I. I., Caspi, Y., Gudes, S., Fishman, D., Lev, S., Hersfinkel, M., … Binshtok, A. M. (2016). Privileged crosstalk between TRPV1 channels and mitochondrial

calcium shuttling machinery controls nociception. *Biochimica et Biophysica Acta (BBA) - Molecular Cell Research*, *1863*(12), 2868–2880. https://doi.org/10.1016/j.bbamcr.2016.09.009

O'Sullivan, D. J., & Swallow, M. (1968). The fibre size and content of the radial and sural nerves. *Journal of Neurology, Neurosurgery, and Psychiatry*, *31*(5), 464–470. https://doi.org/10.1136/jnnp.31.5.464

Obis, È., Irazusta, V., Sanchís, D., Ros, J., & Tamarit, J. (2014). Frataxin deficiency in neonatal rat ventricular myocytes targets mitochondria and lipid metabolism. *Free Radical Biology & Medicine*, *73*, 21–33. https://doi.org/10.1016/j.freeradbiomed.2014.04.016

Ohara, P. T., Vit, J. P., Bhargava, A., Romero, M., Sundberg, C., Charles, A. C., & Jasmin, L. (2009). Gliopathic pain: When satellite glial cells go bad. *Neuroscientist*, *15*(5), 450–63. https://doi.org/10.1177/1073858409336094

Ouahchi, K., Arita, M., Kayden, H., Hentati, F., Hamida, M. Ben, Sokol, R., … Koenig, M. (1995). Ataxia with isolated vitamin E deficiency is caused by mutations in the α–tocopherol transfer protein. *Nature Genetics*, *9*(2), 141–145. https://doi.org/10.1038/ng0295-141

Ozaki, T., Yamashita, T., & Ishiguro, S. (2009). Mitochondrial m-calpain plays a role in the release of truncated apoptosis-inducing factor from the mitochondria. *Biochimica et Biophysica Acta (BBA) - Molecular Cell Research*, *1793*(12), 1848–1859. https://doi.org/10.1016/J.BBAMCR.2009.10.002

Palandri, A., L'hôte, D., Cohen-Tannoudji, J., Tricoire, H., & Monnier, V. (2015). Frataxin inactivation leads to steroid deficiency in flies and human ovarian cells. *Human Molecular Genetics*, *24*(9), 2615–2626. https://doi.org/10.1093/hmg/ddv024

Palomo, G. M., Cerrato, T., Gargini, R., & Diaz-Nido, J. (2011). Silencing of frataxin gene expression triggers p53- dependent apoptosis in human neuron-like cells. *Human Molecular Genetics*, *20*(14), 2807–2822. https://doi.org/10.1093/hmg/ddr187

Palomo, G. M., Cerrato, T., Gargini, R., & Diaz-Nido, J. (2011). Silencing of frataxin gene expression triggers p53-dependent apoptosis in human neuron-like cells. *Human Molecular Genetics*, *20*(14), 2807–2822. https://doi.org/10.1093/hmg/ddr187

Palty, R., & Sekler, I. (2012). The mitochondrial Na+/Ca2+ exchanger. *Cell Calcium*, *52*(1), 9–15. https://doi.org/10.1016/j.ceca.2012.02.010

Palty, R., Silverman, W. F., Hershfinkel, M., Caporale, T., Sensi, S. L., Parnis, J., … Sekler, I. (2010). NCLX is an essential component of mitochondrial Na+/Ca 2+ exchange. *Proceedings of the National Academy of Sciences of the United States of America*, *107*(1), 436–441. https://doi.org/10.1073/pnas.0908099107

Pancani, T., Phelps, J. T., Searcy, J. L., Kilgore, M. W., Chen, K. C., Porter, N. M., & Thibault, O. (2009). Distinct modulation of voltage-gated and ligand-gated Ca2+ currents by PPAR-γ agonists in cultured hippocampal neurons. *Journal of Neurochemistry*, *109*(6), 1800–11. https://doi.org/10.1111/j.1471-4159.2009.06107.x

Pastore, A. (2013). Frataxin: a protein in search for a function, *126*, 43–52. https://doi.org/10.1111/jnc.12220

Pastore, A., & Puccio, H. (2013). Frataxin: a protein in search for a function. *Journal of Neurochemistry*, *126*, 43–52. https://doi.org/10.1111/jnc.12220

Patel, M., Schadt, K., McCormick, A., Isaacs, C., Dong, Y. N., & Lynch, D. R. (2019). Open-label pilot study of oral methylprednisolone for the treatment of patients with

friedreich ataxia. *Muscle and Nerve*, *60*(5), 571–575. https://doi.org/10.1002/mus.26610

Patergnani, S., Suski, J. M., Agnoletto, C., Bononi, A., Bonora, M., De Marchi, E., … Pinton, P. (2011). Calcium signaling around Mitochondria Associated Membranes (MAMs). *Cell Communication and Signaling*, *9*(1), 19. https://doi.org/10.1186/1478-811X-9-19

Patron, M., Granatiero, V., Espino, J., Rizzuto, R., & De Stefani, D. (2019). MICU3 is a tissue-specific enhancer of mitochondrial calcium uptake. *Cell Death and Differentiation*, *26*(1), 179–195. https://doi.org/10.1038/s41418-018-0113-8

Paupe, V., Dassa, E. P., Goncalves, S., Auchère, F., Lönn, M., Holmgren, A., & Rustin, P. (2009). Impaired nuclear Nrf2 translocation undermines the oxidative stress response in Friedreich ataxia. *PLoS ONE*, *4*(1). https://doi.org/10.1371/journal.pone.0004253

Paupe, V., Prudent, J., Dassa, E. P., Rendon, O. Z., & Shoubridge, E. A. (2015). CCDC90A (MCUR1) is a cytochrome c oxidase assembly factor and not a regulator of the mitochondrial calcium uniporter. *Cell Metabolism*, *21*(1), 109–116. https://doi.org/10.1016/j.cmet.2014.12.004

Pedersen, J. I., Ghazarian, J. G., Orme Johnson, N. R., & DeLuca, H. F. (1976). Isolation of chick renal mitochondrial ferredoxin active in the 25 hydroxyvitamin D3 1α hydroxylase system. *Journal of Biological Chemistry*, *251*(13), 3933–41. https://doi.org/10.1016/S0021-9258(17)33338-0

Pendin, D., Greotti, E., & Pozzan, T. (2014). The elusive importance of being a mitochondrial Ca2+ uniporter. *Cell Calcium*, *55*(3), 139–145. https://doi.org/10.1016/j.ceca.2014.02.008

Penner, R., Fasolato, C., & Hoth, M. (1993). Calcium influx and its control by calcium release. *Current Opinion in Neurobiology*, *3*(3), 368–74. https://doi.org/10.1016/0959-4388(93)90130-Q

Penzo, D., Tagliapietra, C., Colonna, R., Petronilli, V., & Bernardi, P. (2002). Effects of fatty acids on mitochondria: Implications for cell death. *Biochimica et Biophysica Acta - Bioenergetics*, *1555*(1–3), 160–5. https://doi.org/10.1016/S0005-2728(02)00272-4

Perdomini, M., Hick, A., Puccio, H., & Pook, M. A. (2013). Animal and cellular models of Friedreich ataxia. *Journal of Neurochemistry*, *126*(Suppl.1), 65–79. https://doi.org/10.1111/jnc.12219

Pickrell, A. M., & Youle, R. J. (2015). The roles of PINK1, Parkin, and mitochondrial fidelity in parkinson's disease. *Neuron*, *85*(2), 257–73. https://doi.org/10.1016/j.neuron.2014.12.007

Piguet, F., de Montigny, C., Vaucamps, N., Reutenauer, L., Eisenmann, A., & Puccio, H. (2018). Rapid and Complete Reversal of Sensory Ataxia by Gene Therapy in a Novel Model of Friedreich Ataxia. *Molecular Therapy*, *26*(8), 1940–1952. https://doi.org/10.1016/j.ymthe.2018.05.006

Pike, B. R., Zhao, X., Newcomb, J. K., Posmantur, R. M., Wang, K. K. W., & Hayes, R. L. (1998). Regional calpain and caspase-3 proteolysis of α-spectrin after traumatic brain injury. *NeuroReport*, *9*(11), 2437–42. https://doi.org/10.1097/00001756-199808030-00002

Puccio, H., Simon, D., Cossée, M., Criqui-filipe, P., Tiziano, F., Melki, J., … Koenig, M. (2001). Mouse models for Friedreich ataxia exhibit cardiomyopathy, sensory nerve defect and Fe-S enzyme deficiency followed by intramitochondrial iron deposits. *Nat Genet*, *27*(2), 181–186. https://doi.org/10.1038/84818

Purroy, R., Britti, E., Delaspre, F., Tamarit, J., & Ros, J. (2018). Mitochondrial pore

opening and loss of Ca 2+ exchanger NCLX levels occur after frataxin depletion. *Biochimica et Biophysica Acta (BBA) - Molecular Basis of Disease*, *1864*(2), 618–631. https://doi.org/10.1016/j.bbadis.2017.12.005

Quarato, G., D'Aprile, A., Gavillet, B., Vuagniaux, G., Moradpour, D., Capitanio, N., & Piccoli, C. (2012). The cyclophilin inhibitor alisporivir prevents hepatitis C virus-mediated mitochondrial dysfunction. *Hepatology*, *55*(5), 1333–1343. https://doi.org/10.1002/hep.25514

Quintanilla, R. A., Utreras, E., & Cabezas-Opazo, F. A. (2014). Role of PPAR γ in the differentiation and function of neurons. *PPAR Research*, *2014*, 768594. https://doi.org/10.1155/2014/768594

Rakovic, A., Grunewald, A., Voges, L., Hofmann, S., Orolicki, S., Lohmann, K., & Klein, C. (2011). PINK1-Interacting Proteins: Proteomic Analysis of Overexpressed PINK1. *Parkinson's Disease*, *2011*, 153979. https://doi.org/10.4061/2011/153979

Rao, G., Dwivedi, S. K. D., Zhang, Y., Dey, A., Shameer, K., Karthik, R., … Mukherjee, P. (2020). Micro RNA -195 controls MICU 1 expression and tumor growth in ovarian cancer. *EMBO Reports*, *21*(10), e48483. https://doi.org/10.15252/embr.201948483

Rasola, A., & Bernardi, P. (2007). The mitochondrial permeability transition pore and its involvement in cell death and in disease pathogenesis. *Apoptosis*, *12*(5), 815–33. https://doi.org/10.1007/s10495-007-0723-y

Rasola, A., & Bernardi, P. (2011). Mitochondrial permeability transition in Ca2+-dependent apoptosis and necrosis. *Cell Calcium*, *50*(3), 222–233. https://doi.org/10.1016/j.ceca.2011.04.007

Reinhold, A. K., & Rittner, H. L. (2020). Characteristics of the nerve barrier and the blood dorsal root ganglion barrier in health and disease. *Experimental Neurology*, *327*, 113244. https://doi.org/10.1016/j.expneurol.2020.113244

Ren, K., Ruda, M. A., & Jacobowitz, D. M. (1993). Immunohistochemical localization of calretinin in the dorsal root ganglion and spinal cord of the rat. *Brain Research Bulletin*, *31*(1–2), 13–22. https://doi.org/10.1016/0361-9230(93)90004-U

Ristow, M., Pfister, M. F., Yee, A. J., Schubert, M., Michael, L., Zhang, C. Y., … Kahn, C. R. (2000). Frataxin activates mitochondrial energy conversion and oxidative phosphorylation. *Proceedings of the National Academy of Sciences of the United States of America*, *97*(22), 12239–12243. https://doi.org/10.1073/pnas.220403797

Robledinos-Antón, N., Fernández-Ginés, R., Manda, G., & Cuadrado, A. (2019). Activators and Inhibitors of NRF2: A Review of Their Potential for Clinical Development. *Oxidative Medicine and Cellular Longevity*, *2019*, 9372182. https://doi.org/10.1155/2019/9372182

Rodríguez-Pascau, L., Britti, E., Calap-Quintana, P., Dong, Y. N., Vergara, C., Delaspre, F., … Pizcueta, P. (2020). PPAR gamma agonist leriglitazone improves frataxin-loss impairments in cellular and animal models of Friedreich Ataxia. *Neurobiology of Disease*, *148*, 105162. https://doi.org/10.1016/j.nbd.2020.105162

Rodríguez, L. R., Calap-Quintana, P., Lapeña-Luzón, T., Pallardó, F. V., Schneuwly, S., Navarro, J. A., & Gonzalez-Cabo, P. (2020). Oxidative stress modulates rearrangement of Endoplasmic reticulum-mitochondria contacts and calcium dysregulation in a Friedreich's Ataxia model. *Redox Biology*, *37*, 101762. https://doi.org/10.1016/j.redox.2020.101762

Rong, Y. P., Bultynck, G., Aromolaran, A. S., Zhong, F., Parys, J. B., De Smedt, H., … Distelhorst, C. W. (2009). The BH4 domain of Bcl-2 inhibits ER calcium release

and apoptosis by binding the regulatory and coupling domain of the IP3 receptor. *Proceedings of the National Academy of Sciences of the United States of America*, *106*(34), 14397–402. https://doi.org/10.1073/pnas.0907555106

Rötig, A., de Lonlay, P., Chretien, D., Foury, F., Koenig, M., Sidi, D., … Rustin, P. (1997). Aconitase and mitochondrial iron–sulphur protein deficiency in Friedreich ataxia. *Nature Genetics*, *17*(2), 215–217. https://doi.org/10.1038/ng1097-215

Rouault, T. A., & Tong, W. H. (2005). Iron-sulphur cluster biogenesis and mitochondrial iron homeostasis. *Nature Reviews Molecular Cell Biology*, *6*(4), 345–51. https://doi.org/10.1038/nrm1620

Roumaud, P., Rwigemera, A., & Martin, L. J. (2017). Transcription factors SF1 and cJUN cooperate to activate the Fdx1 promoter in MA-10 Leydig cells. *Journal of Steroid Biochemistry and Molecular Biology*, *171*, 121–132. https://doi.org/10.1016/j.jsbmb.2017.03.003

Runko, A. P., Griswold, A. J., & Min, K.-T. (2008). Overexpression of frataxin in the mitochondria increases resistance to oxidative stress and extends lifespan in *Drosophila*. *FEBS Letters*, *582*(5), 715–719. https://doi.org/10.1016/j.febslet.2008.01.046

Ryan, Z. C., Craig, T. A., Folmes, C. D., Wang, X., Lanza, I. R., Schaible, N. S., … Kumar, R. (2016). 1α,25-dihydroxyvitamin D3 regulates mitochondrial oxygen consumption and dynamics in human skeletal muscle cells. *Journal of Biological Chemistry*, *291*(3), 1514–28. https://doi.org/10.1074/jbc.M115.684399

Sadan, O., Melamed, E., & Offen, D. (2009). Bone-marrow-derived mesenchymal stem cell therapy for neurodegenerative diseases. *Expert Opinion on Biological Therapy*, *9*(12), 1487–1497. https://doi.org/10.1517/14712590903321439

Sakaki, T., Kagawa, N., Yamamoto, K., & Inouye, K. (2005). Metabolism of vitamin D3 by cytochromes P450. *Frontiers in Bioscience : A Journal and Virtual Library*, *10*, 119–34. https://doi.org/10.2741 / 1514

Samanta, K., Kar, P., Chakraborti, T., & Chakraborti, S. (2010). Calcium-dependent cleavage of the Na+/Ca2+ exchanger by m-calpain in isolated endoplasmic reticulum. *Journal of Biochemistry*, *147*(2), 225–35. https://doi.org/10.1093/jb/mvp176

Sanchez-Casis, G., Cote, M., & Barbeau, A. (1976). Pathology of the heart in Friedreich's ataxia: review of the literature and report of one case. *Can.J.Neurol.Sci.*, *3*(4), 349–354. https://doi.org/10.1017/S0317167100025580

Santos, M. M., Ohshima, K., & Pandolfo, M. (2001). Frataxin deficiency enhances apoptosis in cells differentiating into neuroectoderm. *Human Molecular Genetics*, *10*(18), 1935–44. https://doi.org/10.1093/hmg/10.18.1935

Sawada, N., Sakaki, T., Kitanaka, S., Kato, S., & Inouye, K. (2001). Structure-function analysis of CYP27B1 and CYP27A1. *European Journal of Biochemistry*, *268*(24), 6607–15. https://doi.org/10.1046/j.0014-2956.2001.02615.x

Sazanov, L. A., & Hinchliffe, P. (2006). Structure of the hydrophilic domain of respiratory complex I from Thermus thermophilus. *Science*, *311*(5766), 1430–1436. https://doi.org/10.1126/science.1123809

Schiavi, A., Maglioni, S., Palikaras, K., Shaik, A., Strappazzon, F., Brinkmann, V., … Ventura, N. (2015). Iron-Starvation-Induced Mitophagy Mediates Lifespan Extension upon Mitochondrial Stress in C. elegans. *Current Biology*, *25*(14), 1810–22. https://doi.org/10.1016/j.cub.2015.05.059

Schiavi, A., Torgovnick, A., Kell, A., Megalou, E., Castelein, N., Guccini, I., … Ventura, N. (2013). Autophagy induction extends lifespan and reduces lipid content in response to frataxin silencing in C. elegans. *Experimental Gerontology*,

48(2), 191–201. https://doi.org/10.1016/j.exger.2012.12.002

Schiavone, M., Zulian, A., Menazza, S., Petronilli, V., Argenton, F., Merlini, L., … Bernardi, P. (2017). Alisporivir rescues defective mitochondrial respiration in Duchenne muscular dystrophy. *Pharmacological Research*, *125*, 122–131. https://doi.org/10.1016/j.phrs.2017.09.001

Schmidt, H., Stonkute, A., Jüttner, R., Schäffer, S., Buttgereit, J., Feil, R., … Rathjen, F. G. (2007). The receptor guanylyl cyclase Npr2 is essential for sensory axon bifurcation within the spinal cord. *Journal of Cell Biology*, *179*(2), 331–40. https://doi.org/10.1083/jcb.200707176

Schoenfeld, R. A., Napoli, E., Wong, A., Zhan, S., Reutenauer, L., Morin, D., … Cortopassi, G. A. (2005). Frataxin deficiency alters heme pathway transcripts and decreases mitochondrial heme metabolites in mammalian cells. *Human Molecular Genetics*, *14*(24), 3787–3799. https://doi.org/10.1093/hmg/ddi393

Schreiber, S. L., & Crabtree, G. R. (1992). The mechanism of action of cyclosporin A and FK506. *Immunology Today*, *13*(4), 136–142. https://doi.org/10.1016/0167-5699(92)90111-J

Schulz, J. B., Boesch, S., Bürk, K., Dürr, A., Giunti, P., Mariotti, C., … Pandolfo, M. (2009). Diagnosis and treatment of Friedreich ataxia: A European perspective. *Nature Reviews Neurology*, *5*(4), 222–234. https://doi.org/10.1038/nrneurol.2009.26

Schulz, J. B., Dehmer, T., Schöls, L., Mende, H., Hardt, C., Vorgerd, M., … Bogdanov, M. B. (2000). Oxidative stress in patients with Friedreich ataxia. *Neurology*, *55*(11), 1719–1721. https://doi.org/10.1212/WNL.55.11.1719

Schwaller, B. (2014). Calretinin: From a 'simple' Ca2+ buffer to a multifunctional protein implicated in many biological processes. *Frontiers in Neuroanatomy*, *8*, 3. https://doi.org/10.3389/fnana.2014.00003

Scroggs, R. S., & Fox, A. P. (1992). Calcium current variation between acutely isolated adult rat dorsal root ganglion neurons of different size. *The Journal of Physiology*, *445*, 639–58. https://doi.org/10.1113/jphysiol.1992.sp018944

Selak, M. A., Lyver, E., Micklow, E., Deutsch, E. C., Önder, Ö., Selamoglu, N., … Sarry, J. E. (2011). Blood cells from Friedreich ataxia patients harbor frataxin deficiency without a loss of mitochondrial function. *Mitochondrion*, *11*(2), 342–50. https://doi.org/10.1016/j.mito.2010.12.003

Shan, Y., Napoli, E., & Cortopassi, G. (2007). Mitochondrial frataxin interacts with ISD11 of the NFS1/ISCU complex and multiple mitochondrial chaperones. *Hum Mol Genet*, *16*(8), 929–41. https://doi.org/10.1093/hmg/ddm038

Shan, Y., Schoenfeld, R. A., Hayashi, G., Napoli, E., Akiyama, T., Iodi Carstens, M., … Cortopassi, G. A. (2013). Frataxin deficiency leads to defects in expression of antioxidants and Nrf2 expression in dorsal root ganglia of the Friedreich's ataxia YG8R mouse model. *Antioxidants & Redox Signaling*, *19*(13), 1481–93. https://doi.org/10.1089/ars.2012.4537

Shanmughapriya, S., Tomar, D., Dong, Z., Slovik, K. J., Nemani, N., Natarajaseenivasan, K., … Madesh, M. (2018). FOXD1-dependent MICU1 expression regulates mitochondrial activity and cell differentiation. *Nature Communications*, *9*(1), 3449. https://doi.org/10.1038/s41467-018-05856-4

Sheftel, A. D., Stehling, O., Pierik, A. J., Elsässer, H. P., Mühlenhoff, U., Webert, H., … Lill, R. (2010). Humans possess two mitochondrial ferredoxins, Fdx1 and Fdx2, with distinct roles in steroidogenesis, heme, and Fe/S cluster biosynthesis. *Proceedings of the National Academy of Sciences of the United States of America*, *107*(26), 11775–11780. https://doi.org/10.1073/pnas.1004250107

Shen, X., Wong, J., Prakash, T. P., Rigo, F., Li, Y., Napierala, M., & Corey, D. R. (2020). Progress towards drug discovery for Friedreich's Ataxia: Identifying synthetic oligonucleotides that more potently activate expression of human frataxin protein. *Bioorganic and Medicinal Chemistry*, *28*(11), 115472. https://doi.org/10.1016/j.bmc.2020.115472

Shepherd, D., & Garland, P. B. (1969). The kinetic properties of citrate synthase from rat liver mitochondria. *The Biochemical Journal*, *114*(3), 597–610. https://doi.org/10.1042/bj1140597

Shi, Y., Ghosh, M., Kovtunovych, G., Crooks, D. R., & Rouault, T. A. (2012). Both human ferredoxins 1 and 2 and ferredoxin reductase are important for iron-sulfur cluster biogenesis. *Biochimica et Biophysica Acta - Molecular Cell Research*, *1823*(2), 484–492. https://doi.org/10.1016/j.bbamcr.2011.11.002

Shidara, Y., & Hollenbeck, P. J. (2010). Defects in Mitochondrial Axonal Transport and Membrane Potential without Increased ROS Production in a Drosophila Model of Friedreich Ataxia. *The Journal of Neuroscience : The Official Journal of the Society for Neuroscience*, *30*(2010), 11369–78. https://doi.org/10.1523/JNEUROSCI.0529-10.2010

Shimizu, S., Konishi, A., Kodama, T., & Tsujimoto, Y. (2000). BH4 domain of antiapoptotic Bcl-2 family members closes voltage-dependent anion channel and inhibits apoptotic mitochondrial changes and cell death. *Proceedings of the National Academy of Sciences of the United States of America*, *97*(7), 3100–3105. https://doi.org/10.1073/pnas.97.7.3100

Shioda, N., Han, F., Moriguchi, S., & Fukunaga, K. (2007). Constitutively active calcineurin mediates delayed neuronal death through Fas-ligand expression via activation of NFAT and FKHR transcriptional activities in mouse brain ischemia. *Journal of Neurochemistry*, *102*(5), 1506–1517. https://doi.org/10.1111/j.1471-4159.2007.04600.x

Shishkin, V., Potapenko, E., Kostyuk, E., Girnyk, O., Voitenko, N., & Kostyuk, P. (2002). Role of mitochondria in intracellular calcium signaling primary and secondary sensory neurones of rats. *Cell Calcium*, *32*(3), 121–130. https://doi.org/10.1016/S0143-4160(02)00095-7

Sieber, M., & Baumgrass, R. (2009). Novel inhibitors of the calcineurin/NFATc hub - Alternatives to CsA and FK506? *Cell Communication and Signaling*, *7*, 25. https://doi.org/10.1186/1478-811X-7-25

Šileikytė, J., & Forte, M. (2016). Shutting down the pore: The search for small molecule inhibitors of the mitochondrial permeability transition. *Biochimica et Biophysica Acta - Bioenergetics*, *1857*(8), 1197–1202. https://doi.org/10.1016/j.bbabio.2016.02.016

Siman, R., Baudry, M., & Lynch, G. (1984). Brain fodrin: substrate for calpain I, an endogenous calcium-activated protease. *Proceedings of the National Academy of Sciences*, *81*(11), 3572–3576. https://doi.org/10.1073/pnas.81.11.3572

Smith, H. S. (2009). Calcineurin as a nociceptor modulator. *Pain Physician*, *12*(4), e309-18. https://doi.org/10.36076/ppj.2009/12/E09

Smith, M. A., & Schnellmann, R. G. (2012). Calpains , mitochondria , and apoptosis. *Cardiovascular Research*, *96*(1), 32–7. https://doi.org/10.1093/cvr/cvs163

Steinbach, W. J., Reedy, J. L., Cramer, R. A., Perfect, J. R., & Heitman, J. (2007). Harnessing calcineurin as a novel anti-infective agent against invasive fungal infections. *Nature Reviews Microbiology*, *5*(6), 418–30. https://doi.org/10.1038/nrmicro1680

Steven, A., Friedrich, M., Jank, P., Heimer, N., Budczies, J., Denkert, C., & Seliger, B.

(2020). What turns CREB on? And off? And why does it matter? *Cellular and Molecular Life Sciences*, *77*(20), 4049–4067. https://doi.org/10.1007/s00018-020-03525-8

Stoffler, D., Goldie, K. N., Feja, B., & Aebi, U. (1999). Calcium-mediated structural changes of native nuclear pore complexes monitored by time-lapse atomic force microscopy. *Journal of Molecular Biology*, *287*(4), 741–52. https://doi.org/10.1006/jmbi.1999.2637

Stram, A. R., Wagner, G. R., Fogler, B. D., Pride, P. M., Hirschey, M. D., & Payne, R. M. (2017). Progressive mitochondrial protein lysine acetylation and heart failure in a model of Friedreich's Ataxia cardiomyopathy. *PLoS ONE*, *12*(5), e0178354. https://doi.org/10.1371/journal.pone.0178354

Strushkevich, N., MacKenzie, F., Cherkesova, T., Grabovec, I., Usanov, S., & Park, H.-W. (2011). Structural basis for pregnenolone biosynthesis by the mitochondrial monooxygenase system. *Proceedings of the National Academy of Sciences*, *108*(25), 10139–10143. https://doi.org/10.1073/pnas.1019441108

Sturm, B., Stupphann, D., Kaun, C., Boesch, S., Schranzhofer, M., Wojta, J., … Scheiber-Mojdehkar, B. (2005). Recombinant human erythropoietin: Effects on frataxin expression in vitro. *European Journal of Clinical Investigation*, *35*(11), 711–717. https://doi.org/10.1111/j.1365-2362.2005.01568.x

Sudji, I. R., Subburaj, Y., Frenkel, N., García-Sáez, A. J., & Wink, M. (2015). Membrane disintegration caused by the steroid saponin digitonin is related to the presence of cholesterol. *Molecules*, *20*(11), 20146–60. https://doi.org/10.3390/molecules201119682

Svichar, N., Kostyuk, P., & Verkhratsky, A. (1997). Mitochondria buffer Ca2+ entry but not intracellular Ca2+ release in mouse DRG neurones. *NeuroReport*, *8*(18), 3929–32. https://doi.org/10.1097/00001756-199712220-00017

Swenson, S. A., Moore, C. M., Marcero, J. R., Medlock, A. E., Reddi, A. R., & Khalimonchuk, O. (2020). From Synthesis to Utilization: The Ins and Outs of Mitochondrial Heme. *Cells*, *9*(3), 579. https://doi.org/10.3390/cells9030579

Szabadkai, G., Bianchi, K., Várnai, P., De Stefani, D., Wieckowski, M. R., Cavagna, D., … Rizzuto, R. (2006). Chaperone-mediated coupling of endoplasmic reticulum and mitochondrial Ca2+ channels. *Journal of Cell Biology*, *175*(6), 901–11. https://doi.org/10.1083/jcb.200608073

Tague, S. E., & Smith, P. G. (2011). Vitamin D receptor and enzyme expression in dorsal root ganglia of adult female rats: modulation by ovarian hormones. *Journal of Chemical Neuroanatomy*, *41*(1), 1–12. https://doi.org/10.1016/j.jchemneu.2010.10.001

Tait, S. W. G., & Green, D. R. (2010). Mitochondria and cell death: Outer membrane permeabilization and beyond. *Nature Reviews Molecular Cell Biology*, *11*(9), 621–32. https://doi.org/10.1038/nrm2952

Tajiri, N., Staples, M., Kaneko, Y., Kim, S. U., Zesiewicz, T. A., & Borlongan, C. V. (2014). Autologous stem cell transplant with gene therapy for Friedreich ataxia. *Medical Hypotheses*, *83*(3), 296–298. https://doi.org/10.1016/j.mehy.2014.05.022

Takeuchi, A., Kim, B., & Matsuoka, S. (2013). The mitochondrial Na+-Ca 2+ exchanger, NCLX, regulates automaticity of HL-1 cardiomyocytes. *Scientific Reports*, *3*(1), 1–11. https://doi.org/10.1038/srep02766

Takeuchi, A., Kim, B., & Matsuoka, S. (2020). Physiological functions of mitochondrial Na+-Ca2+ exchanger, NCLX, in lymphocytes. *Cell Calcium*, *85*, 102114. https://doi.org/10.1016/j.ceca.2019.102114

Tamarit, J., Britti, E., Delaspre, F., Medina-Carbonero, M., Sanz-Alcázar, A., Cabiscol,

E., & Ros, J. (2021). Mitochondrial iron and calcium homeostasis in Friedreich ataxia. *IUBMB Life*, *73*(3), 543–553. https://doi.org/10.1002/iub.2457

Tamarit, J., Obis, È., & Ros, J. (2016). Oxidative stress and altered lipid metabolism in Friedreich ataxia. *Free Radical Biology and Medicine*, *100*, 138–146. https://doi.org/10.1016/j.freeradbiomed.2016.06.007

Thierbach, R., Drewes, G., Fusser, M., Voigt, A., Kuhlow, D., Blume, U., … Ristow, M. (2010). The Friedreich's ataxia protein frataxin modulates DNA base excision repair in prokaryotes and mammals. *Biochemical Journal*, *432*(1), 165–72. https://doi.org/10.1042/BJ20101116

Thierbach, R., Schulz, T. J., Isken, F., Voigt, A., Mietzner, B., Drewes, G., … Ristow, M. (2005). Targeted disruption of hepatic frataxin expression causes impaired mitochondrial function, decreased life span and tumor growth in mice. *Human Molecular Genetics*, *14*(24), 3857–64. https://doi.org/10.1093/hmg/ddi410

Thomas, R. E., Andrews, L. A., Burman, J. L., Lin, W., & Pallanck, L. J. (2014). PINK1-Parkin Pathway Activity Is Regulated by Degradation of PINK1 in the Mitochondrial Matrix. *PLoS Genetics*, *10*(5), e1004279. https://doi.org/10.1371/journal.pgen.1004279

Tomar, D., Dong, Z., Shanmughapriya, S., Koch, D. A., Thomas, T., Hoffman, N. E., … Madesh, M. (2016). MCUR1 Is a Scaffold Factor for the MCU Complex Function and Promotes Mitochondrial Bioenergetics. *Cell Reports*, *15*(8), 1673–1685. https://doi.org/10.1016/j.celrep.2016.04.050

Tsai, C.-W., Wu, Y., Pao, P.-C., Phillips, C. B., Williams, C., Miller, C., … Tsai, M.-F. (2017). Proteolytic control of the mitochondrial calcium uniporter complex. *Proceedings of the National Academy of Sciences of the United States of America*, *114*(17), 4388–4393. https://doi.org/10.1073/pnas.1702938114

Tsubuki, S., Saito, Y., Tomioka, M., Ito, H., & Kawashima, S. (1996). Differential inhibition of calpain and proteasome activities by peptidyl aldehydes of di-leucine and tri-leucine. *Journal of Biochemistry*, *119*(3), 572–6. https://doi.org/10.1093/oxfordjournals.jbchem.a021280

Turchi, R., Tortolici, F., Guidobaldi, G., Iacovelli, F., Falconi, M., Rufini, S., … Aquilano, K. (2020). Frataxin deficiency induces lipid accumulation and affects thermogenesis in brown adipose tissue. *Cell Death and Disease*, *11*(3), 165. https://doi.org/10.1038/s41419-020-2253-2

Ulrich, J. D., Kim, M. S., Houlihan, P. R., Shutov, L. P., Mohapatra, D. P., Strack, S., & Usachev, Y. M. (2012). Distinct activation properties of the nuclear factor of activated T-cells (NFAT) isoforms NFATc3 and NFATc4 in neurons. *Journal of Biological Chemistry*, *287*(45), 37594–609. https://doi.org/10.1074/jbc.M112.365197

Unoki, M., & Nakamura, Y. (2001). Growth-suppressive effects of BPOZ and EGR2, two genes involved in the PTEN signaling pathway. *Oncogene*, *20*(33), 4457–65. https://doi.org/10.1038/sj.onc.1204608

Valdivielso, J. M., Cannata-Andía, J., Coll, B., & Fernández, E. (2009). A new role for vitamin D receptor activation in chronic kidney disease. *American Journal of Physiology - Renal Physiology*, *297*(6), F1502-9. https://doi.org/10.1152/ajprenal.00130.2009

Van Buyten, J. P. (2018). Dorsal Root Ganglion Stimulation. In *Essentials of Pain Medicine* (p. 683–692. e1). https://doi.org/10.1016/b978-0-323-40196-8.00075-9

Vaubel, R. A., & Isaya, G. (2013). Iron-sulfur cluster synthesis, iron homeostasis and oxidative stress in Friedreich ataxia. *Molecular and Cellular Neuroscience*, *55*, 50–61. https://doi.org/10.1016/j.mcn.2012.08.003

Vaubel, R. A., Rustin, P., & Isaya, G. (2011). Mutations in the Dimer Interface of Dihydrolipoamide Dehydrogenase Promote Site-specific Oxidative Damages in Yeast and Human Cells. *Journal of Biological Chemistry*, *286*(46), 40232–45. https://doi.org/10.1074/jbc.M111.274415

Vázquez-Manrique, R. P., González-Cabo, P., Ros, S., Aziz, H., Baylis, H. A., & Palau, F. (2006). Reduction of Caenorhabditis elegans frataxin increases sensitivity to oxidative stress, reduces lifespan, and causes lethality in a mitochondrial complex II mutant. *The FASEB Journal*, *20*(1), 172–4. https://doi.org/10.1096/fj.05-4212fje

Ventura, N., Rea, S., Henderson, S. T., Condo, I., Johnson, T. E., & Testi, R. (2005). Reduced expression of frataxin extends the lifespan of Caenorhabditis elegans. *Aging Cell*, *4*(2), 109–12. https://doi.org/10.1111/j.1474-9726.2005.00149.x

Vieth, R. (2020). Vitamin D supplementation: cholecalciferol, calcifediol, and calcitriol. *European Journal of Clinical Nutrition*, *74*(11), 1493–1497. https://doi.org/10.1038/s41430-020-0697-1

Vihma, H., Luhakooder, M., Pruunsild, P., & Timmusk, T. (2016). Regulation of different human NFAT isoforms by neuronal activity. *Journal of Neurochemistry*, *137*(3), 394–408. https://doi.org/10.1111/jnc.13568

Vyas, P. M., Tomamichel, W. J., Pride, P. M., Babbey, C. M., Wang, Q., Mercier, J., … Payne, R. M. (2012). A TAT–frataxin fusion protein increases lifespan and cardiac function in a conditional Friedreich's ataxia mouse model. *Human Molecular Genetics*, *21*(6), 1230–1247. https://doi.org/10.1093/hmg/ddr554

Wagner, G. R., Melanie Pride, P., Babbey, C. M., & Mark Payne, R. (2012). Friedreich's ataxia reveals a mechanism for coordinate regulation of oxidative metabolism via feedback inhibition of the SIRT3 deacetylase. *Human Molecular Genetics*, *21*(12), 2688–2697. https://doi.org/10.1093/hmg/dds095

Wai, T., Saita, S., Nolte, H., Müller, S., König, T., Richter-Dennerlein, R., … Langer, T. (2016). The membrane scaffold SLP2 anchors a proteolytic hub in mitochondria containing PARL and the i-AAA protease YME1L. *EMBO Reports*, *17*, 1844–1856. https://doi.org/10.15252/embr

Wang, K. K. W. (2000). Calpain and caspase: Can you tell the difference? *Trends in Neurosciences*, *23*(1), 20–26. https://doi.org/10.1016/S0166-2236(99)01479-4

Wang, L., Cho, Y.-L., Tang, Y., Wang, J., Park, J.-E., Wu, Y., … Shen, H.-M. (2018). PTEN-L is a novel protein phosphatase for ubiquitin dephosphorylation to inhibit PINK1–Parkin-mediated mitophagy. *Cell Research*, *28*(8), 787–802. https://doi.org/10.1038/s41422-018-0056-0

Wang, L., Wang, J., Tang, Y., & Shen, H. M. (2018). PTEN-L puts a brake on mitophagy. *Autophagy*, *14*(11), 2023–2025. https://doi.org/10.1080/15548627.2018.1502565

Wang, X., Han, D., & Li, G. (2018). Electrocardiographic manifestations in severe hypokalemia. *Journal of International Medical Research*, *48*(1), 300060518811058. https://doi.org/10.1177/0300060518811058

Wanichawan, P., Hafver, T. L., Hodne, K., Aronsen, J. M., Lunde, I. G., Dalhus, B., … Carlson, C. R. (2014). Molecular basis of Calpain cleavage and inactivation of the sodium-calcium exchanger 1 in heart failure. *Journal of Biological Chemistry*, *289*(49), 33984–98. https://doi.org/10.1074/jbc.M114.602581

Warne, J., Pryce, G., Hill, J. M., Shi, X., Lennerås, F., Puentes, F., … Selwood, D. L. (2016). Selective inhibition of the mitochondrial permeability transition pore protects against neurodegeneration in experimental multiple sclerosis. *Journal of Biological Chemistry*, *291*(9), 4356–4373. https://doi.org/10.1074/jbc.M115.700385

Webert, H., Freibert, S. A., Gallo, A., Heidenreich, T., Linne, U., Amlacher, S., … Lill, R. (2014). Functional reconstitution of mitochondrial Fe/S cluster synthesis on Isu1 reveals the involvement of ferredoxin. *Nature Communications*, *5*(1), 1–12. https://doi.org/10.1038/ncomms6013

Wilkins, B. J., Dai, Y. S., Bueno, O. F., Parsons, S. A., Xu, J., Plank, D. M., … Molkentin, J. D. (2004). Calcineurin/NFAT Coupling Participates in Pathological, but not Physiological, Cardiac Hypertrophy. *Circulation Research*, *94*(1), 110–8. https://doi.org/10.1161/01.RES.0000109415.17511.18

Wong, A. O. T., Wong, G., Shen, M., Chow, M. Z. Y., Tse, W. W., Gurung, B., … Li, R. A. (2019). Correlation between frataxin expression and contractility revealed by in vitro Friedreich's ataxia cardiac tissue models engineered from human pluripotent stem cells. *Stem Cell Research and Therapy*, *10*(1), 203. https://doi.org/10.1186/s13287-019-1305-y

Wong, A., Yang, J., Cavadini, P., Gellera, C., Lonnerdal, B., Taroni, F., & Cortopassi, G. (1999). The Friedreich's ataxia mutation confers cellular sensitivity to oxidant stress which is rescued by chelators of iron and calcium and inhibitors of apoptosis. *Human Molecular Genetics*, *8*(3), 425–430. https://doi.org/10.1093/hmg/8.3.425

Wood, J. N., Winter, J., James, I. F., Rang, H. P., Yeats, J., & Bevan, S. (1988). Capsaicin-induced ion fluxes in dorsal root ganglion cells in culture. *Journal of Neuroscience*, *8*(9), 3208–20. https://doi.org/10.1523/jneurosci.08-09-03208.1988

Worby, C. A., & Dixon, J. E. (2014). PTEN. *Annual Review of Biochemistry*, *83*, 641–69. https://doi.org/10.1146/annurev-biochem-082411-113907

Yoon, T., & Cowan, J. A. (2003). Iron-sulfur cluster biosynthesis. Characterization of frataxin as an iron donor for assembly of [2Fe-2S] clusters in ISU-type proteins. *Journal of the American Chemical Society*, *125*(20), 6078–6084. https://doi.org/10.1021/ja027967i

Yoon, T., & Cowan, J. A. (2004). Frataxin-mediated iron delivery to ferrochelatase in the final step of heme biosynthesis. *Journal of Biological Chemistry*, *279*(25), 25943–25946. https://doi.org/10.1074/jbc.C400107200

Zalewski, A., Ma, N. S., Legeza, B., Renthal, N., Flück, C. E., & Pandey, A. V. (2016). Vitamin D-dependent rickets type 1 caused by mutations in CYP27B1 affecting protein interactions with adrenodoxin. *Journal of Clinical Endocrinology and Metabolism*, *101*(9), 3409–18. https://doi.org/10.1210/jc.2016-2124

Zanatta, L., Zamoner, A., Zanatta, A. P., Bouraïma-Lelong, H., Delalande, C., Bois, C., … Silva, F. R. M. B. (2011). Nongenomic and genomic effects of 1α,25(OH)2 vitamin D3 in rat testis. *Life Sciences*, *89*(15–16), 515–523. https://doi.org/10.1016/j.lfs.2011.04.008

Zarse, K., Schulz, T. J., Birringer, M., & Ristow, M. (2007). Impaired respiration is positively correlated with decreased life span in Caenorhabditis elegans models of Friedreich Ataxia. *The FASEB Journal*, *21*(4), 1271–5. https://doi.org/10.1096/fj.06-6994com

Zesiewicz, T., Salemi, J. L., Perlman, S., Sullivan, K. L., Shaw, J. D., Huang, Y., … Klein, M. B. (2018). Double-blind, randomized and controlled trial of EPI-743 in Friedreich's ataxia. *Neurodegenerative Disease Management*, *8*(4), 233–242. https://doi.org/10.2217/nmt-2018-0013

Zhang, Q.-G., Wu, D.-N., Han, D., & Zhang, G.-Y. (2007). Critical role of PTEN in the coupling between PI3K/Akt and JNK1/2 signaling in ischemic brain injury. *FEBS Letters*, *581*(3), 495–505. https://doi.org/10.1016/j.febslet.2006.12.055

Zhang, Z., Larner, S. F., Liu, M. C., Zheng, W., Hayes, R. L., & Wang, K. K. W.

(2009). Multiple alphaII-spectrin breakdown products distinguish calpain and caspase dominated necrotic and apoptotic cell death pathways. *Apoptosis*, *14*(11), 1289–98. https://doi.org/10.1007/s10495-009-0405-z

Zhou, S., Shen, D., Wang, Y., Gong, L., Tang, X., Yu, B., … Ding, F. (2012). microRNA-222 Targeting PTEN Promotes Neurite Outgrowth from Adult Dorsal Root Ganglion Neurons following Sciatic Nerve Transection. *PLoS ONE*, *7*(9), e44768. https://doi.org/10.1371/journal.pone.0044768

Zhou, X. F., Cameron, D., & Rush, R. A. (1998). Endogenous neurotrophin-3 supports the survival of a subpopulation of sensory neurons in neonatal rat. *Neuroscience*, *86*(4), 1155–64. https://doi.org/10.1016/S0306-4522(98)00076-1

Zhu, Y., Hoell, P., Ahlemeyer, B., & Krieglstein, J. (2006). PTEN: A crucial mediator of mitochondria-dependent apoptosis. *Apoptosis*, *11*(2), 197–207. https://doi.org/10.1007/s10495-006-3714-5

Zou, X., Ratti, B. A., O'Brien, J. G., Lautenschlager, S. O., Gius, D. R., Bonini, M. G., & Zhu, Y. (2017). Manganese superoxide dismutase (SOD2): is there a center in the universe of mitochondrial redox signaling? *Journal of Bioenergetics and Biomembranes*, *49*(4), 325–333. https://doi.org/10.1007/s10863-017-9718-8

SITOGRAPHY

SITOGRAPHY

https://epd.epfl.ch//index.php

https://www.addgene.org/protocols/plko

https://www.broadinstitute.org

https://www.coriell.org/

https://www.curefa.org

https://www.curefa.org/pipeline.html

https://www.medchemexpress.com/

https://www.sigmaaldrich.com/

PUBLICATIONS

PUBLICATIONS

Tamarit, J., **Britti, E.**, Delaspre, F., Medina-Carbonero, M., Sanz-Alcázar, A., Cabiscol, E., & Ros, J. (2021) (Review). Mitochondrial iron and calcium homeostasis in Friedreich ataxia. *IUBMB Life*, *73*(3), 543–553. https://doi.org/10.1002/iub.2457

Britti, E., Delaspre, F., Sanz-Alcázar, A., Medina-Carbonero, M., Llovera, M., Purroy, R., … Ros, J. (2021). Calcitriol increases frataxin levels and restores mitochondrial function in cell models of Friedreich Ataxia. *Biochemical Journal*, *478*(1), 1–20. https://doi.org/10.1042/BCJ20200331

Rodríguez-Pascau, L., **Britti, E.**, Calap-Quintana, P., Dong, Y. N., Vergara, C., Delaspre, F., … Pizcueta, P. (2020). PPAR gamma agonist leriglitazone improves frataxin-loss impairments in cellular and animal models of Friedreich Ataxia. *Neurobiology of Disease*, *148*, 105162. https://doi.org/10.1016/j.nbd.2020.105162

Britti, E., Delaspre, F., Tamarit, J., & Ros, J. (2020). Calpain-Inhibitors Protect Frataxin-Deficient Dorsal Root Ganglia Neurons from Loss of Mitochondrial Na^{+}/Ca^{2+} Exchanger, NCLX, and Apoptosis. *Neurochemical Research*, *46*(1), 108–119. https://doi.org/10.1007/s11064-020-03020-3

Britti, E., Ros, J., Esteras, N., & Abramov, A. Y. (2020). Tau inhibits mitochondrial calcium efflux and makes neurons vulnerable to calcium-induced cell death. *Cell Calcium*, *86*, 102150. https://doi.org/10.1016/j.ceca.2019.102150

Britti, E., Delaspre, F., Tamarit, J., & Ros, J. (2018). (Review). Mitochondrial calcium signalling and neurodegenerative diseases. *Neuronal Signaling*, *2*(4), 20180061. https://doi.org/10.1042/ns20180061

Purroy, R., **Britti, E.**, Delaspre, F., Tamarit, J., & Ros, J. (2018). Mitochondrial pore opening and loss of Ca^{2+} exchanger NCLX levels occur after frataxin depletion. *Biochimica et Biophysica Acta (BBA) - Molecular Basis of Disease*, *1864*(2), 618–631. https://doi.org/10.1016/j.bbadis.2017.12.005

Britti, E., Delaspre, F., Feldman, A., Osborne, M., Greif, H., Tamarit, J., & Ros, J. (2018). Frataxin-deficient neurons and mice models of Friedreich ataxia are improved by TAT-MTScs-FXN treatment. *Journal of Cellular and Molecular Medicine*, *22*(2), 834–848. https://doi.org/10.1111/jcmm.13365